



Université
de Lille

Ecole Doctorale Biologie Santé de Lille

THÈSE

Pour l'obtention du grade de

DOCTEUR

Discipline : **Aspects moléculaires et cellulaires de la biologie**

Spécialité : **Biochimie et Biologie moléculaire**

NMR STUDY OF 14-3-3 PROTEIN-PROTEIN INTERACTIONS AND MODULATION THEREOF BY SMALL MOLECULES

.....

ÉTUDE PAR RÉSONANCE MAGNÉTIQUE NUCLÉAIRE DES INTERACTIONS PROTÉINE-PROTÉINE DE 14-3-3 ET LEUR MODULATION AVEC DES PETITES MOLÉCULES

Présenté et soutenue publiquement par

João Filipe SECO MARTINS MARQUES NEVES

Le 2 octobre 2019

Directeur de thèse : **Docteur Isabelle LANDRIEU**

JURY

Docteur Xavier MORELLI

Rapporteur

Docteur Françoise OCHSENBEIN

Rapporteur

Professeur Nicolas WILLAND

Président du jury

Professeur Christian OTTMANN

Examineur

Docteur Isabelle LANDRIEU

Directeur de thèse

ACKNOWLEDGMENTS

These three years made me grow significantly, both scientifically and personally. Along the way, I was lucky to be surrounded by people who, during these three years, have made a very important contribution to my work and to my life.

First, I would like to thank my thesis supervisor, Dr. Isabelle Landrieu for having trusted me for this mission when I was still a pharmacy student, for the continuous support and for all the lessons she taught me along the way. Dr. Isabelle gave me a lot of freedom to apply my own ideas and methods and was the one who was there when I most needed.

Besides Dr. Isabelle, I have to further thank Dr. Xavier Hanouille for his continuous support and supervision. This work would definitely not be the same without the important discussions we had.

I also thank the European Union for supporting the TASPPI project (H2020-MSCA-ITN-2015, grant number 675179) and Prof. Christian Ottmann for having made the extraordinary work of creating and coordinating this European Training Network. I also thank Dr. Inge Van Bussel for the great work as project manager of our network.

I also thank the members of the jury, Prof. Christian Ottmann, Dr. Xavier Morelli, Dr. Françoise Ochsenein and Prof. Nicolas Willand for having accepted my invitation and for having provided me their insights on this work.

I am also grateful to the members of the *Comité de Suivi Individuel*, Prof. Christian Ottmann and Prof. Tomáš Obšil for having followed my work and for the valuable suggestions that changed the course of this project.

I am also extremely grateful to Dr. François-Xavier Cantrelle for helping me setting up the NMR experiments and for being a patient “teacher” of NMR spectroscopy. I will always remember those afternoons in front of the spectrometer trying to solve issues with “invisible compounds”, poor shimming, IconNMR, WaterLOGSY experiments, DMSO, manganese and other complications.

I need to thank Hamida Merzougui for teaching me two very important skills to work in the lab: producing proteins and speaking French.

I am also grateful to Emmanuelle Boll for having set-up some NMR experiments with me when the spectrometer was still a stranger to me.

I could not forget all the colleagues from the lab not yet mentioned: Dr. Davy Sinnaeve, Dr. Robert Schneider, Dr. Caroline Smet-Nocca, Dr. Idir Malki, Dr. Elian Dupré, Dr. Alessia Lasorsa, Dr. Geraldine Levy, Dr. Clément Danis, Dr. Clément Despres, Dr. Luiza Bessa and Orgeta Zejneli. It was a pleasure to meet each and every one of you and to see you in the corridors every day. I wish you all the best for your future.

I also need to thank all those who I met on the 18th of September, 2016 in Eindhoven, the day and the place in which the adventure started. I am of course talking about the TASPPI ESRs: Alice Ballone, Federica Centorrino, Madita Wolter, Sonja Srdanovic, Domenico Lentini Santo (who I met a few months later), Marianna Longo (who I met a few months later), Leire Iralde Lorente, Blaž Andlovic, Dario Valenti, Claire Munier, Francesco Bosica and Lorenzo Soini. I will never forget all the collaborations, support and funny moments I had with you. I hope you all get what you want for your future! You all have a bright future in front of you!

I need to acknowledge Prof. Tomáš Obšil for arranging my secondment in Prague which added tremendous value to my work. I also thank everyone from the Obšil group, especially Dr. Olivia Petrválská and Domenico Lentini Santo for their valuable help in the lab.

I also thank Dr. Gavin O'Mahony for arranging my secondment at AstraZeneca in Gothenburg. The work performed during this secondment was very important for my project and made me learn a lot. I also thank Francesco Bosica for his guidance, valuable help and for being so persistent with our trouble-shooting. Many thanks as well to Dr. Anders Gunnarsson and to Claire Munier for their help with the SPR experiments.

I would like to express my gratitude to all TASPPI and external collaborators contributing to our collaborative projects: Ave Kuusk, Claire Munier, Francesco Bosica, Dr. Gavin O'Mahony, Dr. Helen Boyd, Dr. Hongming Chen, Dr. Mathew Perry (AstraZeneca), Domenico Lentini Santo, Prof. Tomáš Obšil (Charles University of Prague), Femke Meijer, Madita Wolter, Dr. Lech-Gustav Milroy, Dr. Sebastian Andrei, Dr. Xavier Guillory, Prof. Christian Ottmann, Prof. Luc Brunsveld (Eindhoven University of Technology), Dario Valenti, Dr. Dimitrios Tzalis, Dr. Laura M. Levy, Dr. Stanimira Hlstroma (Taros Chemicals), Dr. Seppe Leysen (UCB Biopharma), Dr. Kenny Bravo Rodriguez, Prof. Elsa Sanchez Garcia (University of Duisburg-Essen), Sonja Srdanovic, Prof. Andrew J. Wilson (University of Leeds), Dr. Richard Doveston (University of Leicester).

I could not forget the support of all my friends (those in Lille and those thousands of Kilometers away) who always stayed by my side.

I also thank my partner, Marie, for giving me a second life in Lille besides the PhD and for the enormous support during the best and hardest moments. I also need to thank her for the valuable expertise with illustration software and the advice on figures, posters and presentations.

Finally, I could not forget to thank my family for having constructed the person that I am today and for giving me the conditions to follow the right directions. Without them, I would not be where I am today.

ABSTRACT

14-3-3 proteins are adapter proteins that exert their biological functions by modulating the activity of hundreds of proteins. This remarkable interactome makes 14-3-3 proteins influent actors in many cellular events and, by consequence, in several pathologies. The selective stabilization or inhibition of 14-3-3 protein-protein interactions (PPIs) are therefore seen as promising approaches for finding innovative therapies for a number of conditions like Alzheimer's, cancer or Parkinson.

Our first objective towards finding small molecule modulators of these targets was to obtain the molecular detail of 14-3-3 PPIs. To this end, using Nuclear Magnetic Resonance (NMR), we assigned the backbone chemical shifts of 14-3-3 σ . We then studied the 14-3-3/phosphorylated Tau interaction and found that Tau binds strictly within the amphipathic binding groove of 14-3-3 and can anchor in both monomers of the 14-3-3 dimer. We also studied the 14-3-3/p53 interaction and showed by NMR, that intramolecular interactions within the peptide define a conformation that drives the affinity towards 14-3-3.

We then focused on the optimization of NMR assays for screening and characterization of the effect of small-molecules binding to 14-3-3 or 14-3-3 complexes with target's phosphopeptides. We used, for example, phospho-mimetic peptides to inhibit the Tau/14-3-3 interaction. In a different strategy, we screened a fragment library against 14-3-3 σ and found three hits binding to different regions of the protein. Using our NMR assays we further characterized small molecules binding 14-3-3 complexes with, for example, p53 and p65 peptides and demonstrated the stabilization capacity of some compounds.

Keywords: Nuclear magnetic resonance, 14-3-3, Protein-protein interactions, drug discovery

RÉSUMÉ

Les protéines 14-3-3 sont des protéines adaptatrices qui exercent leurs fonctions biologiques en modulant l'activité de certaines d'autres protéines. De par leur impressionnant interactome, les protéines 14-3-3 sont des acteurs qui influencent de nombreux événements cellulaires et, par conséquent, de maladies associées. La stabilisation ou l'inhibition sélective d'interactions protéine-protéine (IPP) de 14-3-3 sont considérées comme des approches prometteuses pour trouver des thérapies innovantes contre des maladies comme la maladie d'Alzheimer, certains cancers ou la maladie de Parkinson.

Notre premier but afin de trouver des petites molécules capables de moduler ces cibles a été d'étudier au niveau moléculaire des IPP de 14-3-3. Dans ce but, nous avons utilisé la Résonance Magnétique Nucléaire (RMN) pour attribuer les déplacements chimiques des atomes du squelette de 14-3-3 σ . Nous avons ensuite étudié l'interaction entre 14-3-3 et la protéine Tau phosphorylée. Nous avons découvert que Tau se lie strictement dans la cavité amphipathique de 14-3-3 et peut s'ancrer aux deux monomères du dimère de 14-3-3. Nous avons aussi étudié l'interaction 14-3-3/p53 et avons découvert, en utilisant la RMN, que l'affinité du peptide p53 envers 14-3-3 est liée à des interactions intramoléculaires au niveau du peptide.

Nous nous sommes enfin focalisés sur l'optimisation d'expériences RMN visant le criblage et la caractérisation de l'activité des petites molécules qui se lient à 14-3-3 ou à des complexes de 14-3-3 avec des peptides phosphorylés. Nous avons aussi utilisé des peptides phospho-mimétiques pour inhiber l'interaction 14-3-3/Tau. D'autre part, nous avons criblé une bibliothèque de fragments contre 14-3-3 σ et trouvé trois *hits* qui se lient à des régions différentes de la protéine. Des expériences RMN ont ensuite permis de caractériser l'activité de certaines petites molécules actives sur des complexes de 14-3-3 avec, par exemple des peptides de p53 ou p65, et nous avons aussi démontré la capacité de certains de ces composés à stabiliser les complexes.

Mots-clés : Résonance magnétique nucléaire, 14-3-3, interactions protéine-protéine, découverte de médicaments

INDEX

ACKNOWLEDGMENTS	iii
ABSTRACT	vi
RÉSUMÉ	vii
INDEX.....	viii
ABBREVIATIONS	xiii
PUBLICATIONS.....	xvi
COMMUNICATIONS.....	xvii
INTRODUCTION	1
1 14-3-3 Proteins.....	2
1.1 The 14-3-3 Family: Isoforms, structure and function	2
1.2 14-3-3 Protein-Protein Interactions	4
1.3 Modulation of 14-3-3 Protein-Protein Interactions: a new hot-topic in drug discovery	7
1.3.1 Inhibitors of 14-3-3 Protein-Protein Interactions.....	7
1.3.2 Stabilizers of 14-3-3 Protein-Protein Interactions.....	9
1.3.3 Fragment-based approach for the identification of starting points for the modulation of 14-3-3 Protein-Protein Interactions	15
2 Methods to study Proteins, Peptides and Protein-Protein Interactions	18
2.1 Protein Nuclear Magnetic Resonance.....	18
2.1.1 1D and 2D NMR of proteins.....	19
2.1.2 Backbone assignment of proteins	22
2.1.3 Backbone assignments of high molecular weight proteins.....	24
2.1.3.1 Deuteration	25
2.1.3.2 Transverse Relaxation Optimized Spectroscopy	26

2.1.3.3	Selective labeling	28
2.1.4	NMR on the study of Protein-Protein Interactions	29
2.1.4.1	Interaction surface determination	30
2.1.4.2	Dissociation constant	32
2.2	Peptide Nuclear Magnetic Resonance	33
2.3	Analytical Ultracentrifugation as a tool to study protein-protein interactions... ..	35
3	The 14-3-3/Tau Protein-Protein Interaction: a promising therapeutic target for Alzheimer's disease	37
3.1	Alzheimer's disease	37
3.1.1	Aggregation of the β -amyloid peptide: The amyloid hypothesis.....	38
3.1.2	Neurofibrillary tangles: Aggregation of Tau protein	40
3.1.2.1	The discovery of neurofibrillary tangles.....	40
3.1.2.2	Tau protein: the main constituent of neurofibrillary tangles	40
3.1.2.3	Tau in the neurofibrillary tangles	43
3.1.3	Treatment of Alzheimer's disease and new investigational drugs	45
3.2	The 14-3-3/Tau Protein-Protein Interaction	49
3.2.1	Structural insights on the 14-3-3/Tau Protein-Protein Interaction.....	49
3.2.2	Functional effects of the 14-3-3/Tau Protein-Protein Interaction.....	52
3.2.2.1	14-3-3 mediates phosphorylation of Tau	52
3.2.2.2	14-3-3 impacts the aggregation of Tau	52
3.2.2.3	14-3-3 increases neuronal Tau mediated toxicity	55
3.2.3	Inhibition of the 14-3-3/Tau Protein-Protein Interaction	56
4	Fragment-based drug discovery	57
4.1	The Fragment-based approach in drug discovery: an alternative to High Throughput Screening.....	57
4.2	Fragment screening.....	59

4.2.1	NMR methods for fragment screening.....	59
4.2.1.1	Ligand-based NMR for fragment screening	60
4.2.1.1.1	Saturation Transfer Difference (STD)	61
4.2.1.1.2	Water-Ligand Observed via Gradient Spectroscopy (WaterLOGSY) ..	64
4.2.1.1.3	Other techniques.....	67
4.2.1.2	Protein-based NMR for fragment screening.....	68
4.2.1.2.1	^1H - ^{15}N HSQC.....	68
4.2.1.2.2	^1H - ^{13}C HSQC.....	70
4.2.2	Differential Scanning Fluorimetry (DSF) for Fragment Screening.....	70
4.2.3	Surface Plasmon Resonance (SPR) for Fragment Screening	71
	OBJECTIVES.....	74
	RESULTS.....	77
1	Backbone chemical shift assignments of human 14-3-3 σ	78
2	Structural Insights on the 14-3-3/Tau Protein-Protein Interaction	91
2.1	Materials and Methods.....	91
2.1.1	14-3-3 Proteins Production and Purification.....	91
2.1.2	Tau Proteins Production and Purification	92
2.1.3	PKA-catalytic subunit Production and Purification	92
2.1.4	In-vitro phosphorylation of Tau.....	93
2.1.5	^1H - ^{15}N TROSY-HSQC Spectroscopy	93
2.1.6	Backbone chemical shift assignment of the C-terminal stretch (A232-S245) of 14-3-3 σ	94
2.1.7	Analytical Ultracentrifugation	94
2.1.8	Surface Plasmon Resonance.....	95
2.2	Results and Discussion	96
2.2.1	Phosphorylation of Tau by PKA enhances its interaction with 14-3-3.....	96

2.2.2	Tau interacts with 14-3-3 exclusively via the amphipathic binding groove...	99
2.2.3	The C-terminal stretch of 14-3-3 σ does not participate in the interaction with Tau.....	101
2.2.4	Tau phosphorylated by PKA occupies both binding grooves of the 14-3-3 dimer.....	102
2.2.5	The affinity of the 14-3-3/Tau-PKA interaction is in the low μ M range.....	104
2.3	Conclusions.....	105
2.4	Supporting Information.....	106
3	Adoption of a Turn conformation drives the binding affinity of the p53 C-terminal domain peptides to 14-3-3 σ	114
3.1	The 14-3-3/p53 protein-protein interaction.....	114
3.2	Context of the collaboration.....	114
3.3	Manuscript (in preparation).....	115
4	Targeting 14-3-3 protein interface with a fragment-based approach.....	159
5	Fragment Screening for the modulation of 14-3-3 interactions with Kinases: the CaMKK2 and ASK1 cases.....	197
5.1	The Interaction of 14-3-3 with ASK1 and CaMKK2.....	197
5.1.1	Interaction of 14-3-3 with ASK1.....	197
5.1.2	Interaction of 14-3-3 with CaMKK2.....	197
5.2	Context of the collaboration.....	198
5.3	Materials and Methods.....	199
5.3.1	Production of $^{15}\text{N}^{13}\text{C}^2\text{H}$ labeled 14-3-3 ζ	199
5.3.2	Ligand-based NMR experiments: Saturation Transfer Difference and WaterLOGSY.....	199
5.3.3	Protein-based NMR experiments: ^1H - ^{15}N TROSY HSQC.....	200
5.4	Results and discussion.....	200
5.4.1	Ligand-based NMR experiments.....	200

5.4.2	Protein-based experiments: ^1H - ^{15}N TROSY-HSQC.....	201
5.5	Conclusions.....	202
5.6	Supporting Information.....	203
6	Inhibition of 14-3-3/Tau by Hybrid Small-Molecule Peptides Operating via Two Different Binding Modes	209
6.1	Context of the collaboration	209
6.2	Manuscript (published)	209
7	Stabilization of the 14-3-3/p65pS45 PPI by Fusicoccin-A	267
7.1	The 14-3-3 role on the NF- κ B interaction	267
7.2	Context of the collaboration	267
7.3	Materials and Methods.....	268
7.3.1	NMR spectroscopy.....	268
7.4	Results and discussion.....	268
7.5	Conclusions.....	271
7.6	Supporting Information.....	272
8	Stabilization of the 14-3-3/p53 Protein-Protein Interaction	275
8.1	Context of the collaboration	275
8.2	Materials and Methods.....	275
8.2.1	WaterLOGSY experiments	275
8.2.2	^1H - ^{15}N TROSY-HSQC NMR spectroscopy.....	276
8.3	Results and discussion.....	276
8.4	Conclusions.....	279
8.5	Supporting Information.....	280
	GENERAL CONCLUSION AND PERSPECTIVES.....	283
	RÉSUMÉ SUBSTANTIEL EN FRANÇAIS.....	290
	REFERENCES	292

ABBREVIATIONS

AD	Alzheimer's disease
AMP	Adenosine monophosphate
APP	Amyloid precursor protein
ASK1	Apoptosis signal-regulating kinase 1
AUC	Analytical ultracentrifugation
BACE	β -secretase
BME	β -mercaptoethanol
CaMKK2	Calcium/calmodulin-dependent protein kinase kinase 2
c(s)	Diffusion-deconvoluted sedimentation coefficients
ChREBP	Carbohydrate-response element-binding protein
CPMG	Carr–Purcell–Meiboom–Gill
CSP	Chemical shift perturbations
DNA	Deoxyribonucleic acid
DSF	Differential scanning fluorimetry
DSS	4,4-dimethyl-4-silapentane-1-sulfonic acid
DTT	Dithiothreitol
FAX	Fluorine chemical shift anisotropy and exchange for screening
FBA	Fragment-based approach
FBDD	Fragment-based drug discovery
FC-A	Fusicoccin A
FP	Fluorescence polarization
GR	Glucocorticoid receptor
GST	Glutathione S-transferase
HSQC	Heteronuclear single quantum coherence spectroscopy
HTS	High-throughput screening
ITC	Isothermal calorimetry
I κ B α	Nuclear factor of kappa light polypeptide gene enhancer in B-cells inhibitor, alpha

K _d	Dissociation constant
K _{off}	Dissociation rate constant
K _{on}	Association rate constant
LB	<i>Luria Bertani</i>
LBM	Ligand-based NMR methods
MD	Molecular dynamics
MDM2	Murine double minute-2
MS	Mass spectrometry
MTBD	Microtubule-binding domain
MW	Molecular-weight
NCLK	Neuronal Cdc2-like Protein Kinase
NF-κB	nuclear factor kappa-light-chain-enhancer of activated B cells
NFT	Neurofibrillary tangles
NMR	Nuclear Magnetic Resonance
NOESY	Nuclear Overhauser effect spectroscopy
O-GlcNAc	O-glycoside-linked N-acetylglucosamine
PBM	Protein-based NMR methods
PET	Positron emission tomography
PHF	Paired helical filament
PK	Pharmacokinetic
PKA	Protein-Kinase A
PLI	Protein-ligand interactions
PPI	Protein-Protein Interactions
ppm	parts per million
PRD	Proline-rich domain
R2	Transverse-relaxation
RU	Response unit
S/N	Signal to noise
SAR	Structure-activity relationship
SE	Sedimentation equilibrium
SF	Straight filaments

SGK1	Serum and glucocorticoid-induced protein kinase
SPLASTIC	Spin labels attached to protein side chains as a tool to identify interacting compounds
SPR	Surface plasmon resonance
SSP	Secondary structure propensity
STD	Saturation transfer difference
SV	Sedimentation velocity
T1	Longitudinal relaxation time
T2	Transverse relaxation time
Tau-PKA	Tau phosphorylated by Protein Kinase A
TCEP	Tris(2-carboxyethyl)phosphine
TINS	Target Immobilized NMR screening
Tm	Melting temperature
TNF α	Tumor necrosis factor alpha
TOCSY	Total correlation spectroscopy
TROSY	Transverse relaxation-optimized spectroscopy
VHH	variable heavy-chain domain
wt-Tau	Wild-type Tau
τ_c	Correlation time

PUBLICATIONS

Published in peer-review journals :

Valenti, D., Neves, J. F., Cantrelle, F.-X., Hristeva, S., Santo, D. L., Obšil, T., ... Ottmann, C. (2019). Set-up and screening of a fragment library targeting the 14-3-3 protein interface. *MedChemComm*, 10(10), 1796–1802. <https://doi.org/10.1039/C9MD00215D>

Neves, J. F., Landrieu, I., Merzougui, H., Boll, E., Hanouille, X., & Cantrelle, F.-X. (2019). Backbone chemical shift assignments of human 14-3-3 σ . *Biomolecular NMR Assignments*, 13(1), 103–107. <https://doi.org/10.1007/s12104-018-9860-1>

Andrei, S. A., Meijer, F. A., Neves, J. F., Brunsveld, L., Landrieu, I., Ottmann, C., & Milroy, L.-G. (2018). Inhibition of 14-3-3/Tau by Hybrid Small-Molecule Peptides Operating via Two Different Binding Modes. *ACS Chemical Neuroscience*, 9(11), 2639–2654. <https://doi.org/10.1021/acscemneuro.8b00118>

In-press:

Danis, C., Dupré, E., Hanouille, X., Landrieu, I., Lasorsa, A., **Neves, J. F.,** Schneider, R., Smet-Nocca, C. Nuclear magnetic resonance spectroscopy insights into Tau structure in solution: Impact of post-translational modifications. *In press*.

In preparation:

Kuusk, A., Neves, J.F., Rodriguez, K. B., Doveston, R. G., Gunnarsson A., Ehrmann, M., ... Ottmann, C. Adoption of a Turn Conformation Drives the Binding Affinity of p53 C-Terminal Domain Peptides to 14-3-3 σ , *in preparation*.

COMMUNICATIONS

Oral presentations:

NMR guided Fragment-based screening applied to the discovery of modulators of 14-3-3 Protein-Protein Interactions; Presented at Drug Discovery Day, 07/12/2017, University of Lille 2, Lille, France.

NMR as a powerful analytical and screening tool for the discovery of modulators of protein-protein interactions; Presented at 2nd International Symposium on Advances in Pharmaceutical Analysis 2018, 12/7/2018 – 13/7/2018, University of Lille, Lille, France.

Poster presentations:

Neves, J. F., Valenti, D., Cantrelle, F-X., Merzougui, H., Boll, E., Wolter, M., Ballone, A., Centorrino, F., Ottmann, C., Tzalis, D., Karawajczyk, A., Hanouille, X., Landrieu, I. *NMR guided Fragment-based screening applied to the discovery of modulators of 14-3-3 Protein-Protein Interactions*; Poster presented at Drug Discovery Day, 07/12/2017, University of Lille 2, Lille, France.

Neves, J. F., Valenti, D., Cantrelle-F-X., Merzougui, H., Boll, E., Wolter, M., Ballone, A., Centorrino, F., Ottlann, C., Tzalis, D., Karawajczyk, A., Hanouille, X., Landrieu, I. *NMR applied to the discovery of modulators of 14-3-3 Protein-Protein Interactions*; Poster presented at Distal scientific advisory board, 24/01/2018, Pasteur Institute of Lille, Lille, France.

Neves, J. F., Valenti, D., Cantrelle-F-X., Merzougui, H., Boll, E., Wolter, M., Ballone, A., Centorrino, F., Ottlann, C., Tzalis, D., Karawajczyk, A., Hanouille, X., Landrieu, I. *NMR study of the 14-3-3/Tau Protein-Protein Interaction and its modulation by small molecules*; Poster presented at EuroTau 2018, 26/04/2018 – 27/04/2018, LILLIAD conference center, Lille, France.

Neves, J. F., Cantrelle, F-X., Merzougui, H., Boll, E., Valenti, D., Andrei, S., Meijer, F., Wolter, M., Ballone, A., Centorrino, F., Santo, D.L., Brunsveld, L., Tzalis, D., Obšil, T., Milroy, L-G., Ottmann, C., Hanouille, X., Landrieu, I. *NMR as a powerful analytical and screening tool for the*

discovery of modulators of protein-protein interactions; Poster presented at Advances in Pharmaceutical Analysis 2018, 12/7/2018 – 13/7/2018, University of Lille, Lille, France.

INTRODUCTION

1 14-3-3 Proteins

1.1 The 14-3-3 Family: Isoforms, structure and function

14-3-3 proteins have been named after bi-dimensional gel electrophoresis experiments on bovine brain tissue by Moore and Perez in 1967 (B.W. Moore & V. J. Perez, 1967). More precisely the name is attributed to the fact that these proteins were identified in position 3-3 on the two-dimensional gel of fraction 14, yielding the name 14-3-3. These ubiquitous proteins are expressed in all tissues and compartments of all eukaryotic organisms. In humans, the 14-3-3 family encompasses seven different isoforms (β , γ , ϵ , η , σ , τ and ζ). Despite the considerably high homology between different isoforms, 14-3-3 activity is sometimes isoform specific (Fu, Subramanian, & Masters, 2000). Having in mind this isoform specific activity it is not surprising that specific 14-3-3 isoforms are more associated with certain targets and certain pathologies than others are. As an example, 14-3-3 σ is the isoform of 14-3-3 most linked to cancer (Benzinger et al., 2005; Kaplan, Ottmann, & Fournier, 2017).

These adapter proteins do not have a defined enzymatic activity, as the basis for their biological functions relies on the binding to their partners, through protein-protein interactions (PPI). These interactions allow 14-3-3 proteins to modulate their partners' subcellular location, activity and even their binding to target molecules. This modulation of their partners' activity allows 14-3-3 to intervene in many pathways in eukaryotic cells. They are involved in cell cycle regulation, signal transduction, Deoxyribonucleic acid (DNA) damage response, cytoskeletal rearrangement, protein trafficking, and apoptosis control (Steinacker, Aitken, & Otto, 2011).

In physiological conditions, 14-3-3 proteins exist as functional dimers, both as hetero and homodimers. They are acidic proteins and each monomer has a molecular weight of around 30 kDa, being composed by nine parallel α -helices, commonly named α A-I or alternatively, α 1-9 (**Figure 1 A**). The dimerization is achieved through salt bridges and hydrophobic interactions between α A and α B of one monomer and α C and α D of the other (Tomas Obsil & Obsilova, 2011). Differences in the amino acid sequence of these helices explains why there are isoforms that are able to form heterodimers while others (σ and γ) exist strictly as homodimers (Fu et al., 2000). In addition to the dimer interface, the

amphipathic groove is the other important structural feature of 14-3-3 proteins. This channel is formed by the helices α C, α E, α G and α I and is crucial for the interaction with its partners. A particularly interesting feature in this channel is the acceptor site for the phosphate group of its partners. This site is extremely important for 14-3-3 proteins' function since most of its targets are phosphorylated proteins (Tomas Obsil & Obsilova, 2011). The side chains of K49, R56, R129 and Y130 (**Figure 1 B**) (numeration according to isoform σ) constitute this interaction center (Benzinger et al., 2005). The interior of this channel is the most conserved region among the different isoforms, which suggests a similar interaction mode with its targets. The residues that constitute the phosphor-acceptor site (K49, R56, R129 and Y130) are strictly conserved among 14-3-3 isoforms. The least conserved regions of 14-3-3 are mostly located at the protein surface (Benzinger et al., 2005). Immediately following the last helix of 14-3-3 proteins (α I), there is a flexible and highly acidic region, which is, contrarily to the amphipathic groove, the most divergent portion of 14-3-3 proteins. Despite the uncertainty regarding the role of this C-terminal region, it is thought to act as a sort of a gatekeeper that occupies the binding groove when no partner is binding (Silhan et al., 2004).

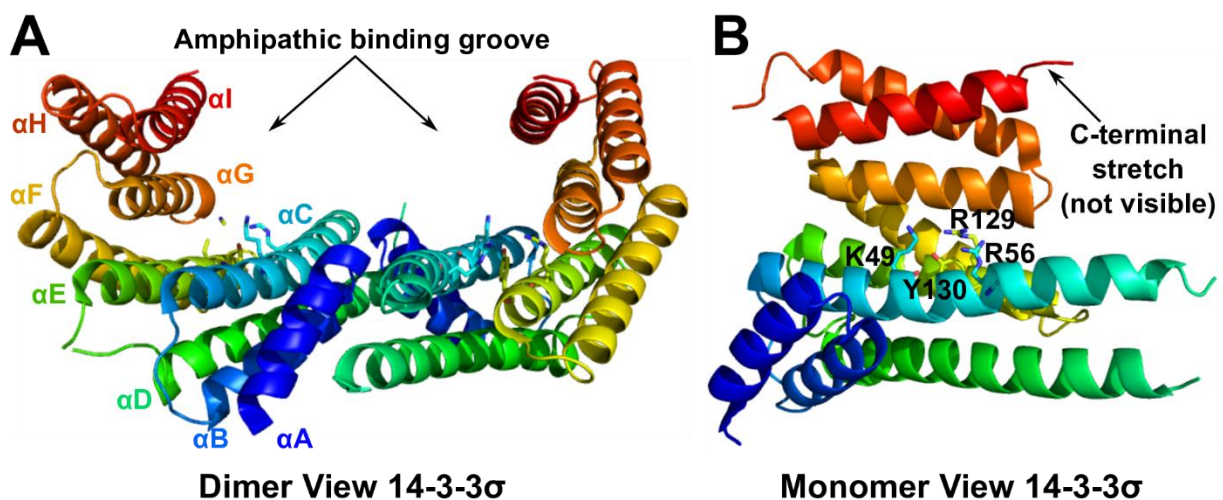


Figure 1 – The crystallographic structure of human 14-3-3 σ (PDB ID: 1YZ5), one of the seven human isoforms of 14-3-3. (A) The dimer of 14-3-3 σ is shown as a cartoon representation. The 9 α -helices and the location of the amphipathic binding grooves are indicated. (B) The monomer of 14-3-3 σ is shown as a cartoon representation. The four residues that constitute the interaction center for the phosphate group of the partner proteins (K49, R56, R129 and Y130) are represented as sticks. The location of the beginning of the C-terminal stretch (at the end of helix α I) is also indicated. This region is not seen in the crystal structure due to high flexibility.

1.2 14-3-3 Protein-Protein Interactions

There are hundreds of known biomolecules interacting with 14-3-3 and sequence analysis revealed that there are three preferred binding motifs: mode-1 (RSXpSXP) (**Figure 2 A**), mode-2 (RXF/YXpSXP, where pS denotes phosphoserine or phosphothreonine) (**Figure 2 B**) and mode-3 (the C-terminal sequence pS/TX₁₋₂-COOH) (**Figure 2 C**) (Coblitz, Wu, Shikano, & Li, 2006; Ganguly et al., 2005). There are also some other proteins that are known to interact with 14-3-3 that do not bind through any of these “preferential” structural motifs (Tomas Obsil & Obsilova, 2011). One of the most curious examples is the one of the p53 peptide phosphorylated at T387 (**Figure 2 D**), which will be discussed in detail ahead. Moreover, there are examples of peptides and proteins, which have been shown to bind to 14-3-3 proteins without a phosphorylated residue. One example is the R18 peptide discovered from a phage display library (**Figure 2 E**). The binding of this peptide to 14-3-3 is somewhat similar to the one shown for phosphorylated partners. In this case, two acidic residues of this peptide “mimick” the phosphate group and are able to interact with the positively charged residues of the amphipathic binding groove (Petosa et al., 1998). NMR studies have also shown that the Tau protein can bind 14-3-3 without being phosphorylated. Nevertheless, these studies suggest that the affinity of the binding is much smaller when compared to the binding of the phosphorylated Tau to 14-3-3 (Milroy et al., 2015). Recently, another chapter has been open on the story of 14-3-3 partners, as Toleman *et al* have shown that 14-3-3 can bind to peptides bearing O-glycoside-linked N-acetylglucosamine (O-GlcNAc) moieties. Despite the differences on steric and electronic characteristics between an O-Phosphate and an O-GlcNAc group, it was shown that the latest could mimic the first and bind in a similar fashion (**Figure 2 F**), establishing polar interactions with the basic residues of the amphipathic binding groove of 14-3-3 (Toleman et al., 2018). Given the number of O-GlcNAcylated targets in the cell and the widely documented cross talk between phosphorylation and O-GlcNAcylation (Bourré et al., 2018), a lot more can be discovered about 14-3-3 biology in the upcoming years. Regarding 14-3-3 binding motifs it is also interesting to mention that the group of Prof. Barton from the University of Dundee, in Scotland, developed the webserver 14-3-3-Pred (Madeira et al., 2015), which constitutes an easy predictor of 14-3-3 binding sites on a protein of interest.

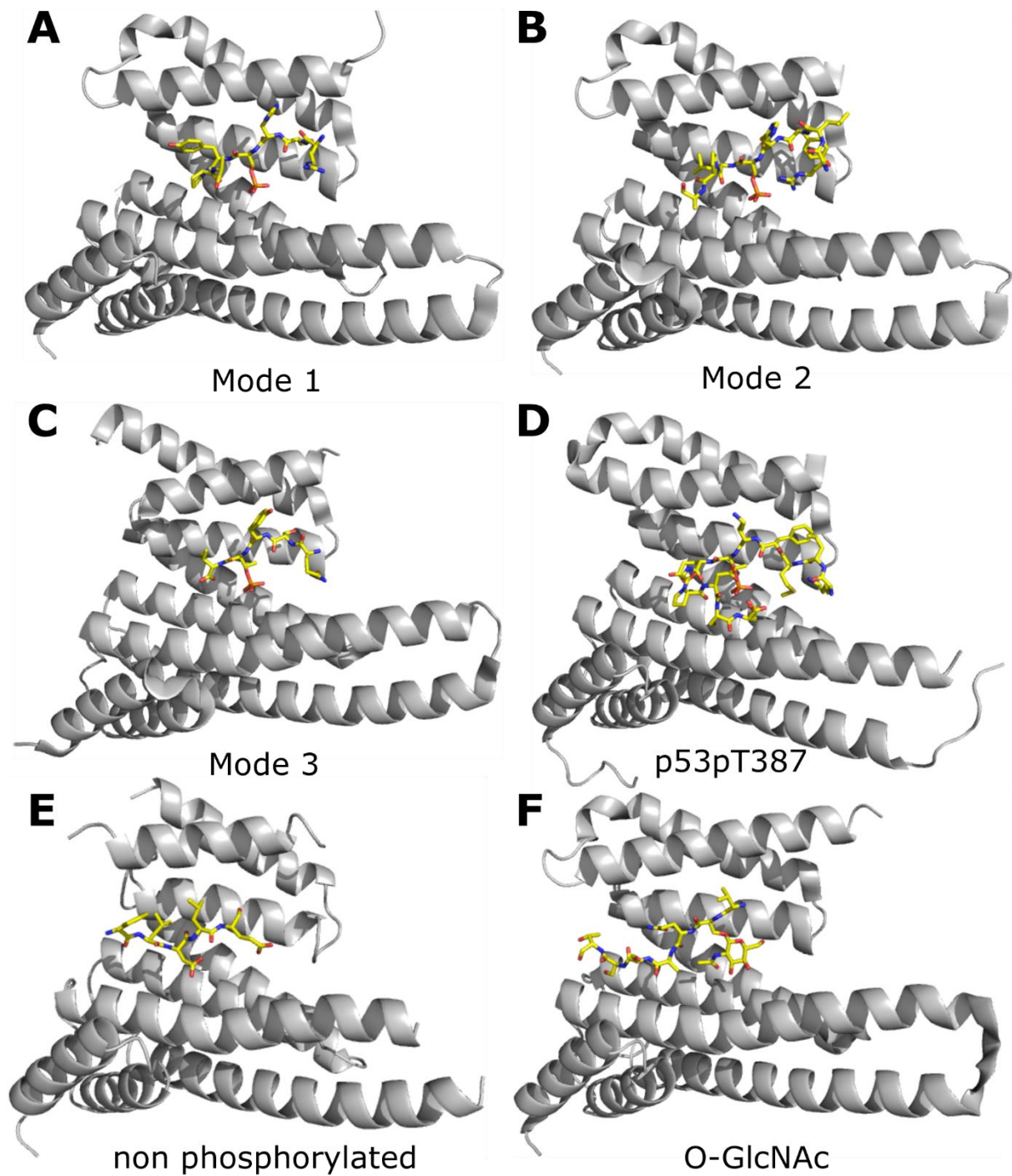


Figure 2 – Examples of the three preferred binding motifs and of other three atypical motifs of 14-3-3 binders. The peptide binders are represented as yellow sticks, while 14-3-3 proteins are represented as a grey cartoon. (A) An example of a Mode 1 binder peptide (ARSHpSYPA) binding in the amphipathic binding groove of 14-3-3 ζ (PDB ID: 1QJB). (B) An example of a Mode 2 binder peptide (RLYHpSLPA) binding in the amphipathic binding groove of 14-3-3 ζ (PDB ID: 1QJA). (C) An example of a Mode 3 binder peptide (PMA2 peptide :QSYpTV-COOH) binding in the amphipathic binding groove of 14-3-3 ζ (PDB ID: 1O9D). (D) An example of an atypical binding mode (p53pT387 peptide: KLMFKpTEGPDS) on 14-3-3 σ (PDB ID: 5MHC) in which the peptide binds in a bended conformation. (E)

An example of a non-phosphorylated peptide (R18 peptide: *PHCVPRDLSWLDLEANMCLP*) binding in the amphipathic binding groove of 14-3-3 ζ . Note that an aspartate residue is pointing towards the phospho-accepting cleft of 14-3-3 ζ (PDB ID: 1A38). (F) An example of an O-GlcNacylated peptide (*TSTTATPPVS-O-GlcNac-QASSTTSTW*) binding to 14-3-3 β . Note that the O-GlcNAc moiety is pointing towards the phospho-accepting cleft of 14-3-3 β (PDB ID: 6BYJ).

Bioinformatics studies have shown that there are more than 500 proteins that are, in theory, able to interact with 14-3-3 (Ottmann, 2013). Recent evidence points to more than 800 partners (Sluchanko, 2018). Tau, p53, Glucocorticoid receptor, Gab2, BAX, Estrogen receptor α , β -cell linker protein and Cdc25C are just some examples among the most famous 14-3-3 partners (Brummer et al., 2008; Hernández, Cuadros, & Avila, 2004; Kim, Kim, Jang, & Ko, 2011; Nomura et al., 2003; Peng et al., 1997; Wakui, Wright, Gustafsson, & Zilliacus, 1997; X. Wang et al., 2012; Waterman, Stavridi, Waterman, & Halazonetis, 1998). In fact, the number of confirmed partners of 14-3-3 is increasing rapidly with the improvement of bioinformatics and molecular/cell biology techniques. Recently, Karl W Barber *et al* (Barber et al., 2018) developed an innovative method to identify more 14-3-3 binders, by screening a library of 110,139 human serine phosphosites designed from the human phosphoproteome. Notably, researchers have identified several hundreds of previously known or new phosphosites capable of binding to 14-3-3. Moreover, several binding epitopes significantly different from the ones that were previously described, were identified. This work also represents a first step towards a platform capable of better understanding the human phosphoproteome and to reveal new PPIs (Barber et al., 2018).

This remarkable interactome makes 14-3-3 an influent actor in many cellular functions and, by consequence, in several diseases. In this sense, 14-3-3 proteins have been associated with several types of cancer (Hermeking, 2003), inflammation (Hirata, Marotta, Gui, Hanami, & Tanaka, 2015), virulence of microorganisms (Fu, Coburn, & Collier, 1993), Parkinson's disease (Rudenko & Cookson, 2010) , as well as AD (Hernández et al., 2004; Umahara et al., 2004). 14-3-3 interactome is also dynamic in a way that when a cell is exposed to a particular type of stress, new 14-3-3 PPIs can arise as an adaptive response (Pennington, Chan, Torres, & Andersen, 2018).

1.3 Modulation of 14-3-3 Protein-Protein Interactions: a new hot-topic in drug discovery

Given their central role in the cell and the opportunity that 14-3-3 PPIs represent for increasing the druggable proteome, 14-3-3 proteins have been attracting the attention of several research groups and the modulation of their activity has been seen as a promising strategy in drug discovery (Milroy, Brunsveld, & Ottmann, 2013). It is therefore not surprising that several groups, including pharmaceutical companies, focus on the characterization and development of inhibitors and stabilizers of 14-3-3 PPIs. A first step towards this aim relies on the structural elucidation of 14-3-3 protein-protein interfaces. Although the number of crystal structures of 14-3-3 in the presence of phosphorylated partners has increased significantly over the last years, there are still hundreds of known 14-3-3 PPIs to elucidate (Ballone, Centorrino, & Ottmann, 2018; Sluchanko, 2018). This is particularly important for the modulation of 14-3-3 PPIs since selectivity for one out of hundreds of PPIs can only be achieved with deep structural understanding of the protein-protein interface.

1.3.1 Inhibitors of 14-3-3 Protein-Protein Interactions

As the binding motifs of 14-3-3 partners are known, it is easier to have a starting point for the development of PPI inhibitors compared to the case of stabilizers. Several classes of inhibitors of 14-3-3 PPIs have already been developed: stapled peptides (Glas et al., 2014), molecular tweezers (Bier et al., 2013), hybrid peptides (Andrei, Meijer, et al., 2018; Milroy et al., 2015) and small molecules (Corradi et al., 2010).

Considering modified peptides in order to achieve PPI inhibition, two fundamental strategies were employed: computer-aided design and modification of a known peptidic epitope. Regarding the first strategy, a virtual screen of macrocyclic peptides based on molecular docking yielded the most potent peptidic inhibitor of a 14-3-3 PPI known up to now (Krüger et al., 2017). This macrocyclic peptide incorporates two unnatural amino acids and docks in the binding groove of 14-3-3 ζ (**Figure 3 A**) with very high affinity ($K_d = 38 \pm 3$ nM). As mentioned above, the other strategy followed for the construction of peptidic inhibitors was the modification of a known epitope. This strategy was followed for the inhibition of the 14-

3-3/Tau PPI. Starting from the Tau epitope surrounding pS214 (R211-P218) (Andrei, Meijer, et al., 2018; Milroy et al., 2015). In this case, the strategy was to expand the peptide in order to increase the affinity through the interaction with lipophilic residues of 14-3-3. This strategy yielded compound 201D (**Figure 3 B**), which was shown to have a ca. 200-fold improved affinity to 14-3-3 when compared to the original epitope ($K_d = 5.9 \pm 1.0 \mu\text{M}$ vs ca. 1330 μM).

Regarding the use of small molecules, the first one was synthesized based on the amino acid sequence of a motif that was shown to bind strongly to 14-3-3 (Kaiser & Ottmann, 2010). In the same year, the group of Professor Maurizio Botta established a mark in the field by synthesizing BV-02, the first non-peptidic small molecule inhibitor of 14-3-3 PPIs (Corradi et al., 2010). This compound developed through an *in silico* structure-based ligand design approach contains a carboxyl group that, according to docking studies, is anchored by polar interactions with the side chains of K49, R56 and R129 in the binding groove of 14-3-3 σ (**Figure 3 C**). Through the inhibition of the c-Abl/14-3-3 PPI, this compound was able to drive leukemia cells to apoptosis, including those that were resistant to Imatinib with an LD₅₀ in the low μM range (Corradi et al., 2010, 2011). Nevertheless, this compound was shown to be chemically unstable in aqueous buffers and therefore, some years later, the same group developed new chemically stable BV-02 derivatives with a remarkable anti-proliferative activity against K-562 cells (Iralde-Lorente et al., 2019). Another example of a small molecule inhibitor of a 14-3-3 PPI is FOBISIN (FOurteen-three-three BInding Small molecule INhibitor) 101 (Zhao et al., 2011). This compound was identified through a Fluorescence Polarization (FP) based screen. It contains a phosphate group interacting with the phospho-accepting site of 14-3-3 and additionally, it binds covalently to K122 side chain through an imide bond (**Figure 3 D**) (Röglin, Thiel, Kohlbacher, & Ottmann, 2012).

From the analysis of the inhibitors of 14-3-3 PPI reported so far, one can see that potency and biological activity shown in functional assays have already been achieved. Nevertheless, selectivity for one particular 14-3-3 PPI was never exhaustively tested for any of the reported inhibitors. Therefore, selectivity is now the greatest challenge for the design of 14-3-3 PPI Inhibitors.

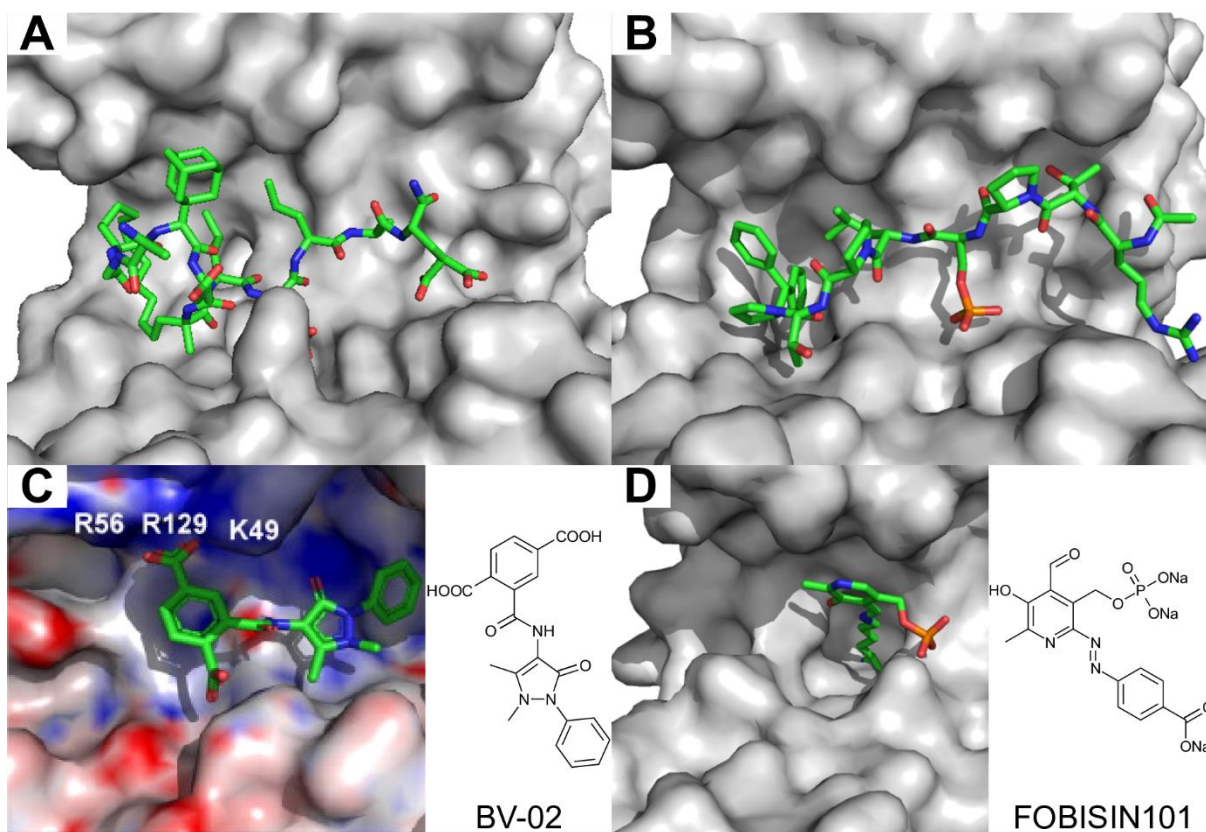


Figure 3 – Inhibitors of 14-3-3 Protein-Protein Interactions. (A) Macrocyclic peptidic inhibitor (green sticks) in complex with 14-3-3 ζ (gray surface) – PDB ID: 5JM4. (B) Peptidomimetic phosphorylated inhibitor 201D (green sticks) in complex with 14-3-3 σ (gray surface) – PDB ID: 5HF3. (C) Left side: docking pose of small molecule inhibitor BV-02 (green sticks) in complex with 14-3-3 σ (gray surfaced colored by charge distribution). Note that the phospho-acceptor pocket is shown at the top of the figure. Figure from (Corradi et al., 2011). Right side: chemical structure of BV-02. (D) Left side: phosphate containing small molecule inhibitor FOBISIN101 (green sticks) covalently bound to the side chain of K122 of 14-3-3 σ (gray surface) through the formation of an imide bond – PDB ID: 3U9X. Right side: chemical structure of FOBISIN101.

1.3.2 Stabilizers of 14-3-3 Protein-Protein Interactions

Although particularly promising, developing a PPI stabilizer is always an extremely challenging process. There are two possible ways to achieve a PPI stabilization: binding to a single protein partner in a way that increases the affinity of the interaction between the two proteins; or binding the complex, interacting with both partners and increasing the mutual binding affinity (Thiel, Kaiser, & Ottmann, 2012). Both these approaches are extremely challenging for several reasons but there are, nevertheless, some examples of PPI stabilizers,

including some approved drugs like paclitaxel or rapamycin (Thiel et al., 2012). The stabilization of PPI involving 14-3-3 has already been shown to have interesting biological effects. The first demonstration comes from nature, more specifically from the fungus *Phomopsis amygdali*, which produces the diterpene glycoside Fusicoccin A (FC-A) (**Figure 4 A**). This secondary metabolite binds at the interface of the complex between the regulatory domain of the plasma membrane H⁺-ATPase (PMA) and 14-3-3 (**Figure 4 B**). The affinity of FC-A to 14-3-3 is relatively low ($K_d = 66 \mu\text{M}$) whereas the affinity of this compound to the complex of 14-3-3 with a phosphorylated PMA peptide increases 100 times ($K_d = 700 \text{ nM}$) (Würtele, Jelich-Ottmann, Wittinghofer, & Oecking, 2003). This fungal toxin binds to a hydrophobic pocket formed by the phosphorylated PMA peptide and a part of the amphipathic groove of 14-3-3 proteins. This stabilizing effect is extremely auspicious since the stabilization of PPI involving 14-3-3 is seen as a promising approach for some pathologies (Benzinger et al., 2005). Since then, Fusicoccin has been tested in many complexes and shown to stabilize a great number of PPIs in which the 14-3-3 binding groove is left partially unoccupied by the binding partner. Some examples of PPIs that are stabilized by FC-A are the 14-3-3/p53pT387 (**Figure 4 C**) (Doveston et al., 2017), 14-3-3/ER α pT594 (**Figure 4 D**) (De Vries-van Leeuwen et al., 2013), 14-3-3/TASK-3pS373 (**Figure 4 E**) (Anders et al., 2013), 14-3-3/CFTRpS753 (Stevens et al., 2016) and 14-3-3/C-RAFpS259 (M. Molzan et al., 2010). The activity of FC-A as a stabilizer of 14-3-3 PPIs has recently been assessed for its capacity to promote axon regeneration (Kaplan, Morquette, et al., 2017). In this study FC-A was found to stabilize the interaction between 14-3-3 and the stress response regulator "General Control Non-Derepressible 1" (GCN1), leading to neurite outgrowth *in vitro* and axon regeneration *in vivo*, when tested in mice. These encouraging results for the activity of FC-A are, nevertheless, not easy to explain. The authors suggest that FC-A may modulate many other 14-3-3 PPIs and that this stabilization of the 14-3-3/GCN1 may not be enough to explain this promotion of neurite outgrowth *in vivo* (Kaplan, Morquette, et al., 2017).

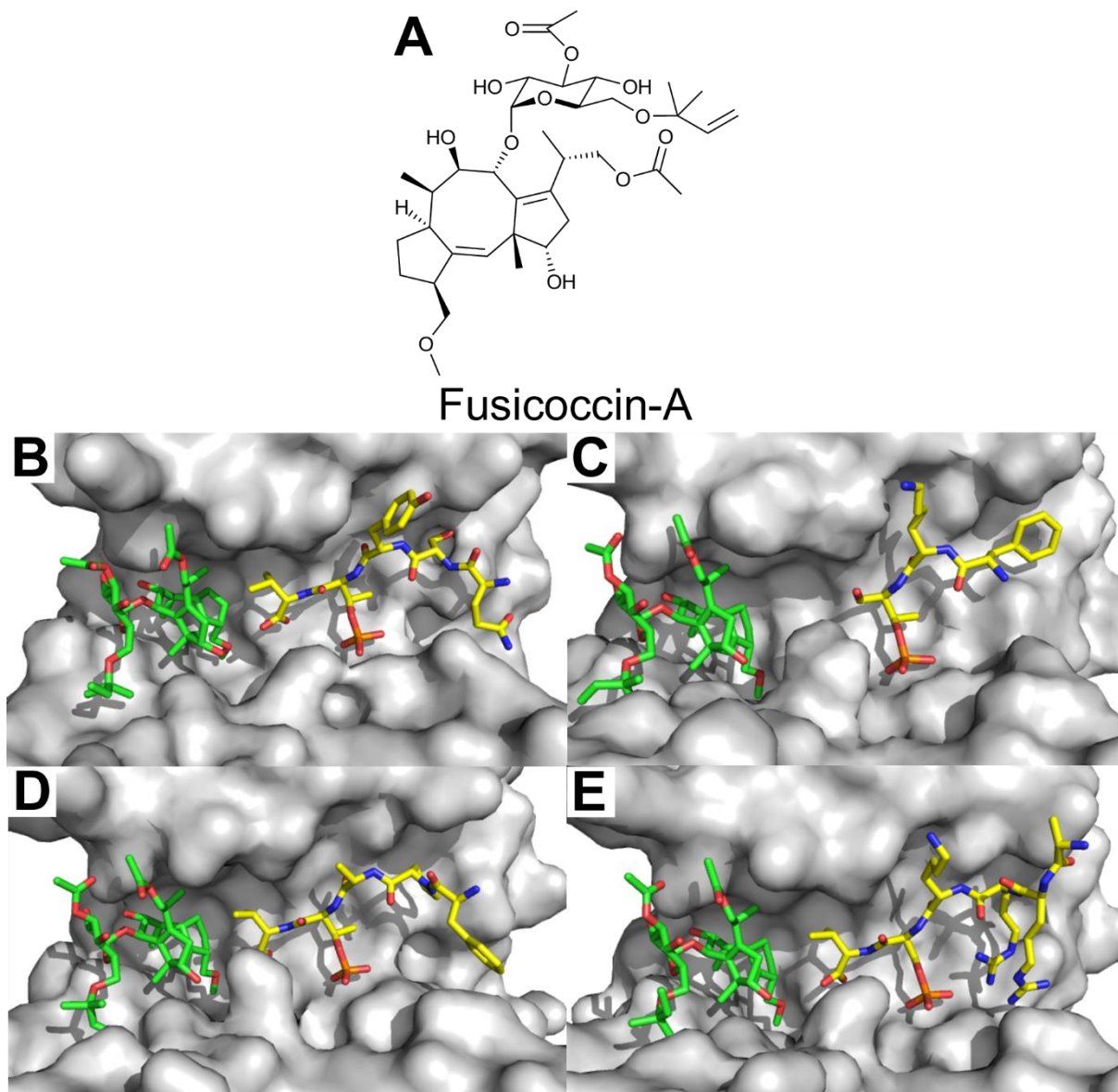


Figure 4 – The natural small molecule Fusicoccin-A (FC-A) stabilizes 14-3-3 PPIs by binding at the interface between 14-3-3 and its partner. (A) Chemical structure of FC-A. (B) FC-A (green sticks) binding at the interface of 14-3-3-like protein C from *Nicotiana Tabacum* (gray surface) and the PMA2pT439 peptide (yellow sticks) – PDB ID: 1O9F. (C) FC-A (green sticks) binding at the interface of 14-3-3 σ (gray surface) and the p53pT387 peptide (yellow sticks) – PDB ID: 5MXO. (D) FC-A (green sticks) binding at the interface of 14-3-3 σ (gray surface) and the ER α pT594 peptide (yellow sticks) – PDB ID: 4JDD. (E) FC-A (green sticks) binding at the interface of 14-3-3 σ (gray surface) and the TASK-3pS373 peptide (yellow sticks) – PDB ID: 3P1O.

FC-A is not the only natural molecule able to stabilize 14-3-3 PPIs. Another natural FC-A related molecule, Cotylenin A (CN-A), was also found to be able to stabilize some PPI involving

14-3-3 in a similar fashion (Ottmann et al., 2009). One example is the complex 14-3-3/N-terminal 14-3-3 recognition motif of C-Raf (**Figure 5 A**), which may explain CN-A anti-cancer properties (Manuela Molzan et al., 2013). The portfolio of natural molecules able to stabilize 14-3-3 PPIs is not restricted to the FC-A family because Mizorribine, an imidazole nucleoside isolated from *Eupenicillium brefeldianum*, was also shown to have this activity. *In vitro* studies have demonstrated that this immunosuppressant molecule is able to stabilize the interaction between 14-3-3 and the Glucocorticoid Receptors (GR) (Takahashi, Wakui, Gustafsson, Zilliacus, & Itoh, 2000). Recently Adenosine Monophosphate (AMP) was also shown to stabilize a 14-3-3 PPI, specifically the one between 14-3-3 β and the Carbohydrate-response element-binding protein (ChREBP) (Sato et al., 2016). This interaction is, contrarily to most of 14-3-3 PPIs, independent of phosphorylation. When AMP is present in the ternary complex, its phosphate group occupies the traditional phospho-binding groove while the adenosine moiety occupies part of the “Stabilizer binding pocket”. This binding of AMP stabilizes the complex between the two proteins leading to the inhibition of the nuclear localization of ChREBP (Sato et al., 2016).

The biological activity demonstrated by these natural compounds inspired the 14-3-3 community to produce semi-synthetic derivatives of these molecules. The group of Kato concentrates on the development of semi-synthetic fusicocanes in order to increase the specificity of these molecules towards specific 14-3-3 PPIs. In this context they have synthesized FC-THF, which stabilizes the binding of 14-3-3 to the potassium channel TASK-3. This leads to an increase of plasma membrane insertion of this channel in *Xenopus* oocytes (Anders et al., 2013). More recently, a broader (Structure-Activity Relationship) SAR study was performed with the aim of identifying more potent fusicocanes. In this work, the authors conducted a rational design of fusicocanes guided by Molecular Dynamics (MD) simulations (Andrei, de Vink, et al., 2018). All fusicocanes were tested for their abilities to stabilize the 14-3-3/TASK-3 PPI. While FC-A promoted a 1.9-fold decrease of the apparent dissociation constant (K_d), its semi-synthetic derivative FC-NAC promoted a 32-fold decrease (18-fold improvement). The key aspect for this improvement in the activity is an additional hydrogen bond with the receptor, between the amide group of FC-NAC (**Figure 5 B**) and one oxygen atom of the carboxylate group of residue D215 of 14-3-3 σ . Further experiments showed that

the compounds capable of establishing the abovementioned extra hydrogen interaction with 14-3-3 had an improved antiproliferative activity when compared to classic fusicocanes (Andrei, de Vink, et al., 2018).

Despite the interesting biological activities demonstrated by Fusicocanes, their lack of selectivity and poor Pharmacokinetic (PK) properties constitute serious barriers for their hypothetical use as therapeutic molecules. For this reason, an effort for finding small molecule stabilizers capable of replacing natural compounds has been made, by classical library screen, yielding compound Pyrrolidone1 (Rose et al., 2010). The crystal structure of this compound bound to the PMA2 peptide/14-3-3 complex shows that Pyrrolidone1 binds, similarly to FC-A, in the same solvent-exposed hydrophobic pocket of the amphipathic binding groove of 14-3-3 (**Figure 5 C**). A follow-up study in which the pyrrolidone scaffold was replaced by a pyrazole yielded new optimized compounds capable of stabilizing the 14-3-3/PMA2 PPI (Richter, Rose, Hedberg, Waldmann, & Ottmann, 2012).

Another stabilizer that deserves to be mentioned is the molecular Tweezer CLR01. This supramolecular ligand is composed by 5 benzene rings alternated with 4 norbornadiene rings disposed in a belt-like structure. Additionally two phosphate groups are bound to the central hydroquinone ring (**Figure 5 D**). The molecular tweezer binds to lysine and arginine residues with an affinity in the μM range, depending on the steric hindrance and the surrounding electronic environment (Bier et al., 2013). The molecular tweezer has been shown to be an inhibitor of the 14-3-3/C-Raf and 14-3-3/Exoenzyme S PPIs (Bier et al., 2013) and a stabilizer of the 14-3-3/Cdc25pS216 PPI (Bier et al., 2017). In this last case, the tweezer recognizes R208 of the Cdc25pS216 peptide and additionally, through its aromatic core, establishes hydrophobic interactions with 14-3-3 ζ (**Figure 5 D**). Additional experiments by Isothermal Calorimetry (ITC) and FP showed that the CLR01 stabilized the 14-3-3/Cdc25pS216 PPI by a factor of 20 (Bier et al., 2017). Recently, a new class of supramolecular stabilizers was discovered from a FP screening of cationic supramolecular peptide-mimetic compounds (Gigante et al., 2019). Some of these compounds were shown to stabilize the complexes 14-3-3/C-RafpS259 and 14-3-3/TaupS214pS324 by up to 84 and 26 fold, respectively.

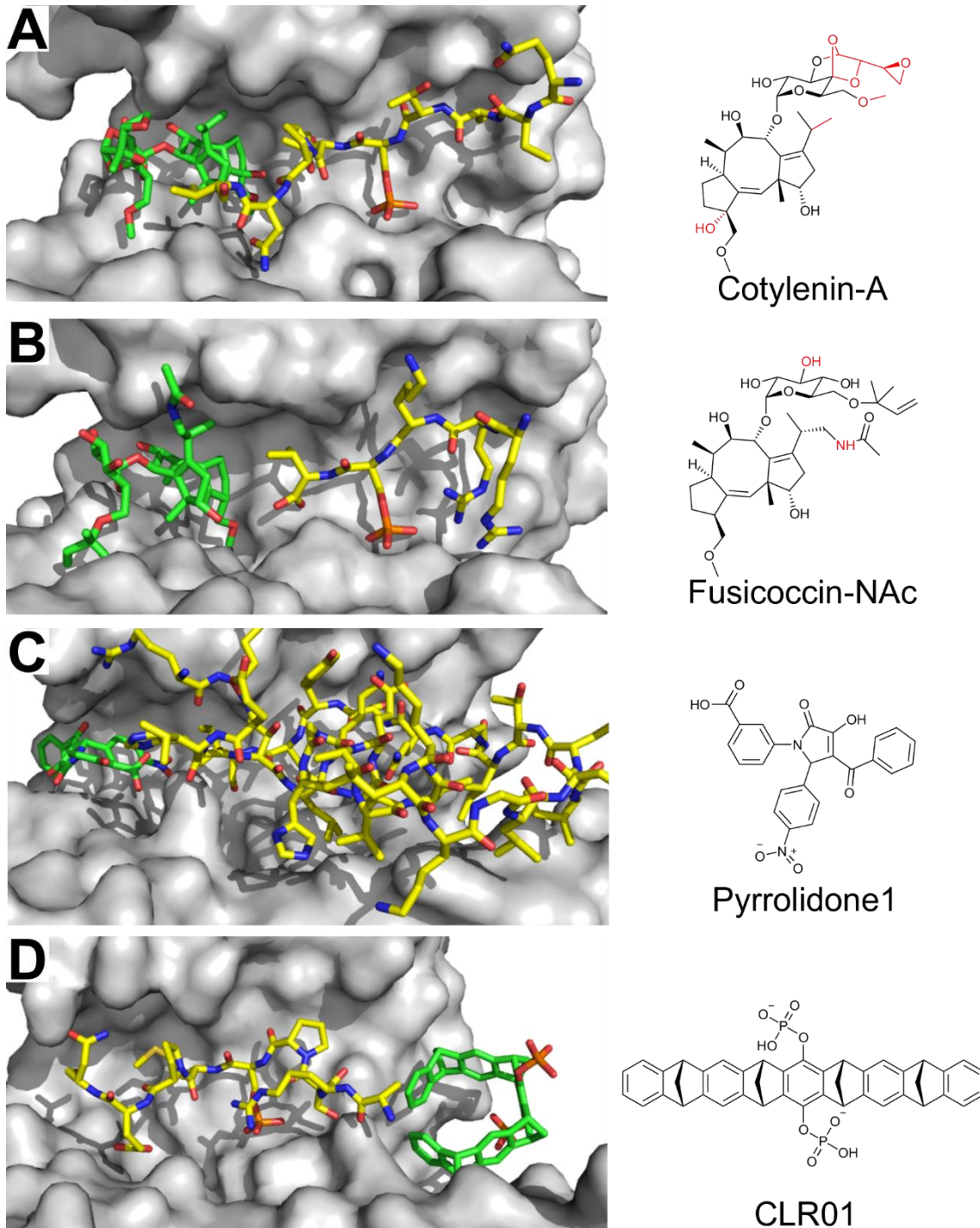


Figure 5 – Several classes of compounds can act as stabilizers of 14-3-3 PPIs. (A) Left side: Cotylenin-A (green sticks) binding at the interface of 14-3-3 ζ (gray surface) and a diphosphorylated C-Raf peptide (yellow sticks) – PDB ID: 4IHL. The interface shown in the figure is the one between 14-3-3 ζ and the region surrounding the pS259 site. Right side: chemical structure of Cotylenin-A. Different structural features from FC-A are drawn in red. (B) Left side: Fusicoccin-NAc (green sticks) binding at the interface of 14-3-3 σ (gray surface) and a TASK-3pS373 peptide (yellow sticks) – PDB ID: 6GHP. Right side: chemical structure of Fusicoccin-NAc. Different structural

features from FC-A are drawn in red. (C) Left side: Pyrrolidone1 (green sticks) binding at the interface of 14-3-3-like protein C from *Nicotiana tabacum* (gray surface) and an unphosphorylated PMA2 peptide (yellow sticks) – PDB ID: 3M51. Right side: chemical structure of Pyrrolidone1. (D) Left side: Molecular Tweezer CLR01 (green sticks) binding at the interface of 14-3-3 ζ (gray surface) and Cdc25pS216 peptide (yellow sticks) – PDB ID: 5M36. Right side: chemical structure of CLR01.

Since the stabilization of PPI involving 14-3-3 may be of therapeutic interest for some pathologies and shows encouraging results, the search for these molecules has grown in recent years and its now being pursued by several academic and industrial laboratories. With the start of several projects aiming to discover 14-3-3 PPI stabilizers, many more exciting molecules are expected to enrich the field in the next few years.

1.3.3 Fragment-based approach for the identification of starting points for the modulation of 14-3-3 Protein-Protein Interactions

The fragment-based approach, which will be discussed in detail in **Introduction - section 4** has also been successfully applied in order to find low MW starting points for the development of 14-3-3 PPIs' modulators. The first example came from Novartis, in which a library of 1408 fragments was screened to find hits to the 14-3-3 ζ /TAZpS89 complex. After preliminary screening by WaterLOGSY and T1 ρ , followed by more robust Protein Based NMR and X-ray crystallography studies, 2 compounds were identified. These compounds were found to bind in two pockets of 14-3-3 ζ that had never been identified before. These compounds sit in conserved regions of 14-3-3 ζ at the top of helices α H and α I (**Figure 6 A,B**). Although far from the binding groove, where most of the protein partners bind, these compounds can be of interest for the modulation of 14-3-3 PPIs where the partners establish contacts with these regions of 14-3-3. The authors stated the cases of the Serotonin N-acetyltransferase (AANAT), PMA2-CT52 from tobacco (*Nicotiana plumbaginifolia*) and Hd3a from rice.

More recently, another study focused on finding tethering fragments able to selectively stabilize the interaction between 14-3-3 σ and a ER α peptide surrounding the pT594 residue (Sijbesma et al., 2019). The authors' strategy was to find a disulfide fragment able to be

tethered by a cysteine residue located in the binding groove of 14-3-3 σ and on the interface with the ER α peptide. Three constructs of 14-3-3 σ were used: wild type, which has the natural occurring C38, 14-3-3 σ (C42) containing the mutations C38N and N42C and 14-3-3 σ (C45) containing the mutations C38N and S45C. The fragments were screened by intact protein mass spectrometry (MS) for binding to the *apo*-14-3-3 σ and 14-3-3 σ /ER α complex. The fragments were selected based on their maximum tethering capacity and preference for the protein-peptide complex over the *apo* form (quantified by MS). Two compounds binding to 14-3-3 σ (C42)/ER α pT594 were pre-selected (**Figure 6 C,D**) and shown to stabilize the complex by 40- and 14-fold, being even more potent than FC-A. Ligand-based NMR experiments further revealed that the binding of the fragments was, despite the tethering, still driven by a non-covalent interaction. A total of 6 fragments were identified by X-ray crystallography (5 for the 14-3-3 σ (C42)/ER α pT594 complex and 1 for the 14-3-3 σ (C45)/ER α pT594 complex). The fragments were then tested against other 14-3-3 complexes in order to test their selectivity and effect on other 14-3-3 PPIs.

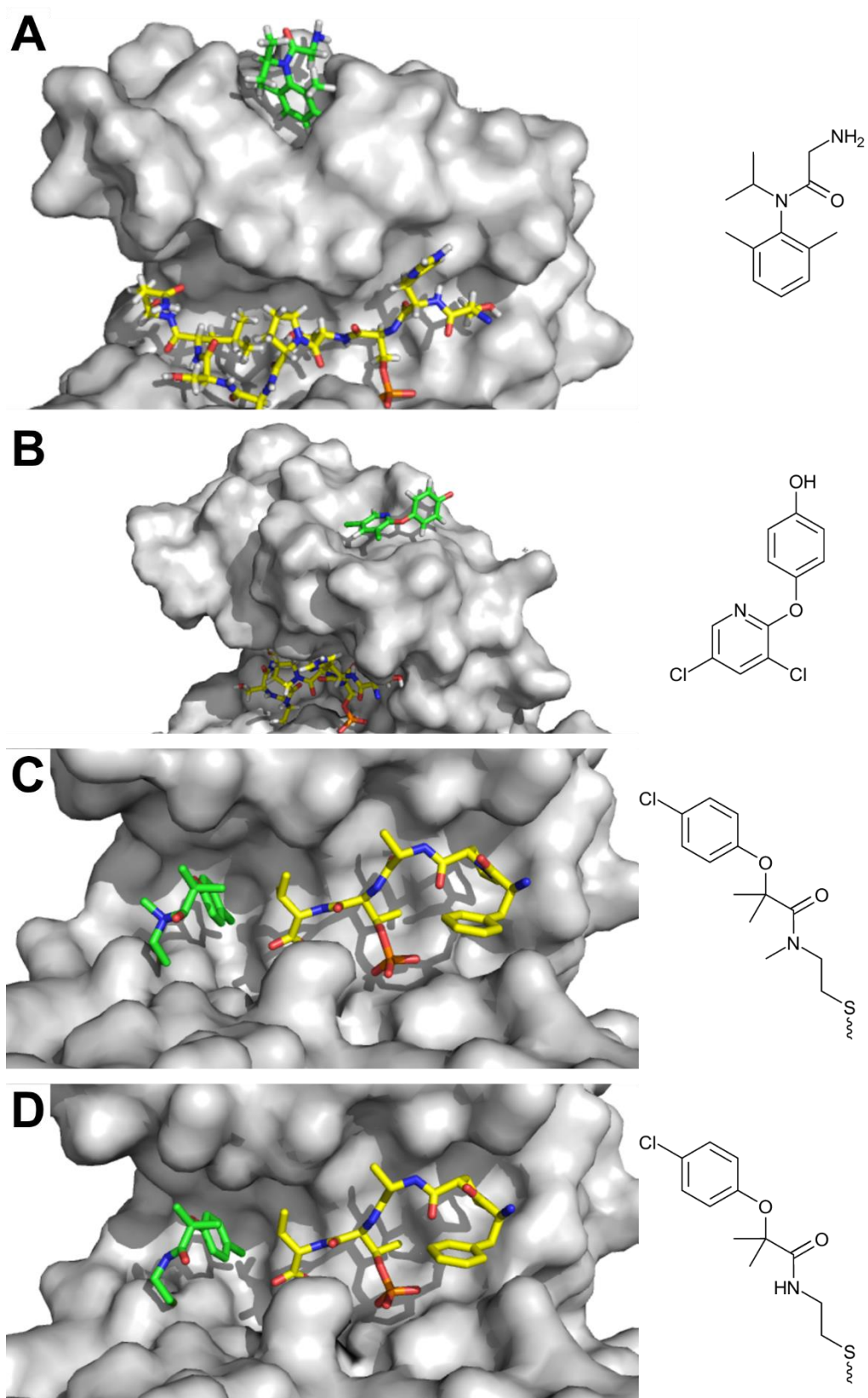


Figure 6 – Examples of fragments binding to 14-3-3. (A) Left side: Example of a fragment (green sticks) binding to 14-3-3 ζ (grey surface) in complex with a TAZpS89 peptide (yellow sticks) – PDB ID: 5N5R. Right side: Chemical

structure of the fragment. (B) Left side: Example of a fragment (green sticks) binding to 14-3-3 ζ (grey surface) in complex with a TAZpS89 peptide (yellow sticks) – PDB ID: 5N5T. Right side: Chemical structure of the fragment. (C) Left side: Example of a fragment (green sticks) binding covalently to 14-3-3 σ (C42) (grey surface) in complex with a ERapT594 peptide (yellow sticks) – PDB ID: 6HHP. Right side: Chemical structure of the fragment. (D) Left side: Example of a fragment (green sticks) binding covalently to 14-3-3 σ (C42) (grey surface) in complex with a ERapT594 peptide (yellow sticks) – PDB ID: 6GMT. Right side: Chemical structure of the fragment.

2 Methods to study Proteins, Peptides and Protein-Protein Interactions

2.1 Protein Nuclear Magnetic Resonance

Nuclear Magnetic Resonance (NMR) is an interesting technique for the study of biological molecules, especially proteins. Today, the diverse group of NMR techniques allows the study of very important topics in chemical-biology such as PPI, Protein-Ligand Interactions (PLI), determination of binding affinities, determination of complex NMR structures or proteins dynamics (Agrawal, 2014). Protein NMR has some genuine complementary features to other biophysical characterization techniques. Regarding the determination of binding affinities, NMR can extend the range of measurable interactions to the mM range, which is hard to achieve with other biophysical assays. Considering PPI and PLI, NMR is specific and sensitive, having low rates of false positives and false negatives (Williamson, 2013). It is also a powerful technique for the study of intrinsically disordered proteins, which cannot be crystallized and are a huge challenge for many techniques due to their dynamic character (Gibbs, Cook, & Showalter, 2017).

Proteins are exclusively composed by Hydrogen, Carbon, Nitrogen and Sulfur. Hydrogen, Carbon and Nitrogen are the nuclei that are observed in Protein NMR. In order to be detected by NMR, nuclei need to be “NMR active”, which means to have a spin $\neq 0$. It is also important that these nuclei are well abundant in order to be reasonably detected. The nuclei that are interesting for Protein NMR are ^1H (spin = $\frac{1}{2}$, abundance = 100 %), ^{13}C (spin = $\frac{1}{2}$, abundance = 1 %) and ^{15}N (spin = $\frac{1}{2}$, abundance = 0.37%). The most abundant form of Carbon (^{12}C) is not magnetically active, as its spin = 0. The magnetically active isotope of Carbon is ^{13}C , which has a spin = $\frac{1}{2}$ and an abundance of only 1%. Therefore, if one wants to detect the Carbon from proteins, it is necessary to enrich them with the ^{13}C isotope. Considering Nitrogen, the

most abundant isotope, ^{14}N is magnetically active but it is a quadrupolar nuclei (spin = 1), which causes its detection to not to be ideal due to broadening of the signals. The ^{15}N isotope, which has a spin = $\frac{1}{2}$ and therefore ideal for NMR, also exists in proteins but in very low abundance (0.37 %). For this reason, ^{15}N enrichment is also necessary when the objective is to use the Nitrogen from proteins. It is therefore not surprising that biomolecular NMR relies on recombinant technologies for sample production. The most popular organism for the production of proteins for NMR is *Escherichia coli* and isotopic enrichment is attained by adding specific isotopically labeled nutrients to the culture medium. ^{15}N isotopic enrichment can be achieved by using $[^{15}\text{N}]\text{NH}_4\text{Cl}$ as the only source of Nitrogen and ^{13}C isotopic enrichment can be achieved by adding ^{13}C D-Glucose as the only source of Carbon.

2.1.1 1D and 2D NMR of proteins

The ^1H spectrum of a protein is very complex due to the high number of signals (at least two per amino acid residue) (**Figure 7 A**). Although it is not the most useful spectrum for analyzing proteins, the ^1H spectrum can still provide information. A ^1H spectrum is routinely performed before any further experiment as an analytical control of the sample preparation. The analysis of the chemical shifts and intensities of the signals of the ^1H NMR spectrum can also serve as a quick method for detecting changes in the protein over time, for example, the occurrence of degradation, aggregation, folding/unfolding or precipitation. In order to acquire a good ^1H spectrum of a protein it is essential to use a pulse sequence set-up for suppressing the water signal since it is by far the most abundant molecule in the samples. Water protons resonate at around 4.7 ppm and therefore prevent the detection of the nearby protein resonances. The ^1H protein spectra of proteins is complex and can be divided in several regions (**Figure 7 A**). The most upfield region of the spectrum contains the methyl protons (CH_3) that can be found for example in Isoleucine, Valine, Methionine or Leucine residues. Other aliphatic protons (CH_2) can be found in the same area or up to 3.5 ppm. From 3.5 ppm up to 5 ppm the ^1H NMR spectrum of the protein is dominated by the H_α protons of the amino acid residues. It is important to note that a precise water suppression is crucial for the detection of these signals. Downfield from this area, the last three types of protons can be identified: the protons of the side chains of glutamine and asparagine residues (each residue contains

two signals in this area), the backbone HN and the aromatic protons. For most applications in protein-based NMR, this is the most interesting region of the spectrum. The main reason for this relies on the fact that all amino acid residues except proline contain a detectable HN resonance and these are well dispersed in the chemical shift scale. Nevertheless, the ^1H spectrum does not provide information about individual resonances and therefore does not allow spectroscopists to obtain residue-specific information. In order to overcome this limitation, 2D NMR spectra are necessary. Therefore, it is not surprising that the ^1H - ^{15}N Heteronuclear Single Quantum Coherence (HSQC) spectrum is the most commonly recorded spectrum in protein NMR. Every resonance in this 2D spectrum corresponds to an N-H bond (**Figure 7 B**). One can virtually say that every amino acid in the protein, except proline, is represented by a resonance. The HN signals from the side chains of glutamine, asparagine, arginine and tryptophan residues are also visible in the spectrum. Several factors affect the chemical shift values of the ^1H - ^{15}N resonances: the type of amino acid residue, the secondary structure motif in which the corresponding amino acid is integrated, the temperature of the acquisition of the spectrum, the pH and the buffering conditions. The ^1H - ^{15}N HSQC of every protein is unique and therefore this spectrum is seen as the "Identity card" of a protein. There are many applications of the ^1H - ^{15}N HSQC spectrum that will be explored in the chapters ahead but in short one can say that it is a spectrum that can follow any modification on the protein (interaction, post-translational modification, degradation) in a residue specific way. The resonances are sensitive probes to any change in electronic or chemical environment of the corresponding N-H bond and can provide useful information. The main drawback of this technique is that it requires ^{15}N isotopic enrichment of the protein. Additionally, due to the low sensitivity of NMR, there is the demand of relatively concentrated sample and/or relatively long acquisition times. Despite these high demands of time and material, the amount of information provided by a ^1H - ^{15}N HSQC justifies its wide application in several areas. In order to maximize the information that can be obtained from the ^1H - ^{15}N HSQC, it is important to know at which amino acid residue each resonance corresponds. In other words, one needs to assign the ^1H - ^{15}N spectrum of the protein, at specific experimental conditions regarding the temperature, pH and buffer.

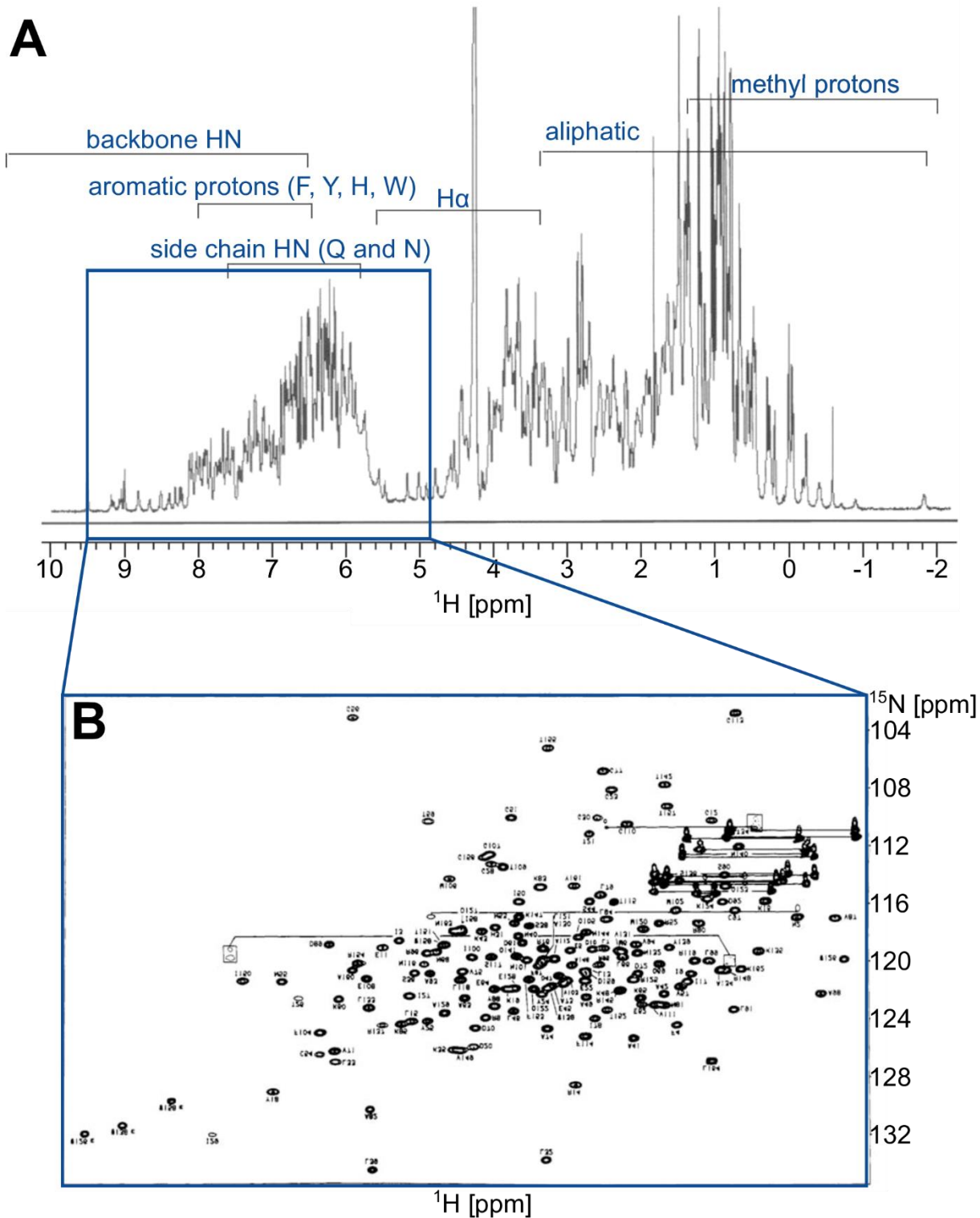


Figure 7 – NMR spectrum of lysozyme, at pH 7.0, 25 °C, recorded on a 600 MHz magnet. (A) ^1H NMR spectrum of lysozyme recorded with water suppression. The approximate regions of different types of protons of amino acid residues are shown. (B) Assigned ^1H - ^{15}N HSQC spectrum of the same protein. Adapted from (James Chou, 2008).

2.1.2 Backbone assignment of proteins

In order to assign the ^1H - ^{15}N HSQC of a protein, 1D and 2D NMR spectra are not enough and 3D NMR spectra are therefore required. For the backbone assignment of a protein, the NMR signals of the carbon atoms of the amino acid residues need to be detected and therefore, ^{13}C isotopic enrichment is necessary. Moreover, usually 3D NMR experiments have poor sensitivity when compared to 2D, and therefore require even higher concentrations of protein (from hundreds of μM to mM) in order to have a reasonable Signal/Noise (S/N) ratio. Another problem related to this poor sensitivity is the fact that acquisition times of several days are usually necessary for 3D NMR experiments. This may be problematic for unstable proteins or proteins undergoing rapid degradation. Despite all these challenges, the backbone assignment can be a powerful tool for the study of the protein. In addition to the already referred possibility of assigning the ^1H - ^{15}N HSQC and performing interaction studies in a specific way, the backbone assignment can also provide information about the secondary structure of the protein. This is possible because the chemical shift values of the carbon atoms are strongly related to dihedral angles and therefore to the secondary structure (D. S. Wishart & Sykes, 1994).

There are several types of 3D NMR spectra that can be acquired for backbone chemical shift assignments and some of the most popular ones are summarized in **Figure 8**.

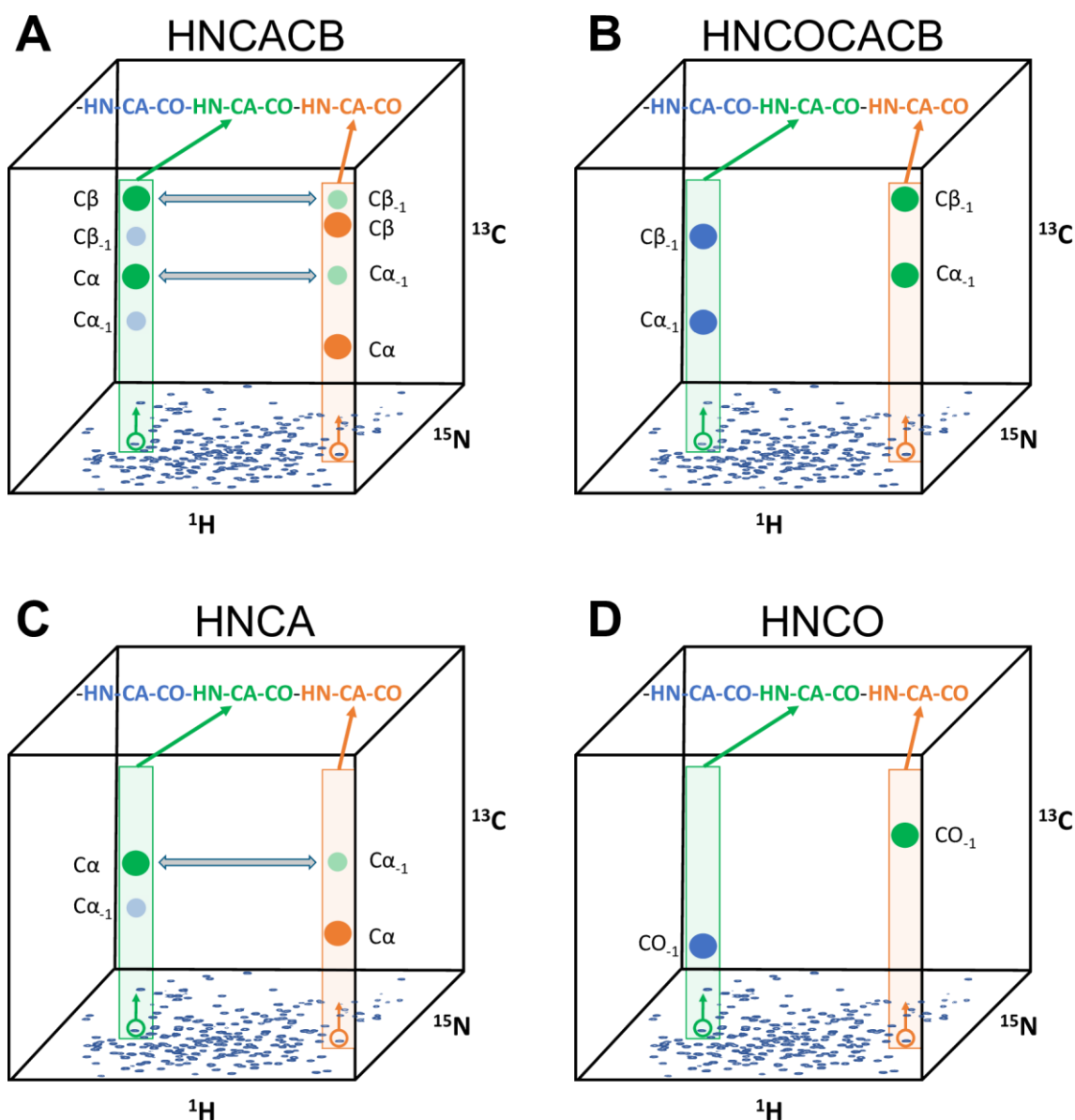


Figure 8 – Examples of some of the most popular 3D NMR experiments for backbone assignment. (A) In the HNCACB spectrum, by navigating through the ^{13}C axis of a fixed ^1H - ^{15}N plan, 4 peaks should in theory be detected: two intense peaks corresponding to $^{13}\text{C}\alpha$ and $^{13}\text{C}\beta$ from the same residue as the ^1H - ^{15}N resonance and two less intense peaks corresponding to the $^{13}\text{C}\alpha$ and $^{13}\text{C}\beta$ from the preceding residue in the protein sequence ($^{13}\text{C}\alpha_{-1}$ and $^{13}\text{C}\beta_{-1}$ respectively). This spectrum allows the sequential assignment of the protein's sequence. (B) In the HNCOCACB spectrum, by navigating through the ^{13}C axis of a fixed ^1H - ^{15}N plan, 2 peaks should in theory be detected: $^{13}\text{C}\alpha$ and $^{13}\text{C}\beta$ from the preceding residue in the protein sequence ($^{13}\text{C}\alpha_{-1}$ and $^{13}\text{C}\beta_{-1}$ respectively). The analysis of this spectrum in parallel with the HNCACB allows the emancipation of ambiguities. (C) In the HNCA spectrum, by navigating through the ^{13}C axis of a fixed ^1H - ^{15}N plan, 2 peaks should in theory be detected: one intense peak corresponding to the $^{13}\text{C}\alpha$ from the same residue as the ^1H - ^{15}N resonance and one less intense peak corresponding to the $^{13}\text{C}\alpha$ from the preceding residue in the protein sequence ($^{13}\text{C}\alpha_{-1}$). This spectrum allows the

sequential assignment of the protein's sequence and its analysis in parallel with the HNCACB allows the emancipation of ambiguities. (D) In the HNCO spectrum, by navigating through the ^{13}C axis of a fixed ^1H - ^{15}N plane, a peak should in theory be detected: ^{13}CO from the preceding residue in the protein sequence, ($^{13}\text{CO}_{-1}$). This is the simplest spectrum for obtaining the chemical shift values of ^{13}CO atoms.

In a practical way, after having recorded and processed the 3D NMR spectra, the first step is the commonly named process of “peak picking”. During the “peak picking”, one must label all visible ^{13}C peaks and identify the type of resonance (for example if it corresponds to the $^{13}\text{C}\alpha$ or the $^{13}\text{C}\beta_{-1}$ of the amino acid residue represented by a given ^1H - ^{15}N resonance). After this step, the assignment can be performed by analyzing manually all the sequential connections found in the spectra or it can also be performed automatically. For automatic assignment, the list of the chemical shifts identified during the peak picking is loaded into a software that tries to find sequential connections between resonances. Several software's and webservers are available today for automatic backbone assignment (Jung & Zweckstetter, 2004). Assignment of the chemical shifts from the atoms of side chains of residues is also possible with different 3D NMR experiments.

2.1.3 Backbone assignments of high molecular weight proteins

Generally, the higher the MW of the protein to be assigned, the more challenging the process will be. With the increase in MW, two main problems will arise that greatly affect the assignment procedure. The first and more obvious is that with the increase of the sequence length, there will be more signals in the ^1H - ^{15}N HSQC spectrum of the protein, which will lead to signal overlap. This spectral crowding is especially relevant as the proportion of disordered regions in the protein increases. Despite the advances in resolution brought by high-field spectrometers, this problem still persists. The second problem, affecting mainly high MW globular proteins, consists on the poor S/N ratio. The higher the MW of a protein, the higher will be its correlation time (τ_c). The correlation time can be defined as the time it takes to a particle to rotate by one radian (Lankhorst, Schriever, & Leyte, 1982). In other words, the higher the MW of the protein is, the slower will be its tumbling in solution. The slow tumbling and high τ_c will be translated into fast transverse relaxation (R_2) and therefore a reduced

transverse relaxation time (T_2) (since $R_2 = 1/T_2$). Increased transverse relaxation rate decreases the remaining magnetization at the end of the pulse sequence to be detected by the receiver. In other words, reduced T_2 leads to faster signal decay, leading to loss of sensitivity and broadening of the signals (Cavanagh, Fairbrother, III, Skelton, & Rance, 2010). A short transverse relaxation time is therefore unfavorable to NMR experiments since the signals become broad and less intense. In proteins with MW higher than 30 KDa it is possible that some of the NMR signals are broaden beyond detection in the ^1H - ^{15}N , preventing its assignment (Gardner & Kay, 1998). The abovementioned strategies for backbone assignment are therefore limited to well-behaving proteins under a MW under ± 30 KDa. If the objective is to assign high MW proteins, unconventional "S/N increasing methods" need to be introduced either on sample preparation or during spectra acquisition. The increase of the acquisition temperature can be a logical solution to promote faster particle tumbling and therefore higher S/N ratios. Unfortunately, this often leads to issues with protein stability, which must always be considered as the first priority. Fortunately, other methods are available to increase S/N ratio without the need to increase the temperature of acquisition.

2.1.3.1 Deuteration

Although expensive, deuteration is a very effective way for improving the detection of resonances of high MW proteins. The objective of deuteration is to tackle the line broadening and consequent loss of S/N ratio caused by low T_2 (Sattler & Fesik, 1996). One of the major contributors to the fast relaxation rate characteristic of big proteins are dipolar couplings with neighboring protons. The objective of deuteration is to reduce the dipolar couplings, decreasing therefore the transverse relaxation rate and with this, increase the S/N ratio. The dipolar relaxation is less effective when the nuclei involved have higher gyromagnetic ratios. The reason why the incorporation of deuterium reduces the contribution of dipolar couplings to transverse relaxation is because deuterium (^2H) has a gyromagnetic ratio 6.5-fold higher than the proton (^1H) (Sattler & Fesik, 1996). This important difference is translated in better relaxation properties (higher T_2), leading to less signal broadening and consequent gain in sensitivity.

In order to produce a deuterated recombinant protein, the totality (in case of perdeuteration) or a part of the ^1H sources of the culture medium (water, glucose, etc.) need to be replaced by ^2H . If only H_2O from the culture medium is replaced by D_2O , while all the carbon sources are standard protonated chemicals, one can estimate an average ^2H enrichment between 60 and 80% (Cavanagh et al., 2010). For the expression of a perdeuterated protein, all the carbon sources used for the preparation of the medium must be perdeuterated. The biggest disadvantage of deuteration is, non-surprisingly, the considerably higher price of the culture medium. Moreover, cell growth is often considerably slower in D_2O and the expression yields are often lower when compared to a non-deuterated protein. In order to tackle this problem and to increase the yield, small amounts of commercially available deuterated rich media can be added to the culture medium.

Once the deuterated protein is produced, it is placed in a protonated buffer and the exchangeable deuterons of the protein (amides, alcohols, and carboxylates) will exchange, to a certain extent, to protons. The protein will still retain an important proportion of ^2H since the aliphatic protons do not exchange, conferring better relaxation properties. Thanks to this, the ^1H - ^{15}N HSQC can be recorded while benefiting from the better sensitivity conferred by the slower transverse relaxation rate. The ^2H to ^1H exchange of labile protons is nevertheless not complete which can prevent the detection of some resonances on the ^1H - ^{15}N HSQC of deuterated proteins. This problem is dependent on the structure of the protein and particularly serious for proteins containing very large regions with poor solvent accessibility (Frueh, 2014).

2.1.3.2 Transverse Relaxation Optimized Spectroscopy

The use of Transverse Relaxation Optimized Spectroscopy (TROSY) pulse sequences is another way to improve the poor S/N ratio in the spectra of large proteins. TROSY is a method that suppresses the T_2 relaxation in multidimensional spectra, first developed in the lab of Kurt Wüthrich (Pervushin, Riek, Wider, & Wüthrich, 1997). The principle is illustrated in **Figure 9**. In a standard ^1H - ^{15}N HSQC, a single resonance is observed for a particular N-H bond of an amino acid residue. This happens because the ^1H - ^{15}N HSQC is recorded with decoupling. If the spectrum is recorded without ^{15}N decoupling, a multiplet of 4 peaks is visible (**Figure 9 A**)

instead of one single resonance as in the conventional decoupled ^1H - ^{15}N HSQC (**Figure 9 B**). In the conventional ^1H - ^{15}N HSQC, in order to avoid spectral crowding, decoupling averages the relaxation contributions and consequently the intensities of the signals of the multiplet, leading only to one resonance. We can therefore say that the resonance observed on a decoupled HSQC is in fact the average of the 4 components of the multiplet. These four resonances have different linewidths and consequently different intensities and the most intense resonance of the multiplet (**Figure 9 A, bottom-right corner**) is logically more intense than the single resonance observed in the conventional HSQC. With the application of the TROSY only the most intense resonance of the multiplet will be selected (**Figure 9 C**) leading to improved signal to noise ratio (although the absolute intensity is lower). It should be noted that the efficiency of the TROSY is better for perdeuterated samples since the replacement of ^1H spins with ^2H leads to a decrease in dipole-dipole interactions (Cavanagh et al., 2010). Moreover, theoretical studies suggest that the TROSY efficiently is ideal for ^1H frequencies close to 1000 MHz (Pervushin et al., 1997), which corresponds to the highest-field spectrometers commercialized nowadays. TROSY pulse sequences have also been shown to increase the sensitivity in some 3D experiments and are now being used to assign high molecular weight proteins (Salzmann, Pervushin, Wider, Senn, & Wüthrich, 1998).

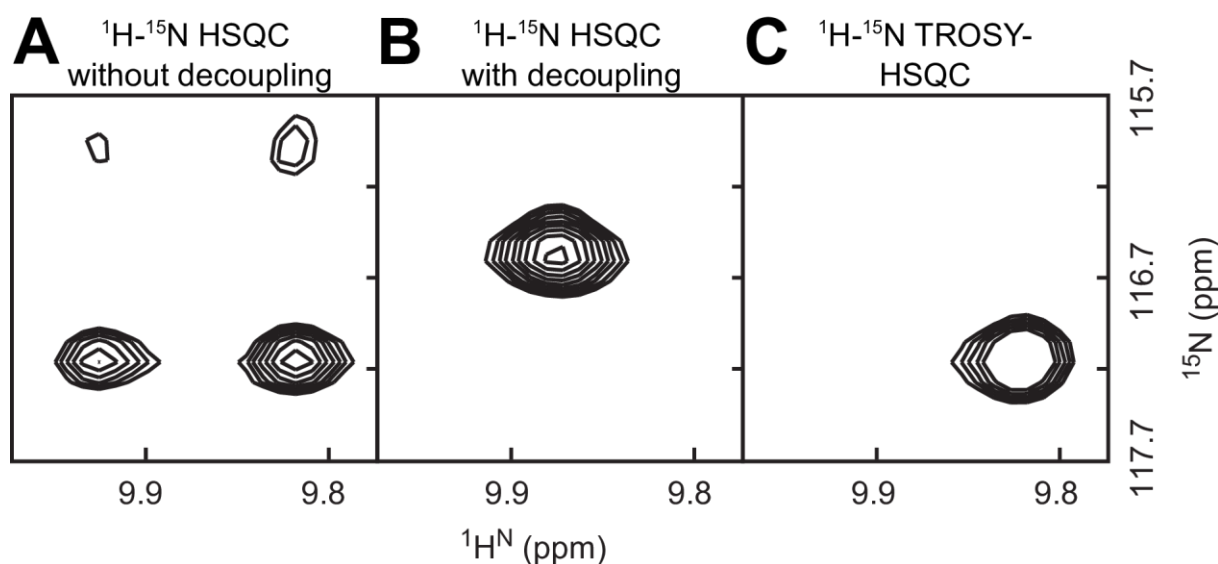


Figure 9 – Principle of TROSY. (A) The ^1H - ^{15}N HSQC recorded without decoupling is presented as a multiplet containing 4 components. (B) In the ^1H - ^{15}N HSQC with decoupling (spectrum that is performed in routine) a single signal is observed. The resultant signal is as an average, in intensity and in chemical shift, of the 4 components of

the multiplet. (C) In the ^1H - ^{15}N TROSY-HSQC only the most intense signal is presented. Adapted from (Cavanagh et al., 2010).

2.1.3.3 Selective labeling

Selective labeling can be both a strategy to simplify a crowded spectrum or a method for getting spectra with higher sensitivity. The objective of selective labelling is to detect in the NMR spectra a selective set of amino acid residues (**Figure 10**). One of the main uses of selective labeling is to help on backbone assignment of proteins presenting a ^1H - ^{15}N HSQC spectrum with extreme overlap. In this case, the most common strategy is to produce the protein in a minimal medium containing only natural abundance Nitrogen sources and feed the bacteria with a particular ^{15}N enriched amino acid just before induction (Tugarinov, Kanelis, & Kay, 2006).

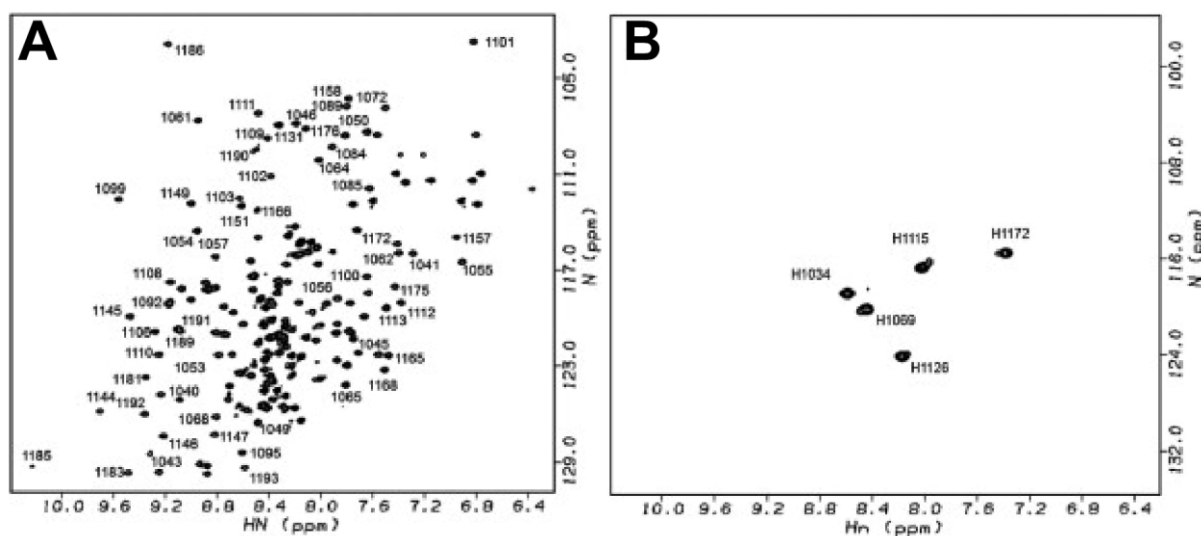


Figure 10 – Selective labeling applied to backbone assignment. (A) ^1H - ^{15}N HSQC of Uniformly labeled N-domain of Wilson disease protein (2ARF) recorded on a 600 MHz spectrometer. (B) ^1H - ^{15}N HSQC of natural abundance N-domain of Wilson disease protein (2ARF) selectively labeled with ^{15}N Histidine recorded on a 600 MHz spectrometer. Adapted from (O’Grady, Rempel, Sokaribo, Nokhrin, & Dmitriev, 2012).

Another application is the inclusion of ^{13}C labeled amino acid residue(s) or biosynthetic precursors of specific amino acid residue(s) on a perdeuterated culture

containing only ^{12}C sources. In this case, when a 2D ^1H - ^{13}C spectrum is recorded, only the ^1H - ^{13}C resonances of the selected amino acid residue(s) will be detected. This method can be applied to alanine, threonine, methionine, leucine, isoleucine and valine. One obvious advantage of this technique relies on the fact that each singlet in the spectrum is originating from three equivalent hydrogen atoms from the methyl group, which is additionally very mobile. This results in increased S/N ratio compared to the ^1H - ^{15}N resonance of backbone amides, where only one hydrogen is bound to the heteroatom. Resonance assignments of isoleucine, leucine and valine methyl groups are usually performed for large proteins in which backbone chemical shift assignments are impossible to obtain (Kerfah, Plevin, Sounier, Gans, & Boisbouvier, 2015). As no sequential connectivities can be obtained from 3D spectra for the side-chain methyl groups, assignment relies mainly on mutation, simulation and distance restraints (Sprangers & Kay, 2007). This method allows the assignments of methyl resonances in proteins with MW in the range of hundreds of kDa. An example is the study conducted on the 670 kDa 20S proteasome performed using a deuterated protein with selective isotopic ^{13}C - ^1H labeling on isoleucine, leucine and valine methyl groups (Sprangers & Kay, 2007). In this case labeling of methyl groups allowed to perform quantitative dynamic studies and to identify the binding interface of the 20S proteasome with a protein partner. This methyl labelling schemes also allowed the characterization of the inhibitory effect of chloroquine on the function of the 20S proteasome (Sprangers et al., 2008).

2.1.4 NMR on the study of Protein-Protein Interactions

The assignment of the ^1H - ^{15}N HSQC spectrum of a certain protein is a powerful tool to study the interactions of that particular protein with its partners. With the acquisition of one or more ^1H - ^{15}N HSQC spectra of a ^{15}N labeled protein in the presence of its partner, one can approximately localize the interaction surface, calculate the dissociation constant of the interaction or even predict if there are conformational changes or oligomerization/aggregation.

2.1.4.1 Interaction surface determination

The proximity of other nuclei from the ^{15}N - ^1H nuclei of the ^{15}N labeled protein changes their electronic environment and therefore induces Chemical Shift Perturbations (CSP). However, it cannot be directly deduced from a CSP that a residue is in direct interaction with the ligand or partner. In fact CSP may also arise due to conformational changes occurring sometimes far away from the binding site. Another aspect that can lead to difficulties interpreting the binding site based on CSP from the ^1H - ^{15}N resonances is the fact that hydrophobic interactions are usually downplayed (Williamson, 2013). Chemical shifts can also be affected by minor changes in buffer composition, temperature, and pH or by the presence of some substances (i.e. DMSO) (Williamson, 2013). For this reason, the ranking of the most affected resonances does not allow the exact determination of the residues directly in the binding site. Nevertheless, this ranking provides an approximation of the region of the ^{15}N labeled protein that directly contacts with its partner, in solution.

There is no defined cut-off for picking the CSPs that are directly linked to the binding of a partner. Some authors propose that a CSP is significant when the measured value is higher than the double of the standard deviation of the measurement for all residues (Williamson, 2013). Yet, the threshold is usually defined by the author on an individual basis. Two properties can be measured for quantifying the CSP upon addition of the partner: either the shift in the position of the resonance (in ppm) if the system is in fast exchange or the change on the intensity of the resonance if the system is in intermediate or slow exchange on the NMR timescale. If the system is in fast exchange the resonances will move from their initial coordinates (in ppm) upon addition of the partner. In a titration, the signal observed translates the averaged populations of free and bound protein (**Figure 11 A**).

If the system is in slow exchange, then the rate at which the conversion between the free and bound forms occurs is considerably slower than the difference in frequency between the free and bound forms. As a consequence, two peaks are observed in the spectrum for one single resonance: one peak representing the free form, whose intensity should decrease during a titration and another peak, close to this one, representing the bound form and whose intensity increases during a titration (**Figure 11 B**). Slow exchange can drastically complicate

the determination of the binding site since the presence of two resonances for only one ^1H - ^{15}N bond may prevent the assignment of some residues.

If the rate of conversion between the free and the bound form is similar to the NMR time scale, then the system is in intermediate exchange. In this type of exchange only one resonance is observed and the signals may also, in some cases shift like in fast exchange. Nevertheless, what characterizes intermediate exchange is the progressive broadening of the resonances in the spectrum when adding increasing concentrations of the ligand. In intermediate exchange, resonances may even broaden beyond detection. Logically, the exchange between free and bound forms is usually faster for low affinity interactions, typically in the mM or μM range (Williamson, 2013). Finally, a resonance can be broadened due to a decreased local mobility induced by the binding.

Nevertheless, the Kinetics (and not the affinity) of the interaction is what will define the exchange rate. Therefore, although a slower exchange rate typically means a higher affinity interaction, this assumption cannot be made directly (Fielding, 2007).

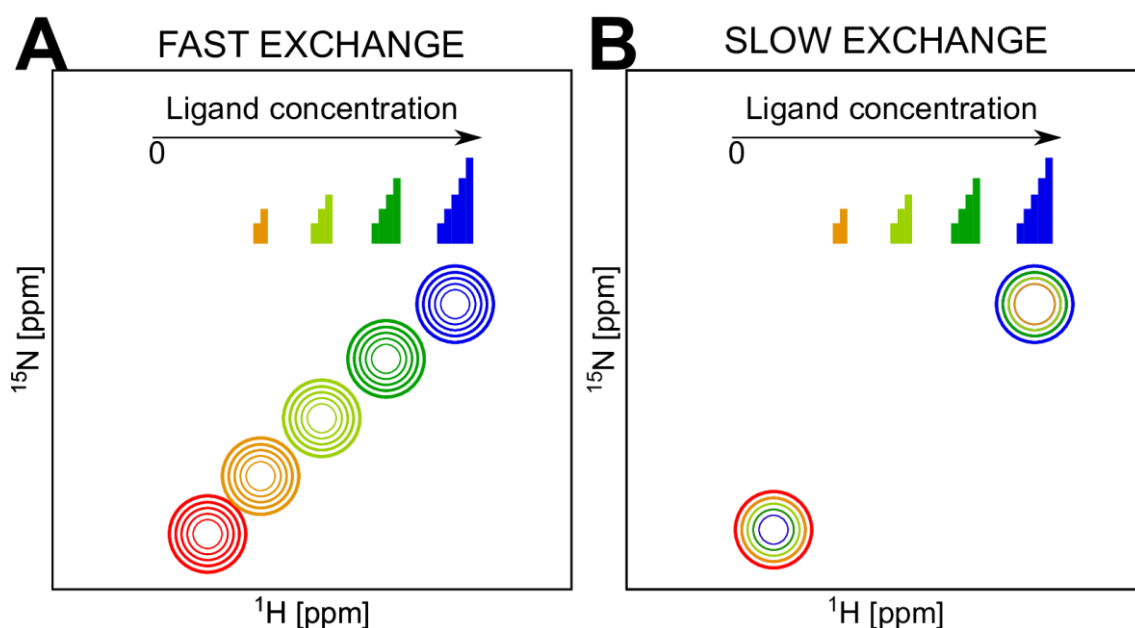


Figure 11 – Fast and slow exchange regimes observed in the ^1H - ^{15}N HSQC during a protein-ligand interaction. (A) In the fast-exchange regime, the peaks do not significantly change intensity and move slightly from their original position (red) upon addition of a ligand (highest concentration in blue). (B) In the slow-exchange regime, once the ligand is added, two signals are observed: one for the bound and one for the free form. During a titration, the

intensity of the signal correspondent to the free form decreases and the intensity of the signal correspondent to the bound form increases. Adapted from (Williamson, 2013).

2.1.4.2 Dissociation constant

NMR has the intrinsic advantage of allowing the determination of dissociation constants of very weak interactions that are hard to obtain with other biophysical techniques. NMR can be used to estimate K_d values in the mM and μM range. It is estimated that K_d values as high as 10 mM can be optimally determined by ^1H - ^{15}N HSQC titration (Williamson, 2013). Nevertheless, in order to accurately determine the K_d by a protein-observed NMR titration, the system must be in fast exchange. The chemical shift in fast exchange regime is indeed a direct measurement of the amount of complex in the solution. In this case the monitoring of the CSP (in ppm) upon the titration of the ^{15}N labeled protein with increasing concentration of the ligand (for example from a L/P ratio = 0.1 up to a L/P ratio = 3 or 5) (**Figure 12 A**) allows the determination of the K_d after fitting the gradual chemical change with a saturation curve (**Figure 12 B**). This analysis is often done for more than one peak and the calculated K_d is the average of the result obtained for all the peaks analyzed (Fielding, 2007; Williamson, 2013; Xu & Van Doren, 2016).

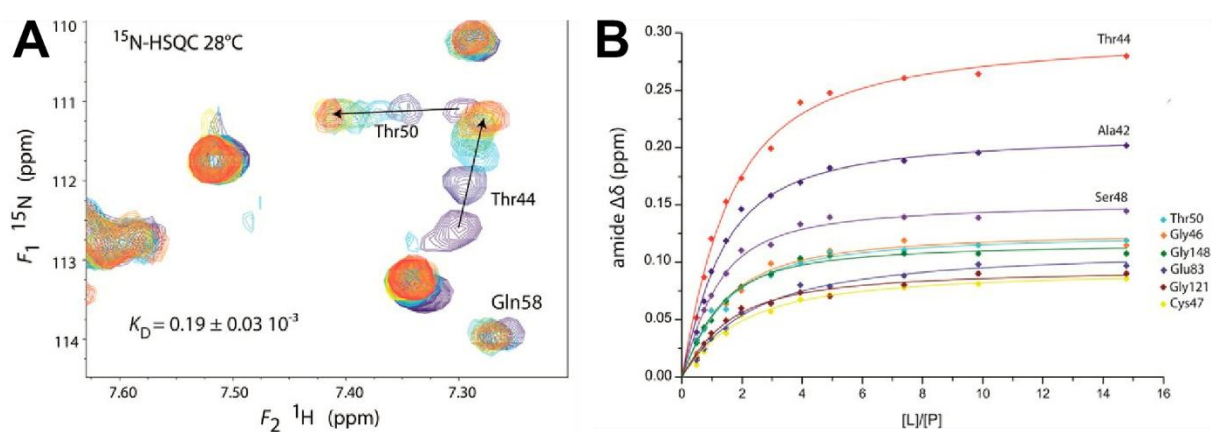


Figure 12 – Determination of the dissociation constant of a protein-ligand system in fast exchange regime. (A) ^1H - ^{15}N HSQC of reduced human peroxiredoxin 5, recorded at 28°C, in the presence of increasing concentration of ligand. The CSP induced by the ligand on T44 and T50 show that the system is in fast exchange. (B) Plot of CSP (in ppm) (y axis) versus the $[L]/[P]$ ratio for 9 residues of reduced human peroxiredoxin 5 in the presence of increasing concentration of the ligand. The fitting for each individual residue allows the determination of a dissociation constant. The final value is an average of all the 9 values obtained. Adapted from (Chow et al., 2016).

2.2 Peptide Nuclear Magnetic Resonance

NMR is a very useful method for studying the structure, secondary structure propensity and dynamics of peptides. As for proteins, the first step on NMR driven projects for peptides is the assignment. Here there is one important difference from proteins, which relies on the fact that peptides do not always need to be isotopically enriched to be assigned. Peptides are smaller than proteins and have therefore less signal overlap, smaller τ_c and thus more favorable relaxation properties. Additionally peptides can be concentrated to mM samples and natural abundance detection of ^{15}N or ^{13}C is feasible to achieve a complete assignment of the peptide chemical shifts (backbone amides and side chain chemical shifts) (S. Raghothama, 2010). In case it is not possible to assign a non-labeled peptide, then the approach to follow is to produce the isotopically enriched peptide and to assign it using 3D spectra in a similar fashion as it is done with proteins.

Assuming that the peptide can be assigned without isotopic ^{13}C and ^{15}N enrichment, ^1H - ^{15}N HSQC and ^1H - ^{13}C HSQC are typically recorded for obtaining nearly all ^1H - ^{15}N and ^1H - ^{13}C correlations. In addition 2D spectra, named Total Correlation Spectroscopy (TOCSY) and Nuclear Overhauser Effect Spectroscopy (NOESY) are recorded. The TOCSY spectrum is a 2D ^1H - ^1H experiment in which each strip contains the ^1H resonances of one spin system (Cavanagh et al., 2010). Non aromatic amino acids contain only one spin system and therefore what is observed is a unique strip containing all the ^1H chemical shift of each amino acid residue, as exemplified in **Figure 13**. Each amino acid type contains a specific TOCSY pattern allowing its differentiation from others. In practice, a specific amino acid can rarely be identified directly from a TOCSY strip but several possibilities can be discarded directly. In order to assign the TOCSY spectrum, another spectrum needs to be recorded for establishing sequential links between each amino acid residue. This is accomplished by the NOESY spectrum. The NOESY spectrum is based on the Nuclear Overhauser Effect. In the NOESY spectrum, an NOE cross peak arises when two protons are located less than approximately 5 Å away from each other. These cross peaks are due to dipolar couplings resulting from interactions of spins via space (Derome, 1987). Therefore, contrarily to what happens in the TOCSY, signals in the NOESY spectrum depend exclusively on the distance and not on the number of bonds separating the nuclei. The detection of NOE between the ^1HN of one residue and the $^1\text{H}\alpha$ of neighboring

residues allows the establishment of sequential relationships between the amino acid residues. The utility of the NOE is not restricted to the assignment of peptides. The establishment of distance constraints on peptides can also identify structural motifs like α -helices, β -strands or turns (Wüthrich, Spitzfaden, Memmert, Widmer, & Wider, 1991). Once the ^1H chemical shifts are assigned, the corresponding ^1H - ^{13}C and ^1H - ^{15}N resonances can be assigned with the ^1H - ^{13}C HSQC and ^1H - ^{15}N HSQC, respectively. Chemical shift values of a peptide or protein, especially $^{13}\text{C}\alpha$ and $^{13}\text{C}\beta$ which are linked to dihedral angles, are excellent reporters of the secondary structure motif in which a particular residue is taking part (David S. Wishart & Sykes, 1994). Several methods are available for predicting the secondary structure from chemical shifts: CSI 3.0 server (Hafsa, Arndt, & Wishart, 2015), Talos + (Shen, Delaglio, Cornilescu, & Bax, 2009), Talos N (Shen & Bax, 2013), PECAN (Bahrami, Assadi, Markley, & Eghbalnia, 2009) or Secondary Structure Propensity (SSP) score (Marsh, Singh, Jia, & Forman-Kay, 2006). All those methods are based on the difference between the experimental chemical shifts and the random coil chemical shift for each amino acid reported in a database, like for example the RefDB database (H. Zhang, Neal, & Wishart, 2003). From the methods mentioned above, the SSP score differs in the fact that it takes into account the intrinsic probability of an amino acid to be found in a specific secondary structure (Marsh et al., 2006). For this reason, the SSP score is mostly applied to disordered proteins or peptides in order to detect small tendencies to form a secondary structure. Hence, for structures known or predicted to contain stable secondary structure, other methods than the SSP score are more suitable.

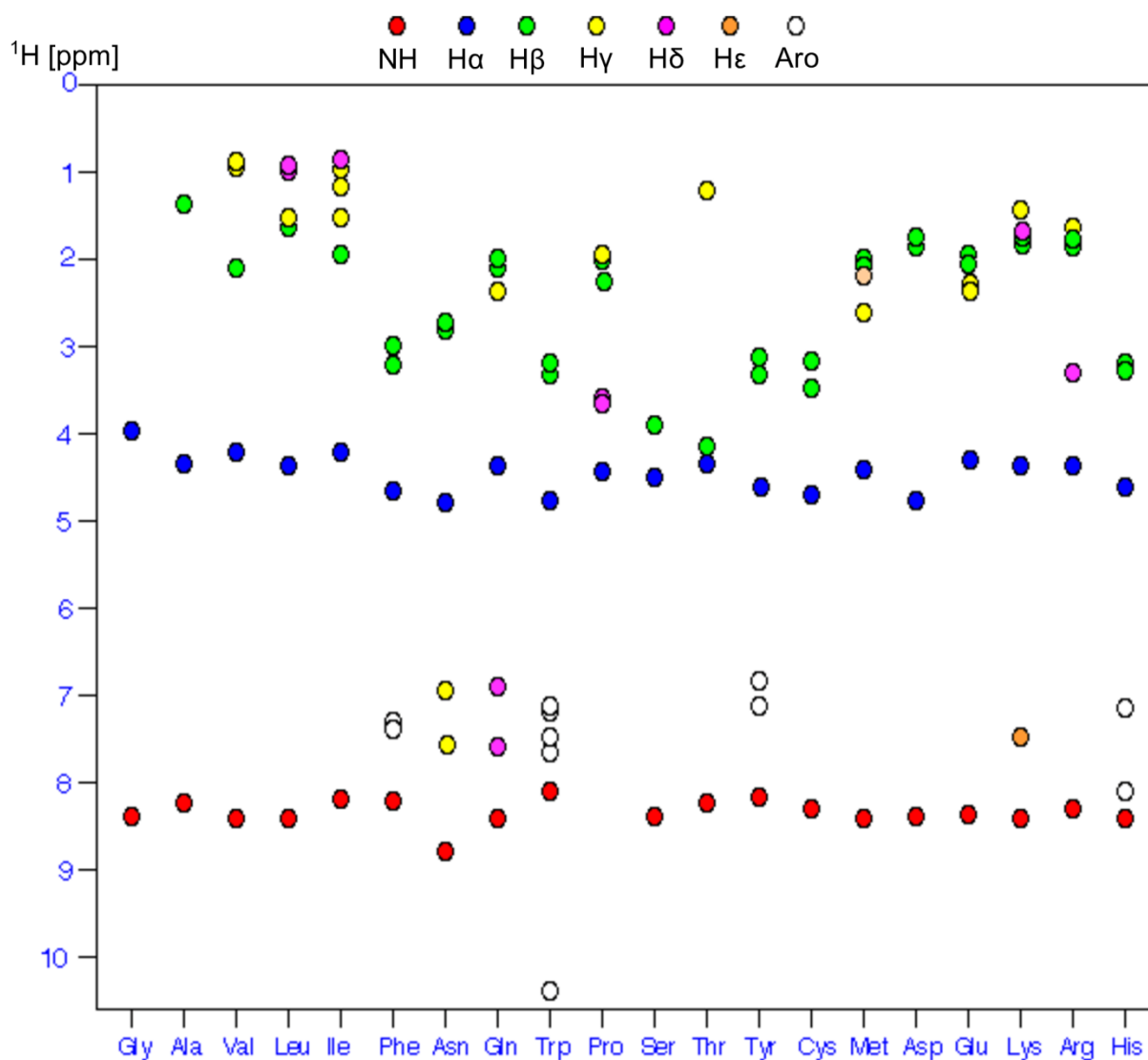


Figure 13 – TOCSY patterns of the different amino acid residues. This diagram does not take in consideration the different spin systems and presents all the ^1H chemical shifts expected for each amino acid residue. Adapted from (Teodor Parella).

2.3 Analytical Ultracentrifugation as a tool to study protein-protein interactions

Analytical ultracentrifugation (AUC) is a free solution technique that enables the study of several aspects of PPIs such as stoichiometry, dissociation constants or reversibility (Harding & Rowe, 2010). In practice, species in solution are monitored by absorption or interference detection systems while the sample is being centrifuged at high rotor speeds. In

order to allow the correction of the signal, centrifuge cells are equipped with two cavities, one to contain the sample and the other to contain the reference buffer. There are two types of AUC experiments: sedimentation equilibrium (SE) and sedimentation velocity (SV). The first is conducted at lower centrifuge forces in order to allow an equilibrium between sedimentation (opposite to the center of rotation) and diffusion forces (towards the center of rotation). SE experiments require considerably more acquisition time than SV since the measurements must be performed during a few days (Cole, Lary, Moody, & Laue, 2008). The greatest advantage of SE relies on the fact that the measurements are not affected by hydrodynamic effects. For this reason it allows the calculation of the Molar mass of the biomolecules with high precision when compared to SV (Harding, 1993). SV is conducted at high centrifuge forces in order to let the proteins flow away from the center of the rotor, concentrating all the species at the bottom of the cell. The concentration of proteins in each point of the cuvette is measured over time throughout the run (**Figure 14**) (Lebowitz, Lewis, & Schuck, 2002). This raw data can then be used for the calculation of the diffusion-deconvoluted sedimentation coefficients ($c(s)$) based on calculations performed by softwares such as SEDFIT (Schuck, 2000). The recorded data can also be used to derive a dissociation constant by direct modelling using an appropriate software package to fit the data (Dam, Velikovskiy, Mariuzza, Urbanke, & Schuck, 2005). SV is the ideal technique for studying the distribution of species in solution, for determining their sedimentation coefficients and for deriving the stoichiometry of a reaction. Nevertheless, contrarily to SE, SV does not allow a precise determination of the molar mass. Both SV and SE allow the determination of the dissociation constant of the reaction between two proteins (Cole et al., 2008).

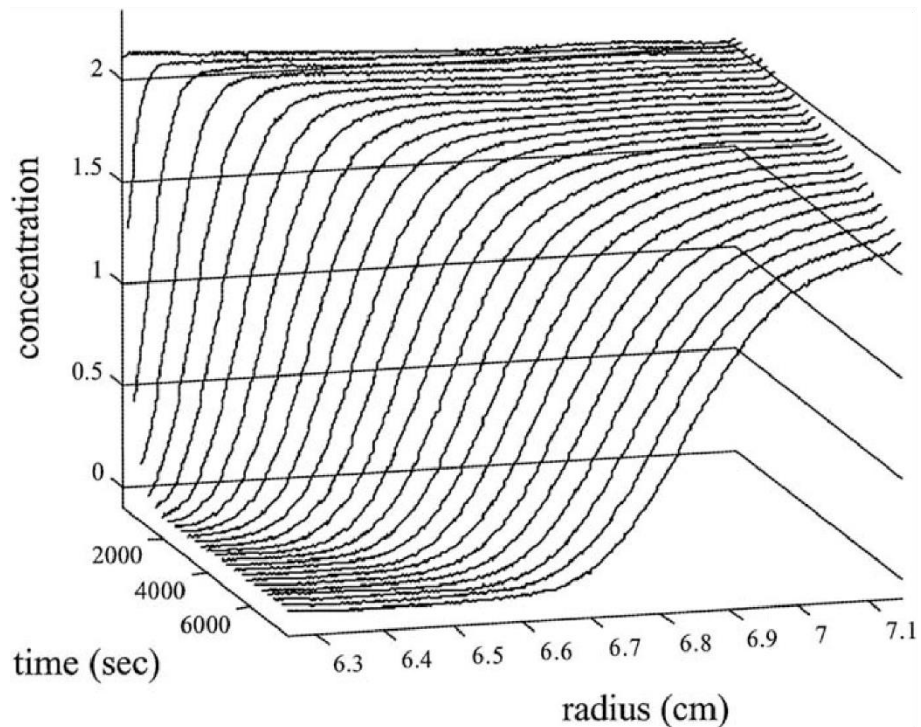


Figure 14 - SV data of a protein sample. The concentration is shown as a function of the radius (cm) over time in (s) after the start of the sedimentation process. In this example, SV data from a sample containing bovine serum albumin centrifuged at 50 000 rpm is shown. Concentrations are in units of fringe displacement in the interference optical system, which corresponds to ~ 0.3 mg/mL per fringe. Figure from (Lebowitz et al., 2002).

3 The 14-3-3/Tau Protein-Protein Interaction: a promising therapeutic target for Alzheimer's disease

3.1 Alzheimer's disease

According to The World Alzheimer report 2018 ('World Alzheimer Report 2018: The state of the art of dementia research: New frontiers', 2018) the number of people living with Alzheimer's disease (AD) has already reached 50 million. According to the same source, one new case is diagnosed every 3 seconds and the global figures are predicted to triple to 150 million by 2050. The estimated worldwide cost of dementia in 2018 is estimated to have reached 1 Trillion US\$.

AD is characterized clinically by a progressive decline in cognitive function. AD can cause a multitude of symptoms that have a wide patient variability. The most famous symptom of

AD is short-term memory impairment, which is the most commonly reported first cognitive symptom of the disease. Memory impairment is not necessarily the first cognitive symptom of the disease as impairment in judging and changes in linguistic and visuospatial functions are also often reported, especially for early onset of the disease (Barnes et al., 2015). Other important group of symptoms are the neuropsychiatric symptoms, present in 97% of patients (Lanctôt et al., 2017). In the late-stage of the disease, there is a complete loss of independence and permanent care is needed. Once patients get into the late stage of the disease they are not expected to live more than 2-3 years (Neugroschl & Wang, 2011).

The etymology of this pathology's name comes from the doctor who first characterized clinically and histologically what was considered as a normal collateral effect of ageing. The German doctor Alois Alzheimer followed a 51 years old patient presenting signs of severe cognitive impairment, behavioral abnormalities and an overall progressive loss of autonomy (Hippius & Neundörfer, 2003). What differentiated Dr. Alzheimer from others of the same time was the fact of having proceeded to an autopsy in the quest of the origin of the problem. The observations of the autopsy of his 51 years old patient showed a brain with severe signs of atrophy. Dr. Alzheimer went further with his analysis and analyzed brain tissue under his microscope. He detected aggregated fibrous material both inside and outside of neurons (Vishal, Sourabh, & Harkirat, 2011). These two histopathological observations reported in 1907, remain as the two main hallmarks of Alzheimer's disease up to date.

3.1.1 Aggregation of the β -amyloid peptide: The amyloid hypothesis

Extracellular senile plaques are one of the hallmarks of AD and are mainly constituted by the β -amyloid peptide ($A\beta$). This peptide is originating from the cleavage of APP (amyloid precursor protein). APP can be processed by two different enzymes: α -secretase and BACE (β -secretase) (**Figure 15**). Upon the cleavage by one of these two enzymes, an N-terminal fragment ($sAPP-\alpha$ for cleavage by α -secretase or $sAPP-\beta$ for cleavage by β -secretase) and a C-terminal fragment are formed (C83 for cleavage by α -secretase or C99 for cleavage by β -secretase). After this, independently of the pathway, the C-terminal fragment undergoes an additional cleavage step by an enzyme complex called γ -secretase (constituted by Presenilin 1 or 2, Nicastrin, Presenilin Enhancer 2 and Anterior Pharynx Defective 1). The second

cleavage of this proteolytic cascade yields AICD (APP intracellular domain), and either the p3 peptide in the case of the pathway involving α -secretase or the A β peptide in the case of the β -secretase pathway (Teich & Arancio, 2012).

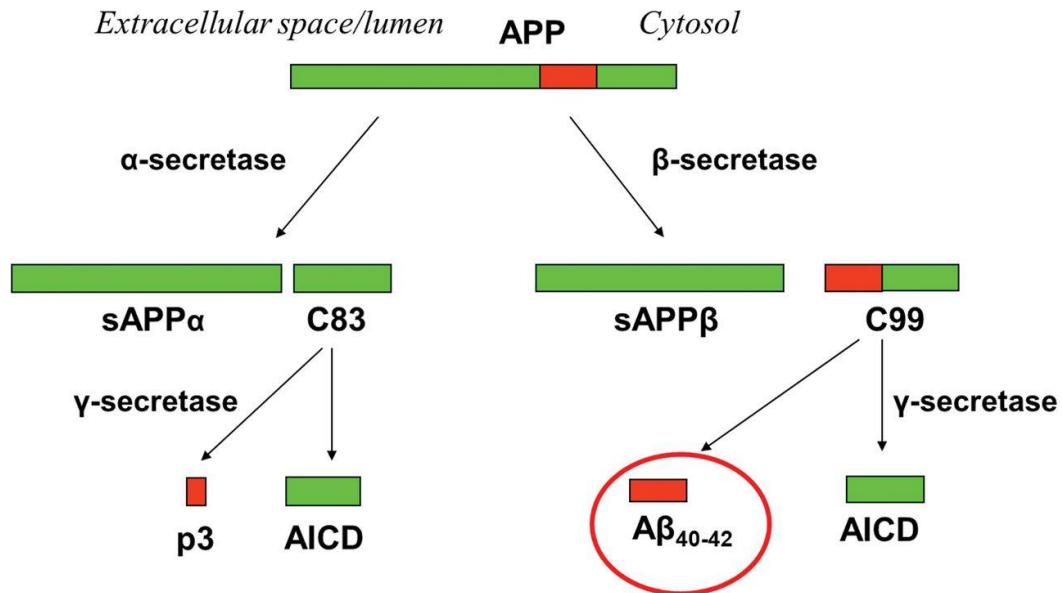


Figure 15 – Non-amyloidogenic and amyloidogenic metabolic pathways of APP. The pathway starting with the cleavage by α -secretase is represented on the left and the pathway starting with the cleavage by β -secretase is represented on the right. From (Teich & Arancio, 2012).

In the brains of AD patients, the A β peptide resulting from the APP cleavage by the β -secretase pathway aggregates forming extracellular oligomers and senile plaques. The amyloid hypothesis defends that the accumulation of this peptide and the formation of the aggregates is the key starting point for the complex turn of events happening in AD. This hypothesis is highly supported by the fact that the three main genes linked to familial AD, which accounts for 1-6% of the total cases of AD, are involved in the APP cascade. These genes codify for APP itself, Presenilin 1 and Presenillin 2. Inversely, the presence of a missense mutation in APP leading to the decrease of A β aggregation was shown to be protective against AD (Selkoe & Hardy, 2016). In fact, the totality of AD patients experience progressive A β deposition followed by adjoining neuritic and glial cytopathology in brain regions controlling memory and cognition (Selkoe & Hardy, 2016). Supporters of the amyloid hypothesis also state that the aggregation of the A β peptide is linked to the origin of the other hallmark of AD:

the neurofibrillary tangles. Indeed, human A β 42 oligomers were shown to indirectly induce Tau hyperphosphorylation (the main constituent of the neurofibrillary tangles) at AD-relevant epitopes and cause neuritic dystrophy in cultured rat neurons (Jin et al., 2011). Despite the existence of evidence supporting the amyloid hypothesis and therefore the suggestion that the aggregation of the A β peptide is the trigger for the pathology, there are pieces missing on the puzzle and the scientific community is divided in this regard (Selkoe & Hardy, 2016).

3.1.2 Neurofibrillary tangles: Aggregation of Tau protein

3.1.2.1 The discovery of neurofibrillary tangles

Apart from the extracellular aggregates that later were found to be A β aggregates, Dr. Alois Alzheimer also detected, in 1907, an intracellular accumulation of a fibrous material. These intracellular aggregates were studied in more detail by Kidd, in 1963, using electron microscopy for the analysis of neurons of the cerebral cortex of 3 AD patients. In some neurons, Kidd observed long double-helical parallel fibers with varying sizes (Kidd, 1963). Nowadays these fibers described by Kidd are called Paired Helical Filaments (PHFs). Today we also know that the main constituent of these PHF's is the abnormally phosphorylated neuronal protein Tau, but this was only confirmed more than 20 years after the description of the PHFs by Kidd (Brion, Flament-Durand, & Dustin, 1986; Grundke-Iqbal et al., 1986). After this discovery, the scientific community turned its attention to the study of the function of this protein.

3.1.2.2 Tau protein: the main constituent of neurofibrillary tangles

Nowadays, Tau is considered one of the most important biomolecules on the pathogenesis of AD and for some, it represents the best opportunity for pharmacological interventions. Human Tau is encoded by the MAPT gene, whose pre-ribonucleic acid (RNA) is spliced differently according to the cellular type and degree of maturation. This alternative splicing is responsible for the existence of six different isoforms of Tau. The classification of these isoforms is based on the presence of zero, one or two N-terminal inserts (0N, 1N and 2N, respectively) and on the presence of three or four microtubule binding repeats (3R and

4R, respectively) (Buée, Bussi re, Bu e-Scherrer, Delacourte, & Hof, 2000; Guo, Noble, & Hanger, 2017). Tau protein has an overall basic character and is an intrinsically disordered protein with a key role on the polymerization of tubulin and therefore on the stability of microtubules (Kolarova, Garc a-Sierra, Bartos, Ricny, & Ripova, 2012). The fact of being intrinsically disordered means that Tau has no defined structure in solution and what happens in reality is that Tau adopts a wide range of different conformations. Due to its flexibility, Tau is impossible to study by X-ray crystallography and therefore structural studies of Tau rely frequently on NMR (Lippens et al., 2016).

Four regions can be distinguished in the structure of Tau: the N-terminal domain, the proline-rich domain, the microtubule-binding domain and the C-terminal domain. The N-terminal domain does not bind directly to microtubules but is involved in microtubule dynamics and function. It is also known that this domain is involved on the interaction of Tau with molecules from the neural plasma membrane and on a signaling cascade that influences axon transport in neurons (Chen, Kanai, Cowan, & Hirokawa, 1992). This domain also influences the protein interaction partners of Tau and interestingly the number of N-terminal inserts has a key role on this topic (Liu, Song, Nisbet, & G tz, 2016). The proline-rich domain of Tau contains seven Pro-X-X-Pro motifs and is directly implicated in the interaction of Tau with Src homology-3 (SH3) domain containing proteins (Lasorsa et al., 2018; G. Lee, Newman, Gard, Band, & Panchamoorthy, 1998; Gloria Lee, 2005). It has also been reported that this domain is a binding site for nucleic acids and that it is implicated in the regulation of microtubule assembly (Guo et al., 2017; Qi et al., 2015). The microtubule binding domain contains the microtubule binding repeats and the flanking sequences. This region is directly involved on the binding to microtubules (Bibow et al., 2011; Sillen et al., 2007), a key cellular event for neuronal cells and the most important biological function of Tau (Weingarten, Lockwood, Hwo, & Kirschner, 1975). Considering the C-terminal region, despite the fact that its function is poorly known, it has been reported that changes in this domain have a strong influence on the global function of the protein (Guo et al., 2017). A scheme regarding this protein's structure is represented in **Figure 16**.



Figure 16 – Schematic representation of Tau isoforms. Above each protein the domains are presented as N (N-terminal domain), PRD (Proline-rich domain), MTBD (Microtubule binding domain) and C (C-terminal domain). The actual molecular weight is presented for each isoform. From (Guo et al., 2017).

The interactome and the wide range of functions of Tau are markedly influenced by the post-translational modifications that the protein is subjected to (Buée et al., 2000). Phosphorylation is the most studied post-translational modification and is markedly increased under pathological conditions. Tau phosphorylation at key residues, mainly S214, S262, S293, S324 and S356 has been shown to dramatically decrease the affinity of Tau to microtubules (Hasegawa, 2016). Phosphorylation of Tau has also other consequences as it increases the transport of Tau from axons into the somatodendritic compartment, disrupts its degradation and influences its interaction with other cellular biomolecules. Eventually this leads to Tau-mediated toxicity, which occurs through several mechanisms, many of them still unknown (Guo et al., 2017). Tau has several important functions, such as nuclear protection, cell signaling and maintenance of microtubule stability (Buée et al., 2000; Guo et al., 2017; Jadhav et al., 2019). Consequently, Tau pathway dysregulations are also associated with several pathological events such as axonal transport deficiencies (Terwel, Dewachter, & Van Leuven, 2002), cell-signaling dysfunction (Burnouf et al., 2013), nuclear damage (Frost, Hemberg, Lewis, & Feany, 2014; Hamdane et al., 2005) and aggregation in NFT's (Musi et al., 2018). In

fact, as seen in **Figure 17** some of the pathological events related to Tau pathway dysregulations are directly linked to impairments of its physiological functions.

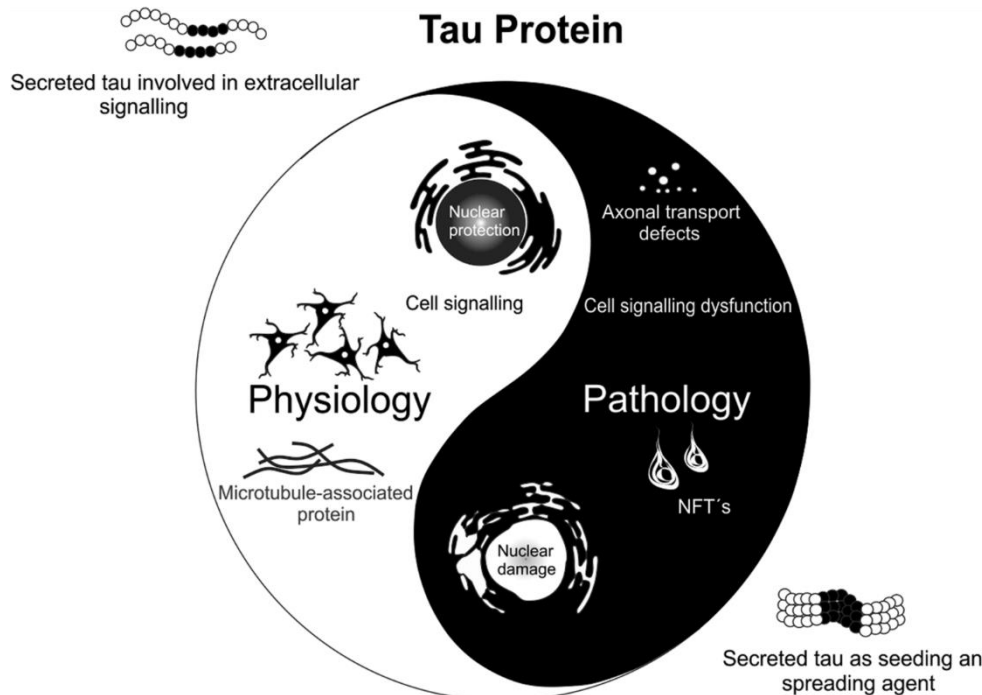


Figure 17 – Yin and Yang of the Tau protein. Tau pathology is linked to Tau physiological functions. Figure from (Jadhav et al., 2019).

Given its involvement in many pathological processes, targeting Tau, its interacting partners and the enzymes responsible for its post-translational modifications are promising therapeutic approaches, not only for Alzheimer’s disease, but also for other Tauopathies (Bakota & Brandt, 2016; Jadhav et al., 2019).

3.1.2.3 Tau in the neurofibrillary tangles

One finding that highlights the importance of the Tau containing neurofibrillary tangles in the pathology of AD is the fact that, contrarily to the deposits of β -amyloid plaques, it is very well correlated to the progression of the disease and with the severity of the symptoms (Teich & Arancio, 2012). These findings were recently confirmed in a study based on Positron

emission tomography (PET) observations. This study showed that A β accumulation precedes Tau accumulation and that the latest is extremely well correlated with the symptoms of AD. Therefore, it is suggested that A β accumulation can be seen as an early marker of AD (as proposed by the amyloid hypothesis) while the formation of neurofibrillary tangles, tracked by PET-scan is the best way to track disease progression, the rate of accumulation being linked to the disease severity (Hanseeuw et al., 2019).

Although PHFs are the major component of NFTs, they are not the only type of Tau aggregates found on the NFTs. Straight filaments (SF) were identified in 1981 (Yagishita, Itoh, Nan, & Amano, 1981) and are another type of Tau filaments that can be found in the brain of AD patients. Since 1991 it is known that both types of filaments share the same C-shaped packing unit (Crowther, 1991). Recently, high resolution cryo-electron microscopy (cryo-EM) structures of Tau filaments purified from the brain neurofibrillary lesions of an AD patient were presented (Fitzpatrick et al., 2017). These structures confirm the C-shaped architecture of the aggregation core in both the PHF and SF (**Figure 18 A, B**). Each C-shaped core is comprised by a β -helix region. The region of Tau involved in this C-shaped core is the one located between V306 and F376. What differentiates the two types of filaments is the organization of the two protofilaments around the C-shaped core. In PHFs the protofilaments are organized in a helical symmetrical fashion (**Figure 18 C**). In SFs the two protofilaments are not packed symmetrically (**Figure 18 D**).

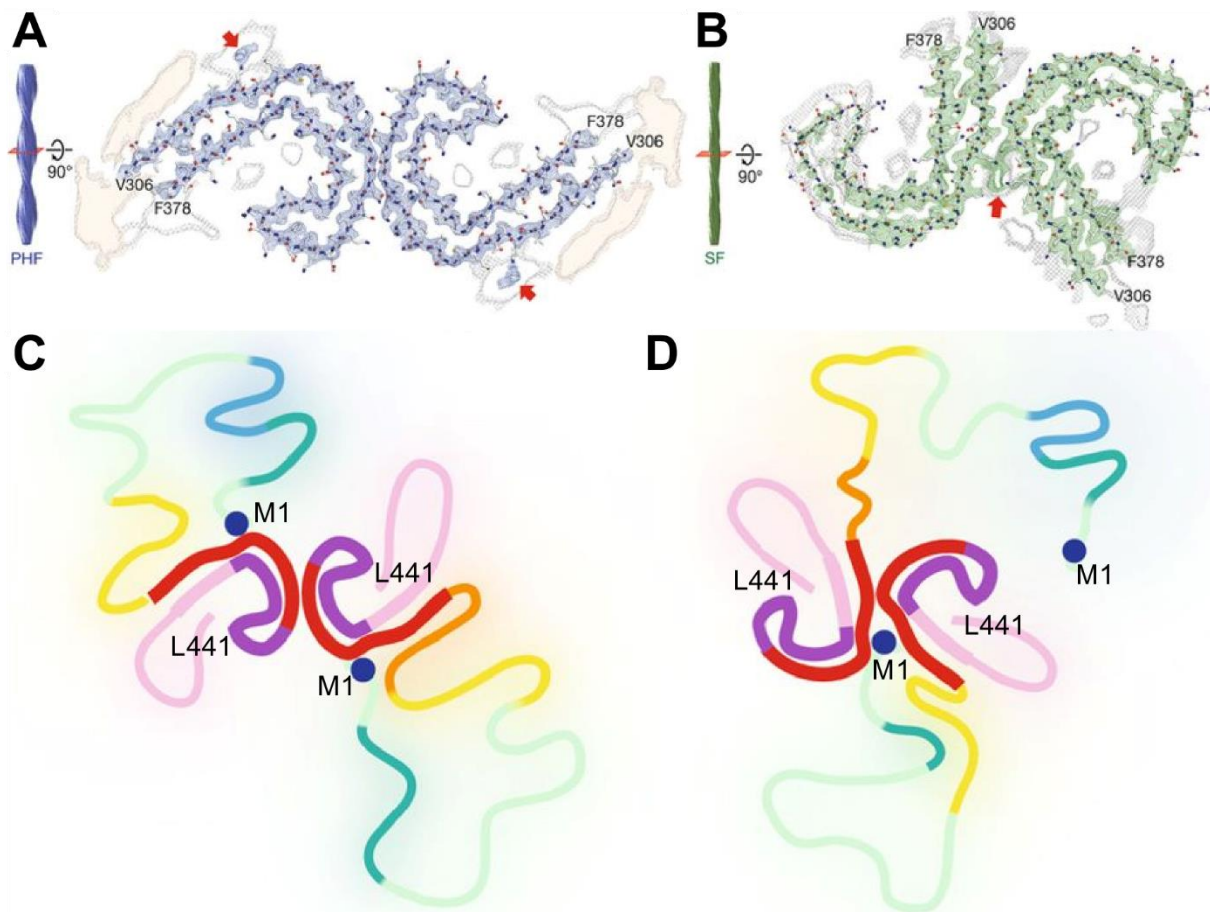


Figure 18 – Schematic representation of PHFs and SFs. Cryo-EM density and atomic models of PHFs (A) and SFs (B). The first (V306) and last (F376) residues of the C-shaped core are indicated. Schematic representation of the full-length Tau protein in a PHF (C) and in a SF (D). The first (M1) and last (L441) residues of Tau are indicated. Adapted from (Fitzpatrick et al., 2017).

3.1.3 Treatment of Alzheimer’s disease and new investigational drugs

The treatment of AD remains one of the biggest challenges for the scientific community. The truth is that after decades of research and investment, current treatment for AD has not changed since many years. There are currently only two classes of approved drugs for AD: the cholinesterase inhibitors, which prevent acetylcholine/butrylcholine deprivation in the brain and an N-methyl-D-aspartate antagonist, which prevents the toxic effects associated with excess glutamate. From the first group, donepezil, rivastigmine and galantamine are approved for all stages of AD. Regarding the only approved N-methyl-D-aspartate antagonist,

memantine, it is approved for moderate to severe cases of AD. These treatments are usually combined with other pharmacological and non-pharmacological interventions in order to reduce the symptoms and the associated comorbidities (Fertalova & Ondrioiva, 2019). All approved drugs show a significant improvement of the symptoms but do not interfere with the rate of cognitive decline (Weller & Budson, 2018) and therefore are not a treatment for AD. For treating this disease, the scientific community is now targeting molecules and processes that are on the origin of the pathology using more biological information than ever. **Table 1** summarizes the status of investigated disease modifying therapies for Alzheimer’s disease.

Table 1 – Current targets and investigational disease modifying treatments for Alzheimer’s disease as per April 2019. Adapted from (Weller & Budson, 2018) with further contributions from (Medina, 2018), (Sigurdsson, 2018), (Cummings, Lee, Ritter, & Zhong, 2018) (Makin, 2018), clinicaltrials.gov (accessed 06/05/2018).

Target	Drug	Study phase	Expected completion date	Remarks
β-Amyloid	CAD106	2	May 2024	
	CNP520	2	May 2024	
	BAN2401	2	November 2018	
	LY3002813 *	2	December 2020	
	Crenezumab #	3	Terminated January 2019	Not effective
	Aducanumab	3	Terminated April 2022	Not effective
	UB-311	2	December 2018	
	Gantenerumab	3	May 2023	Already failed 1 phase 3 CT
	Solanezumab	3	Terminated May 2017	Not effective
	CT1812	2	Completed October 2016	Safe for phase 3
	Thiethylperazine	2	July 2021	
	ID1201	2	December 2018	

	NPT088	1	Completed Februar 2019	
	Lu AF20513	1	January 2020	
	ABvac40	2	February 2021	
	Ponezumab	2	Completed June 2011	Not effective
	ACC-001	2	Completed February 2014	Safe for phase 3
	KHK6640	1	Completed December 2017	
	GSK933776	2	Completed	Not effective
	ABvac40	1	Completed July 2015	Safe for phase 2
BACE1 (β-site Amyloid precursor protein Cleaving Enzyme)	Lanabecestat	2	September 2019	
	JNJ-54861911	2	October 2022	
	Elenbecestat	3	June 2021	
	<u>LY3202626 *</u>	2	December 2020	
	Verubecestat	3	March 2021	
	LY450139	3	Completed April 2011	Not effective
p-Tau (hyperpho sphorylate d Tau)	IONIS-MAPTRx	1, 2	February 2020	
	JNJ-63733657	1	March 2020	
	RO7105705	2	September 2022	
	ABBV-8E12	2	June 2021	
	AADvac1	2	June 2019	
	BIIB-092	2	September 2020	
	BIIB-080	1	February 2020	

	TPI-287	1	Completed May 2017	
	TRx0237	3	December 2020	
	LY3303560	1	June 2019	
	ACI-35	1	-	
	UCB0107	1	Completed December 2018	
APP (Amyloid Precursor Protein)	Posiphen	1	December 2019	
RAGE (Receptor for Advanced Glycation End products)	Azeliragon	3	Terminated January 2019	Not effective
Retinoid receptor	Acitretin	2	Completed February 2018	Not effective
	Bexarotene	2	Completed February 2016	Not effective

*Medications under investigation as combination therapy.

Phase 2 clinical trial still ongoing

Table 1 does not include drugs that are currently in clinical trials for the treatment of AD's associated comorbidities. An example of one of these drugs targeting AD's associated comorbidities is zolpidem, which is being studied for improvement of sleep disorders in AD patients (Cummings et al., 2018). **Table 1** leaves no doubt on the challenge of the development of new disease-modifying therapeutics for AD. Some therapies have already reached Phase 3 Clinical trials and have achieved what they were meant to achieve in the biological context but did not reach the clinical endpoints. An example is Aducanumab, which effectively reduced beta amyloid plaques in the brains of AD patients (Sevigny et al., 2016) but its phase 3 clinical trials were prematurely interrupted because it did not have a significant effect on the symptoms of the disease when compared to placebo. The failure of several investigational drugs, at both pre-clinical and clinical levels, intensified the urge for finding new targets for the treatment of this pathology.

3.2 The 14-3-3/Tau Protein-Protein Interaction

Numerous PPIs play a role in AD. PPIs are undoubtedly popular drug targets nowadays but as seen in **Table 1**, they remain somewhat unexplored for AD. As mentioned above, Tau is involved in many PPIs that influence its behavior in the cell. The 14-3-3 family of proteins has been shown to directly interact with Tau (Hashiguchi, Sobue, & Paudel, 2000) and has even been shown to be one of the components of the NFT (Layfield et al., 1996). After these two discoveries, further work has been done in order to structurally characterize this PPI and to study its biological relevance.

3.2.1 Structural insights on the 14-3-3/Tau Protein-Protein Interaction

In 1996, 14-3-3 proteins have been identified as one of the components of the NFT, but only 4 years later, in 2000, the physical interaction between 14-3-3 and wild-type Tau (wt-Tau) was confirmed on a Glutathione S-transferase (GST) pull-down assay (Hashiguchi et al., 2000). In this study, through the detection of the intensity of the bands on the blot, the K_d of the 14-3-3/Tau PPI was estimated to be 0.9 μ M. The same study reported that the interaction was independent of phosphorylation. Nevertheless, some years later, several studies have shown that phosphorylation of Tau at specific residues (**Table 2**) increase its affinity to 14-3-3 (Milroy et al., 2015; Sadik et al., 2009; Sluchanko, Seit-Nebi, & Gusev, 2009).

Table 2 – Binding motifs of Tau reported to bind to 14-3-3 proteins.

Residue	Motif	14-3-3 binding reported
pS214	SRT pS ²¹⁴ LPTP	(Joo et al., 2015; Milroy et al., 2015; Sadik et al., 2009; Sluchanko et al., 2009)
pS324	SKCG S ³²⁴ LGNI	(Joo et al., 2015; Milroy et al., 2015; Sluchanko et al., 2009)
pS356	SKIG S ³⁵⁶ LDNI	(Sluchanko et al., 2009)

All these phospho-sites, especially the motif surrounding pS214, represent considerable similarity with the 14-3-3 binding motifs (Tugaeva, Tsvetkov, & Sluchanko, 2017). The serine residues mentioned in **Table 2** are phosphorylated by the Protein Kinase A (PKA) kinase, which is known to “prepare” targets for 14-3-3 binding since it optimally phosphorylates target proteins at (R/K)RX(S/T) sequences, which are often suitable for 14-3-3 binding (Kemp, Graves, Benjamini, & Krebs, 1977; Tugaeva et al., 2017). All the sites above have effectively been found phosphorylated in human brains. Phosphorylation of S214 and S356 have only been reported in AD brains, while phosphorylation of S324 happens in physiological conditions (Martin et al., 2013).

NMR studies on ¹⁵N-labeled full-length Tau phosphorylated by PKA (Tau-PKA) in the presence of 14-3-3 σ identified strong CSP on resonances corresponding to residues surrounding pS214 and pS324 (Joo et al., 2015). Hence, these results identified these epitopes as the key anchoring points of Tau on 14-3-3 σ . Co-crystallization of the peptides mimicking both anchoring sites with 14-3-3 σ has revealed that, in both cases, the binding occurs in the amphipathic groove of 14-3-3 (**Figure 19**). Despite the fact that only 3 residues of the pS324 epitope are resolved, it seems clear that both peptides bind in an extended way. The pS214 epitope is comparable to a mode 2 14-3-3 binding motif. Yet, P218 introduces a kink in the backbone (**Figure 19 A**), therefore making a unique binding motif (Joo et al., 2015).

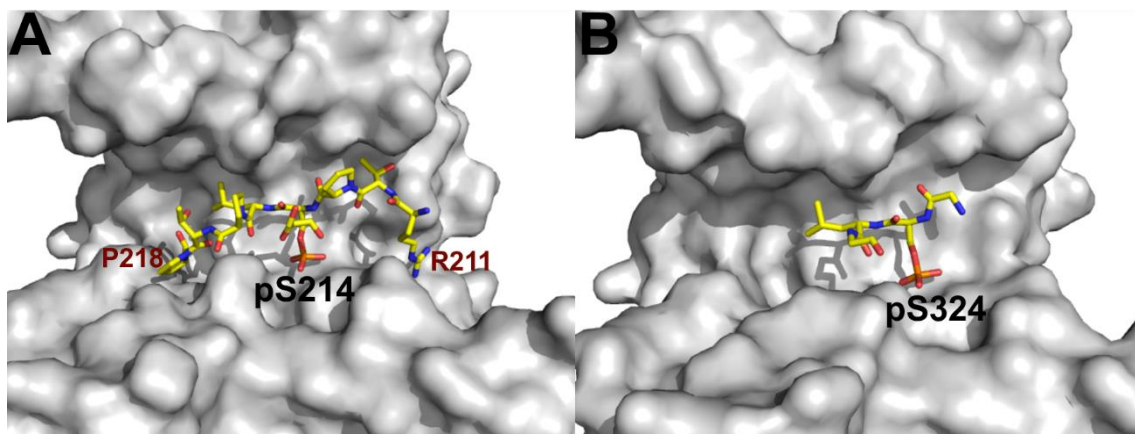


Figure 19 –Crystal structures of 14-3-3 σ (grey surface) in the presence of Tau peptides (yellow sticks). (A) Crystal structure of 14-3-3 σ in complex with a Tau peptide surrounding pS214 (residues 210-218). (B) Crystal structure of 14-3-3 σ in complex with a Tau peptide surrounding pS324 (residues 320-328).

In the same study the authors shed some light on the affinity of this PPI and on the individual contribution of each epitope. The K_d of the complex of Tau-PKA (phosphorylated on both S214 and S324) and 14-3-3 σ was $6.5 \pm 1.9 \mu\text{M}$ (determined by ^1H - ^{15}N HSQC titration). The K_d of the monophosphorylated peptides on pS214 and pS324 was $102 \pm 31 \mu\text{M}$ and $140 \pm 2.5 \mu\text{M}$, respectively (determined by Microscale thermophoresis). Moreover a diphosphorylated peptide containing both pS214 and pS324 epitopes was designed and interacted with 14-3-3 with a very similar K_d value as the full-length Tau phosphorylated by PKA ($2 \pm 0.2 \mu\text{M}$ determined by Microscale thermophoresis). The fact that the K_d value of the diphosphorylated peptide is considerably lower than the arithmetic difference of the K_d of the monophosphorylated peptides, suggests that the peptide is capable of binding to both monomers of 14-3-3, establishing a 1:2 stoichiometry. It seems therefore possible that one molecule of diphosphorylated Tau can bind to both monomers of the 14-3-3 dimer. (Joo et al., 2015). Some years before, and using cross-linked 14-3-3 ζ and Tau-PKA, Sluchanko *et al*, identified bands in gel electrophoresis of complexes with apparent MW of 80 kDa (suggesting 1:1 stoichiometry), 120 kDa (suggesting 1:2 stoichiometry) and 150 kDa (suggesting 2:2 stoichiometry (Sluchanko, Sudnitsyna, Seit-Nebi, Antson, & Gusev, 2011). They have also produced mutants of 14-3-3 ζ partially or totally incapable of assembling as a dimer and concluded that the amount of Tau bound to 14-3-3 was proportional to the dimerization capacity of 14-3-3 (Sluchanko et al., 2011). These results, despite originating from cross-linking studies and not from free biomolecules in solution, are an extra argument to the hypothesis that phosphorylated Tau can bind to both monomers of 14-3-3, with the pS214 epitope binding to one monomer and the pS324 epitope binding to the other monomer. Nevertheless, further studies are necessary to effectively prove the stoichiometry(ies) in solution for the PPI between phosphorylated Tau and 14-3-3.

Regarding the affinity of this interaction, the value obtained by Joo et al ($K_d = 6.5 \pm 1.9 \mu\text{M}$, determined by ^1H - ^{15}N HSQC titration) is not the only value reported in the literature for the 14-3-3/Tau-PKA PPI. In 2009, Sadik *et al* determined the affinity of 14-3-3 ζ for wt-Tau and PKA-phosphorylated Tau by Surface Plasmon Resonance (SPR). They obtained a K_d value of $312 \pm 102 \text{ nM}$ for 14-3-3 ζ /wt-Tau and a K_d value of $27.4 \pm 1.3 \text{ nM}$ for 14-3-3 ζ /Tau-PKA (Sadik et al., 2009). The value of the K_d calculated by Joo et al., 2015 for 14-3-3/Tau-PKA is 3 orders

of magnitude higher. There is therefore a lack of consensus in literature regarding, not only the stoichiometry, but also the affinity of this PPI.

3.2.2 Functional effects of the 14-3-3/Tau Protein-Protein Interaction

3.2.2.1 14-3-3 mediates phosphorylation of Tau

One of the most important consequences of the 14-3-3/Tau PPI is the fact that 14-3-3 enhances Tau phosphorylation. The first evidence came in 2000, when it was shown that the phosphorylation of Tau at S262 by PKA was enhanced by the presence of 14-3-3 ζ (Hashiguchi et al., 2000). As the 14-3-3 dimer can bind simultaneously a Kinase and a protein substrate, 14-3-3 can indeed, by this mechanism, enhance phosphorylation of its target proteins. This is also the case for the phosphorylation of Tau by Glycogen Synthase Kinase-3 β (GSK3 β), which was shown to be enhanced 10-fold by the presence of 14-3-3 ζ (Agarwal-Mawal et al., 2003). In addition it was shown that 14-3-3 τ mediates the phosphorylation of S214 of Tau by the Serum and Glucocorticoid-induced Protein Kinase 1 (SGK1) and that 14-3-3 ζ mediates the phosphorylation of Tau at S262 by the Neuronal Cdc2-like Protein Kinase (NCLK) (Qureshi, Han, MacDonald, & Paudel, 2013). The increase in phosphorylation of S214 and S262 of Tau by the overexpression of 14-3-3 was also verified *in vivo*, in a *Drosophila* model (Papanikolopoulou, Grammenoudi, Samiotaki, & Skoulakis, 2018).

3.2.2.2 14-3-3 impacts the aggregation of Tau

Mutations, polyanions (such as nucleic acids or heparin), post-translational modifications, proteolysis and PPIs are factors that stimulate Tau aggregation, *in vitro* and *in vivo* (Chirita, Congdon, Yin, & Kuret, 2005). 14-3-3 has been proposed in some studies to promote the aggregation of wt-Tau *in vitro*. Hernández *et al*, in 2004 found that 14-3-3 ζ promotes the aggregation of wt-Tau and that Tau phosphorylated by PKA decreases the 14-3-3 induced aggregation, without abolishing it completely (Hernández et al., 2004). It has indeed been shown that phosphorylation of S214, the strongest anchoring epitope of Tau on 14-3-3, reduced significantly Tau affinity for microtubules but, pS214 by itself, inhibited the aggregation of Tau into PHFs (Schneider, Biernat, von Bergen, Mandelkow, & Mandelkow,

1999). By monitoring the fluorescence emitted by Thioflavin S, Sadik *et al*, studied the aggregation of Tau, PKA-phosphorylated Tau, PKB-phosphorylated Tau and GSK3-phosphorylated Tau induced by 14-3-3 (**Figure 20**) (Sadik *et al.*, 2009). Two important conclusions can be taken out of this study. First, Tau only aggregated in the presence of 14-3-3 in the conditions of this assay. Then, Tau when phosphorylated by PKA or PKB was shown to be resistant to 14-3-3 induced aggregation (**Figure 20 A**), as already described by Hernandez *et al* (Hernández *et al.*, 2004). In order to confirm the influence of the phosphorylation of S214 on the protection against aggregation, a S214A mutant was tested. The results show that the S214A mutant phosphorylated by PKA was not aggregation resistant in the presence of 14-3-3 (**Figure 20 B**). The authors suggest that the phosphorylation of S214 by PKA or PKB create a strong anchoring point for Tau on 14-3-3, protecting Tau from aggregation. As it was mentioned before, the phosphorylation of Tau at S214 inhibits by itself the aggregation (Schneider *et al.*, 1999). Therefore, it might be that these results are not related to the interaction of phosphorylated Tau with 14-3-3, but to Tau itself. It should be noted that in our lab, we tried to reproduce these studies in several occasions but we never found evidence that 14-3-3 induces the aggregation of wt-Tau or Tau phosphorylated by PKA.

In another study 14-3-3 ζ was shown to promote equally the aggregation of both wt-Tau and Tau phosphorylated by a rat brain extract (Qureshi, Li, *et al.*, 2013). In this study, phosphorylation did not show a significant effect on Tau aggregation induced by 14-3-3.

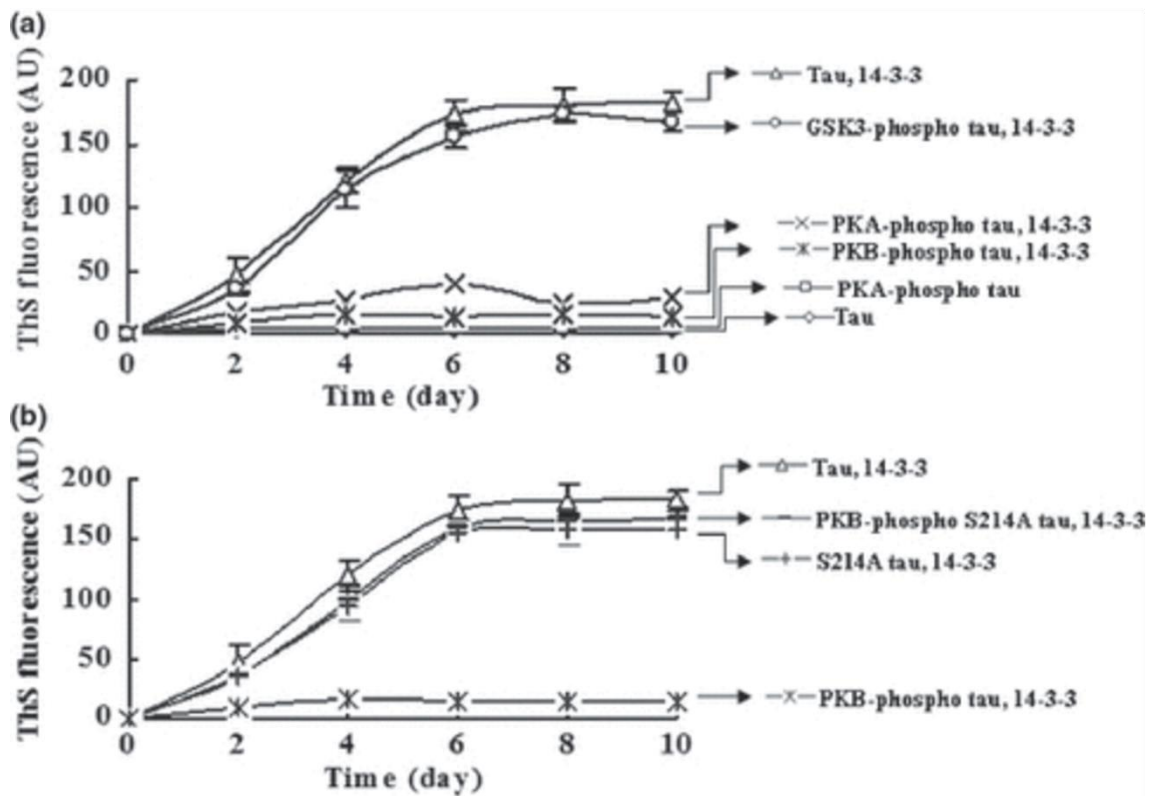


Figure 20 – Tau aggregation induced by 14-3-3 followed by ThS fluorescence. (A) Evaluation of the effect of the addition of 14-3-3 on the aggregation of Tau and evaluation of the effect of phosphorylation by GSK3, PKB and PKA on the 14-3-3 induced aggregation of Tau. (B) Evaluation of the effect of the S214A mutation on the 14-3-3 induced aggregation of Tau phosphorylated by PKB or non-phosphorylated. Figure from (Sadik et al., 2009).

More recently the aggregation of Tau induced by 14-3-3 was studied in human neuroblastoma M17 cells (Li & Paudel, 2016). In this study, phosphorylation of Tau by PKA caused its detachment from microtubules, which ultimately lead to 14-3-3 induced Tau aggregation. On the other hand wt-Tau did not aggregate in the presence of 14-3-3 because it bound to microtubules, suggesting that maybe the results presented before are not relevant in a cellular context. Nevertheless, wt-Tau aggregated when cells were exposed to colchicine, a microtubule-destabilizing drug. These results suggest that in a cellular environment, phosphorylated Tau is more susceptible to 14-3-3-induced aggregation because it is not attached to microtubules. Nevertheless, these studies do not explain how exactly 14-3-3 intervenes in the process or if there are other actors involved.

Although several research has been done to investigate the role of 14-3-3 on Tau aggregation, it is still not clear if it effectively depends on Tau phosphorylation and if it is relevant in a cellular context. The mechanisms by which it happens were never disclosed. 14-3-3 is indeed a highly acidic protein, containing several negatively charged residues and therefore it is in theory possible that these can start the aggregation process of Tau (in the same manner as heparin). Nevertheless, the fact that the interaction of wt-Tau with 14-3-3 is of very low affinity (as it will be shown on the results chapter), also raises some doubts on the specific role of 14-3-3 for promoting aggregation. The available research might indeed point to the fact that 14-3-3 can induce the aggregation of Tau but more research is needed to understand in detail how this happens in a cellular environment and how it is relevant to the global Tau pathology.

3.2.2.3 14-3-3 increases neuronal Tau mediated toxicity

Since 14-3-3 mediates Tau phosphorylation, it is no surprise that this interaction promotes Tau-related toxic effects in neuronal cells. As mentioned before it was shown that 14-3-3 ζ promoted Tau phosphorylation on S262. Further studies found that this lead to proteosomal degradation of synaptophysin in rat primary hippocampal neurons in culture (Qureshi, Han, et al., 2013). It was further shown that this effect was preceded by the destabilization of microtubules. Synaptophysin has an important role on the function of brain synapses and its degradation is pointed as an indicator of synaptic dysfunction in AD (Masliah et al., 2001; Selkoe, 2002). In a more recent study, overexpression of 14-3-3 σ was shown to disrupt the tubulin cytoskeleton and to promote Tau detachment from microtubules. As a consequence of this severe impairment of microtubule stability, neuritic growth of cells overexpressing 14-3-3 σ was reduced as well as its survival rate. In addition, it was observed that these cells have accumulated Tau (Joo et al., 2015). In a *Drosophila* model, overexpression of one of 14-3-3 isoforms (isoform Leo) induced Tau pathology, while elevation of the other isoform (isoform D14-3-3 ϵ) did not induce Tau-mediated toxicity (Papanikolopoulou et al., 2018).

3.2.3 Inhibition of the 14-3-3/Tau Protein-Protein Interaction

Considering the abovementioned evidence that 14-3-3 mediates Tau phosphorylation, induced its aggregation and promotes Tau-related cytotoxicity, one can state the reasoning that the pharmacological inhibition of this PPI can be of benefit for AD patients. The first compounds synthesized specifically for this purpose were peptidomimetic compounds based on the strongest anchor of Tau on 14-3-3, the pS214 epitope (Milroy et al., 2015). Superposition of co-crystal structures of 14-3-3 in the presence of Fusicoccin and 14-3-3 in the presence of the Tau peptide surrounding pS214 reveal that there is a superposition of P218 of Tau with the A-ring of Fusicoccin (**Figure 21 A, B**). The strategy, already explained in **Introduction-section 1.3.1**, involved the addition of bulky groups to P218 of the Tau peptide surrounding pS214 (comprising residues R211 to P218). This yielded peptidomimetic compounds occupying both the phospho-binding pocket of 14-3-3 and the Fusicoccin-binding pocket (**Figure 21 C**). The bulky aromatic moieties allowed a very important increase in affinity thanks to additional interactions with lipophilic residues of 14-3-3. From the library synthesized, the most potent compound, 201D, was shown to have a ca. 200-fold improved affinity for 14-3-3 when compared to the original epitope ($K_d = 5.9 \pm 1.0 \mu\text{M}$ vs ca. $1330 \mu\text{M}$). An NMR assay based on ^1H - ^{15}N HSQC spectra of ^{15}N labeled Tau-PKA in the presence of 14-3-3 and increasing concentrations of 201D showed that this peptidomimetic compound inhibits the PPI in a concentration dependent manner.

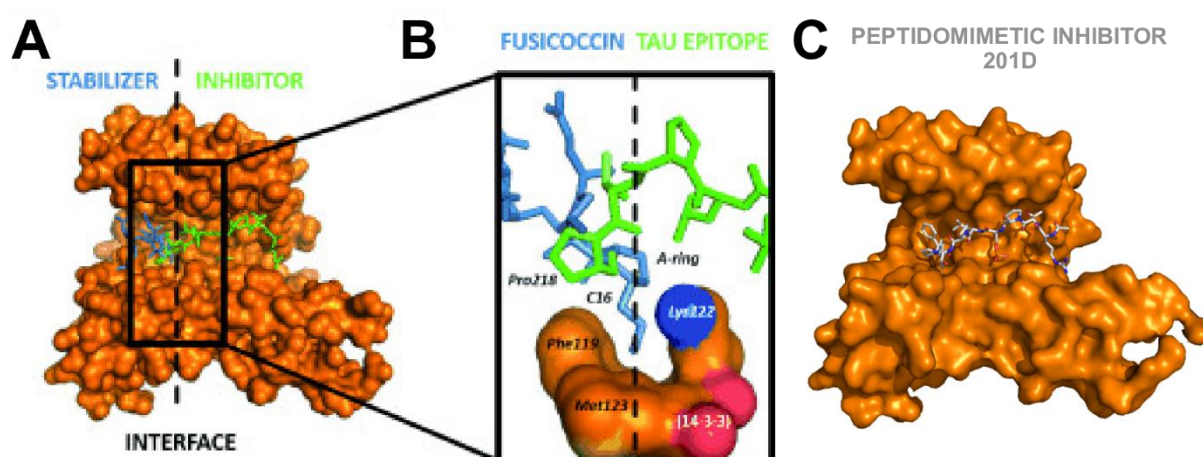


Figure 21 – Strategy for the development of the peptidomimetic inhibitor 201D. (A) Overlay of the crystal structures of 14-3-3 (orange spheres) in the presence of Fusicoccin (blue sticks) and in the presence of the Tau

epitope surrounding pS214 (green sticks). (B) Detailed view of the interface between the A-ring of Fusicoccin and P218 of the Tau peptide surrounding pS214. (C) Crystal structure of 14-3-3 σ (orange surface) in the presence of 201D (white sticks) – PDB ID: 5HF3. Panels A and B from (Milroy et al., 2015).

4 Fragment-based drug discovery

4.1 The Fragment-based approach in drug discovery: an alternative to High Throughput Screening

In the 1990s, the drug discovery community was mostly relying on the combination of High Throughput screening (HTS) and combinatorial chemistry in order to drive the quest for new drugs. Nevertheless, the community reported some pitfalls on this approach and recognized that the number of drug approvals was below the expectations. Fragment-based drug discovery (FBDD) emerged as an alternative to this approach for finding high quality hits. The central idea of FBDD is to find small ligands that perfectly fit binding pockets of the target (**Figure 22**), binding with high ligand efficiency (ligand efficiency = (pKi or pIC50) / number of heavy atoms) and allowing further optimization into a drug-like compound (Velvadapu, Farmer, & Reitz, 2015). The first and most obvious difference between HTS and FBDD is the nature of the compounds. While the set-up of an HTS library is guided by the rule of 5 (Lipinski, Lombardo, Dominy, & Feeney, 1997; Ma, Wang, Wu, & Ruan, 2016), the set-up of a fragment library is usually guided by the rule of 3 (Congreve, Carr, Murray, & Jhoti, 2003; Ma et al., 2016). The rule of 5 sets that molecules should have a MW \leq 500 Da, cLogP \leq 5 and that the number of H-bond donors and acceptors should not exceed 5 and 10, respectively (Lipinski et al., 1997) (**Figure 22**). The rule of 3 sets that fragments should have a MW \leq 300 Da, cLogP \leq 3, a polar surface area not exceeding 60 Å² and that the number of H-bond donors, acceptors and rotatable bonds should not exceed 3 (Congreve et al., 2003) (**Figure 22**). HTS employs therefore more complex molecules aiming at the identification of more mature chemical starting points. In spite of higher potency of the hits, when compared to FBDD, HTS usually yields molecules with a lower Ligand Efficiency and harder to optimize (Velvadapu et al., 2015). Another important difference between HTS and FBDD, is the size of the libraries to

screen. While in HTS up to millions of compounds can be screened with a considerable cost, in FBDD the libraries to screen typically do not contain more than 10000 compounds (Hajduk, 2006). These smaller libraries of low MW compounds enable to cover more efficiently the chemical space than libraries of higher MW compounds (Ma et al., 2016). In FBDD, as the compounds are smaller, it is more likely to find key structural motifs that are able to bind to the target's binding site. However, as they do not contain many functional groups, the number of interactions with the target is also limited and therefore these compounds bind weakly (normally in the high μM – mM range) (Dias et al., 2014) (**Figure 22**). This fact represents the biggest challenge in the Fragment Based approach (FBA) and its major disadvantage over HTS, as very sensitive biophysical techniques are required in order to detect such weak binding.

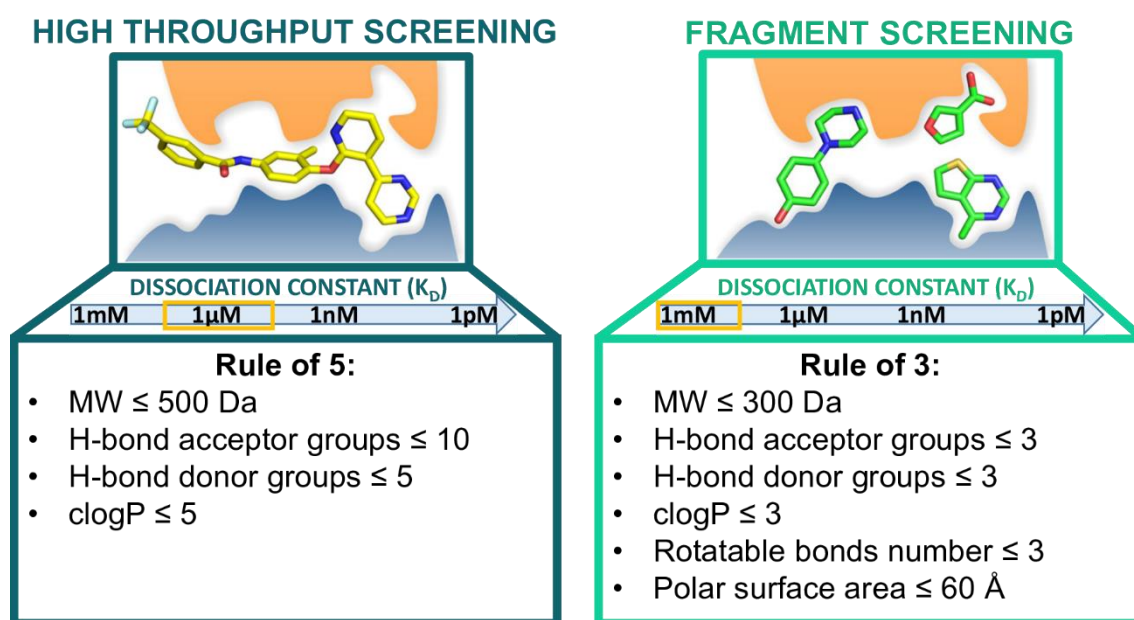


Figure 22 – Differences between High Throughput Screening and Fragment-based drug discovery. Molecules screened in HTS tend to be robust, following the rule of 5 and typical dissociation constants of the hits are within the μM - high nM range. Molecules screened on the scope of a FBDD project tend to be small and to fit a precise pocket in a target, following the rule of 3 and typical dissociation constants of the hits are within the mM – high μM range. Images of molecules and targets from (Scott, Coyne, Hudson, & Abell, 2012).

4.2 Fragment screening

Despite considerable advances on sensitivity improvement of biophysical techniques, the fragment screening continues to be one of the biggest challenges of the FBA. The selection of the techniques for the screening campaign takes always into account the balance between throughput and robustness. Due to the low affinity and low mass, the signals originated from fragment binding are usually close to the limits of sensitivity of the screening techniques. For this reason, there is usually a considerable number of false positives and therefore fragment screening campaigns rarely depend on only one screening method, but rather rely on orthogonal validation. Typically, the fragment library is screened by a medium-high throughput method for a primary screening. Ligand-based NMR, SPR, Fluorescence-based techniques or Differential Scanning Fluorimetry (DSF) are the most popular methods for primary screening (Ciulli, 2013; Velvadapu et al., 2015). Typically during the primary screening, fragments are not screened individually. Instead they are combined in cocktails, usually containing from 5 to 15 fragments. For the assembly of the cocktails, care needs to be taken to not mix chemical motifs able to react in the same cocktail (for example aldehydes and primary amines) (Stark, Eghbalnia, Lee, Westler, & Markley, 2016). Moreover, the number and nature of the compounds in each cocktail should be optimized according to the screening methods that will be employed. The fragments selected by this procedure are typically confirmed by another method on a secondary screening. Often the secondary screening is performed by Protein-based NMR or X-ray crystallography, which provide information regarding the binding site (Ciulli, 2013). This information is essential for elaborating the fragment into a more potent molecule. In the next sections, fragment screening methods will be reviewed, with special emphasis on NMR methods.

4.2.1 NMR methods for fragment screening

NMR is especially suitable to detect weak and very weak interactions (μM – mM range) (Williamson, 2013), which is a major reason for its employment in the FBA. In addition, NMR has also some additional advantages compared to other techniques. NMR allows, for example, the pre-screening of the compound library for purity or aggregation between compounds

(Begley, Moen, Pierce, & Zartler, 2013). It is also possible to detect modifications on the target protein such as degradation, impurity, unfolding or aggregation, which can significantly affect the screening. The application of NMR in drug discovery can be roughly divided into Protein based methods (PBM) and Ligand based methods (LBM) (Howard, Abell, & Royal Society of Chemistry (Great Britain), 2015; Ma et al., 2016).

4.2.1.1 Ligand-based NMR for fragment screening

A free fragment in solution has an apparent MW of around 300 Da, while a fragment bound to a protein acquires, in solution, the apparent MW of the target protein. This important difference in apparent MW is also translated into an important difference in relaxation properties. While a free ligand tumbles quickly in solution, a fragment bound to the protein tumbles slowly and therefore it acquires the relaxation properties of the protein. Most of the Ligand-based methods rely on the detection of this binding-induced relaxation of the ligand to screen a library of fragments (Gossert & Jahnke, 2016).

When compared to PBM, LBM have two very important advantages in nowadays drug discovery setting: they are cheaper and faster to apply. PBM require isotopic labeling of the target protein and assay concentrations in the range of 50 μM – 100 μM of protein. LBM require considerably less concentrated protein (as low as 100 nM) and most importantly do not require isotopic labelling (World Intellectual Property Organization Patent No. WO2003104824A2, 2003). In LBM, depending on the experiment, a pool of ligands can be screened in a few minutes, while in PBM, the need for the acquisition of 2D experiments makes it impossible to screen a pool of ligands in less than a couple of hours. Another advantage of LBM is that it is unlimited by the size of the target protein. In the case of screening of cocktails, LBM also allows, in a straightforward way, the determination of the fragment of the cocktail that is binding the target. This identification is not possible in a PBM.

Nevertheless LBM have some important disadvantages. The first and most obvious is the fact that they do not allow the detection of the binding site of the ligand. The second is that the detection of the ligand depends on the kinetics of the binding. In fact, in order to be detected by a LBM, the off-rate should be fast or intermediate regarding the relaxation time-scale (Unione, Galante, Díaz, Cañada, & Jiménez-Barbero, 2014). Given this kinetic constraints,

these methods are therefore suitable to detect mostly molecules that bind with low or moderate affinity, which is the reason behind its application on Fragment screening. Molecules that dissociate slowly from the receptor (in slow exchange considering the NMR time-scale), which are typically potent binders, are therefore not detected by LBM. This is also the case for irreversible covalent binders. Another disadvantage of LBM is the fact that the results can be affected by compound aggregation. An aggregated compound may have an apparent MW and relaxation properties of a protein and can therefore originate false positives (Dalvit, Caronni, Mongelli, Veronesi, & Vulpetti, 2006; LaPlante et al., 2013). For this reason, it is a good practice to perform, for each fragment/cocktail, a control experiment in the absence of the protein.

Overall, LBM are easy to implement, sensitive and are characterized by a favorable cost/throughput balance. Nevertheless, they do not allow the detection of the binding site and they are also subjected to a higher rate of both false positives and false negatives than PBM (Barile & Pellecchia, 2014; Harner, Frank, & Fesik, 2013). For this reason, they are very frequently employed as a primary screening or orthogonal confirmation technique and the binders are usually confirmed by a more robust technique such as a PBM or X-ray crystallography.

4.2.1.1.1 *Saturation Transfer Difference (STD)*

According to a survey conducted by the “Practical Fragments” blog, Ligand-based NMR was, in 2016, the most frequently used technique for fragment screening and Saturation Transfer Difference (STD) was the most used NMR method for this purpose (Erlanson, 2016). For screening a compound/cocktail by STD, two ^1H spectra are recorded for the same sample: an off-resonance spectrum where there is no saturation of signal of any species in solution (**Figure 23 A**) and an on-resonance spectrum, where there is selective saturation of the protein’s signals (**Figure 23 B**). The spectra routinely called STD spectra are in fact, a difference between the off-resonance spectrum and the on-resonance spectrum (**Figure 23 C**) (Mayer & Meyer, 1999). Saturation of the protein’s signals can be achieved by a selective radiation targeting the methyl protons of the protein (between -1 ppm and 1 ppm). After the selective radiation, saturation will be transmitted to all the protons of the protein by spin diffusion. The

key event in the STD experiment is that, thanks to the NOE effect, this saturation also spreads to the protons of the ligands that interact with the molecule. The consequence of this transfer of saturation is the attenuation of the intensity of the signals (Viegas, Manso, Nobrega, & Cabrita, 2011). Therefore, if a compound does not interact with the target (**Figure 23, blue compound**), there is no saturation transfer during the on-resonance spectrum and therefore the intensities of the NMR signals are unaffected. In this case, no signal of this compound is seen in the difference spectrum. If a compound interacts, the intensity of its ^1H resonances will drop because of the transfer of saturation and therefore, a difference will exist on the difference spectrum, observed as signals (**Figure 23, red compound**). This principle is therefore used to distinguish which molecules from a pool of compounds bind the protein (Krishnan, 2005). Regarding sample preparation, STD requires little protein consumption (as little as 100 nM concentration) and requires a ratio of Ligand/Protein ranging from 10:1 up to 100:1, depending on the system and on the mass of the protein. The sensitivity of the experiment is also increased when the sample is prepared in 100% D_2O , since that there are no sensitivity losses due to spin diffusion between the biomolecule protons and bulk water protons (Mayer & James, 2002)

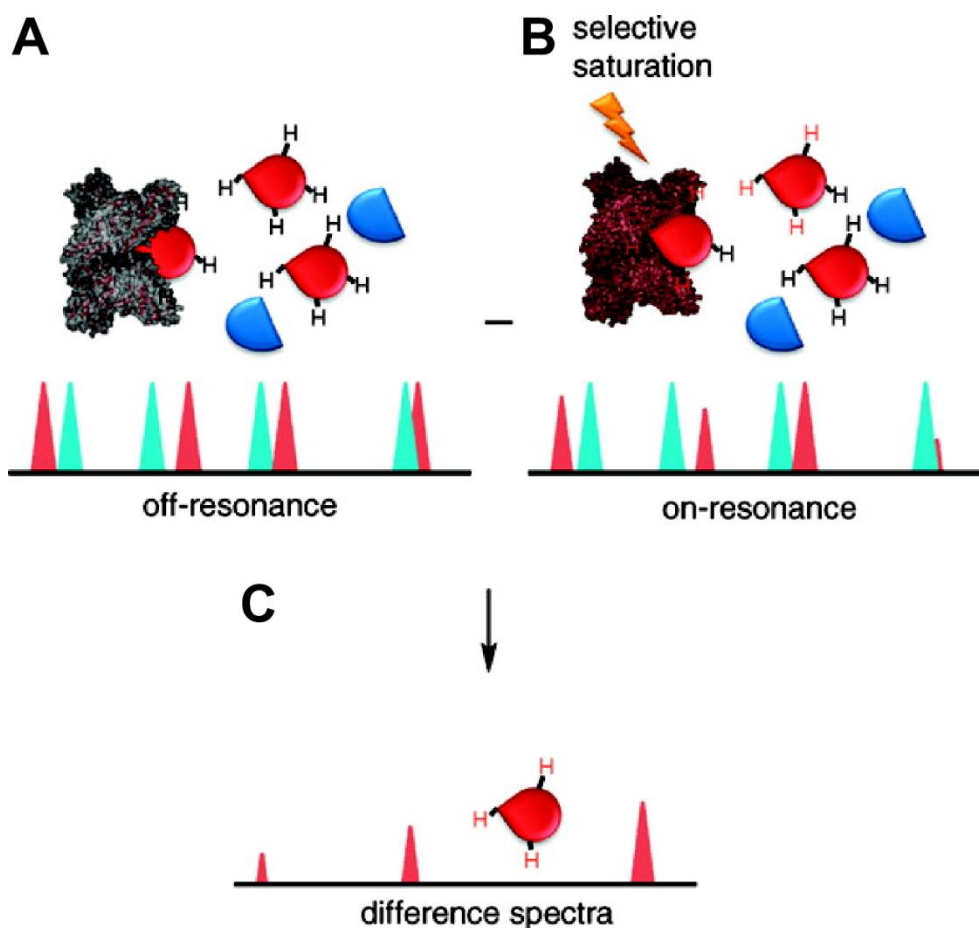


Figure 23 – Scheme of the STD experiment. (A) Two ligands, blue and red, are screened for binding to the protein. An off-resonance spectrum is recorded without selective saturation of the protein's signals. (B) An on-resonance spectrum is recorded. Note that the intensity of the ^1H signals of the red compound (which interacts with the protein) drops and that the ^1H signals of the blue compound (which does not interact with the protein) are unaffected. (C) The two spectra are subtracted and in the difference spectrum only the signals of the interacting compound are observed. Adapted from (Viegas et al., 2011).

Fragment screening is by far, the most common application of STD but this experiment can also be used to study the binding mode of the ligand (Cala & Krimm, 2015). As seen in **Figure 23**, not all the ^1H signals of the compound are affected equally by the saturation transfer. Those which are more buried in the binding cavities are more affected than the protons which are more solvent exposed and therefore will be less intense in the on-resonance spectrum and more intense in the difference spectrum (**Figure 23 B, C**). This principle, called “Group Epitope Mapping” can be used in order to study the orientation of a ligand upon binding to the receptor (Mayer & Meyer, 2001). This information is very useful to

drive molecular docking and can be used to compare the binding modes of similar compounds (Stark & Powers, 2011). Unquestionably, this is only possible if the intensities of the STD signals of the same type of protons are compared (protons from aromatic rings for example). Another application of STD, is the determination of dissociation constants (Angulo, Enríquez-Navas, & Nieto, 2010). Nevertheless this method is not one of the most suitable ones for this application (Fielding, 2007).

4.2.1.1.2 *Water-Ligand Observed via Gradient Spectroscopy (WaterLOGSY)*

Proposed by Dalvit and collaborators (Dalvit, Fogliatto, Stewart, & Veronesi, 2001) just a few years after the development of STD, WaterLOGSY, is one of the most important ligand-based methods. In a practical way, one can visually identify the hits among a mixture of compounds since the NMR signals of hits are positive whereas those of non-binding molecules are negative (**Figure 24**). Similarly to the STD experiment, an off-resonance and an on-resonance spectra are recorded. The uniqueness of this experiment is that it is based on the ePHOGSY-NOE principle and therefore the selective on-resonance irradiation is applied at 4.7 ppm, which corresponds to the water signal (Dalvit et al., 2001; Ludwig et al., 2008). After this selective irradiation, magnetization is transferred to the other components of the solution during the mixing time, which is typically 0.8-1.2 seconds (Gossert & Jahnke, 2016). The magnetization is transferred to the protein by two main pathways: through the water molecules present in the protein's cavities and through hydrogen exchange with the labile protons of the amino acid residues. Spin diffusion, similarly to what happens in STD is responsible for the transfer of the magnetization through the protein. If it is the case that there is a hit among the compounds tested, then the magnetization is transferred from the protein to the ligand via the water molecules located at the cavities of the binding site. It is true that magnetization is also transferred to the compounds that do not bind the protein, but it can be easily distinguished in the WaterLOGSY spectrum, since the NMR signals of binders and non-binders have opposite phases (World Intellectual Property Organization Patent No. WO2003104824A2, 2003; Dalvit et al., 2001). The explanation of how this happens relies on one of the golden rules of biomolecular NMR. Small molecules have small correlation times and positive NOEs, while large MW molecules like proteins have long correlation times and

negative NOEs (Becker, Bhattiprolu, Gubensäk, & Zangger, 2018). When a ligand is bound to a protein, it acquires the apparent MW of the protein-ligand complex, therefore experiencing negative NOEs. On the other hand, for free molecules in solution, the NOE is positive. This reveals why the phase of NMR signals of hits and non-hits is different. For convenience, in most cases, the WaterLOGSY spectra are phased so that the NMR signals of the ligands are positive and those of non-ligands are negative.

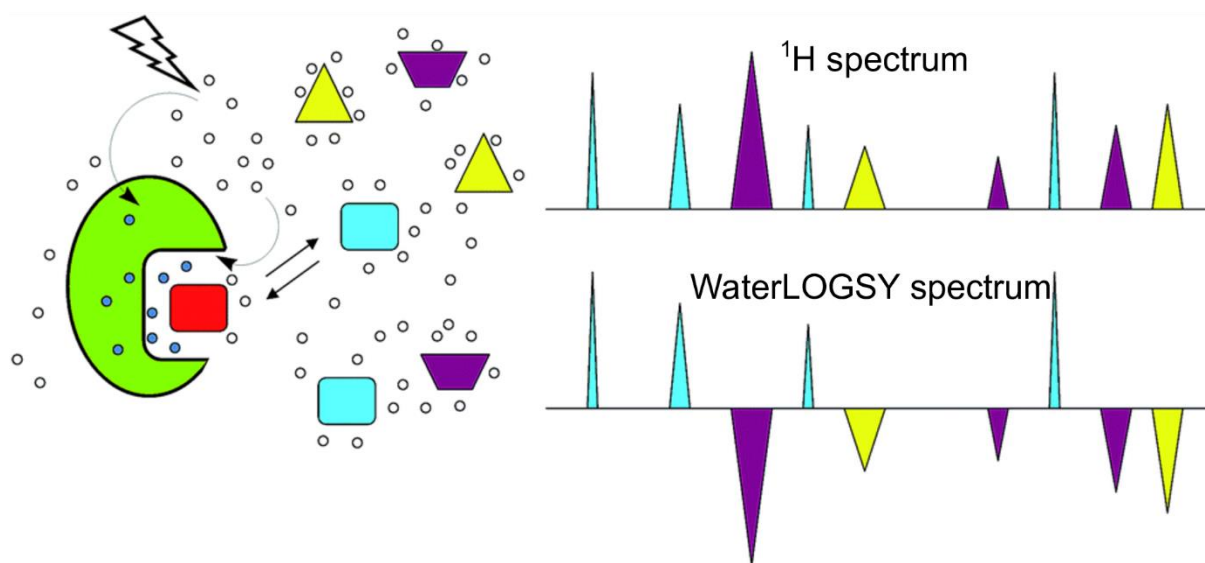


Figure 24 –Schematic representation of the WaterLOGSY experiment. Water is saturated by a selective pulse and the magnetization is transferred to all the molecules in solution. In the case of the non-binders (yellow and purple molecules), the magnetization is transferred directly. In the case of the binder (blue), the magnetization is transferred from the water to the protein and from the protein to the ligand. In the ^1H spectrum of this mixture all the signals are phased positive (spectrum above). In the WaterLOGSY spectrum, the signals of the binder are phased positive, while the signals of non-binders are phased negative. Adapted from (Unione et al., 2014).

As a ligand-based method, WaterLOGSY does not require high concentrations of protein since concentrations as little as 100 nM can be used. Similarly to STD, the ratio between ligand and protein is usually in the range of 10:1 to 100:1 (Gossert & Jahnke, 2016). In addition to the convenience of not requiring large amounts of protein and of being possible to screen a cocktail in just a few minutes, this technique is extremely sensitive to binding since even compounds that only bind transiently are detected. In a comparative study against STD, WaterLOGSY was shown to be more time-efficient and sensitive (Antanasijevic, Ramirez, &

Caffrey, 2014). Another important advantage of WaterLOGSY over STD is the fact that the first, contrarily to the second does not rely only on spin diffusion for the transfer of magnetization along the target. This enables WaterLOGSY to be used in targets with low density of protons, such as RNA (Meyer & Peters, 2003).

Despite its many advantages, WaterLOGSY also has its pitfalls, which demand particular attention and the necessary control experiments. First, and similarly to STD, aggregation of compounds is a very important issue, leading to false positives (Dalvit et al., 2006). Another important aspect to keep in mind is that the presence of labile protons in the ligands will generate strong positive signals. In order to overcome these two limitations of this method, a negative control experiment with the free ligands is necessary. The other limitation of WaterLOGSY, shared with other ligand-based methods as STD and T1 relaxation, is the fact that it is not suitable to detect the binding of molecules that bind the target with a high affinity (K_d in the nM range). This limitation comes from the fact that in order to be detected, a bound ligand needs to have fast dissociation and take into the “free state” the magnetization transmitted via the protein complex during the mixing time. In a more objective way, the T1 relaxation time of the ligand needs to be greater than the dissociation rate constant (K_{off}) (Gossert & Jahnke, 2016). The WaterLOGSY signal is a sum of the negative signal from the free ligand and the positive signal from the bound-ligand. It may happen, for hit molecules binding with very low affinity, that there is no inversion of the 1H signal when a WaterLOGSY spectrum is recorded. In this case what happens is that the signal disappears or remains negative but less intense than it would be if the WaterLOGSY spectrum would have been recorded in the absence of the protein (Lepre, Moore, & Peng, 2004). This can also happen for very hydrophobic pockets, in which there is poor contact with hyperpolarized water stuck at the cavities of the protein’s surface (Seifert & Wieland, 2005). This is another reason why it is imperative to record a control WaterLOGSY spectrum in the absence of the protein.

Although the simple detection of hits from a fragment pool is the most common application from WaterLOGSY, other useful data can be obtained from this technique. One other application is the determination of the binding orientation of ligands through the SALMON method (Solvent Accessibility, Ligand binding, and Mapping of ligand Orientation by NMR spectroscopy) (Ludwig et al., 2008). The authors that developed this concept in 2008,

were able to obtain, from WaterLOGSY spectra, information that allowed to determine the binding orientation of the ligand CB1954 to Quinone oxidoreductase 2. The principle is that signals corresponding to protons that are buried in the protein surface will show up in the WaterLOGSY spectrum as positive peaks, whose intensity is similar to the intensity of the same peak in the 1D spectrum. Protons that are more exposed to the bulk water and less buried in the protein surface will show a positive signal whose intensity is lower than the signal on the original 1D spectrum or even a negative peak but less intense than the correspondent one in the WaterLOGSY spectrum of the compound alone (Ludwig et al., 2008). By applying this principle, the authors were able to disclose the binding orientation of the small molecule, which was unclear on the X-ray data.

4.2.1.1.3 Other techniques

Although STD and WaterLOGSY are, by far, the most widely applied LBM, there are many others that may be applied. Carr–Purcell–Meiboom–Gill (CPMG) experiments are based on the fast T_2 relaxation times of proteins relative to ligands. When a ligand binds a protein, its relaxation time will decrease, which will result in line broadening and in intensity drop of its NMR signals (C. Wang, Grey, & Palmer, 2001). Although it is also applied to fragments, CPMG is more suitable for compounds with binding processes in the intermediate and slow exchange regimes, and therefore, in general, more potent compounds. Techniques based on ^{19}F NMR are also frequently employed for fragment screening due to the high sensitivity of ^{19}F resonances to binding events (Dalvit & Vulpetti, 2019). Fluorine chemical shift anisotropy and exchange for screening (FAXS) is one of the most famous methods in ^{19}F NMR in which there is the screening of compounds containing a ^{19}F atom. Binding is identified by the broadening of the ^{19}F signal. This experiment can also be conducted in a competition format, where the molecules to screen (containing ^{19}F or not) compete with a spy-molecule containing a ^{19}F atom (Dalvit, Fagerness, Hadden, Sarver, & Stockman, 2003). For poorly expressed or very expensive targets, the TINS methodology (Target Immobilized NMR screening) can be applied. This methodology allows to recycle the receptor for screening multiple compounds (Vanwetswinkel et al., 2005). The incorporation of paramagnetic moieties containing unpaired

electrons on protein residues can also be applied to fragment screening. This method, developed in 2001 is named SPLASTIC (Spin labels attached to protein side chains as a tool to identify interacting compounds) (Jahnke, Rüdiger, & Zurini, 2001). NOESY experiments can also be employed in Fragment screening since the binding of a fragment to a protein can also be monitored by changes in the 2D NOESY spectrum. The NOE peaks detected in these methods can be between a ligand and the protein or even inter-ligand NOEs, if two ligands bind to the same site (Aguirre, Cala, & Krimm, 2015; Megy et al., 2006).

4.2.1.2 Protein-based NMR for fragment screening

Despite more expensive and time-consuming, protein-based methods are more robust and provide information on the binding site. Protein-based NMR methods rely almost exclusively on ^1H - ^{15}N HSQC or ^1H - ^{13}C HSQC. Less often, ligand binding can be detected by CSP in the aliphatic region of a simple ^1H spectrum of the protein in the presence of the ligand (Barile & Pellecchia, 2014; Rega et al., 2011).

4.2.1.2.1 ^1H - ^{15}N HSQC

The ^1H - ^{15}N HSQC is by far the most widely used experiment for protein-based fragment screening. For detecting a protein-ligand interaction, the backbone chemical shifts assignment is not mandatory. However, the binding site of the fragment, which is the most interesting information of fragment screening by ^1H - ^{15}N HSQC, can only be achieved if the protein is assigned. The principle used for detecting the binding of a fragment is the same as the one used for detecting the binding site of another molecule, which was already explained in **Introduction - section 2.1.4.1**. Due to the high cost and the consumption of high amounts of isotopically enriched protein, the ^1H - ^{15}N HSQC is mostly applied as a secondary screening technique (Harner et al., 2013). However, there are examples in the literature in which primary screening campaigns were performed by ^1H - ^{15}N HSQC. One of these, was the one performed by Abbot (Petros et al., 2006) that led to the discovery of the approved drug venetoclax (Valenti, Hristeva, Tzalis, & Ottmann, 2019).

The ^1H - ^{15}N HSQC can also be used for starting the fragment elaboration process. In this context, after identifying a first hit and identifying its binding site, another screening can be performed in order to find a second fragment, binding adjacently to the first one. The two fragments can then be linked in order to obtain a more potent molecule (**Figure 25**). This principle of fragment elaboration by linking fragments using NMR data was named as “SAR by NMR” (Shuker, Hajduk, Meadows, & Fesik, 1996). Ideally this process is assisted by more detailed structural information either by NMR-guided docking, X-ray crystallography or NMR structure determination (Hajduk, Meadows, & Fesik, 1997).

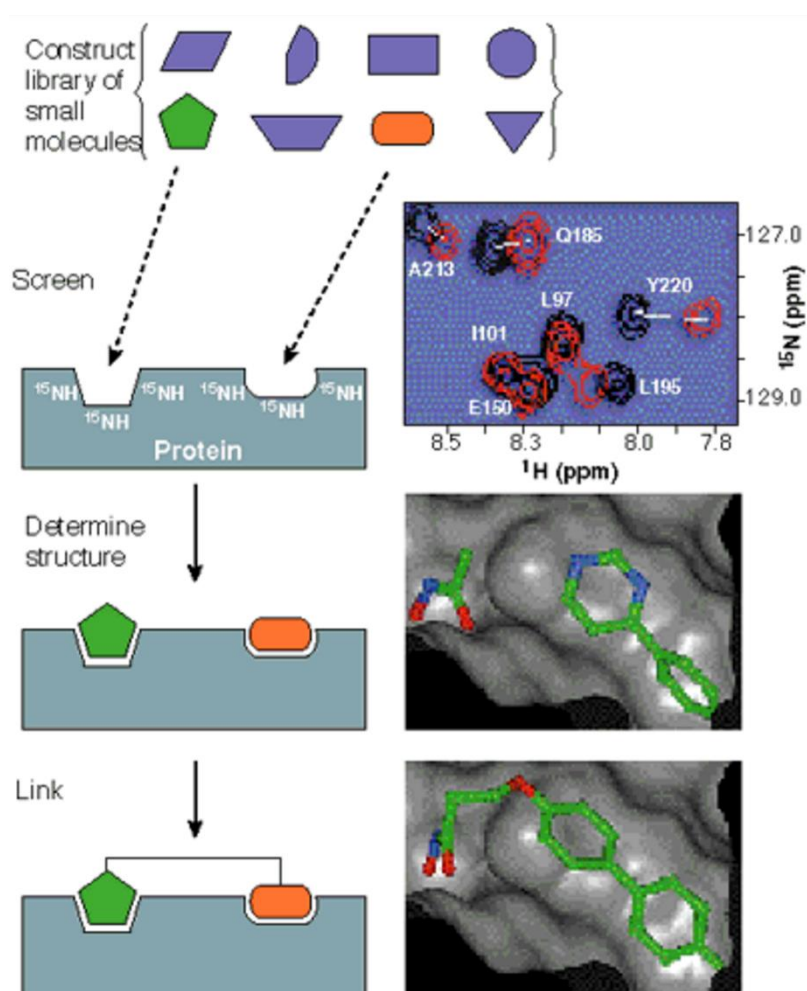


Figure 25 – The “SAR by NMR” process. From the screening of a library of compounds, two fragments are identified by NMR and shown to bind to pockets in spatial proximity. The structure of the protein in the presence of both compounds is resolved which provides information for planning the design of the linker. The two fragments are then linked, yielding a potent compound. Figure from (Hajduk et al., 1997).

4.2.1.2.2 ^1H - ^{13}C HSQC

Due to the fact that ^1H - ^{13}C resonances cannot be assigned sequentially by 3D NMR experiments, fragment screening on ^1H - ^{13}C labeled proteins is far less applied when compared to PBM based on ^1H - ^{15}N labeled proteins. Still, sometimes there are a few advantages on the detection of ^1H - ^{13}C resonances that justify its application in certain screening campaigns (Huth et al., 2007). Methyl groups are often found on hydrophobic cavities and interaction surfaces. Additionally methyl groups are much more resistant to pH variations than amide groups, which is an important advantage for fragment screening since the CSP caused by pH variations are an important source of false positives in ^1H - ^{15}N HSQC based screening campaigns. The other advantage is the fact that ^1H - ^{13}C resonances are more influenced by direct binding and less by structural changes when compared to ^1H - ^{15}N resonances, leading to, in certain cases, a better identification of the binding site (Williamson, 2013). Observing the ^1H - ^{13}C resonances can also be used for screening of compounds targeting very high MW proteins for which the ^1H - ^{15}N HSQC spectrum is crowded and has poor S/N ratio. In this case a deuterated protein containing ^{13}C - ^1H labeled methyl groups should be used (Hajduk et al., 2000). Nevertheless, CSPs are less pronounced in ^1H - ^{13}C resonances than for the amide ^1H - ^{15}N resonances which can be problematic for the detection of the binding of low affinity compounds (Williamson, 2013).

4.2.2 Differential Scanning Fluorimetry (DSF) for Fragment Screening

DSF is based on the ability of a compound to induce a shift in the melting temperature (T_m) of the protein. T_m is defined as the temperature in which 50% of the protein is denatured (Gorania, Seker, & Haris, 2010). In DSF, the solution containing the protein and the fragment/cocktail is progressively heated and the temperature at which 50% of the protein is denatured is monitored. The most common way to follow the protein's denaturation is to use fluorescent dyes that bind preferably to the denatured state, as SYPRO Orange. Upon denaturation, the hydrophobic residues of the protein become surface exposed and are available to interact with SYPRO Orange (Ciulli, 2013). Upon binding to a hydrophobic surface, the fluorescent signal is emitted and can be monitored in real-time. In practice what happens is that for temperature values close to the T_m , the fluorescence increases yielding a melting

curve with a sigmoidal form (**Figure 26 A**). The inflexion point of the sigmoidal curve corresponds to the T_m and can be calculated by plotting the first derivative of this curve against the temperature (**Figure 26 B**). The minimum value of the first derivative corresponds to the T_m (Bai, Roder, Dickson, & Karanicolas, 2019).

The major advantages of DSF are the low consumption of material (can be performed with protein concentrations as low as 0.5 μM) and the relatively high throughput since the mixtures can be prepared in 96 or even in 384-well plates and read simultaneously (Kranz & Schalk-Hihi, 2011). The assay is mainly limited by compound solubility and the main artifacts arise due to high concentrations of ligands or irreversible protein aggregation (Cimpmperman et al., 2008).

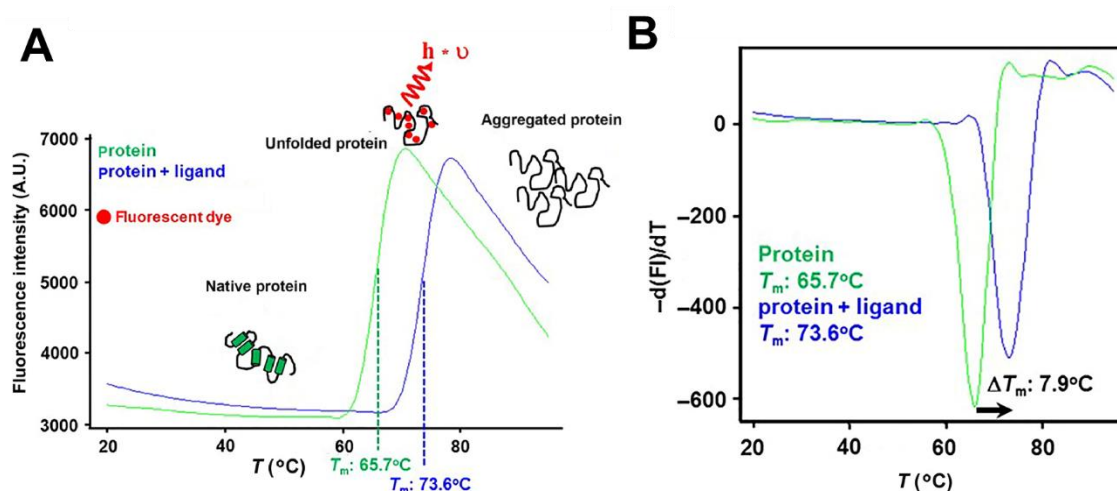


Figure 26 – Principle of DSF. (A) The melting curve of a protein is presented in green as the variation of fluorescence intensity (y axis) with the temperature ($^\circ\text{C}$) (x axis). The melting curve of the same protein in the presence of a ligand is presented in blue. Note that the compound induces a Thermal shift since T_m increases from 65.7°C to 73.8 °C. (B) First derivatives of the melting curves presented in (A). Adapted from (Bergsdorf & Wright, 2018).

4.2.3 Surface Plasmon Resonance (SPR) for Fragment Screening

SPR became, since the 1990's, one of the most important techniques for characterizing protein-ligand interactions and protein-protein interactions. SPR allows not only the detection of binding but also the determination of the dissociation constant and of the kinetic

parameters (K_{off} and K_{on}) of an interaction. SPR also allows one to obtain insight on the thermodynamics of the interaction.

The principle behind SPR is the measure of the change in refractive index at the surface interface produced by a molecular interaction. For most applications, a protein is immobilized, covalently or not, onto a biosensor surface. The ligand, which can be a fragment, a small molecule or even a biomolecule is injected into the biosensor and allowed to flow past on it. The binding is detected by an increase in the mass, which is followed in real time by the increase in the Response Units (RUs) (Ciulli, 2013). When the target is covalently immobilized, the molecule of interest can be flown and the chip can be recycled after washing the ligand. When the choice for immobilization is a non-covalent immobilization, then the protein must be immobilized at the beginning of each cycle and the SPR chip should be regenerated before the next cycle. For non-covalent immobilization, the protein can be immobilized through the use of affinity tags (i.e his-tag) (Fischer, Leech, & Hubbard, 2011; Nieba et al., 1997) or through the use of a capturing molecule (i.e. switchavidin) (Zauner et al., 2016). The amount of protein, the amount of injected molecule, the time of injection, the speed of injection and the regeneration step should be carefully optimized in order to achieve reproducible sensorgrams and allow the precise determination of the binding parameters (Navratilova & Hopkins, 2010).

In a typical sensorgram (**Figure 27**), the association phase is observed when the injection of the ligand starts, reaching eventually a *plateau* when the system is at equilibrium. When the injection of ligand stops, the molecules start to dissociate and the number of RUs starts to decrease (Ciulli, 2013). When using a covalently immobilized target, one must wait for the complete dissociation of the ligand. When using a non-covalently immobilized target, there is no need to wait for the total dissociation, since the surface is regenerated and the protein immobilized again for the next cycle. The rate at which the association happens is influenced by the K_{on} and the rate at which the dissociation happens is influenced by the K_{off} . The concentration of ligand to inject in order to achieve the maximum response is influenced by the amount of immobilized protein and by the K_d . For the calculation of the K_d , the simple determination of the K_{on} and K_{off} with a single injection of ligand would in theory be enough. Nevertheless, for a more precise determination, increasing concentrations of the ligand are

injected and the maximum values of RU obtained (R_{max}) are plotted against the concentration of ligand in order to derive a K_d value (Navratilova & Hopkins, 2010).

In fragment screening, SPR can be used both as a primary screening technique and as a characterization technique in order to determine the affinity of fragments already identified by another technique (Velvadapu et al., 2015). One good advantage of this technique is the fact that it requires a low amount of protein to be immobilized (25-50 μ g) that, if it is covalently immobilized, can even be reused to screen an entire library (Navratilova & Hopkins, 2010). Another advantage is that it is relatively fast and straightforward to implement the screening assay.

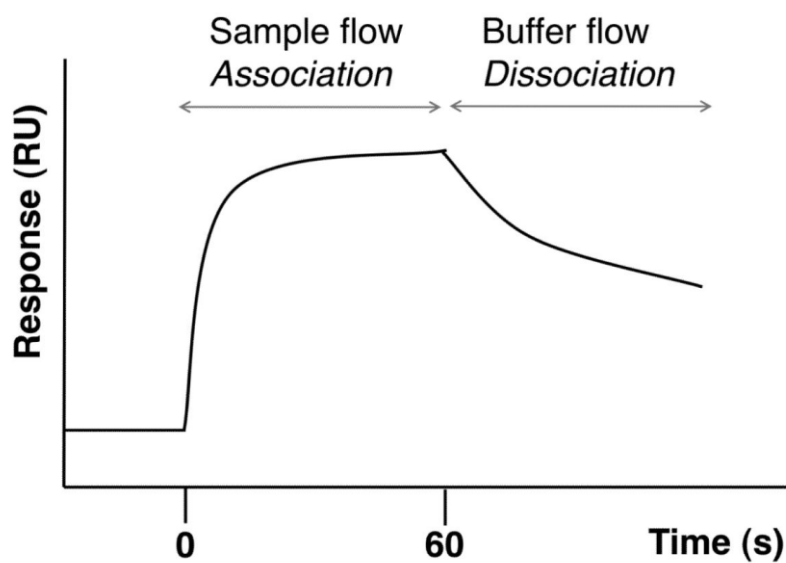


Figure 27 – Representation of a typical SPR sensorgram. The sensorgram starts at $t=0$ s from a stable baseline and with a protein previously immobilized in the SPR chip. At $t=0$ s, the binding partner is injected and allowed to flow over the SPR chip surface. As soon as the partner is injected, the association is observed by an increase in the RUs because more material is accumulated in the surface. The amplitude of the increase in the RUs depends on the mass of the molecule that is injected. The rate at which the association happens depends on the K_{on} of the reaction. Once the system reaches equilibrium, a signal plateau is achieved and is maintained until the injection of the ligand stops. Once the injection of ligand stops at $t=60$ s, the dissociation starts to happen and is translated by a decrease in the RUs. The rate at which the dissociation takes place depends on the K_{off} of the reaction. The SPR chip should be regenerated after this cycle. From (Ciulli, 2013).

OBJECTIVES

This research work is integrated in the Targeted Small-molecule Stabilization of Protein-Protein Interactions (TASPPI) European Training Network. The TASPPI consortium employs 13 PhD students integrated in 6 universities and 5 industrial partners around Europe. The primary goal of the TASPPI project is to find small-molecule selective stabilizers of 14-3-3 protein-protein interactions by making use of collaborations between the labs integrated in the consortium. Other goals of the TASPPI project included the study of 14-3-3 PPIs, the development of screening assays specific for finding small-molecule modulators of 14-3-3 PPIs and the development of inhibitors of 14-3-3 PPIs. Our work in this consortium was linked to all these objectives and was mainly divided in four milestones.

First, we had the objective of assigning the backbone chemical shifts of 14-3-3 σ . This task was considered as a key milestone for the TASPPI project since the assignment allows to get residue-specific information for studying the interaction of 14-3-3 with its partners or small molecules.

The second milestone was to get further insights on the 14-3-3/Tau PPI from a structural point of view. This interaction had already been characterized in some studies published in the last two decades but many questions were still to be answered. In order to achieve this goal, the NMR experiments performed in Lille and the analytical ultracentrifugation and SPR experiments performed during the secondments at the Charles University and AstraZeneca were essential.

The third milestone was the development of NMR assays for the screening of small-molecules/fragments intended to bind 14-3-3 or to modulate specific 14-3-3 PPIs. In this sense, we developed both ligand-based (WaterLOGSY, STD and ^1H NMR) and protein-based NMR assays (^1H - ^{15}N HSQC) directed to 14-3-3 or 14-3-3 PPIs. We have then applied our methods to screen a fragment library against 14-3-3 and to screen compounds received from collaborators against a variety of 14-3-3/peptide complexes.

The fourth milestone was to integrate the expertise and the methodologies developed on the scope of the first three milestones at the service of the TASPPI consortium in order to assist on the study of 14-3-3 PPIs and on the quest for small-molecule modulators of 14-3-3 PPIs. In this regard, 8 research collaborations were established. From these, 1 collaboration was set in order to get further insights on a 14-3-3 PPI (the 14-3-3/p53 PPI), while the others

were devoted to screen or characterize small molecules/fragments intended to target 14-3-3 or a particular 14-3-3 PPI.

RESULTS

1 Backbone chemical shift assignments of human 14-3-3 σ

The work developed on this topic is summarized in a manuscript that is currently published:

Neves, J. F., Landrieu, I., Merzougui, H., Boll, E., Hanouille, X., & Cantrelle, F.-X. (2019). Backbone chemical shift assignments of human 14-3-3 σ . *Biomolecular NMR Assignments*, 13(1), 103–107. <https://doi.org/10.1007/s12104-018-9860-1>.

The manuscript is presented ahead. To respect copyright constraints, the manuscript is presented as it was originally submitted to the journal and before the minor modifications performed upon peer-review.

Backbone chemical shift assignments of human 14-3-3 σ

João Filipe Neves¹, Isabelle Landrieu^{1*}, Hamida Merzougui¹, Emmanuelle Boll¹, Xavier Hanouille¹, François-Xavier Cantrelle¹

¹UMR 8576 CNRS-Lille University, 59000 Lille, France

ORCID ID for authors:

JFN: 0000-0003-0582-1193

IL: 0000-0002-4883-2637

XH: 0000-0002-3755-2680

*Corresponding author: Isabelle Landrieu, isabelle.landrieu@univ-lille1.fr

+33 (0)3 62 53 17 02

Abstract

14-3-3 proteins are a group of seven dimeric adapter proteins that exert their biological function by interacting with hundreds of phosphorylated proteins, thus influencing their sub-cellular localization, activity or stability in the cell. Due to this remarkable interaction network, 14-3-3 proteins have been associated with several pathologies and the protein-protein interactions established with a number of partners are now considered promising drug targets. The activity of 14-3-3 proteins is often isoform specific and to our knowledge only one out of seven isoforms, 14-3-3 ζ , has been assigned. Despite the availability of the crystal structures of all seven isoforms of 14-3-3, the additional NMR assignments of 14-3-3 proteins are important for both biological mechanism studies and chemical biology approaches. Herein, we present a robust backbone assignment of 14-3-3 σ , which will allow advances in the discovery of potential therapeutic compounds. This assignment is now being applied to the discovery of both inhibitors and stabilizers of 14-3-3 protein-protein interactions.

Keywords

Protein-Protein Interactions, 14-3-3 proteins, Drug discovery, NMR resonance assignments

Biological context

The 14-3-3 family includes seven different isoforms (β , γ , ϵ , η , σ , τ and ζ) expressed in all eukaryotic organisms. 14-3-3 proteins are adapter proteins, expressed in an ubiquitous manner in all tissues and cell compartments. Despite the considerably high structural homology between different isoforms, 14-3-3 activity is often isoform specific (Fu et al., 2000). To our knowledge, 14-3-3 ζ is the only isoform of 14-3-3 whose assignment is reported (Killoran, Fan, Yang, Shilton, & Choy, 2015). 14-3-3 proteins exert their biological functions through the modulation of the activity of hundreds of phosphorylated proteins. This remarkable interactome makes 14-3-3 proteins influent actors in many cellular events and, by consequence, in several pathologies like cancer, Alzheimer's disease, Parkinson's disease, among others (Kaplan, Ottmann, et al., 2017). With the rise of the interest on the modulation of Protein-Protein Interactions (PPIs) in modern drug discovery, 14-3-3 proteins are being seen as promising targets for several pathologies. Especially over the last 10 years, there has been a remarkable effort towards the discovery of compounds capable of inhibiting or stabilizing 14-3-3 PPIs (Stevens et al., 2018). In particular, we have been interested in modulating the Tau/14-3-3 interaction, which is thought to have detrimental effects in neuronal cells in Alzheimer's disease (Joo et al., 2015). Peptidomimetic compounds have been designed and shown to inhibit this PPI (Andrei, Meijer, et al., 2018; Milroy et al., 2015). Assignment of 14-3-3 σ spectra will further help the development of these promising compounds.

In physiological conditions, 14-3-3 proteins exist as functional dimers, both as hetero and homodimers (Fu et al., 2000). They are acidic proteins and each monomer has a molecular weight (MW) of around 30 kDa, being composed by nine α -helices, commonly named α A-I, disposed in an antiparallel fashion. At the C-terminus of the last helix of 14-3-3 proteins (α I), there is a flexible and highly acidic tail, which is the less conserved region of 14-3-3 (Tomas Obsil & Obsilova, 2011).

Here we report the backbone assignments ($^{13}\text{C}_\alpha$, $^{13}\text{C}_\beta$, ^{13}CO , ^{15}N and $^1\text{H}^{\text{N}}$) of 14-3-3 σ (a truncated form comprising residues 1-231 out of 248). Due to the large number of partners of 14-3-3 σ , the assignment of this protein opens new possibilities for the study of hundreds of PPIs. Our assignment is currently being applied to drug screening and to the study of the effect

of small molecules on the modulation of 14-3-3 PPIs. In the future, it may have a role on the development of new 14-3-3 PPI modulators that can be employed as tool compounds and hopefully, be the basis for the development of new therapeutic molecules.

Sample preparation

The plasmids used for protein expression were kindly provided by Dr. Christian Ottmann from the Eindhoven University of Technology, The Netherlands. The cDNA coding for human 14-3-3 σ (residues 1-248) or 14-3-3 $\sigma\Delta$ C17 (residues 1-231) was cloned into the pProExHtb vector between the *Bam*HI and *Not*I sites. A Tobacco Etch Virus (TEV) cleavage site followed by a linker (GAMGS) are present between the regions coding for the N-terminal His₆-tag and for the protein, yielding a recombinant expression plasmid with the following configuration: His₆ tag-TEV cleavage site-Linker-14-3-3 σ /14-3-3 $\sigma\Delta$ C17. Therefore, 14-3-3 σ and 14-3-3 $\sigma\Delta$ C17 were both expressed as N-terminally His₆-tagged proteins.

¹⁵N¹³C²H labeled 14-3-3 σ or 14-3-3 $\sigma\Delta$ C17 were expressed in *E. coli* BL21 (DE3) cells. A 20 ml pre-culture in *Luria-Bertani* (LB) medium containing 100 mg/L ampicillin was grown overnight at 310 K and was used to inoculate 1 L of deuterated M9 minimal medium supplemented with 2 g/L ¹³C₆²H₇ D-Glucose, 1 g/L ¹⁵N Ammonium Chloride, 0.4 g/L Isogro ¹⁵N¹³C²H Powder – Growth Medium (Sigma Aldrich) and 100 mg/L ampicillin. The culture was grown at 310 K to an OD₆₀₀ of 0.9 and induced with 0.5 mM Isopropyl- β -D-Thiogalactopyranoside (IPTG). Incubation was continued for 15h at 301 K with vigorous shaking. Cells were harvested by centrifugation, resuspended in a buffer containing 50 mM Tris-HCl, 500 mM NaCl, 5% (v/v) glycerol, 25 mM imidazole, 2 mM β -Mercaptoethanol (BME), pH 8.0 and lysed with a homogenizer. The cellular debris were then eliminated by centrifugation and the supernatant was loaded into a Ni-NTA column (GE Healthcare). Elution of proteins was performed with a buffer containing 50 mM Tris-HCl, 500 mM NaCl, 5% (v/v) glycerol, 250 mM imidazole, 2 mM BME, pH 8.0. The N-terminal His₆-tag was then cleaved by the TEV protease for 2 hours at 293 K, followed by 12 hours at 277 K, while being dialyzed against 100 mM sodium phosphate, pH 6.8 and 50 mM NaCl (NMR buffer). The molar ratio between 14-3-3 σ or 14-3-3 $\sigma\Delta$ C17 and TEV protease was 50:1. The protein without His₆-tag was collected in the flow-through of a Ni-NTA column, using NMR buffer for the elution, while

the uncleaved fraction and the His₆-tagged peptide were retained on the column. The protein was then concentrated to 2 mM, aliquoted, flash frozen and stored at 193 K. Typical yields were in the range of 45-70 mg of protein per liter of culture.

NMR spectroscopy

All NMR experiments were recorded using a 900 MHz Bruker Avance spectrometer, equipped with a cryoprobe. Samples, in a buffer containing 100 mM sodium phosphate, pH 6.8, 50 mM NaCl, 1mM DTT (Dithiothreitol), EDTA-free Protease Inhibitor Cocktail (Roche, Switzerland) and 10% (v/v) D₂O, were transferred to *Shigemi* tubes and experiments were acquired at 305 K. The concentration of ¹⁵N¹³C²H labeled protein for assignment experiments ranged from 0.8 mM to 1.0 mM. Backbone assignments were obtained from TROSY-HNCACB, TROSY-HN(CO)CACB, BEST-TROSY-HNCO and ¹H-¹⁵N-NOESY-HMQC spectra on ¹⁵N¹³C²H labeled 14-3-3 σ or 14-3-3 σ Δ C17 samples. The mixing time of the ¹H-¹⁵N-NOESY-HMQC spectrum was 120 ms. Non-Uniform Sampling was employed for the acquisition of all 3D spectra. The reference for the ¹H chemical shift was relative to Trimethyl silyl propionate. The ¹⁵N and ¹³C chemical shifts were referenced indirectly. All spectra were collected and processed with Topspin 3.5 (Bruker Biospin) and analyzed with Sparky 3.12 (T. D. Goddard and D. G. Kneller, SPARKY 3, University of California, San Francisco). Automatic assignments were performed with MARS version 1.2 (Jung & Zweckstetter, 2004) and with PINE-NMR server (Bahrami et al., 2009).

Assignments and data deposition

For sequence numbering purposes, the residues of the linker left after TEV cleavage (GAMGS) were not considered. Accordingly, residue 1 corresponds to the first Methionine residue of 14-3-3 σ . Similarly to what has been reported for the assignment of 14-3-3 ζ (Killoran et al., 2015), we also observed the presence of highly intense peaks in the ¹H-¹⁵N TROSY-HSQC spectrum of the full-length 14-3-3 σ (residues 1-248). Because these intense signals were overlapping with signals corresponding to the ordered core-region, we decided to use a construct of 14-3-3 σ without the C-terminal flexible region (14-3-3 σ Δ C17, containing residues 1-231) for the backbone assignment. The elimination of the resonances corresponding to this

flexible region indeed allowed to detect more resonances on the ^1H - ^{15}N TROSY-HSQC spectrum and additionally improved the overall quality of the 3D spectra. Removal of the disordered terminal tail did not affect the structure of the protein in solution as resonances in the 2D spectra of the protein with or without the tail superimposed. The final construct, after cleavage of the N-terminus by the TEV protease, yielded a 14-3-3 $\sigma\Delta\text{C17}$ protein with a MW of 26.51 KDa. Given its association as a dimer and therefore the formation of a biomolecule with a MW higher than 50 KDa, it was necessary to produce a deuterated protein, to use a high-field spectrometer and to extend acquisition times. A good coverage of the protein assignment was reached although it should be noted that not all the amide peaks of the protein were detected on the ^1H - ^{15}N TROSY-HSQC (shown in **figure 1 a**) and in some cases, backbone signals in the ^{13}C dimension were of low intensity. The incomplete $^2\text{H}/^1\text{H}$ exchange may have been a factor that prevented the detection of some resonances, in particular those corresponding to residues located at the dimer interface.

Overall, we were able to obtain a robust assignment of 14-3-3 $\sigma\Delta\text{C17}$ comprising 177 out of 226 $^1\text{H}^{\text{N}}$ and ^{15}N resonances (78%), 200 out of 231 $^{13}\text{C}_{\alpha}$ resonances (87%), 187 out of 219 $^{13}\text{C}_{\beta}$ resonances (85%) and 176 out of 231 ^{13}CO resonances (77%). The assignment covers homogeneously the protein's sequence (**figure 1 b**). The assigned chemical shifts were deposited into the Biological Magnetic Resonance Database (<http://www.bmrb.wisc.edu/>) under the BMRB accession number 27563.

Secondary structure

The obtained chemical shift assignments were further used for the analysis of the secondary structure of 14-3-3 σ by two different methods. On one hand, the ensemble of backbone chemical shifts ($^{13}\text{C}_{\alpha}$, $^{13}\text{C}_{\beta}$, ^{13}CO , ^{15}N and $^1\text{H}^{\text{N}}$) was submitted to CSI 3.0 sever (Hafsa et al., 2015) in order to obtain the Chemical Shift Indexes predictive of the secondary structure. On the other hand, the $^{13}\text{C}_{\alpha}$ and $^{13}\text{C}_{\beta}$ chemical shift values were used to calculate the Secondary Structure Propensity (SSP) scores (Marsh et al., 2006). Prediction by SSP scores allowed comparison with the secondary structure analysis of the previously assigned 14-3-3 isoform (Killoran et al., 2015).

The results of the predictions made by both softwares are summarized in **figure 2**. Indeed, the results obtained from both methods are coherent and well correlated with what is reported in the crystal structure of 14-3-3 σ (PDB ID: 1YZ5). The SSP scores of 14-3-3 σ presented here are almost identical to the ones of 14-3-3 ζ showing that the secondary structures of both isoforms in solution are very similar. The only remarkable difference is the length of helix α D, which is shorter in 14-3-3 σ at its N-terminus due to the replacement of Q₇₉ of 14-3-3 ζ by a proline residue.

Figures

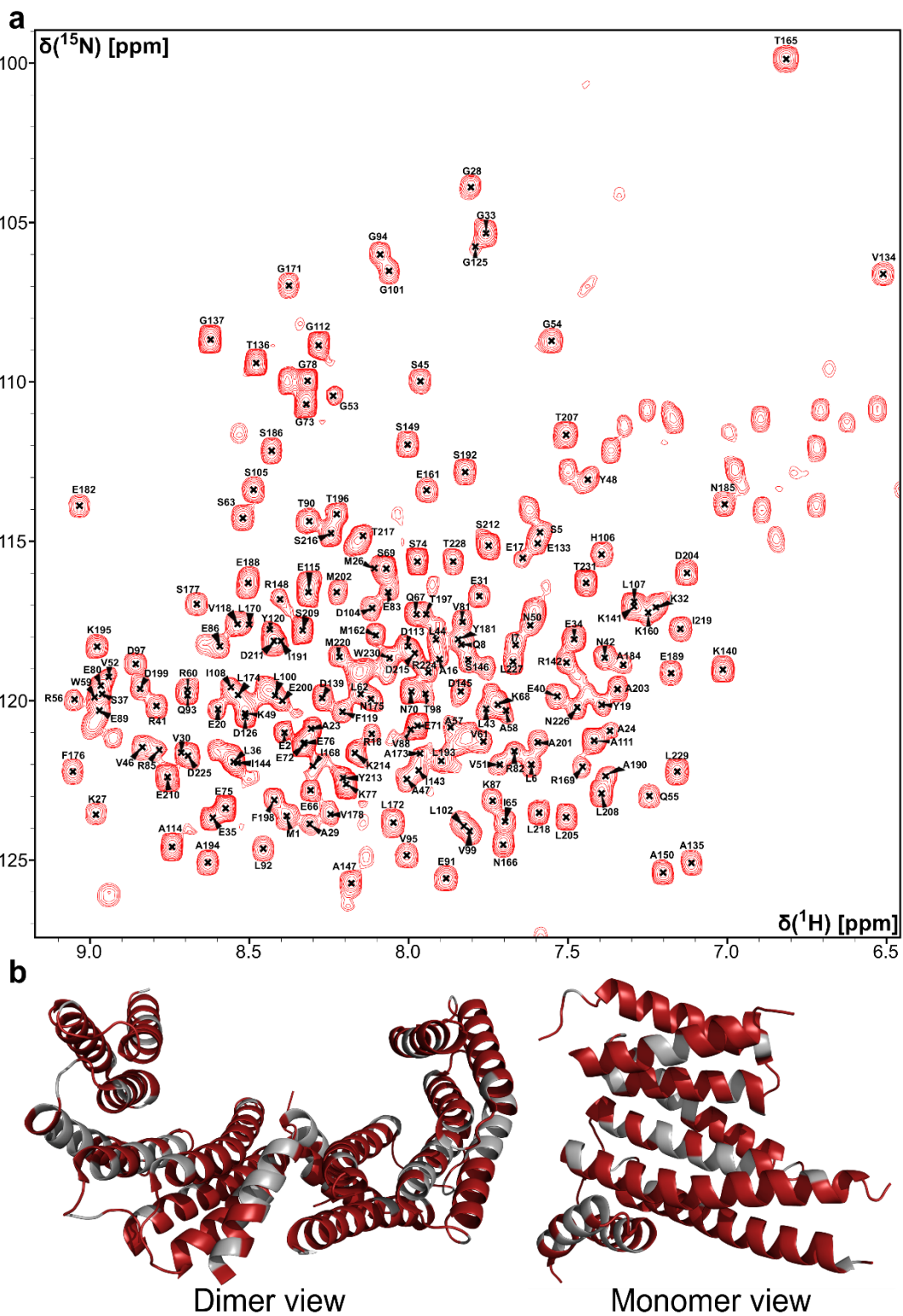


Figure 1 - Assignment of 14-3-3 σ is robust and covers homogeneously the protein's surface. a) Annotated ^1H - ^{15}N TROSY-HSQC spectrum of $^{15}\text{N}^{13}\text{C}^2\text{H}$ labeled 14-3-3 $\sigma\Delta\text{C17}$ 0.8 mM acquired at 305 K in a buffer containing 100 mM sodium phosphate, pH 6.8, 50 mM NaCl, 1mM DTT, EDTA-free Protease Inhibitor Cocktail (Roche, Switzerland)

and 10% (v/v) D₂O. The spectrum was acquired with 3426 complex points in the ¹H dimension and 256 complex points in the ¹⁵N dimension with 64 scans per increment. The spectral window was between 4.72 ppm and 14.64 ppm for the ¹H dimension and between 80.2 ppm and 140.1 ppm for the ¹⁵N dimension. The selected window contains all the assigned backbone resonances. b) Cartoon representation of the crystal structure of 14-3-3σ (PDB ID: 1YZ5, gray cartoon) with the assigned residues colored in red. The structure is shown both as a dimer and as a monomer of 14-3-3σ.

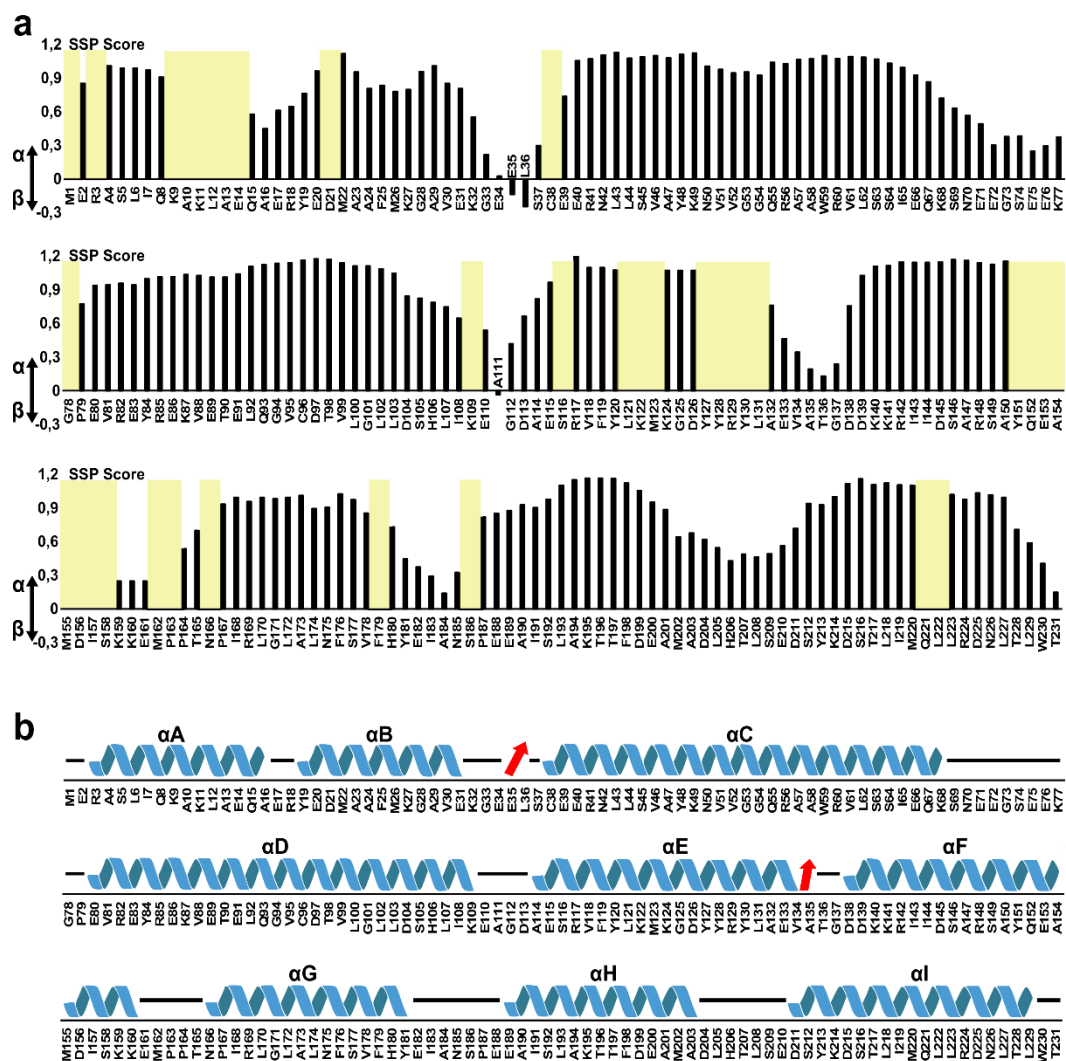


Figure 2 - Secondary Structure analysis of 14-3-3σ by calculation of the SSP scores and by the CSI 3.0 server reveals that 14-3-3σ is composed by nine α-helices, as expected from the crystal structure. a) SSP scores calculation for 14-3-3σ. The y axis of the plot represents the score (~ 1 for α-helix, ~ 0 for random coil, ~ -1 for β-strand) for each residue of 14-3-3σ (represented on the x axis). Yellow bars correspond to non-assigned residues or to residues preceding prolines, which were not considered for the SSP score calculation. Random coil chemical shift values used for the calculation of SSP scores were taken from RefDB database (H. Zhang et al., 2003). The plot is divided

in 3 lines. b) Output of the CSI 3.0 server in a residue specific-way (blue cartoon stands for α -helix, red arrow stands for β -strand and black line stands for random coil). The plot is divided in 3 lines. The identification of the helices of 14-3-3 σ (α A- α) is shown above the output of the CSI 3.0 server.

Acknowledgments

We thank MSc. Eline Sijbesma and Dr. Christian Ottmann from the Eindhoven University of Technology for kindly providing us the plasmids of both 14-3-3 σ and 14-3-3 $\sigma\Delta$ C17. We also thank Dr. Elian Dupré from Lille University for his help with the automatic assignments software.

The research is supported by funding from the European Union through the TASPPI project (H2020-MSCA-ITN-2015, grant number 675179) and by the LabEx (Laboratory of Excellence) DISTALZ (ANR, ANR-11-LABX- 009). The NMR facilities were funded by the Nord Region Council, CNRS, Institut Pasteur de Lille, the European Community (ERDF), the French Ministry of Research and the University of Lille and by the CTRL CPER cofunded by the European Union with the European Regional Development Fund (ERDF), by the Hauts de France Regional Council (contract n°17003781), Métropole Européenne de Lille (contract n°2016_ESR_05), and French State (contract n°2017-R3-CTRL-Phase 1). We acknowledge support for the NMR facilities from TGE RMN THC (CNRS, FR-3050) and FRABio (Univ. Lille, CNRS, FR-3688).

Conflict of interest

The authors declare that they have no conflict of interest.

References

Andrei SA, Meijer FA, Neves JF, et al (2018) Inhibition of 14-3-3/Tau by Hybrid Small-Molecule Peptides Operating via Two Different Binding Modes. *ACS Chem Neurosci*. doi: 10.1021/acscchemneuro.8b00118

Bahrami A, Assadi AH, Markley JL, Eghbalnia HR (2009) Probabilistic Interaction Network of Evidence Algorithm and its Application to Complete Labeling of Peak Lists from Protein NMR Spectroscopy. *PLOS Computational Biology* 5:e1000307. doi: 10.1371/journal.pcbi.1000307

Fu H, Subramanian RR, Masters SC (2000) 14-3-3 proteins: structure, function, and regulation. *Annual review of pharmacology and toxicology* 40:617–647

Hafsa NE, Arndt D, Wishart DS (2015) CSI 3.0: a web server for identifying secondary and super-secondary structure in proteins using NMR chemical shifts. *Nucleic Acids Res* 43:W370–W377. doi: 10.1093/nar/gkv494

Joo Y, Schumacher B, Landrieu I, et al (2015) Involvement of 14-3-3 in tubulin instability and impaired axon development is mediated by Tau. *The FASEB Journal* 29:4133–4144. doi: 10.1096/fj.14-265009

Jung Y-S, Zweckstetter M (2004) Mars - robust automatic backbone assignment of proteins. *J Biomol NMR* 30:11–23. doi: 10.1023/B:JNMR.0000042954.99056.ad

Kaplan A, Ottmann C, Fournier AE (2017) 14-3-3 adaptor protein-protein interactions as therapeutic targets for CNS diseases. *Pharmacological Research* 125:114–121. doi: 10.1016/j.phrs.2017.09.007

Killoran RC, Fan J, Yang D, et al (2015) Structural Analysis of the 14-3-3 ζ /Chibby Interaction Involved in Wnt/ β -Catenin Signaling. *PLOS ONE* 10:e0123934. doi: 10.1371/journal.pone.0123934

Marsh JA, Singh VK, Jia Z, Forman-Kay JD (2006) Sensitivity of secondary structure propensities to sequence differences between α - and γ -synuclein: Implications for fibrillation. *Protein Sci* 15:2795–2804. doi: 10.1110/ps.062465306

Milroy L-G, Bartel M, Hemen MA, et al (2015) Stabilizer-Guided Inhibition of Protein-Protein Interactions. *Angewandte Chemie International Edition* 54:15720–15724. doi: 10.1002/anie.201507976

Obsil T, Obsilova V (2011) Structural basis of 14-3-3 protein functions. *Seminars in Cell & Developmental Biology* 22:663–672. doi: 10.1016/j.semcdb.2011.09.001

Stevens LM, Sijbesma E, Botta M, et al (2018) Modulators of 14-3-3 Protein-Protein Interactions. *J Med Chem* 61:3755–3778. doi: 10.1021/acs.jmedchem.7b00574

Zhang H, Neal S, Wishart DS (2003) RefDB: A database of uniformly referenced protein chemical shifts. *J Biomol NMR* 25:173–195. doi: 10.1023/A:1022836027055

2 Structural Insights on the 14-3-3/Tau Protein-Protein Interaction

2.1 Materials and Methods

2.1.1 14-3-3 Proteins Production and Purification

14-3-3 σ or 14-3-3 $\sigma\Delta C$ (cleaved after T231 – used for NMR experiments to improve the quality of spectra) were expressed in *E. coli* BL21 (DE3) cells transformed with a pProExHtb vector carrying the cDNA to express an N-terminally His₆-tagged human 14-3-3 σ or 14-3-3 $\sigma\Delta C$. An overnight 20 mL pre-culture in *Luria-Bertani* (LB) medium was used to inoculate 1 L of culture medium. For the expression of the natural abundance proteins, cells were inoculated in 1 L of M9 minimal medium supplemented with 4 g/L D-Glucose, 1 g/L Ammonium Chloride, 5% (v/v) LB medium and 100 $\mu\text{g/mL}$ ampicillin. For ¹⁵N¹³C²H labeling, the cells were inoculated in 1 L of deuterated M9 minimal medium supplemented with 2 g/L ¹³C₆²H₇ D-Glucose, 1 g/L ¹⁵N Ammonium Chloride, 0.4 g/L Isogro ¹⁵N¹³C²H Powder – Growth Medium (Sigma Aldrich) and 100 $\mu\text{g/mL}$ ampicillin. Cells were grown at 37 °C to an OD₆₀₀ of 0.9 and induced with 0.5 mM IPTG. Incubation was continued for 12 h at 25 °C for the natural abundance proteins and for 15 h at 28 °C for the ¹⁵N¹³C²H labelled protein. Cells were harvested by centrifugation, lysed with a homogenizer and the proteins were purified using a Ni-NTA column (GE Healthcare). The selected fractions were then mixed with the TEV protease in NMR buffer (100 mM Sodium Phosphate, pH 6.8, 50 mM NaCl) during 2 hours at 20°C and 12 hours at 4°C for cleavage of the N-terminal His₆-tag. The cleavage was performed during dialysis and the molar ratio between 14-3-3 σ /14-3-3 $\sigma\Delta C$ and the TEV protease was 50:1. The cleaved protein was separated from the uncleaved fraction and from the His₆-tagged TEV protease by flowing the proteins in NMR buffer through the same Ni-NTA column. The cleaved 14-3-3 σ or 14-3-3 $\sigma\Delta C$ proteins were then concentrated, aliquoted, flash frozen and stored at -80 °C. Typical yields were in the range of 40 to 80 mg of protein per liter of culture. A detailed protocol can be found at (Neves et al., 2019).

2.1.2 Tau Proteins Production and Purification

E.coli BL21 (DE3) cells were transformed with the pET15b vector carrying the gene coding for wild-type Tau (2N4R, 441 residues – for NMR experiments) or His₆-tagged Tau Y394W (2N4R, 441 residues - for Analytical Ultracentrifugation and Surface Plasmon Resonance Experiments). A 20 ml pre-culture in Luria–Bertani (LB) medium containing 100 µg/mL ampicillin was grown overnight at 37 °C and was used to inoculate a 1 L culture in M9 minimal medium supplemented with 4 g/L D-Glucose, 1 g/L NH₄Cl, 5% (v/v) LB medium and 100 µg/mL ampicillin. For ¹⁵N labeling, cells were inoculated in 1L of M9 minimal medium supplemented with 4 g/L D-Glucose, 1 g/L ¹⁵NH₄Cl, 500 mg Isogro ¹⁵N¹²C¹H Powder – Growth Medium (Sigma Aldrich) and 100 µg/mL ampicillin. The culture was grown at 37 °C to an OD₆₀₀ of 0.8 and induced with 0.5 mM IPTG. Incubation was continued for 3h at 37 °C and the culture was then harvested by centrifugation. The lysate was lysed using a homogenizer and centrifuged at 30 000 g for 30 minutes. A first purification step was achieved by heating the sample at 75°C for 15 min, followed by centrifugation at 15 000 g for 20 minutes to eliminate the precipitate. The recombinant Tau protein, dissolved in buffer containing 50 mM sodium phosphate pH 6.6 and 2mM EDTA (buffer A) was then loaded on a cation-exchange chromatography column (GE Healthcare). Elution was performed with a gradient from 0% to 50% using a buffer containing 50 mM sodium phosphate pH 6.6 and 2mM EDTA, 1M NaCl (buffer B). The selected fractions were further buffer-exchanged with 50 mM ammonium bicarbonate using a desalting column (GE Healthcare) before lyophilization. Protein concentration was estimated by absorption at 280 nm. A more detailed protocol can be found in (Danis et al., 2016). Typical yields were in the range of 5-15 mg of recombinant Tau protein per liter of culture.

2.1.3 PKA-catalytic subunit Production and Purification

E.coli BL21 (DE3) cells were transformed with the pet15b Vector (Addgene plasmid # 14921) carrying the gene coding for the N-terminally His₆-tagged PKA catalytic subunit α from *Mus musculus* (PKAc). A 20 mL pre-culture in LB medium containing 100 µg/ml ampicillin was grown overnight at 37 °C and was used to inoculate a 1 L culture in LB medium. The culture was grown at 37 °C to an OD₆₀₀ of 0.8 and production was induced with 0.5 mM IPTG.

Incubation was continued for 20 h at 20 °C and the culture was then harvested by centrifugation. After being suspended in a buffer containing 50 mM Tris, pH 8.0, 500 mM NaCl, 2 mM β -mercaptoethanol and 10 mM Imidazole, the pellet was lysed using an homogeneizer, followed by centrifugation at 30,000 g for 30 minutes. The His₆-tagged PKAc was then loaded on a Ni-NTA column (GE Healthcare) and eluted with a buffer containing 50 mM Tris, pH 8.0, 500 mM NaCl, 2 mM BME and 250 mM Imidazole. The pure fractions were then buffer-exchanged with 250 mM potassium phosphate pH 6.5, 0.1 mM DTT on a desalting column (GE Healthcare). The protein was aliquoted, flash frozen in liquid nitrogen and stored at -80 °C. Typical yields were in the range of 10-15mg per liter of culture.

2.1.4 In-vitro phosphorylation of Tau

Recombinant Tau or TauY394W proteins (100 μ M) were incubated with 1.5 μ M recombinant PKAc at 30 °C for 3 h, in a buffer consisting of 50 mM Hepes pH 8.0, 5 mM ATP, 12.5 mM MgCl₂, 50 mM NaCl, 5 mM DTT, 1 mM EDTA. The reaction was heat-inactivated at 75 °C for 15 min and the solution was centrifuged in order to eliminate the precipitated PKAc. Buffer exchange with 50 mM ammonium bicarbonate on a desalting column (GE Healthcare) was performed before lyophilization. Tau phosphorylation by PKAc was accessed by ¹H NMR (Danis et al., 2016; Landrieu et al., 2006).

2.1.5 ¹H-¹⁵N TROSY-HSQC Spectroscopy

¹H-¹⁵N TROSY-HSQC (Transverse Relaxation Optimized Spectroscopy- Heteronuclear Single Quantum Coherence Spectroscopy) spectra were acquired in 3 mm tubes (sample volume 200 μ L) using a 900 MHz Bruker Avance NEO spectrometer, equipped with a cryoprobe. The spectra were recorded with 3426 complex data points in the direct dimension and 128 complex data points in the indirect dimension, with 300 scans per increment, at 32 °C, in a buffer containing 100 mM sodium phosphate, 50 mM NaCl, pH 6.8, 1 mM DTT, EDTA-free protease inhibitor cocktail (Roche) and 10% (v/v) D₂O. Experiments on 125 μ M ¹⁵N¹³C²H labeled 14-3-3 σ (full-length, comprising residues 1-248) were acquired in the presence and absence of Tau-PKA 80 μ M. Experiments on 125 μ M ¹⁵N¹³C²H labeled 14-3-3 σ Δ C (comprising

residues 1-231 out of 248) were acquired in the presence or in the absence of 500 μ M wt-Tau, 500 μ M Tau-PKA, 500 μ M Tau peptide surrounding pS214 (R₂₁₁TPpSLPTP₂₁₈) and 500 μ M Tau peptide surrounding pS214+pS324 (5,6-FAM-R₂₁₁TPpSLPT₂₁₇GGSGGGSGGGS₃₂₀KCGpSLGNIHHK₃₃₁). The reference for the ¹H chemical shift was relative to trimethylsilyl propionate. ¹⁵N chemical shifts were referenced indirectly. Spectra were collected and processed with Topspin 4.0 (Bruker Biospin) and analyzed with Sparky 3.12 (T. D. Goddard and D. G. Kneller, SPARKY 3, University of California, San Francisco). The backbone resonance assignments of 14-3-3 σ Δ C were previously reported (Neves et al., 2019).

2.1.6 Backbone chemical shift assignment of the C-terminal stretch (A232-S245) of 14-3-3 σ

Backbone assignment experiments were recorded using a 900 MHz Bruker Avance NEO spectrometer, equipped with a cryoprobe. Samples, in a buffer containing 100 mM sodium phosphate, pH 6.8, 50 mM NaCl, 1mM DTT (Dithiothreitol), EDTA-free Protease Inhibitor Cocktail (Roche, Switzerland) and 10% (v/v) D₂O, were transferred to Shigemi tubes (sample volume of 330 μ L) and experiments were acquired at 32 °C. The concentration of ¹⁵N¹³C²H labeled protein for assignment was 1.0 mM. Backbone assignments were obtained from TROSY-HNCACB, TROSY-HNCA, TROSY-HN(CO)CACB and TROSY-HNCO spectra on ¹⁵N¹³C²H labeled 14-3-3 σ (full-length, comprising residues 1-245). Non-Uniform Sampling was employed for the acquisition of all 3D spectra. The reference for the ¹H chemical shift was relative to Trimethyl silyl propionate. The ¹⁵N and ¹³C chemical shifts were referenced indirectly. All spectra were collected and processed with Topspin 3.5 (Bruker Biospin) and analyzed with Sparky 3.12 (T. D. Goddard and D. G. Kneller, SPARKY 3, University of California, San Francisco).

2.1.7 Analytical Ultracentrifugation

Analytical Ultracentrifugation (AUC)-Sedimentation velocity (SV) experiments were conducted in a ProteomeLabTM XL-I analytical ultracentrifuge (Beckman Coulter), as described

previously (Kosek et al., 2014). Prior to measurement, proteins were dialyzed against a buffer containing Tris-HCl 50 mM pH 6.7, NaCl 30 mM, EDTA 2.5 mM and Tris(2-carboxyethyl)phosphine (TCEP) 1 mM. Samples were loaded in charcoal-filled Epon centerpieces with 12 mm optical path length and centrifuged at 20 °C, during 24 hours at 45 000 rpm/ 163 004 g rotor speed (An-50 Ti rotor, Beckman Coulter). All sedimentation profiles were recorded using both interference and absorption optics at 280 nm. The diffusion-deconvoluted sedimentation coefficients distributions $c(s)$ were calculated using the SEDFIT software (Schuck, 2000). A Tau construct containing a Tryptophan (TauY394W) was used for improving its detection by absorption optics. In order to study the effect of the phosphorylation of Tau on the formation of a complex with 14-3-3 σ , solutions containing 14-3-3 σ 24 μ M in the presence and absence of 12 μ M wt-Tau or 12 μ M Tau-PKA were analyzed. In order to study the stoichiometry of the 14-3-3 σ /Tau-PKA complex, solutions containing 14-3-3 σ /Tau-PKA in the proportions of 1:1 (14-3-3 σ 20 μ M: Tau-PKA 20 μ M) and 2:1 (14-3-3 σ 24 μ M: Tau-PKA 12 μ M) were analyzed. In order to determine the apparent K_d of the 14-3-3 σ /Tau-PKA complex, sedimentation velocity analysis of solutions containing 14-3-3 σ 8.4 μ M and different concentrations of Tau-PKA (0.42 μ M, 1.4 μ M, 4.2 μ M, 12.6 μ M and 42 μ M) was performed. The apparent K_d was estimated using the global Lamm equation modeling with a 1:1 Langmuir binding model implemented in the SEDPHAT software (Dam et al., 2005) considering the interaction of one molecule of Tau-PKA with one dimer (two molecules) of 14-3-3 σ . Figures of normalized continuous sedimentation coefficient distributions were prepared using GUSSE 1.4.2 (Brautigam, 2015).

2.1.8 Surface Plasmon Resonance

SPR experiments were conducted with a Biacore 3000 optical biosensor instrument (Biacore, Inc) equipped with a research-grade BDM500M sensor chip (XanTec Bioanalytics). For the determination of the dissociation constant between phosphorylated Tau and 14-3-3 σ or 14-3-3 ζ , the Tau mutant Y394W was used for more accurate determination of protein concentration. Biotinylation reactions of 14-3-3 σ /14-3-3 ζ were conducted by mixing the proteins at 350 μ M with the EZ-Link NHS-PEG12-Biotin reagent (Thermo Scientific) at 385 μ M for 2 hours at room temperature, at pH 7.4. The biotinylated 14-3-3 σ or 14-3-3 ζ proteins were

mixed with Switchavidin before immobilization (1:1 or 2:1 ratio, ~ 2500 RUs). Measurements were carried out at 20°C, at a flow rate of 5 μ L/min in HBSP+ buffer (10 mM Hepes, pH 7.4, 150 mM NaCl, 0.05% surfactant Tween 20). Binding of Tau-PKA was accessed by injecting 12 different concentrations of Tau-PKA, as 3-fold serial dilutions, for 5 minutes in two channels of the sensor chip. One channel was used as a blank surface and the other contained immobilized 14-3-3 σ or 14-3-3 ζ . After each cycle, the surface was regenerated with a 5 M GUSCN solution acidified with 5 mM TCEP. Dissociation constants (K_d) were calculated with GraphPad Prism 8.1.2 Software using a nonlinear regression analysis.

2.2 Results and Discussion

2.2.1 Phosphorylation of Tau by PKA enhances its interaction with 14-3-3

We first confirmed that in our experimental system we could detect the stimulation of Tau binding to 14-3-3 by specific phosphorylations. It has been reported that Tau can bind to 14-3-3 even without being phosphorylated (Hashiguchi et al., 2000) and that phosphorylation by PKA increases the affinity of Tau to 14-3-3 (Sadik et al., 2009). The increase in the affinity upon phosphorylation was shown to be related to the pS214 (Joo et al., 2015; Sadik et al., 2009) and pS324 epitopes (Joo et al., 2015).

The ^1H - ^{15}N TROSY-HSQC spectra of 125 μM $^{15}\text{N}^{13}\text{C}^2\text{H}$ labeled 14-3-3 $\sigma\Delta\text{C}$ in the presence of either 500 μM wt-Tau (**Figure 1 A**) or 500 μM Tau-PKA (**Figure 1 B**) were recorded. We used 14-3-3 $\sigma\Delta\text{C}$ (containing residues 1-231 out of 248), lacking the 17-residue disordered C-terminal tail since it significantly improves the quality of NMR spectra. The spectrum of the 14-3-3 $\sigma\Delta\text{C}$ /wt-Tau complex does not show a remarkable difference compared to the spectra of 14-3-3 $\sigma\Delta\text{C}$ alone (**Figure 1 A**, **Figure S1**) except a loss of intensity for a number of resonances. On the other hand, it is possible to detect marked changes in the spectrum of 14-3-3 $\sigma\Delta\text{C}$ in the presence of Tau-PKA, as it can be seen in **Figure 1 B**. In some cases, the broadening of the resonances was so pronounced that the peaks cannot even be detected. In spite of not being an objective measure of interaction affinities, this shows that Tau interacts more tightly with 14-3-3 $\sigma\Delta\text{C}$ when phosphorylated by PKA. For further characterization, we performed Analytical Ultracentrifugation – Sedimentation Velocity (AUC-SV) experiments in

order to study the formation of 14-3-3 σ /wt-Tau and 14-3-3 σ /Tau-PKA complexes. The normalized continuous sedimentation coefficient distributions $c(s)$ calculated from the absorbance data (A_{280}) are shown in **Figure 1 C**. The sedimentation profiles of the 14-3-3 σ , wt-Tau and Tau-PKA display single peaks suggesting homogeneity and well defined stoichiometries of all the isolated proteins (orange, violet and blue curves). The sedimentation profile of a solution containing both wt-Tau and 14-3-3 σ (**Figure 1 C, light blue curve**) seems to be a combined profile of the 14-3-3 σ and wt-Tau alone as it contains only peaks at exactly the same positions as both isolated proteins. This suggests that the interaction between wt-Tau and 14-3-3 σ either does not exist or that it is too weak to form a stable complex in solution. On the other hand, when Tau-PKA and 14-3-3 σ are centrifuged together, the formation of a complex is clear (**Figure 1 C, green curve**) as both peaks of the isolated proteins disappear and one new peak appears, whose position is shifted towards higher values of sedimentation coefficients suggesting a new particle with higher molecular mass.

Both NMR and AUC-SV data clearly showed that the phosphorylation of Tau by PKA enhanced the interaction with 14-3-3 σ , to the point of being essential for the formation of a stable complex in solution.

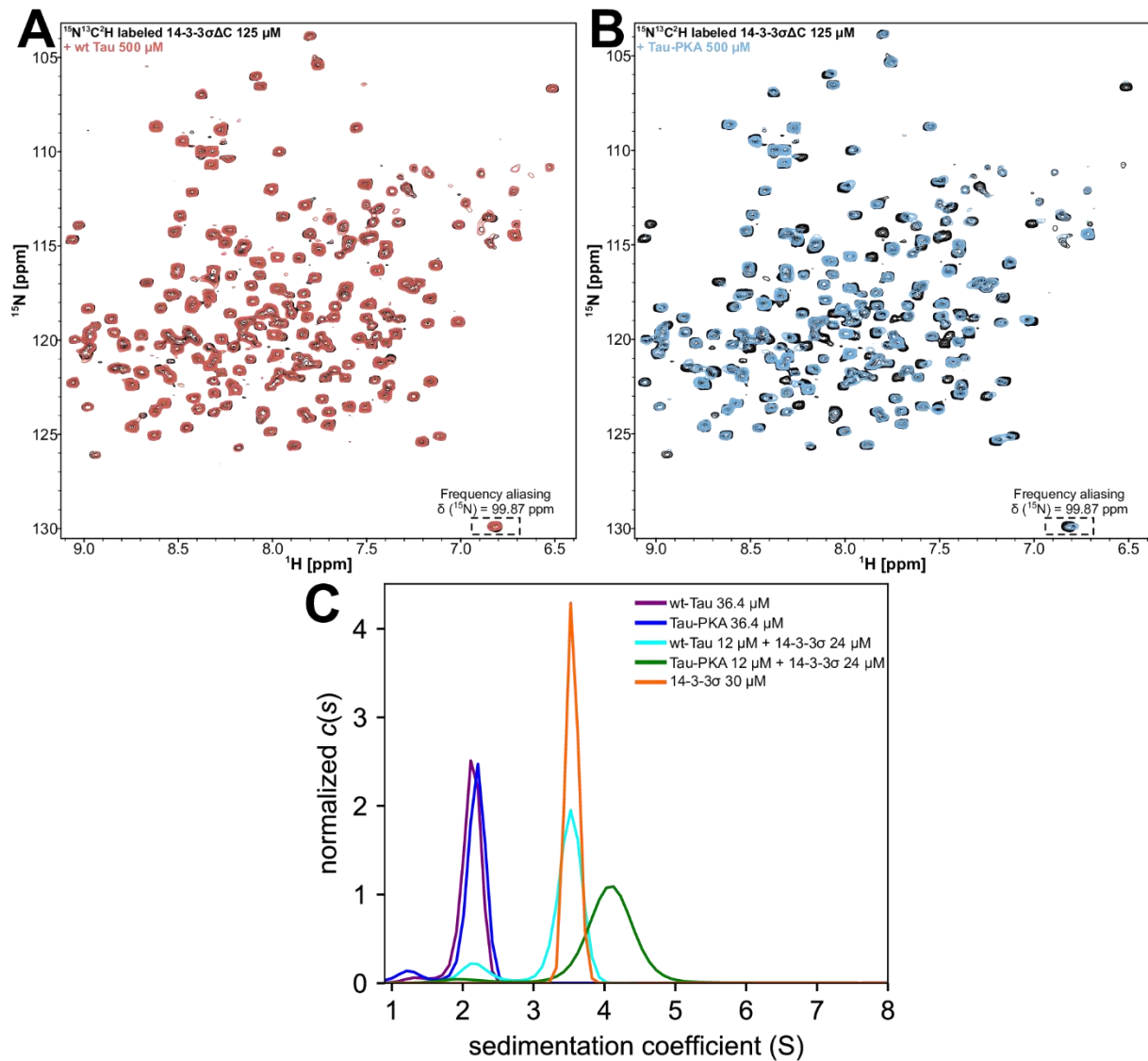


Figure 1 – Phosphorylation of Tau by PKA increases the affinity of Tau to 14-3-3. (A) ^1H - ^{15}N TROSY-HSQC spectra of $^{15}\text{N}^{13}\text{C}^2\text{H}$ labeled 14-3-3 $\sigma\Delta\text{C}$ 125 μM alone (in black), or in the presence of 500 μM wt-Tau (superimposed in red). (B) ^1H - ^{15}N TROSY-HSQC spectra of $^{15}\text{N}^{13}\text{C}^2\text{H}$ labeled 14-3-3 $\sigma\Delta\text{C}$ 125 μM alone (in black), or in the presence of 500 μM Tau-PKA (superimposed in blue). Note that the CSP on the spectrum of 14-3-3 $\sigma\Delta\text{C}$ are much more pronounced in the presence of Tau-PKA than in the presence of wt-Tau. (C) The normalized continuous sedimentation coefficient distributions for wt-Tau 36 μM alone (purple), Tau-PKA 36 μM alone (dark blue), 14-3-3 σ 30 μM alone (orange), wt-Tau 12 μM mixed with 14-3-3 σ 24 μM (light blue) and Tau-PKA 12 μM mixed with 14-3-3 σ 24 μM (green). Note that for the Tau-PKA/14-3-3 σ mixture, a new peak shifted towards higher S values is formed (complex), whereas for the wt-Tau/14-3-3 σ mixture no such a particle is formed.

2.2.2 Tau interacts with 14-3-3 exclusively via the amphipathic binding groove

Here, we analyzed the complex formed by full-length Tau-PKA and 14-3-3 to define the interface of these proteins. Definition of this interface is of interest in regards to the efforts underway to modulate the interaction of these proteins (Milroy et al., 2015). In this context, it is of importance to understand whether the interaction is mediated only by the phosphorylated Tau epitopes or rather required additional contacts with 14-3-3 surface, as reported in some complexes whose structures have been investigated using full-length proteins (Alblova et al., 2017; T. Obsil, Ghirlando, Klein, Ganguly, & Dyda, 2001; Ottmann et al., 2007; Psenakova et al., 2018; Sluchanko et al., 2017; Taoka et al., 2011). It was previously shown, by X-ray crystallography, that the epitopes of pS214 and pS324 of Tau anchor in the phospho-accepting pocket of the amphipathic binding groove of 14-3-3 (Joo et al., 2015). By the analysis of the ^1H - ^{15}N HSQC of Tau-PKA in the presence of 14-3-3, CSP are detected mainly closer to the phosphorylation sites, specially pS214 and pS324. In order to further explore the interface, we recorded ^1H - ^{15}N TROSY-HSQC of $^{15}\text{N}^{13}\text{C}^2\text{H}$ labeled 14-3-3 $\sigma\Delta\text{C}$ in the presence of Tau-PKA (**Figure 1 B**) and compared the effect caused by the full-length protein to the one caused by peptides containing only the pS214 epitope (**Figure S2**) or both pS214 and pS324 epitopes (**Figure S3**). Addition of the full-length Tau-PKA and of peptides containing the Tau peptides surrounding pS214 and both pS214 and pS324 to $^{15}\text{N}^{13}\text{C}^2\text{H}$ labeled 14-3-3 $\sigma\Delta\text{C}$ induced, as expected broadening of certain resonances in the spectrum of 14-3-3 $\sigma\Delta\text{C}$. The broadening of a resonance causes a drop of its intensity and consequently of its I/I0 ratio - being I the intensity of the resonance in the analyzed spectrum and I0 the intensity of the resonance in the control spectrum ($^{15}\text{N}^{13}\text{C}^2\text{H}$ labeled 14-3-3 $\sigma\Delta\text{C}$ 125 μM alone). The previously reported backbone assignment of 14-3-3 σ (Neves et al., 2019) allows the link of a resonance to a specific residue of 14-3-3 σ . By analyzing the intensity plots corresponding to the formation of the three complexes along the 14-3-3 σ sequence, a similar profile is observed (**Figure 2 A**). Nevertheless the magnitude of the intensity decrease is gradual from the peptide surrounding pS214 (**Figure 2 A, red plot**) that showed the lower decrease, followed by the pS214+pS324 doubly-phosphorylated peptide (**Figure 2 A, green plot**) and finally the full-length PKAc phosphorylated Tau protein (**Figure 2 A, blue plot**). This data suggests that, as expected, the affinity of the diphosphorylated peptide for 14-3-3 σ ($K_d = 2 \pm 0.2 \mu\text{M}$ determined

by (Joo et al., 2015) on the homologous 14-3-3ζ) is considerably higher than the one surrounding pS214 ($K_d = 102 \pm 31 \mu\text{M}$ determined by (Joo et al., 2015) on the homologous 14-3-3ζ). In the case of the full-length protein, the magnitude of the I/I0 ratio is even higher. Nonetheless, we cannot state that this effect shows that the affinity of Tau-PKA to 14-3-3σ is higher than the one of the peptides as the more pronounced decrease of the I/I0 can also be caused by the formation of a high MW complex (14-3-3/Tau-PKA) that possesses a higher correlation time and thus a smaller relaxation time leading to a general decrease of the resonance intensities. The analysis of the residues corresponding to the resonances of the spectrum of $^{15}\text{N}^{13}\text{C}^2\text{H}$ labeled 14-3-3σΔC the most affected by the presence of Tau-PKA indicates that it anchors in the amphipathic binding groove of 14-3-3 (Figure 2 B). Moreover the I/I0 plots show a similar profile for the three spectra which indicates that all the three molecules share approximately the same binding surface on 14-3-3σ. Keeping in mind that the peptides only bind to the amphipathic binding groove and that no other contact regions are detected for Tau-PKA, our study suggests that the contacts of Tau with 14-3-3 are strictly with the residues that compose the amphipathic binding groove, similarly to the peptides.

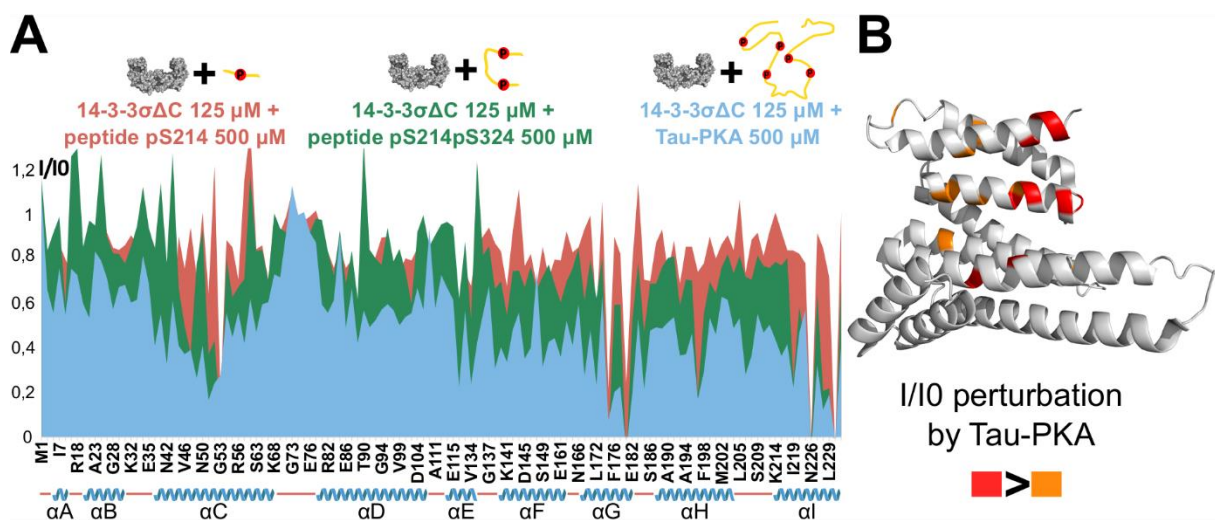


Figure 2 – Tau-PKA interacts with 14-3-3σ through the amphipathic binding groove. (A) Plot of the I/I0 values of $^1\text{H}^{15}\text{N}$ correlation peak intensities in the spectrum of $125 \mu\text{M}$ $^{15}\text{N}^{13}\text{C}^2\text{H}$ labeled 14-3-3σΔC in the presence of $500 \mu\text{M}$ Tau peptide surrounding pS214 (red plot), $500 \mu\text{M}$ Tau peptide surrounding pS214 and pS324 (green plot) and $500 \mu\text{M}$ full-length Tau-PKA (blue plot) (I) compared to corresponding resonances in the reference spectrum of $125 \mu\text{M}$ 14-3-3σΔC (I0) (y axis) versus 14-3-3σΔC amino acid sequence (x axis). A total of 135 correlation peak intensity ratios are shown. The x axis is not proportional to the sequence length. The helices of 14-3-3σ are

identified below the x axis as blue cartoons, while disordered regions are represented by red lines. (c) Mapping on the crystal structure of 14-3-3 σ (PDB ID: 1YZ5, represented as a grey cartoon) of the amino acid residues corresponding to the 20 most affected resonances by the presence of 500 μ M Tau-PKA. The residues corresponding to the 10 most affected resonances are colored in red and the following 10 are colored in orange. Note that the most affected residues are almost entirely located in the amphipathic binding groove.

2.2.3 The C-terminal stretch of 14-3-3 σ does not participate in the interaction with Tau

Our data obtained from the spectra of 14-3-3 σ Δ C seems to suggest that the binding of Tau-PKA occurs exclusively through the amphipathic binding groove. Nevertheless, the data acquired with this C-truncated form (comprising residues 1-231 out of 248) which is normally used for crystallographic and NMR studies does not allow us to exclude a possible participation of the disordered C-terminal stretch (residues A232-S248). Due to a better quality of the NMR spectra, the reported backbone chemical shift assignments of 14-3-3 σ were performed on the C-truncated form of 14-3-3 σ , which means that the chemical shift assignments of this C-terminal stretch are not available. Therefore, in order to study the effect of this C-terminal stretch on the interaction of 14-3-3 σ with Tau, the first step was to obtain the backbone chemical shift assignments of these residues. As reported before (Neves et al., 2019), the signals correspondent to this C-terminal stretch are very intense (**Figure S4**), which allowed the straightforward assignment of the corresponding backbone chemical shifts using standard 3D NMR experiments (**Table 1**). After the assignment, a ^1H - ^{15}N TROSY HSQC of ^{15}N ^{13}C ^2H labeled full-length 14-3-3 σ in the presence and absence of Tau-PKA was recorded (**Figure S5**) and the corresponding I/I0 ratios were plotted (**Figure 3**). The I/I0 plot shows that the intensities of the resonances corresponding to residues of the C-terminal stretch are not affected by the presence of Tau, indicating that these residues do not interfere in the interaction.

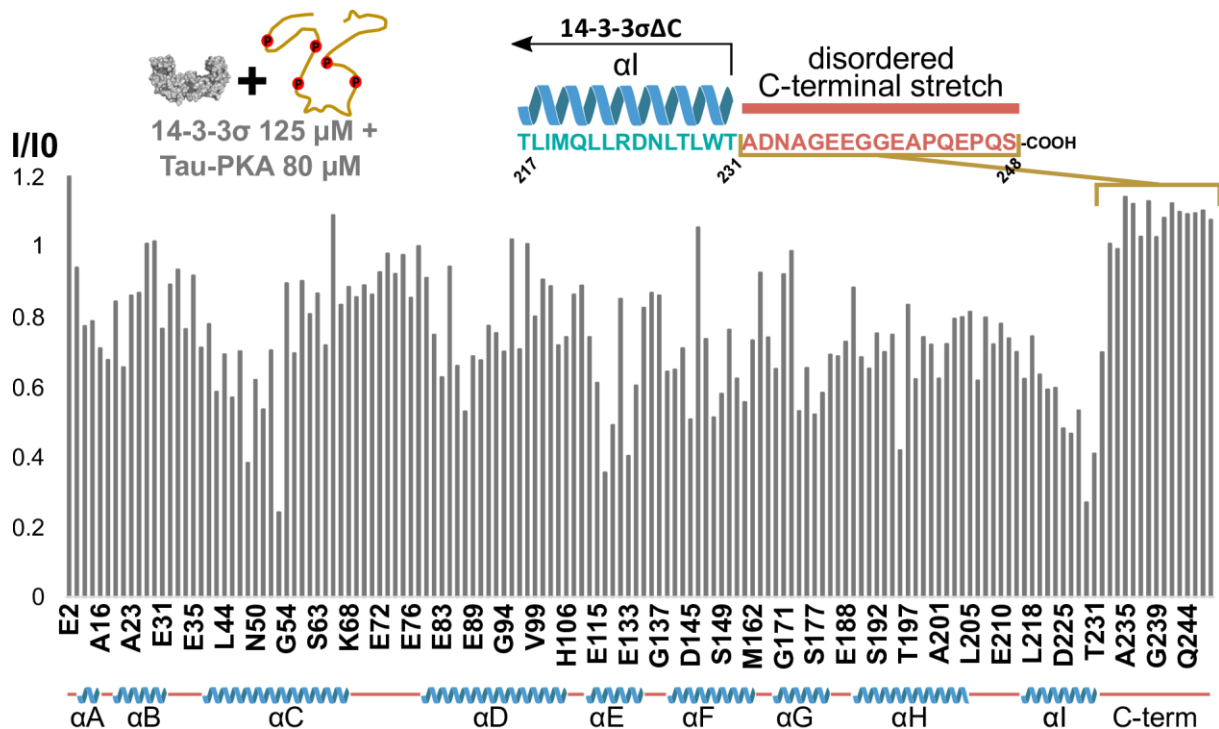


Figure 3 – The C-terminal stretch of 14-3-3σ is not involved in the interaction with Tau-PKA. Plot of the I/I0 values of ^1H - ^{15}N correlation peak intensities in the spectrum of 125 μM ^{15}N / ^{13}C labeled 14-3-3σ in the presence of 80 μM Tau-PKA (I) compared to corresponding resonances in the reference spectrum of 125 μM 14-3-3σ (I0) (y axis) versus 14-3-3σ amino acid sequence (x axis). A total of 148 correlation peak intensity ratios are shown. The x axis is not proportional to the sequence length. The helices of 14-3-3σ are identified below the x axis as blue cartoons, while disordered regions are represented by red lines. A diagram of the location of the C-terminal stretch in the sequence of 14-3-3σ is presented above the plot.

2.2.4 Tau phosphorylated by PKA occupies both binding grooves of the 14-3-3 dimer

In previous studies using cross-linking, Sluchanko *et al* identified bands in gel electrophoresis of 14-3-3ζ/Tau-PKA complexes with apparent MW of 80 KDa (suggesting 1:1 stoichiometry), 120 KDa (suggesting 1:2 stoichiometry) and 150 KDa (suggesting 2:2 stoichiometry (Sluchanko *et al.*, 2011)). Joo *et al.*, also hypothesized that the 1-fold improvement on K_d of the peptide containing both pS214 and pS324 sites over peptides containing only one phosphorylation site, could be due to the occupation of both binding grooves of 14-3-3. Nevertheless, the capacity of the full-length Tau-PKA to bind to two monomers of 14-3-3 in solution was never shown experimentally. We therefore decided to get further insights on the Tau-PKA/14-3-3σ complex using AUC-SV. When Tau-PKA and 14-3-

3 σ are mixed in equimolar ratio, it can be clearly seen that the complex is formed but that there is some free Tau-PKA remaining in solution (**Figure 4 A, light blue curve**). On the other hand, when Tau-PKA and 14-3-3 σ are mixed in 1:2 molar ratio, a complex with the same value of sedimentation coefficient is formed and there are no traces of free Tau-PKA in solution (**Figure 4 A, green curve**). In addition, the observed value of weight averaged sedimentation coefficient $s_{w(20,w)}$ of 4.2 S for the 14-3-3/Tau-PKA complex corresponds approximately to the molecular mass of 100 kDa. Given that the theoretical mass for a complex containing one molecule of Tau-PKA (considering 5 phosphorylation sites) and two 14-3-3 molecules is 102.6 kDa, this experiment confirms that in solution Tau-PKA occupies simultaneously both subunit binding sites of a 14-3-3 σ dimer (**Figure 4 B**).

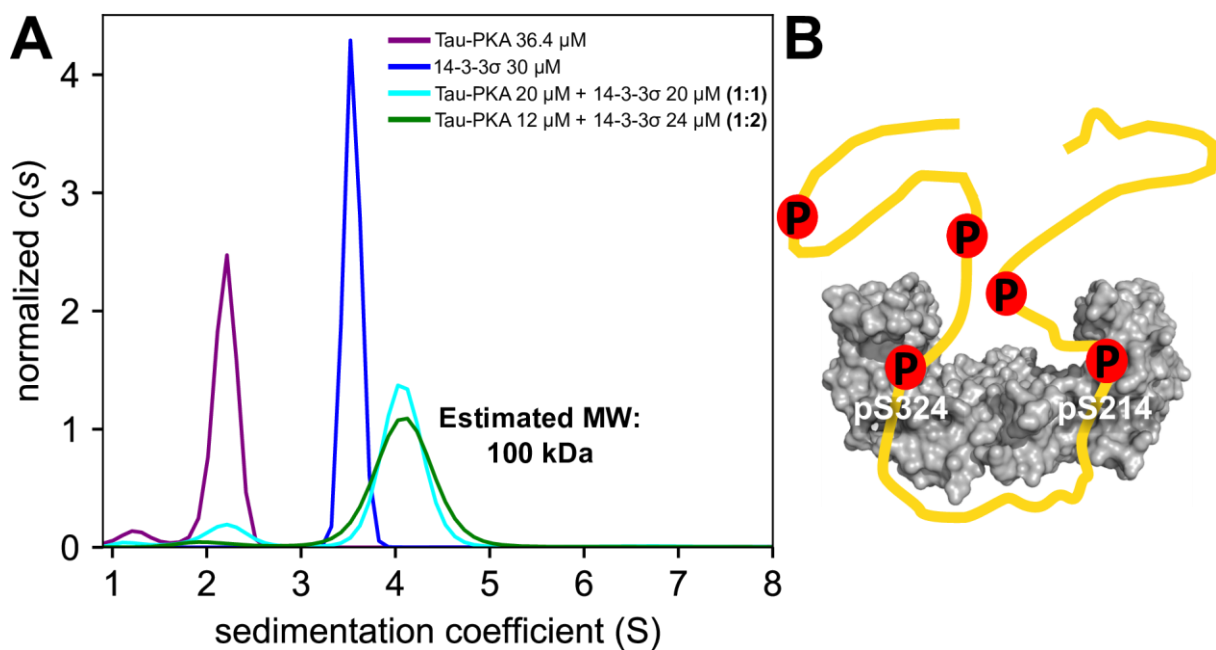


Figure 4 – Tau-PKA occupies both binding grooves of the 14-3-3 dimer. (A) Normalized continuous sedimentation coefficient distributions of Tau-PKA 36 μ M alone (purple), 14-3-3 σ 30 μ M alone (dark blue), Tau-PKA 20 μ M mixed with 14-3-3 σ 20 μ M (light blue) and Tau-PKA 12 μ M mixed with 14-3-3 σ 24 μ M (green). Note that in the mixtures containing both proteins there is the presence of a complex with $s_{w(20,w)}$ of 4.2 S (estimative MW of 100 kDa), confirming that one molecule of Tau-PKA can bind simultaneously both monomers of 14-3-3 σ . (B) Proposed model for the 14-3-3/Tau-PKA protein-protein interaction in which Tau-PKA anchors in each monomer of 14-3-3 with the pS214 and pS324 epitopes.

According to previous NMR studies, the pS214 and the pS324 epitopes are the epitopes of Tau-PKA with the highest affinity for 14-3-3 proteins (Joo et al., 2015). Moreover, these sites are the first to be phosphorylated by PKA (Landrieu et al., 2006) and are the only ones totally phosphorylated by this kinase (Landrieu et al., 2006; Milroy et al., 2015). All this information suggests that when Tau is phosphorylated by PKA, these two epitopes (pS214 and pS324) are the ones anchoring in the amphipathic binding grooves of the 14-3-3 dimer (**Figure 4 B**).

2.2.5 The affinity of the 14-3-3/Tau-PKA interaction is in the low μM range

There are two reported values for the dissociation constant (K_d) of the interaction between Tau-PKA and 14-3-3. In 2009, Sadik *et al* determined the affinity of 14-3-3 ζ for wt-Tau and Tau-PKA by Surface Plasmon Resonance (SPR). They obtained a K_d value of 27.4 ± 1.3 nM for 14-3-3 ζ /PKA-phosphorylated Tau (Sadik et al., 2009). In 2015, the K_d value for the Tau-PKA/14-3-3 σ complex measured by NMR was almost 3 orders of magnitude higher ($K_d = 6.5 \pm 1.9$ μM) (Joo et al., 2015). There is therefore a lack of consensus in literature regarding the affinity of this PPI. Again, this information is of importance when trying to modulate the interaction by small molecules. We decided therefore to determine the K_d of this interaction using two different techniques, AUC-SV and SPR. By titrating 14-3-3 σ with increasing concentrations of Tau and recording the sedimentation profiles of these solutions, a K_d of 1.3 ± 0.2 μM was derived from AUC-SV data (**Figure 5 A**). By injecting increasing concentrations of Tau-PKA over surface-immobilized biotinylated 14-3-3 σ (**Figure 5 B**), a K_d of 12.66 ± 0.47 μM was obtained (**Figure 5 C**). These values which differ in approximately one order of magnitude, suggest that the K_d of the 14-3-3 σ /Tau-PKA is in the low μM range, similarly to what had been determined by NMR ($K_d = 6.5 \pm 1.9$ μM) (Joo et al., 2015). Further SPR experiments were performed in order to evaluate whether there was a difference between the σ and ζ isoforms regarding the affinity for Tau-PKA. A K_d of 1.35 ± 0.46 μM was derived for the 14-3-3 ζ /Tau-PKA interaction (**Table S2**). This value, despite being almost one order of magnitude lower than for the 14-3-3 σ /Tau-PKA interaction determined using the same technique, also falls within the low μM range.

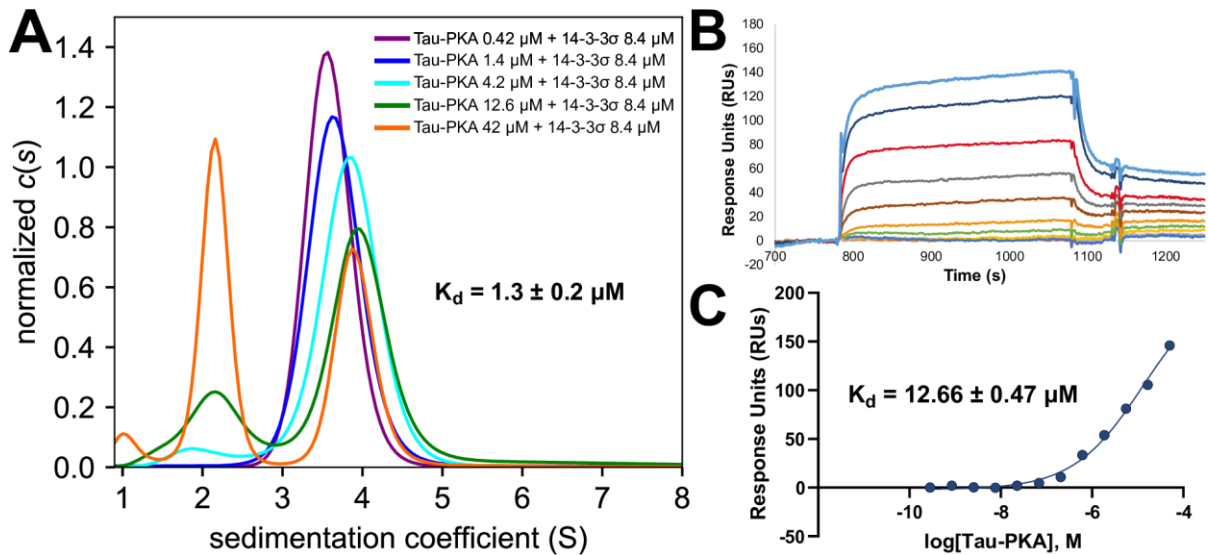


Figure 5 – The dissociation constant of the 14-3-3 σ /Tau PPI is in the low μM range. (A) Area normalized continuous sedimentation coefficient distributions of mixtures of 14-3-3 σ 8.4 μM with 0.42 μM Tau-PKA (purple curve), 1.4 μM Tau-PKA (dark blue curve), 4.2 μM Tau-PKA (light blue curve), 12.6 μM Tau-PKA (green curve) and 42 μM Tau-PKA (orange curve). (B) Example of an SPR sensorgram in which increasing concentrations of Tau-PKA was allowed to flow over a chip containing immobilized biotinylated 14-3-3. The Response Units (RUs) achieved (y axis) are presented in function of the time after the start of the immobilization of 14-3-3, in seconds (x axis). For each curve, the values at equilibrium response (i.e. binding coverage) where extrapolated and fitted in a dose-response curve, shown in (C), against the log of the molar concentration of Tau-PKA.

2.3 Conclusions

Here we elucidate, using a diversified range of biophysical techniques, several important aspects of the interaction of 14-3-3 and Tau-PKA. We first show that the interaction between 14-3-3 and Tau is greatly enhanced by the phosphorylation of Tau by PKA and that the interaction between wt-Tau and 14-3-3 σ is too weak to form a complex in solution detectable by AUC-SV. We further show that, similarly to the peptides surrounding the phospho epitopes of Tau, the full-length phosphorylated Tau + protein seems to only interact with 14-3-3 σ through the amphipathic binding groove. This aspect is an important consideration for the pharmacological modulation of this PPI since it reinforces the strategy already followed in previous work where this PPI was targeted by competitive inhibitors binding to the amphipathic binding groove of 14-3-3 (Milroy et al., 2015).

We also confirm that in solution, Tau phosphorylated by PKA occupies the amphipathic binding grooves of the two monomers of 14-3-3, leading to a low μM affinity interaction. All summed up, our work provides valuable structural insights about the 14-3-3/Tau interaction that can be of great importance for future drug discovery projects aiming at the pharmacological modulation of the 14-3-3/Tau interaction, a promising target for Alzheimer's disease.

2.4 Supporting Information

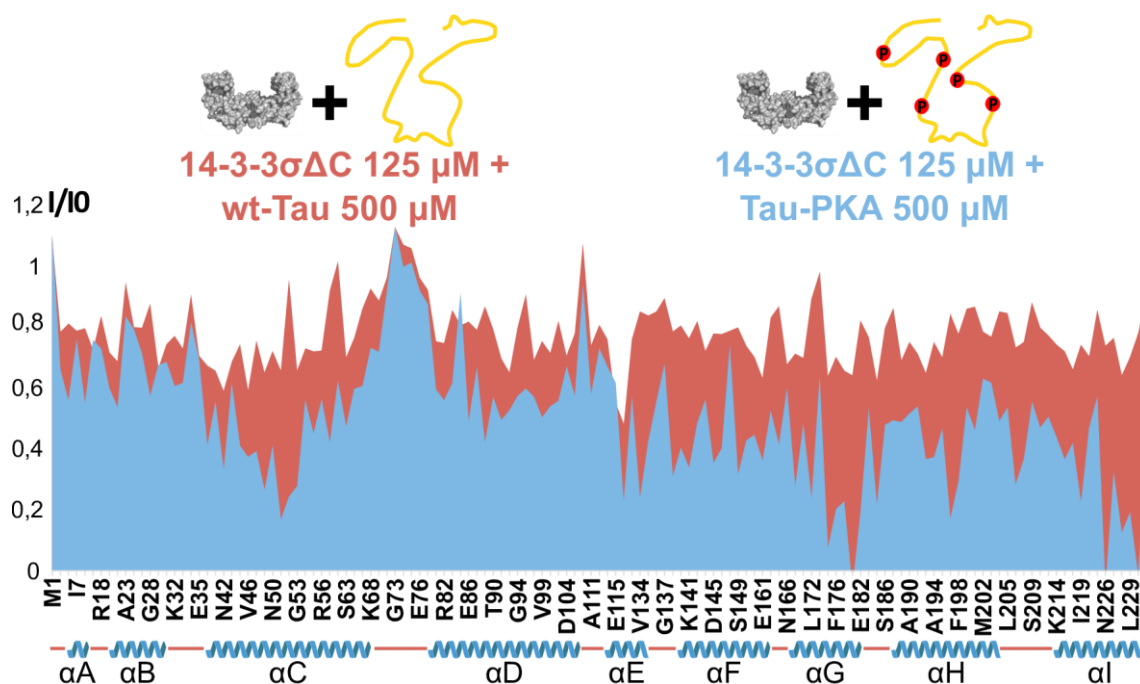


Figure S1 – Plot of the I/I_0 values of ^1H - ^{15}N correlation peak intensities in the spectrum of 125 μM ^{15}N / ^{13}C / ^2H labeled 14-3-3 $\sigma\Delta\text{C}$ in the presence of 500 μM wt-Tau (red plot) and 500 μM full-length Tau-PKA (blue plot) (I) compared to corresponding resonances in the reference spectrum of 125 μM 14-3-3 $\sigma\Delta\text{C}$ (I_0) (y axis) versus 14-3-3 $\sigma\Delta\text{C}$ amino acid sequence (x axis). A total of 135 correlation peak intensity ratios are shown. The x axis is not proportional to the sequence length. The helices of 14-3-3 σ are identified below the x axis as blue cartoons, while disordered regions are represented by red lines.

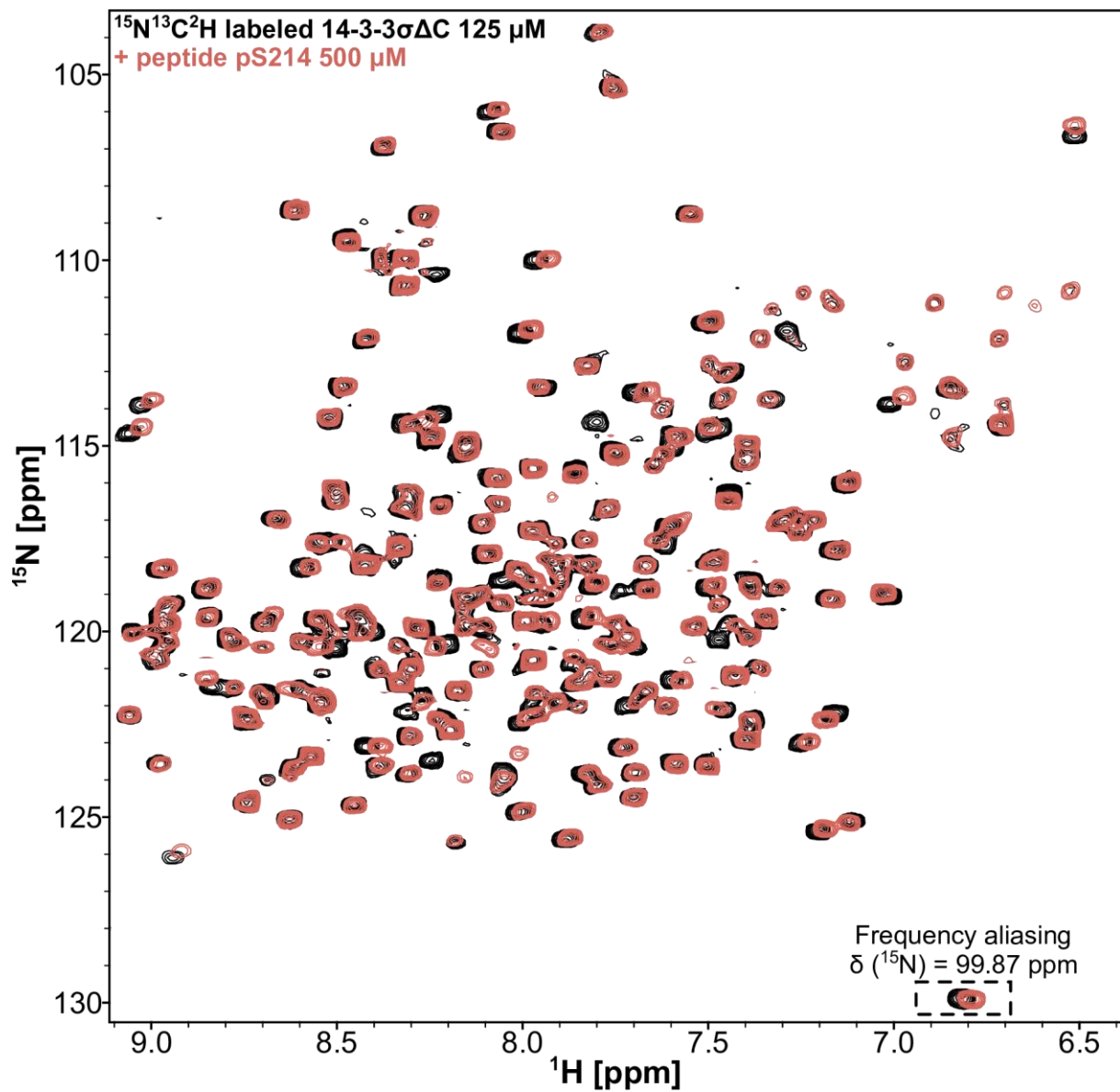


Figure S2 - ^1H - ^{15}N TROSY-HSQC spectra of $^{15}\text{N}^{13}\text{C}^2\text{H}$ labeled 14-3-3 $\sigma\Delta\text{C}$ 125 μM alone (in black), or in the presence of 500 μM Tau peptide surrounding pS214 (superimposed in red).

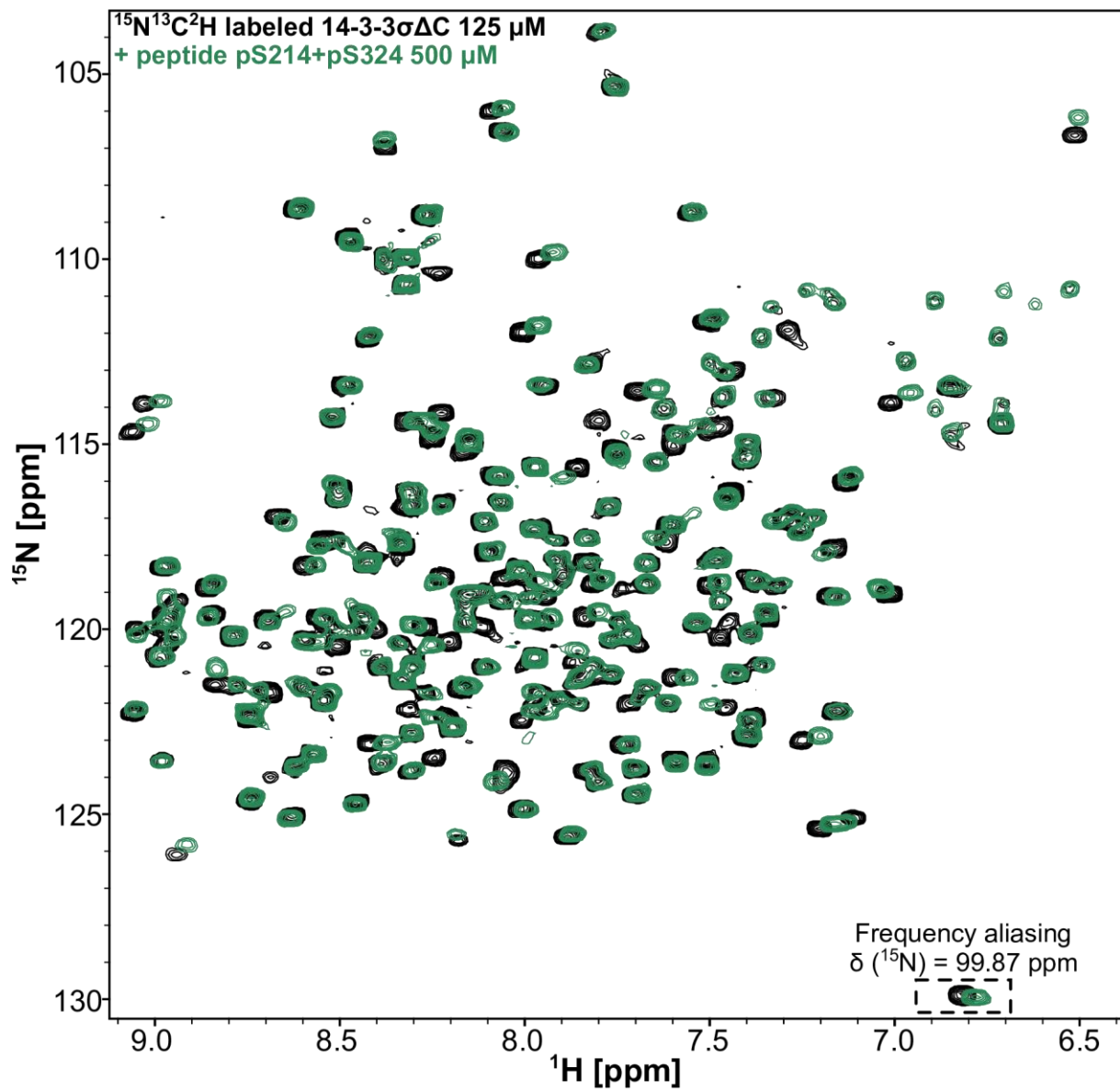


Figure S3 - ¹H-¹⁵N TROSY-HSQC spectra of ¹⁵N¹³C²H labeled 14-3-3σΔC 125 μM alone (in black), or in the presence of 500 μM Tau peptide surrounding pS214 and pS324 (superimposed in green).

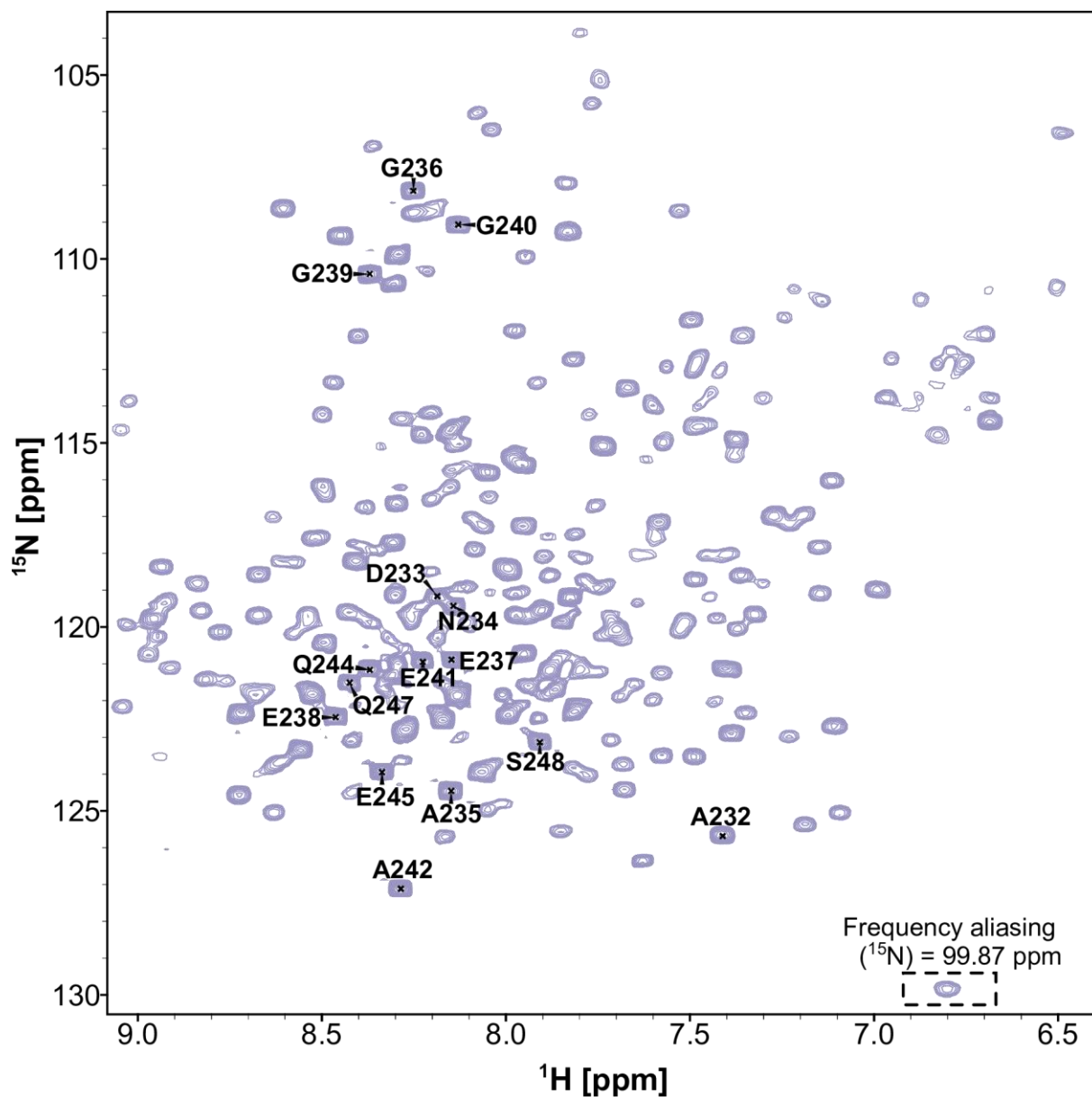


Figure S4 - ^1H - ^{15}N TROSY-HSQC spectra of $^{15}\text{N}^{13}\text{C}^2\text{H}$ labeled full-length 14-3-3 σ 125 μM (purple). The assignments of the ^1H - ^{15}N resonances corresponding to the backbone amide function of the amino acid residues constituting the C-terminal stretch of 14-3-3 σ (residues 232-248) are presented. Note that all these resonances are more intense than the average resonances of the protein's spectrum.

Table S1 –Backbone chemical shift assignments of the C-terminal stretch (residues A232-S248) of 14-3-3 σ .

Residue number	$\delta(^{15}\text{N})$	$\delta(^1\text{H})$	$\delta(^{13}\text{C})$		
	[ppm]	[ppm]	[ppm]		
	N^{H}	H^{N}	C_{α}	C_{β}	CO
A232	125.7	7.410	53.09	18.06	175.3
D233	119.2	8.184	54.27	40.53	173.6
N234	119.4	8.141	52.94	38.50	172.4
A235	124.5	8.150	52.73	18.31	175.7
G236	108.2	8.251	44.85	-	171.6
E237	120.9	8.147	56.00	29.62	174.2
E238	122.5	8.461	56.41	29.50	174.5
G239	110.5	8.369	44.99	-	172.1
G240	109.1	8.124	44.71	-	171.3
E241	120.9	8.147	55.68	29.69	173.4
A242	127.1	8.287	50.03	17.23	-
P243	-	-	-	-	174.3
Q244	121.2	8.369	55.10	29.07	173.2
E245	124.0	8.337	53.96	28.87	-
P246	-	-	-	-	174.3
Q247	121.5	8.425	55.32	29.06	172.7
S248	123.1	7.908	59.54	64.30	-

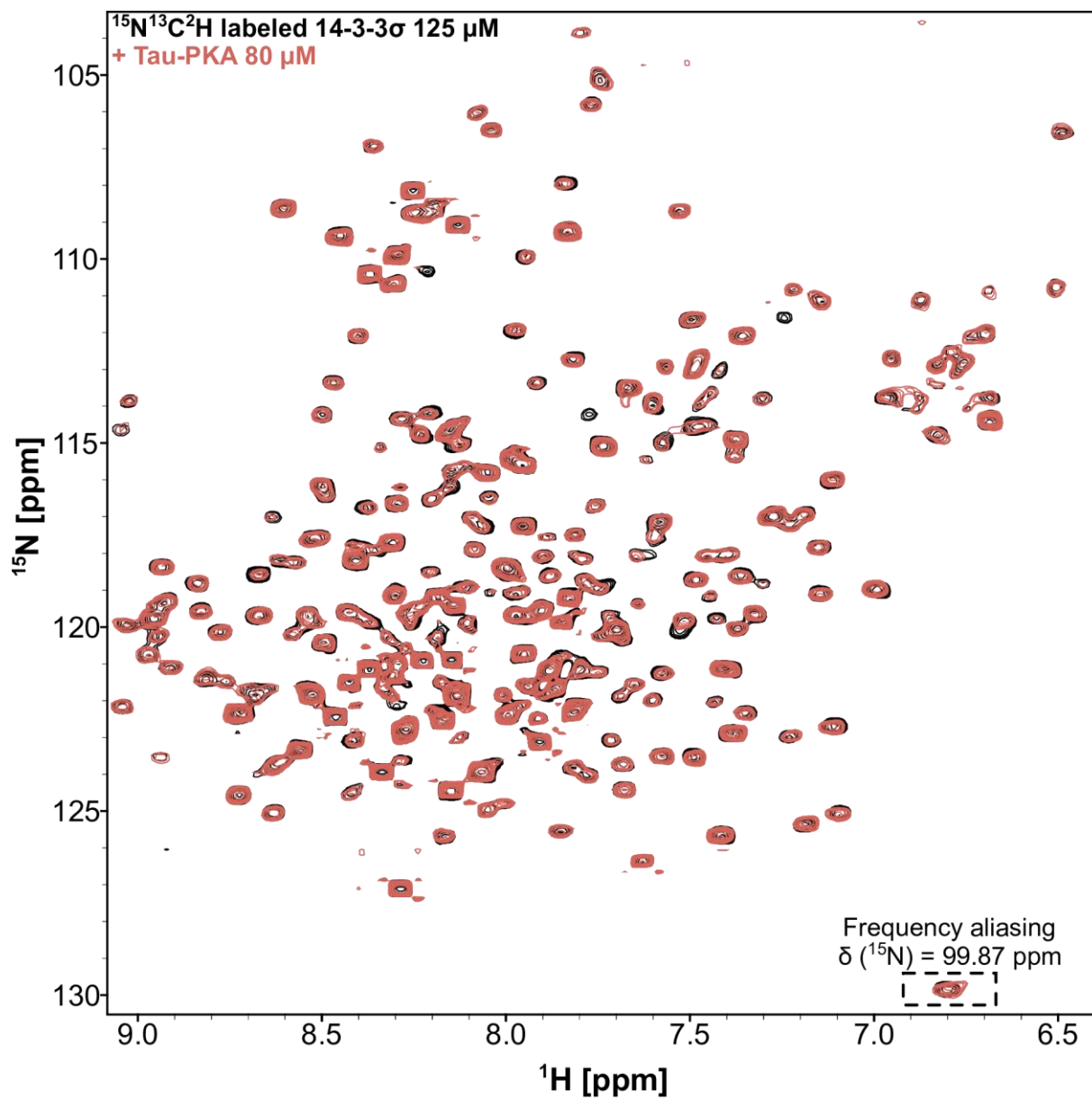


Figure S5 - ¹H-¹⁵N TROSY-HSQC spectra of ¹⁵N¹³C²H labeled full-length 14-3-3σ 125 μM alone (in black), or in the presence of 80 μM Tau-PKA (superimposed in red).

Table S2 – Determination of dissociation constants (K_d) by SPR for the interactions between Tau-PKA with 14-3-3 σ and 14-3-3 ζ .

	14-3-3σ/Tau-PKA	14-3-3ζ/Tau-PKA
First experiment	$K_d = 13.12 \mu\text{M}$	$K_d = 0.883 \mu\text{M}$
Second experiment	$K_d = 12.19 \mu\text{M}$	$K_d = 1.808 \mu\text{M}$
Average	$K_d = 12.66 \pm 0.47 \mu\text{M}$	$K_d = 1.35 \pm 0.46 \mu\text{M}$

3 Adoption of a Turn conformation drives the binding affinity of the p53 C-terminal domain peptides to 14-3-3 σ

3.1 The 14-3-3/p53 protein-protein interaction

p53 is a tumor suppressor protein that plays a key role in the cellular response upon DNA damage (Lakin & Jackson, 1999). p53 is considered as one of the proteins with the tightest link to cancer since mutations on p53 are observed in 50% of human cancers (Freed-Pastor & Prives, 2012). 14-3-3 σ is the isoform of 14-3-3 most considered in regard to cancer (Benzinger et al., 2005; Kaplan, Ottmann, et al., 2017) and was shown to interact with p53 in response to DNA damage. The binding of 14-3-3 σ to the C-terminal domain of p53 was shown to protect the tumor suppressor protein from murine double minute 2 (MDM2)-mediated degradation and nuclear export (Yang, Wen, Chen, Lozano, & Lee, 2003). 14-3-3 σ was also shown to stabilize p53 by promoting its tetramerization (Rajagopalan, Jaulent, Wells, Veprintsev, & Fersht, 2008). The tetramerization of p53 is critical for DNA binding and therefore for the tumor suppressing activity of p53 (Yang et al., 2003).

The phosphorylation of the residue T387, located in the C-terminal domain of p53 was shown to be the binding epitope on 14-3-3. As mentioned in **Introduction - section 1.2**, the co-crystallization of 14-3-3 with the p53 peptide surrounding pT387 revealed a unique binding motif, completely different from the 3 typical 14-3-3 binding motifs (**Introduction - Figure 2 D**). The reason behind this unique interaction interface with 14-3-3 is unknown. Further studies have shown that FC-A is capable of stabilizing this PPI since its pocket is left unoccupied by the p53 peptide (Doveston et al., 2017).

All available information points to the important role of 14-3-3 σ on the upregulation of p53 activity. The stabilization of the 14-3-3 σ /p53 PPI is therefore seen as a promising strategy for targeting cancer.

3.2 Context of the collaboration

Our collaborators synthesized 5 different p53 peptides of different lengths surrounding the pT387 epitope. All 5 peptides (12mer, 14mer, 15mer, 20mer and 32mer) contained the residues that, according to the crystal structure, are essential for the interaction (F385-D393).

It was observed, through ITC and SPR experiments that the affinities of these peptides towards 14-3-3 varied considerably. Given that all peptides contained the fundamental residues for the interaction, they were not able to explain these biophysical studies. We were then contacted in order to find an explanation for this data.

3.3 Manuscript (in preparation)

The manuscript containing this work is, at the moment, in preparation and is presented in the next pages. Our contribution to this work included protein production for NMR experiments, setting up of protein and peptide-based NMR experiments, interpretation of data and writing of the manuscript. In a more detailed way we contributed with:

- RESULTS AND DISCUSSION: NMR spectroscopy of the p53 peptide-14-3-3 σ Δ C17 complexes, NMR spectroscopic studies on the structure of 12mer and 15mer;
- METHODS: 14-3-3 σ protein expression and purification, ^1H - ^{15}N HSQC Spectroscopy on $^{15}\text{N}^{13}\text{C}^2\text{H}$ labeled 14-3-3 σ Δ C17, NMR Spectroscopy on 12mer and 15mer peptides;
- FIGURES: 3, 4, S2, S3, S4, S5, S6;
- TABLES: S1, S2;

Adoption of a Turn Conformation Drives the Binding Affinity of p53 C-Terminal Domain Peptides to 14-3-3 σ

Ave Kuusk^{1,2‡}, João Filipe Neves^{3‡}, Kenny Bravo Rodriguez^{4,5‡}, Richard G. Doveston^{6‡}, Anders Gunnarsson¹, Michael Ehrmann⁵, Hongming Chen¹, Isabelle Landrieu^{3,*}, Elsa Sanchez-Garcia^{4,*}, Helen Boyd^{7,*}, Christian Ottmann^{2,,8,*}

¹ Discovery Sciences, IMED Biotech Unit, AstraZeneca, Mölndal, Sweden

² Laboratory of Chemical Biology, Department of Biomedical Engineering and Institute for Complex Molecular Systems, Eindhoven University of Technology, The Netherlands

³ UMR 8576 CNRS-Lille University, 59000 Villeneuve d'Ascq, France

⁴ Department of Computational Biochemistry, University of Duisburg-Essen, Germany

⁵ Department of Microbiology, University of Duisburg-Essen, Germany

⁶ Leicester Institute of Structural and Chemical Biology and Department of Chemistry, University of Leicester, University Road, Leicester LE1 7RH, UK

⁷ Drug Safety and Metabolism, IMED Biotech Unit, AstraZeneca, Cambridge, UK

⁸ Department of Chemistry, University of Duisburg-Essen, Germany

Keywords: protein – protein interaction, 14-3-3 proteins, p53 protein, surface plasmon resonance, isothermal titration calorimetry, nuclear magnetic resonance, molecular dynamics simulations

ABSTRACT

The interaction between the adapter protein 14-3-3 σ and transcription factor p53 is important for preserving the tumor-suppressor functions of p53 in the cell. A phosphorylated motif within the C-terminal domain of p53 has been shown to be the key for binding to the amphipathic groove of 14-3-3. This motif is unique amongst 14-3-3 binding partners and the precise dynamics of the interaction are not yet fully understood.

Here, we investigate this interaction at the molecular level by analysing the binding of different p53 CTD peptides to 14-3-3 σ using ITC, SPR, NMR and MD simulations. We observed that the disordered character of p53 and its tendency to form a turn play an important role in the binding to the 14-3-3 σ protein. Our study contributes to elucidate the molecular

mechanism of the 14-3-3 σ /p53 binding and provides useful insight for therapeutic discovery and development.

The tumor suppressor protein p53 plays an important role in the cellular response to DNA damage [1, 2]. Activation of p53 upregulates genes involved in cell cycle arrest, DNA repair, senescence and apoptosis [3, 4]. Mutations to p53 occur by several mechanisms and are observed in 50% of all human cancers. These can lead to inactivation of p53 and tumor growth [5, 6].

14-3-3 proteins belong to a family of highly conserved adapter proteins present in all eukaryotic cells [7, 8]. In mammals, seven isoforms with distinct differences in discrete regions have been described: β , γ , ϵ , ζ , η , τ and σ [9, 10]. 14-3-3 proteins bind to phosphoserine- and phosphothreonine motif-containing proteins and regulate their sub-cellular localization, enzymatic activity or interaction with other proteins [11, 12]. Of all the isoforms, 14-3-3 σ has been directly linked to tumor formation [9, 13]. The expression of 14-3-3 σ is down-regulated in several types of cancer including breast cancer, gastric cancer, prostate cancer, lung cancer and ovarian cancer [14]. Significantly, over-expression of 14-3-3 σ has been shown to inhibit the growth of oncogene-expressing cells in nude mice and reduce the transformation and growth of breast cancer cells [15, 16]. 14-3-3 σ is recruited by p53 upon phosphorylation of the transcription factor in response to DNA damage to mediate cell cycle arrest [14, 17]. Its binding to the C-terminal domain of p53 protects the tumor suppressor protein from MDM2-mediated degradation by inhibiting MDM2's ubiquitin ligase activity and blocking the nuclear-exporting activity of MDM2 toward p53 [15, 18]. Tetramerization of p53 is crucial for DNA binding and plays an important role in the regulation of p53's transcriptional activity [19, 20]. 14-3-3 σ facilitates the formation of p53 dimer-dimer interaction thus stabilizing the tumor suppressor protein-DNA binding and potentiating p53's transcriptional activity [15].

The 14-3-3 σ protein has been shown to bind partners containing either a mode 1 (RSXpSXP), mode 2 (RXF/YXpSXP) or mode 3 (pS/TX₁₋₂-COOH) motif (pS representing phosphoserine, X representing any amino acid and –COOH the C-terminus) [21, 22]. The interaction of 14-3-3 with p53 involves phosphorylation of S378, S366 or T387 at the C-terminus of p53 [23, 24]. In 2010 Schumacher et al. reported that p53 binds to 14-3-3 σ via a

distinctive recognition motif, different from the classical 1 and 2 models. This binding enables p53 to establish a rather unique interaction with 14-3-3 σ . The binary crystal structure of 14-3-3 σ in complex with the CTD 9mer peptide of p53 showed that the glycine residue at position +2 of the phosphorylated threonine followed by a proline at position +3 caused a kink in the peptide backbone, resulting 14-3-3 σ binding the peptide in a turn conformation. The extreme C-terminus of p53 peptide is engaged in a salt-bridge with an arginine of 14-3-3 σ and consequently, the p53 peptide occupies only around 2/3 of the 14-3-3 σ peptide-binding channel and forms an interface pocket able to accommodate a small-molecule PPI stabilizer [25]. In 2017 Doveston et al. provided the first evidence that this pocket could indeed be targeted with small-molecules showing that Fusicoccin-A acts as a stabilizer for the 14-3-3 σ - p53 PPI [26].

Further characterization of the molecular and structural basis of the binding of p53 to 14-3-3 σ might give valuable insights into the design of novel PPI stabilizers. To this end we first examined the effect of the p53 peptide length on binding to 14-3-3 σ by measuring the binding affinities of 9mer, 12mer, 14mer, 15mer, 20mer and 32mer peptides of p53 CTD using isothermal titration calorimetry (ITC) and surface plasmon resonance (SPR) assays. The biophysical data demonstrated that the 15mer peptide bound the 14-3-3 σ protein more tightly as compared to 12mer peptide, which surprisingly did not show any binding activity to the protein when analyzed by ITC, despite its presence in binary complexes successfully used for protein crystallography. This indicated the possibility that variations in the length of p53-derived peptides have a significant influence on the binding affinity to 14-3-3. Nuclear magnetic resonance (NMR) and molecular dynamic simulation analysis were performed to further provide a structural rationale for this observation. The analysis of the NMR experiments and the MD simulations indicated that the binding affinities of the peptides are related to the disordered character of p53 and its propensity to form a dynamic turn.

Such a finding could reveal important insights into the molecular characteristics of this PPI. Furthermore, it has implications for *in vitro* assay and structure-based drug design as modulation of this or indeed other PPIs mature as therapeutic strategies.

RESULTS AND DISCUSSION

Analysis of peptide binding affinity to 14-3-3 by ITC and SPR

ITC experiments were performed to measure the thermodynamic characteristics of the 14-3-3 σ – p53 PPI and to compare the binding constants of p53 peptides of different lengths to 14-3-3 σ . Mono-phosphorylated 9mer, 12mer, 14mer, 15mer, 20mer and 32mer peptides (Table 1) were titrated stepwise into a solution of 14-3-3 σ protein at fixed concentration. The saturation curve was fitted to a single-site binding model. The thermodynamic parameters and dissociation constants obtained are summarized in Figure 1a, 1b and S1. To our surprise, the ITC data revealed that both 9mer and 12mer peptides do not show any binding to the protein. Binding of the 15mer, 20mer and 32mer peptides to 14-3-3 σ was in the same order of magnitude with affinity constants of 25.7, 61 and 13.6 μ M, respectively. This indicated that three additional positively charged amino acid residues (R379, H380 and K381) at the N-terminus of the 15mer peptide have a significant positive effect on the binding affinity to 14-3-3 σ . In addition, the deletion of R379 alone already remarkably reduced the binding affinity of the 14mer peptide, to a K_d of 119.6 μ M. The thermodynamic parameters (ΔH , $T\Delta S$) of the binding of the 14mer and the 15mer to 14-3-3 σ indicate that the increase in binding affinity is mainly due to the more negative enthalpy change (ΔH) upon the addition of one amino acid residue. In contrast, calorimetric studies clearly indicate that the binding of weaker binders (14mer and 20mer) is largely driven by the increase of entropy associated with the formation of hydrophobic interactions upon binding to 14-3-3 σ (Figure 1b).

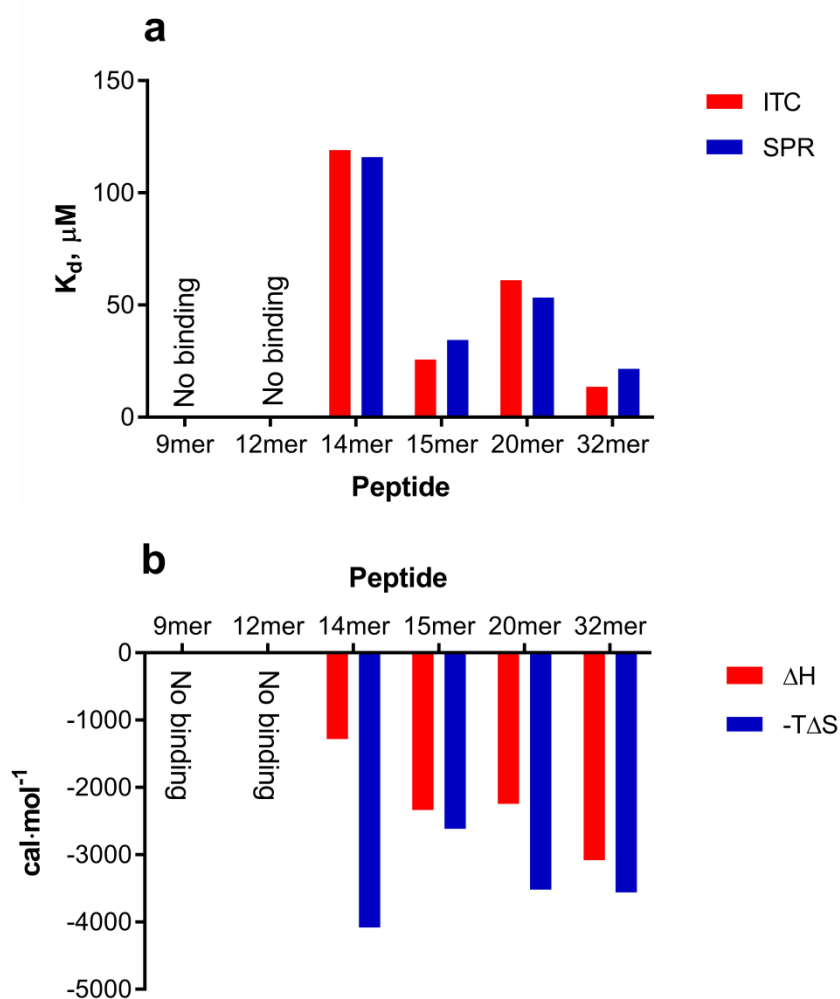


Figure 1 - Dissociation constants (a) and thermodynamic parameters (b) obtained by ITC and SPR.

To confirm and further characterize the binding data obtained by ITC, a surface plasmon resonance (SPR) assay was employed. To this end, the 14-3-3 σ protein was covalently immobilized on the sensor surface. Data obtained from the injection of 9mer, 12mer, 14mer, 15mer, 20mer and 32mer peptides of p53 over the protein-bound surface was fitted to a nonlinear regression model and dissociation constants were calculated (Figure 1a, 2). Dissociation constants measured by SPR were in a good agreement with the values determined by ITC. SPR experiments confirmed the positive effect of R379, H380 and K381 residues in the peptide on the binding affinity to the protein.

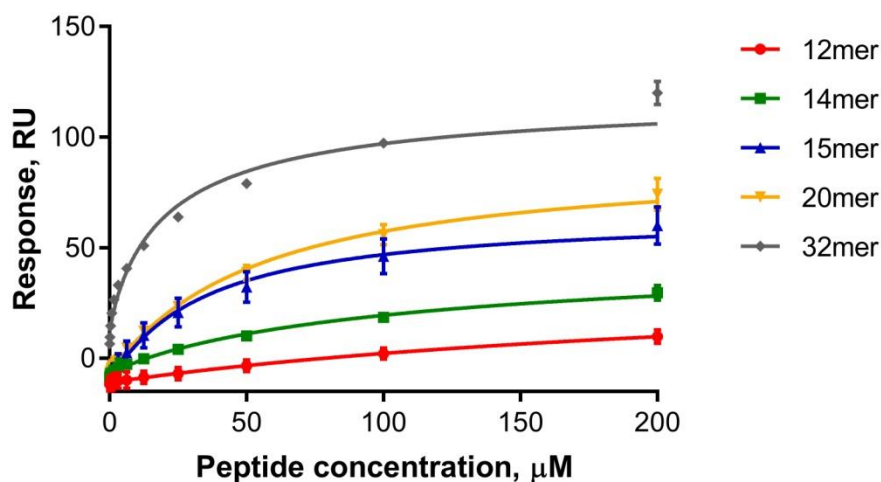


Figure 2 - SPR dose-response curves of 12mer, 14mer, 15mer, 20mer and 32mer peptides of p53. Data shown are mean of three separate experiments.

NMR spectroscopy of the p53 peptide-14-3-3 σ Δ C17 complexes

Because the K_d values linked to various lengths of p53 peptides could not be directly rationalized from the crystal structure of 14-3-3 σ with the 12-mer, an NMR analysis of the complexes formed by $^{15}\text{N}^{13}\text{C}^2\text{H}$ labeled C-terminally truncated 14-3-3 σ (14-3-3 σ Δ C17) and p53 CTD peptides was initiated. 2D ^1H - ^{15}N HSQC spectra of 14-3-3 σ Δ C17 were recorded in the presence and absence of each p53 peptide in order to get further insights on the complex formation. The experiments were performed for the 12mer, 14mer, 15mer, 20mer and 32mer, all at a molar stoichiometry of 1:2.5 for 14-3-3 σ Δ C17:peptide. The intensities of the correlation peaks corresponding to specific amino acid residues along the 14-3-3 σ Δ C17 sequence (I) were monitored in NMR spectra of 14-3-3 σ Δ C17 in the presence of each peptide and compared to the intensities of the same correlation peaks in the spectrum of 14-3-3 σ Δ C17 alone (I_0). The addition of each p53 peptide similarly led to peak broadening for a discrete number of resonances in the spectra of 14-3-3 σ Δ C17 (Figure 3, S2). The intensities of resonances corresponding to amino acid residues remote from the phospho-binding pocket remained unaffected and similar to the control spectrum ($I/I_0 \approx 1$) (Figure 3a and 3c, S3). In contrast, the I/I_0 ratio of resonances corresponding to amino acid residues located in, or close, to the phospho-anchoring region of the amphipathic binding groove decreased (Figure 3b, 3d and

S3). Figure 3b illustrates that the magnitude of the decrease of the I/I₀ ratio of the affected peaks was different, depending on the added peptide. The I/I₀ decrease was higher when the protein was exposed to the 32mer, followed by the 15mer, the 20mer, the 14mer, and finally by the 12mer. This series reversely correlates with the measured binding affinities, with the lowest K_d for the 32mer inducing the highest decrease of intensity. This is not unexpected as the magnitude of the broadening of correlation peak intensities, and therefore the drop of the I/I₀ ratio, is proportionally correlated with the amount of 14-3-3σΔC17 bound to peptide in solution during the acquisition period. In other words, the comparison of the amplitude of resonance broadening among the spectra allowed us to establish a ranking that matched the ranking of K_d values obtained by SPR and ITC (K_d 12mer>14mer>20mer>15mer>32mer). Therefore, these experiments confirmed that the 32mer is the peptide with the highest affinity to 14-3-3, followed by the 15mer, the 20mer, the 14mer and the 12mer.

In addition, the plots in Figure 3e showed that I/I₀ profiles obtained by NMR are similar for all the peptides, establishing that the binding interface is conserved. This result also suggested that the longer peptides did not establish extra-contacts with the protein when compared to the 12mer, which could have explained the measured variation in the K_d. This observation led us to consider that the basis for the differences in the binding affinities may not rely on the bound-peptide in the complex, but rather on the properties of the free-peptide.

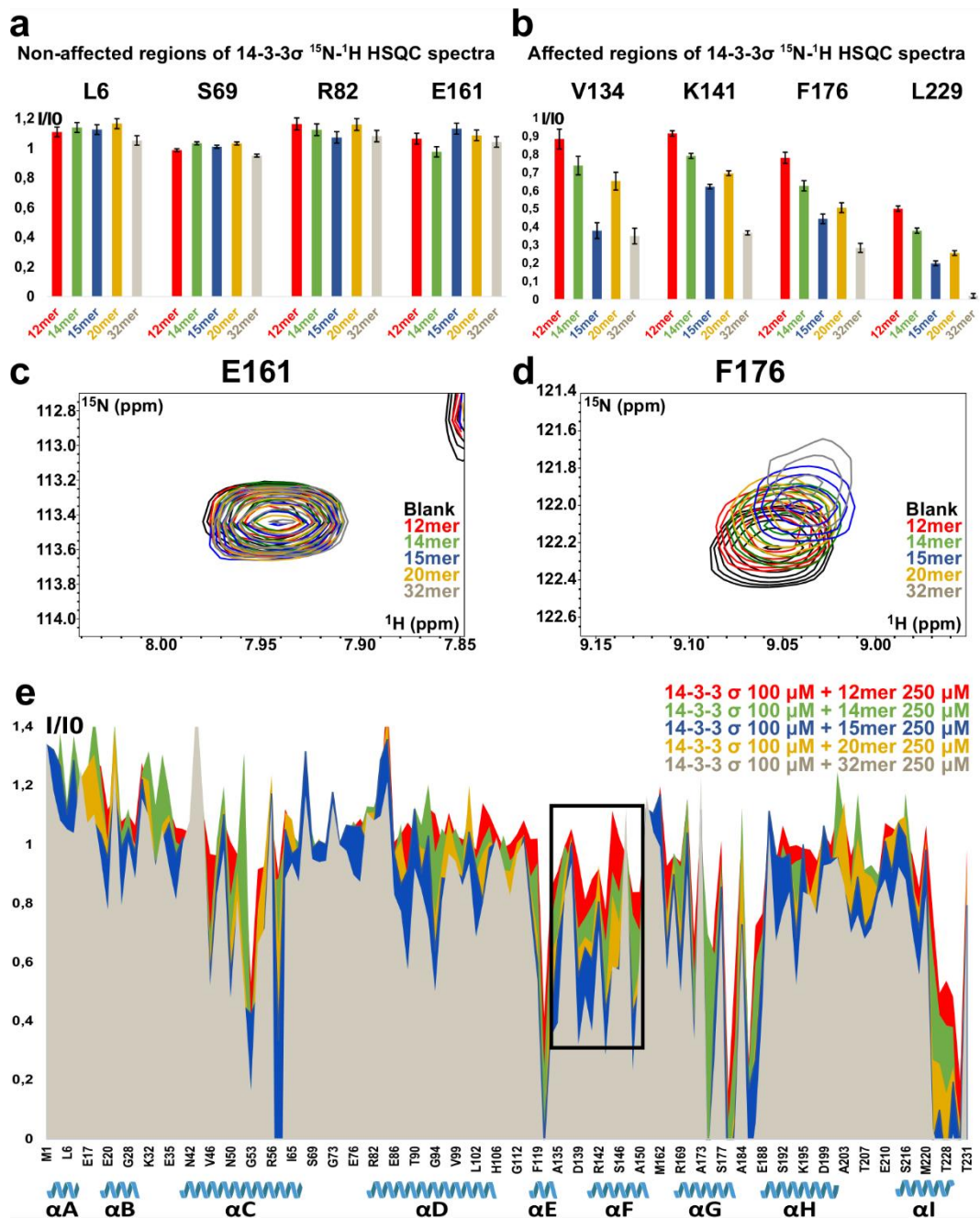


Figure 3 - Interaction of p53 peptides with 14-3-3 σ Δ C17. Plot of the ratios of the bound (I)/free (I0) ^1H - ^{15}N HSQC correlation peak intensities of individual resonances corresponding to residues of the protein, remote from the interaction site (a) or close to the interaction site (b), in the presence of 12mer (red bar), 14mer (green bar), 15mer (blue bar), 20mer (yellow bar) and 32mer (grey bar). Error bars of I/I0 ratios were calculated based on the maximum noise estimate of each spectrum. The intensities of peaks shown in panel (c) were not altered when 14-3-3 σ Δ C17 was exposed to any of the peptides (a). To the contrary, in panel (d), broadening of resonances due to the presence of each peptide lead to decrease of I/I0 ratios (b), with the highest decrease for the 32mer, followed by the 15mer, the 20mer, the 14mer and the 12mer. (c) Enlarged region of overlaid ^1H - ^{15}N HSQC spectra showing an individual resonance corresponding to residue E161 (remote from the binding site, see panel a) of: in black:

14-3-3 σ Δ C17 and overlaid in red, green, blue, yellow, gray: 14-3-3 σ Δ C17 in the presence of the 12mer, 14mer, 15mer, 20mer and 32mer peptide, respectively. (d) same as (c) for an individual resonance corresponding to residue F176 (close to the binding site, see panel (b)). Note that the extent of the chemical shift perturbation caused by the peptides was higher for the 32mer, followed by the 15mer, the 20mer, the 14mer and the 12mer. The intensities of peaks shown in panel (c) were not altered when 14-3-3 σ Δ C17 was exposed to any of the peptides (a). To the contrary, in panel (d), broadening of resonances due to the presence of each peptide lead to decrease of I/I0 ratios (b), with the highest decrease for the 32mer, followed by the 15mer, the 20mer, the 14mer and the 12mer. (e) Plot of the ratios of the bound (I)/free (I0) ^1H - ^{15}N correlation peak intensities of 14-3-3 σ Δ C17 (y axis) versus the amino acid sequence (x axis) in the presence of 12mer (red plot); 14mer (green plot); 15mer (blue plot), 20mer (yellow plot) and 32mer (gray plot). A total of 136 correlation peak intensities are shown. The x axis is not proportional. The helices of 14-3-3 σ Δ C17 are identified below the x axis. The squared region of the plot best exemplifies the gradual increase in broadening of specific resonances in 14-3-3 σ Δ C17 spectra, induced by the series of peptides. The concentration of 14-3-3 σ Δ C17 in all the experiments was 100 μM and the concentration of peptide, 250 μM .

NMR spectroscopic studies on the structure of 12mer and 15mer

Although the NMR interaction experiments strikingly confirmed the ranking of relative affinities observed for the peptides by both ITC and SPR, these experiments did not provide any indication to explain the differences in affinities, as contact surfaces were not modified from one peptide to the other. As the difference could not be found at the interface, we reasoned that it could arise from the conformational properties of the peptide itself, which could also affect the interaction. We thus next performed a set of NMR experiments directed at the 12mer and 15mer free peptides, in order to investigate whether distinct conformational propensity could be observed and potentially be linked to the differences in the binding affinity to 14-3-3 σ Δ C17. The recorded spectra, based on ^1H and natural abundance of ^{15}N or ^{13}C of the unlabeled peptides, allowed us to obtain chemical shift assignments (Tables S1, S2). The chemical shift values of $^{13}\text{C}\alpha$ and $^{13}\text{C}\beta$ were first used as an indication of the presence of local secondary structure, as these values are linked to the dihedral angles of each amino-acid residue. Calculation of the Secondary Structure Propensity scores (Figure S4) showed a tendency to adopt β -strand conformation (negative scores), although the chemical shift values clearly indicated that both peptides had a dynamic disordered structure. The SSP score profile along the sequence of the 12mer and 15mer peptides was found to be different, an

unexpected observation for short peptides with high dynamics that usually lead to averaging of the NMR parameters. An additional NOESY spectrum was thus used to search NOE contacts between the atoms of the peptides in solution, indicative of spatial proximity (Figure 4a) and potential local dynamic structuration. Interestingly, in both peptides, the presence of three NOEs between protons of non-sequential residues confirmed that their structures are not completely disordered (Figure 4a). NOE cross-peaks could be observed between the H α of F385 and the HN of pT387, between the HN of pT387 and the HN of G389 and finally between the H α of G389 and the HN of D391 (Figure 4a). This data suggested that among the multiple conformations experienced by these predominately disordered peptides in solution, there was formation of a dynamic turn, whose prevalence is however high enough to be detected by NMR. This NOE profile seemed well-correlated with the position of these atoms in the crystal structure of 14-3-3 σ in complex with the 12mer (Figure 4b). This fact suggested that in solution, a population of the peptides has a bended conformation that is compatible with the one observed in the crystal structure (PDB ID: 5MHC) [26].

We observed in the dynamic ensemble of peptide conformations a tendency to adopt a bended conformation, involving residues pT387 to D391. In addition, β -strand propensity is observed along the peptide sequence. This conformational preference is in line with the unbalanced charge distribution, with four positive charges in the first N-terminal half matched by four negative charges in the C-terminal half, including pT387, in the 15mer. The presence of the turn suggested that electrostatic contribution allowed the peptide to fold on itself, forming a dynamic short β -sheet. The 12mer, in contrast, lost the three first positive charges, inducing a charge unbalance that could explain the observed smaller propensity to adopt the turn conformation. Accordingly, the normalized intensities of the three medium range NOEs that identify the turn were higher for the 15mer than for the 12mer (Figure 4c), suggesting that the population of this bended conformation in solution is higher on the 15mer than on the 12mer.

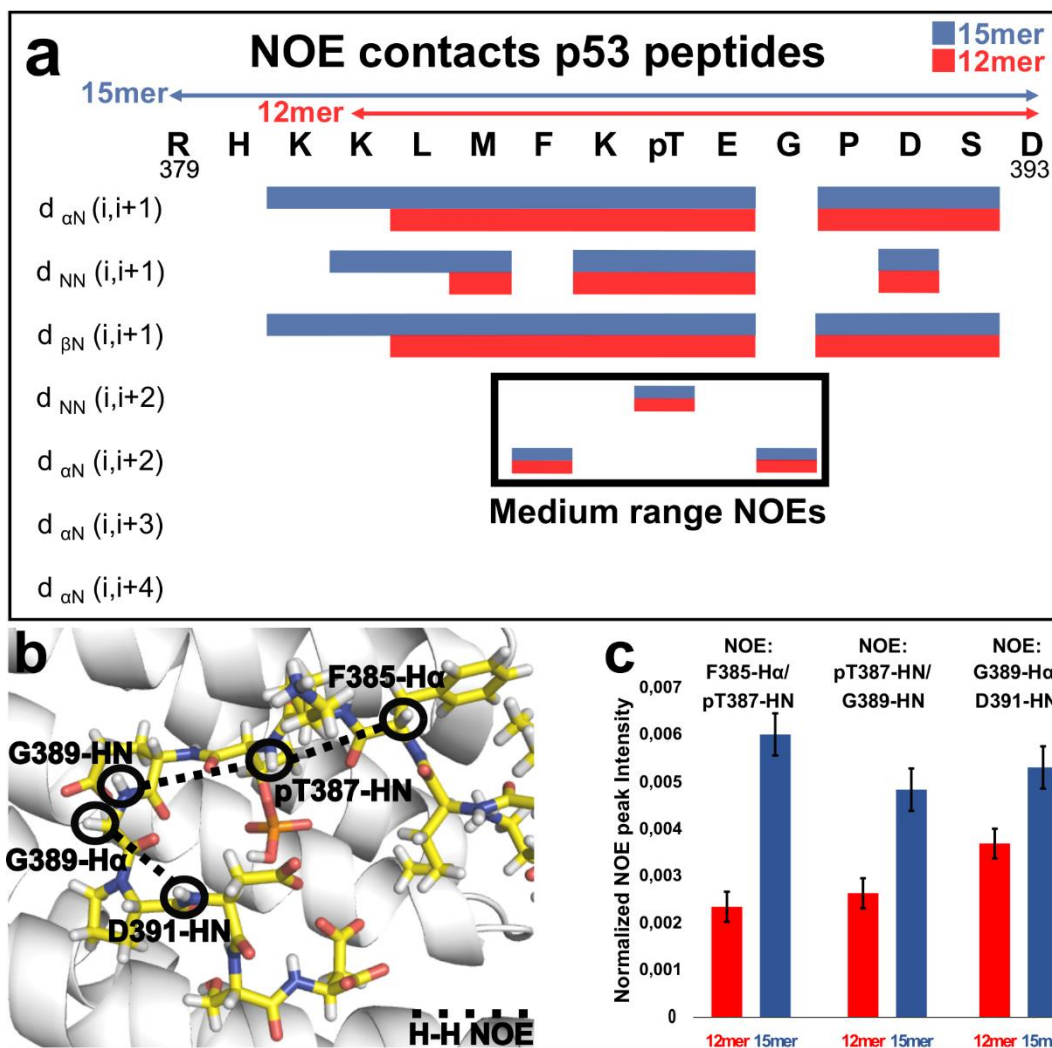


Figure 4 - Peptides adopt a conformation in solution that corresponds to the 14-3-3 binding conformation. (a) NOE summary diagram for 15mer (in blue) and for 12mer (in red) in 100 mM Sodium Phosphate, 50 mM NaCl, pH 6.8 at 4°C. NOE intensities were classified as strong (for sequential NOEs) and weak (for non-sequential NOEs) and are proportional to bar thickness. Sections of NOESY spectra are presented in S5 and S6. (b) Detailed view of the amphipathic binding groove of 14-3-3 σ (white cartoon representation) in the presence of 12mer (yellow sticks representation) on the crystal structure (PDB ID: 5MHC) [26]. The atoms involved on the mid-range NOEs are surrounded by a black circle and identified on the structure. The NOE profile of the peptides in solution seems well correlated with the position of the atoms on the crystal structure. (c) Plot of the normalized intensities of the NOE correlation peaks for medium range NOEs (F385-H α /pT387-HN; pT387-HN/G391-HN; G391-H α -D393-HN) for the 12mer (red bars) and for the 15mer (blue bars). The intensities of the peaks are normalized to the intensity of the diagonal peak on the NOESY spectrum corresponding to the HN of pT387. The most intense cross-peak for each medium-range NOE was used for the intensity calculation. Error bars of I/I₀ ratios were calculated based on the maximum noise estimate of each spectrum. The bars show that the intensities of all the medium-range NOEs are higher for the 15mer.

Molecular dynamics (MD) simulations of 12mer and 15mer peptides

As the NMR data suggested a preferential turn conformational for the 15-mer peptide in solution, additional MD experiments were used to explore the 14-3-3 σ -bound or free in solution, 12-mer and 15-mer peptide conformations. As a first step, to characterize the 14-3-3 σ – peptide binding we performed MD simulations for the 14-3-3 σ – 12mer and 14-3-3 σ – 15mer complexes (see details in the SI). The MD simulations revealed subtle differences in the interaction pattern of the 12mer and 15mer complexes with 14-3-3 σ that confirmed the hypothesis that the improved binding of the 15mer could be related to the differential conformations explored by the peptides in solution. To pursue this issue, MD simulations were started for each peptide under two different setups. In one case the initial structure of the peptide was the conformation found when the peptide is bound to 14-3-3 σ (bound conformation) and in the other simulation setup an extended conformation of the peptide was used (see Computational details). For the 12mer peptide, the MD simulations in the absence of 14-3-3 σ show the peptide adopting conformations similar to the 14-3-3 σ bound conformation (RMSD less than 0.8 Å, Figure S8) in 1 and 16% of the trajectories starting in the bound and extended conformation, respectively. When the peptide adopts geometries different to the 14-3-3 σ bound conformation, intra-molecular interactions between the N and C-terminus of the peptide are scarce. The interaction Kp386NZ – Dp391CG is found in 38% of the trajectory starting from the bound conformation and in only 10% of the trajectory starting from the extended conformation (Figure S9). In the case of the 15mer, both simulations show the peptide adopting the 14-3-3 σ bound conformation in 67% and 13% of the trajectories for simulations starting from the bound and extended conformation, respectively. For the trajectory starting from the bound conformation, the Kp386NZ – Dp391CG interaction is found in 79% of the trajectory frames. Conversely, in simulations starting from the extended conformation the Kp386NZ – Dp391CG interaction is not established and Kp386 interacts with pTp387. The simulation starting from the bound conformation shows that, in the absence of 14-3-3 σ , the 15mer peptide may establish a stabilizing intra-peptide interaction network not found in the 12mer (Figure 5).

To further explore how accessible is the bound conformation to both peptides in the absence of 14-3-3 σ , we performed free energy calculations using the ABF [27] formalism and

the RMSD value of the backbone atoms of residues Kp386 to Dp391 as the collective variable. The 14-3-3 σ bound conformation was taken as the reference structure to calculate the RMSD values. The average RMSD value for the MD simulations of the 14-3-3 σ -peptide complexes was approximately 0.6 Å (Figure S8). The obtained potential of mean force (PMF) is shown in Figure 5b. Our results indicate that the adoption of a bound-like conformation is more favorable in the 15mer than in the 12mer. For the 12mer, the minimum in the PMF closer to the bound structure has a ΔG value of 2.2 kcal/mol at a RMSD value of 1.4 Å. In the case of the 15mer, there are two minima below 1.4 Å. The first minimum is located at 1.2 Å and has a ΔG value of only 0.7 kcal/mol. The second minimum is shallower than the first and it is located at 0.9 Å with a ΔG value of 1.4 kcal/mol. Even more, for the 12mer the barrier to reach the minimum is 2.8 kcal/mol while for the 15mer the maximum barrier to reach the two minima below 1.4 Å is 1.6 kcal/mol. The ABF calculations showed that, although the bound-like conformation is not the most stable conformation for the peptides in solution, it is more accessible for the 15mer than for the 12mer.

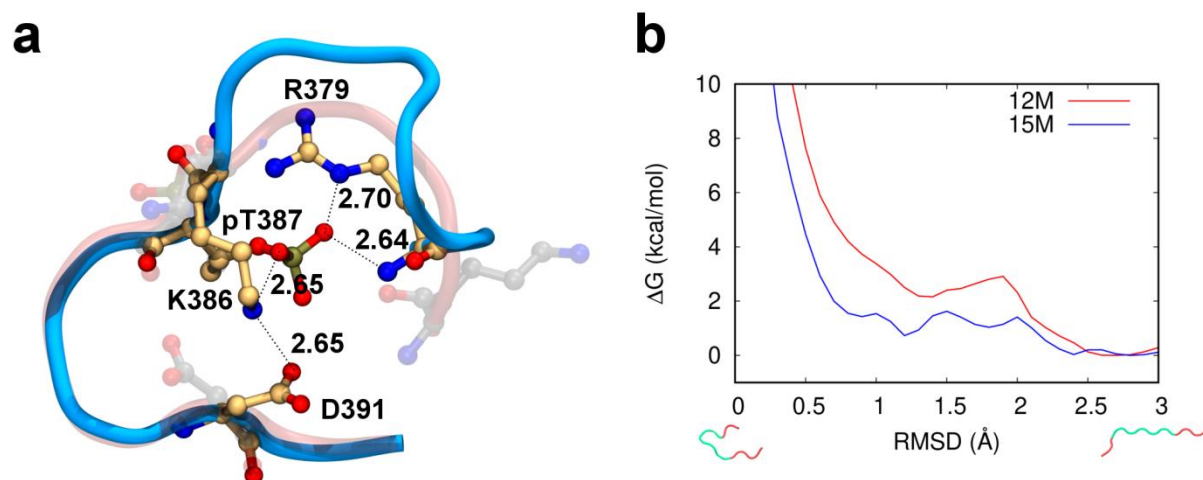


Figure 5 - (a) R_p379 helps to stabilize the 14-3-3 σ bound-like conformation during the MD simulation of the 15mer in the absence of 14-3-3 σ . The populations for the interaction between R_p379 and pT_p387 are 55% and 0% for the simulations starting from the bound and extended conformation, respectively. The populations for the interaction between K_p381 and pT_p387 in the 12mer are 35% and 3%. In the figure the 15mer is shown in blue with carbon atoms in orange while the 12mer is shown in transparent-red with carbon atoms in transparent-gray. Distances are in Å. (b) PMF profile for the conformational change between the bound-like and the extended conformation in the peptides. The bound-like and extended conformations for the 12mer are shown below the

RMSD axis. The backbone atoms of residues colored in green (K_p386 to D_p391) are the ones used for the calculation of the RMSD.

The MD simulations of the peptide in solution support the NOE data suggesting the formation of a dynamic turn since the calculations indicate that the 15mer has higher propensity to form a loop (residues K_p386 to D_p391) than the 12mer, which is related to R_p379 favoring an interaction network involving residues K_p386, pT_p387 and D_p391. This network stabilizes the turn conformation. We concluded that conformational selection, at least in part, drives the binding of the p53 peptide to 14-3-3 σ , and that the ability of the p53 peptide to adopt a conformation close to that in the bound state is related to the preferential binding. Our study provides the first detailed molecular and structural characterization of this important PPI. NMR and MD simulations indicated that the disordered character of p53 and its propensity to form a dynamic turn might be a driving force of the unpredictable binding affinities of different lengths of p53 peptides as observed in SPR and ITC. These results might broaden our understanding of 14-3-3/p53 PPI and give valuable insights for further structure-based drug design.

METHODS

14-3-3 σ protein expression and purification

His₆-tagged full-length 14-3-3 σ protein for ITC and SPR was expressed in NiCo21 (DE3) competent cells with a pProExHTb plasmid and purified using Ni⁺² affinity chromatography according to well established procedures. 14-3-3 σ protein was dialysed against ITC buffer (25 mM HEPES pH 7.5, 100 mM NaCl, 10 mM MgCl₂, 0.5 mM TCEP) or a standard buffer (10 mM HEPES pH 7.5, 150 mM NaCl, 0.1% Tween 20).

The ¹⁵N¹³C²H labeled 14-3-3 σ Δ C17 protein for NMR studies was expressed in *E. coli* BL21 (DE3) cells transformed with a pProExHtb vector carrying the cDNA to express an N-terminally His₆-tagged human 14-3-3 σ Δ C17. A 20 mL pre-culture in *Luria–Bertani* (LB) medium containing 100 mg/L ampicillin was grown overnight at 37°C and was used to inoculate 1 L of deuterated M9 minimal medium supplemented with 2 g/L ¹³C₆²H₇ Glucose, 1 g/L ¹⁵N Ammonium Chloride, 0.4

g/L Isogro ¹⁵N¹³C²H Powder – Growth Medium (Sigma Aldrich) and 100 mg/L ampicillin. The culture was grown at 37°C to an OD₆₀₀ of 0.9 and induced with 0.5 mM isopropyl-β-D-Thiogalactopyranoside (IPTG). Incubation was continued for 15h at 28°C. Cells were harvested by centrifugation and the protein was then purified by affinity chromatography using a Ni-NTA column (GE Healthcare). The N-terminal His₆-tag was then cleaved by the tobacco etch virus (TEV) protease for 2 hours at 20°C, followed by 12 hours at 4°C, while being dialyzed against 100 mM sodium phosphate and 50 mM NaCl, pH 6.8 (NMR buffer). The molar ratio between 14-3-3σΔC17 and TEV protease was 50:1. The 14-3-3σΔC17 protein without His₆-tag was collected in the flow-through of a Ni-NTA column, using NMR buffer for the elution, while the uncleaved fraction and the His₆-tag peptide were retained on the column.

Peptide synthesis and purification

CTD Thr387 phosphorylated 9mer, 12mer, 14mer, 15mer and 20mer peptides of p53 were synthesized by Fmoc solid phase chemistry using an Intavis MultiPep RSi peptide synthesizer and purified using a preparative LC-MS on a reverse-phase C18 column (Atlantis T3 prep OBD, 5 μm, 150 x 19 mm, Waters). The purification was conducted using a 17-21% gradient of acetonitrile in water (with 0.1% trifluoroacetic acid) over 12 min at 20 mL min⁻¹. CTD Thr387 phosphorylated 32mer peptide was obtained from commercial sources. Peptide sequences are summarized in Table 1. LC-MS analysis for 12mer, 14mer, 15mer and 20mer peptides is shown in SI.

Table 1 - Peptide sequences

Peptide	Sequence
9mer	H ₂ N-FK(pT)EGPDSD-COOH
12mer	H ₂ N -KLMFK(pT)EGPDSD-COOH
14mer	H ₂ N -HKKLMFK(pT)EGPDSD-COOH
15mer	H ₂ N -RHKKLMFK(pT)EGPDSD-COOH
20mer	H ₂ N -GQSTSRHKKLMFK(pT)EGPDSD-COOH
32mer	H ₂ N-SRAHSSHLKSKKGQSTSRHKKLMFK(pT)EGPDSD-COOH

Isothermal titration calorimetry (ITC)

Isothermal titration calorimetry (ITC) experiments were performed using Malvern MicroCal ITC200 and MicroCal Auto-iTC200 instruments. Binding experiments were carried out at 25°C in ITC buffer (25 mM HEPES pH 7.5, 100 mM NaCl, 10 mM MgCl₂, 0.5 mM TCEP). 2 µL aliquots of 1 mM (12mer, 15mer, 20mer) or 2 mM (9mer, 14mer, 32mer) p53 peptide were titrated stepwise into the sample cell containing 0.1 mM (12mer, 15mer, 20mer) or 0.05 mM (9mer, 14mer, 32mer) of 14-3-3σ.

1% v/v DMSO was added to both cell and titrant. The dissociation constant (K_d), binding enthalpy (ΔH) and entropy (ΔS), Gibbs free energy (ΔG) and binding stoichiometry (n) were calculated using nonlinear least square regression analysis with Origin 7.0.

Surface Plasmon resonance (SPR)

SPR experiments were performed using a Biacore 3000 optical biosensor equipped with research-grade HC200 sensor chip (XanTec Bioanalytics). All measurements were carried out at 25°C at a flow rate of 20 µL/min. Immobilization of 14-3-3σ protein was conducted in HBSP⁺ buffer (0.01 M HEPES pH 7.4, 0.2 M NaCl, 0.1% v/v Surfactant P20) and peptide titration experiments in HBSP⁺ buffer containing 1% DMSO. The carboxylate groups on the surface were activated with 1:1 mixture of 0.4 M N-ethyl-N'-(3-dimethylaminopropyl)-carbodiimide (EDC) and 0.1 M N-hydroxysuccinimide (NHS). His₆-tagged 14-3-3σ (3 µM in 10 mM sodium acetate pH 5.5) was covalently immobilized onto the activated surface with a density of 6000 RU (6 ng/mm²). Remaining active groups were blocked by injection of 0.5 M ethanolamine in HBSP⁺ buffer. Binding of p53 peptides to 14-3-3σ was measured by injecting 2-fold serial dilutions of peptide in the running buffer over the sensor chip for 2 min followed by a dissociation of unbound peptide for 3 min. Dissociation constants (K_d) were calculated with GraphPad Prism 7.02 Software using a nonlinear regression analysis.

^1H - ^{15}N HSQC Spectroscopy on $^{15}\text{N}^{13}\text{C}^2\text{H}$ labeled 14-3-3 ΔC17

^1H - ^{15}N TROSY-HSQC (Transverse Relaxation Optimized Spectroscopy- Heteronuclear Single Quantum Coherence Spectroscopy) spectra were acquired in 3 mm tubes (sample volume 200 μL) using a 900 MHz Bruker Avance spectrometer, equipped with a cryoprobe. The spectra were recorded with 3426 complex data points in the direct dimension and 128 complex data points in the indirect dimension, with 300 scans per increment, at 32 $^\circ\text{C}$, in a buffer containing 100 mM sodium phosphate, 50 mM NaCl, pH 6.8, 1 mM DTT, EDTA-free protease inhibitor cocktail (Roche, Basel, Switzerland) and 10% (v/v) D_2O . The experiments were performed with samples containing 100 μM $^{15}\text{N}^{13}\text{C}^2\text{H}$ labeled 14-3-3 ΔC17 in the presence or in the absence of 250 μM p53 peptide. The experiments were performed on the 12mer, 14mer, 15mer, 20mer and 32mer peptides. The reference for the ^1H chemical shift was relative to trimethylsilyl propionate. Spectra were collected and processed with Topspin 4.0 (Bruker Biospin, Karlsruhe, Germany) and analyzed with Sparky 3.12 (T. D. Goddard and D. G. Kneller, SPARKY 3, University of California, San Francisco). The backbone resonance assignments of 14-3-3 ΔC17 were recently reported by us in the Biological Magnetic Resonance Database (<http://www.bmrb.wisc.edu/>) under the BMRB accession number 27563.

NMR Spectroscopy on 12mer and 15mer peptides

All 2D NMR spectra of natural abundance 12mer and 15mer peptides were acquired in a buffer containing 100 mM sodium phosphate, 50 mM NaCl, pH 6.8 and 10% (v/v) D_2O at 4 $^\circ\text{C}$ using a 600 MHz Bruker Avance I spectrometer equipped with a CPQCI cryoprobe. The spectra were recorded in *Shigemi* NMR tubes at a peptide concentration of 2.25 mM and in the absence of 14-3-3. The set of NMR experiments consisted of a ^1H - ^{15}N HSQC (^{15}N natural abundance), a ^1H - ^{13}C HSQC (^{13}C natural abundance), a TOCSY (Total Correlation Spectroscopy) and a NOESY (Nuclear Overhauser Effect Spectroscopy). ^1H - ^{15}N HSQC experiments were recorded with 2048 complex data points in the direct dimension and 64 complex data points in the ^{15}N dimension with 300 scans per increment. ^1H - ^{13}C HSQC experiments were recorded with 1440 complex data points in the direct dimension and 128 complex data points in the ^{13}C dimension with 32 scans per increment. TOCSY and NOESY spectra were acquired with 8192

x 512 complex data points, with a recycle delay of 1s and with 32 and 64 scans per increment, respectively. The mixing times were 69 ms for the TOCSY and 400 ms for the NOESY experiments. The reference for the ^1H chemical shift was relative to trimethylsilyl propionate. Spectra were collected and processed with Topspin 3.5 (Bruker Biospin, Karlsruhe, Germany) and analyzed with Sparky 3.12 (T. D. Goddard and D. G. Kneller, SPARKY 3, University of California, San Francisco). The assignment of chemical shifts of peptides reached a completeness of 88 % for the 12mer and 86 % for the 15mer concerning the chemical shift values of ^{15}N , $^1\text{H}^{\text{N}}$, $^1\text{H}\alpha$, $^1\text{H}\beta$, $^{13}\text{C}\alpha$ and $^{13}\text{C}\beta$. The Secondary Structure Propensity (SSP) scores [28] were calculated for both peptides based on $^{13}\text{C}\alpha$ and $^{13}\text{C}\beta$ chemical shift values. Random coil chemical shift values used for the calculation of the SSP score were taken from RefDB database [29]. The $^{13}\text{C}\alpha$ and $^{13}\text{C}\beta$ random coil chemical shift values for phosphorylated Threonine used for the calculation of the SSP scores were taken from literature [30].

Computational details

The starting point for the molecular dynamics simulations (MD) was the crystal structure of the complex between a p53 C-terminal 12mer phosphopeptide (KLMFKpTEGPDSD) and 14-3-3 σ (PDB code 5MHC) [26]. In addition to the 12mer peptide, the 15mer phosphopeptide (RHKKLMFKpTEGPDSD) was also considered. All missing residues in 14-3-3 σ were built using the program Modeller 9.15 [31]. The 15mer peptide was bound to 14-3-3 σ similar to the 12mer structure. The phosphorylated threonine residue was simulated with charge -2 in the phosphate group since the binding site in 14-3-3 σ contains several positively charged residues in close proximity to the phosphate group. The systems were placed in a water box with 20 Å distance between the protein and the walls of the box. The TIP3P water model was used in all simulations [32]. All systems were neutralized before the beginning of the simulations. MD simulations were carried out in the NPT ensemble for 250 ns and three independent replicas of each simulation were performed with CHARMM36 as force field [33]. A time step of 2 fs was used. The cutoff used was 12 Å while the pair list distance was set to 13.5 Å. All simulations were performed with NAMD 2.11 [34]. The analysis of the trajectories was performed with VMD [35]. The cutoff used for the analysis of the distances was 4 Å while for the RMSD was 0.8 Å. The same setup was employed for shorter MD simulations (120 ns) of both peptides in

the absence of 14-3-3 σ . Two starting geometries were considered for the peptides, the conformation adopted in the 14-3-3 σ – peptide complexes (bound conformation) and an extended structure in which the peptide appears as a linear β -strand. The objective of these simulations was to provide insights on the conformations adopted by the peptides in the absence of 14-3-3 σ . For these studies, a cubic water box with edges of 80 Å was used. The peptides were placed in the center of the box at the beginning of the simulations. The rest of the setting was as described above for the 14-3-3 σ -peptide simulations.

The ABF [27] calculations were performed by dividing the collective variable in six equal windows of 0.5 Å and setting the bin width to 0.1 Å. Each window was simulated for 20 ns (Figure S10). 100 samples were taken in each bin before the starting applying the force. The collective variable was the RMSD of the backbone atoms of residues Kp386 to Dp391 (Figure S9). The extended Lagrangian [36] formalism was used and the final PMF was obtained with the corrected z-averaged restraint estimator [37].

ASSOCIATED CONTENT

Supporting information

ITC titration curves of p53 peptides; 15N-1H TROSY-HSQC spectra of 14-3-3 σ Δ C17 in the presence of p53 peptides; mapping of the crystal structure of 14-3-3 σ Δ C17 in complex with 12mer; 15N, 1H and 13C Chemical shift values of 12mer and 15mer; SSP Scores of p53 peptide; NOE contacts in 12mer and 15mer; molecular dynamics of the 14-3-3 – 12mer/15mer complexes; RMSD values; average distances for selected interactions; structure of the bound conformation of the 12mer peptide; time evolution of the PMF profiles for the 15mer and 12mer; LC-MS data of p53 peptides.

AUTHOR INFORMATION

Corresponding authors

*E-mail: c.ottmann@tue.nl

helen.boyd@astrazeneca.com

isabelle.landrieu@univ-lille1.fr

elsa.sanchez-garcia@uni-due.de

Author Contributions

All authors have given approval to the final version of the manuscript. / ‡These authors contributed equally.

ACKNOWLEDGEMENTS

The research is supported by funding from the European Union through the AEGIS project (H2020-MSCA-ITN-2015, grant number 67555), TASPPI project (H2020-MSCA-ITN-2015, grant number 675179) and MSCA IEF (H2020-MSCA-IEF-2016, grant number 705188, R.G.D). J.F.N and I.L acknowledge LabEx (Laboratory of Excellence) for financial support on the scope of the DISTALZ consortium (ANR, ANR-11-LABX-009). E.S.-G. acknowledges a Plus-3 Grant of the Boehringer-Ingelheim Foundation and the computational time provided by the Computing and Data Facility of the Max Planck Society. The German Research Foundation (DFG) supported this work via the Collaborative Research Center SFB1093 (K.B.-R., C.O., and E.S.-G.) and the Excellence Cluster RESOLV EXC1069 (E.S.-G., infrastructure support).

We would like to acknowledge François-Xavier Cantrelle for assistance on NMR data acquisition. The NMR facilities were funded by the Nord Region Council, CNRS, Institut Pasteur de Lille, the European Community (ERDF), the French Ministry of Research and the University of Lille and by the CTRL CPER cofunded by the European Union with the European Regional Development Fund (ERDF), by the Hauts de France Regional Council (contract n°17003781), Métropole Européenne de Lille (contract n°2016_ESR_05), and French State (contract n°2017-R3-CTRL-Phase 1). We acknowledge support for the NMR facilities from TGE RMN THC (CNRS, FR-3050) and FRABio (Univ. Lille, CNRS, FR-3688).

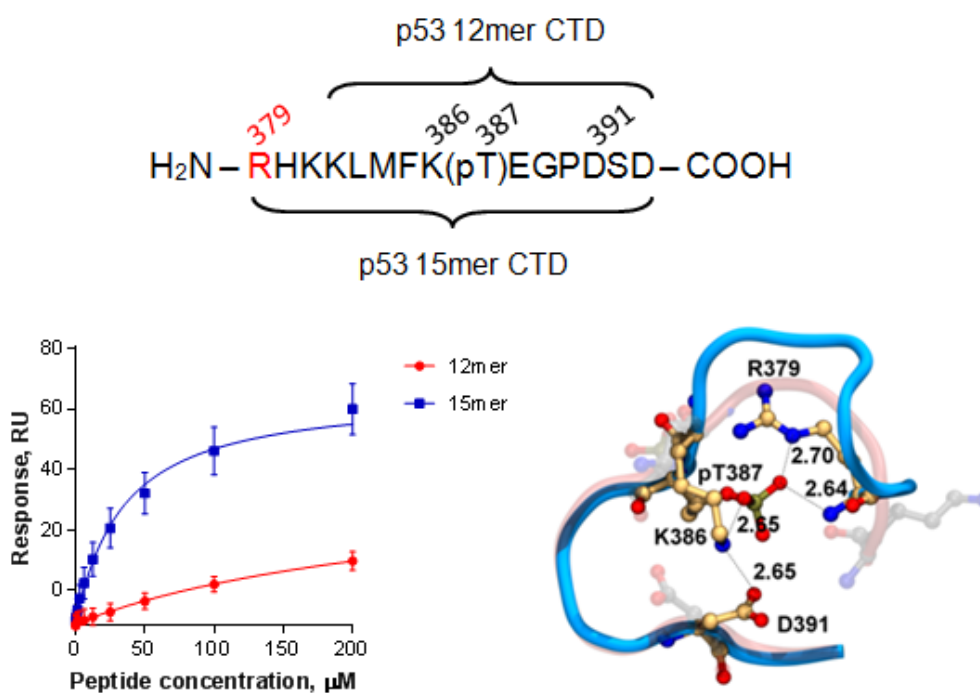
REFERENCES

1. Brown CJ, Lain S, Verma CS, Fersht AR, Lane DP (2009) Awakening guardian angels: drugging the p53 pathway. *Nat Rev Cancer* 9, 862-73
2. Yuangang Liu, Molly Kulesz-Martin (2001) p53 protein at the hub of cellular DNA damage response pathways through sequence-specific and non-sequence-specific DNA binding. *Carcinogenesis* 22, 851–860
3. Joerger AC, Fersht AR (2008) Structural biology of the tumor suppressor p53. *Annu Rev Biochem* 77, 557-82
4. Lakin ND, Jackson SP (1999) Regulation of p53 in response to DNA damage. *Oncogene* 18, 7644–7655
5. Alejandro Parrales, Tomoo Iwakuma (2015) Targeting Oncogenic Mutant p53 for Cancer Therapy. *Frontiers in Oncology* 5, 288
6. Toshinori Ozaki, Akira Nakagawara (2011) Role of p53 in Cell Death and Human Cancers. *Cancers* 3, 994-1013
7. van Heusden GP (2005) 14-3-3 proteins: regulators of numerous eukaryotic proteins. *IUBMB Life* 57, 623-9
8. Andrew Kaplan, Mardja Bueno, Alyson E. Fournier (2017) Extracellular functions of 14-3-3 adaptor proteins. *Cellular Signalling* 31, 26-30
9. Hermeking H (2003) The 14-3-3 cancer connection. *Nat Rev Cancer* 3, 931-43.
10. Aitken A, Collinge DB, van Heusden BP, Isobe T, Roseboom PH, Rosenfeld G, Soll J (1992) 14-3-3 proteins: a highly conserved, widespread family of eukaryotic proteins. *Trends Biochem Sci* 17, 498-501
11. Tomas Obsil, Veronika Obsilova (2011) Structural basis of 14-3-3 protein functions. *Seminars in Cell & Developmental Biology* 22, 663-672
12. Manuela Molzan, Benjamin Schumacher, Corinna Ottmann, Angela Baljuls, Lisa Polzien, Michael Weyand, Philipp Thiel, Rolf Rose, Micheline Rose, Philipp Kuhenne, Markus Kaiser, Ulf R. Rapp, Jürgen Kuhlmann, Christian Ottmann (2010) Impaired binding of 14-3-3 to C-RAF in Noonan syndrome suggests new approaches in diseases with increased Ras signaling. *Mol Cell Biol* 30, 4698-711

13. Dellambra E, Golisano O, Bondanza S, Siviero E, Lacal P, Molinari M, D'Atri S, De Luca M (2000) Downregulation of 14-3-3sigma prevents clonal evolution and leads to immortalization of primary human keratinocytes. *J Cell Biol* 149, 1117-30
14. Mong-Hong Lee, Guillermina Lozano (2006) Regulation of the p53-MDM2 pathway by 14-3-3 σ and other proteins. *Seminars in Cancer Biology* 16, 225-234
15. Heng-Yin Yang, Yu-Ye Wen, Chih-Hsin Chen, Guillermina Lozano, and Mong-Hong Lee (2003) 14-3-3 σ Positively Regulates p53 and Suppresses Tumor Growth. *Mol Cell Biol* 23, 7096-107
16. Laronga C, Yang HY, Neal C, Lee MH (2000) Association of the cyclin-dependent kinases and 14-3-3 sigma negatively regulates cell cycle progression. *J Biol Chem* 275, 23106-12
17. Verdoodt B, Benzinger A, Popowicz GM, Holak TA, Hermeking H (2006) Characterization of 14-3-3sigma dimerization determinants: requirement of homodimerization for inhibition of cell proliferation. *Cell Cycle* 5, 2920-6
18. Liem Phan, Ping-Chieh Chou, Guermarie Velazquez-Torres, Ismael Samudio, Kenneth Parreno, Yaling Huang, Chieh Tseng, Thuy Vu, Chris Gully, Chun-Hui Su, Edward Wang, Jian Chen, Hyun-Ho Choi, Enrique Fuentes-Mattei, Ji-Hyun Shin, Christine Shiang, Brian Grabiner, Marzenna Blonska, Stephen Skerl, Yiping Shao, Dianna Cody, Jorge Delacerda, Charles Kingsley, Douglas Webb, Colin Carlock, Zhongguo Zhou, Yun-Chih Hsieh, Jaehyuk Lee, Andrew Elliott, Marc Ramirez, Jim Bankson, John Hazle, Yongxing Wang, Lei Li, Shaofan Weng, Nibal Rizk, Yu Ye Wen, Xin Lin, Hua Wang, Huamin Wang, Aijun Zhang, Xuefeng Xia, Yun Wu, Mouhammed Habra, Wei Yang, Lajos Pusztai, Sai-Ching Yeung, Mong-Hong Lee (2015) The cell cycle regulator 14-3-3 σ opposes and reverses cancer metabolic reprogramming. *Nat Commun* 6, 7530
19. Tomohiro Kawaguchi, Shunsuke Kato, Kazunori Otsuka, Gou Watanabe, Toshihiro Kumabe, Teiji Tominaga, Takashi Yoshimoto, Chikashi Ishioka (2005) The relationship among p53 oligomer formation, structure and transcriptional activity using a comprehensive missense mutation library. *Oncogene* 24, 6976–6981
20. Patrick Chène (2001) The role of tetramerization in p53 function. *Oncogene* 20, 2611-7

21. Michael B Yaffe, Katrin Rittinger, Stefano Volinia, Paul R Caron, Alastair Aitken, Henrik Leffers, Steven J Gamblin, Stephen J Smerdon, Lewis C Cantley (1997) The Structural Basis for 14-3-3:Phosphopeptide Binding Specificity. *Cell* 91, 961–971
22. Surajit Ganguly, Joan L. Weller, Anthony Ho, Philippe Chemineau, Benoit Malpoux, David C. Klein (2005) Melatonin synthesis: 14-3-3-dependent activation and inhibition of arylalkylamine N-acetyltransferase mediated by phosphoserine-205. *PNAS* 102, 1222-1227
23. Rajagopalan S, Jaulent AM, Wells M, Veprintsev DB, Fersht AR (2008) 14-3-3 activation of DNA binding of p53 by enhancing its association into tetramers. *Nucleic Acids Res* 36, 5983-5991
24. Rajagopalan S, Sade RS, Townsley FM, Fersht AR (2009) Mechanistic differences in the transcriptional activation of p53 by 14-3-3 isoforms. *Nucleic Acids Res* 38, 893-906
25. Schumacher B1, Mondry J, Thiel P, Weyand M, Ottmann C (2010) Structure of the p53 C-terminus bound to 14-3-3: Implications for stabilization of the p53 tetramer. *FEBS Letters* 584, 1443–1448
26. Doveston RG, Kuusk A, Andrei SA, Leysen S, Cao Q, Castaldi MP, Hendricks A, Brunsveld L, Chen H, Boyd H, Ottmann C (2017) Small-molecule stabilization of the p53 - 14-3-3 protein-protein interaction. *FEBS Letters* 591, 2449-2457
27. E. Darve, D. Rodríguez-Gómez, A. Pohorille.(2008) Adaptive biasing force method for scalar and vector free energy calculations. *J. Chem. Phys* 128, 144120
28. Marsh JA, Singh VK, Jia Z, Forman-Kay JD (2006) Sensitivity of secondary structure propensities to sequence differences between alpha- and gamma-synuclein: implications for fibrillation. *Protein Science* 15, 2795-2804
29. Zhang H, Neal S, Wishart DS (2003) RefDB: a database of uniformly referenced protein chemical shifts. *J Biomol NMR* 25, 173-95
30. Ewa A. Bienkiewicz, Kevin J. Lumb (1999) Random-coil chemical shifts of phosphorylated amino acids. *Journal of Biomolecular NMR* 15, 203–206
31. Eswar N, Webb B, Marti-Renom MA, Madhusudhan MS, Eramian D, Shen MY, Pieper U, Sali A (2007) Comparative protein structure modeling using MODELLER. *Curr Protoc Protein Sci* 50, 2.9.1-2.9.31

32. W. L. Jorgensen, J. Chandrasekhar, J. D. Madura, R. W. Impey, M. L. Klein (1983) Comparison of simple potential functions for simulating liquid water. *J. Chem. Phys* 79, 926
33. Vanommeslaeghe K, MacKerell AD Jr. (2015) CHARMM additive and polarizable force fields for biophysics and computer-aided drug design. *Biochim Biophys Acta* 1850, 861-871
34. Phillips JC, Braun R, Wang W, Gumbart J, Tajkhorshid E, Villa E, Chipot C, Skeel RD, Kalé L, Schulten K (2005) Scalable molecular dynamics with NAMD. *J Comput Chem* 26, 1781-802
35. William Humphrey, Andrew Dalke, Klaus Schulten (1996) VMD: Visual molecular dynamics. *J Mol Graph* 14, 27-8
36. M. Iannuzzi, A. Laio, M. Parrinello (2003) Efficient Exploration of Reactive Potential Energy Surfaces Using Car-Parrinello Molecular Dynamics. *Phys. Rev. Lett* 90, 238302
37. A. Lesage, T. Lelièvre, G. Stoltz, J. Hénin (2017) Smoothed Biasing Forces Yield Unbiased Free Energies with the Extended-System Adaptive Biasing Force Method. *J. Phys. Chem. B* 121, 3676



For Table of Contents Only: Higher binding affinity of the 15mer peptide to 14-3-3 σ observed in biophysical assays can structurally be explained by arginine 379 at the N-terminus of the 15mer peptide stabilizing the 14-3-3 bound-like conformation.

Adoption of a Turn Conformation Drives the Binding Affinity of p53 C-Terminal Domain Peptides to 14-3-3 σ

Supporting Information

Ave Kuusk^{1,2‡}, João Filipe Neves^{3‡}, Kenny Bravo Rodriguez^{4,5‡}, Richard G. Doveston⁶, Anders Gunnarsson¹, Michael Ehrmann⁵, Hongming Chen¹, Isabelle Landrieu^{3,*}, Elsa Sanchez-Garcia^{4*}, Helen Boyd^{7*}, Christian Ottmann^{2,8*}

¹ Discovery Sciences, IMED Biotech Unit, AstraZeneca, Mölndal, Sweden

² Laboratory of Chemical Biology, Department of Biomedical Engineering and Institute for Complex Molecular Systems, Eindhoven University of Technology, The Netherlands

³ UMR 8576 CNRS-Lille University, 59000 Villeneuve d'Ascq, France

⁴ Department of Computational Biochemistry, University of Duisburg-Essen, Germany

⁵ Department of Microbiology, University of Duisburg-Essen, Germany

⁶ Leicester Institute of Structural and Chemical Biology and Department of Chemistry, University of Leicester, University Road, Leicester LE1 7RH, UK

⁷ Drug Safety and Metabolism, IMED Biotech Unit, AstraZeneca, Cambridge, UK

⁸ Department of Chemistry, University of Duisburg-Essen, Germany

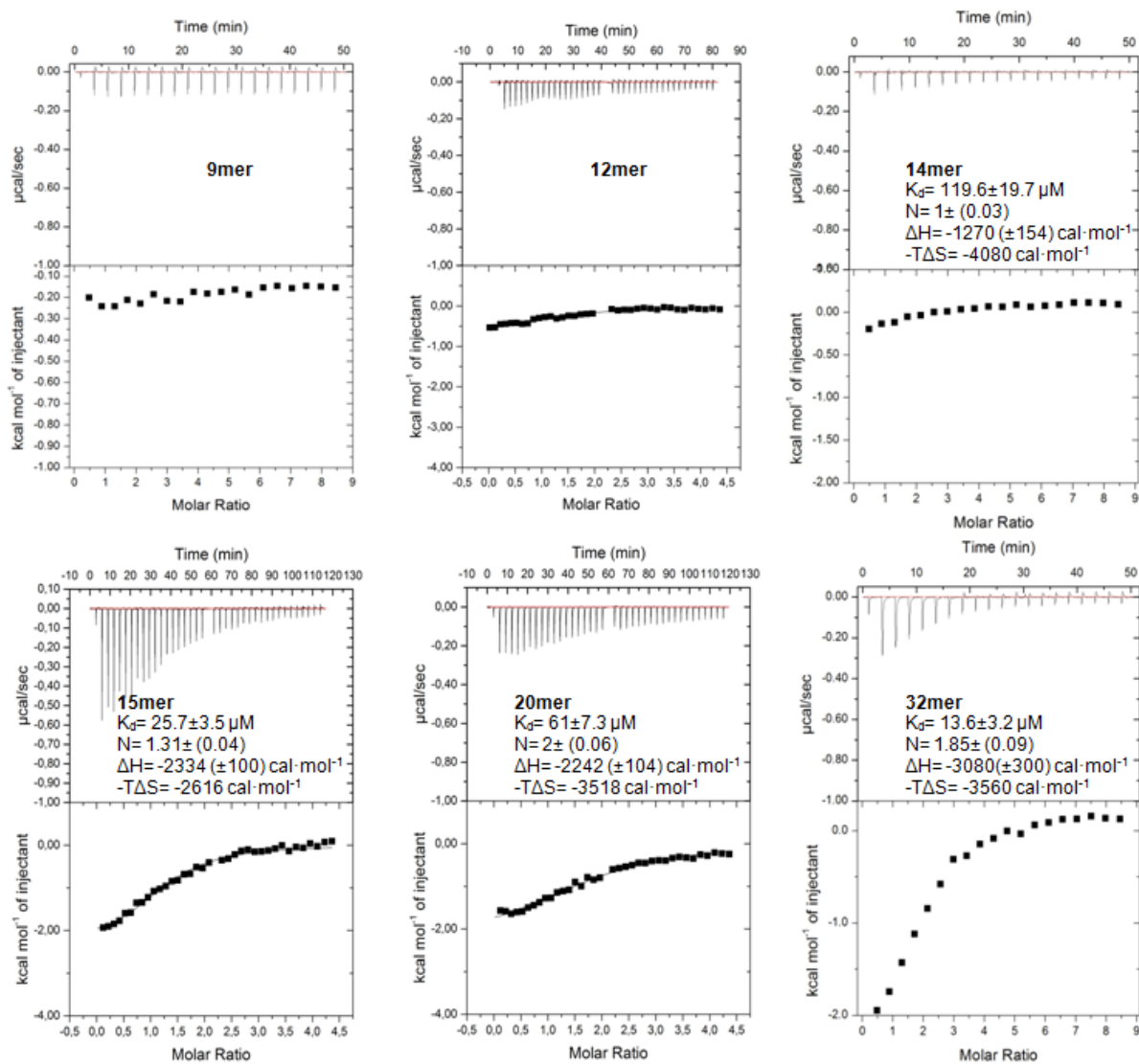


Figure S1 - Titration curves of 9mer, 12mer, 14mer, 15mer, 20mer and 32mer peptides of p53.

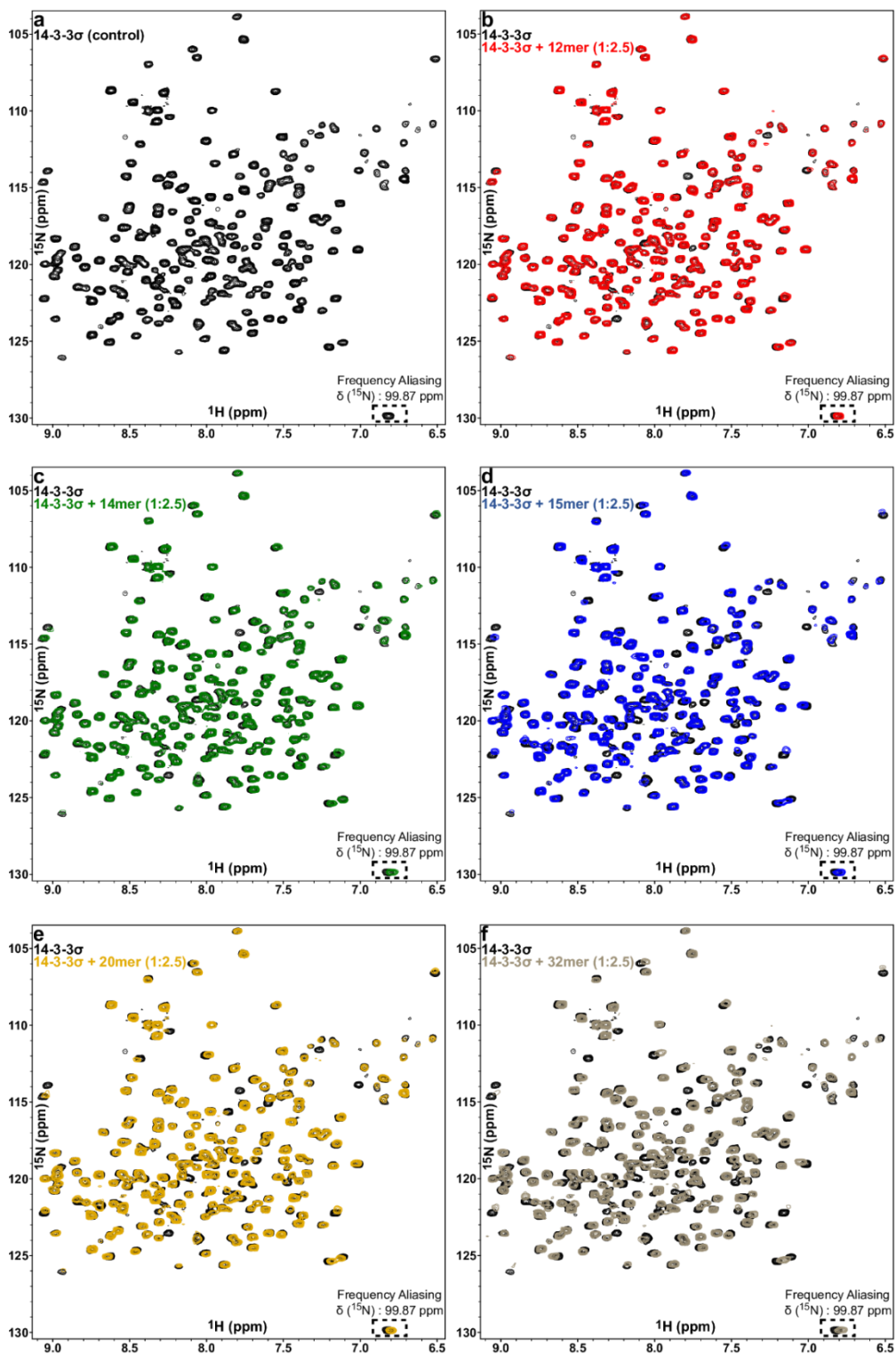


Figure S2 - ^{15}N - ^1H TROSY-HSQC spectra of $^{15}\text{N}^{13}\text{C}^2\text{H}$ labelled 14-3- $3\sigma\Delta\text{C}17$ in the presence of p53 peptides. The spectra of $100\ \mu\text{M}$ $^{15}\text{N}^{13}\text{C}^2\text{H}$ labelled 14-3- $3\sigma\Delta\text{C}17$ alone is shown in A (in black). The spectra of $100\ \mu\text{M}$ $^{15}\text{N}^{13}\text{C}^2\text{H}$ labelled 14-3- $3\sigma\Delta\text{C}17$ in the presence of $250\ \mu\text{M}$ of each of the p53 peptides are shown overlaid to the spectrum of $100\ \mu\text{M}$ $^{15}\text{N}^{13}\text{C}^2\text{H}$ labelled 14-3- $3\sigma\Delta\text{C}17$ alone (in black) in panels B (12mer, red spectrum); C (14mer, green spectrum); D (15mer, blue spectrum); E (20mer, yellow spectrum) and F (32mer, grey spectrum).

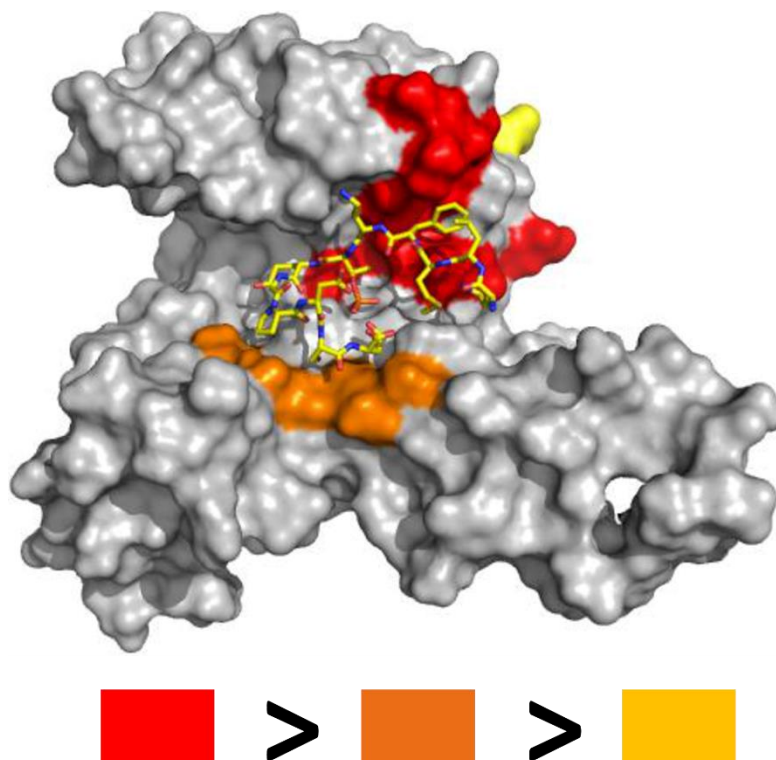


Figure S3 - p53 peptides interact with 14-3-3 through the amphipathic binding groove. Mapping on the crystal structure of 14-3-3 Δ C17 in complex with 12mer (PDB ID: 5MHC) of the amino acid residues whose correspondent correlation peak intensities were the most affected by the presence of 12mer. The 1-10 residues whose correspondent correlation peak intensities were the most affected are colored in red, the 11-20 are colored in brown and the 20-25 are colored in yellow. The results for 14mer, 15mer, 20mer and 32mer were identical.

Table S1 - ^{15}N , ^1H and ^{13}C NMR Chemical shift values of 12mer in 100 mM Sodium Phosphate, 50 mM NaCl, pH 6.8 at 4°C.

	$\delta(^{15}\text{N})$ [ppm]	$\delta(^1\text{H})$ [ppm]			$\delta(^{13}\text{C})$ [ppm]	
	N	HN	H $_{\alpha}$	H $_{\beta}$	C $_{\alpha}$	C $_{\beta}$
K382	-	-	-	-	-	-
L383	125.2	8.798	4.317	1.478, 1.611	55.39	42.19
M384	122.2	8.560	4.447	1.923, 1.924	54.95	32.82
F385	121.5	8.351	4.633	2.982, 3.132	57.53	39.92
K386	123.9	8.335	4.350	1.729, 1.802	55.92	33.55
pT387	121.3	9.306	4.167	4.402	63.27	72.41
E388	125.4	8.857	4.342	1.966, 2.053	56.59	30.48
G389	110.9	8.467	4.079, 4.167	-	44.69	-
P390	-	-	4.450	1.974, 2.2267	63.21	32.32
D391	120.7	8.617	4.639	2.611, 2.748	54.45	41.04
S392	116.3	8.287	4.456	3.835, 3.890	58.25	64.27
D393	128.0	8.196	4.401	2.579, 2.672	56.10	41.98

Table S2 - ^{15}N , ^1H and ^{13}C NMR Chemical shift values of 15mer in 100 mM Sodium Phosphate, 50 mM NaCl, pH 6.8 at 4°C.

	$\delta(^{15}\text{N})$ [ppm]	$\delta(^1\text{H})$ [ppm]			$\delta(^{13}\text{C})$ [ppm]	
	N	HN	H $_{\alpha}$	H $_{\beta}$	C $_{\alpha}$	C $_{\beta}$
R379	-	-	-	-	-	-
H380	-	-	-	-	-	-
K381	124.3	8.766	4.260	1.734, 1.788	56.46*	33.17*
K382	123.7	8.671	4.257	1.753, 1.792	56.46*	33.17*
L383	124.1	8.494	4.292	1.484, 1.640	55.06	42.18
M384	120.7	8.379	4.402	1.913, 1.913	56.02	32.67
F385	120.8	8.294	4.622	2.987, 3.151	57.45	39.81
K386	123.1	8.258	4.343	1.732, 1.805	55.97	33.17
pT387	121.1	9.312	4.167	4.399	63.26	72.36
E388	125.2	8.864	4.347	1.963, 2.105	56.68	30.47
G389	110.7	8.464	4.112, 4.096	-	44.73	-
P390	-	-	4.448	2.213	63.20	32.28
D391	120.5	8.618	4.638	2.615, 2.748	54.44	41.01
S392	116.1	8.278	4.453	3.832, 3.892	58.20	64.19
D393	127.8	8.197	4.400	2.587, 2.676	55.01	41.98

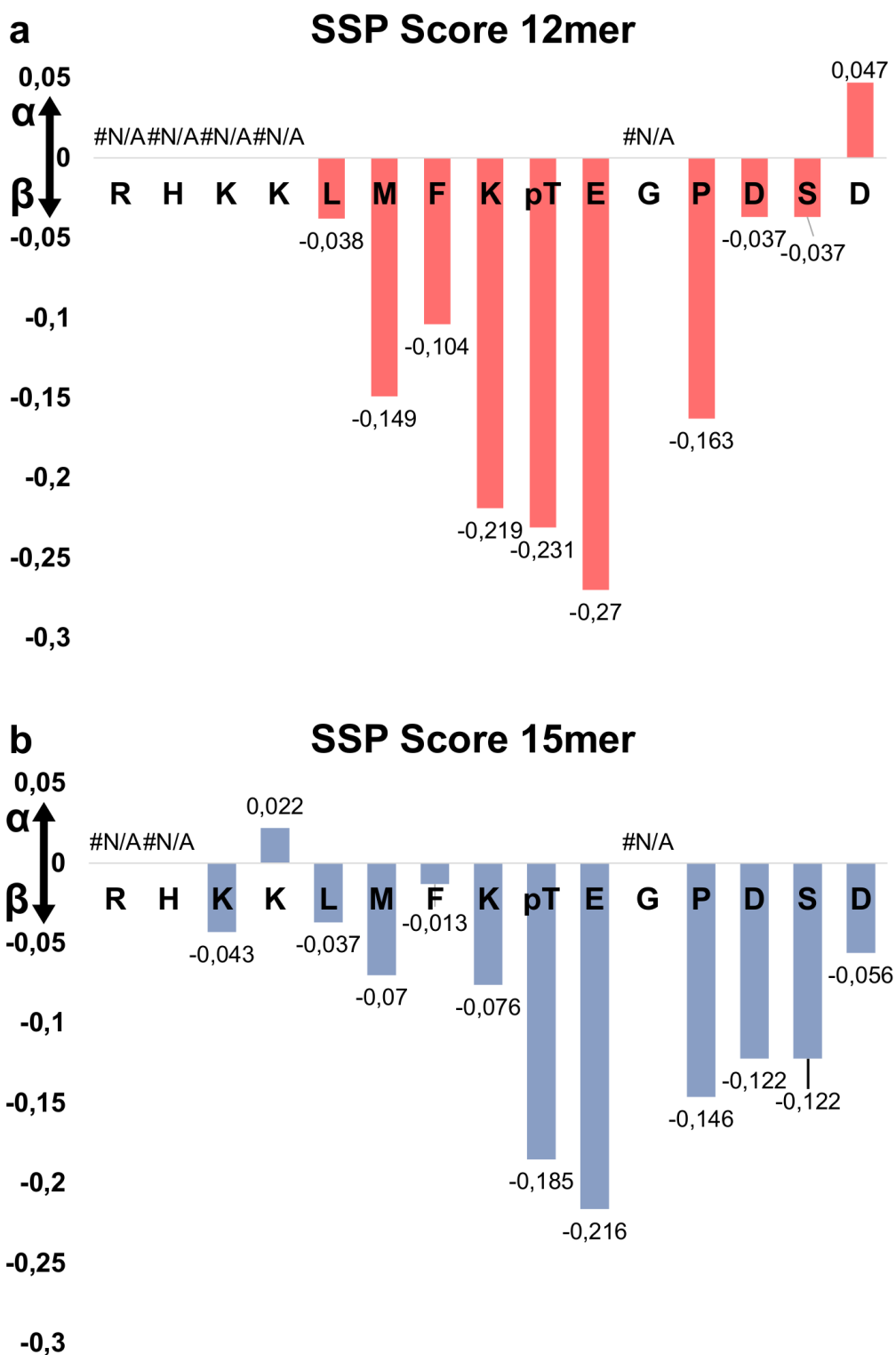


Figure S4 - SSP Scores of p53 peptides reveal a predominantly disordered structure with a small tendency to β -strand. The plots of SSP scores for the 12mer and 15mer are shown in A and B respectively. The bars represent the chemical shift indexes (~ 1 for α -helix, ~ 0 for random coil, ~ -1 for β -strand). The SSP score for G389 was not calculated since residues preceding a proline are usually outliers.

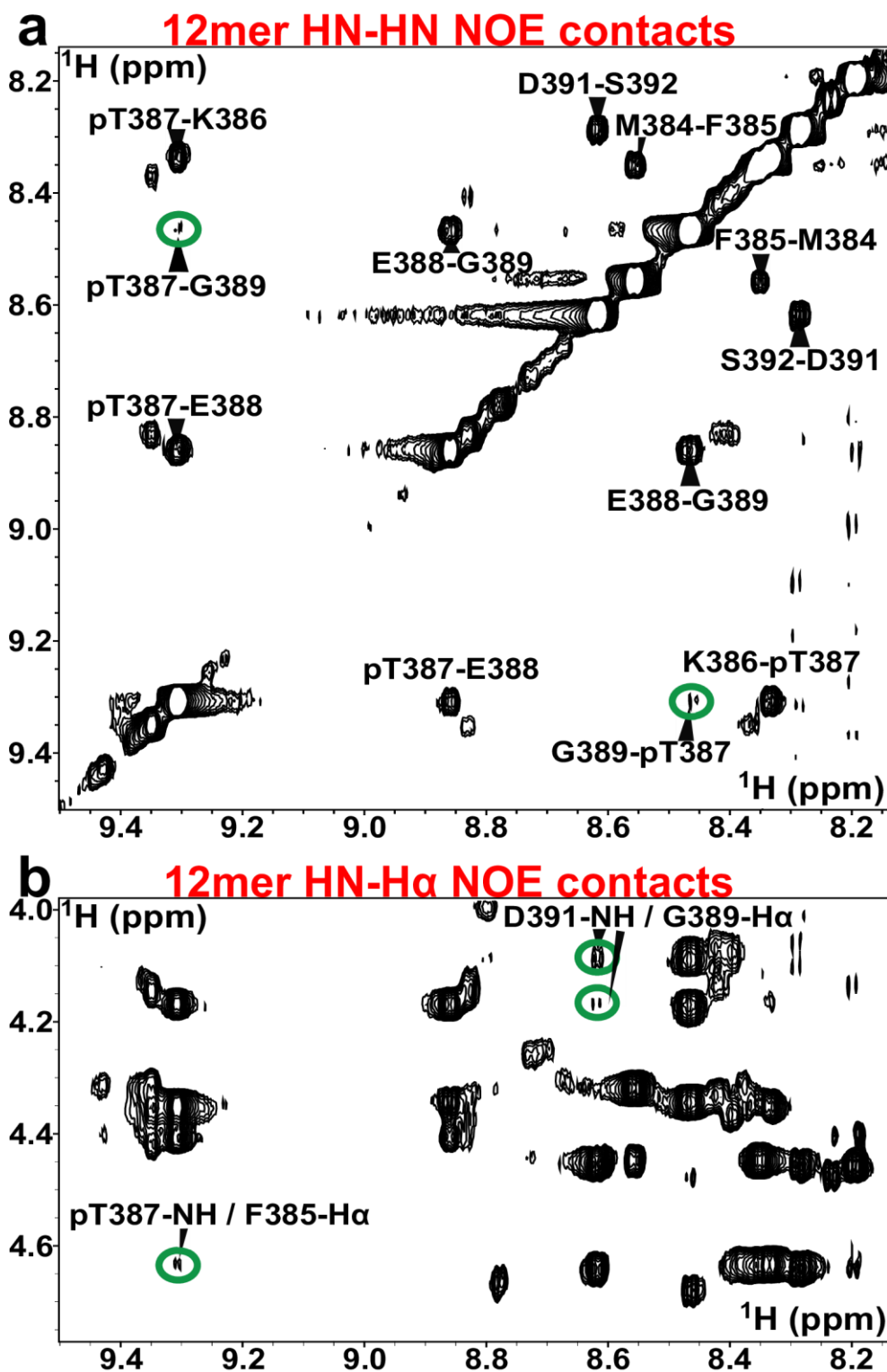


Figure S5 - NOE contacts in 12mer. (A) Section of the NOESY spectrum of 12mer where it is possible to see the HN-HN NOE peaks. Only the majoritarian forms are assigned. The medium-range NOEs are identified with a green circle. (B) Section of the NOESY spectrum of 12mer where it is possible to see the HN-H α NOE peaks. Only the medium-range NOEs are assigned and are identified with a green circle. The NOE summary diagram is presented in Figure 4 of the manuscript.

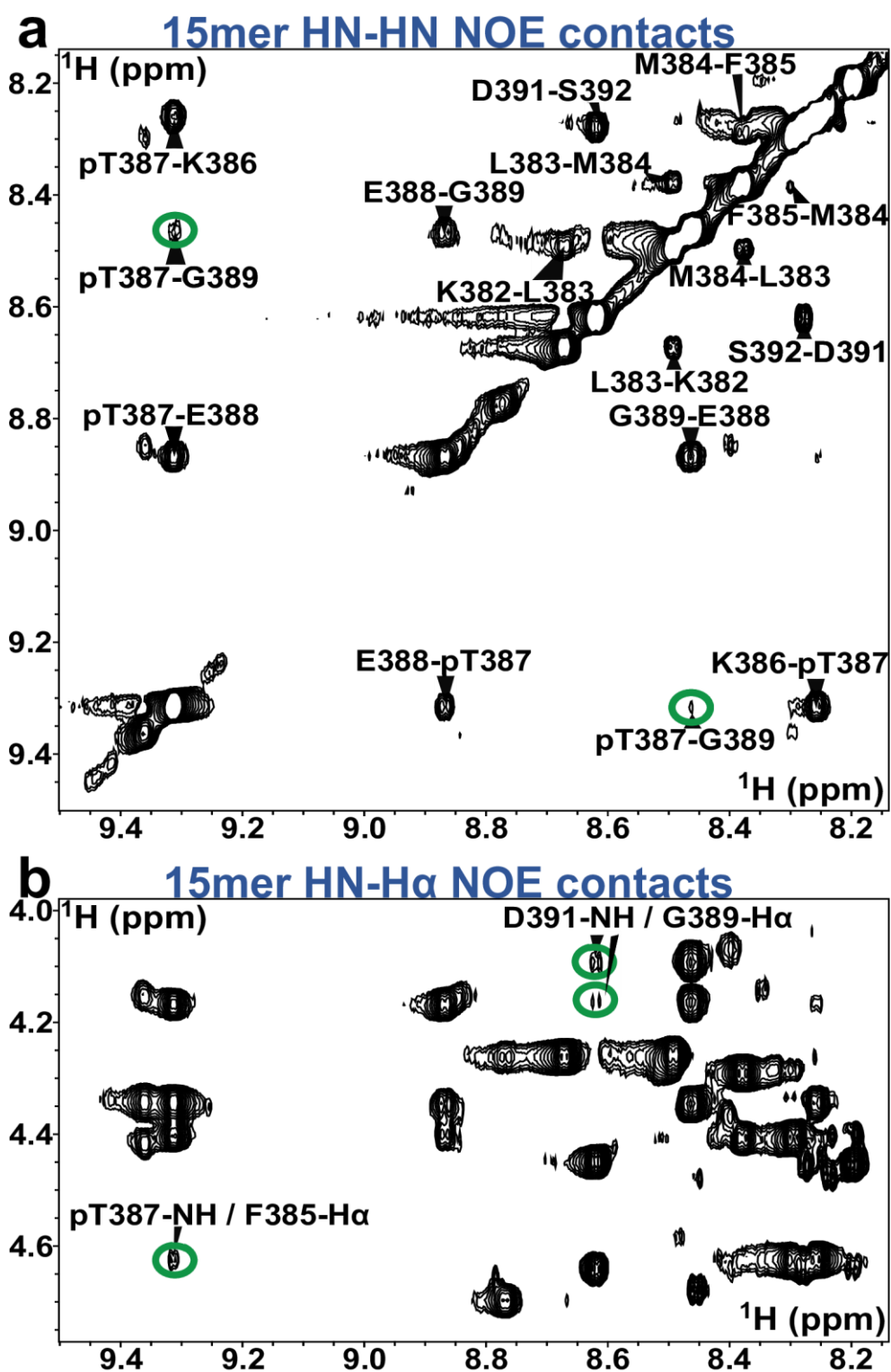


Figure S6 - NOE contacts in 15mer. (A) Section of the NOESY spectrum of 15mer where it is possible to see the HN-HN NOE peaks. Only the major forms are assigned. The medium-range NOEs are identified with a green circle. (B) Section of the NOESY spectrum of 15mer where it is possible to see the HN-H α NOE peaks. Only the medium-range NOEs are assigned and are identified with a green circle. The NOE summary diagram is presented in Figure 4 of the manuscript.

Molecular dynamics (MD) of the 14-3-3 σ – 12mer and 14-3-3 σ – 15mer complexes

The analysis of the MD simulations shows that both, the 12mer and the 15mer, remain bound to 14-3-3 σ during the trajectories. The residues of 14-3-3 σ that are in contact with the peptides are similar in both cases (Figure S7), in agreement with the NMR observations. Binding of the peptides to 14-3-3 σ involves the formation of a loop comprising residues K_p386 to D_p391 (peptides residues are identified with the subscript p and residues of 14-3-3 σ with the σ subscript). This loop is conserved during the MD simulations as indicated by the small RMSD values adopted by the backbone atoms of residues K_p386 to D_p391 (Figure S8). The binding of the peptides to 14-3-3 σ is mainly driven by the positioning of pT_p387 in the binding site. There, pT_p387 establishes conserved salt bridges with residues K _{σ} 49, R _{σ} 56, R _{σ} 129 and Y _{σ} 130. In addition, E_p388 forms a salt bridge with K _{σ} 122 (Table S3) and F_p385 remains docked in a small cavity formed by V _{σ} 178, Y _{σ} 181, E _{σ} 182, L _{σ} 229 and W _{σ} 230. This explains why the I/I0 ratio for L _{σ} 229 experiences the changes shown in Figure 3. In case of the 12mer peptide, there are two additional interactions with 14-3-3 σ that are conserved for more than 50% of the MD simulations (Table S3). The interaction between E _{σ} 182 and K_p382 is found in 78% of the conformations and effectively restricts the movement of the N-terminus of the 12mer peptide. The salt bridge between D _{σ} 225 and K_p386 is found in 56% of the conformations. On the other hand, for the 12mer peptide intra-peptide interactions are scarce while K_p386 of the 15mer preferentially interacts with D_p391 (intra-peptide interaction) and not with D _{σ} 225 (peptide-protein interaction). Furthermore, the interaction between E _{σ} 182 and K_p382 is considerably less favored in the 15mer (Table S3). In general, the introduction of R_p379, H_p380 and K_p381 residues at the N-terminus of the peptide increases the flexibility of the 15mer peptide. As mentioned above, the interaction between K_p382 and E _{σ} 182 is almost lost and R_p379 explores a wide area around the binding cleft establishing contacts with E _{σ} 182, D _{σ} 225 and T _{σ} 231. The populations of conformations showing distances below 4 Å for the interaction of R_p379 with a) E _{σ} 182, b) D _{σ} 225 and c) T _{σ} 231 are 32%, 3% and 9%, respectively. In addition, an intra-peptide interaction between R_p379 and D_p393 was found in 5% of the conformations during the 15mer-14-3-3 σ simulations. Contrarily, the N-terminal K_p382 of the 12mer does not interact with D_p393.

12M (4 Å)

15M (4 Å)

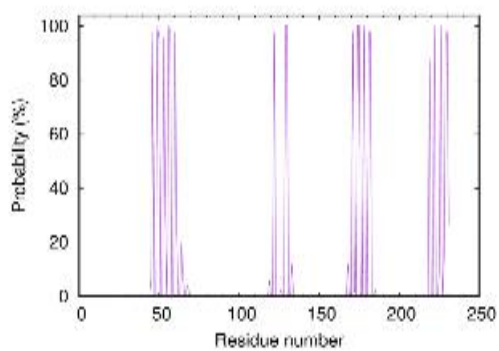
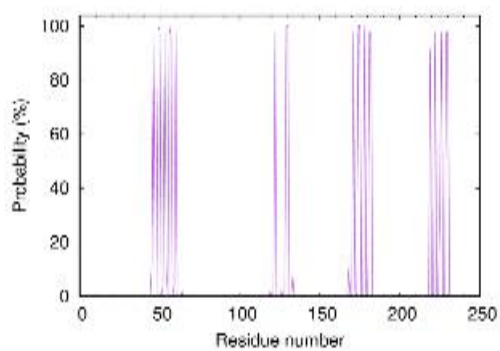
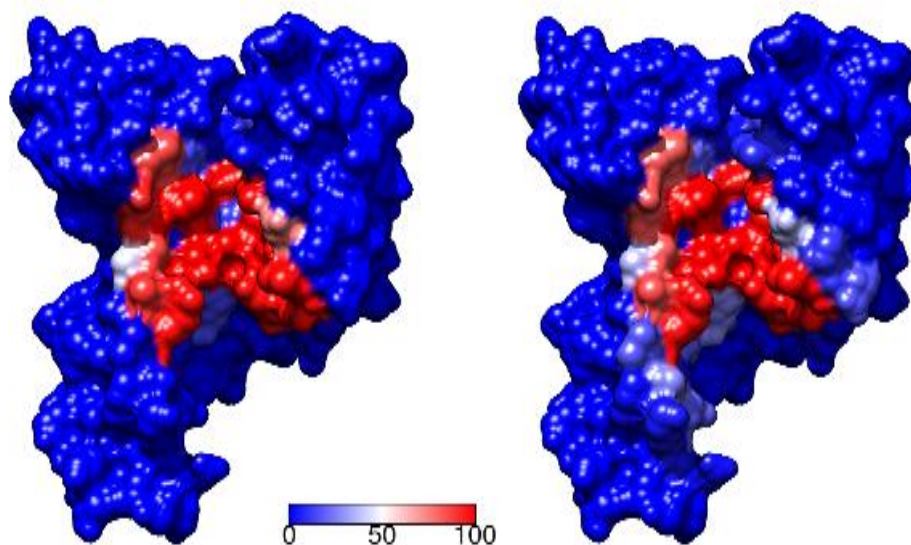


Figure S7 - Residue wise probability to find the peptide closer than 4 Å to 14-3-3 σ residues. The values shown are averaged over the three replicas of the MD simulations.

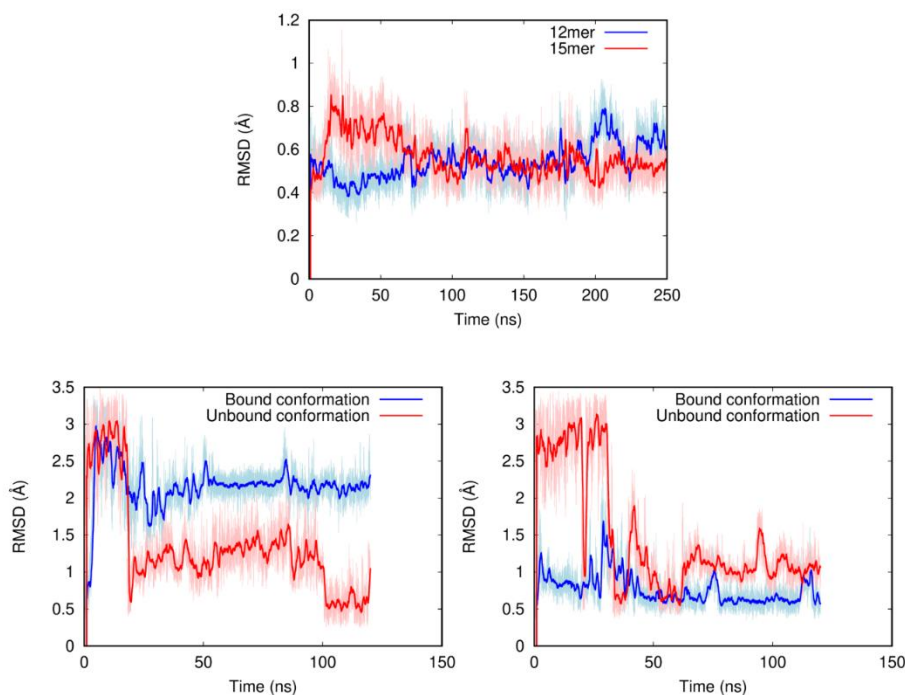


Figure S8 - RMSD values for the backbone atoms of residues Kp386 to Dp391 during the MD simulations. Top: Average of the three MD replicas performed with the 12mer and 15mer peptides bound to 14-3-3 σ . Bottom left: Results for the two MD simulations with the 12mer in the absence of 14-3-3 σ . The starting conformation of the peptide is indicated in the legend of the figure. Bottom right: Results for the two MD simulations with the 15mer in the absence of 14-3-3 σ .

Table S3 - Average distances (\AA) for selected interactions. Population values are given for conformations in which the corresponding distance takes values below 4.0 \AA . The atoms used to measure the distances are given in the name of the interaction as superscripts. Three independent replicas of the simulations are considered.

Interactions	Distances (\AA)		Population (%)	
	12mer	15mer	12mer	15mer
14-3-3 σ – Peptide interactions				
$E_{\sigma}182^{\text{CD}} - K_{\text{p}}382^{\text{NZ}}$	4.4 ± 2.4	9.6 ± 5.0	78	28
$D_{\sigma}225^{\text{CG}} - K_{\text{p}}386^{\text{NZ}}$	5.9 ± 3.0	8.8 ± 3.0	56	20
$K_{\sigma}122^{\text{NZ}} - E_{\text{p}}388^{\text{CD}}$	3.6 ± 0.4	3.9 ± 0.7	97	87
Intra-peptide interactions				
$K_{\text{p}}386^{\text{NZ}} - D_{\text{p}}391^{\text{CG}}$	7.0 ± 2.6	5.4 ± 2.9	28	62

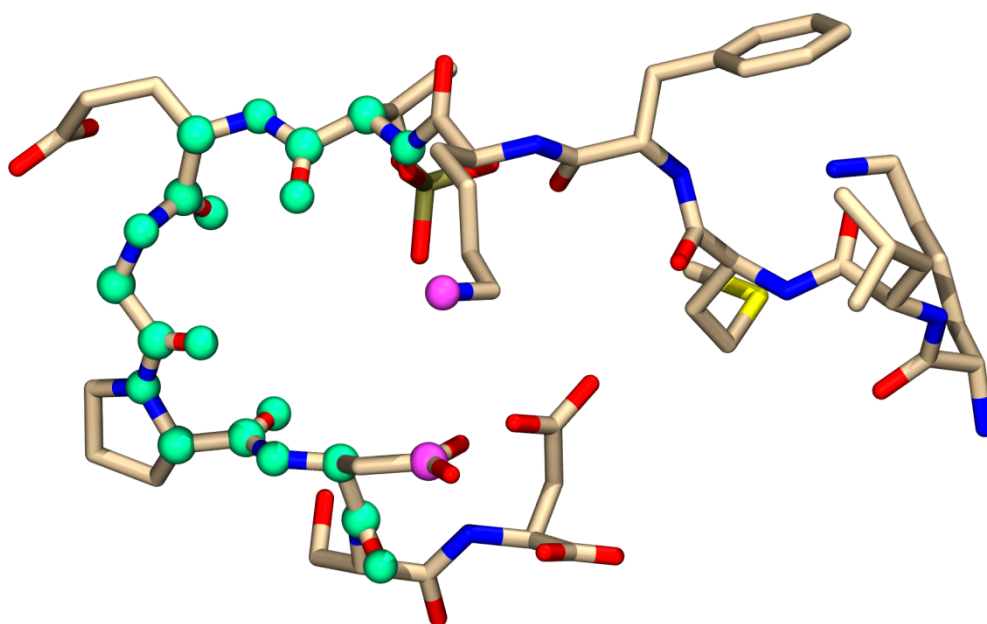


Figure S9 - Structure of the bound conformation of the 12mer peptide. Atoms used to define the collective variable used in the ABF calculations are highlighted as green spheres. Atoms involved in the important interaction between Kp386NZ and Dp391CG are highlighted as pink spheres.

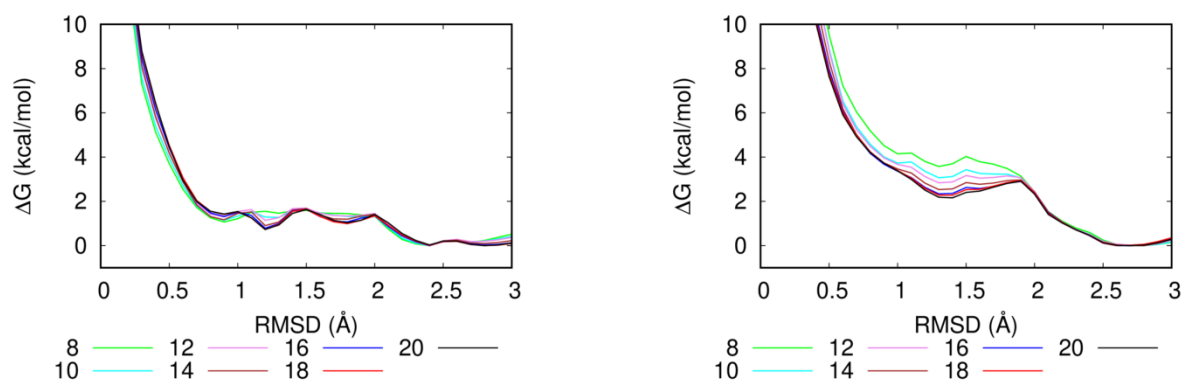


Figure S10 - Time evolution of the PMF profiles for the 15mer (left) and 12mer (right). The PMF was plotted for a simulated time of 8, 10, 12, 14, 16, 18 and 20 ns per window.

LC-MS data of p53 peptides

p53-9mer-COOH

H₂N-FK(pT)EGPDSD-COOH

Chemical Formula: C₄₂H₆₃N₁₀O₂₁P

Exact Mass: 1074.39

Molecular Weight: 1074.99

[M⁺H]: 1075.39 (100.0%), [M^{+2H}]²⁺ 538.2; [M^{+3H}]³⁺ 359.1

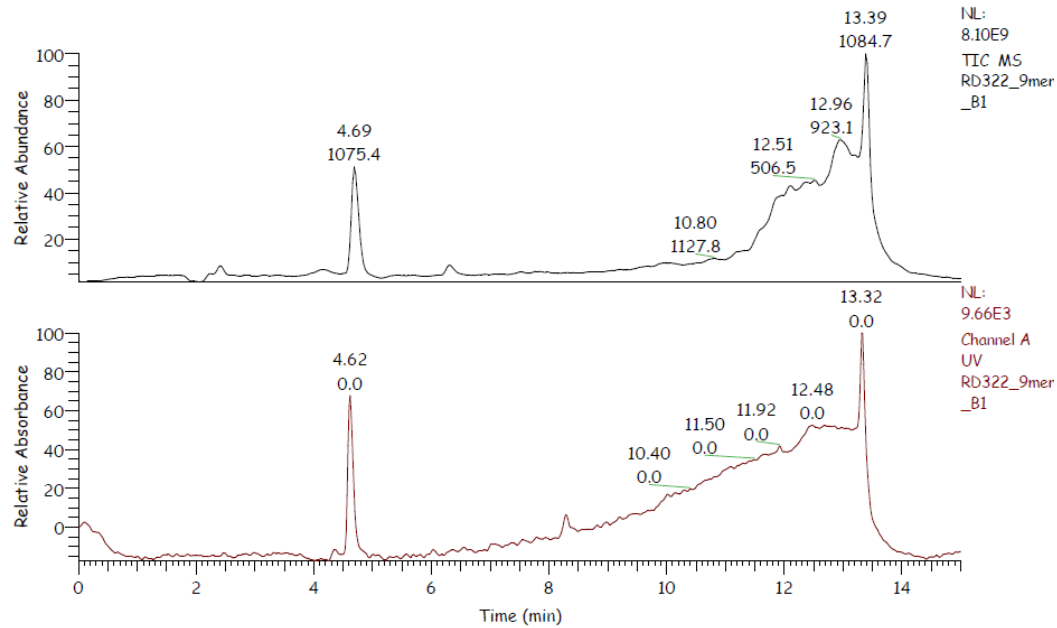
D:\data\...\RichardD\RD322_9mer_B1

7/10/2017 10:07:56

B:24

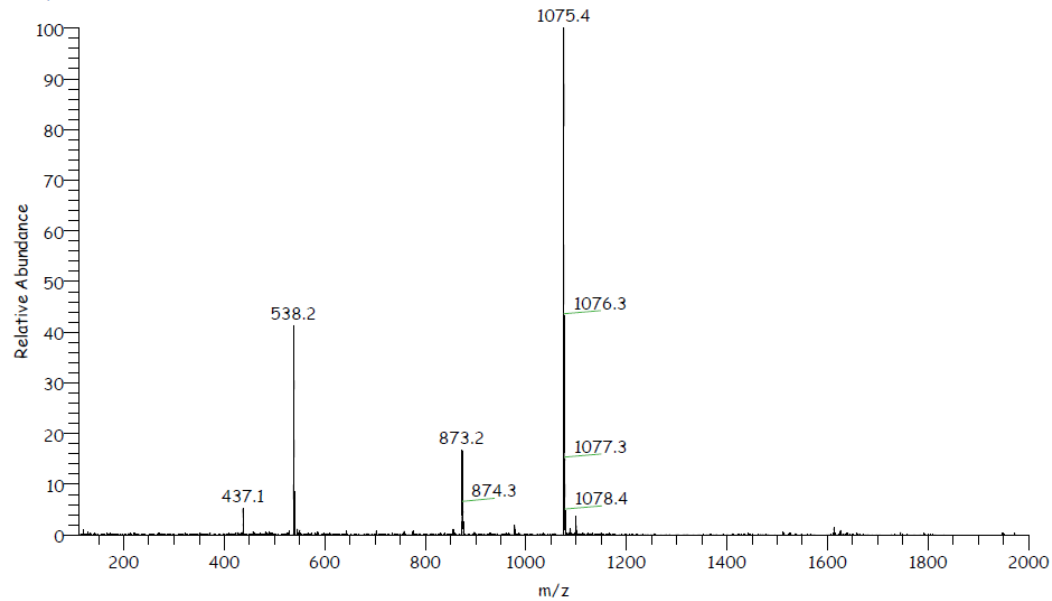
D:\Method\Richard\general method analytical.meth

RT: 0.00 - 15.00 SM: 76



RD322_9mer_B1 #167-183 RT: 4.47-4.90 AV: 17 SM: 56 NL: 4.99E7

T: + p ESI Full ms [110.00-2000.00]



p53-12mer-COOH

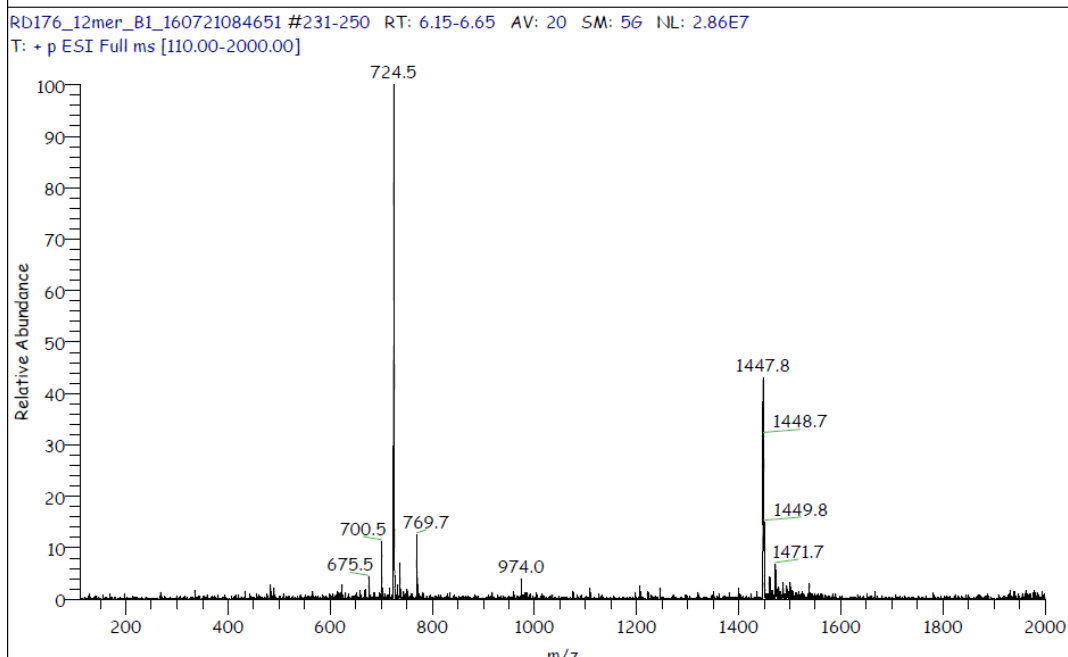
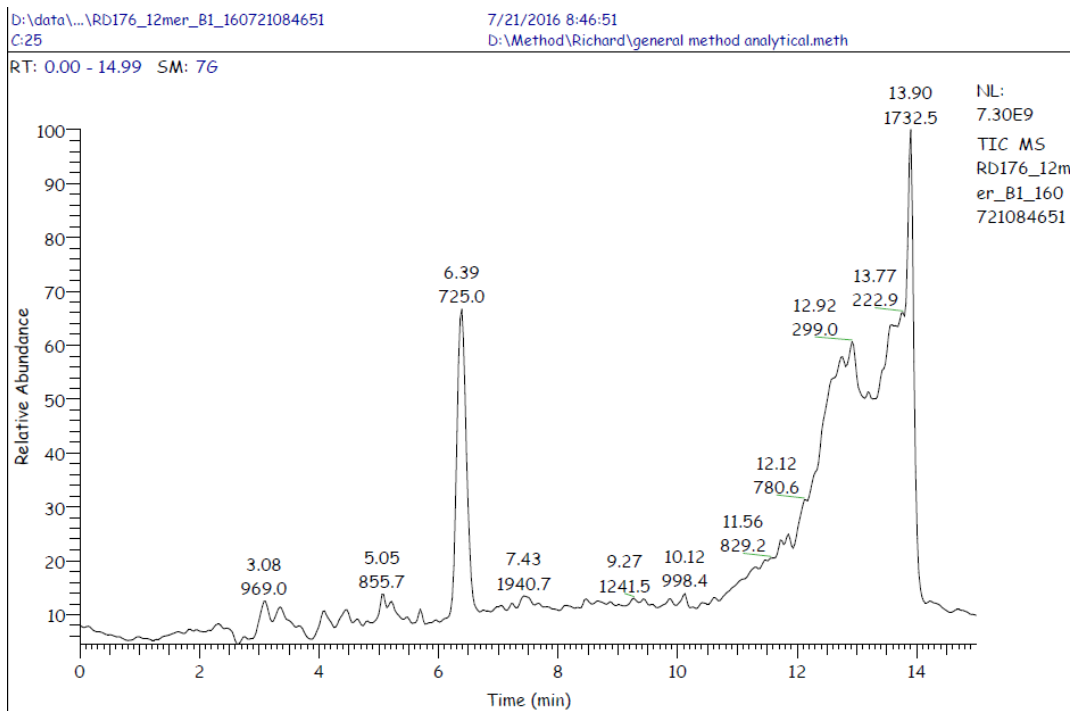
H2N-KLMFK(pT)EGPDS-D-OH

Chemical Formula: C₅₉H₉₅N₁₄O₂₄PS

Exact Mass: 1446.61

Molecular Weight: 1447.52

[M+H]⁺: 1447.61 (100.0%), [M+2H]²⁺: 724.76; [M+3H]³⁺: 483.50



p53-14mer-COOH

H₂N-HKCLMFK(pT)EGPDS-D-COOH

Chemical Formula: C₇₁H₁₁₄N₁₉O₂₆PS

Exact Mass: 1711.76

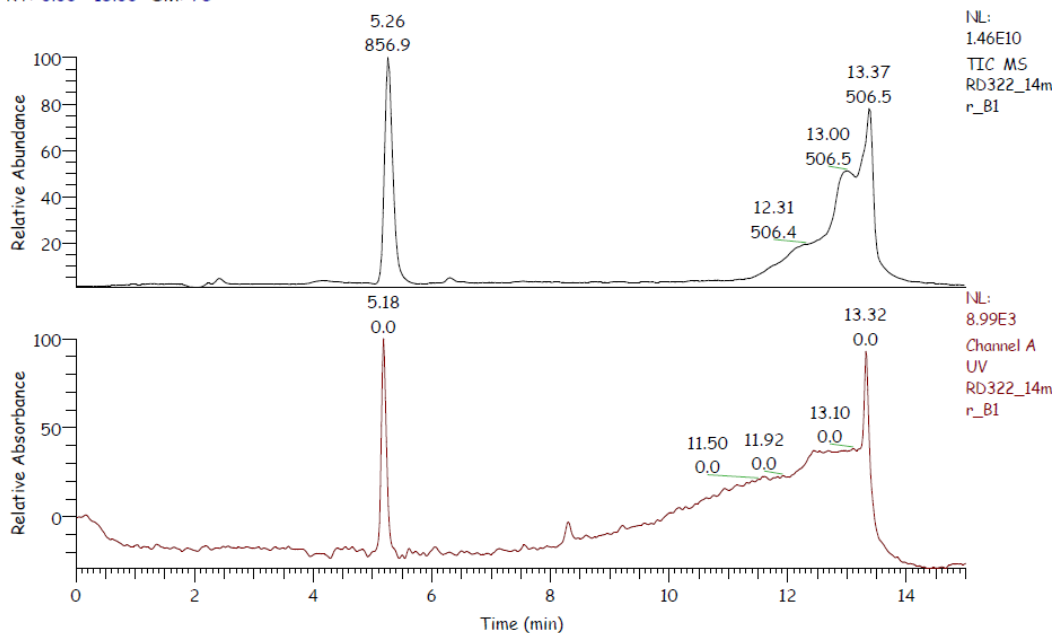
Molecular Weight: 1712.83

[M⁺H]: 1712.76 [M^{+2H}]²⁺: 857.4; [M^{+3H}]³⁺: 571.9

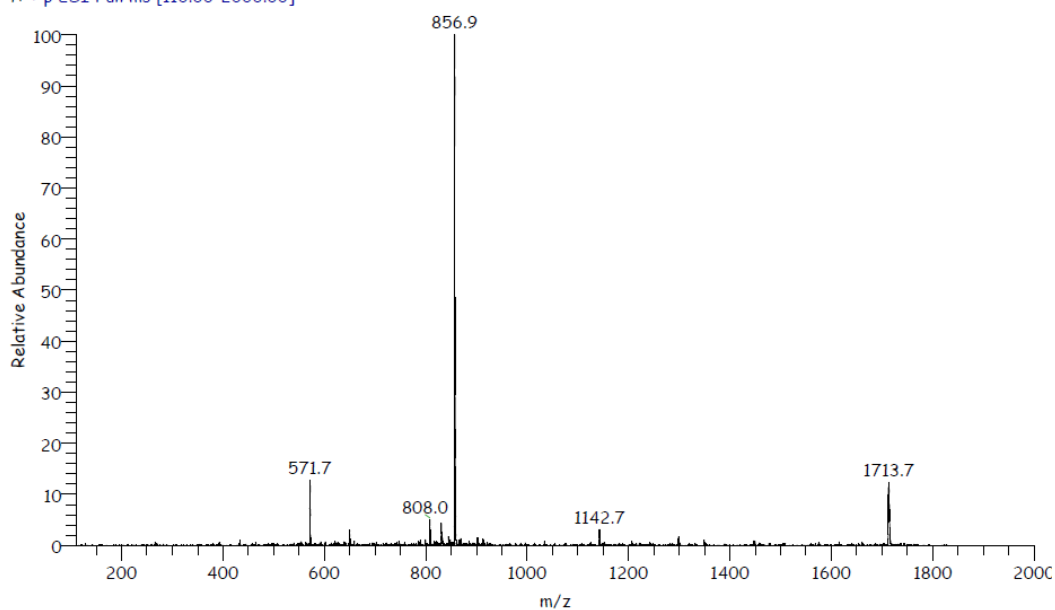
D:\data\...\RichardD\RD322_14mer_B1
B:26

7/10/2017 10:38:51
D:\Method\Richard\general method analytical.meth

RT: 0.00 - 15.00 SM: 76



RD322_14mer_B1 #186-204 RT: 4.99-5.47 AV: 19 SM: 56 NL: 1.31E8
T: + p ESI Full ms [110.00-2000.00]



p53-15mer-COOH

H₂N-RHKLMFK(pT)EGPDSD-COOH

Chemical Formula: C₇₇H₁₂₆N₂₃O₂₇PS

Exact Mass: 1867.87

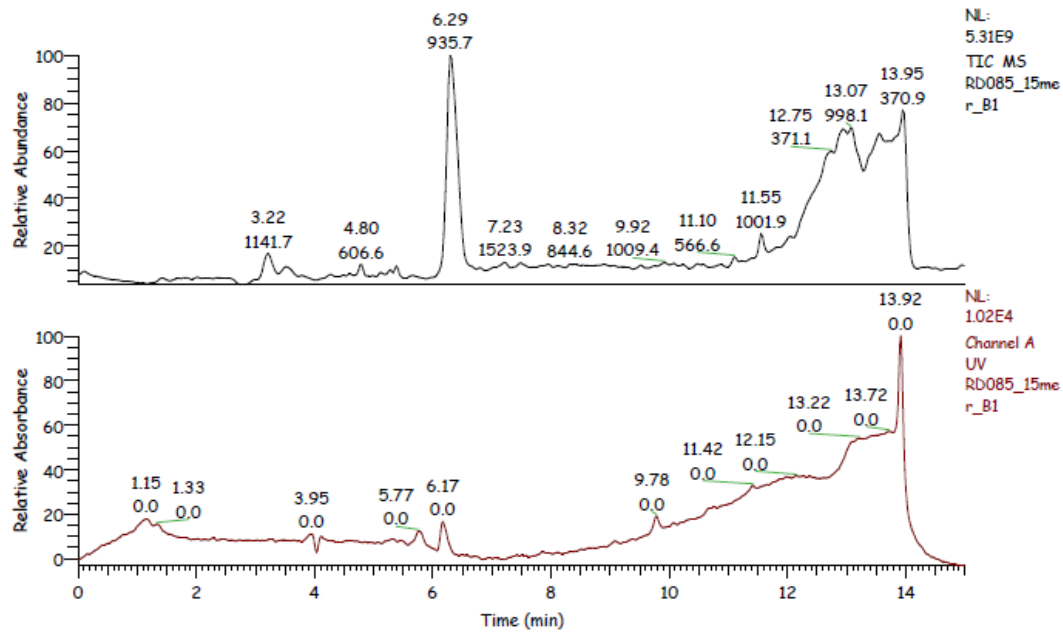
Molecular Weight: 1869.02

[M⁺H]: 1867.87 (100.0%); [M^{+2H}]²⁺: 934.90; [M^{+3H}]³⁺: 623.62; [M^{+4H}]⁴⁺: 467.97

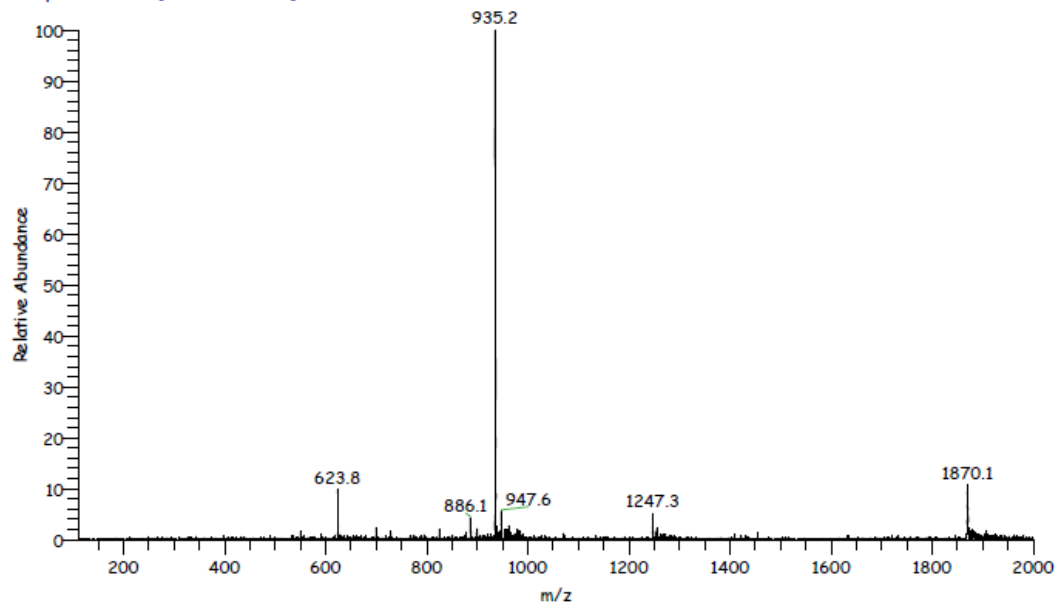
D:\data\...\Richard\RD085_15mer_B1
D-24

8/5/2016 8:06:45
D:\Method\Richard\general method analytical.meth

RT: 0.00 - 15.00 SM: 76



RD085_15mer_B1 #226-246 RT: 6.03-6.56 AV: 21 SM: 56 NL: 4.56E7
T: + p ESI Full ms [110.00-2000.00]



p53-20mer-COOH

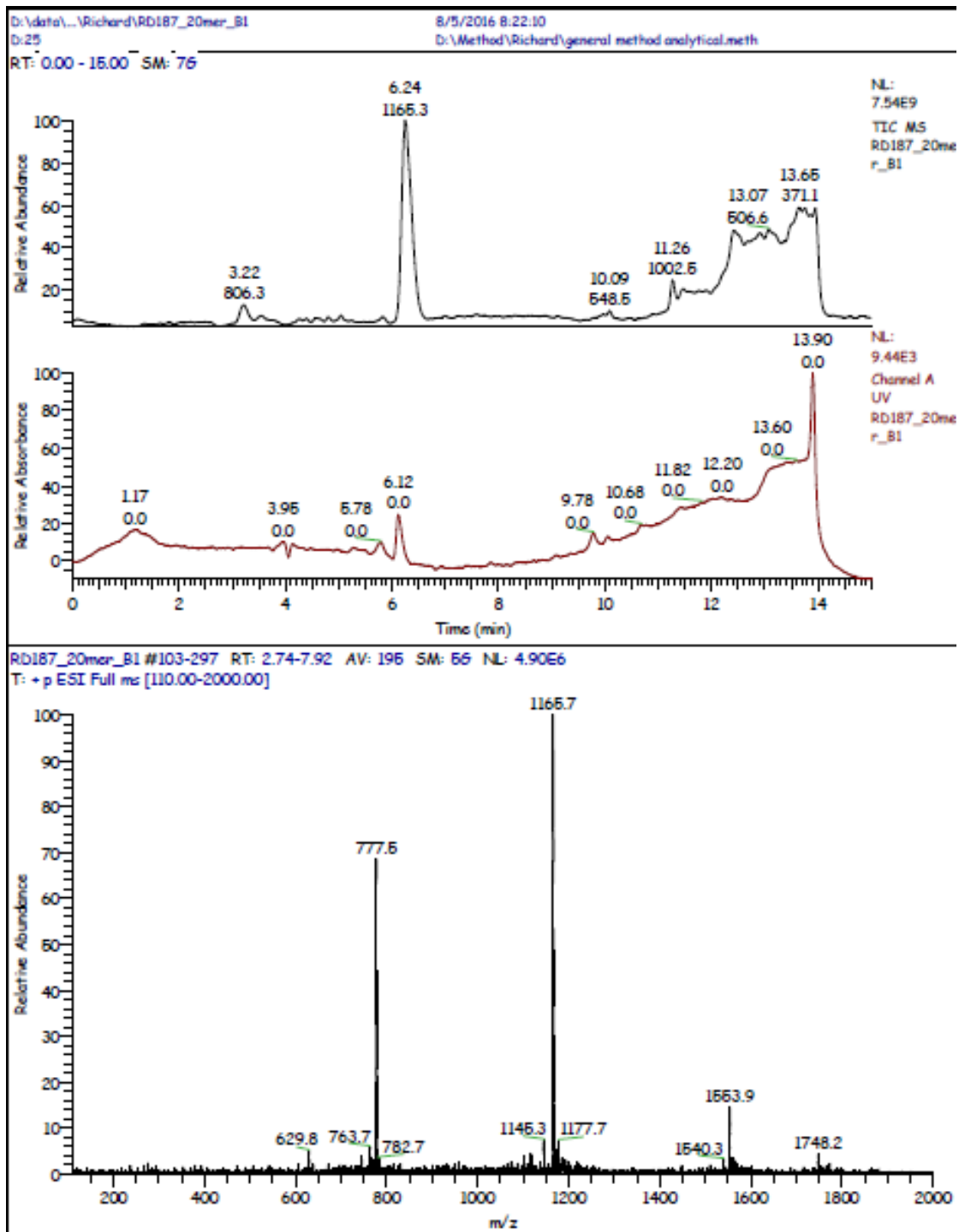
H₂N-GQSTSRHKKLMFK(pT)EGPDS-D-COOH

Chemical Formula: C₉₄H₁₅₄N₂₉O₃₆PS

Exact Mass: 2328.06

Molecular Weight: 2329.47

[M⁺H]: 2329.06 (100.0%); [M^{+2H}]²⁺: 1165.03; [M^{+3H}]³⁺: 777.02; [M^{+4H}]⁴⁺: 583.02



4 Targeting 14-3-3 protein interface with a fragment-based approach

This work was a collaboration with Taros Chemicals, on the scope of the TASPPI project. Taros Chemicals set-up a library of fragments tailored to target PPIs and we were in charge of screening the fragment library in order to find small-molecule binders of 14-3-3 σ . The manuscript containing this work was published:

Valenti, D., Neves, J. F., Cantrelle, F.-X., Hristeva, S., Santo, D. L., Obšil, T., ... Ottmann, C. (2019). Set-up and screening of a fragment library targeting the 14-3-3 protein interface. *MedChemComm*, 10(10), 1796–1802. <https://doi.org/10.1039/C9MD00215D>

The manuscript is presented ahead. To respect copyright constraints, the manuscript is presented as it was originally submitted to the journal and before the modifications performed upon peer-review.

Targeting 14-3-3 protein interface with a fragment-based approach

Dario Valenti,^{a,b†} João Filipe Neves,^{c†} François-Xavier Cantrelle,^c Stanimira Hristeva,^a Domenico Lentini Santo,^d Tomáš Obšil,^{d,e} Xavier Hanouille,^c Laura M. Levy,^{a†} Dimitrios Tzalis,^{*a} Isabelle Landrieu^{*c†} and Christian Ottmann^{*b†}

^a*Medicinal Chemistry, Taros Chemicals GmbH & Co. KG, Emil-Figge-Straße 76a, 44227, Dortmund, Germany. Email: dtzalis@taros.de*

^b*Department of Biomedical Engineering and Institute for Complex Molecular Systems, Technische Universiteit Eindhoven, Den Dolech 2, 5612, AZ, Eindhoven, the Netherlands. Email: c.ottmann@tue.nl*

^c*Univ. Lille, CNRS, UMR 8576 - UGSF - F-59000 Lille, France. Email: isabelle.landrieu@univ-lille.fr*

^d*Department of Physical and Macromolecular Chemistry, Faculty of Science, Charles University, 12843 Prague, Czech Republic*

^e*Department of Structural Biology of Signaling Proteins, Division BIOCEV, Institute of Physiology of the Czech Academy of Sciences, Prumyslova 595, 252 50 Vestec, Czech Republic*

^f*Department of Chemistry, University of Duisburg-Essen, Universitätsstraße 7, 45117, Essen, Germany*

† Equal contribution.

ABSTRACT

Protein-protein interactions (PPIs) are at the core of regulation mechanisms in biological systems and consequently became an attractive target for therapeutical intervention. PPIs involving the adapter protein 14-3-3 are representative examples given the broad range of partner proteins forming a complex with one of its seven human isoforms. Given the challenges represented by the nature of these interactions, fragment-based approaches offer a valid alternative for the development of PPIs modulators. After having assembled a fragments set tailored on PPIs' modulation, we started a screening campaign on the sigma isoform of 14-3-3 adapter proteins. Through the use of both mono- and bi-dimensional Nuclear Magnetic Resonance spectroscopy measurements, coupled with Differential Scanning Fluorimetry, three fragment hits were identified. These molecules bind the protein at two different regions distant from the usual binding groove highlighting new possibilities for selective modulation of 14-3-3 complexes.

INTRODUCTION

Adapter proteins play a crucial role in the occurrence of complexes formation, and their stabilization in regulatory pathways. Given their function – to mediate interactions between two proteins and therefore to regulate the activity or localization of their partners – this protein class represents an attractive point for therapeutic intervention. An example of adapter proteins is represented by the 14-3-3 protein's family that – through its seven human isoforms¹ – is involved in the regulation of numerous biological functions such as cellular signalling,² protein translocation,³ enzymatic activity modulation,⁴ cell cycle regulation,⁵ structural maintenance⁶ and many others. 14-3-3 proteins are dimers composed by two 30 kDa monomers constituted by 9 α helices, named αA - αI .¹ Nowadays, PPIs attract significant interest by the pharma industry but are also challenging targets in drug discovery. PPIs involved in regulation are generally weak, ensuring a turn-over and mainly correspond to superficial interactions between two – or more – proteins. Nonetheless, the multiplicity of hydrogen bonds,⁷ lipophilic interactions, π -stacking, π -cation stacking⁸ and ionic interactions⁹ observed in these interactions constitute a complex and dynamic network that is hard to emulate. Their modulation has been studied intensively and several approaches have emerged to improve the discovery of small molecules able to offer therapeutic interventions. In a previous work¹⁰ the rise of fragment-based approaches in this field was discussed as a good opportunity for developing successful modulators. Circa one third of the clinical candidates or approved drugs modulating PPIs has been indeed developed by application of a fragment-based campaign. The central idea of fragment-based approach (FBA) is to develop a ligand for its own target, building it piece-by-piece from a low molecular weight (MW) molecule. Because of this principle, this strategy offers numerous advantages such as the possibility to constantly validate the molecules' evolution and to cover a very broad chemical space using one binding pharmacophore. This multidisciplinary strategy is generally constituted by a multistep workflow that allows scientists to go relatively fast from a fragment – an entity with a MW \leq 300 Da – to a drug-like molecule ready to enter the clinical phase. Considering the fragments' nature – resumed by the *Congreeves' Rule of Three*¹¹ – the chances to find key structural motifs able to address the target's binding site with higher ligand efficiency are increased. However, as fragments do not contain many functional groups, the

number of interactions with the target is also limited and therefore these compounds bind weakly (normally in the high μM – mM range). Among the broad range of biophysical techniques involved in the primary screening, Nuclear Magnetic Resonance (NMR) is especially suitable to detect weak and very weak interactions (μM – mM range),¹² which is a major reason for its employment in the FBA. NMR fragment screening methods can be divided in two classes: Ligand-based methods and Protein-based methods. While Ligand-based methods allow the fast and sensitive screening of fragment mixtures with little material consumption,¹³ Protein-based methods are more robust and allow, in cases where a protein assignment is available, the determination of the approximate binding site.¹⁴

In recent years, a considerable effort has been put on the development of modulators of 14-3-3 PPIs, ranging from covalent¹⁵ and non-covalent fragments,¹⁶ peptidomimetic inhibitors,^{17,18} semi-synthetic derivatives of natural compounds¹⁹ and molecular tweezers.^{20,21} Considering that 14-3-3 proteins have hundreds of different protein-partners with a variety of binding interfaces, the discovery of small attaching points in their structures is important towards the selective modulation of 14-3-3 PPIs. The results presented here contribute to the enrichment of the portfolio of 14-3-3 binders with three novel fragments binding to two different areas of 14-3-3 σ .

EXPERIMENTAL

Setup of the fragment collection

With the aim to identify novel chemical entities as a starting point in the development of modulators (either disruptive or stabilizing) of 14-3-3 σ interactions, we performed a fragment screening campaign. The first step on this pathway is the set-up of a fragments' pool. Currently Taros proprietary fragments collection counts a subdivision dedicated to the PPIs' modulation with circa 1230 entries comprising both commercially available and novel structures. In this paragraph we describe the guidelines used for building up this fragments' set and the criteria applied for its growth. In a usual practice, the Congreve's "Rule of Three" (Ro3) would be applied. It represents one of the main guidelines for identifying molecules presenting the optimal physico-chemical properties required for being considered as a reliable

member of the set. These attributes can be listed as follows: Molecular Weight ≤ 300 Da, clogP ≤ 3 as well as the number of rotatable bonds and hydrogen-bond acceptors (HBAs) and donors (HBDs), Polar Surface Area (PSA) $\leq 60 \text{ \AA}^2$. However, considering the superficial nature of PPIs as well as the dynamic behaviour of a pocket formed by two proteins, we decided to apply a higher tolerance regarding these original selection parameters. Thus, we considered as optimal parameters Molecular Weight ≤ 330 Da, clogP ≤ 3.4 , number of rotatable bonds ≤ 4 as well as the hydrogen-bond acceptors (HBAs) and donors (HBDs), and at last a Polar Surface Area $\leq 70 \text{ \AA}^2$. Nonetheless, in order to include also very attractive and chemically accessible structures that otherwise would not have passed the filtering phase, we decided to perform a pre-filtering on the whole Taros internal compounds collection (ca. 20000 entries) fixing a threshold of 350 Da for the MW. This pre-filtering phase was followed by a visual inspection of the molecules (ca. 300) with a mass between 330 Da (our parameters for the final physico-chemical filtering) and 350 Da. As anticipated, the process started from the whole Taros' compounds collection and after the two rounds of physico-chemical properties filtering we reached a pool of ca. 4000 entries. Internal IP verification of all novel structures within this set decreased the number of molecules to 3200, which were submitted to additional considerations. The aim of this second step was to remove the entries presenting undesired structural features and to create a diversified collection. Inspecting the collection from a medicinal chemistry point of view led us to exclude extremely reactive functions, such as alkylating or acylating features like aliphatic halides, acyl chlorides, epoxides, imines, oximes and acetals. We also excluded Michael acceptors and isocyanates due to their strong electrophilic character. On the other hand, polycyclic and heterocyclic compounds as well as sp^3 -enriched compounds, when possible, were always preferred in order to enrich the collection with a higher three-dimensional character. Another consideration applied in this phase was the synthetic accessibility of the molecules and the presence of exit points for further derivatization. Moreover, in order to keep the reactivity of the molecules under control and at the same time to enhance the synthetic tractability of any eventual hit, we considered the isosteric members of the collection. For a given molecule, the carboxylic acid was preferred to the corresponding boronic acid or nitro group. For maintaining a high diversity between the cores composing the set, we picked up – after visual inspection – one

of the three possible positions for mono substituted aromatic rings keeping the other two as backup molecules. Physical availability of the selected entries was evaluated and compounds available in less than 30 mg were discarded. A quality control was performed by uHPLC-MS integrated systems and – when necessary – purification by preparative HPLC was carried out. Applying this workflow, we built up a collection of circa 900 compounds, this last set was further enriched by the design and synthesis of novel cores. Fig. 1 shows the workflow applied for the set-up of the Taros' fragment library. Currently, the PPIs-dedicated section of the Taros' fragment collection counts circa 1230 entries and is in constant growing. For a statistical analysis of the physico-chemical properties, we remand to Fig. S1 and S2. Finally, for the aim of this project, we selected circa 800 fragments that were first combined in cocktails containing five fragments each and then screened against 14-3-3 σ applying a multistep approach.

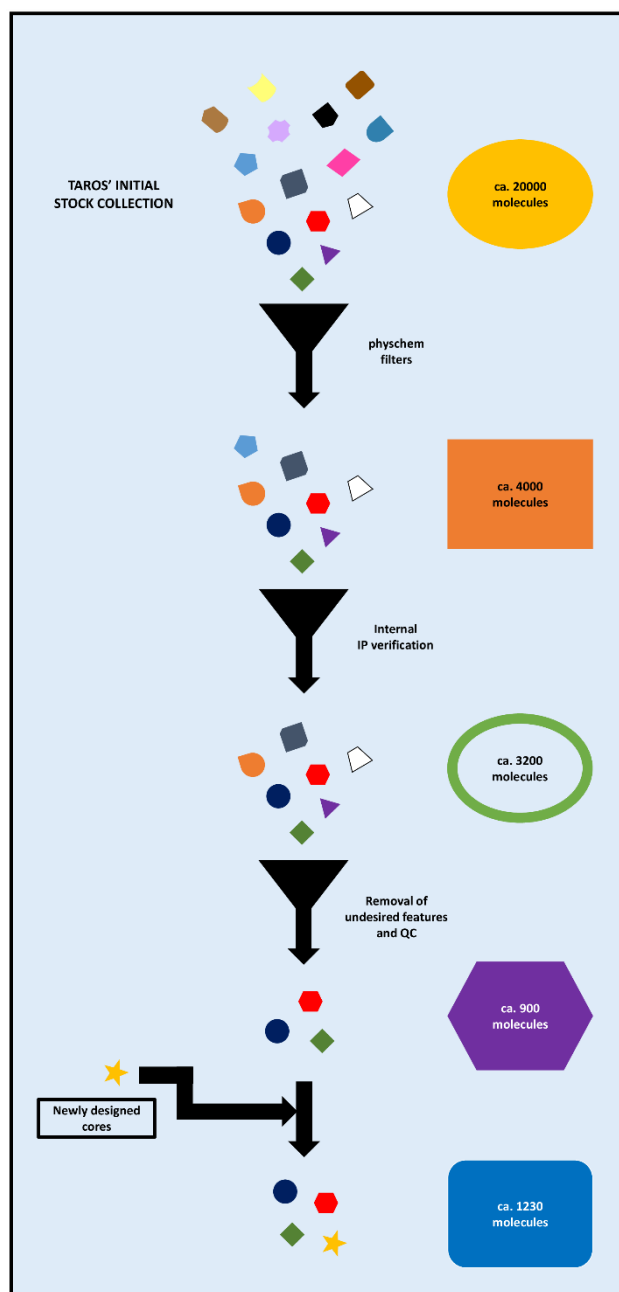


Figure 1 - Workflow applied for setting up the Taros' PPIs fragment library.

Physico-chemical Filtering

Physico-chemical properties have been calculated by ChemAxon JChem for Excel (version 16.10.1700.1231).

Fragments' quality control and purification

The initial purity of each fragment was analysed by uHPLC-MS integrated systems. For each sample, 100 mg were weighted and dissolved in a mixture of Acetonitrile and Methanol in ratio 1:1. The non-soluble fragments were excluded from the collection. uHPLC-MS checks were performed using uHPLC Agilent Technologies 1290 Infinity coupled with Agilent Technologies 6120 Quadrupole LC/MS, Column: ACQUITY UPLC®BEH C18 1.7 μm , mobile phase: mixture of Acetonitrile + 0.1% Formic Acid and Water + 0.1% Formic Acid. When purity was below the 85% threshold, preparative HPLC was performed using UPLC Agilent Technologies 1260 Infinity coupled with Agilent Technologies 6120 Quadrupole LC/MS, Column: XBridge EH C18 5 μm , 19 mm x 150 mm, mobile phase: mixture of Acetonitrile + 0.1% Formic Acid and Water + 0.1% Formic Acid.

Protein Production and Purification

14-3-3 σ (for Differential Scanning Fluorimetry experiments) or 14-3-3 $\sigma\Delta\text{C17}$ (cleaved after T231 – used for NMR experiments to improve the quality of spectra) were expressed in *E. coli* BL21 (DE3) cells transformed with a pProExHtb vector carrying the cDNA to express an N-terminally His₆-tagged human 14-3-3 σ or 14-3-3 $\sigma\Delta\text{C17}$. An overnight 20 mL pre-culture in *Luria-Bertani* (LB) medium was used to inoculate 1 L of culture medium. For the natural abundance proteins, cells were inoculated in 1 L of M9 minimal medium supplemented with 4 g/L Glucose, 1 g/L Ammonium Chloride, 5% (v/v) LB medium and 100 $\mu\text{g}/\text{mL}$ ampicillin. For ¹⁵N²H labelling, the cells were inoculated in 1 L of deuterated M9 minimal medium supplemented with 2 g/L ¹²C₆²H₇ Glucose, 1 g/L ¹⁵N Ammonium Chloride, 0.4 g/L Isogro ¹⁵N¹²C²H Powder – Growth Medium (Sigma Aldrich) and 100 $\mu\text{g}/\text{mL}$ ampicillin. Cells were grown at 37 °C to an OD₆₀₀ of 0.9 and induced with 0.5 mM IPTG. Incubation was continued for 12 h at 25 °C for the natural abundance proteins and for 15 h at 28 °C for the ¹⁵N²H labelled protein. Cells were harvested by centrifugation, lysed with a homogenizer and the proteins were purified using a Ni-NTA column (GE Healthcare). The N-terminal His₆-tag was then cleaved by the TEV protease and the proteins were further dialyzed overnight at 4 °C against NMR buffer (100 mM Sodium Phosphate, pH 6.8, 50 mM NaCl), concentrated, aliquoted, flash

frozen and stored at -80 °C. Typical yields were in the range of 40 to 80 mg of protein per liter of culture. A detailed protocol can be found at Neves *et al.*²²

Differential Scanning Fluorimetry

Differential Scanning Fluorimetry (DSF) Thermal melting points were recorded using a LightCycler® 480 (Roche, Switzerland). Measurements were performed in 96-well plates with samples containing 7 µM 14-3-3σ in the presence or absence of each cocktail (2500 µM per fragment). The buffer contained 100 mM Hepes, pH 7.5, 150 mM NaCl and 4% (v/v) DMSO. The fluorescent probe SYPRO Orange (Sigma Aldrich) was added at a dilution of 1:600. The excitation filter for SYPRO Orange was set to 465 nm and the emission filter was set to 580 nm. The temperature was increased from 20 °C to 95 °C at a rate of 0.6 °C per minute. Melting temperature values were determined using the LightCycler® 480 software version 1.5.1.62 by plotting the first derivative of the melting curves (Fig. S3). All the measurements were performed in triplicates and the deviations of melting temperatures (ΔT_m) presented for each cocktail were calculated relatively to three control samples (7 µM 14-3-3σ in the absence of compound) measured in the same 96-well plate.

WaterLOGSY Experiments

WaterLOGSY spectra were acquired in 5 mm tubes (sample volume 530 µL) using a 600 MHz Bruker Avance III HD spectrometer equipped either with a CPQCI cryogenic probe or with a TXI non-cryogenic probe. The spectra were recorded with 32768 complex data points and with a mixing time of 1.7s. Number of scans per increment was 384 when the spectrometer was equipped with a cryogenic probe (acquisition time of 35 minutes per experiment) and 1280 when the spectrometer was equipped with a non-cryogenic probe (acquisition time of 118 minutes). The spectra were acquired at 16 °C, in a buffer containing 100 mM sodium phosphate, 50 mM NaCl, pH 6.8 and 10% (v/v) D₂O. The final concentration of DMSO-d₆ was 2% and was kept constant for all the experiments. The spectra were performed with samples containing 25 µM 14-3-3σΔC17 in the presence or in the absence of each cocktail (500 µM per fragment) or each fragment (at 500 µM). Additional control experiments were performed in

the presence of the cocktail/fragment and in the absence of protein. Spectra were collected and processed with Topspin 3.5 (Bruker Biospin, Karlsruhe, Germany).

2D Nuclear Magnetic Resonance Experiments

^1H - ^{15}N TROSY-HSQC spectra were acquired in 3 mm tubes (sample volume 200 μL) using a 900 MHz Bruker Avance-NEO spectrometer, equipped with a cryoprobe. The spectra were recorded with 3072 complex data points in the direct dimension and 120 complex data points in the indirect dimension, with 128 scans per increment (acquisition time of 4 hours per experiment), at 32 $^\circ\text{C}$, in a buffer containing 100 mM sodium phosphate, 50 mM NaCl, pH 6.8, 1 mM DTT, EDTA-free protease inhibitor cocktail (Roche, Basel, Switzerland) and 10% (v/v) D_2O . The final concentration of DMSO-d_6 was 2% and was kept constant for all the experiments. The spectra were performed with samples containing 75 μM $^{15}\text{N}^2\text{H}$ labelled 14-3-3 $\sigma\Delta\text{C17}$ in the presence or in the absence of each cocktail (2000 μM per fragment). Backbone assignments of $^{15}\text{N}^2\text{H}$ labelled 14-3-3 $\sigma\Delta\text{C17}$ were previously reported.²² The reference for the ^1H chemical shift was relative to trimethylsilyl propionate (TMSP) or 4,4-dimethyl-4-silapentane-1-sulfonic acid (DSS). ^{15}N chemical shifts were referenced indirectly. Spectra were collected and processed with Topspin 4.0 (Bruker Biospin, Karlsruhe, Germany) and analyzed with Sparky 3.12 (T. D. Goddard and D. G. Kneller, SPARKY 3, University of California, San Francisco). CSPs in the form of chemical shift value modifications (in ppm) on the ^1H - ^{15}N TROSY-HSQC were calculated using the following equation:

$$\Delta\delta = \sqrt{\Delta\delta(^1\text{H})^2 + [0.14 * \Delta\delta(^{15}\text{N})^2]}$$

RESULTS AND DISCUSSION

Design of new cores: the “SARs by BioCores” concept

Nowadays, numerous natural product-derived molecules for modulation of relevant biological targets are available.^{23,24} Particularly, several natural products (NPs) have been identified also as valuable tools and starting points for PPI modulation programs.²⁵⁻³⁰ There have been examples described for Neuronal Acetylcholine Receptors³¹ and 11 β -

Hydroxysteroid Dehydrogenases.³² Further targets were addressed for cancer^{33,34} and diseases like malaria and African Trypanosomiasis.³⁵ We took this strategy in consideration during the design phase of our fragment collection. In this case we started from Nicotine (Fig. 2, a), a natural alkaloid that is widely known in drug discovery for its activity on the cholinergic system. Noteworthy, its structure presents one heteroaromatic ring (pyridine) directly connected to an aliphatic heterocycle (N-methylpyrrolidine) forming a chiral centre with S-configuration. Molecules bearing these specific structural features (a heteroaromatic ring and an aliphatic heterocycle connected by no more than a three carbon chain) have been ascribed into the BioCores – structural motifs which are frequently observed in marketed drugs.³⁶ Another advantage of this class of compounds – considering its intrinsic isosteric character – is its suitability for a straightforward scaffold hopping approach during an eventual follow-up phase. Since, incorporation of NPs-derived cores – especially BioCores – into a compounds set enhances the drug likeness of each member of the library,³⁶ we seized the opportunity for structural elaboration of the Nicotine's core in order to further explore its chemical space. As Fig. 2 shows, Nicotine (a) offers just one exit point for diversification represented by the pyrrolidine nitrogen. The aim of the design of Nicotine-like structures was to maintain both its pharmacophoric features and its three-dimensional character while introducing additional points for diversification. The first example of this structural evolution is represented by the *2-(pyrrolidin-2-yl)-imidazole* series (Fig. 2, b) where an additional exit point has been introduced directly in the hetero-aromatic ring. Going further in the core elaboration, we also applied an easily accessible chemistry that would support our design strategy. The *1,4-disubstituted triazoles* series (Fig. 2, c) allowed us to keep once more the aforementioned features of interest as well as to synthesize analogues where the connection between the two rings is either direct or mediated by one methylene. Additionally, we were able to synthesize selectively the 1,4-regio-isomer with good yields by applying Cu-catalysed Huisgen cycloaddition,³⁷ using various terminal alkynes. It is worth mentioning that in one subsection of this series we extended also saturated hetero-cycle from a 3-substituted pyrrolidine to a 3- or 4-substituted piperidine ring, thus reaching a structural core related to another alkaloid – Anabastine. Eventually, we also introduced a third diversification point in the BioCore including *1,2,4-trisubstituted triazoles* (Fig. 2, d). This was possible through the application of

the one-step triazole synthesis by Castanedo *et al.*³⁸ This last reference described how BioCore showcases a new concept – named as “SARs by BioCores” – that could be included in the toolbox for designing of fragments libraries. In general, applying an accessible and robust synthetic strategy during the design phase allows a fast and systematic probing for favourable interactions by introduction of a small substituent (or no substituent) at one exit vector whilst diversifying the other two positions by parallel chemistry or multistep approaches. Since, the three exit points are designed to be pointing in three different spatial vectors (Fig. 2, black box), the substituents’ orientation and their nature permit not only to rapidly explore the chemical space but also to proceed to a fast identification of the target’s space by using only one scaffold. Such a strategy would provide important information concerning the SARs of a series directly after the initial screenings thus saving valuable time and resources – an idea showing how big the contribution and importance of BioCores-based entities in design of fragments libraries could be.

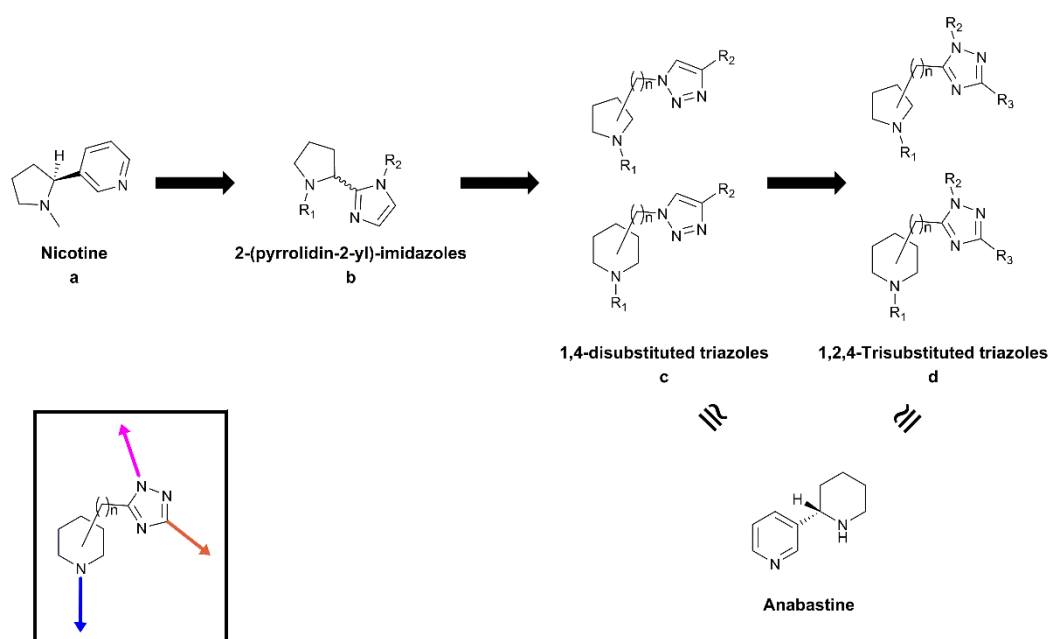


Figure 2 - Example of new core’s design: Nicotine evolution (n between 0 and 3). Within the black box an example of BioCore (n between 0 and 3) is shown where the diversification points lay on different spatial vectors.

Fragment screening strategy

A library of 785 fragments grouped in 157 cocktails of 5 compounds each was screened for binding to 14-3-3 σ with the objective of finding low MW starting points for the development of PPI modulators. Initially, ^1H - ^{15}N TROSY-HSQC were directly recorded for 55 out of the 157 cocktails. For the screening of the rest of the library, DSF and WaterLOGSY were introduced in order to allow a primary screening of the cocktails before confirmation by ^1H - ^{15}N TROSY-HSQC, which is costly and time consuming, but offers the additional advantage of identifying the binding pocket. DSF screening was used for 156 out of the 157 cocktails and WaterLOGSY was applied for the 102 cocktails that were not directly screened by ^1H - ^{15}N TROSY-HSQC. The cocktails which showed binding by either WaterLOGSY or DSF were furthermore screened by ^1H - ^{15}N TROSY-HSQC (secondary screening). The fragments contained in the cocktails showing binding by ^1H - ^{15}N TROSY-HSQC were further screened individually initially by WaterLOGSY and finally by ^1H - ^{15}N TROSY-HSQC for the determination of the binding site. A diagram illustrating this screening strategy is presented in Fig. 3.

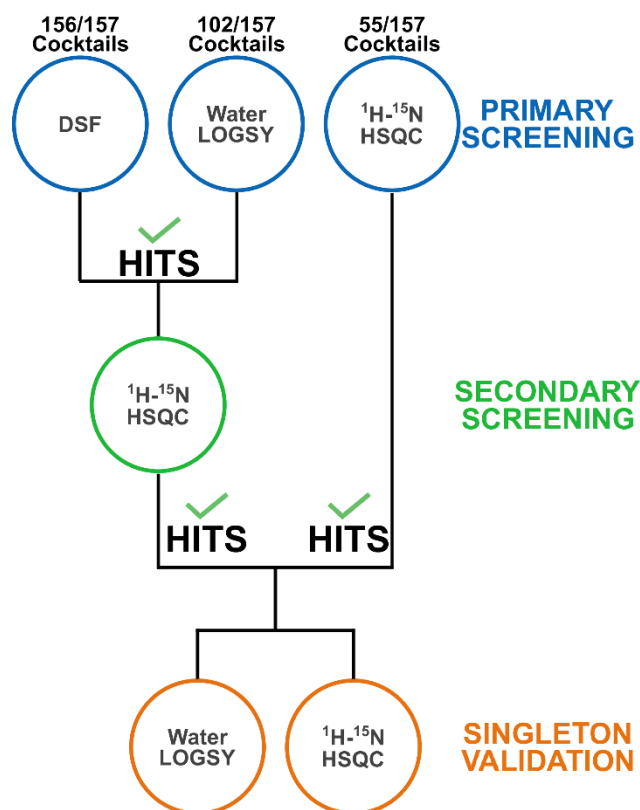


Figure 3 - Workflow of the fragment screening campaign. DSF, Water LOGSY and ^1H - ^{15}N TROSY-HSQC were employed for primary screening. Secondary screening by ^1H - ^{15}N TROSY-HSQC was performed for the cocktails that showed binding by either DSF or WaterLOGSY. Water LOGSY and ^1H - ^{15}N TROSY-HSQC were performed for singleton validation.

Primary Screening by WaterLOGSY

WaterLOGSY is a ligand-based NMR screening method that allows the fast screening of fragment libraries based on the Nuclear Overhauser Effect (NOE).³⁹ WaterLOGSY requires less amount of protein in comparison with protein-based NMR methods and does not require isotopic labelling of the target. Moreover, this method allows a straightforward hit identification since the NMR signals of binders and non binders have a different phase in the WaterLOGSY spectrum (Fig. S4). WaterLOGSY was performed for the 102 cocktails that were not directly screened by ^1H - ^{15}N TROSY-HSQC. Binding was detected for 43 out of the 102 cocktails, which were selected for secondary screening by ^1H - ^{15}N TROSY-HSQC.

Primary Screening by Differential Scanning Fluorimetry

Differential Scanning Fluorimetry (DSF) is a fast method to screen a fragment library with little material consumption. The principle relies on monitoring the thermal melting curve of the protein upon gradual heating of the protein's solution and on the determination of the melting temperature (T_m). A Protein-Ligand Interaction is therefore detected when the binder induces a shift in the melting temperature of the protein.⁴⁰ Unlike most proteins, the thermal denaturation profile of 14-3-3 σ exhibits two sigmoidal curves, suggesting that there are two unfolding transitions (Fig. S3). Both melting temperatures were determined for all the samples and the binding effect was considered significant upon the induction of a thermal shift higher than 1 °C in the sum of both melting temperatures ($\Delta T_{m1} + \Delta T_{m2} > 1$ °C). After the primary screening, 22 out of the screened 156 cocktails showed a significant thermal shift effect (Table S1). These cocktails were therefore selected for secondary screening. 15 cocktails out of these 22 also showed binding by WaterLOGSY.

Primary/Secondary Screening by ^1H - ^{15}N TROSY-HSQC

^1H - ^{15}N HSQC is the most popular method for protein-based NMR screening. In spite of being more expensive and time-consuming when compared to ligand-based NMR methods, ^1H - ^{15}N HSQC is a more robust method and has the important advantage of identifying the binding site of the ligands.⁴¹ ^1H - ^{15}N TROSY-HSQC was used for the screening of 55 out of 157 cocktails and as a secondary screening technique for the 50 cocktails that showed binding by either WaterLOGSY (43), DSF (22) or both (15). From these, 6 cocktails showed a significant effect on the ^1H - ^{15}N TROSY-HSQC of 14-3-3 σ . All 6 cocktails were positive by WaterLOGSY and 4 were positive by DSF as well.

False positives in the DSF screening could be due to aggregates of compounds since a considerable part of the hits showed solubility problems at the tested concentration.

Compared to ^1H - ^{15}N TROSY-HSQC, WaterLOGSY also provided a very high hit rate. Probably some of the hits detected were just binding transiently to the protein and were too weak to be detected by ^1H - ^{15}N TROSY-HSQC. Although negative controls were performed for all the WaterLOGSY tested cocktails, aggregation cannot be excluded as a source of false positives in this method. It is also possible that some of the WaterLOGSY hits were not

confirmed due to the fact that around 15% of the amide resonances of 14-3-3 σ Δ C17 are undetected in the ^1H - ^{15}N TROSY-HSQC.

Confirmation of hits from cocktails and binding site identification

After the identification and orthogonal validation of 6 hit cocktails, we decided to test the components of the cocktails as singletons. Thirty singletons were further screened individually by Water-LOGSY. Six out of these 30 singletons (1 per cocktail) showed a positive effect and were submitted to the final confirmation by ^1H - ^{15}N TROSY-HSQC. Two out of these 6 singletons failed to cause a significant effect on the 2D spectrum of 14-3-3 σ Δ C17. One singleton caused chemical shift perturbations but also induced protein precipitation and was, for this reason, excluded from the screening. Three out of the 6 singletons were successfully confirmed as binders by ^1H - ^{15}N TROSY-HSQC, producing the same effect in the spectrum as their respective corresponding cocktail. These 3 fragments were therefore validated by both a ligand-based method (Fig. S5, S6 and S7) and a protein-based method (Fig. S8, S9 and S10). Fragments **1** and **2** were seen to bind at the top of helices αH and αI (Fig. S8, S9, and 4) and fragment **3** was seen to bind at the dimer interface (Fig. S10 and 4). Interestingly, the cocktails containing the fragments that were seen to bind at the top of helices αH and αI did not produce a significant effect by DSF while the cocktail containing fragment **3** induced a significant thermal shift. This fact suggests that binding at the upper region of the protein does not have an influence on its denaturation.

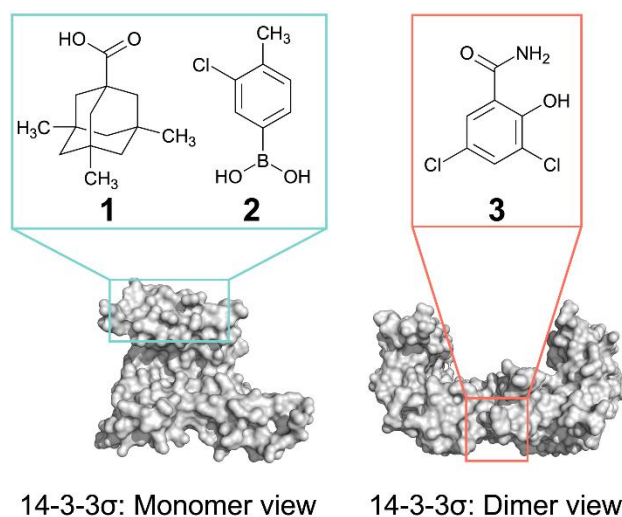


Figure 4 - Identification of the binding sites of the hits by ^1H - ^{15}N TROSY-HSQC. The structures of the hits are represented and their binding sites are shown in the crystal structure of 14-3-3 σ (gray surface - PDB ID: 1YZ5). Fragments **1** and **2** induce chemical shift perturbations in resonances corresponding to amino acid residues located on the top of helices αH and αI . Fragment **3** induces chemical shift perturbations in resonances corresponding to amino acid residues located at the dimer interface of 14-3-3 σ .

CONCLUSIONS

Here we discussed the strategy applied in the set-up of a fragment collection dedicated to PPI modulation. The “SARs by BioCores” concept would address the exploration of the ligand’s chemical space in a more rapid way enabling researchers to perform an immediate first round of SARs directly on the target. Moreover, according to the distribution of its physico-chemical properties, the presented fragment collection fits very well the characteristics needed for a wider application in the PPIs modulation.

In this work, we screened the fragment library on the adapter protein 14-3-3 σ using a multi-technique approach. Application of mono- and bi-dimensional NMR coupled with DSF provided us a robust and orthogonally validated dataset of molecules, rapidly excluding false positives and reintegrating false negative hits.

Eventually we identified three fragment hits binding two different sites from the classic amphipathic groove of 14-3-3 σ , where most of the protein partners bind. Nevertheless there are some examples in which the protein partners establish contacts with different regions of

14-3-3.⁴²⁻⁴⁷ In these cases, fragments that bind remotely from the classic amphipathic binding groove represent a unique opportunity for a selective modulation of the PPIs.

The hits disclosed by this integrated screening campaign represent a new starting point for modulating the 14-3-3 PPIs and highlight an important opportunity for a selectivity improvement towards a specific protein complex.

CONFLICTS OF INTEREST

There are no conflicts to declare.

ACKNOWLEDGMENTS

The research is supported by funding from the European Union through the TASPPi project (H2020-MSCA-ITN-2015, grant number 675179). DV acknowledge Dr. Martin Corpet for the fruitful scientific discussion. J.F.N, F-X.C, X.H and I.L acknowledge LabEx (Laboratory of Excellence) for financial support on the scope of the DISTALZ consortium (ANR, ANR-11-LABX-009). The NMR facilities were funded by the Nord Region Council, CNRS, Institut Pasteur de Lille, the European Community (ERDF), the French Ministry of Research and the University of Lille and by the CTRL CPER cofunded by the European Union with the European Regional Development Fund (ERDF), by the Hauts de France Regional Council (contract n°17003781), Métropole Européenne de Lille (contract n°2016_ESR_05), and French State (contract n°2017-R3-CTRL-Phase 1). We acknowledge support for the NMR facilities from TGE RMN THC (CNRS, FR-3050) and FRABio (Univ. Lille, CNRS, FR-3688).

NOTES AND REFERENCES

- 1 T. Obsil and V. Obsilova, *Semin. Cell Dev. Biol.*, 2011, 22, 663–672.
- 2 R. J. Daly, H. Gu, J. Parmar, S. Malaney, R. J. Lyons, R. Kairouz, D. R. Head, S. M. Henshall, B. G. Neel and R. L. Sutherland, *Oncogene*, 2002, 21, 5175–5181.
- 3 C. Aguilera, V. Fernández-Majada, J. Inglés-Esteve, V. Rodilla, A. Bigas and L. Espinosa, *J Cell Sci*, 2006, 119, 3695–3704.
- 4 S. C. Masters, H. Yang, S. R. Datta, M. E. Greenberg and H. Fu, *Mol. Pharmacol.*, 2001, 60, 1325–1321.

- 5 K. H. Vousden and C. Prives, *Cell*, 2009, 137, 413–431.
- 6 N. N. Sluchanko and N. B. Gusev, *J. Alzheimers Dis.*, 2011, 27, 467–476.
- 7 L.-G. Milroy, T. N. Grossmann, S. Hennig, L. Brunsveld and C. Ottmann, *Chem. Rev.*, 2014, 114, 4695–4748.
- 8 M. G. Wuo, A. B. Mahon and P. S. Arora, *J. Am. Chem. Soc.*, 2015, 137, 11618–11621.
- 9 B. Schumacher, J. Mondry, P. Thiel, M. Weyand and C. Ottmann, *FEBS Lett.*, 2010, 584, 1443–1448.
- 10 D. Valenti, S. Hristeva, D. Tzalis and C. Ottmann, *Eur. J. Med. Chem.*, 2019, 167, 76–95.
- 11 M. Congreve, R. Carr, C. Murray and H. Jhoti, *Drug Discov. Today*, 2003, 8, 876–877.
- 12 M. P. Williamson, *Prog. Nucl. Magn. Reson. Spectrosc.*, 2013, 73, 1–16.
- 13 L. Unione, S. Galante, D. Díaz, F. J. Cañada and J. Jiménez-Barbero, *MedChemComm*, 2014, 5, 1280–1289.
- 14 A. D. Gossert and W. Jahnke, *Prog. Nucl. Magn. Reson. Spectrosc.*, 2016, 97, 82–125.
- 15 E. Sijbesma, K. K. Hallenbeck, S. Leysen, P. J. de Vink, L. Skóra, W. Jahnke, L. Brunsveld, M. R. Arkin and C. Ottmann, *J. Am. Chem. Soc.*, 2019, 141, 3524–3531.
- 16 E. Sijbesma, L. Skora, S. Leysen, L. Brunsveld, U. Koch, P. Nussbaumer, W. Jahnke and C. Ottmann, *Biochemistry (Mosc.)*, 2017, 56, 3972–3982.
- 17 S. A. Andrei, F. A. Meijer, J. F. Neves, L. Brunsveld, I. Landrieu, C. Ottmann and L.-G. Milroy, *ACS Chem. Neurosci.*, 2018, 9, 2639–2654.
- 18 L.-G. Milroy, M. Bartel, M. A. Henen, S. Leysen, J. M. C. Adriaans, L. Brunsveld, I. Landrieu and C. Ottmann, *Angew. Chem. Int. Ed.*, 2015, 54, 15720–15724.
- 19 S. A. Andrei, P. de Vink, E. Sijbesma, L. Han, L. Brunsveld, N. Kato, C. Ottmann and Y. Higuchi, *Angew. Chem. Int. Ed.*, 2018, 57, 13470–13474.
- 20 D. Bier, R. Rose, K. Bravo-Rodriguez, M. Bartel, J. M. Ramirez-Angueta, S. Dutt, C. Wilch, F.-G. Klärner, E. Sanchez-Garcia, T. Schrader and C. Ottmann, *Nat. Chem.*, 2013, 5, 234–239.
- 21 D. Bier, S. Mittal, K. Bravo-Rodriguez, A. Sowislok, X. Guillory, J. Briels, C. Heid, M. Bartel, B. Wettig, L. Brunsveld, E. Sanchez-Garcia, T. Schrader and C. Ottmann, *J. Am. Chem. Soc.*, 2017, 139, 16256–16263. DOI: 10.1021/jacs.7b07939.
- 22 J. F. Neves, I. Landrieu, H. Merzougui, E. Boll, X. Hanouille and F.-X. Cantrelle, *Biomol. NMR Assign.*, DOI:10.1007/s12104-018-9860-1.

- 23 S. Wetzel, R. S. Bon, K. Kumar and H. Waldmann, *Angew. Chem. Int. Ed.*, 2011, 50, 10800–10826.
- 24 A. L. Harvey, R. Edrada-Ebel and R. J. Quinn, *Nat. Rev. Drug Discov.*, 2015, 14, 111–129.
- 25 P. Thiel, M. Kaiser and C. Ottmann, *Angew. Chem. Int. Ed.*, 2012, 51, 2012–2018.
- 26 R. Rose, S. Erdmann, S. Bovens, A. Wolf, M. Rose, S. Hennig, H. Waldmann and C. Ottmann, *Angew. Chem. Int. Ed.*, 2010, 49, 4129–4132.
- 27 D. Bier, M. Bartel, K. Sies, S. Halbach, Y. Higuchi, Y. Haranosono, T. Brummer, N. Kato and C. Ottmann, *ChemMedChem*, 2016, 11, 911–918.
- 28 L.-G. Milroy, L. Brunsveld and C. Ottmann, *ACS Chem. Biol.*, 2013, 8, 27–35.
- 29 C. Ottmann, *Bioorg. Med. Chem.*, 2013, 21, 4058–4062.
- 30 F. Giordanetto, A. Schäfer and C. Ottmann, *Drug Discov. Today*, 2014, 19, 1812–1821.
- 31 C. Dallanoce, P. Bazza, G. Grazioso, M. D. Amici, C. Gotti, L. Riganti, F. Clementi and C. D. Micheli, *Eur. J. Org. Chem.*, 2006, 2006, 3746–3754.
- 32 M. A. Koch, A. Schuffenhauer, M. Scheck, S. Wetzel, M. Casaulta, A. Odermatt, P. Ertl and H. Waldmann, *Proc. Natl. Acad. Sci.*, 2005, 102, 17272–17277.
- 33 Y. Zhang, Z. Zhang, B. Wang, L. Liu and Y. Che, *Bioorg. Med. Chem. Lett.*, 2016, 26, 1885–1888.
- 34 D. J. Newman, G. M. Cragg, S. Holbeck and E. A. Sausville, *Curr. Cancer Drug Targets*, 2002, 2, 279–308.
- 35 D. Camp, R. A. Davis, M. Campitelli, J. Ebdon and R. J. Quinn, *J. Nat. Prod.*, 2012, 75, 72–81.
- 36 R. Kombarov, A. Altieri, D. Genis, M. Kirpichenok, V. Kochubey, N. Rakitina and Z. Titarenko, *Mol. Divers.*, 2010, 14, 193–200.
- 37 M. Meldal and C. W. Tornøe, *Chem. Rev.*, 2008, 108, 2952–3015.
- 38 G. M. Castanedo, P. S. Seng, N. Blaquiere, S. Trapp and S. T. Staben, *J. Org. Chem.*, 2011, 76, 1177–1179.
- 39 C. Dalvit, G. Fogliatto, A. Stewart, M. Veronesi and B. Stockman, *J. Biomol. NMR*, 2001, 21, 349–359.
- 40 A. Ciulli, in *Protein-Ligand Interactions: Methods and Applications*, eds. M. A. Williams and T. Daviter, Humana Press, Totowa, NJ, 2013, pp. 357–388.

- 41 R. Ma, P. Wang, J. Wu and K. Ruan, *Molecules*, 2016, 21, 854.
- 42 M. Alblova, A. Smidova, V. Docekal, J. Vesely, P. Herman, V. Obsilova and T. Obsil, *Proc. Natl. Acad. Sci.*, 2017, 114, E9811–E9820.
- 43 T. Obsil, R. Ghirlando, D. C. Klein, S. Ganguly and F. Dyda, *Cell*, 2001, 105, 257–267.
- 44 C. Ottmann, S. Marco, N. Jaspert, C. Marcon, N. Schauer, M. Weyand, C. Vandermeeren, G. Duby, M. Boutry, A. Wittinghofer, J.-L. Rigaud and C. Oecking, *Mol. Cell*, 2007, 25, 427–440.
- 45 K. Psenakova, O. Petrvalska, S. Kylarova, D. Lentini Santo, D. Kalabova, P. Herman, V. Obsilova and T. Obsil, *Biochim. Biophys. Acta BBA - Gen. Subj.*, 2018, 1862, 1612–1625.
- 46 N. N. Sluchanko, S. Beelen, A. A. Kulikova, S. D. Weeks, A. A. Antson, N. B. Gusev and S. V. Strelkov, *Structure*, 2017, 25, 305–316.
- 47 K. Taoka, I. Ohki, H. Tsuji, K. Furuita, K. Hayashi, T. Yanase, M. Yamaguchi, C. Nakashima, Y. A. Purwestri, S. Tamaki, Y. Ogaki, C. Shimada, A. Nakagawa, C. Kojima and K. Shimamoto, *Nature*, 2011, 476, 332–335.

Targeting 14-3-3 protein interface with a fragment-based approach

Dario Valenti,^{a,b,†} João Filipe Neves,^{c,†} François-Xavier Cantrelle,^c Stanimira Hristeva,^a Domenico Lentini Santo,^d Tomáš Obšil,^{d,e} Xavier Hanouille,^c Laura Mariana Levy,^{a,†} Dimitrios Tzalis,^{*a} Isabelle Landrieu^{*c,†} and Christian Ottmann^{*b,f,†}

^{a.} *Medicinal Chemistry, Taros Chemicals GmbH & Co. KG, Emil-Figge-Straße 76a, 44227, Dortmund, Germany. Email: dtzalis@taros.de*

^{b.} *Department of Biomedical Engineering and Institute for Complex Molecular Systems, Technische Universiteit Eindhoven, Den Dolech 2, 5612, AZ, Eindhoven, the Netherlands. Email: c.ottmann@tue.nl*

^{c.} *Univ. Lille, CNRS, UMR 8576 - UGSF - F-59000 Lille, France. Email: isabelle.landrieu@univ-lille.fr*

^{d.} *Department of Physical and Macromolecular Chemistry, Faculty of Science, Charles University, 12843 Prague, Czech Republic*

^{e.} *Department of Structural Biology of Signaling Proteins, Division BIOCEV, Institute of Physiology of the Czech Academy of Sciences, Prumyslova 595, 252 50 Vestec, Czech Republic*

^{f.} *Department of Chemistry, University of Duisburg-Essen, Universitätsstraße 7, 45117, Essen, Germany*

† Equal contribution.

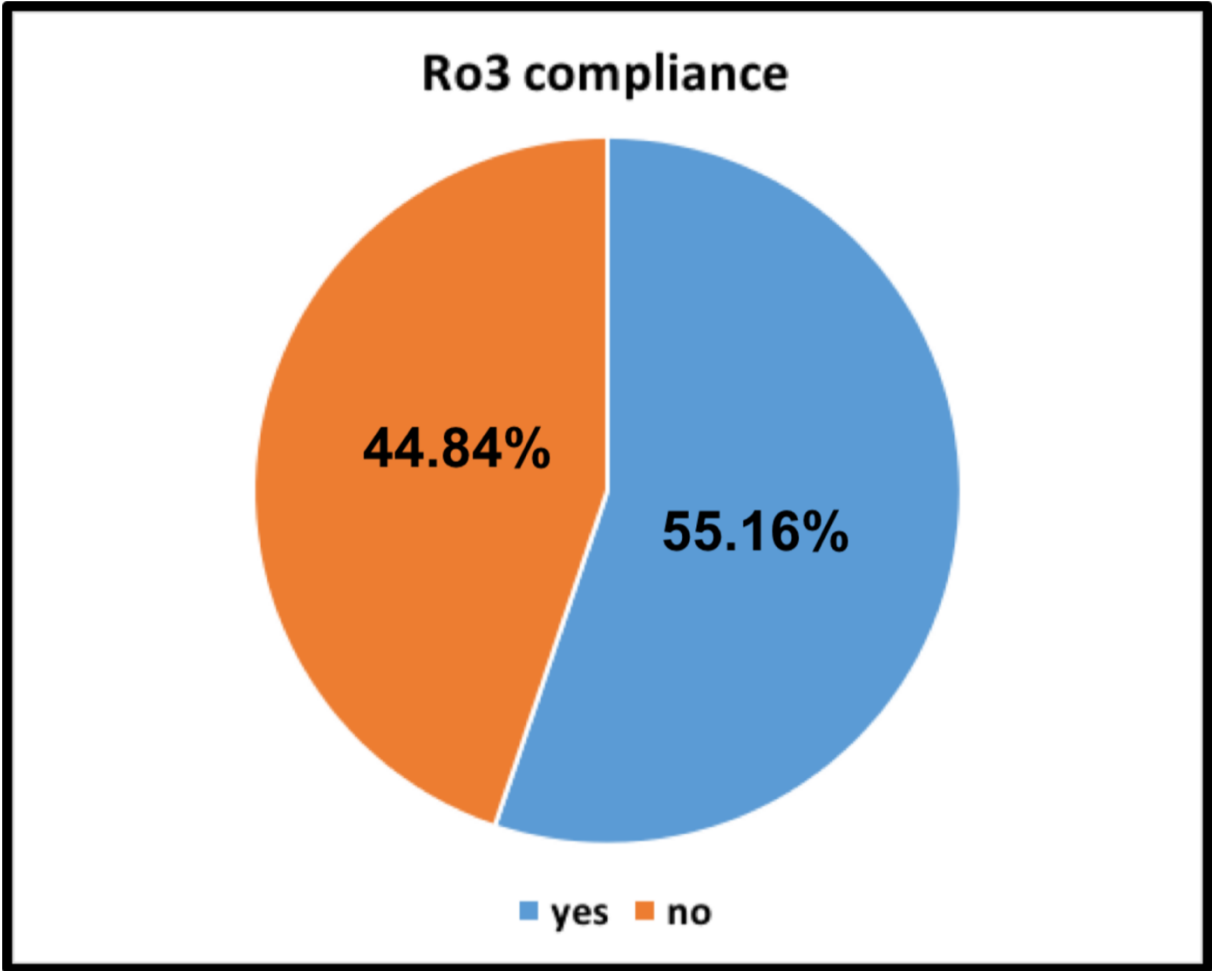


Chart S1 - Ro3 compliance of the fragment collection.

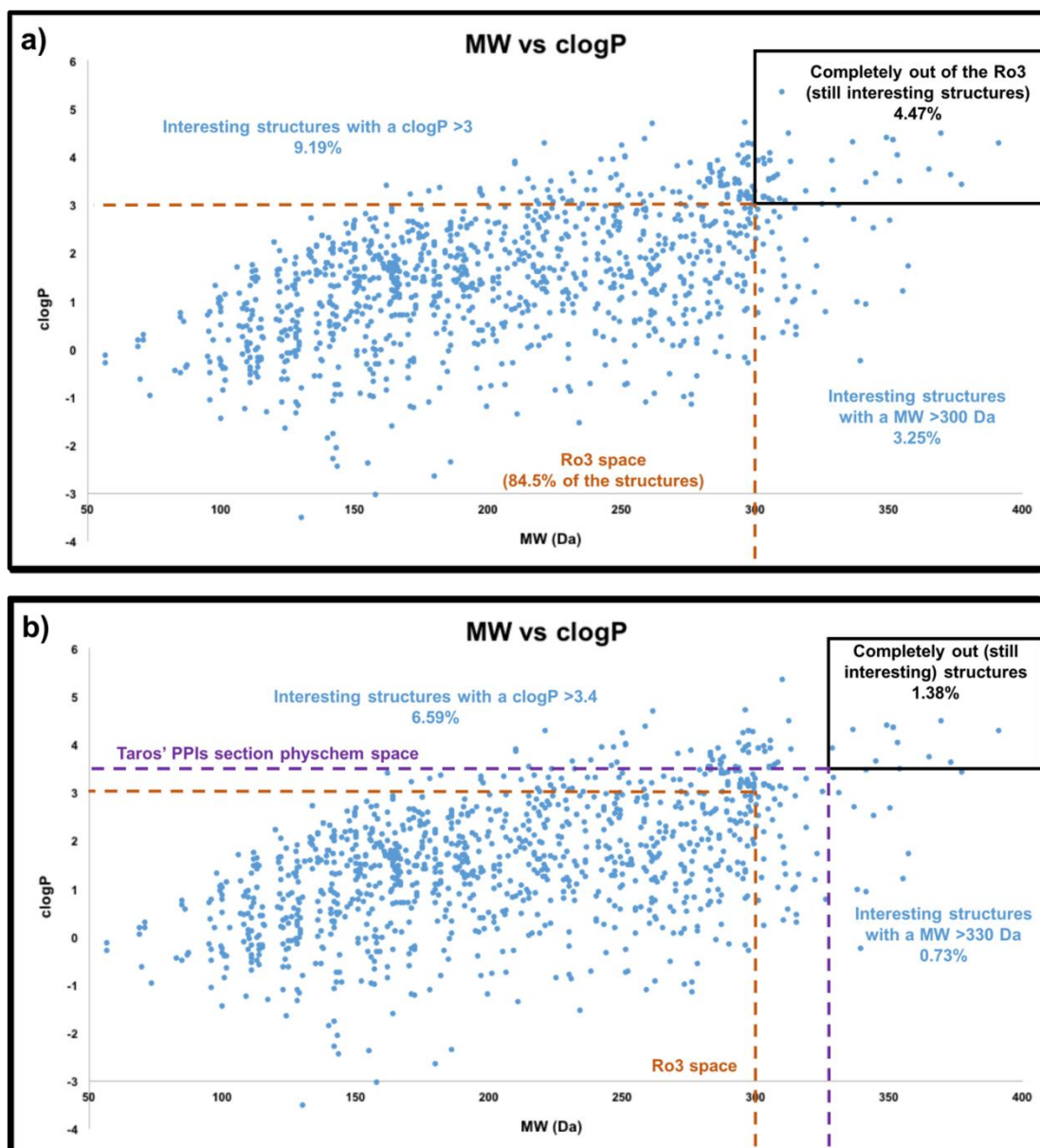


Figure S1 - Fragments' MW and clogP distribution. Correlation between MW and clogP considering the classical Rule of Three parameters (A) or the revised limits (MW 330 Da and clogP 3.4) used for setting up the collection (B). Orange dashed line delimitates the Rule of Three (Ro3) space that is included into the wider parameters selected for this particular subset of the Taros' fragment library (purple dashed lines, (B)) while the black box on the top right includes the entries with both MW and clogP out of the Ro3 space (A) or out of the Taros' PPIs physchem space (B). (A) 12% of the structures have at least one parameter out of the rule and only 4% of the entries have both MW and clogP outside of the rule but present promising structures. (B) The percentage of structures with MW or clogP parameters over the settings decrease to 7.3% (compared to (A)) while 1.4% present both MW and clogP over the set limits but nonetheless have attractive structures.

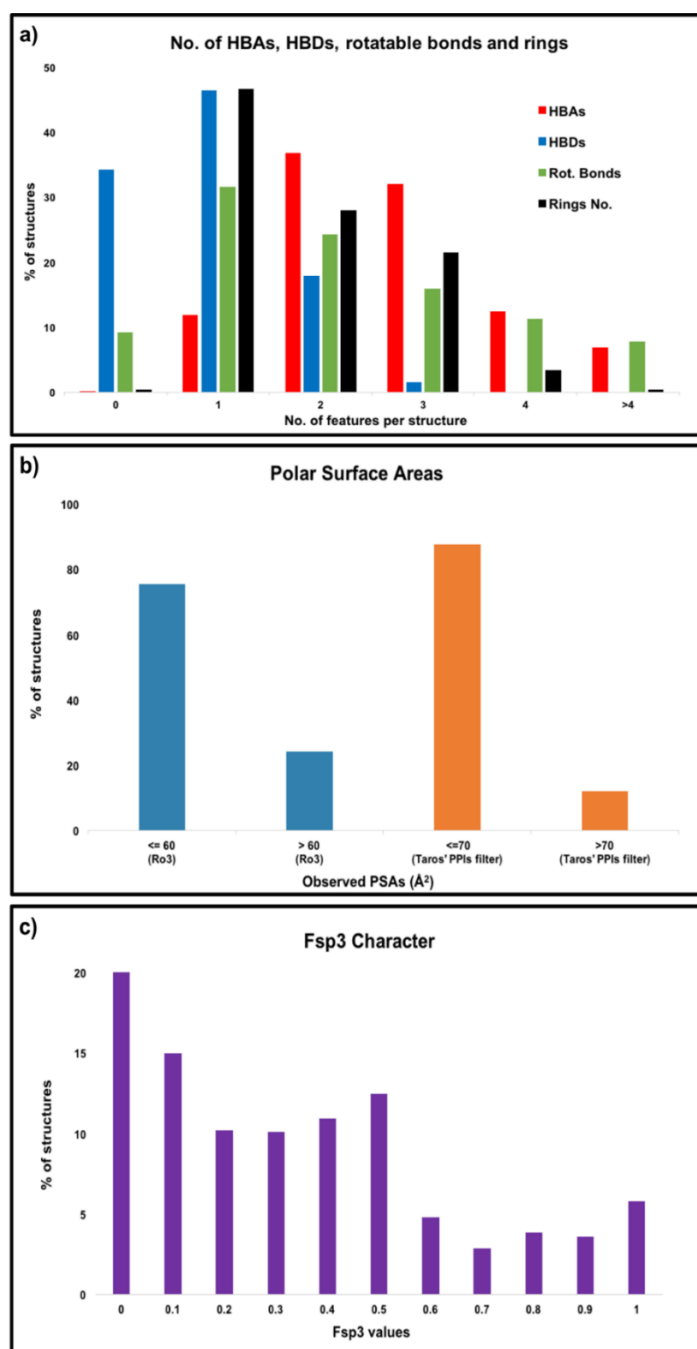


Figure S2 - (A) Number of H-bond acceptors (HBAs), donors (HBDs), rotatable bonds (Rot. Bonds) and rings. The totality of the molecules presents no more than 3 HBDs while 80.7% has no more than 3 HBAs. Number of entries with no more than 3 rotatable bonds covers a similar percentage (80.9%). 96.4% of the structures contains no more than 3 rings. (B) Distribution of Polar Surface Areas, according to the Ro3 (cyan) and to the Taros' PPIs section parameters (orange). 75.7% has a PSA value below or equal the 60 Å² threshold. According to our parameters (PSA ≤ 70 Å²) 87.9% of the molecules fit well the requirements. (C) Saturation character (Fsp3) distribution. More than half of the structures (55.8%) present a completely flat core while 28.2% have an intermediate saturation character and 16.1% of them show a fully three-dimensional character.

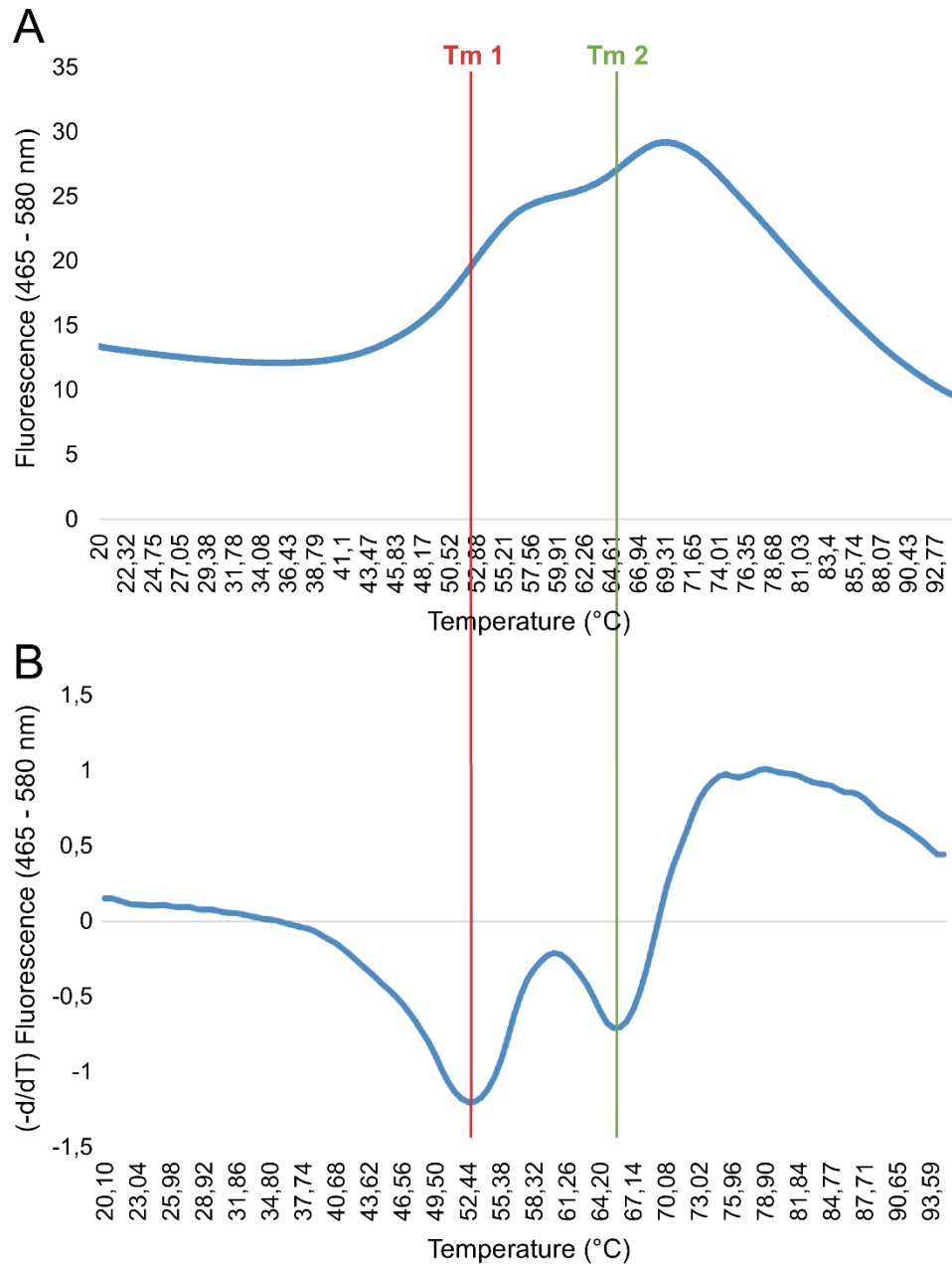


Figure S3 - DSC analysis of melting temperatures of 14-3-3 σ in the presence of compounds. The melting curve of 14-3-3 σ 7 μ M in the presence of 4% DMSO is presented in A as the variation of fluorescence (y axis) as a function of the temperature (x axis). Two different melting temperatures, identified as Tm 1 (in red) and Tm 2 (in green) are observed in the melting curve of the protein. The first derivative of the melting curve is presented in B. The x axis represents the temperature, same scale as in A.

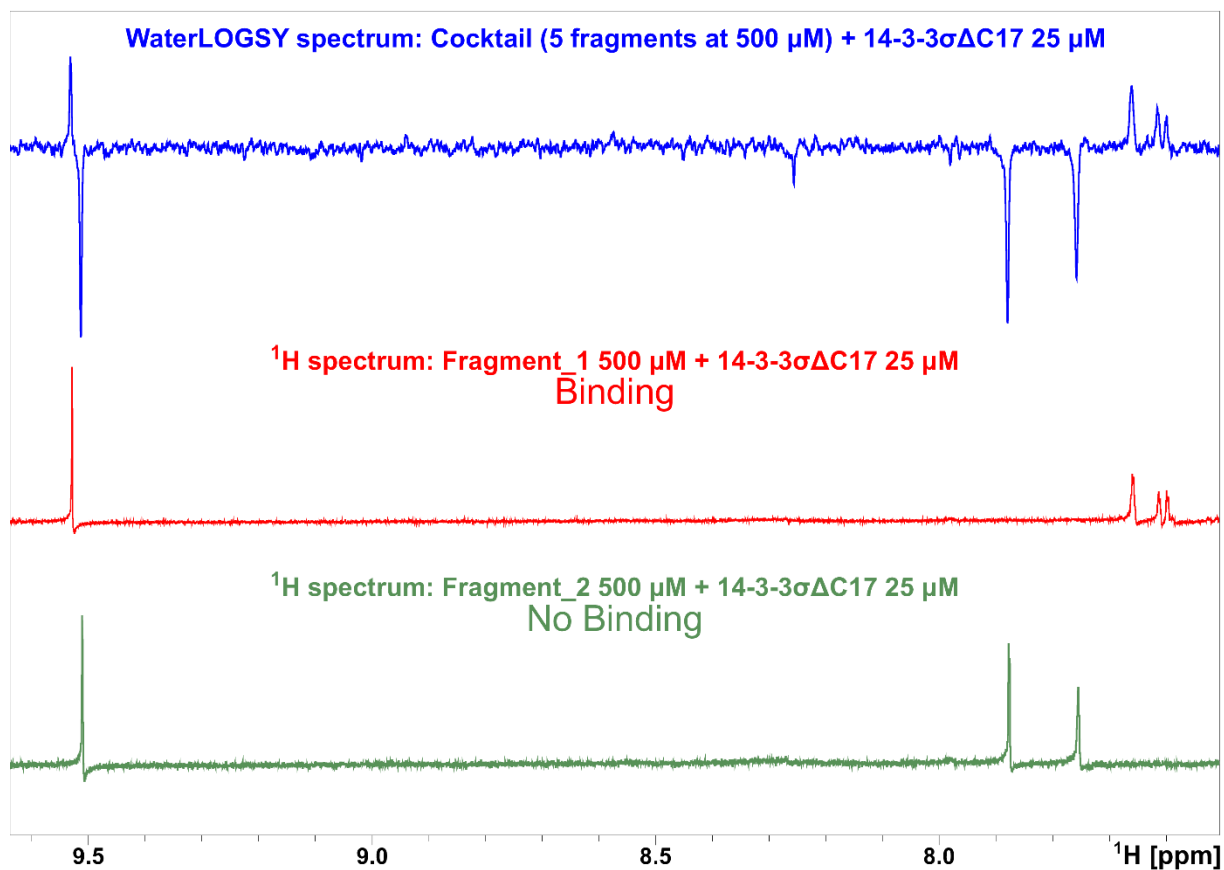


Figure S4 - WaterLOGSY allows the determination of which singleton of the cocktail is binding to 14-3-3 $\sigma\Delta\text{C17}$. A WaterLOGSY spectrum of a Cocktail is shown at the top, in blue. A ^1H spectrum of a hit singleton of the same cocktail is presented below the WaterLOGSY spectrum, in red (Fragment_1). Note that the resonances of this molecule are positive in the WaterLOGSY spectrum of the cocktail, meaning that this compound binds to 14-3-3 $\sigma\Delta\text{C17}$. Below the red spectrum, a ^1H spectrum of a non-binder singleton is shown in green (Fragment_2). Note that the resonances of this molecule are negative in the WaterLOGSY spectrum, showing that this molecule does not bind to 14-3-3 $\sigma\Delta\text{C17}$. The three spectra are referenced equally and were acquired in the same conditions.

Table S1 - DSF melting temperature data for the screened cocktail library. The average melting temperatures, standard deviations and induced thermal shifts (ΔT_m) are reported for each cocktail.

COCKTAIL	Average T _m 1 (°C) n=3	SD T _m 1 (°C) n=3	ΔT_m 1 (°C)	Average T _m 2 (°C) n=3	SD T _m 2 (°C) n=3	ΔT_m 2 (°C)	ΔT_m 1 + ΔT_m 2 (°C)
1	52,54	0,11	-0,31	65,69	0,19	-0,03	0,35
2	53,02	0,06	0,16	66,33	0,06	0,60	0,76
3	52,92	0,15	0,06	66,35	0,25	0,63	0,69
4	52,80	0,11	-0,06	65,82	0,20	0,09	0,15
5	52,73	0,05	-0,13	65,76	0,06	0,03	0,16
6	52,89	0,15	0,03	66,04	0,20	0,31	0,35
7	52,98	0,06	0,13	66,20	0,27	0,47	0,60
8	52,57	0,10	-0,28	65,60	0,09	-0,13	0,41
9	52,54	0,05	-0,32	65,88	0,00	0,15	0,47
10	51,50	0,11	-1,35	66,07	0,10	0,35	1,70
11	-	-	-	-	-	-	-
12	51,57	0,11	-1,29	66,13	0,11	0,41	1,70
13	52,81	0,06	-0,05	65,79	0,17	0,06	0,11
14	52,76	0,10	-0,09	65,82	0,24	0,09	0,19
15	53,11	0,14	0,25	66,23	0,24	0,50	0,75
16	53,17	0,10	0,31	66,20	0,11	0,47	0,78
17	52,95	0,10	0,10	65,95	0,14	0,22	0,32
18	52,64	0,24	-0,22	65,69	0,16	-0,03	0,25
19	53,14	0,28	0,28	66,32	0,22	0,60	0,88
20	53,20	0,14	0,35	66,42	0,14	0,69	1,04
21	52,54	0,20	-0,32	65,73	0,11	0,00	0,32
22	52,98	0,38	0,13	66,20	0,05	0,47	0,60
23	52,95	0,10	0,10	66,13	0,11	0,41	0,50
24	53,11	0,20	0,25	66,39	0,11	0,66	0,91
25	52,67	0,19	-0,19	66,04	0,31	0,31	0,50
26	52,73	0,11	-0,12	66,20	0,11	0,47	0,59
27	53,11	0,20	0,25	66,48	0,05	0,75	1,01
28	53,05	0,10	0,19	66,23	0,24	0,50	0,69
29	52,86	0,00	0,00	66,17	0,00	0,44	0,45
30	53,02	0,14	0,16	66,26	0,17	0,54	0,70
31	52,73	0,20	0,19	66,07	0,10	-0,03	0,22
32	52,67	0,17	0,12	65,76	0,29	-0,35	0,47
33	52,54	0,33	0,00	66,13	0,29	0,03	0,03
34	52,58	0,43	0,03	66,04	0,24	-0,06	0,10
35	52,48	0,10	-0,07	66,04	0,20	-0,06	0,13
36	43,32	0,25	-9,22	65,09	0,11	-1,01	10,23

37	52,94	0,42	0,40	66,04	0,13	-0,06	0,46
38	52,51	0,11	-0,04	65,94	0,11	-0,16	0,20
39	52,32	0,28	-0,22	66,04	0,15	-0,06	0,29
40	52,79	0,45	0,25	65,88	0,10	-0,22	0,47
41	52,83	0,06	0,28	65,69	0,16	-0,41	0,69
42	52,67	0,00	0,13	66,17	0,00	0,07	0,19
43	52,56	0,36	0,02	66,10	0,06	0,02	0,19
44	52,48	0,43	-0,07	65,82	0,24	-0,28	0,35
45	52,13	0,49	-0,41	66,20	0,43	0,09	0,50
46	52,60	0,24	0,06	66,04	0,11	-0,06	0,12
47	51,82	0,33	-0,72	65,69	0,10	-0,41	1,13
48	52,58	0,34	0,03	65,91	0,14	-0,19	0,22
49	52,42	0,38	-0,13	65,72	0,14	-0,38	0,51
50	52,20	0,29	-0,35	65,88	0,17	-0,22	0,57
51	51,25	0,34	-1,29	65,28	0,11	-0,82	2,11
52	52,51	0,33	-0,03	65,76	0,29	-0,35	0,38
53	52,60	0,24	0,06	65,98	0,10	-0,13	0,19
54	52,67	0,41	0,13	66,01	0,11	-0,10	0,22
55	52,48	0,28	-0,06	65,91	0,14	-0,19	0,25
56	52,32	0,14	-0,22	65,72	0,06	-0,38	0,60
57	52,98	0,43	0,44	65,60	0,25	-0,50	0,94
58	52,95	0,10	0,41	65,98	0,00	-0,12	0,53
59	52,86	0,10	0,31	65,88	0,17	-0,22	0,53
60	52,86	0,10	0,31	65,76	0,14	-0,35	0,66
61	52,80	0,29	0,28	65,85	0,24	0,00	0,28
62	52,76	0,34	0,25	66,09	0,32	0,24	0,49
63	53,08	0,29	0,56	66,07	0,10	0,22	0,79
64	51,66	0,14	-0,85	65,60	0,09	-0,25	1,10
65	52,45	0,14	-0,07	65,95	0,14	0,10	0,16
66	52,57	0,10	0,06	65,91	0,07	0,06	0,12
67	51,82	0,48	-0,69	65,88	0,10	0,03	0,73
68	52,70	0,05	0,19	66,01	0,05	0,16	0,35
69	52,54	0,20	0,03	65,76	0,14	-0,09	0,12
70	52,92	0,11	0,41	66,42	0,14	0,57	0,98
71	52,57	0,20	0,06	65,79	0,10	-0,06	0,12
72	52,54	0,15	0,03	65,79	0,10	-0,06	0,09
73	50,40	0,10	-2,11	65,26	0,11	-0,59	2,70
74	51,03	0,11	-1,48	66,67	0,15	0,82	2,30
75	52,26	0,05	-0,25	65,88	0,10	0,03	0,29
76	52,83	0,14	0,31	65,88	0,10	0,03	0,35
77	52,57	0,17	0,06	65,79	0,25	-0,06	0,12
78	52,57	0,10	0,06	66,01	0,11	0,16	0,22

79	52,64	0,06	0,12	65,91	0,06	0,06	0,19
80	52,67	0,00	0,16	65,88	0,17	0,03	0,19
81	52,73	0,20	0,22	66,01	0,11	0,16	0,37
82	53,14	0,00	0,63	66,23	0,28	0,38	1,01
83	52,83	0,14	0,31	65,85	0,15	0,00	0,31
84	52,10	0,10	-0,41	66,42	0,38	0,57	0,98
85	52,95	0,28	0,44	66,48	0,20	0,63	1,07
86	52,80	0,22	0,28	66,04	0,31	0,19	0,47
87	53,02	0,06	0,50	66,04	0,45	0,19	0,69
88	52,92	0,27	0,40	66,23	0,20	0,38	0,78
89	52,70	0,20	0,19	66,20	0,28	0,35	0,54
90	52,71	0,41	0,34	65,73	0,29	0,00	0,34
91	52,59	0,14	0,22	66,20	0,00	0,47	0,69
92	52,65	0,05	0,28	66,26	0,15	0,53	0,82
93	52,43	0,09	0,06	65,69	0,11	-0,03	0,10
94	52,40	0,14	0,03	65,79	0,05	0,06	0,09
95	51,93	0,21	-0,44	65,88	0,14	0,16	0,60
96	52,49	0,05	0,12	66,32	0,07	0,60	0,72
97	52,40	0,05	0,03	65,82	0,09	0,09	0,13
98	52,24	0,17	-0,12	65,91	0,10	0,19	0,31
99	52,40	0,05	0,03	65,91	0,32	0,19	0,22
100	52,81	0,00	0,44	66,16	0,11	0,44	0,88
101	51,87	0,11	-0,50	65,88	0,19	0,16	0,66
102	52,52	0,16	0,16	65,82	0,09	0,09	0,25
103	52,68	0,28	0,31	66,13	0,33	0,41	0,72
104	52,52	0,16	0,16	66,20	0,41	0,47	0,63
105	52,46	0,10	0,09	65,91	0,19	0,19	0,28
106	52,40	0,05	0,03	66,10	0,19	0,37	0,41
107	48,60	0,30	-3,77	66,29	0,17	0,57	4,34
108	52,52	0,10	0,16	66,51	0,05	0,78	0,94
109	52,49	0,05	0,12	66,26	0,05	0,53	0,66
110	52,46	0,10	0,09	65,88	0,05	0,15	0,25
111	52,43	0,25	0,06	66,32	0,20	0,60	0,66
112	52,49	0,11	0,13	66,16	0,11	0,44	0,56
113	52,49	0,14	0,13	66,13	0,24	0,41	0,53
114	52,43	0,09	0,06	66,17	0,06	0,44	0,50
115	51,74	0,14	-0,63	66,10	0,10	0,38	1,01
116	52,81	0,00	0,44	66,45	0,20	0,72	1,17
117	52,40	0,20	0,03	66,54	0,36	0,82	0,85
118	52,71	0,34	0,35	66,32	0,14	0,60	0,94
119	52,52	0,10	0,16	66,54	0,05	0,81	0,97
120	52,57	0,17	0,10	66,04	0,15	0,28	0,38

121	52,48	0,17	0,00	66,20	0,20	0,44	0,44
122	52,60	0,14	0,13	66,07	0,10	0,32	0,44
123	50,84	0,19	-1,63	65,22	0,16	-0,53	2,17
124	48,54	0,45	-3,94	65,22	0,25	-0,53	4,47
125	52,48	0,10	0,00	65,92	0,11	0,16	0,16
126	52,64	0,14	0,16	66,39	0,39	0,64	0,80
127	51,19	0,11	-1,29	65,82	0,11	0,06	1,35
128	52,42	0,11	-0,06	65,82	0,05	0,06	0,12
129	52,42	0,24	-0,06	66,04	0,34	0,28	0,34
130	50,50	0,49	-1,98	63,87	0,43	-1,89	3,87
131	52,29	0,09	-0,19	65,57	0,14	-0,19	0,38
132	52,48	0,00	0,00	65,63	0,10	-0,13	0,13
133	52,51	0,11	0,03	66,04	0,20	0,28	0,31
134	52,70	0,22	0,22	66,35	0,41	0,60	0,82
135	52,35	0,05	-0,13	65,75	0,11	0,00	0,13
136	52,73	0,05	0,25	66,17	0,16	0,41	0,66
137	52,63	0,29	0,16	66,48	0,14	0,73	0,88
138	48,76	0,11	-3,71	66,83	0,00	1,07	4,79
139	52,54	0,15	0,06	65,85	0,22	0,10	0,16
140	52,29	0,00	-0,19	65,85	0,33	0,10	0,28
141	52,67	0,10	0,19	66,48	0,14	0,73	0,92
142	52,57	0,19	0,09	66,11	0,22	0,35	0,44
143	52,45	0,06	-0,03	65,76	0,06	0,00	0,03
144	52,79	0,36	0,32	66,32	0,24	0,57	0,88
145	52,54	0,05	0,06	66,26	0,17	0,51	0,57
146	52,20	0,10	-0,28	65,60	0,09	-0,16	0,44
147	50,25	0,11	-2,23	65,98	0,19	0,22	2,45
148	52,35	0,14	-0,12	65,98	0,35	0,22	0,34
149	48,13	0,02	-4,01	66,45	0,09	0,60	4,61
150	51,54	0,32	-0,60	66,14	0,06	0,29	0,89
151	52,22	0,46	0,09	66,45	0,34	0,60	0,68
152	51,94	0,20	-0,19	65,66	0,19	-0,19	0,38
153	51,79	0,36	-0,35	65,79	0,10	-0,06	0,41
154	52,10	0,00	-0,04	65,85	0,05	0,00	0,04
155	52,14	0,11	0,00	66,18	0,10	0,33	0,33
156	52,24	0,05	0,10	65,92	0,11	0,07	0,17
157	52,20	0,00	0,06	65,82	0,05	-0,03	0,09

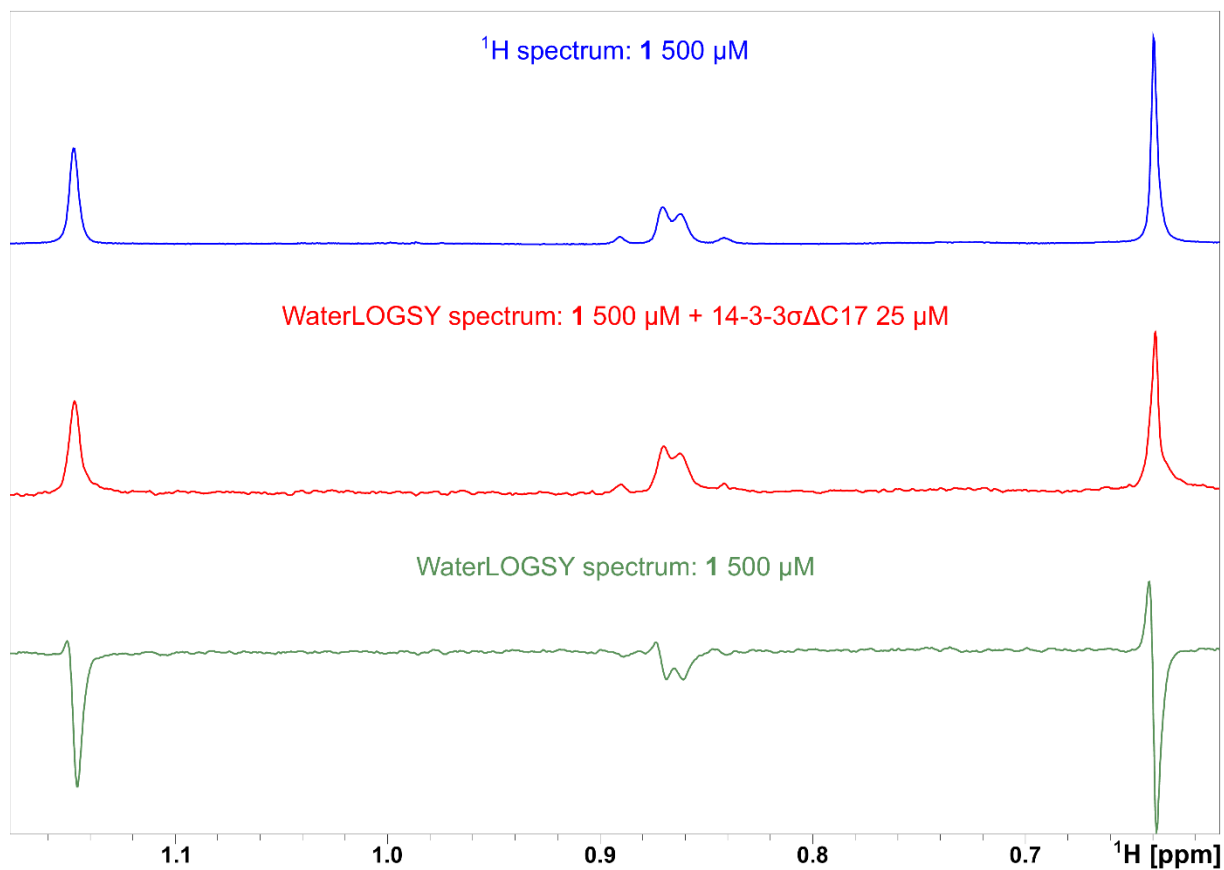


Figure S5 - WaterLOGSY detects the binding of **1** to 14-3-3 $\sigma\Delta\text{C17}$. ^1H spectrum of **1** 500 μM (blue spectrum, on top). The WaterLOGSY spectrum of a solution containing **1** 500 μM and 14-3-3 $\sigma\Delta\text{C17}$ 25 μM (in red) shows that the NMR signals of **1** are phased positive, indicating binding. The control WaterLOGSY spectrum of a solution containing **1** 500 μM alone (in green) shows that in the absence of 14-3-3 $\sigma\Delta\text{C17}$ the NMR signals of **1** 500 μM are all phased negative.

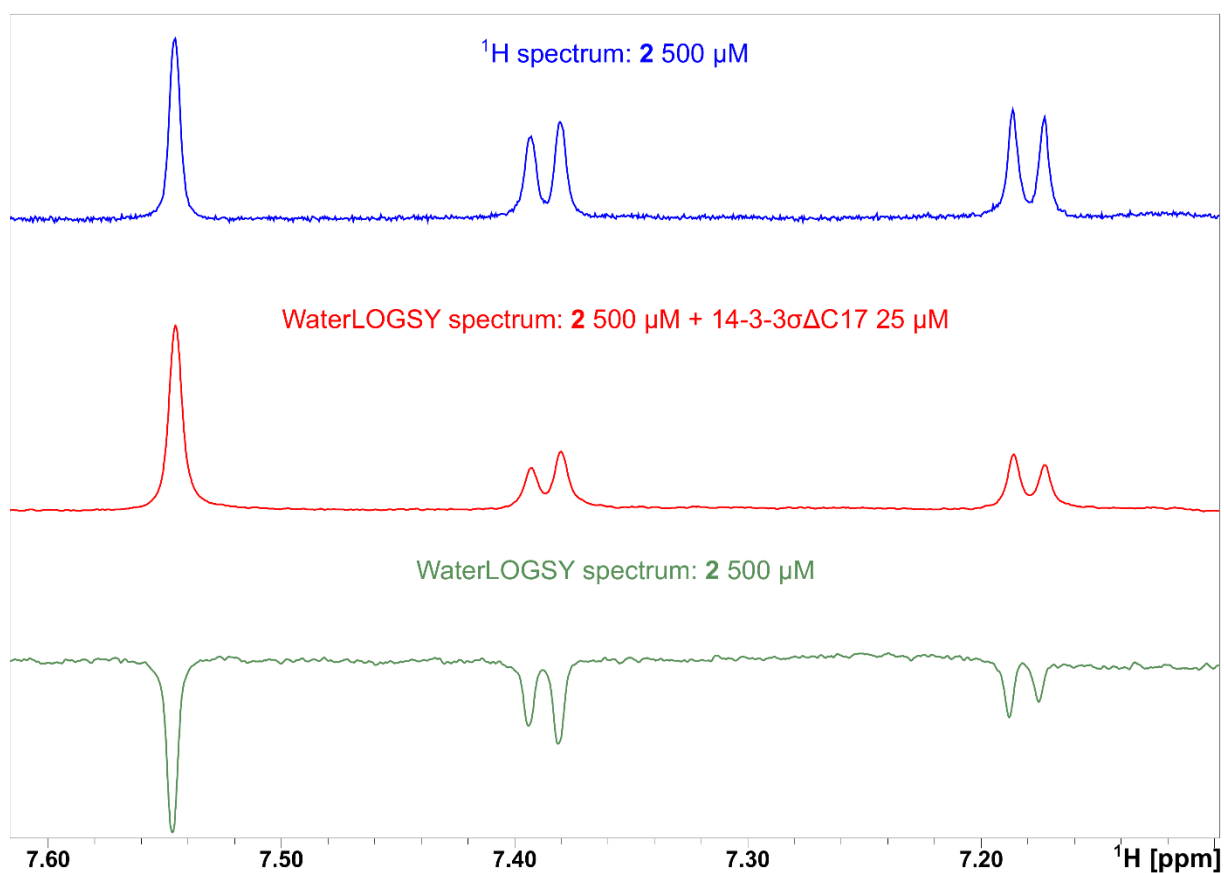


Figure S6 - WaterLOGSY detects the binding of **2** to 14-3-3 $\sigma\Delta$ C17. ^1H spectrum of **2** 500 μM (blue spectrum, on top). The WaterLOGSY spectrum of a solution containing **2** 500 μM and 14-3-3 $\sigma\Delta$ C17 25 μM (in red) shows that the NMR signals of **2** are phased positive, indicating binding. The control WaterLOGSY spectrum of a solution containing **2** 500 μM alone (in green) shows that in the absence of 14-3-3 $\sigma\Delta$ C17 the NMR signals of **2** 500 μM are all phased negative.

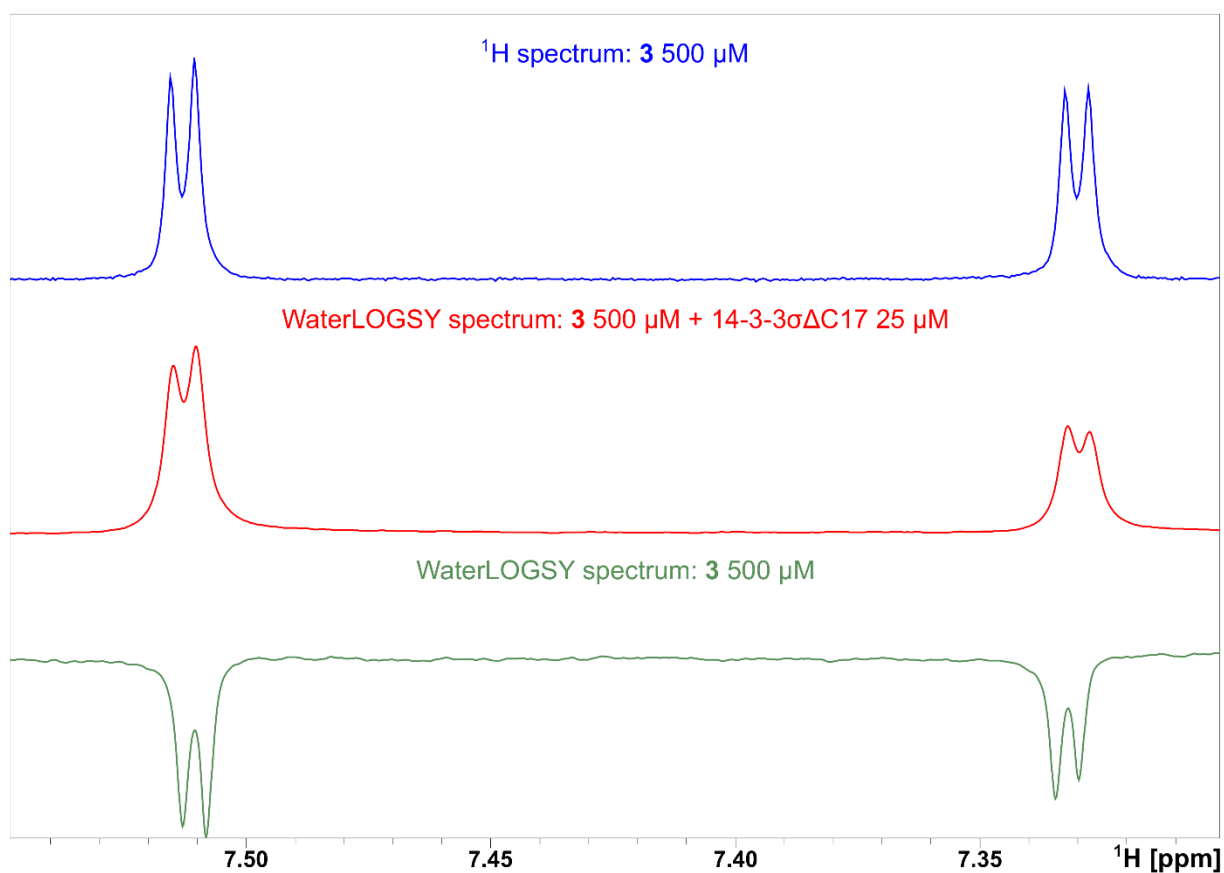


Figure S7 - WaterLOGSY detects the binding of **3** to 14-3-3 $\sigma\Delta$ C17. ^1H spectrum of **3** 500 μM (blue spectrum, on top). The WaterLOGSY spectrum of a solution containing **3** 500 μM and 14-3-3 $\sigma\Delta$ C17 25 μM (in red) shows that the NMR signals of **3** are phased positive, indicating binding. The control WaterLOGSY spectrum of a solution containing **3** 500 μM alone (in green) shows that in the absence of 14-3-3 $\sigma\Delta$ C17 the NMR signals of **3** 500 μM are all phased negative.

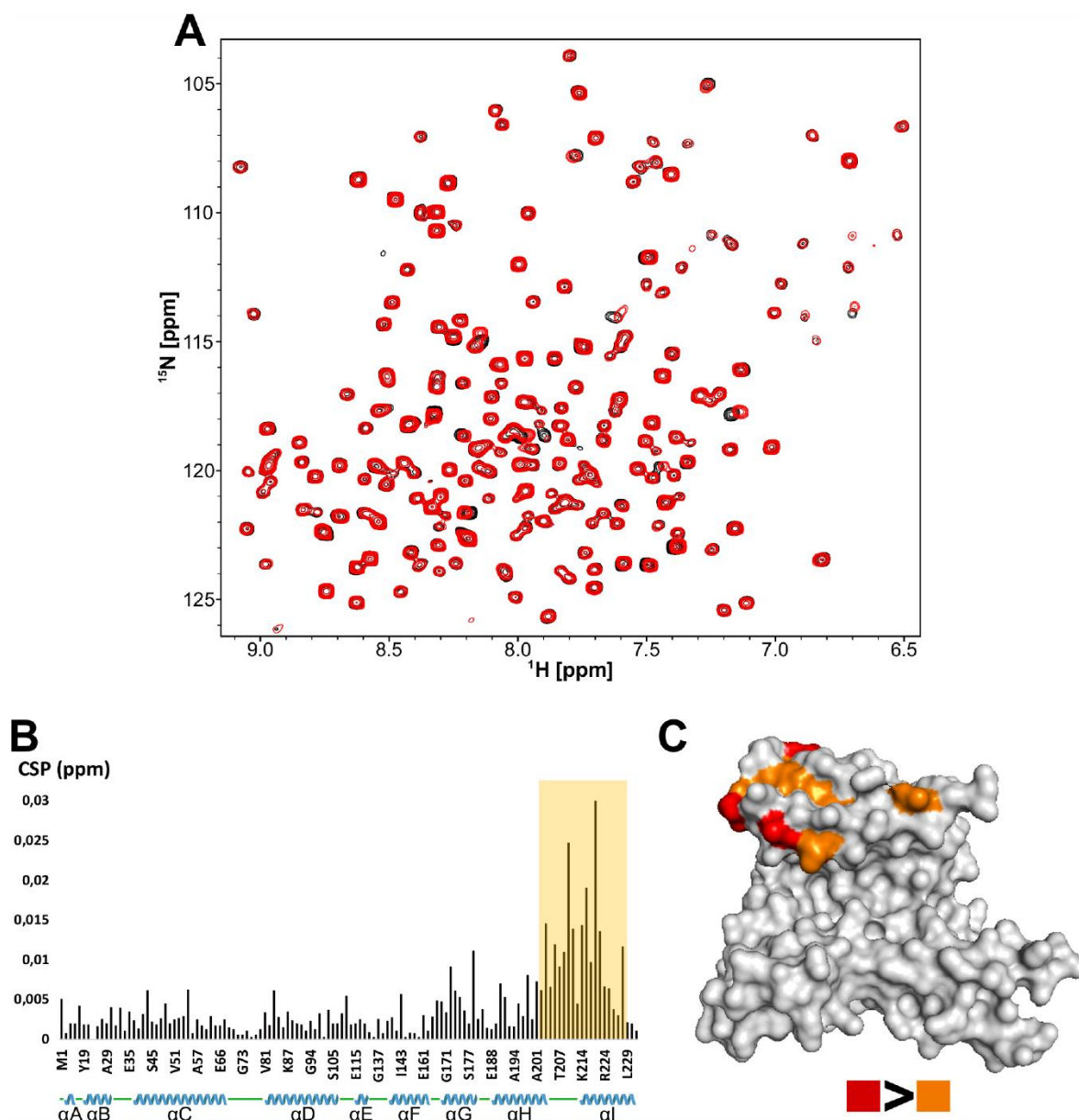


Figure S8 - **1** binding site on 14-3-3 σ Δ C17 identified by ^1H - ^{15}N TROSY-HSQC. (A) Superimposed ^1H - ^{15}N TROSY-HSQC spectra of $^{15}\text{N}^2\text{H}$ labelled 14-3-3 σ Δ C17 75 μM in the presence of 2% DMSO- d_6 (v/v) (in black) and **1** 2000 μM (in red). (B) Plot of the CSP values (in ppm) of ^1H - ^{15}N correlation peaks of 75 μM 14-3-3 σ Δ C17 in the presence of 2000 μM **1** compared to the reference 14-3-3 σ Δ C17 spectrum (75 μM) (y axis) versus the amino acid sequence (x axis). A total of 128 correlation peak CSP are shown. The x axis is not proportional. The helices of 14-3-3 σ are identified below the x axis as blue cartoons, while disordered regions are represented by green lines. The area highlighted in yellow shows the region of the protein affected by the presence of **1**. (C) Mapping on the crystal structure of 14-3-3 σ (PDB ID: 1YZ5) of the amino acid residues corresponding to the 10 most affected resonances by the presence of **1**. The residues corresponding to the 5 most affected resonances are colored in red and an additional 5 are colored in orange.

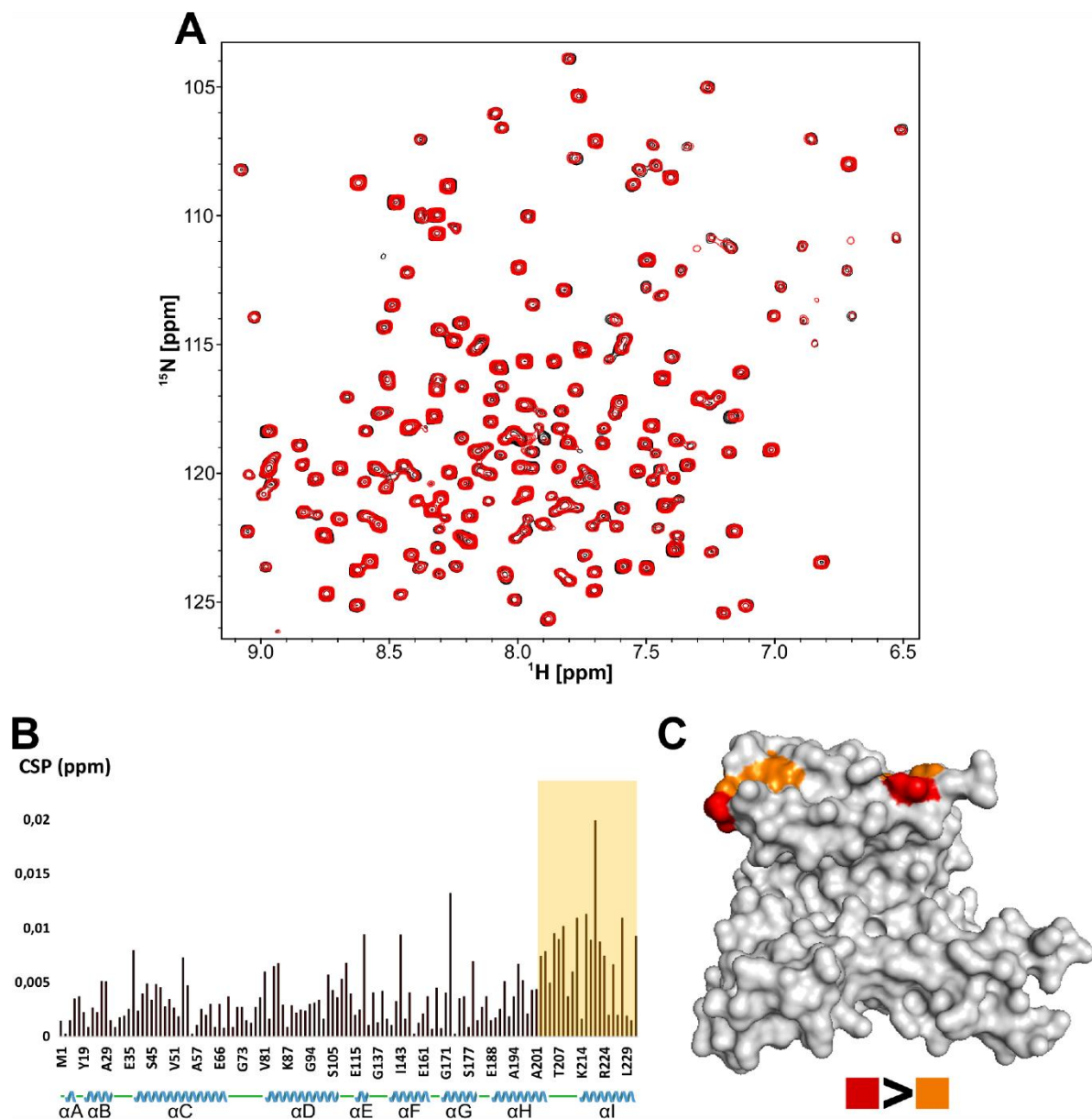


Figure S9 - 2 binding site on 14-3-3 $\sigma\Delta$ C17 identified by ^1H - ^{15}N TROSY-HSQC. (A) Superimposed ^1H - ^{15}N TROSY-HSQC spectra of $^{15}\text{N}^2\text{H}$ labelled 14-3-3 $\sigma\Delta$ C17 75 μM in the presence of 2% DMSO- d_6 (v/v) (in black) and **2** 2000 μM (in red). (B) Plot of the CSP values (in ppm) of ^1H - ^{15}N correlation peaks of 75 μM 14-3-3 $\sigma\Delta$ C17 in the presence of 2000 μM **2** compared to the reference 14-3-3 $\sigma\Delta$ C17 spectrum (75 μM) (y axis) versus the amino acid sequence (x axis). A total of 128 correlation peak CSP are shown. The x axis is not proportional. The helices of 14-3-3 σ are identified below the x axis as blue cartoons, while disordered regions are represented by green lines. The area highlighted in yellow shows the region of the protein affected by the presence of **2**. (C) Mapping on the crystal structure of 14-3-3 σ (PDB ID: 1YZ5) of the amino acid residues corresponding to the 10 most affected resonances by the presence of **2**. The residues corresponding to the 5 most affected resonances are colored in red and an additional 5 are colored in orange.

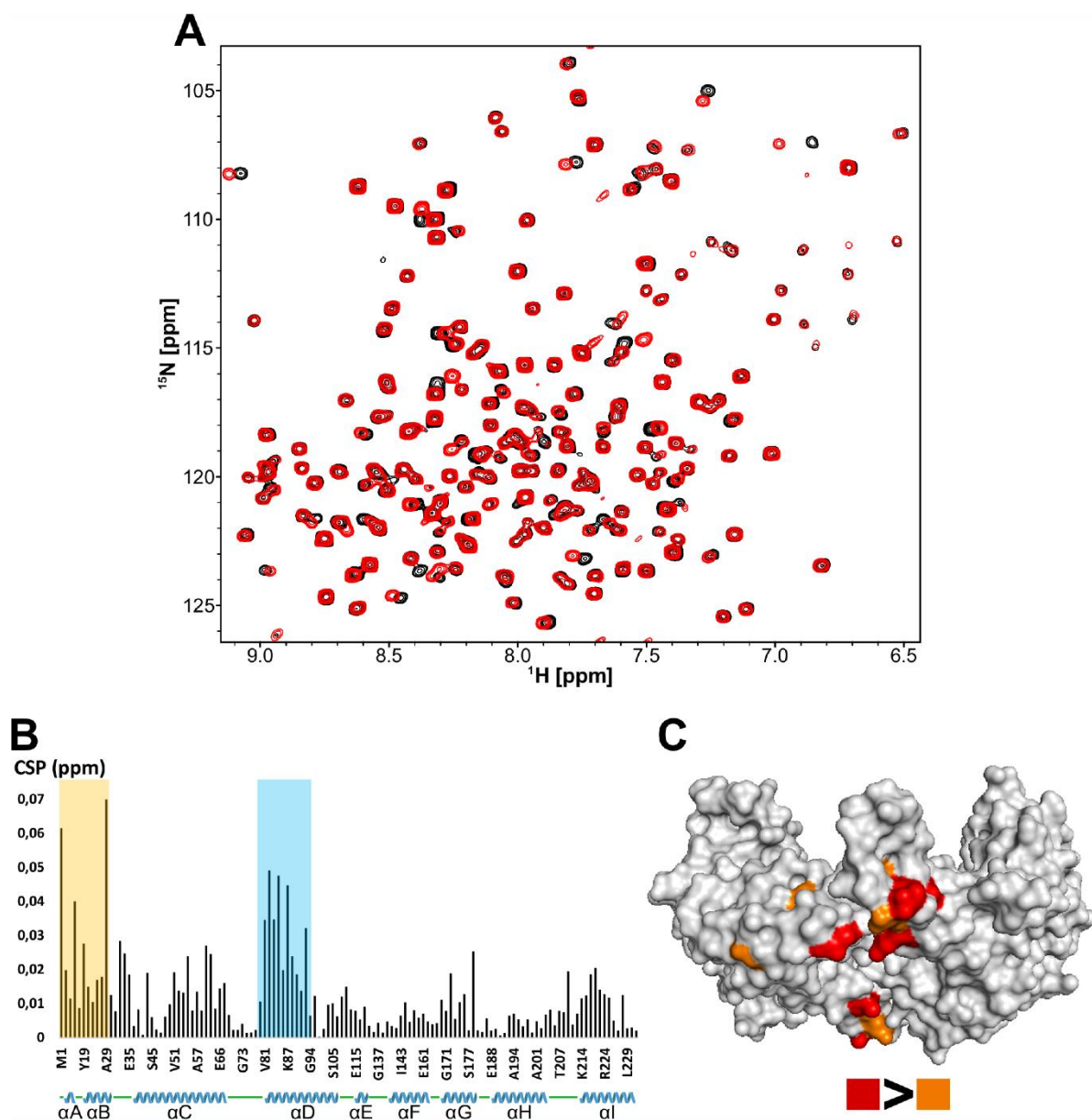


Figure S10 - **3** binding site on 14-3-3 $\sigma\Delta$ C17 identified by ^1H - ^{15}N TROSY-HSQC. (A) Superimposed ^1H - ^{15}N TROSY-HSQC spectra of $^{15}\text{N}^2\text{H}$ labelled 14-3-3 $\sigma\Delta$ C17 75 μM in the presence of 2% DMSO- d_6 (v/v) (in black) and **3** 2000 μM (in red). (B) Plot of the CSP values (in ppm) of ^1H - ^{15}N correlation peaks of 75 μM 14-3-3 $\sigma\Delta$ C17 in the presence of 2000 μM **3** compared to the reference 14-3-3 $\sigma\Delta$ C17 spectrum (75 μM) (y axis) versus the amino acid sequence (x axis). A total of 128 correlation peak CSP are shown. The x axis is not proportional. The helices of 14-3-3 σ are identified below the x axis as blue cartoons, while disordered regions are represented by green lines. The areas highlighted in yellow and blue show the region of the protein affected by the presence of **3**. (C) Mapping on the crystal structure of 14-3-3 σ (PDB ID: 1Y25) of the amino acid residues corresponding to the 10 most affected resonances by the presence of **3**. The residues corresponding to the 5 most affected resonances are colored in red and an additional 5 are colored in orange.

5 Fragment Screening for the modulation of 14-3-3 interactions with Kinases: the CaMKK2 and ASK1 cases

5.1 The Interaction of 14-3-3 with ASK1 and CaMKK2

5.1.1 Interaction of 14-3-3 with ASK1

Apoptosis signal-regulating kinase 1 (ASK1) is a member of the mitogen-activated protein kinase kinase kinase (MAP3K) family. It is involved in the regulation of diverse cellular processes, such as apoptosis, cytokine secretion or differentiation (Shiizaki, Naguro, & Ichijo, 2013). As a result of its remarkable influence in the cell, ASK1 has been linked to several pathologies such as cancer, inflammation and metabolic diseases, including diabetes (Kawarazaki, Ichijo, & Naguro, 2014). 14-3-3 is known to bind to the pS966 epitope of ASK1 and to inhibit this kinase by mechanisms that are still to be elucidated (Goldman, Chen, & Fu, 2004; Petrvalska et al., 2016). X-ray crystallography studies revealed that the ASK1pS966 epitope anchors in the binding groove of 14-3-3 in an extended way, like most of 14-3-3 complexes. The 14-3-3 ζ /ASK1pS966 complex was shown to be dynamic and the affinity of this interaction was estimated to be in the low μ M range (Petrvalska et al., 2016). The biological impact of this interaction was confirmed in a cellular system since the replacement of S966 by an Alanine accelerates ASK1 induced cell-death (L. Zhang, Chen, & Fu, 1999). 14-3-3 was shown to regulate ASK1 signaling and the stabilization of this PPI, and consequent inhibition of ASK1 activity, is suggested to be of therapeutic interest for metabolic pathologies like diabetic cardiomyopathy (Thandavarayan et al., 2008). Nevertheless, it should be noted that in certain conditions, ASK1 seems to have a protective role, while in others it can have harmful effects (Kawarazaki et al., 2014).

5.1.2 Interaction of 14-3-3 with CaMKK2

The Calcium/calmodulin-dependent protein kinase kinase 2 (CaMKK2) is a member of the Ca²⁺/calmodulin-dependent kinase (CaMK) family (Haribabu et al., 1995). This family is involved in important physiological processes such as glucose homeostasis, neuronal development and cell cycle regulation (Racioppi & Means, 2012; Santiago et al., 2018).

CaMKK2 has been shown to be partly inhibited upon phosphorylation by PKA, which was shown to phosphorylate CaMKK2 at 4 sites (S100, T145, S495, and S511) (Matsushita & Nairn, 1999; Okuno, Kitani, & Fujisawa, 2001). Biochemical assays have shown that CaMKK2 binds to various 14-3-3 isoforms (especially to the 14-3-3 γ isoform) and that the conserved motif containing pS100 is suggested to be the main anchoring epitope on 14-3-3 proteins (Davare, Saneyoshi, Guire, Nygaard, & Soderling, 2004; Ichimura, Taoka, Hozumi, Goto, & Tokumitsu, 2008). The crystal structures of 14-3-3 in complex with the pS100 and pS511 epitopes of CaMKK2 show that both peptides interact with the amphipathic groove of 14-3-3 similarly to most 14-3-3 complexes. An interesting observation is that an intramolecular interaction within the pS100 epitope induces a change in the direction of the polypeptidic chain, leaving the FC binding pocket unoccupied (Psenakova et al., 2018). This difference on the PPI interface, compared to the fully extended binding mode of most other 14-3-3 partners, can be an excellent opportunity to target this interface with a specific stabilizer, which would inhibit CaMKK2 activity. This strategy could potentially yield therapeutic candidates against cancer (Penfold et al., 2018) or metabolic disorders (Price et al., 2018).

5.2 Context of the collaboration

A fragment library was screened by DSF in cocktails of 5 for binding to the 14-3-3 ζ ΔC/ASK1pS966 and to the 14-3-3 γ /CaMKK2pS100 complexes. The fragments of the cocktails found to induce a significant thermal shift in any of the complexes were further validated as singletons by DSF. After validation of the singletons, 4 were validated as binders of the 14-3-3 ζ ΔC/ASK1pS966 complex and 7 were validated as binders of the 14-3-3 γ /CaMKK2pS100 complexes. Our collaboration was requested in order to validate the binding of the 11 selected fragments by Ligand-based NMR techniques. In the case of binders of the 14-3-3 ζ ΔC/ASK1pS966 complex, as a backbone assignment of 14-3-3 ζ is available in the literature (Killoran et al., 2015), we were further challenged to identify the binding sites of the hits.

5.3 Materials and Methods

5.3.1 Production of $^{15}\text{N}^{13}\text{C}^2\text{H}$ labeled 14-3-3 ζ

This $^{15}\text{N}^{13}\text{C}^2\text{H}$ labeled His₆-tagged 14-3-3 ζ (full-length) had been previously produced in the group according to a similar protocol to the one used for 14-3-3 σ (explained in chapter **Backbone chemical shift assignments of human 14-3-3 σ**). Prior to NMR experiments, the protein was dialyzed against a buffer containing 50 mM sodium phosphate pH 6.8 and 100 mM NaCl.

5.3.2 Ligand-based NMR experiments: Saturation Transfer Difference and WaterLOGSY

WaterLOGSY and STD spectra were acquired at the temperature of 16 °C in 5 mm tubes (sample volume 530 μL) using a 600 MHz Bruker Avance III HD spectrometer equipped with a CPQCI cryogenic probe. WaterLOGSY spectra were recorded with 32768 complex data points, with 1024 scans per increment and with a mixing time of 1.7s (acquisition time of 93 minutes). STD spectra were recorded with 32768 complex data points and with 640 scans per increment (acquisition time of 146 minutes). Saturation of protein's signals was achieved by selective saturation at -0.5 ppm in the on-resonance spectra. Non-saturation controls were performed using a selective pulse at -18 ppm (off-resonance spectra). Saturation time for STD experiments was 4 seconds. All samples were prepared in a buffer containing 50 mM sodium phosphate, 100 mM NaCl, pH 6.8 and 10% (v/v) D₂O. The final concentration of DMSO was 0.5% (v/v) and was kept constant for all experiments. For screening of compounds for binding to the 14-3-3 $\zeta\Delta\text{C}$ /ASK1pS966 complex, WaterLOGSY and STD spectra were performed with samples containing 25 μM 14-3-3 $\zeta\Delta\text{C}$ and 50 μM ASK1pS966 peptide in the presence and absence of each fragment (at 500 μM). For screening of compounds for binding to the 14-3-3 γ /CaMKK2pS100 complex, WaterLOGSY and STD spectra were performed with samples containing 25 μM 14-3-3 γ and 50 μM CaMKK2pS100 peptide in the presence and absence of each fragment (at 500 μM). A ^1H spectrum with water-suppression was additionally recorded for each sample. Spectra were collected, processed and analyzed with Topspin 3.6 (Bruker Biospin, Karlsruhe, Germany).

5.3.3 Protein-based NMR experiments: ^1H - ^{15}N TROSY HSQC

^1H - ^{15}N TROSY-HSQC spectra were acquired in 3 mm tubes (sample volume 200 μL) using a 900 MHz Bruker Avance-NEO spectrometer, equipped with a cryoprobe. The spectra were recorded with 3072 complex data points in the direct dimension and 120 complex data points in the indirect dimension, with 184 scans per increment (acquisition time of 6 hours per experiment), at 25 $^\circ\text{C}$, in a buffer containing 50 mM sodium phosphate pH 6.8, 100 mM NaCl, EDTA-free protease inhibitor cocktail (Roche) and 10% (v/v) D_2O . The final concentration of DMSO was 2% (v/v) and was kept constant for all the experiments. The spectra were performed with samples containing 100 μM $^{15}\text{N}^{13}\text{C}^2\text{H}$ labeled 14-3-3 ζ in the presence or in the absence of each fragment (at 2000 μM). Backbone assignments of $^{15}\text{N}^2\text{H}$ labeled 14-3-3 ζ were previously reported in the literature (Killoran et al., 2015). The reference for the ^1H chemical shift was relative to 4,4-dimethyl-4-silapentane-1-sulfonic acid (DSS). ^{15}N chemical shifts were referenced indirectly. Spectra were collected and processed with Topspin 4.0 (Bruker Biospin, Karlsruhe, Germany) and analyzed with Sparky 3.12 (T. D. Goddard and D. G. Kneller, SPARKY 3, University of California, San Francisco). CSPs in the form of chemical shift value modifications (in ppm) on the ^1H - ^{15}N TROSY-HSQC were calculated using the following equation:

$$\Delta\delta = \sqrt{\Delta\delta(^1\text{H})^2 + [0.14 * \Delta\delta(^{15}\text{N})^2]}$$

5.4 Results and discussion

5.4.1 Ligand-based NMR experiments

The fragments identified previously by DSF for binding to the 14-3-3 ζ ΔC /ASK1pS966 complex or to the 14-3-3 γ /CaMKK2pS100 were further screened by two different Ligand-based NMR experiments: WaterLOGSY and STD. Initially the compounds were screened only by WaterLOGSY but due to the ambiguity of some spectra and the absence of another screening technique more robust than DSF, we decided to confirm the results by repeating the screening using STD. The results are summarized in **Table 1**. Out of the four fragments screened for the 14-3-3 ζ ΔC /ASK1pS966 complex, binding was detected for two (C61_S352 –

Figure S1), (C63_S325 – **Figure S2**). Out of the seven fragments screened for binding to the 14-3-3 γ /CaMKK2pS100 complex, binding was detected for one (C35_S39 – **Figure S3**). The outcome of WaterLOGSY and STD experiments – positive or negative for binding - was the same for all compounds.

Table 1 – Results of the fragment screening by Ligand-based NMR techniques (STD and WaterLOGSY) for the identification of hits for the 14-3-3 ζ Δ C/ASK1pS966 and 14-3-3 γ /CaMKK2pS100 complexes.

COMPOUND	COMPLEX	STD	WaterLOGSY
C25_S35	14-3-3 ζ Δ C/ASK1pS966	No binding	No binding
C25_S105	14-3-3 ζ Δ C/ASK1pS966	No binding	No binding
C61_S352	14-3-3 ζ Δ C/ASK1pS966	Binding	Binding
C63_S325	14-3-3 ζ Δ C/ASK1pS966	Binding	Binding
C11_S82	14-3-3 γ /CaMKK2pS100	No binding	No binding
C11_S108	14-3-3 γ /CaMKK2pS100	No binding	No binding
C11_S115	14-3-3 γ /CaMKK2pS100	No binding	No binding
C35_S39	14-3-3 γ /CaMKK2pS100	Binding	Binding
C35_S182	14-3-3 γ /CaMKK2pS100	No binding	No binding
C109_S297	14-3-3 γ /CaMKK2pS100	No binding	No binding
C152_S521*	14-3-3 γ /CaMKK2pS100	No binding	No binding

* identified in another project as a covalent binder and therefore binding cannot be detected by WaterLOGSY/STD.

5.4.2 Protein-based experiments: ^1H - ^{15}N TROSY-HSQC

As there is a partial backbone assignment reported for 14-3-3 ζ in the literature (Killoran et al., 2015), we decided to perform further experiments by ^1H - ^{15}N TROSY-HSQC in order to try to identify the binding site of the fragments identified by WaterLOGSY and STD for binding to the 14-3-3 ζ Δ C/ASK1pS966. Surprisingly, contrarily to what happened with 14-3-3 ζ Δ C (experiments performed by our collaborators, not shown), the ASK1pS966 peptide did not interact with the full-length $^{15}\text{N}^{13}\text{C}^2\text{H}$ 14-3-3 ζ used for ^1H - ^{15}N TROSY-HSQC acquisition (data

not shown). For this reason, protein-based experiments were performed with samples containing only 14-3-3 ζ and the fragments to identify the binding site of the fragments on 14-3-3 ζ . With this technique, we were able to detect the binding of the two fragments (C61_S352 – **Figure S4** and C63_S325 – **Figure S5**) and to identify their binding sites on 14-3-3 ζ . C61_S352 induced significant CSP in the form of chemical shift value modifications on resonances corresponding to residues I65, T69, E70, G71 and A72. These perturbations are indicative of binding in the region of the loop separating helices α C and α D of 14-3-3 ζ (**Figure S4**). C63_S325 induced pronounced broadening of resonances located at the beginning of helices α H and α I, highlighting a pocket at the surface of the protein, above the amphipathic binding groove (**Figure S5 C, red area**). Additionally, the resonances corresponding to residues located between the end of helix α A and helix α B of 14-3-3 ζ were affected (**Figure S5 C, yellow area**), although to a fewer extent compared to the area above the binding groove. This data suggests that either the compound has two binding sites or that the binding at the top of helices α H and α I causes a long range conformational effect, which seems a less likely hypothesis.

Table 2 – Results for the ^1H - ^{15}N TROSY HSQC NMR experiments performed for the identification of the binding site of fragment hits on $^{15}\text{N}^{13}\text{C}^2\text{H}$ labeled 14-3-3 ζ .

COMPOUND	^1H - ^{15}N TROSY-HSQC
C61_S352	Binding – binding site identified
C63_S325	Binding – binding site identified

5.5 Conclusions

Through the use of Ligand-based NMR, we identified two fragments binding to 14-3-3 ζ or to the 14-3-3 ζ AC/ASK1pS966 complex and one fragment binding to the 14-3-3 γ /CaMKK2pS100 complex. We were further able to identify the binding sites for two fragments on 14-3-3 ζ using a protein-based NMR method. Both fragments were shown to bind in pockets remote from the amphipathic binding groove. Further work will include the co-

crystallization of these compounds with 14-3-3 ζ and the corresponding peptides in order to obtain more detailed information regarding the binding sites.

5.6 Supporting Information

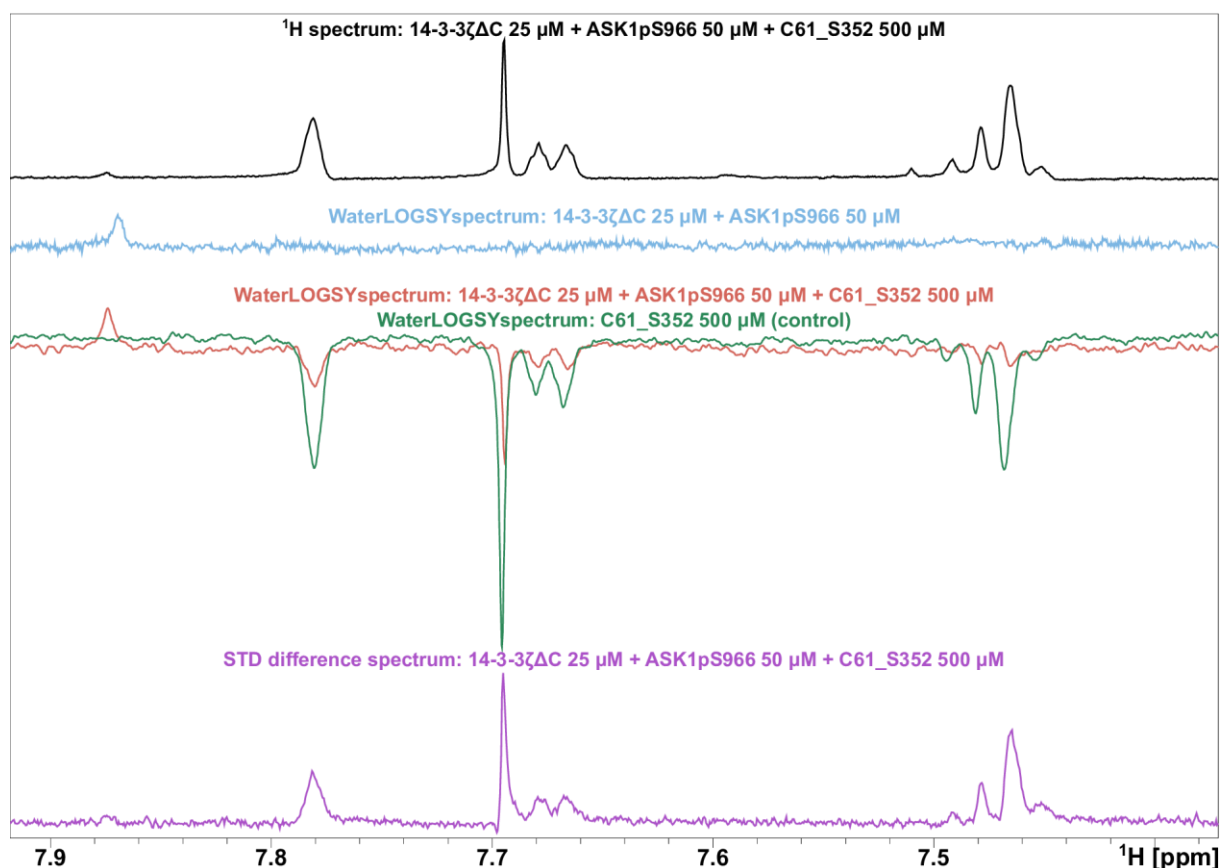


Figure S1 – C61_S352 binding to the 14-3-3 ζ Δ C/ASK1pS966 complex detected by WaterLOGSY and STD. ^1H spectrum of 500 μM C61_S352 in the presence of 25 μM 14-3-3 ζ Δ C and 50 μM ASK1pS966 peptide (in black). WaterLOGSY spectra of 25 μM 14-3-3 ζ Δ C and 50 μM ASK1pS966 peptide, without compound (in blue), 25 μM 14-3-3 ζ Δ C and 50 μM ASK1pS966 peptide in the presence of 500 μM C61_S352 (in red) and of 500 μM C61_S352 alone (superimposed in green). STD difference spectrum of a solution containing 500 μM C61_S352 in the presence of 25 μM 14-3-3 ζ Δ C and 50 μM ASK1pS966 peptide (in purple). Note that there are considerable differences in the compound's signals between the green and the red spectrum indicating binding to the 14-3-3 ζ Δ C/ASK1pS966 complex. Note that the same signals are detected in the STD difference spectrum (in purple), also indicating binding.

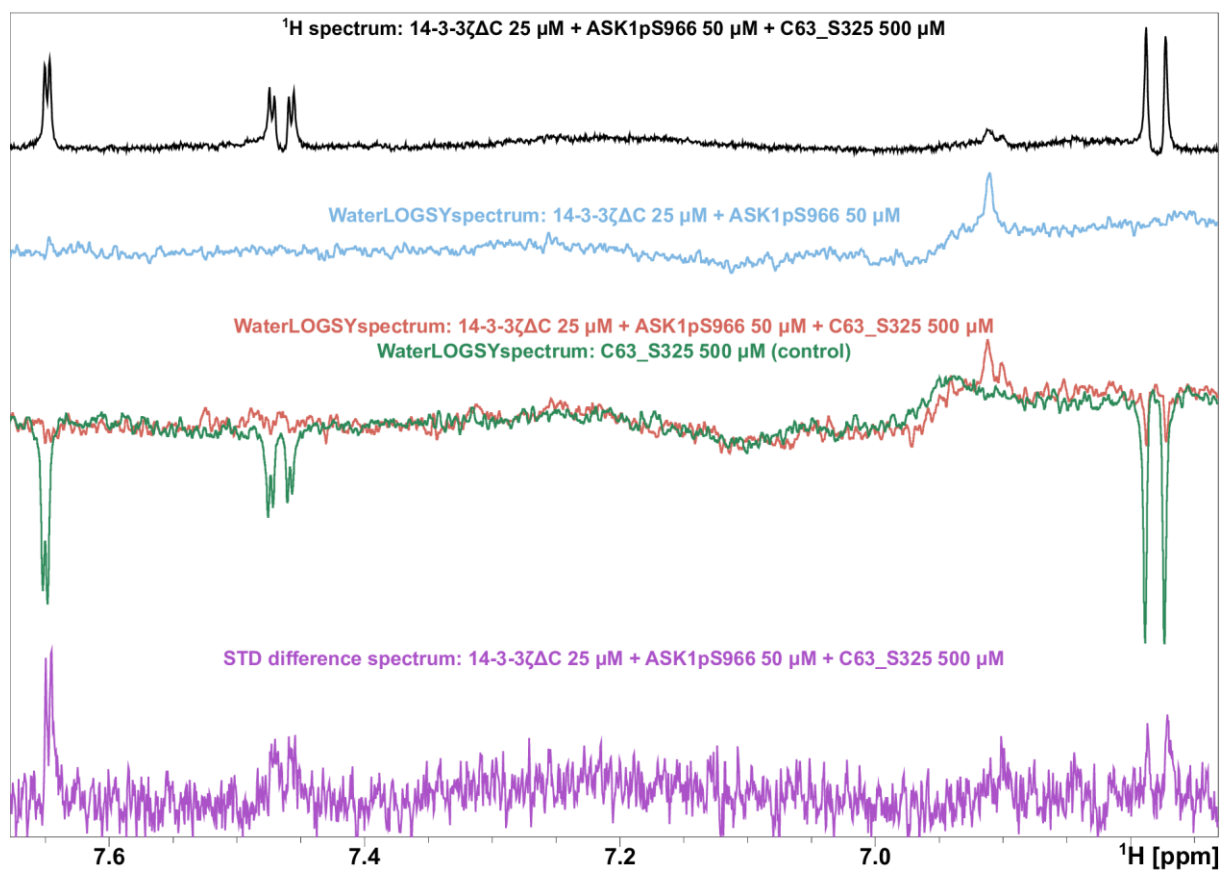


Figure S2 - C63_S325 binding to the 14-3-3 ζ Δ C/ASK1pS966 complex detected by WaterLOGSY and STD. ^1H spectrum of 500 μM C63_S325 in the presence of 25 μM 14-3-3 ζ Δ C and 50 μM ASK1pS966 peptide (in black). WaterLOGSY spectra of 25 μM 14-3-3 ζ Δ C and 50 μM ASK1pS966 peptide, without compound (in blue), 25 μM 14-3-3 ζ Δ C and 50 μM ASK1pS966 peptide in the presence of 500 μM C63_S325 (in red) and of 500 μM C63_S325 alone (superimposed in green). STD difference spectrum of a solution containing 500 μM C63_S325 in the presence of 25 μM 14-3-3 ζ Δ C and 50 μM ASK1pS966 peptide (in purple). Note that there are considerable differences in the compound's signals between the green and the red spectrum indicating binding to the 14-3-3 ζ Δ C/ASK1pS966 complex. Note that the same signals are detected in the STD difference spectrum (in purple), also indicating binding.

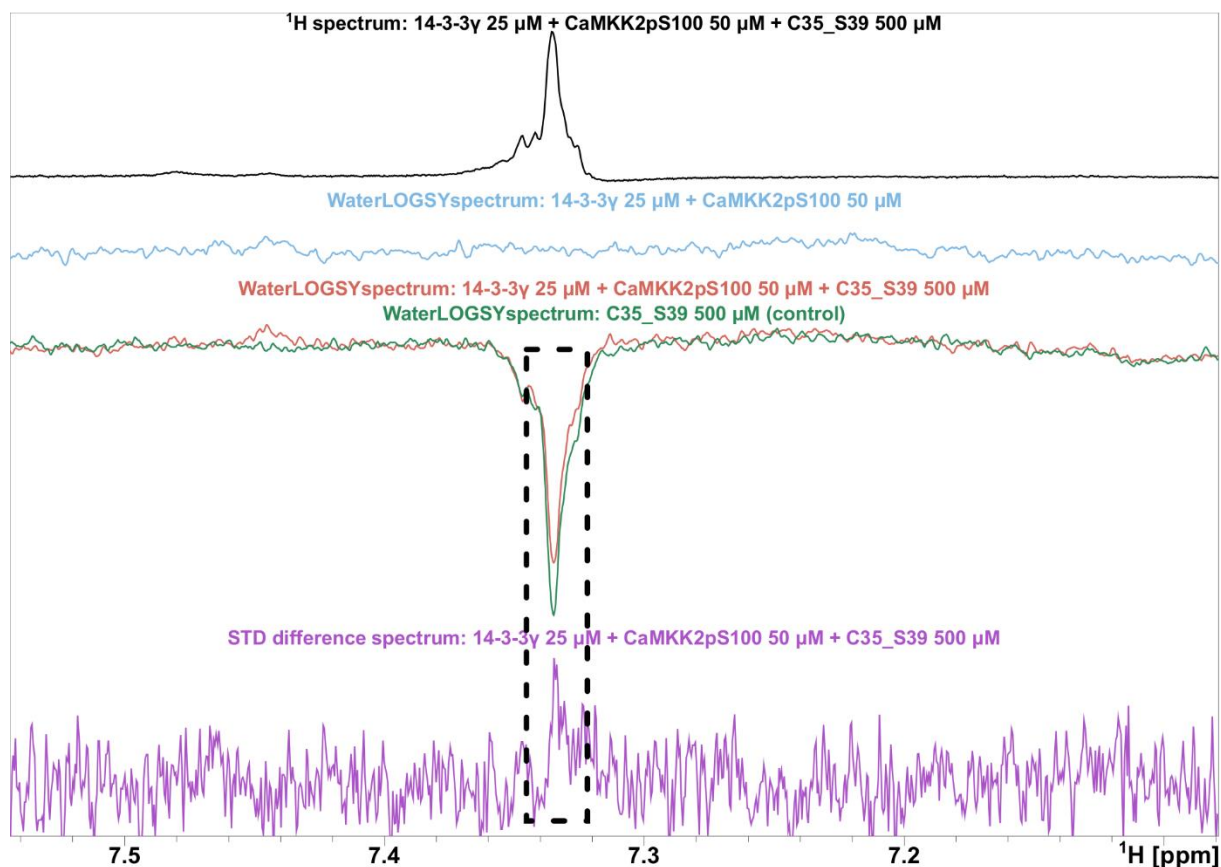


Figure S3 - C35_S39 binding to the 14-3-3 γ /CaMKK2pS100 complex detected by WaterLOGSY and STD. ^1H spectrum of 500 μM C35_S39 in the presence of 25 μM 14-3-3 γ and 50 μM CaMKK2pS100 peptide (in black). WaterLOGSY spectra of 25 μM 14-3-3 γ and 50 μM CaMKK2pS100 peptide, without compound (in blue), 25 μM 14-3-3 γ and 50 μM CaMKK2pS100 peptide in the presence of 500 μM C35_S39 (in red) and of 500 μM C35_S39 alone (superimposed in green). STD difference spectrum of a solution containing 500 μM C35_S39 in the presence of 25 μM 14-3-3 γ and 50 μM CaMKK2pS100 peptide (in purple). Note that for the compound signal at 7.34 ppm there is a difference between the green and the red spectrum indicating binding to the 14-3-3 γ /CaMKK2pS100 complex. Note that the same signal is detected in the STD difference spectrum (in purple), also indicating binding.

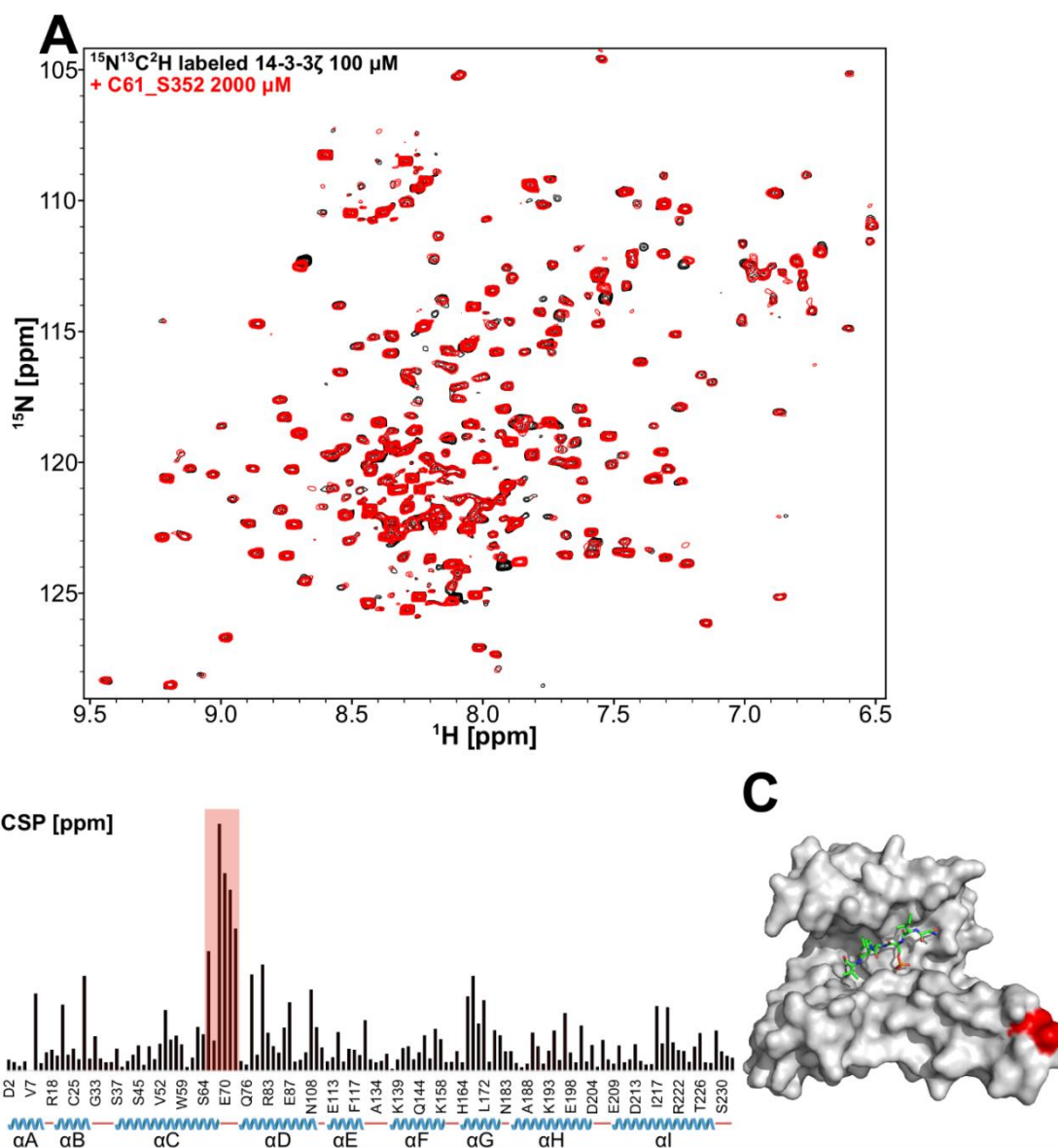


Figure S4 – C61_S352 binding site on 14-3-3 ζ identified by ^1H - ^{15}N TROSY-HSQC. (A) Superimposed ^1H - ^{15}N TROSY-HSQC spectra of $^{15}\text{N}^{13}\text{C}^2\text{H}$ labeled 14-3-3 ζ 100 μM in the presence of 2% DMSO (v/v) (in black) and C61_S352 2000 μM (in red). (B) Plot of the CSP values (in ppm) of ^1H - ^{15}N correlation peaks of 100 μM 14-3-3 ζ in the presence of 2000 μM C61_S352 compared to the reference 14-3-3 ζ spectrum (100 μM) (y axis) versus the amino acid sequence (x axis). A total of 135 correlation peak CSP are shown. The x axis is not proportional. The helices of 14-3-3 ζ are identified below the x axis as blue cartoons, while disordered regions are represented by red lines. The area highlighted in red shows the region of the protein affected by the presence of C61_S352. (C) Mapping on the crystal structure of 14-3-3 ζ in the presence of the ASK1pS966 peptide (PDB ID: 6EJL, protein represented as grey surface, peptide represented as green sticks) of the amino acid residues (colored in red) corresponding to the 5 most affected resonances by the presence of C61_S352.

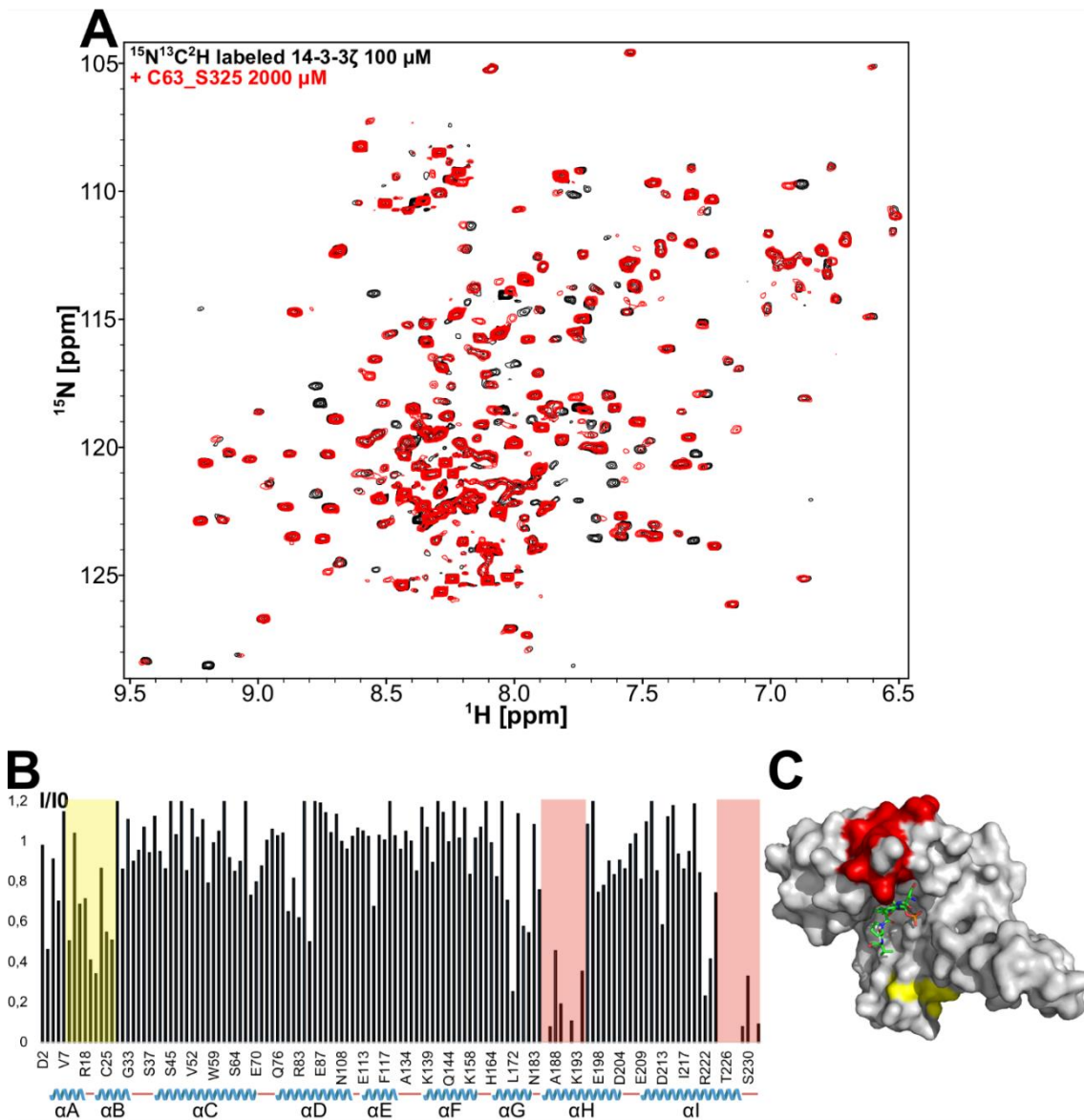


Figure S5- C63_S325 binding site on 14-3-3 ζ identified by ^1H - ^{15}N TROSY-HSQC. (A) Superimposed ^1H - ^{15}N TROSY-HSQC spectra of $^{15}\text{N}^{13}\text{C}^2\text{H}$ labeled 14-3-3 ζ 100 μM in the presence of 2% DMSO (v/v) (in black) and C63_S325 2000 μM (in red). (B) Plot of the I/I0 ratio of ^1H - ^{15}N correlation peaks of 100 μM 14-3-3 ζ in the presence of 2000 μM C63_S325 compared to the reference 14-3-3 ζ spectrum (100 μM) (y axis) versus the amino acid sequence (x axis). A total of 135 correlation peak intensities are shown. The x axis is not proportional. The helices of 14-3-3 ζ are identified below the x axis as blue cartoons, while disordered regions are represented by red lines. The area highlighted in red shows the region of the protein the most affected by the presence of C63_S325, while the area highlighted in yellow shows an additional area affected by the compound. (C) Mapping on the crystal structure of 14-3-3 ζ in the presence of the ASK1pS966 peptide (PDB ID: 6EJL, protein represented as grey surface, peptide represented as green sticks) of the amino acid residues affected by the presence of C63_S325. The amino acid residues colored in red correspond to the area highlighted in red in panel B and the amino acid residues colored in yellow correspond to the area highlighted in yellow in panel B.

6 Inhibition of 14-3-3/Tau by Hybrid Small-Molecule Peptides Operating via Two Different Binding Modes

6.1 Context of the collaboration

Our collaborators synthesized in 2015 the first peptidomimetic inhibitors of the 14-3-3/Tau PPI based on the pS214 epitope. This work yielded the hybrid peptidomimetic inhibitor 201D, binding to 14-3-3 with high affinity (Milroy et al., 2015). They kept working on this project and synthesized 18 new derivatives of 201D. Through FP assays, our collaborators confirmed that the new inhibitors successfully inhibited the interaction between 14-3-3 and a diphosphorylated peptide containing both pS214 and pS324 epitopes. Our collaboration was requested in order to access if the new inhibitors were capable of inhibiting the interaction between the two full-length proteins.

6.2 Manuscript (published)

The manuscript containing this work was published:

Andrei, S. A., Meijer, F. A., Neves, J. F., Brunsveld, L., Landrieu, I., Ottmann, C., & Milroy, L.-G. (2018). Inhibition of 14-3-3/Tau by Hybrid Small-Molecule Peptides Operating via Two Different Binding Modes. *ACS Chemical Neuroscience*, 9(11), 2639–2654. <https://doi.org/10.1021/acscchemneuro.8b00118>

Our contribution to this manuscript included protein production for NMR experiments, phosphorylation of recombinant Tau protein by PKAc, setting up of protein and ligand-based NMR experiments, interpretation of data and writing of the manuscript. In a more detailed way we contributed with:

- RESULTS AND DISCUSSION: Inhibition of the interaction of 14-3-3 with full-length phosphorylated Tau protein;
- METHODS: ¹⁵N labelled Tau Protein Expression and Purification, PKA catalytic subunit expression and Purification, In vitro Tau Phosphorylation, ¹⁵N-¹H HSQC spectroscopy; on full-length PKA-phosphorylated Tau (fl-pTau), ¹H NMR spectroscopy on 4.2e-l;

- FIGURES: 5, S36, S37, S38, S39;

The manuscript is presented ahead. To respect copyright constraints, the manuscript is presented as it was originally submitted to the journal and before the minor modifications performed upon peer-review. Given that the Supporting information associated with this manuscript is extremely extensive (100 pages), only Figures S36, S37, S38 and S39 will be presented here.

Inhibition of 14-3-3/Tau by hybrid small-molecule-peptides operating via two different binding modes.

Sebastian A. Andrei,^{†,ζ} Femke A. Meijer,^{†,ζ} João Filipe Neves,[§] Luc Brunsveld,[†] Isabelle Landrieu,^{§} Christian Ottmann,^{†,ζ*} and Lech-Gustav Milroy^{†*}*

[†] Laboratory of Chemical Biology, Department of Biomedical Engineering and Institute for Complex Molecular Systems, Technische Universiteit Eindhoven, Den Dolech 2, 5612 AZ Eindhoven, The Netherlands

[§] UMR 8576 CNRS-Lille University, 59000 Villeneuve d'Ascq, France

^ζ Department of Chemistry, University of Duisburg-Essen, Universitätsstrasse 7, 45117 Essen, Germany

^ξ These authors contributed equally to the work.

Abstract Current molecular hypotheses have yet not delivered marketable treatments for Alzheimer's disease (AD), arguably due to a lack of understanding of AD biology, and an overreliance on conventional drug modalities. Protein-protein interactions (PPIs) are emerging drug targets, which show promise for the treatment of e.g. cancer, but are still underexploited for treating neurodegenerative diseases. 14-3-3 binding to phosphorylated Tau is a promising PPI drug target based on its reported destabilizing effect on microtubules, leading to enhanced neurofibrillary tangle formation as a potential cause of AD-related neurodegeneration. Inhibition of 14-3-3/Tau may therefore be neuroprotective. Previously, we reported the structure-guided development of modified peptide inhibitors of 14-3-3/Tau. Here, we report further efforts to optimize the binding mode and activity of our modified Tau peptides through a combination of chemical synthesis, biochemical assays, X-ray crystallography. Most notably, we were able to characterize two different high-affinity binding modes, both of which inhibited 14-3-3-binding to full-length hyperphosphorylated Tau protein in vitro as measured by NMR spectroscopy. Our findings, besides producing useful tool inhibitor compounds for studying 14-3-3/Tau, have enhanced our understanding of the molecular parameters for inhibiting 14-3-3/Tau, which are important milestones toward the establishment of our 14-3-3 PPI hypothesis.

Keywords. 14-3-3 • Tau • Protein-Protein Interactions • Inhibitors • Drug Discovery • Peptide Chemistry

Introduction.

Despite the best efforts of academia and pharma, there are currently no marketed drugs, and a dearth of agents in development that treat the underlying pathology of AD – so-called disease modify therapies (DMTs).¹ While the drug mechanisms of current agents in Phases I-III are heterogeneous, they can nonetheless be broadly classified as targeting either the amyloid cascade or the downstream pathophysiology, including Tau pathway. Noticeably, more than half of agents in Phase III are anti-amyloids compared to only 4% directly targeting Tau.¹ The vast preponderance of all agents in the pipeline is either monoclonal antibodies or β -site amyloid precursor protein cleaving enzyme (BACE) inhibitors. Given that no treatment has yet been found, there is considerable incentive to address the relatively unexplored Tau pathway. The major one being that, in AD, the severity of cognitive decline is more correlated with the evolution of Tau neurofibrillary tangles (NFTs) than with that of amyloid deposits.² However, the effective targeting of NFTs might require a shift to new molecular modalities,³ the solution to which could be found in previously intractable molecular targets. Protein-protein interactions (PPIs) are, by conventional standards, emerging drug targets,⁴⁻⁸ which show promise for the treatment of other disease types, such as cancer,⁹ but are as yet underexploited for treating neurodegenerative diseases, including AD, despite the clear potential.¹⁰ We therefore bring forward the PPI between 14-3-3 proteins and Tau, as a potential therapeutic target to treat AD.¹¹⁻¹³

14-3-3 proteins are adapter proteins,¹⁴⁻¹⁶ which preferentially form complexes with phosphorylated proteins, thereby modulating their folding or function.¹⁷ While abundantly expressed in the body, 14-3-3 proteins are most abundantly in CNS compartments.¹⁸ 14-3-3 proteins make important PPIs in diverse pathophysiological settings such as cancer,¹⁹ metabolic diseases,²⁰ and in neurodegeneration. In the latter case, 14-3-3 proteins bind to a number of client proteins implicated in CNS diseases, among them Tau, α -synuclein, parkin and LRRK2.²¹ Therefore, 14-3-3 proteins are fundamentally interesting targets for neurodegenerative drug therapy,¹³ in which either inhibition or stabilization of 14-3-3 PPIs may prove to be viable therapeutic strategies.²²⁻²⁵

Tau protein similarly exerts its multiple neuronal functions by binding a range of partners, the most well-documented being the binding and stabilizing of microtubules.^{26,27} This interaction, as is the case for many Tau interactions, is physiologically regulated by phosphorylation.²⁸ However, hyperphosphorylation of Tau, associated with its aggregation inside neurons as PHF, are well-known hallmarks of AD.²⁹ The Tau/14-3-3 association has been found to impact several aspects of the Tau pathway in neurodegeneration. First, 14-3-3 ζ has been described to stimulate Tau phosphorylation by GSK3 β kinase in cell model and in brain,³⁰⁻³² and cAMP-dependent protein kinase *in vitro*.³⁰ Additionally, 14-3-3 ζ is reported to be associated with the neurofibrillary tangles composed of Tau PHF in AD brain extracts and to stimulate Tau aggregation in an *in vitro* assay.^{33,34}

Our group has provided X-ray crystallographic evidence for the preferential, bivalent binding of 14-3-3 proteins to phosphoepitope sites, pS214 and pS324, with affinity in the μ M range according to additional biochemical and biophysical data.¹¹ We additionally showed that the interaction could be decreased through 14-3-3 σ overexpression in SH-SY5Y cells.¹¹ Taken together, these data led us to hypothesize that 14-3-3 binding to phosphorylated Tau (pTau) occurs at the expense of a stabilizing PPI between Tau and microtubules,¹¹ which is concomitantly known to be decreased by the phosphorylation of Tau on S214.³⁵ Small molecule stabilization of microtubules (MTs) is a promising therapeutic strategy to compensate for the loss of Tau-mediated stabilization.³⁶ Indeed BMS-241027 and TPI 287 are two MT stabilizer compounds currently in clinical development for the treatment of AD³⁷. Small molecule inhibition of Tau aggregation, e.g. using cell permeable D-peptides,³⁸ may also prove to be a complementary therapeutic strategy. Alternatively, inhibition of 14-3-3/Tau, for example through the targeted development of modified peptide inhibitors, could potentially exert a neuroprotective effect by decreasing its phosphorylation level, while increasing the pool of soluble Tau protein for the stabilization of microtubules and by preventing its aggregation – the 14-3-3 PPI hypothesis.

Towards testing our 14-3-3 PPI hypothesis, we previously demonstrated the potential to inhibit 14-3-3/Tau *in vitro*, with small molecules developed using a structure-guided approach.¹² With the Tau-derived pS214 phosphopeptide epitope as the chemical starting point, we targeted chemical modifications specifically at the fusicoccin (FC) binding site of

Mode III 14-3-3 PPIs³⁹ to produce a potent inhibitor of 14-3-3 ζ binding to full-length (fl)-pTau. In this paper, we report the results of studies in which we attempt structure-guided optimization of our Tau-derived 14-3-3 inhibitors. Most notably we were able to improve the activity of the lead compound from our previous study, and characterize two distinct high affinity modes of interaction by fluorescence polarization (FP) and isothermal calorimetry (ITC) measurements, which we correlate to an “open” and “closed” state based on seven new X-ray co-crystal structures. Both binding modes were shown to inhibit the binding of 14-3-3 ζ to fl-pTau in a concentration-dependent manner, lending further weight to our 14-3-3 PPI hypothesis.

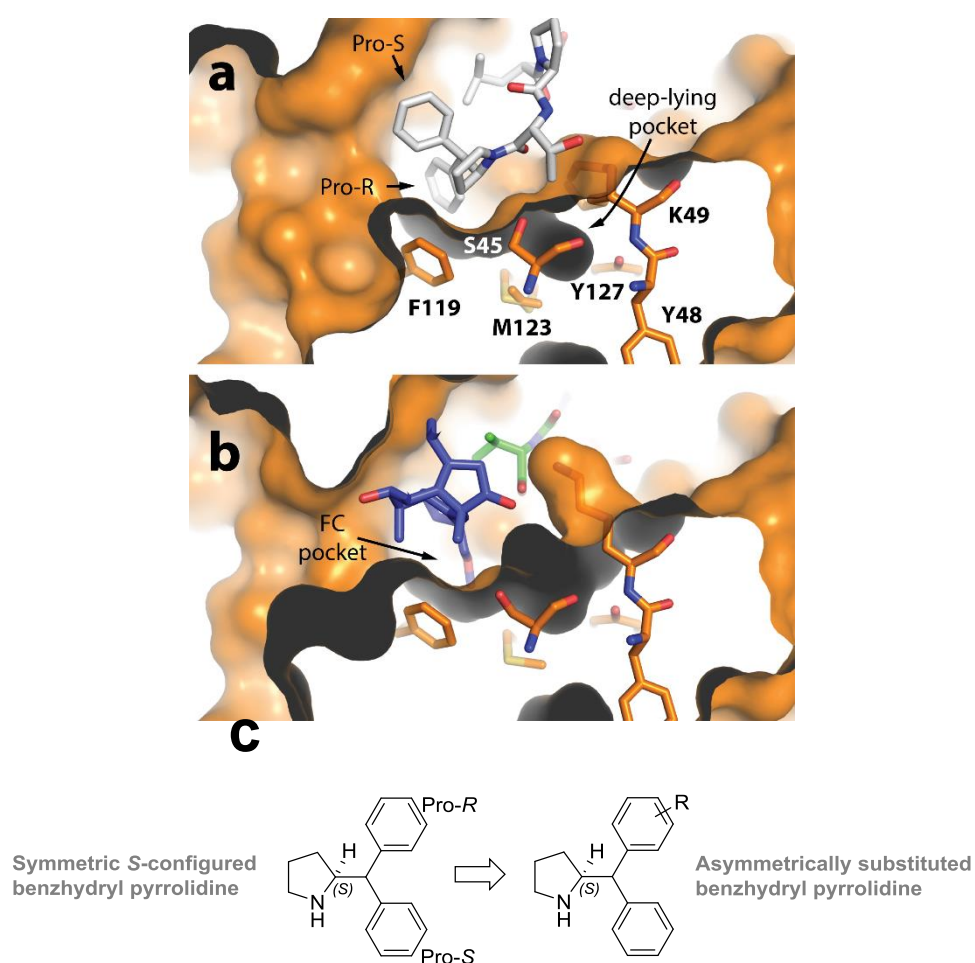
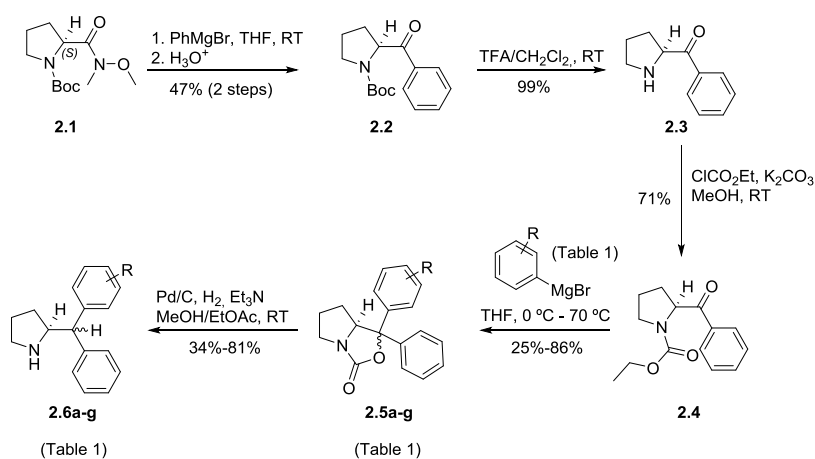


Figure 1 - a) Zoomed in perspective of deep-lying pocket, adjacent to the fusicoccin A (FC) pocket, present in previously published co-crystal structure of a synthetic Tau peptide, modified with a benzhydryl pyrrolidine moiety, bound to 14-3-3 $\sigma\Delta$ C (PDB: 5HF3).¹² The modified Tau peptide is depicted in white sticks, the protein surface and residues in orange and the protein interior surface in dark grey. Pocket-forming amino acid residues

are labelled. b) The same deep-lying pocket present in the ternary complex of 14-3-3 $\sigma\Delta$ C bound to the C-terminal ER α phosphopeptide and FC. The ER α peptide is depicted in green sticks, FC is depicted in purple sticks, the protein surface and residues in orange and the protein interior surface in dark grey. c) Chemical structure of symmetric *S*-configured benzhydryl pyrrolidine & general structure of asymmetrically substituted benzhydryl pyrrolidines.

Results and Discussion

Rational design of new 14-3-3 inhibitors. In a previous study,⁸ we discovered that a synthetic derivative of a pS214-Tau peptide epitope modified at the C-terminus with a benzhydryl pyrrolidine moiety bound more strongly to the 14-3-3 protein than the unmodified Tau epitope. In the resulting crystal structure the benzhydryl moiety – specifically, the pro-*R* phenyl ring – can be seen to occupy the fusicoccin (FC) pocket (Figure 1A), thus explaining the improved activity observed in the biochemical and biophysical assays. Closer inspection of the FC pocket identified a deep-lying pocket proximal to the pro-*R* phenyl group lined by seven amino acid residues derived from the same 14-3-3 protomer – Ser45, Tyr48, Lys49, Phe119, Lys122, Met123, and Tyr 127 (Figure 1A). Interestingly, a similar pocket is also present in other 14-3-3 protein–ligand crystal structure complexes (e.g. the 14-3-3–ER α complexed stabilized by FC – Figure 1B).²² The *ortho* and *meta* positions of the pro-*R* phenyl ring are located closest to the deep-lying pocket (Figure 1C). Based on these observations, we hypothesized that the affinity of our modified peptides might be further improved through structural variation of the benzhydryl pyrrolidine group, potentially addressing the deep-lying pocket in the process (Figure 1C). We therefore targeted the synthesis of a structurally diverse collection of mono-substituted benzhydryl pyrrolidine analogs (Tables 1-3), in which the phenyl substituent group differed in size and the polarity (i.e. H \rightarrow Cl \rightarrow Me \rightarrow OMe \rightarrow OCH₂CH₂OCH₃ – see Table 1).



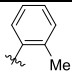
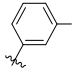
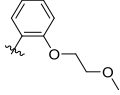
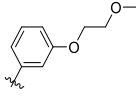
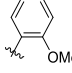
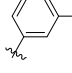
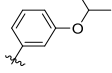
Scheme 1 - Synthesis of asymmetrically substituted benzhydryl pyrrolidine derivatives **2.6a-g** (Table 1).

Synthesis of substituted benzhydryl pyrrolidine derivatives. The synthesis of asymmetrically substituted benzhydryl pyrrolidine derivatives belonging to the generic structure depicted in Figure 1C was complicated by the absence of any literature precedent. Therefore, we elected for a synthesis based on the stereoretentive synthesis of symmetrically substituted (*S*)-2-diphenylmethylpyrrolidine (Scheme 1),⁴⁰ starting from enantiopure L-proline ester, though cognizant of the lack of obvious stereocontrol in the formation of the asymmetric centre at the benzhydryl carbon, and therefore the likely formation of diastereomers.

In brief, the addition of phenylmagnesium bromide to commercial Weinreb amide **2.1**, followed by acid work-up produced benzoylpyrrolidine **2.2** in a 47% yield over the two steps (Scheme 1). Deprotection of the Boc group yielded the substituted pyrrolidine **2.3**, which was followed by protection of the amine group as the ethyl carbamate **2.4**. At this juncture, treatment of **2.4** with a range of structurally diverse substituted Grignard reagents (Table 1) produced a small library of pyrrolooxazolones **2.5a-g**, in isolated yields ranging from 25-86%. The Grignard reagents used to make pyrrolooxazolones **2.5c** and **2.5d** are derived from 1-bromo-2-(2-methoxyethoxy)benzene and 1-bromo-3-(2-methoxyethoxy)benzene, respectively, which could be themselves prepared in one step from commercial compounds (supporting information). These were converted to the corresponding asymmetrically substituted benzhydryl pyrrolidines **2.6a-g** using palladium catalyzed hydrogenation conditions, a step which had been shown to occur without loss of stereopurity for the synthesis

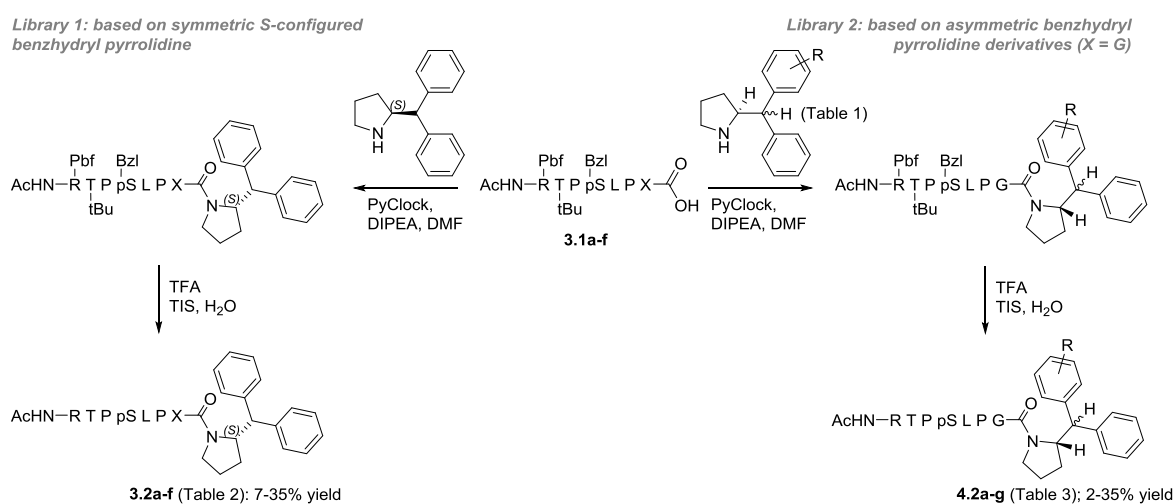
of (*S*)-2-diphenylmethylpyrrolidine, as evidenced by chiral HPLC and X-ray analysis.⁴⁰ For the series **2.5a-g**, we were unable to detect more than one diastereomer by either NMR or LC-MS. For the series **2.6a-g** by contrast, analogs **2.6c-f** yielded diastereomers, which were separable by reverse-phase (RP) HPLC, with combined yields in the range of 33-71% and diastereomeric ratios (drs) in the range 63:37-86:14 (Table 1). We were unable to detect the formation of diastereomers in the case of analogs **2.6a**, **2.6b** and **2.6g**.

Table 1 - Summary of structures, yields & diastereomeric ratios (dr) for pyrrolooxazolone (**2.5a-g**) and benzhydryl derivatives (**2.6a-g**) described in Scheme 1.

Derivative	Substituent group	2.5		2.6		dr ^[b]
		% yield ^[a]	dr	% yield ^[a]		
				I	II	
a		86	-	77 ^[c]		63:37
b		41	-	59 ^[c]		76:24
c		57	-	4	44	74:26 ^[d]
d		80	-	55	16	72:28 ^[d]
e		32	-	17	28	63:37 ^[d]
f		25	-	26	7	86:14 ^[d]
g		86	-	81 ^[c]		66:34

[a] isolated yields of diastereomers either combined or separated by RP-HPLC (denoted I or II). [b] dr determined by comparing integral values in ¹H NMR of crude. [c] Inseparable diastereomers. [d] diastereomers separable by RP-HPLC (Supporting Information).

Synthesis of the first library of modified Tau peptides. With the library of asymmetrically substituted pyrrolidine derivatives in hand, we proceeded with the synthesis of the corresponding modified Tau peptides. The synthesis of **3.2a** has been described in a previous communication.⁸ The appearance of the *R*-epimer in the co-crystal structure of **3.2a** with 14-3-3 σ – likely caused by racemization of the threonine α -stereocentre during the synthesis – was unexpected because the *S*-epimer was observed to bind 14-3-3 σ in co-crystal structures for analogous structures reported in same study, prepared using the same synthetic strategy.¹² An inspection of all structural data, superposed, suggested that the bulky benzhydryl moiety disfavors binding of the *S*-epimer of **3.2a** through a steric clash between the benzhydryl group and the threonine sidechain residue (an effect presumably absent in the case of the *R*-epimer). To test this hypothesis, and specifically probe the steric and stereochemical preferences of the modified Tau peptides for 14-3-3 binding, we synthesized a library of analogous modified Tau peptides in which the C-terminal L-Thr (**3.2a**) had been systematically replaced by either Gly (**3.2b**) or a short series of other *S*- and *R*-configured natural amino acid residues with different sidechains – L-Ala (**3.2c**), D-Ala (**3.2d**), L-Val (**3.2e**) and D-Val (**3.2f**) – Scheme 2.



Scheme 2 - Synthesis of modified Tau peptides **3.2a-f** (Table 2) and **4.2a-g** (Table 3). For the synthesis of **3.2a-f**, $X = L$ -Thr (**3.2a**), Gly (**3.2b**), L-Ala (**3.2c**), D-Ala (**3.2d**), L-Val (**3.2e**), D-Val (**3.2f**) – see Table 2. For the synthesis of **4.2a-g**, $R =$ see Table 3.

Partially protected Tau peptides **3.1a-f** were first synthesized as described for a previous synthesis of **3.1a** (referred to as **3b** in reference),¹² and characterized by LC-MS analysis (supporting information). Each partially protected peptide was then coupled to (S)-benzhydryl pyrrolidine using PyClock as coupling reagent followed by resin cleavage and deprotection of the side-chain protecting groups (TFA, TIS, H₂O) to afford **3.2a-f** in yields of 8-36% after purification by RP-HPLC (Scheme 2). While we could not conclusively exclude the possibility of diastereomer impurities in the final compounds, all modified Tau peptides were purified by RP-HPLC on an optimized gradient (see Methods section). Please refer to the Supporting Information for LC-MS spectra of all compounds after purification.

Biochemical evaluation of first library of modified Tau peptides. We next investigated the activity of our first library of modified Tau peptides in a competitive fluorescence polarization (FP) assay – Table 2 and Figure S34 (Supporting Information) – and compared their activities to that of our reference compound, **3.2a**. The FP data shows that under the specific assay conditions used, all new modified peptides (**3.2b-f**) inhibit binding of the competitor FAM-labeled diphosphorylated Tau competitor peptide to 14-3-3 ζ , with IC₅₀ values in the same low micromolar range as the reference, **3.2a** (Table 2).

Table 2 - Summary of structures, and associated IC_{50} (FP), and K_d values for the modified Tau peptides **3.2a-f**, the synthesis of which is described in Scheme 2. The confidence interval (CI) & \pm standard error (SE) are reported.

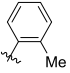
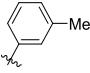
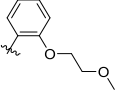
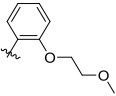
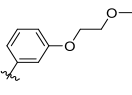
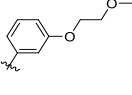
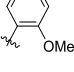
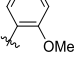
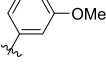
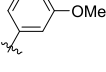
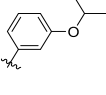
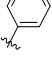
Derivative	Amino acid residue, X (Scheme 2)	FP		ITC	
		$IC_{50}/\mu\text{M}$	95% CI	$K_d/\mu\text{M}$	(\pm SE)
3.2a	L-Thr	8.1	7.3-8.9	5.4	0.4
3.2b	Gly	5.9	5.2-6.8	5.6	0.5
3.2c	L-Ala	5.3	4.7-5.8	3.3	0.7
3.2d	D-Ala	6.2	5.8-6.6	3.0	0.6
3.2e	L-Val	6.2	5.8-6.5	2.2	0.7
3.2f	D-val	7.6	7.2-8.1	3.4	0.6

ITC measurements were next performed in duplicate on modified Tau peptides **3.2a-f** to determine their association constant (K_a), stoichiometry (N), and enthalpy (ΔH) and entropy change (ΔS) on binding to 14-3-3 (Supporting Information). Although the two sets of duplicate measurements are consistent with one another, one set of data are used here for a quantitative comparison of the different analogs. Collectively, the calculated K_d values for analogs **3.2a-f** (Table 2) are of the same magnitude as the IC_{50} values determined by FP. The stoichiometries of binding (N) are also all approximately 1.0, which indicates a 1:1 binding between modified peptide and protein. Individually, the K_d (2.2-5.6 μM) & ΔG (-7.5 – -8.1 kcal mol⁻¹) values for each modified peptide are also very similar across the series, which indicates that they all bind with similar affinity to 14-3-3. In the two cases where the activities of L- and D-isomers could be directly compared – for Ala and Val analogs – similar binding data was measured e.g. compare the data for the L-Ala analog, **3.2c** ($K_d = 3.3 \mu\text{M}$, $\Delta G = -7.8 \text{ kcal mol}^{-1}$), and the D-Ala analog, **3.2d** ($K_d = 3.0 \mu\text{M}$, $\Delta G = -7.8 \text{ kcal mol}^{-1}$). There is additional evidence that increasing sterics and hydrophobicity at the C-terminal amino acid produce marginal gains in activity in the series Gly/**3.2b** ($K_d = 5.6 \mu\text{M}$, $\Delta G = -7.5 \text{ kcal mol}^{-1}$) \rightarrow L-Ala/**3.2c** ($K_d = 3.3 \mu\text{M}$, ΔG

= -7.8 kcal mol⁻¹) → L-Val/**3.2e** ($K_d = 2.2 \mu\text{M}$, $\Delta G = -8.1 \text{ kcal mol}^{-1}$). The thermodynamic binding parameters – ΔH and $-\Delta S$ – are also similar for all Tau peptide inhibitors in this library (Supporting Information), with the ΔH value in the range -1.7 – -2.5 kcal mol⁻¹, and the ΔS value in the range 5.0-6.6 kcal mol⁻¹. Notably, the K_d , ΔH , ΔS and ΔG values are near identical bearing either threonine (**3.2a**) or glycine (**3.2b**) at the C-terminus of the modified Tau peptide. Collectively, the similar FP and ITC data imply that the analogs **3.2a-f** are binding to 14-3-3 with a similar binding mode, the hypothesis being that the benzhydryl group in each case binds the FC pocket in a mode similar to the one observed in the crystal structure for **3.2a** (Figure 1A).¹² Furthermore, increasing the steric bulk and hydrophobicity produces a marginal increase in activity, while inverting the stereochemistry of the C-terminal amino acid residue importantly has no significant effect on the modified Tau peptide's binding and inhibitory properties.

Synthesis of the second library of modified Tau peptides. In view of the measured equipotency and similar thermodynamic profiles of the L-Thr (**3.2a**) and Gly analogs (**3.2b**), we elected to prepare a second library of modified Tau peptides based on **3.2b**. We reasoned that replacing L-Thr with Gly would simplify the synthesis while retaining the ability to explore the FC pocket, potentially addressing the adjacent deep-lying pocket (Figure 1A) through the introduction of asymmetrically substituted benzhydryl pyrrolidine derivatives. A second library of modified Tau peptides, **4.2a-g**, was therefore synthesized, of which the details are outlined in Scheme 2 and the structures summarized in Table 3. For some of the derivatives, two diastereomers were separated by RP-HPLC – denoted I and II – in yields of between 3-32% for the individual diastereomers, and overall combined isolated yields of between 34-57% (see Methods section).

Table 3 - Summary of structures, and associated IC_{50} (FP), and K_d values for the modified Tau peptides **4.2a-g** described in Scheme 3. The confidence interval (CI) & \pm standard error (SE) are reported.

Derivative	Substituent group	FP		ITC	
		$IC_{50}/\mu M$	95% CI	$K_d/\mu M$	(\pm SE)
4.2a ^[a]		6.0	5.7-6.5	8.9	0.7
4.2b ^[a]		5.9	5.6-6.3	9.3	2.0
4.2c-I		2.8	2.2-3.6	2.7	0.3
4.2c-II		4.2	4.0-4.5	9.0	0.5
4.2d-I		5.5	5.0-6.1	6.3	0.6
4.2d-II		12.1	10.7-13.7	20.6	2.4
4.2e-I		5.0	4.8-5.3	3.6	0.6
4.2e-II		10.4	9.6-11.2	12.7	0.9
4.2f-I		5.8	5.5-6.0	4.7	0.6
4.2f-II		11.4	10.7-12.2	16.5	2.0
4.2g ^[a]		7.2	6.5-7.8	6.2	1.2
3.2b []]		5.9	5.2-6.8	5.6	0.5

[a] A mixture of diastereomers.

Biochemical evaluation of second library of modified Tau peptides. As for the first library, we used FP and ITC to characterize the 14-3-3 binding properties of our second library of modified Tau peptides. The findings of this short study are summarized in Table 3. The FP data (Figure S35) shows that all analogs from this library function as competitive inhibitors of 14-3-3 σ with IC₅₀ values in the range 2.8-12.1 μ M. Our ITC data show that all analogs bind to 14-3-3 σ with K_d values in the range 2.7-20.6 μ M and Δ G values between -6.7 – -7.9 kcal mol⁻¹. The most active analog in the series was the 2-(methoxyethoxy)- derived **4.2c-I** (K_d = 2.7 μ M/ Δ G = -7.9 kcal mol⁻¹) and the least active, its regioisomer, analog **4.2d-II** (K_d = 20.6 μ M/ Δ G = -6.7 kcal mol⁻¹). Besides **4.2c-I**, analog **4.2e-I** (K_d = 3.6 μ M/ Δ G = -7.7 kcal mol⁻¹) and methoxy-derivative **4.2f-I** (K_d = 4.7 μ M/ Δ G = -7.5 kcal mol⁻¹) were also strong binders.

X-ray crystallography studies. To provide a molecular explanation for the high affinity binding of our new modified tau peptide inhibitors, the co-crystal structures of symmetrically substituted benzhydryl derivatives, **3.2d** (1.70 Å), and **3.2e** (2.00 Å), and asymmetrically substituted variants **4.2b** (1.50 Å), **4.2c-I** (1.40 Å), **4.2e-I** (1.25 Å), **4.2f-I** (1.40 Å) and **4.2f-II** (1.45 Å) bound to 14-3-3 σ DC were solved to their respective resolutions in parentheses (Figure 2 and supporting information). Figure 2A depicts a superimposition of the three modified Tau peptides, **3.2a** (white),¹² **3.2d** (blue) and **4.f-II** (green), in their 14-3-3-bound state, in which all three peptides clearly bind with a similar extended mode within the amphipathic groove of the protein. However, the structural differences between the three peptides at the C-terminus is observed to perturb the positioning of the peptide backbone and the leucine side-chain C-terminal to the phosphoserine residue. This general trend is representative for all co-crystallized modified Tau peptides. In Figures 2B-I, a panel comparing zoomed-in perspectives of the FC pocket of the seven different co-crystallized modified Tau peptides can be seen: the two benzydryl-derived (**3.2d** & **3.2e**) and five asymmetrically substituted analogs (**4.2b**, **4.2c-I**, **4.2e-I**, **4.2f-I** & **4.2f-II**), compared to **3.2a**. In contrast to analogs **3.2d** and **3.2e**, in which the pyrrolidine group were logically determined to be *S*-configured (derived from commercial (*S*)-2-(diphenylmethyl)pyrrolidine), all five asymmetrically substituted analogs were unexpectedly observed to be *R*-configured at the α -carbon of the pyrrolidine ring, counter to our expectations (Figure 2E-I).⁴⁰ Interestingly as well, all of the five peptides modified with an

asymmetrically substituted benzhydryl group bound in a similar “open” state, which contrasted with the “closed” state observed in the case of the three symmetric benzhydryl analogs. A closer examination of this data reveals that the oxygen of the methoxy substituent on **4.2f-I** (Figure 2H) is sufficiently close (3.1 Å) to engage in a hydrogen bond with the side chain of residue Asn-42 – an interaction witnessed previously between the sugar ring-oxygen of the natural product fusicoccin A (FC) and Asn-42 of 14-3-3 σ for stabilization of TASK-3 (PDB: 5D3F; 2.7 Å)²³ and 14-3-3 ζ for stabilization of CFTR (PDB: 3P1Q; 3.2 Å).⁴¹ By comparison, an analogous hydrogen bond interaction is absent from the crystal structure of the less potent diastereomer **4.2f-II** (Figure 2I). The ITC data for diastereomers **4.2f-I** & **4.2f-II** indicate that their 2-fold difference in affinity by FP and a 3.5-fold difference by ITC is entropically driven (Figure 3 & Table S2 in the supporting information). An explanation for the potency of analog **4.2c-I** – the most potent of the series – can be observed in the crystal structure in which the methoxyethoxy side chain clearly addresses the FC pocket. A more detailed discussion of all the co-crystal structures can be found in the supporting information.

Stereochemical outcome of modified Tau peptide synthesis. Logically, the *R*-configuration of the D-Ala-derived modified Tau peptide was found in the 14-3-3/**3.2d** co-crystal structure (Figure 2C). Interestingly, the *R*-epimer was also observed in the co-crystal structure of the Val-derived modified Tau peptide **3.2e** (Figure 2D), which parallels the result obtained previously¹² for the L-Thr-derived modified Tau peptide **3.2a** (Figure 2A). While the origin of the epimer formation in both cases remains unclear (both syntheses began with enantiomerically pure L-amino acids), it is hypothesized that the *S*-epimer of β -branched amino acids is sterically less favored for binding at the peptide C-terminus than the corresponding *R*-epimer. Significantly, the introduction of a glycine residue at the same C-terminal position of our peptides, which will not be dependent on epimerization, did not significantly affect the affinity of our modified Tau peptides. The electron densities clearly show that the *R*-epimer is bound to 14-3-3 for each of the five asymmetrically substituted analogs (**4.2b**, **4.2c-I**, **4.2e-I**, **4.2f-I** & **4.2f-II**), which was unexpected because the synthesis of the corresponding mono-substituted benzhydryl pyrrolidine in each case commenced with *S*-configured L-proline, and was based on an enantioretentive synthesis of (*S*)-2-

(diphenylmethyl)pyrrolidine.⁴⁰ However, we did not monitor the stereochemical outcome at each step during the synthesis of our mono-substituted benzhydryl pyrrolidine derivatives.

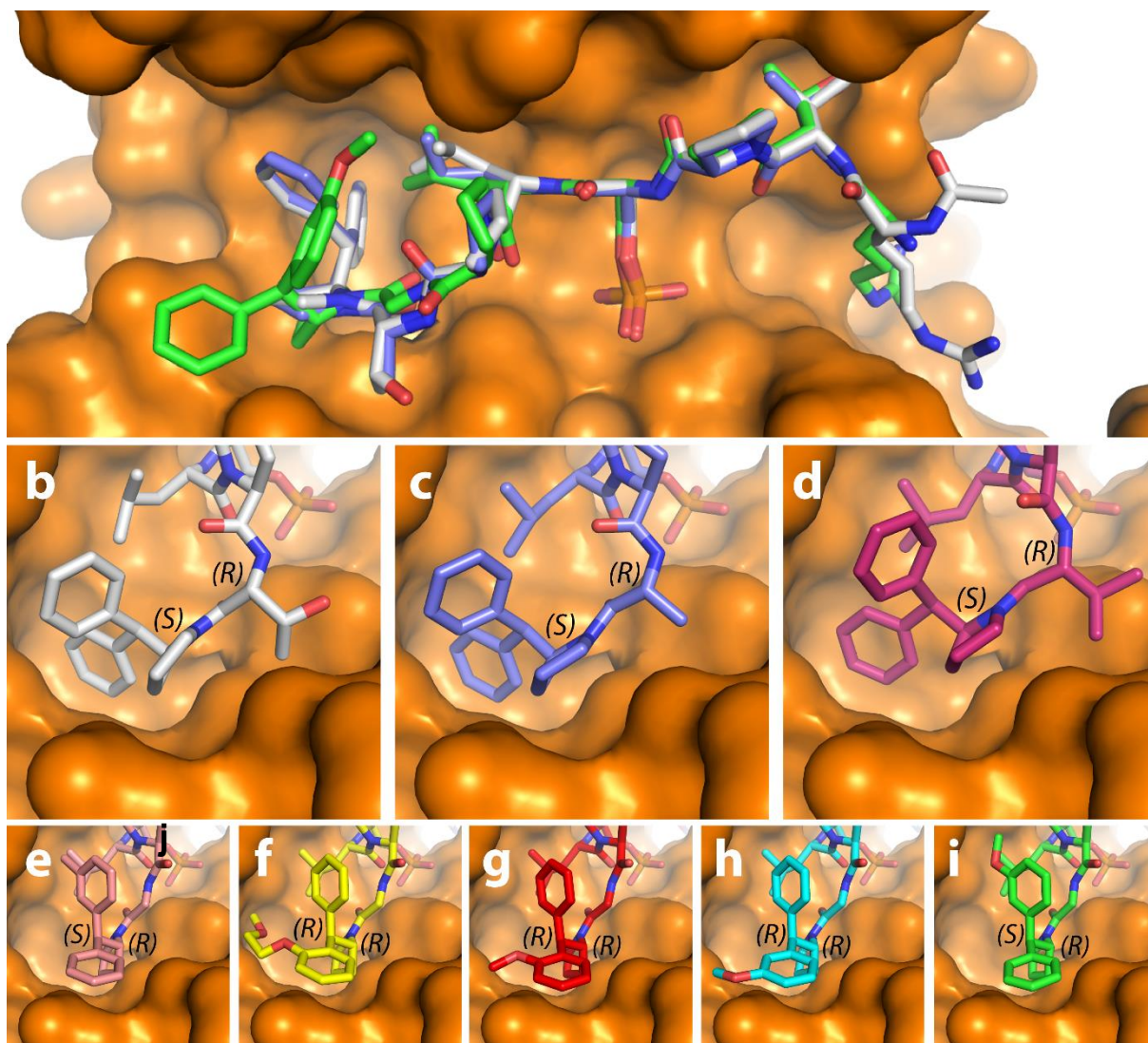


Figure 2 - a) Overlay of the co-crystal structures of the modified peptides **3.2a** (white)(PDB: 5HF3)¹² **3.2d** (blue) & **4.2f-II** (green) bound to 14-3-3 $\sigma\Delta$ C. b-i) Zoom-in of FC pocket for the co-crystal structures of the modified peptides **3.2a** (b),(PDB: 5HF3)¹² **3.2d** (c),(PDB; 6FI5) **3.2e** (d),(PDB; 6FI4) **4.2b** (e),(PDB; 6FBY) **4.2c-I** (f),(PDB; 6FAW) **4.2e-I** (g),(PDB; 6FAW) **4.2f-I** (h),(PDB; 6FAV) & **4.2f-II** (i)(PDB; 6FBW) bound to 14-3-3 $\sigma\Delta$ C. The stereochemical assignment (*S* and *R* notation) of the C-terminal amino acid and benzhydryl pyrrolidine solved in complex with the 14-3-3 protein have been added to each panel.

Analysis of thermodynamic parameters of binding. A clear difference was observed between the thermodynamic parameters for the asymmetrically substituted and those measured for the symmetrically substituted benzhydryl pyrrolidine-modified Tau peptides. In the case of the asymmetrically substituted analogs, the enthalpy change (ΔH) was in general more negative and the entropy change ($-T\Delta S$) more positive than for the symmetrically substituted benzhydryl pyrrolidine-modified Tau peptides. For example, while **3.2e** ($K_d = 2.2 \mu\text{M}$, $\Delta G = -8.1 \text{ kcal}$) and **4.2f-I** gave similar binding parameters ($K_d = 4.7 \mu\text{M}$, $\Delta G = -7.5 \text{ kcal mol}^{-1}$), their corresponding thermodynamic components significantly diverge (Figure 4). In the case of **3.2e**, the entropic factor ($-T\Delta S = -6.6 \text{ kcal mol}^{-1}$) contributed significantly more to the free energy of binding than the enthalpic factor ($\Delta H = -1.5 \text{ kcal mol}^{-1}$), while for analog **4.2f-I**, the opposite was true (i.e. $\Delta H = -4.7 \text{ kcal mol}^{-1}$ & $-T\Delta S = -2.8 \text{ kcal mol}^{-1}$). The same divergent behavior was observed across all Tau peptide inhibitors reported in Tables 2 and 3 such that compound binding could be classified as being either predominantly entropically driven (i.e. the symmetric benzhydryl analogs **3.2a-f**) or enthalpically driven (i.e. the asymmetric analogs **4.2a-g**).

A structural explanation for the two classifications of ITC data could be found in the crystallography data (Figure 4). The predominantly entropically driven binding profile characterized by ITC could be explained by the “closed” binding mode characterized by X-ray crystallography (illustrated by **3.2a**, Figure 4A), in which the *S*-configured symmetric benzhydryl moiety is observed to fill the FC-binding pocket to the exclusion of water molecules. By contrast, the predominantly enthalpically driven binding profile (illustrated by **4.2f-I**, Figure 4B) could be explained by a more “open” binding mode in the X-ray crystal structure, in which the now *R*-configured asymmetrically substituted benzhydryl moiety is found in a more solvent-exposed state, which permits the binding of more water molecules. A similar correlation between the ITC and the crystallography data for all other solved structures was observed, which suggests that all derivatives bearing the same, either enthalpic or entropic, binding profile by ITC (whether co-crystallized or not with the 14-3-3 protein) bind via the aforescribed “closed” or “open” binding modes by X-ray crystallography. The reason for the two different binding modes is most likely for two reasons: first, the difference in *R* and *S* configuration between the asymmetrically substituted benzhydryl pyrrolidine moieties

(*R*-configured), which all bind in the “open” state, and the *S*-configured symmetric benzhydryl pyrrolidines, which bind in the “closed” state. Second, a steric clash between the asymmetrically substituted benzhydryl group and the protein surface may disfavor a “closed” binding mode, which the ligand would relieve by adopting the more “open” binding state. In view of the ITC data for the Gly-derivative **3.2b**, the suggestion is the benzhydryl group of this derivative binds in a similar “closed” state as observed for e.g. **3.2a**, **3.2d** and **3.2e**. This result would suggest the added conformational freedom introduced by the C-terminal glycine residue would apparently not significantly influence the binding mode of **3.2b**, and by extension analogs from within the **4.2** series. While the modifications at the C-terminus of our modified Tau peptides do not address the targeted deep-lying pocket of the 14-3-3 protein (Figure 1C), as hypothesized, they have enabled the potent targeting of chemically distinct sites within the adjacent FC pocket.

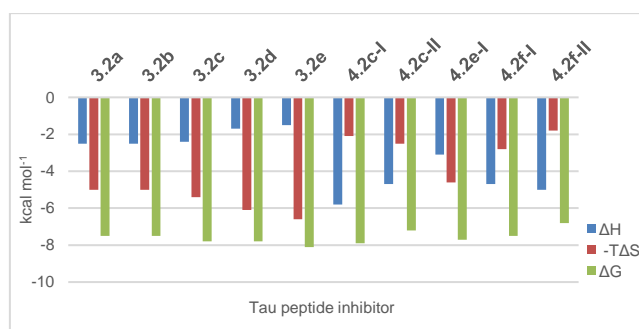


Figure 3 - Comparison of enthalpic (ΔH , blue) and entropic contributions ($-T\Delta S$, red) to the Gibbs free energy of binding (ΔG , green) at 310 K for modified Tau peptides **3.2a**, **3.2b**, **3.2e** & **4.2f-I**. For a comprehensive comparison of thermodynamic parameters for all modified Tau peptides see the supporting information (Table S2).

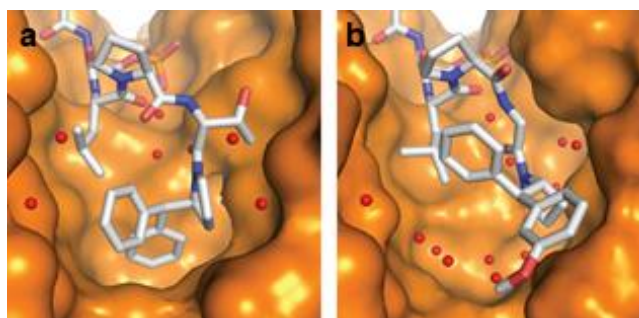


Figure 4 - Crystal structure of a) **3.2a** at 1.8 Å resolution (PDB: 5HF3) and b) **4.2f-I**(PDB; 6FAV) at 1.4 Å resolution, in complex with 14-3-3 σ . A difference in the amount of water molecules (red spheres) in the pocket can be observed, which may explain the difference in entropy observed in the ITC data.

Inhibition of the interaction of 14-3-3 with full-length phosphorylated Tau protein. We next investigated the potential of the three most potent analogs towards the inhibition of the interaction between 14-3-3 ζ and full-length PKA-phosphorylated Tau (pTau). From the analogs tested, one (**3.2e**), binds to 14-3-3 *via* an “open” binding mode, while the other two, (**4.2c-I** and **4.2e-I**), *via* the “closed” binding mode. NMR spectroscopy was used to assess the modulation of this PPI in solution. The 2D ^{15}N - ^1H HSQC spectra of ^{15}N -labelled pTau in the presence of unlabelled 14-3-3 ζ were acquired with or without each of the inhibitors. The intensities of the correlation peaks corresponding to specific amino acid residues along pTau sequence (I) were monitored in each experiment and compared to the intensities of the corresponding correlation peaks in the spectrum of pTau alone (I₀). The binding of 14-3-3 ζ to pTau led to peak broadening and consequently, to the decrease of the (I/I₀) ratio for resonances corresponding specifically to residues located in the binding region of 14-3-3 (Figure 5A and 5B). The addition of **4.2e-I** to the solution containing ^{15}N pTau/14-3-3 ζ led to a dose-dependent recovery of the intensity of these same resonances (Figure 5A and 5B). This effect is well illustrated by the resonances corresponding to the amide groups of the PKA-phosphorylated serines of Tau that showed intensity recovery with addition of each analog (Figure 5B, Figures S36). The same set of 2D experiments was performed for inhibitors **3.2e** and **4.2c-I** resulting in a similar I/I₀ profile (Figure 5, Figures S37 and S38), which confirmed the capacity of these analogs to decrease the formation of the complex 14-3-3 ζ /pTau. To get further insights on the inhibitory effect of these analogs, a series of ^1H spectra of **4.2e-I** was recorded in the presence of increasing concentrations of 14-3-3 ζ (Figure 5C). By monitoring one well-isolated resonance of the spectrum of the small-molecule, a concentration dependent intensity decrease upon the addition of 14-3-3 ζ was observed, which can be attributed to the interaction, as the sharp signal of the free ligand get broadened when complexed with the protein. Additionally, the spectrum of **4.2e-I** was recorded in the presence and absence of pTau, which did not reveal any sign of interaction (Figure S39) as both spectra

were identical. Based on these results, it can be concluded that **3.2e**, **4.2c-I** and **4.2e-I** inhibited the interaction pTau/14-3-3 ζ in a concentration dependent manner, by binding to 14-3-3 ζ and competing with pTau.

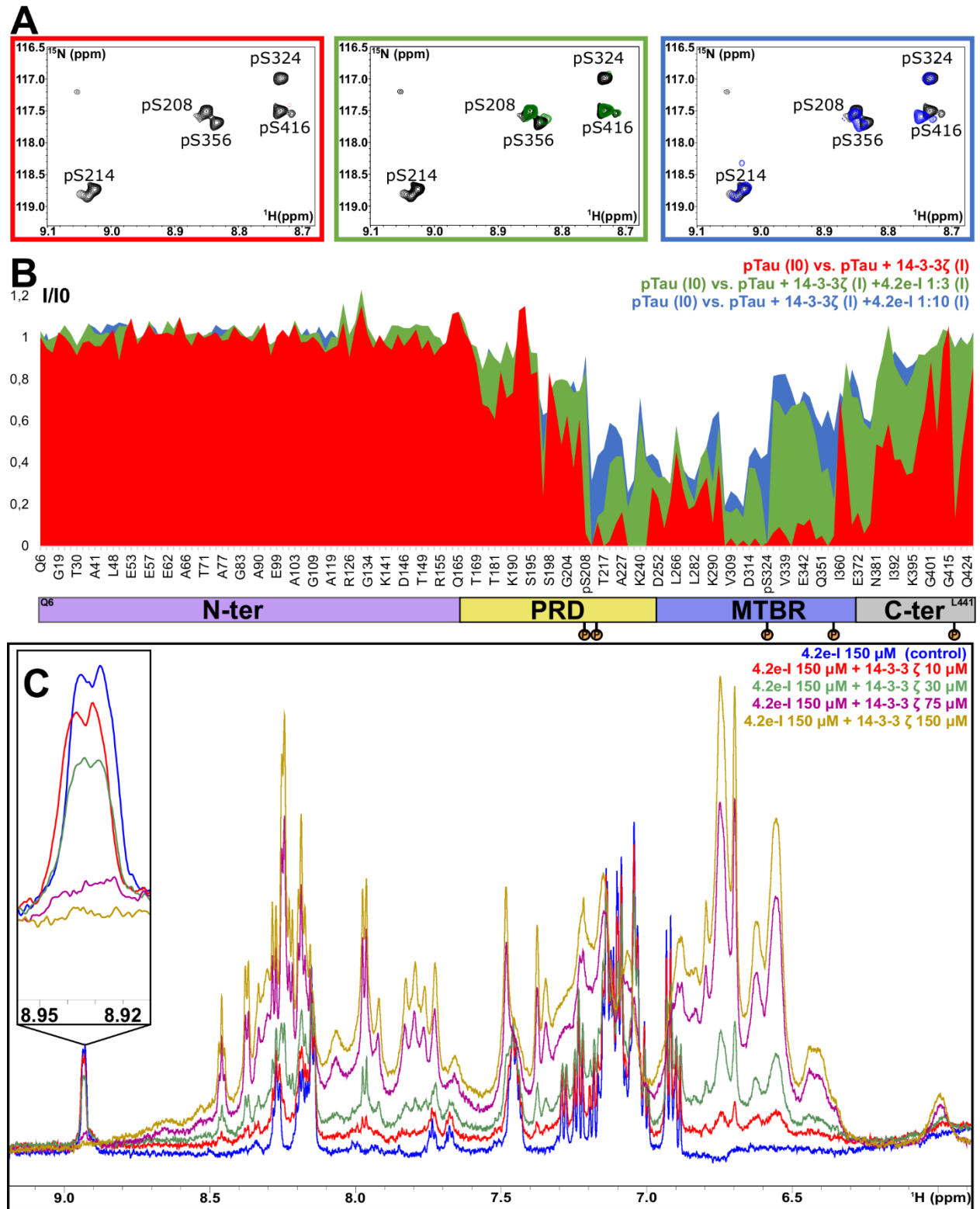


Figure 5 - **4.2e-I** inhibits the binding of pTau to 14-3-3 ζ in a concentration-dependent manner. A) Selected enlarged regions of the overlaid ^{15}N - ^1H HSQC spectra showing the intensity recovery of the correlation peaks correspondent to the amide groups of the PKA-phosphorylated Serines after the addition of **4.2e-I**. The spectra are shown superimposed to the pTau spectrum, which is colored in black. With the addition of a 3-fold excess of **4.2e-I** (considering 14-3-3 ζ concentration) it is possible to remark the intensity recovery of the weakest epitopes (pS208, pS356 and pS416) and finally, with the addition of a 10-fold, it is possible to detect pS214 and pS324. B) Plot of the ratios of the bound (I)/free (I₀) ^1H - ^{15}N correlation peak intensities of full length pTau 60 μM (y axis) versus the amino acid sequence (x axis) in the presence of 14-3-3 ζ 120 μM (red plot); 14-3-3 ζ 120 μM + **4.2e-I** 360 μM (green plot) and 14-3-3 ζ 120 μM + **4.2e-I** 1200 μM (blue plot). A total of 155 correlation peak intensities are shown. The x axis is not proportional. The domains of full-length pTau (N-ter for N-terminal; PRD for Proline-Rich Domain; MTBR for Microtubule Binding Region; C-ter for C-terminal) and the phosphorylation sites (S208, S214, S356, S314 and S416) are identified below the x axis. C) Section of overlaid ^1H spectra of **4.2e-I** 150 μM alone (blue) and in the presence of 14-3-3 ζ 10 μM (red), 30 μM (green), 75 μM (purple) and 150 μM (gold). The enlarged region shows a well-isolated resonance correspondent to a **4.2e-I** proton.

Conclusions

Here, we describe the synthesis of a novel seventeen-membered collection of modified Tau peptide inhibitors, targeting increase binding affinity at the fusicocin A (FC) pocket and proximal deep-lying pocket. In the case of the peptides bearing a symmetric, S-configured benzhydryl pyrrolidine group, exchanging the C-terminal Thr residue during the synthesis with a number of other L- and D-amino acid residues at the C-terminus of the Tau peptide, including non-chiral Gly, did not produce a significant change in the IC₅₀ and K_d and associated thermodynamic parameters. This result suggested that the C-terminal amino acid in the modified Tau peptide can be flexibly replaced by amino acids bearing different side chains and stereochemistry. All resulting Tau peptide analogs (Table 2 & 3) were active inhibitors of 14-3-3/Tau. Interestingly, using a combination of FP, ITC and X-ray crystallography data, we characterized two binding modes for our modified Tau peptides – one “closed” entropically-driven state, the other an “open” enthalpic state at the peptide C-terminus. The different binding modes is most likely caused by the inverted stereochemistry at the α -carbon between the commercial S-configured symmetric benzhydryl pyrrolidine (“closed”) and the synthetic R-configured asymmetric benzhydryl pyrrolidine (“open”) – an unexpected outcome of the

synthesis – and steric factors induced by mono-substitution of the benzhydryl group. While neither of these two modes were capable of addressing the deep-lying pocket (Figure 1C), both inhibited 14-3-3-binding to full-length hyperphosphorylated Tau protein in vitro. Considering the manner in which the Tau-derived phosphoepitope has been studied presently, it could also be envisaged as a non-covalent tether to investigate new chemotypes to address the FC pocket, thus potentially opening the door to new non-phosphorylated inhibitors or novel stabilizers of Mode III 14-3-3 PPIs.

Methods

Synthesis of substituted benzhydryl pyrrolidine derivatives

General methods

Unless otherwise stated, all solvents employed were commercially available and used without purification. Water was purified using a Millipore purification train. Dry solvents were obtained from a MBRAUN Solvent Purification System (MB-SPS-800). Deuterated solvents were obtained from Cambridge Isotope laboratories. All reagents were commercially available, supplied by Sigma-Aldrich, and used without purification. NMR data were recorded on a Bruker Cryomagnet for NMR spectroscopy (400 MHz for ^1H -NMR and 100 MHz for ^{13}C -NMR). Proton experiments were reported in parts per million (ppm) downfield of TMS. All ^{13}C spectra were relative to the residual chloroform signal (77.16 ppm). ^1H -NMR spectra are reported as follows: chemical shift, multiplicity (s = singlet, d = doublet, t = triplet, q = quartet, m = multiplet, dd = doublet of doublets, td = triplet of doublets), integration, and coupling constant (J) in Hertz (Hz). Analytical Liquid Chromatography coupled with Mass Spectrometry (LC-MS) was performed on a C4 Jupiter SuC4300A 150 x 2.0 mm column using H_2O with 0.1% Formic Acid (F.A.) and Acetonitrile with 0.1% F.A., in general with a gradient of 5% to 100% Acetonitrile in H_2O in 15 min (connected to a Thermo Fischer LCQ Fleet Ion Trap Mass Spectrometer). Preparative High Pressure Liquid Chromatography (HP-LC) was performed on a Gemini S4 110A 150 x 21.20 mm column using H_2O with 0.1% F.A. and Acetonitrile with 0.1% F.A. Silica column chromatography was performed manually using silica gel with particle size

60–200 μm (60 \AA). Reaction progress was monitored by thin-layer chromatography using Merck TLC silica gel 60 F254 plates.

tert-butyl (S)-2-benzoylpyrrolidine-1-carboxylate (2.2). To an oven dried 100 mL two-necked flask was added magnesium turnings (1.18 g, 48.4 mmol) and anhydrous THF (10 mL) under argon pressure. A small amount of iodine was added followed by the slow addition of bromobenzene (3.80 g, 24.2 mmol). The reaction was slowly heated using a heat gun to start the reaction and it was then stirred at room temperature for 30 min. Subsequently, the reaction was cooled down to 0 $^{\circ}\text{C}$, at which time the Weinreb amide **2.1** (2.50 g, 9.7 mmol) in THF (6 mL) was added slowly. The resultant mixture was stirred at 0 $^{\circ}\text{C}$ for 3 h, then quenched with saturated NH_4Cl (15 mL) and extracted with EtOAc (3 x 30 mL). The combined organic layers were washed with brine, dried over Na_2SO_4 , filtered and concentrated *in vacuo*. The product was purified by column chromatography, eluting with heptane/EtOAc 72:28 v/v to yield tert-butyl (S)-2-benzoylpyrrolidine-1-carboxylate (**2.2**) as a white powder (1.24 g, 4.50 mmol, 47%). Silica gel TLC R_f = 0.23 (Heptane/EtOAc 72:28 v/v); LC-MS (ESI): calc. for $\text{C}_{16}\text{H}_{21}\text{NO}_3$ [M+H-BOC] $^+$: 176.10, observed 176.25, LC, R_t = 6.76 min; ^1H NMR (400 MHz, CDCl_3): δ (ppm) 8.02 – 7.91 (m, 2H), 7.62 – 7.52 (m, 1H), 7.51 – 7.41 (m, 2H), 5.37 – 5.16 (m, 1H), 3.73 – 3.42 (m, 2H), 2.40 – 2.24 (m, 1H), 2.02 – 1.85 (m, 3H), 1.47 (s, 9H); ^{13}C NMR (100 MHz, CDCl_3): δ 198.92, 154.45, 135.29, 133.19, 128.70, 128.69, 128.52, 128.51, 79.78, 61.36, 46.81, 29.82, 28.21, 28.20, 28.19, 24.18.

(S)-phenyl(pyrrolidin-2-yl)methanone (2.3). The *t*-Boc-protected amine **2.2** (1.14 g, 4.1 mmol) was dissolved in dichloromethane (25 mL) and a solution of trifluoroacetic acid (10 mL) (70:30 v/v) was added. The reaction was stirred at room temperature for 2 hours. The solvent was evaporated, yielding (S)-phenyl(pyrrolidin-2-yl)methanone (**2.3**) (718 mg, 4.1 mmol, 99%), which was directly used without purification. LC-MS (ESI): calc. for $\text{C}_{11}\text{H}_{13}\text{NO}$ [M+H] $^+$: 176.10, observed 176.25, LC, R_t = 2.38 min; ^1H NMR (400 MHz, CDCl_3): δ (ppm) 7.98 (d, J = 7.6 Hz, 2H), 7.72 (t, J = 7.6 Hz, 1H), 7.60 – 7.52 (m, 2H), 5.56 – 5.47 (m, 1H), 3.69 – 3.52 (m, 2H), 2.80 – 2.68 (m, 1H), 2.30 – 2.18 (m, 1H), 2.16 – 1.97 (m, 2H); ^{13}C NMR (100 MHz, CDCl_3): δ 193.67, 135.79, 131.26, 129.33, 129.32, 129.21, 129.19, 63.18, 47.47, 30.22, 24.32.

Ethyl (S)-2-benzoylpyrrolidine-1-carboxylate (2.4). (S)-phenyl(pyrrolidin-2-yl)methanone (**2.3**) (500 mg, 2.58 mmol) was dissolved in methanol (25 mL). K₂CO₃ (1.58 g, 11.4 mmol) was added followed by ethyl chloroformate (340 mg, 3.1 mmol) and the reaction mixture was stirred for 24 h at room temperature. The reaction mixture was quenched with NH₄Cl (15 mL) and extracted with EtOAc (3 x 30 mL). The combined organic layers were washed with brine, dried over Na₂SO₄ and filtered. Evaporation of solvent afforded ethyl (S)-2-benzoylpyrrolidine-1-carboxylate (**2.4**) (501 mg, 2.0 mmol, 71%) as a yellow oil. LC-MS (ESI): calc. for C₁₄H₁₇NO₃ [M+H]⁺: 248.12, observed 248.08, LC, R_t = 5.89 min; ¹H NMR (400 MHz, CDCl₃): δ (ppm) 8.04 – 7.91 (m, 2H), 7.63 – 7.53 (m, 1H), 7.52 – 7.43 (m, 2H), 5.44 – 5.19 (m, 1H), 4.27 – 3.90 (m, 2H), 3.77 – 3.43 (m, 2H), 2.44 – 2.22 (m, 1H), 2.02 – 1.86 (m, 3H), 1.28 (t, J = 6.8 Hz, 3H); ¹³C NMR (100 MHz, CDCl₃): δ 198.31, 155.15, 135.06, 133.30, 128.73, 128.73, 128.53, 128.52, 61.39, 61.15, 47.00, 30.90, 24.25, 14.77.

General procedure for the synthesis of pyrrolooxazolones 2.5a-g

To an oven-dried, either 50 or 100 mL two-necked flask were added the magnesium turnings and anhydrous THF under an argon atmosphere. A catalytic (spatula end) amount of iodine was added, followed by slow addition of the substituted bromobenzene neat via Hamilton gastight syringe. The reaction was gently heated to initiate the reaction, and stirred at room temperature for 30 min. Subsequently, the reaction was cooled down to 0 °C and a 1 mL solution of **2.4** in THF introduced through slow drop-wise addition. The resulting mixture was stirred at 0 °C for 2 h, and then warmed to 70 °C. With the exception of analog **2.5a**, which was heated for 3 h and worked up directly, in the general case, the reaction was monitored by measuring LC-MS on small aliquots of the reaction, and heated for 24 h. For the work-up, the reaction mixture was cooled to room temperature, quenched through addition of sat. aq. NH₄Cl (5 mL) and extracted with EtOAc (3 x 30 mL). The combined organic layers were washed with brine, dried over Na₂SO₄, filtered and then concentrated *in vacuo*. Except with the synthesis of analogs **2.5a**, **2.5b**, and **2.5g**, which proceeded directly to the purification step, the crude material was dissolved in methanol (3 mL) and treated with either 100 mg NaOH (**2.5c** and **2.5d**) or 500 mg KOH (**2.5e** and **2.5f**) to promote further ring-closure to the

pyrrolooxazolone. In these latter cases, the reaction was stirred at room temperature for 24 h and worked up as described previously. The isolated crude was purified by either silica gel column chromatography (**2.5a**, **2.5b**, **2.5c**, **2.5d** and **2.5g**) or reversed-phase flash chromatography on a Biotage Isolera system (**2.5e** and **2.5f**) to yield the pure pyrrolooxazolone after evaporation of elution solvents under reduced pressure.

Pyrrolooxazolone 2.5a. The synthesis was performed in accordance with the general method using magnesium turnings (39 mg, 1.6 mmol) suspended in 5 mL anhydrous THF, 2-bromotoluene (138 mg, 0.81 mmol) and **2.4** (95 mg, 384 μmol). The product was purified by silica gel column chromatography, eluting with heptane/EtOAc 70:10 v/v to yield pyrrolooxazolone **2.5a** as a yellow oil (129 mg, 330 μmol , 86%). Silica gel TLC R_f = 0.30 (Heptane/EtOAc 70:30 v/v); LC-MS (ESI): calc. for $\text{C}_{19}\text{H}_{19}\text{NO}_2$ $[\text{M}+\text{H}]^+$: 294.14, observed 294.17, LC, R_t = 7.08 min; ^1H NMR (400 MHz, CDCl_3): δ (ppm) 7.55 – 7.50 (m, 1H), 7.34 – 7.26 (m, 5H), 7.22 – 7.13 (m, 3H), 4.81 (dd, J = 9.0, 6.2 Hz, 1H), 3.69 – 3.59 (m, 1H), 3.28 – 3.19 (m, 1H), 2.11 (s, 3H), 1.95 – 1.76 (m, 2H), 1.63 – 1.49 (m, 1H), 1.28 – 1.16 (m, 1H); ^{13}C NMR (100 MHz, CDCl_3): δ 159.64, 140.15, 139.03, 138.69, 133.00, 128.65, 128.21, 128.20, 127.65, 125.87, 125.87, 125.52, 125.24, 87.98, 67.66, 45.35, 27.96, 26.00, 21.56.

Pyrrolooxazolone 2.5b. The synthesis was performed in accordance with the general method using magnesium turnings (39 mg, 1.6 mmol) suspended in 5 mL anhydrous THF, 3-bromotoluene (138mg, 0.81 mmol) and **2.4** (95 mg, 384 μmol). The product was purified by silica gel column chromatography, eluting with heptane/EtOAc 70:30 v/v to yield pyrrolooxazolone **2.5b** as a yellow oil (46 mg, 157 μmol , 41%). Silica gel TLC R_f = 0.29 (Heptane/EtOAc 70:30 v/v); LC-MS (ESI): calc. for $\text{C}_{19}\text{H}_{19}\text{NO}_2$ $[\text{M}+\text{H}]^+$: 294.14, observed 294.08, LC, R_t = 7.11 min; ^1H NMR (400 MHz, CDCl_3): δ (ppm) 7.42 – 7.28 (m, 7H), 7.25 – 7.21 (m, 1H), 7.12 (d, J = 7.5 Hz, 1H), 4.54 (dd, J = 10.5, 5.5 Hz, 1H), 3.78 – 3.68 (m, 1H), 3.29 – 3.20 (m, 1H), 2.34 (s, 3H), 2.04 – 1.62 (m, 3H), 1.18 – 1.06 (m, 1H); ^{13}C NMR (100 MHz, CDCl_3): δ 160.48, 143.24, 140.43, 138.34, 129.07, 128.39, 128.28, 128.28, 127.63, 126.58, 125.45, 125.44, 122.90, 85.91, 69.24, 46.02, 28.98, 24.93, 21.59.

Pyrrolooxazolone 2.5c. The synthesis was performed in accordance with the general method using magnesium turnings (49 mg, 2.0 mmol) suspended in 4 mL anhydrous THF, 1-bromo-2-(2-methoxyethoxy)-benzene (280 mg, 0.81 mmol) and **2.4** (80 mg, 324 μ mol). The product was purified by silica gel column chromatography, eluting with heptane/EtOAc 60:40 v/v to yield pyrrolooxazolone **2.5c** as a yellow oil (65 mg, 184 μ mol, 57%). Silica gel TLC R_f = 0.34 (Heptane/EtOAc 60:40 v/v); LC-MS (ESI): calc. for $C_{21}H_{23}NO_4$ $[M+H]^+$: 354.16, observed 354.00, LC, R_t = 6.83 min; 1H NMR (400 MHz, $CDCl_3$): δ (ppm) 7.71 (dd, J = 7.9, 1.7 Hz, 1H), 7.52 – 7.46 (m, 2H), 7.34 – 7.27 (m, 3H), 7.25 – 7.18 (m, 1H), 7.03 – 6.90 (m, 2H), 4.85 (dd, J = 9.0, 6.2 Hz, 1H), 4.23 – 4.16 (m, 2H), 3.81 – 3.69 (m, 2H), 3.69 – 3.61 (m, 1H), 3.41 (s, 3H), 3.19 – 3.09 (m, 1H), 2.03 – 1.93 (m, 1H), 1.90 – 1.80 (m, 2H), 1.39 – 1.25 (m, 1H); ^{13}C NMR (100 MHz, $CDCl_3$): δ 159.53, 154.38, 140.42, 131.80, 129.39, 127.83, 127.83, 127.58, 127.18, 126.39, 126.39, 121.38, 112.03, 86.80, 70.74, 68.46, 66.96, 58.78, 45.24, 28.76, 25.81.

Pyrrolooxazolone 2.5d. The synthesis was performed in accordance with the general method using magnesium turnings (49 mg, 2.0 mmol) suspended in 4 mL anhydrous THF, 1-bromo-3-(2-methoxyethoxy)-benzene (280 mg, 0.81 mmol) and **2.4** (100 mg, 404 μ mol). The product was purified by silica gel column chromatography, eluting with heptane/EtOAc 60:40 v/v to yield pyrrolooxazolone **2.5d** as a yellow oil (114 mg, 323 μ mol, 80%). Silica gel TLC R_f = 0.24 (Heptane/EtOAc 60:40 v/v); LC-MS (ESI): calc. for $C_{21}H_{23}NO_4$ $[M+H]^+$: 354.16, observed 353.92, LC, R_t = 6.68 min; 1H NMR (400 MHz, $CDCl_3$): δ (ppm) 7.40 – 7.27 (m, 6H), 7.15 – 7.08 (m, 2H), 6.88 – 6.83 (m, 1H), 4.52 (dd, J = 10.4, 5.5 Hz, 1H), 4.11 – 4.07 (m, 2H), 3.77 – 3.66 (m, 3H), 3.43 (s, 3H), 3.28 – 3.19 (m, 1H), 2.02 – 1.78 (m, 2H), 1.75 – 1.65 (m, 1H), 1.18 – 1.04 (m, 1H); ^{13}C NMR (100 MHz, $CDCl_3$): δ 160.33, 158.89, 144.89, 140.18, 129.54, 128.29, 128.28, 127.71, 125.43, 125.43, 118.40, 113.83, 113.14, 85.80, 70.97, 69.22, 67.26, 59.21, 45.99, 28.96, 24.95.

Pyrrolooxazolone 2.5e. The synthesis was performed in accordance with the general method using magnesium turnings (49 mg, 2.0 mmol) suspended in 4 mL anhydrous THF, 2-bromoanisole (151 mg, 0.81 mmol) and **2.4** (100 mg, 404 μ mol). The product was purified by reversed-phase flash chromatography on a Biotage Isolera system, eluting with a gradient of

5-100% ACN in H₂O to yield pyrrolooxazolone **2.5e** as a yellow oil (40 mg, 129 μmol, 32%). LC-MS (ESI): calc. for C₁₉H₁₉NO₃ [M+H]⁺: 310.14, observed 310.08, LC, R_t = 6.49 min; ¹H NMR (400 MHz, CDCl₃): δ (ppm) 7.67 (dd, *J* = 7.8, 1.7 Hz, 1H), 7.41 – 7.27 (m, 5H), 7.25 – 7.20 (m, 1H), 7.06 – 6.91 (m, 2H), 4.72 (dd, *J* = 8.7, 6.2 Hz, 1H), 3.86 (s, 3H), 3.72 – 3.60 (m, 1H), 3.21 – 3.09 (m, 1H), 1.98 – 1.90 (m, 1H), 1.89 – 1.80 (m, 2H), 1.45 – 1.32 (m, 1H); ¹³C NMR (100 MHz, CDCl₃): δ 159.32, 155.28, 140.27, 131.63, 129.49, 127.95, 127.94, 127.68, 127.10, 126.29, 126.28, 121.34, 111.63, 87.13, 68.72, 55.21, 45.19, 28.68, 25.92.

Pyrrolooxazolone 2.5f. The synthesis was performed in accordance with the general method using magnesium turnings (49 mg, 2.0 mmol) suspended in 4 mL anhydrous THF, 3-bromoanisole (151 mg, 0.81 mmol) and **2.4** (100 mg, 404 μmol). The product was purified by reversed-phase flash chromatography on a Biotage Isolera system, eluting with a gradient of 5-100% ACN in H₂O to yield pyrrolooxazolone **2.5f** as a yellow oil (31 mg, 100 μmol, 25%). LC-MS (ESI): calc. for C₁₉H₁₉NO₃ [M+H]⁺: 310.14, observed 310.17, LC, R_t = 6.43 min; ¹H NMR (400 MHz, CDCl₃): δ (ppm) 7.42 – 7.26 (m, 6H), 7.12 (d, *J* = 8.0 Hz, 1H), 7.06 (t, *J* = 2.2 Hz, 1H), 6.84 (dd, *J* = 8.0, 2.4 Hz, 1H), 4.53 (dd, *J* = 10.5, 5.5 Hz, 1H), 3.78 (s, 3H), 3.75 – 3.68 (m, 1H), 3.32 – 3.18 (m, 1H), 2.04 – 1.80 (m, 2H), 1.77 – 1.67 (m, 1H), 1.20 – 1.05 (m, 1H); ¹³C NMR (100 MHz, CDCl₃): δ 160.36, 159.72, 144.93, 140.21, 129.56, 128.30, 128.30, 127.72, 125.42, 125.42, 118.07, 113.44, 112.23, 85.83, 69.29, 55.32, 45.99, 28.98, 24.95.

Pyrrolooxazolone 2.5g. The synthesis was performed in accordance with the general method using magnesium turnings (49 mg, 2.0 mmol) suspended in 4 mL anhydrous THF, 3-bromophenyl isopropyl ether (217 mg, 1.0 mmol) and **2.4** (100 mg, 404 μmol). The product was purified by silica gel column chromatography, eluting with CH₂Cl₂/heptane 80:20 v/v to yield pyrrolooxazolone **2.5g** as a yellow oil (117 mg, 347 μmol, 86%). Silica gel TLC R_f = 0.29 (DCM/Heptane 80:20 v/v); LC-MS (ESI): calc. for C₂₁H₂₃NO₃ [M+H]⁺: 338.17, observed 338.08, LC, R_t = 7.12 min; ¹H NMR (400 MHz, CDCl₃): δ (ppm) 7.42 – 7.26 (m, 5H), 7.26 – 7.22 (m, 1H), 7.10 – 7.03 (m, 2H), 6.82 (dd, *J* = 8.0, 2.0 Hz, 1H), 4.57 – 4.47 (m, 2H), 3.78 – 3.67 (m, 1H), 3.29 – 3.19 (m, 1H), 2.00 – 1.80 (m, 2H), 1.76 – 1.66 (m, 1H), 1.30 (dd, *J* = 7.8, 6.1 Hz, 6H), 1.18 – 1.04 (m, 1H); ¹³C NMR (101 MHz, CDCl₃): δ 160.39, 158.00, 144.94, 140.27, 129.52, 128.29,

128.27, 127.67, 125.45, 125.44, 117.91, 114.95, 114.19, 85.83, 69.89, 69.27, 45.99, 28.99, 24.95, 22.00, 21.98.

General procedure for the synthesis of asymmetrically substituted benzhydryl pyrrolidine analogs 2.6a-g

A 25 mL, glass round-bottomed flask was loaded with the pyrrolooxazolone precursor, dissolved in either pure ethyl acetate or a methanol/ethyl acetate solvent mixture, and treated with the catalyst, Pd/C (10%). The flask was flushed with hydrogen gas for 15 minutes. (50 μ L of triethylamine were added to the reaction mixture, and the reaction stirred at room temperature under a hydrogen atmosphere for 24 h. The catalyst was filtered off by passing the reaction mixture through celite, eluting with EtOAc. The solvent was removed under reduced pressure to obtain the benzhydryl pyrrolidine analog. For analogs 2.6a, 2.6b and 2.6g, the material was used without further purification. Analogs 2.6c, 2.6d, 2.6e and 2.6f, were further purified by reversed-phase preparative HPLC to isolated separable diastereomers.

Benzhydryl pyrrolidine analog 2.6a. The synthesis was performed in accordance with the general method using **2.5a** (50 mg, 170 μ mol) and Pd/C (10%) (25 mg) in methanol (1.5 mL) and ethyl acetate (0.5 mL) to form **2.6a** (33 mg, 131 μ mol, 77%), which was directly used without purification. LC-MS (ESI): calc. for $C_{18}H_{21}N$ $[M+H]^+$: 252.17, observed 252.17, LC, R_t = 4.94 min; 1H NMR (400 MHz, $CDCl_3$): δ (ppm) 7.42 – 7.28 (m, 7H), 7.25 – 7.21 (m, 1H), 7.12 (d, J = 7.5 Hz, 1H), 4.54 (dd, J = 10.5, 5.5 Hz, 1H), 3.78 – 3.68 (m, 1H), 3.29 – 3.20 (m, 1H), 2.34 (s, 3H), 2.04 – 1.62 (m, 3H), 1.18 – 1.06 (m, 1H); ^{13}C NMR (100 MHz, $CDCl_3$): δ 160.48, 143.24, 140.43, 138.34, 129.07, 128.39, 128.28, 128.28, 127.63, 126.58, 125.45, 125.44, 122.90, 85.91, 69.24, 46.02, 28.98, 24.93, 21.59.

Benzhydryl pyrrolidine analog 2.6b. The synthesis was performed in accordance with the general method using **2.5b** (45 mg, 153 μ mol) and Pd/C (10%) (25 mg) in methanol (1.5 mL) and ethyl acetate (0.5 mL) to form **2.6b** (22 mg, 88 μ mol, 59%), which was directly used without purification. LC-MS (ESI): calc. for $C_{18}H_{21}N$ $[M+H]^+$: 252.17, observed 252.25, LC, R_t =

4.52; ¹H NMR (400 MHz, CDCl₃): δ (ppm) 7.36 (d, *J* = 7.2 Hz, 1H), 7.30 – 7.24 (m, 2H), 7.19 – 7.06 (m, 5H), 6.97 (d, *J* = 7.1 Hz, 1H), 3.95 – 3.83 (m, 1H), 3.77 (d, *J* = 10.2 Hz, 1H), 3.04 – 2.80 (m, 2H), 2.30 (s, 3H), 1.86 – 1.70 (m, 3H), 1.50 – 1.38 (m, 1H); ¹³C NMR (100 MHz, CDCl₃): δ 143.40, 143.24, 138.03, 128.86, 128.66, 128.66, 128.36, 128.07, 128.07, 127.19, 126.47, 124.95, 62.18, 57.88, 45.92, 30.57, 24.57, 21.51.

Benzhydryl pyrrolidine analog 2.6c. The synthesis was performed in accordance with the general method using **2.5c** (56 mg, 158 μmol) and Pd/C (10%) (35 mg) in methanol (1.9 mL) and ethyl acetate (0.6 mL) to form **2.6c**, which was purified further by preparative HPLC (gradient of 15-40% ACN in 12 min.), to obtain the two different diastereomers **2.6c-I** (2 mg, 7 μmol, 4%) and **2.6c-II** (22 mg, 71 μmol, 44%) as pure compounds. **2.6c-I**: LC-MS (ESI): calc. for C₂₀H₂₅NO₂ [M+H]⁺: 312.19, observed 312.25, LC, R_t = 4.44 min; ¹H NMR (400 MHz, CDCl₃): δ (ppm) 7.41 (d, *J* = 7.6 Hz, 2H), 7.30 (t, *J* = 7.6 Hz, 2H), 7.23 – 7.14 (m, 2H), 7.04 (d, *J* = 7.6 Hz, 1H), 6.93 – 6.79 (m, 2H), 4.84 (d, *J* = 8.3 Hz, 1H), 4.58 – 4.49 (m, 1H), 4.17 – 4.06 (m, 2H), 3.89 – 3.72 (m, 2H), 3.53 (s, 3H), 3.05 – 2.95 (m, 1H), 2.88 – 2.73 (m, 1H), 2.10 – 1.99 (m, 1H), 1.94 – 1.81 (m, 1H), 1.79 – 1.65 (m, 2H); ¹³C NMR (100 MHz, CDCl₃): δ 155.47, 140.05, 130.00, 129.99, 129.29, 129.27, 128.74, 128.70, 128.41, 127.01, 121.42, 111.73, 70.57, 67.52, 61.60, 59.44, 47.41, 45.34, 29.50, 24.08. **2.6c-II**: LC-MS (ESI): calc. for C₂₀H₂₅NO₂ [M+H]⁺: 312.19, observed 312.33, LC, R_t = 4.55 min; ¹H NMR (400 MHz, CDCl₃): δ (ppm) 7.37 – 7.27 (m, 5H), 7.23 – 7.16 (m, 2H), 6.95 (t, *J* = 7.6 Hz, 1H), 6.84 (d, *J* = 8.4 Hz, 1H), 4.56 – 4.44 (m, 2H), 4.14 (t, *J* = 4.7 Hz, 2H), 3.81 – 3.61 (m, 2H), 3.44 (s, 3H), 3.15 (m, 1H), 2.98 (m, 1H), 2.02 (m, 1H), 1.96 – 1.87 (m, 2H), 1.67 (m, 1H); ¹³C NMR (100 MHz, CDCl₃): δ 167.99, 155.41, 140.72, 129.94, 128.65, 128.60, 128.59, 128.28, 128.28, 126.92, 121.76, 111.95, 70.64, 66.81, 61.60, 59.06, 48.83, 45.35, 30.88, 24.06.

Benzhydryl pyrrolidine analog 2.6d. The synthesis was performed in accordance with the general method using **2.5d** (110 mg, 311 μmol) and Pd/C (10%) (50 mg) in methanol (2.6 mL) and ethyl acetate (0.9 mL) to form **2.6d**, which was purified further by preparative HPLC (gradient of 15-40% ACN in 12 min.), to obtain two different diastereomers **2.6d-I** (53 mg, 170 μmol, 55%) and **2.6d-II** (16 mg, 51 μmol, 16%) as pure compounds. **2.6d-I**: LC-MS (ESI): calc.

for $C_{20}H_{25}NO_2$ $[M+H]^+$: 312.19, observed 312.25, LC, $R_t = 4.14$ min; 1H NMR (400 MHz, $CDCl_3$): δ (ppm) 7.40 (d, $J = 7.7$ Hz, 2H), 7.33 – 7.26 (m, 2H), 7.22 – 7.11 (m, 2H), 6.87 – 6.79 (m, 2H), 6.74 (d, $J = 8.4$ Hz, 1H), 4.17 – 4.10 (m, 2H), 4.05 (t, $J = 4.4$ Hz, 2H), 3.72 (t, $J = 5.2$, 2H), 3.44 (s, 3H), 2.75 – 2.66 (m, 2H), 1.92 – 1.83 (m, 2H), 1.81 – 1.71 (m, 1H), 1.68 – 1.57 (m, 1H); ^{13}C NMR (100 MHz, $CDCl_3$): δ 159.01, 143.13, 140.43, 129.85, 128.90, 128.90, 128.11, 128.10, 127.15, 120.16, 114.34, 112.67, 70.98, 67.15, 62.11, 59.25, 54.75, 44.89, 30.76, 23.82. **2.6d-II**: LC-MS (ESI): calc. for $C_{20}H_{25}NO_2$ $[M+H]^+$: 312.19, observed 312.25, LC, $R_t = 4.40$ min; 1H NMR (400 MHz, $CDCl_3$): δ (ppm) 7.26 – 7.16 (m, 6H), 7.11 – 7.00 (m, 2H), 6.76 (d, $J = 8.1$ Hz, 1H), 4.24 – 4.10 (m, 4H), 3.72 (t, $J = 4.4$ Hz, 2H), 3.42 (s, 3H), 2.91 (t, $J = 7.1$ Hz, 2H), 2.00 – 1.77 (m, 3H), 1.73 – 1.60 (m, 1H); ^{13}C NMR (100 MHz, $CDCl_3$): δ 159.04, 130.18, 128.91, 128.91, 127.60, 127.60, 127.22, 120.56, 114.26, 113.91, 71.08, 67.20, 62.81, 59.19, 54.80, 45.37, 30.67, 23.71.

Benzhydryl pyrrolidine analog 2.6e. The synthesis was performed in accordance with the general method using **2.5e** (40 mg, 129 μ mol) and Pd/C (10%) (30 mg) in methanol (1.0 mL) and ethyl acetate (0.6 mL) to form **2.6e**, which was purified further by preparative HPLC (19% ACN in 15 min.), to obtain the two different diastereomers **2.6e-I** (6 mg, 22 μ mol, 17%) and **2.6e-II** (10 mg, 37 μ mol, 28%) as pure compounds. **2.6e-I**: LC-MS (ESI): calc. for $C_{18}H_{21}NO$ $[M+H]^+$: 268.16, observed 268.25, LC, $R_t = 3.67$ min; 1H NMR (400 MHz, $CDCl_3$): δ (ppm) 7.38 – 7.32 (m, 2H), 7.24 – 7.07 (m, 5H), 6.92 – 6.77 (m, 2H), 4.61 (d, $J = 11.3$ Hz, 1H), 4.53 – 4.38 (m, 1H), 3.81 (s, 3H), 2.88 – 2.73 (m, 2H), 1.99 – 1.81 (m, 3H), 1.75 – 1.62 (m, 1H); ^{13}C NMR (100 MHz, $CDCl_3$): δ 156.50, 139.97, 129.44, 128.66, 128.65, 128.41, 128.30, 128.24, 128.23, 127.00, 120.99, 111.15, 62.11, 55.45, 47.48, 45.49, 29.95, 23.70. **2.6e-II**: LC-MS (ESI): calc. for $C_{18}H_{21}NO$ $[M+H]^+$: 268.16, observed 268.25, LC, $R_t = 3.70$ min; 1H NMR (400 MHz, $CDCl_3$): δ (ppm) 7.35 (dd, $J = 7.6, 1.6$ Hz, 1H), 7.26 – 7.20 (m, 4H), 7.20 – 7.11 (m, 2H), 6.88 (td, $J = 7.5, 1.1$ Hz, 1H), 6.77 (dd, $J = 8.3, 1.1$ Hz, 1H), 4.47 (d, $J = 11.7$ Hz, 1H), 4.45 – 4.35 (m, 1H), 3.74 (s, 3H), 2.88 – 2.68 (m, 2H), 2.01 – 1.83 (m, 4H); ^{13}C NMR (100 MHz, $CDCl_3$) δ 157.06, 140.61, 128.61, 128.61, 128.44, 128.13, 128.12, 128.11, 127.95, 127.01, 120.83, 110.87, 61.72, 55.28, 48.28, 45.37, 30.83, 23.80.

Benzhydryl pyrrolidine analog 2.6f. The synthesis was performed in accordance with the general method using **2.5f** (30 mg, 97 μmol) and Pd/C (10%) (25 mg) in methanol (1.0 mL) and ethyl acetate (1.0 mL) to form **2.6f**, which was purified further by preparative HPLC (20% ACN in 15 min.), to obtain the two different diastereomers **2.6f-I** (7 mg, 26 μmol , 26%) and **2.6f-II** (2 mg, 7 μmol , 7%) as pure compounds. **2.6f-I**: LC-MS (ESI): calc. for $\text{C}_{18}\text{H}_{21}\text{NO}$ $[\text{M}+\text{H}]^+$: 268.16, observed 268.25, LC, $R_t = 3.55$ min. ^1H NMR (400 MHz, CDCl_3): δ (ppm) 7.39 (d, $J = 7.6$ Hz, 2H), 7.31 – 7.27 (m, 2H), 7.21 – 7.13 (m, 2H), 6.84 (d, $J = 8.0$ Hz, 1H), 6.79 (t, $J = 2.0$ Hz, 1H), 6.72 (dd, $J = 8.0, 2.0$ Hz, 1H), 4.17 – 4.04 (m, 2H), 3.75 (s, 3H), 2.78 – 2.69 (m, 2H), 1.93 – 1.82 (m, 2H), 1.81 – 1.73 (m, 1H), 1.67 – 1.56 (m, 1H); ^{13}C NMR (100 MHz, CDCl_3): δ 159.79, 143.41, 140.91, 129.83, 128.87, 128.86, 128.09, 128.08, 127.09, 119.95, 113.75, 112.07, 62.09, 55.18, 55.17, 44.96, 30.69, 23.92. **2.6f-II**: LC-MS (ESI): calc. for $\text{C}_{18}\text{H}_{21}\text{NO}$ $[\text{M}+\text{H}]^+$: 268.16, observed 268.25, LC, $R_t = 3.63$ min; ^1H NMR (400 MHz, CDCl_3): δ (ppm) 7.40 – 7.27 (m, 2H), 7.26 – 7.16 (m, 5H), 7.06 (d, $J = 7.7$ Hz, 1H), 7.02 (t, $J = 2.1$ Hz, 1H), 6.72 (dd, $J = 8.3, 2.4$ Hz, 1H), 4.24 – 4.10 (m, 2H), 3.82 (s, 3H), 2.86 (t, $J = 7.2$ Hz, 2H), 1.98 – 1.74 (m, 3H), 1.72 – 1.60 (m, 1H); ^{13}C NMR (100 MHz, CDCl_3): δ 159.86, 141.86, 141.27, 130.08, 128.96, 128.94, 127.61, 127.60, 127.22, 120.37, 113.62, 113.36, 99.99, 62.66, 55.33, 54.88, 45.36, 30.82, 23.74.

Benzhydryl pyrrolidine analog 2.6g. The synthesis was performed in accordance with the general method using **2.5g** (95 mg, 282 μmol) and Pd/C (10%) (50 mg) in ethyl acetate (3.0 mL) to form **2.6g** (67 mg, 227 μmol , 81%), which was used directly without further purification. LC-MS (ESI): calc. for $\text{C}_{20}\text{H}_{25}\text{NO}$ $[\text{M}+\text{H}]^+$: 296.19, observed 296.25, LC, $R_t = 4.16$ min; ^1H NMR (400 MHz, CDCl_3): δ (ppm) 7.40 – 7.26 (m, 4H), 7.22 – 7.12 (m, 2H), 6.90 – 6.80 (m, 2H), 6.72 – 6.65 (m, 1H), 4.56 – 4.44 (m, 1H), 3.90 – 3.78 (m, 1H), 3.72 (dd, $J = 10.3, 2.4$ Hz, 1H), 3.07 – 2.82 (m, 2H), 1.87 – 1.70 (m, 3H), 1.49 – 1.39 (m, 1H), 1.31 (dd, $J = 6.1, 1.6$ Hz, 6H); ^{13}C NMR (100 MHz, CDCl_3): δ 157.85, 145.01, 143.43, 129.35, 128.65, 128.65, 128.04, 128.03, 126.47, 120.28, 116.19, 112.98, 69.66, 62.15, 58.22, 45.98, 30.48, 24.61, 22.08, 22.04.

General procedure for the synthesis of partially protected Tau peptides 3.1a-f

The partially protected Tau peptides **3.1a-f** were prepared in accordance with a previous published synthesis of **3.1a**.¹² In each case, the peptides were synthesized on a 50 μ mol scale by automated peptide synthesis (Intavis MultiPep RSi) using a Fmoc SPPS strategy performed on a 2-chlorotrityl resin (Iris Biotech GmbH & AGTC Bioproducts) preloaded with the corresponding C-terminal amino acid. The Fmoc-protected amino acid building blocks (4.2 eq., 0.5 M, Novabiochem®) were dissolved in *N*-methyl-2-pyrrolidone (NMP) and coupled sequentially to the resin using *N,N*-diisopropylethylamine (DIPEA, 8 eq., prepared as 1.6 M stock solution in NMP, Biosolve) and (2-(1H-benzotriazol-1-yl)-1,1,3,3-tetramethyluronium hexafluorophosphate (HBTU, 4 eq., 0.4 M stock solution in NMP, Biosolve). Each amino acid coupling was repeated once to ensure complete conversion. Fmoc-deprotection was performed using 20% piperidine in NMP (twice per cycle). The peptide N-terminus was *N*-acetylated prior to resin cleavage using Ac₂O/pyridine/NMP (1:1:3). Resin cleavage of the partially protected peptide was performed using 30% hexafluoroisopropanol (HFIP, Sigma-Aldrich) in CH₂Cl₂ (1 mL per 100 mg resin, 1 x 20 min., 1 x 10 min.) and the organic solvents removed to dryness by rotary evaporation. The isolated material was then re-dissolved in acetonitrile/water/0.1% trifluoroacetic acid (TFA) and lyophilized to obtain a white powder. The yields of the crude partially protected peptides were typically >90% yield. The partially protected peptides were characterized by Analytical Liquid Chromatography coupled with Mass Spectrometry (LC-MS), either via,

Method A: using a C4 Jupiter SuC4300A 150 x 2.0 mm column using H₂O with 0.1% Formic Acid (F.A.) and Acetonitrile with 0.1% F.A. with a gradient of 5% to 100% Acetonitrile in H₂O in 15 min (connected to a Thermo Fischer LCQ Fleet Ion Trap Mass Spectrometer, or

Method B: using a C18 Atlantis T3 5 μ m 150 x 1mm column using H₂O with 0.1% Trifluoroacetic Acid (T.F.A.) and Acetonitrile with 0.1% T.F.A. with a gradient of 5% to 100% Acetonitrile in H₂O in 15 min (connected to a Thermo Finnigan LCQ Deca XP MAX Mass Spectrometer) (see supporting information for LC-MS spectra).

General procedure for the synthesis of modified Tau peptides **3.2b-f** and **4.2a-g**

The modified Tau inhibitors **3.2b-f** and **4.2a-g** were prepared in accordance with a previously published synthesis of **3.2a**.¹² A 25 mL round-bottomed flask fitted with a magnetic stirring bar was charged with the partially protected Tau peptide (**3.1b-f**, 1.1 eq.). The peptide was dissolved in *N,N*-dimethylformamide (DMF, 0.06 M) and treated with 6-chloro-benzotriazole-1-yl-oxy-tris-Pyrrolidino-Phosphonium Hexafluorophosphate (PyClock) (Novabiochem[®], 1.5 eq). The reaction mixture was stirred for 15 minutes, which was followed by the sequential addition of *N,N*-diisopropylethylamine (DIPEA, 5 eq) and 1 eq. of either (*S*)-2-(diphenylmethyl)pyrrolidine, for the synthesis of modified tau peptides **3.2a-f**, or benzhydryl pyrrolidine analogs **2.6a-g**, for the synthesis of modified tau peptides **4.2a-g**. The reaction was left to stir, conversion monitored by LC-MS, and then worked up after 24 h by evaporating the organic solvent under reduced pressure to obtain the crude material. Deprotection of the side-chain protecting groups was performed by stirring the crude material for 3 h in a 95/2.5/2.5 (v/v) mixture of TFA/H₂O/triisopropylsilane (TIS) (0.016 M). The peptide was then precipitated into 40 mL ice-cold diethyl ether (Et₂O), stored at -30 °C for 10 min., centrifuged at 2500 rpm for 10 min. and the supernatant decanted. Fresh ice-cold Et₂O (40 mL) was added to pellet, and the subsequent step repeated. The crude pellet was dissolved in H₂O/ACN + 0.1% TFA and then purified by reversed-phase HPLC using a C18 column (Atlantis T3 prep OBD, 19 x 150 mm) using the optimized gradient conditions described below beside each modified peptide. After purification the aqueous organic solvent mixture was removed by lyophilization to obtain the modified Tau inhibitors **3.2 a-f** and **4.2a-g**, typically as white amorphous powders. Afterwards, the modified tau peptides were characterized by Analytical Liquid Chromatography coupled with Mass Spectrometry (LC-MS) using a C18 Atlantis T3 5µm 150 x 1mm column using H₂O with 0.1% Trifluoroacetic Acid (TFA) and Acetonitrile with 0.1% TFA with a gradient of 5% to 100% Acetonitrile in H₂O in 15 min (connected to a Thermo Finnigan LCQ Deca XP MAX Mass Spectrometer) (see supporting information for LC-MS spectra). In the case of Tau inhibitors **4.2c-f**, two diastereomers (**I** and **II**) were separated, which were studied separately in the subsequent biochemical and X-ray crystallography studies.

Modified Tau peptide 3.2a. The synthesis was performed in accordance with the general method using (*S*)-2-(diphenylmethyl)pyrrolidine (9 mg, 37 μ mol) and purification performed by preparative reversed-phase HPLC using a linear gradient of 40-45% MeCN to form **3.2a** (3 mg, 3 μ mol, 8%). LC-MS (ESI): calc. for $C_{52}H_{78}N_{11}O_{14}P_1$ $[M+H]^+$: 1112.55, observed 1112.6, LC, R_t = 7.62 min.

Modified Tau peptide 3.2b. The synthesis was performed in accordance with the general method using (*S*)-2-(diphenylmethyl)pyrrolidine (10 mg, 42 μ mol) and purification performed by preparative reversed-phase HPLC using a linear gradient of 40-45% MeCN to form **3.2b** (11 mg, 10 μ mol, 24%). LC-MS (ESI): calc. for $C_{50}H_{74}N_{11}O_{13}P_1$ $[M+H]^+$: 1068.52, observed 1068.5, LC, R_t = 7.87 min.

Modified Tau peptide 3.2c. The synthesis was performed in accordance with the general method using (*S*)-2-(diphenylmethyl)pyrrolidine (10 mg, 42 μ mol) and purification performed by preparative reversed-phase HPLC using a linear gradient of 40-45% MeCN to form **3.2c** (16 mg, 15 μ mol, 36%). LC-MS (ESI): calc. for $C_{51}H_{76}N_{11}O_{13}P_1$ $[M+H]^+$: 1082.54, observed 1082.6, LC, R_t = 8.00 min.

Modified Tau peptide 3.2d. The synthesis was performed in accordance with the general method using (*S*)-2-(diphenylmethyl)pyrrolidine (10 mg, 42 μ mol) and purification performed by preparative reversed-phase HPLC using a linear gradient of 40-45% MeCN to form **3.2d** (13 mg, 12 μ mol, 29%). LC-MS (ESI): calc. for $C_{51}H_{76}N_{11}O_{13}P_1$ $[M+H]^+$: 1082.54, observed 1082.6, LC, R_t = 8.02 min.

Modified Tau peptide 3.2e. The synthesis was performed in accordance with the general method using (*S*)-2-(diphenylmethyl)pyrrolidine (8 mg, 34 μ mol) and purification performed by preparative reversed-phase HPLC using a linear gradient of 40-45% MeCN to form **3.2e** (10 mg, 9 μ mol, 26%). LC-MS (ESI): calc. for $C_{53}H_{80}N_{11}O_{13}P_1$ $[M+H]^+$: 1110.57, observed 1110.7, LC, R_t = 8.82 min.

Modified Tau peptide 3.2f. The synthesis was performed in accordance with the general method using (*S*)-2-(diphenylmethyl)pyrrolidine (8 mg, 34 μmol), and purification performed by preparative reversed-phase HPLC using a linear gradient of 40-45% MeCN to form **3.2f** (4 mg, 4 μmol , 12%). LC-MS (ESI): calc. for $\text{C}_{53}\text{H}_{80}\text{N}_{11}\text{O}_{13}\text{P}_1$ $[\text{M}+\text{H}]^+$: 1110.57, observed 1110.7, LC, $R_t = 8.83$ min.

Modified Tau peptide 4.2a. The synthesis was performed in accordance with the general method using benzhydryl pyrrolidine analog **2.6a** (7 mg, 28 μmol), and purification performed by preparative reversed-phase HPLC using a linear gradient of 38-43% MeCN to form **4.2a** as an inseparable mixture of diastereomers (9 mg, 8 μmol , 29%). LC-MS (ESI): calc. for $\text{C}_{51}\text{H}_{76}\text{N}_{11}\text{O}_{13}\text{P}_1$ $[\text{M}+\text{H}]^+$: 1082.54, observed 1082.6, LC, $R_t = 8.38$ min.

Modified Tau peptide 4.2b. The synthesis was performed in accordance with the general method using benzhydryl pyrrolidine analog **2.6b** (8 mg, 32 μmol), and purification performed by preparative reversed-phase HPLC using a linear gradient of 37-42% MeCN to form **4.2b** as an inseparable mixture of diastereomers (5 mg, 5 μmol , 16%). LC-MS (ESI): calc. for $\text{C}_{51}\text{H}_{76}\text{N}_{11}\text{O}_{13}\text{P}_1$ $[\text{M}+\text{H}]^+$: 1082.54, observed 1082.6, LC, $R_t = 8.42$ min.

Isomeric modified Tau peptide 4.2c-I. The synthesis was performed in accordance with the general method using isomeric benzhydryl pyrrolidine analog **2.6c-I** (2 mg, 6 μmol), and purification performed by preparative reversed-phase HPLC using a linear gradient of 37-42% MeCN to form **4.2c-I** (1 mg, 1 μmol , 17%). LC-MS (ESI): calc. for $\text{C}_{53}\text{H}_{80}\text{N}_{11}\text{O}_{15}\text{P}_1$ $[\text{M}+\text{H}]^+$: 1142.56, observed 1142.7, LC, $R_t = 8.05$ min.

Isomeric modified Tau peptides 4.2c-II. The synthesis was performed in accordance with the general method using isomeric benzhydryl pyrrolidine analog **2.6c-II** (9 mg, 29 μmol), and purification performed by preparative reversed-phase HPLC using a linear gradient of 37-42% MeCN to form **4.2c-II** (7 mg, 6 μmol , 21%). LC-MS (ESI): calc. for $\text{C}_{53}\text{H}_{80}\text{N}_{11}\text{O}_{15}\text{P}_1$ $[\text{M}+\text{H}]^+$: 1142.56, observed 1142.6, LC, $R_t = 8.35$ min.

Isomeric modified Tau peptide 4.2d-I. The synthesis was performed in accordance with the general method using isomeric benzhydryl pyrrolidine analog **2.6d-I** (12 mg, 39 μmol), and purification performed by preparative reversed-phase HPLC using a linear gradient of 37-42% MeCN to form **4.2d-I** (1 mg, 1 μmol , 3%). LC-MS (ESI): calc. for $\text{C}_{53}\text{H}_{80}\text{N}_{11}\text{O}_{15}\text{P}_1$ $[\text{M}+\text{H}]^+$: 1142.56, observed 1142.8, LC, $R_t = 8.07$ min.

Isomeric modified Tau peptides 4.2d-II. The synthesis was performed in accordance with the general method using isomeric benzhydryl pyrrolidine analog **2.6d-II** (4 mg, 13 μmol), and purification performed by preparative reversed-phase HPLC using a linear gradient of 35-40% MeCN to form **4.2d-II** (4 mg, 4 μmol , 31%). LC-MS (ESI): calc. for $\text{C}_{53}\text{H}_{80}\text{N}_{11}\text{O}_{15}\text{P}_1$ $[\text{M}+\text{H}]^+$: 1142.56, observed 1142.7, LC, $R_t = 8.23$ min.

Isomeric modified Tau peptide 4.2e-I. The synthesis was performed in accordance with the general method using isomeric benzhydryl pyrrolidine analog **2.6e-I** (4 mg, 15 μmol), and purification performed by preparative reversed-phase HPLC using a linear gradient of 37-42% MeCN to form **4.2e-I** (4 mg, 4 μmol , 27%). LC-MS (ESI): calc. for $\text{C}_{51}\text{H}_{76}\text{N}_{11}\text{O}_{14}\text{P}_1$ $[\text{M}+\text{H}]^+$: 1098.53, observed 1098.9, LC, $R_t = 7.60$ min.

Isomeric modified Tau peptides 4.2e-II. The synthesis was performed in accordance with the general method using isomeric benzhydryl pyrrolidine analog **2.6e-II** (7 mg, 26 μmol), and purification performed by preparative reversed-phase HPLC using a linear gradient of 35-40% MeCN to form **4.2e-II** (6 mg, 5 μmol , 19%). LC-MS (ESI): calc. for $\text{C}_{51}\text{H}_{76}\text{N}_{11}\text{O}_{14}\text{P}_1$ $[\text{M}+\text{H}]^+$: 1098.53, observed 1098.7, LC, $R_t = 8.32$ min.

Isomeric modified Tau peptide 4.2f-I. The synthesis was performed in accordance with the general method using isomeric benzhydryl pyrrolidine analog **2.6f-I** (6 mg, 22 μmol), and purification performed by preparative reversed-phase HPLC using a linear gradient of 37-42% MeCN to form **4.2f-I** (8 mg, 7 μmol , 32%). LC-MS (ESI): calc. for $\text{C}_{51}\text{H}_{76}\text{N}_{11}\text{O}_{14}\text{P}_1$ $[\text{M}+\text{H}]^+$: 1098.53, observed 1098.7, LC, $R_t = 8.38$ min.

Isomeric modified Tau peptides 4.2f-II. The synthesis was performed in accordance with the general method using isomeric benzhydryl pyrrolidine analog **2.6f-II** (2 mg, 8 μ mol), and purification performed by preparative reversed-phase HPLC using a linear gradient of 35-40% MeCN to form **4.2f-II** (2 mg, 2 μ mol, 25%). LC-MS (ESI): calc. for $C_{51}H_{76}N_{11}O_{14}P_1$ $[M+H]^+$: 1098.53, observed 1098.7, LC, R_t = 8.28 min.

Modified Tau peptide 4.2g. The synthesis was performed in accordance with the general method using benzhydryl pyrrolidine analog **2.6g** (11 mg, 37 μ mol), and purification performed by preparative reversed-phase HPLC using a linear gradient of 40-45% MeCN to form **4.2g** as an inseparable mixture of diastereomers (1 mg, 1 μ mol, 3%). LC-MS (ESI): calc. for $C_{53}H_{80}N_{11}O_{14}P_1$ $[M+H]^+$: 1126.56, observed 1126.7, LC, R_t = 8.68 min.

Biochemical evaluation of modified tau peptides 3.2a-f and 4.2a-g

Fluorescence polarization assays

FP assays were performed using 100 nM FAM-labeled tethered Tau peptide (5,6-FAM)-RTP(ps)LPTG(GGS)₃GSKCG(ps)LGNIHHK in buffer containing 10 mM HEPES (pH 7.4), 10 mM NaCl, 0.1% (v/v) Tween20 and 0.1% (w/v) Bis(trimethylsilyl)acetamide (BSA). First, a dilution series of His-14-3-3 ζ to the labeled peptide was made in order to obtain a K_d value and select an appropriate concentration for the subsequent inhibition experiments. For the determination of IC_{50} values, dilution series of the inhibitor peptides were made to a solution containing 100 nM labeled peptide and 10 μ M His-14-3-3 ζ (EC_{80}). The assays were performed in Corning black, round-bottom, low-volume, 384 microwell plates (ref. 4514). The polarization was measured by use of a filter-based microplate reader (Tecan Infinite F500) using a fluorescein filterset (λ_{ex} : 485 nm/20nm, λ_{em} : 535 nm/25 nm) (10 reads per well). All experiments were performed in triplicate. To obtain K_d and IC_{50} values, the resulting curve was fitted by use of GraphPad Prism 6.0 for Windows (GraphPad Software Inc., CA, USA).

Isothermal titration calorimetry

ITC experiments were performed on a Malvern ITC₂₀₀ Isothermal Titration Calorimeter (Microcal Inc. USA). The peptide and protein were separately dissolved in ITC-buffer containing 25 mM HEPES (pH 7.5), 100 mM NaCl, 10 mM MgCl₂ and 0.5 mM TCEP (Tris(2-carboxyethyl)phosphine). In the sample cell, a solution of 0.1 mM 14-3-3 ζ protein was placed and the syringe was loaded with a solution of 1 mM peptide inhibitor, which was titrated stepwise into the cell with 2 μ L aliquots (with a delay of 180 seconds between each titration). For each measurement, a series of 19 injections was performed using the following settings: reference power: 5 μ Cal/sec., initial delay: 60 sec., stirring speed: 750 rpm, temperature: 37 °C. All measurements were performed in duplicate. The data was analyzed using Origin 7.0 software. A non-linear regression analysis was performed, using a single-site binding model with varying stoichiometry (N), association constant ($K_a = 1/K_d$), and molar binding enthalpy (ΔH), to determine the thermodynamic parameters.

X-ray crystallography studies

Sitting drop crystallization of 14-3-3 σ -peptide complexes

The 14-3-3 σ protein used for crystallization was truncated C-terminally after the Thr-231 residue to enhance crystallization, called 14-3-3 $\sigma\Delta C$. Crystallization was attempted for all Tau inhibitors **3.2a-f** and **4.2a-g** with 14-3-3 $\sigma\Delta C$. The 14-3-3 $\sigma\Delta C$ -peptide complex was dissolved in crystallization buffer (20 mM HEPES (pH 7.5), 2 mM MgCl₂, 2 mM BME) at a 1:1.5 and 1:5 molar ratio with a resulting protein concentration of 12.5 mg/mL and this incubated overnight at 4 °C. A sitting drop crystal screen was set up on a 96-wells plate (Corning pZero 3550). First, 75 μ L of the optimized 14-3-3 $\sigma\Delta C$ screening conditions (5% glycerol, 0.19 M CaCl₂, varying concentration of PEG400 (24%-29% (v/v)), 0.095 M HEPES at varying pH of 7.1, 7.3, 7.5 and 7.7) were pipetted into the reservoirs. Then, by use of a pipetting robot (Mosquito), 500 nL drops were made by pipetting 250 nL of the screening conditions into 250 nL of protein-peptide complex. The plate was covered with an air-tight foil, and incubated at 4 °C. Crystals were harvested after 1-12 weeks and were flash-cooled in liquid nitrogen before measuring.

Data collection and processing

Diffraction data for **3.2a-d** were collected at the Petra(III) synchrotron in Hamburg , and data for **4.2b**, **4.2c-I**, **4.2e-I**, **4.2f-I** and **4.2f-II** were collected on a Rigaku Compact HomeLab beamline (home source). The data was processed using iMosflm⁴⁶ in the ccp4i package or XDS and the structures were phased by molecular replacement (using PDB: 4Y3B) in Phenix Phaser.⁴⁷ Refinement and model building were done with Phenix.refine⁴⁸ and Coot⁴⁹ software packages. Figures were made by PyMol (DeLano Scientific LLC, version 0.99rc6).

NMR spectroscopy studies on full-length hyperphosphorylated Tau protein

¹⁵N labelled Tau Protein Expression and Purification

E.coli BL21 cells were transformed with the pET15b vector carrying the longest Tau isoform (2N4R, 441 amino acid residues). A 20 ml pre-culture in Luria–Bertani (LB) medium containing 100 µg/mL ampicillin was grown overnight at 37 °C and was used to inoculate a 1 L culture in M9 minimal medium supplemented with 4 g/L Glucose, 1 g/L ¹⁵NH₄Cl and 0.4 g/L ¹⁵N rich-medium (Isogro ¹⁵N, Isotec). The culture was grown at 37 °C to an OD₆₀₀ of 0.8 and induced with 0.5 mM IPTG. Incubation was continued for 4 h at 37 °C and the culture was then harvested by centrifugation. Purification of recombinant Tau protein was achieved by first heating the sample at 75°C for 15 min followed by a cation exchange chromatography. The pure fractions were further buffer exchanged with 50 mM ammonium bicarbonate using a desalting column before lyophilization. Protein concentration was estimated by absorption at 280 nm. Detailed protocols can be found in Danis C, et al. *J. Vis. Exp.* 2016 and Qi H, et al., *Methods Mol Biol.* 2017.^{50,51}

PKA catalytic subunit expression and Purification

E.coli BL21 cells were transformed with the pet15b Vector (Addgene plasmid # 14921) carrying the gene coding for the N-terminally His-tagged PKA catalytic subunit alpha from *M. musculus*. A 20 mL pre-culture in Luria–Bertani (LB) medium containing 100 µg/ml ampicillin was grown overnight at 37 °C and was used to inoculate a 1 L culture in LB medium. The culture

was grown at 20 °C to an OD₆₀₀ of 0.8 and induced with 0.5 mM IPTG. Incubation was continued for 20 h at 20 °C and the culture was then harvested by centrifugation. The His-tagged PKA catalytic subunit alpha was purified by affinity chromatography using a Ni-NTA column (GE Healthcare, Uppsala, Sweden) and buffer-exchanged with 250 mM potassium phosphate, 0.1 mM DTT pH 6.5 on a desalting column. The protein was aliquoted, flash frozen in liquid nitrogen and stored at -80 °C.

In vitro Tau Phosphorylation

Recombinant ¹⁵N labelled Tau protein (100 μM) was incubated with 1.5 μM recombinant PKA catalytic subunit (PKA_c) at 30 °C for 3 h, in a buffer consisting of 50 mM Hepes pH 8.0, 5 mM ATP, 12.5 mM MgCl₂, 50 mM NaCl, 5 mM DTT, 1 mM EDTA. The reaction was heat-inactivated at 75 °C for 15 min and the solution was centrifuged in order to eliminate the precipitated PKA_c. Buffer exchange with 50 mM ammonium carbonate on a desalting column was performed before lyophilization.

¹⁵N-¹H HSQC spectroscopy on full-length PKA-phosphorylated Tau (fl-pTau)

¹⁵N-¹H HSQC spectra were acquired in 3mm tubes (sample volume 200 μL) using a 900 MHz Bruker Avance spectrometer, equipped with a cryoprobe. Spectra were recorded at 25 °C in a buffer containing 50 mM Tris pH 6.7, 30 mM NaCl, 2.5 mM EDTA, 1 mM DTT, EDTA-free Protease Inhibitor Cocktail (Roche, Switzerland) and 10% (v/v) D₂O. The experiments were performed with samples containing 60 μM ¹⁵N labelled PKA-phosphorylated Tau, 120 μM 14-3-3ζ and either 360 μM or 1200 μM of modified Tau peptide (3 and 10-fold excess to 14-3-3ζ concentration). The experiments were performed on compounds **3.2e**, **4.2c-I** and **4.2e-I**. The backbone resonance assignments of the Tau protein, including the phosphorylated residues, were previously reported in the literature. The reference for the ¹H chemical shift was relative to Trimethyl silyl propionate. Spectra were collected and processed with Topspin 3.5 (Bruker Biospin, Karlsruhe, Germany) and analyzed with Sparky 3.12 (T. D. Goddard and D. G. Kneller, SPARKY 3, University of California, San Francisco).^{42,45}

¹H NMR spectroscopy on 4.2e-I

¹H spectra containing **4.2e-I** were acquired in 3mm tubes (sample volume 200 μL) using a 600 MHz Bruker Avance I spectrometer equipped with a CPQCI cryoprobe, at 25 °C in a buffer containing 50 mM Tris pH 6.7, 30 mM NaCl, 2.5 mM EDTA and 10% (v/v) D₂O. The experiments were performed with 150 μM **4.2e-I** alone or in the presence of either 10 μM, 30 μM, 75 μM or 150 μM 14-3-3ζ or 150 μM PKA-phosphorylated Tau. The reference for the ¹H chemical shift was relative to Trimethyl silyl propionate. Spectra were collected and processed with Topspin 3.5 (Bruker Biospin, Karlsruhe, Germany).

AUTHOR INFORMATION

Corresponding Author

*l.milroy@tue.nl

Author Contributions

SAA and FAM contributed equally to this work. The manuscript was written through contributions of all authors. FAM performed synthesis and biochemical studies; SAA, JN and CO performed structural characterization and analysis; JFN performed the NMR experiments; IL, LB, CO & LGM designed the studies; All authors have given approval to the final version of the manuscript.

Funding Sources

Funded by the Netherlands Organization for Scientific Research via ECHO grant 717014001, VICI grant 016150366, Gravity Program 024.001.035, by the Initial Training Network TASPPI, funded by the H2020 Marie Curie Actions of the European Commission under Grant Agreement 675179 and by the LabEx (Laboratory of Excellence) DISTALZ (ANR, ANR-11-LABX-009). Parts of this research were carried out at PETRA III at DESY, a member of the Helmholtz Association (HGF). We would like to thank Anja Burkhardt for assistance in using the P11 beamline and François-Xavier Cantrelle for NMR data acquisition. Some other crystallographic experiments were performed on the X06SA beamline at the Swiss Light

Source, Paul Scherrer Institut, Villigen, Switzerland. The NMR facilities were funded by the Nord Region Council, CNRS, Institut Pasteur de Lille, the European Community (ERDF), the French Ministry of Research and the University of Lille and by the CTRL CPER cofunded by the European Union with the European Regional Development Fund (ERDF), by the Hauts de France Regional Council (contrat n°17003781), Métropole Européenne de Lille (contract n°2016_ESR_05), and French State (contract n°2017-R3-CTRL-Phase 1). We acknowledge support for the NMR facilities from TGE RMN THC (CNRS, FR-3050) and FRABio (Univ. Lille, CNRS, FR-3688).

The authors declare no competing financial interest.

ASSOCIATED CONTENT

Supporting Information

Additional information found in the supporting information: synthesis details and characterization data for 1-bromo-2-(2-methoxyethoxy)benzene and 1-bromo-3-(2-methoxyethoxy)benzene; ¹H-NMR, ¹³C-NMR and LC-MS or GC-MS spectra for intermediates **2.2**, **2.3**, **2.4**, pyrrolooxazolones **2.5a-g**, and benzhydryl pyrrolidine derivatives **2.6a-g**; LC-MS data of purified final modified Tau peptides, **3.2a-f** and **4.2a-g**; thermograms of duplicate ITC measurements of **3.2a-f** and **4.2a-g** and a summary of the corresponding thermodynamic parameters in table form; data collection and refinement statistics and an in-depth discussion of all crystal structures reported in the manuscript; supplementary ¹⁵N-¹H HSQC spectra and intensity plots.

Accession Codes

Atomic coordinates and structure factors for the crystal structures of 14-3-3 σ with ligands **3.2d**, **3.2e**, **4.2b**, **4.2c-I**, **4.2e-I**, **4.2f-I** and **4.2f-II** can be accessed using PDB codes 6FI5, 6FI4, 6FBY, 6FAW, 6FAW, 6FAV and 6FBW, respectively. Authors will release the atomic coordinates and experimental data upon article publication.

References

- (1) Cummings, J.; Lee, G.; Mortsdorf, T.; Ritter, A.; Zhong, K. Alzheimer's Disease Drug Development Pipeline: 2017. *Alzheimers Dement. Transl. Res. Clin. Interv.* 2017, 3 (3), 367–384.
- (2) Nelson, P. T.; Alafuzoff, I.; Bigio, E. H.; Bouras, C.; Braak, H.; Cairns, N. J.; Castellani, R. J.; Crain, B. J.; Davies, P.; Del Tredici, K.; et al. Correlation of Alzheimer Disease Neuropathologic Changes with Cognitive Status: A Review of the Literature. *J. Neuropathol. Exp. Neurol.* 2012, 71 (5), 362–381.
- (3) Valeur, E.; Guéret, S. M.; Adihou, H.; Gopalakrishnan, R.; Lemurell, M.; Waldmann, H.; Grossmann, T. N.; Plowright, A. T. New Modalities for Challenging Targets in Drug Discovery. *Angew. Chem. Int. Ed.* 2017, 56 (35), 10294–10323.
- (4) Arkin, M. R.; Wells, J. A. Small-Molecule Inhibitors of Protein–protein Interactions: Progressing towards the Dream. *Nat. Rev. Drug Discov.* 2004, 3 (4), 301–317.
- (5) Wells, J. A.; McClendon, C. L. Reaching for High-Hanging Fruit in Drug Discovery at Protein–protein Interfaces. *Nature* 2007, 450 (7172), 1001–1009.
- (6) Arkin, M. R.; Tang, Y.; Wells, J. A. Small-Molecule Inhibitors of Protein-Protein Interactions: Progressing toward the Reality. *Chem. Biol.* 2014, 21 (9), 1102–1114.
- (7) Milroy, L.-G.; Grossmann, T. N.; Hennig, S.; Brunsveld, L.; Ottmann, C. Modulators of Protein–Protein Interactions. *Chem. Rev.* 2014, 114 (9), 4695–4748.
- (8) Pelay-Gimeno, M.; Glas, A.; Koch, O.; Grossmann, T. N. Structure-Based Design of Inhibitors of Protein-Protein Interactions: Mimicking Peptide Binding Epitopes. *Angew. Chem. Int. Ed Engl.* 2015, 54 (31), 8896–8927.
- (9) Petta, I.; Lievens, S.; Libert, C.; Tavernier, J.; Bosscher, K. D. Modulation of Protein–Protein Interactions for the Development of Novel Therapeutics. *Mol. Ther.* 2016, 24 (4), 707–718.
- (10) Ballatore, C.; Brunden, K. R.; Trojanowski, J. Q.; Lee, V. M.-Y.; Smith, A. B.; Hurn, D. M. Modulation of Protein-Protein Interactions as a Therapeutic Strategy for the Treatment of Neurodegenerative Tauopathies. *Curr. Top. Med. Chem.* 2011, 11 (3), 317–330.

- (11) Joo, Y.; Schumacher, B.; Landrieu, I.; Bartel, M.; Smet-Nocca, C.; Jang, A.; Choi, H. S.; Jeon, N. L.; Chang, K.-A.; Kim, H.-S.; et al. Involvement of 14-3-3 in Tubulin Instability and Impaired Axon Development Is Mediated by Tau. *FASEB J.* 2015, 29 (10), 4133–4144.
- (12) Milroy, L.-G.; Bartel, M.; Henen, M. A.; Leysen, S.; Adriaans, J. M. C.; Brunsveld, L.; Landrieu, I.; Ottmann, C. Stabilizer-Guided Inhibition of Protein-Protein Interactions. *Angew. Chem. Int. Ed Engl.* 2015, 54 (52), 15720–15724.
- (13) Kaplan, A.; Ottmann, C.; Fournier, A. E. 14-3-3 Adaptor Protein-Protein Interactions as Therapeutic Targets for CNS Diseases. *Pharmacol. Res.* 2017, 125 (Pt B), 114–121.
- (14) Fu, H.; Subramanian, R. R.; Masters, S. C. 14-3-3 Proteins: Structure, Function, and Regulation. *Annu. Rev. Pharmacol. Toxicol.* 2000, 40 (1), 617–647.
- (15) Yaffe, M. B. How Do 14-3-3 Proteins Work? – Gatekeeper Phosphorylation and the Molecular Anvil Hypothesis. *FEBS Lett.* 2002, 513 (1), 53–57.
- (16) Aitken, A. 14-3-3 Proteins: A Historic Overview. *Semin. Cancer Biol.* 2006, 16 (3), 162–172.
- (17) Yaffe, M. B.; Rittinger, K.; Volinia, S.; Caron, P. R.; Aitken, A.; Leffers, H.; Gamblin, S. J.; Smerdon, S. J.; Cantley, L. C. The Structural Basis for 14-3-3:Phosphopeptide Binding Specificity. *Cell* 1997, 91 (7), 961–971.
- (18) Aghazadeh, Y.; Papadopoulos, V. The Role of the 14-3-3 Protein Family in Health, Disease, and Drug Development. *Drug Discov. Today* 2016, 21 (2), 278–287.
- (19) Freeman, A. K.; Morrison, D. K. 14-3-3 Proteins: Diverse Functions in Cell Proliferation and Cancer Progression. *Semin. Cell Dev. Biol.* 2011, 22 (7), 681–687.
- (20) Kleppe, R.; Martinez, A.; Døskeland, S. O.; Haavik, J. The 14-3-3 Proteins in Regulation of Cellular Metabolism. *Semin. Cell Dev. Biol.* 2011, 22 (7), 713–719.
- (21) Shimada, T.; Fournier, A. E.; Yamagata, K. Neuroprotective Function of 14-3-3 Proteins in Neurodegeneration <https://www.hindawi.com/journals/bmri/2013/564534/> (accessed Feb 11, 2018).
- (22) De Vries-van Leeuwen, I. J.; da Costa Pereira, D.; Flach, K. D.; Piersma, S. R.; Haase, C.; Bier, D.; Yalcin, Z.; Michalides, R.; Feenstra, K. A.; Jiménez, C. R.; et al. Interaction of 14-3-3 Proteins with the Estrogen Receptor Alpha F Domain Provides a Drug Target Interface. *Proc. Natl. Acad. Sci. U. S. A.* 2013, 110 (22), 8894–8899.

- (23) Anders, C.; Higuchi, Y.; Koschinsky, K.; Bartel, M.; Schumacher, B.; Thiel, P.; Nitta, H.; Preisig-Müller, R.; Schlichthörl, G.; Renigunta, V.; et al. A Semisynthetic Fusicoccane Stabilizes a Protein-Protein Interaction and Enhances the Expression of K⁺ Channels at the Cell Surface. *Chem. Biol.* 2013, 20 (4), 583–593.
- (24) Andrei, S. A.; Sijbesma, E.; Hann, M.; Davis, J.; O’Mahony, G.; Perry, M. W. D.; Karawajczyk, A.; Eickhoff, J.; Brunsveld, L.; Doveston, R. G.; et al. Stabilization of Protein-Protein Interactions in Drug Discovery. *Expert Opin. Drug Discov.* 2017, 12 (9), 925–940.
- (25) Stevers, L. M.; Sijbesma, E.; Botta, M.; MacKintosh, C.; Obsil, T.; Landrieu, I.; Cau, Y.; Wilson, A. J.; Karawajczyk, A.; Eickhoff, J.; et al. Modulators of 14-3-3 Protein-Protein Interactions. *J. Med. Chem.* 2017.
- (26) Cleveland, D. W.; Hwo, S. Y.; Kirschner, M. W. Purification of Tau, a Microtubule-Associated Protein That Induces Assembly of Microtubules from Purified Tubulin. *J. Mol. Biol.* 1977, 116 (2), 207–225.
- (27) Himmler, A.; Drechsel, D.; Kirschner, M. W.; Martin, D. W. Tau Consists of a Set of Proteins with Repeated C-Terminal Microtubule-Binding Domains and Variable N-Terminal Domains. *Mol. Cell. Biol.* 1989, 9 (4), 1381–1388.
- (28) Lindwall, G.; Cole, R. D. Phosphorylation Affects the Ability of Tau Protein to Promote Microtubule Assembly. *J. Biol. Chem.* 1984, 259 (8), 5301–5305.
- (29) Grundke-Iqbal, I.; Iqbal, K.; Tung, Y. C.; Quinlan, M.; Wisniewski, H. M.; Binder, L. I. Abnormal Phosphorylation of the Microtubule-Associated Protein Tau (Tau) in Alzheimer Cytoskeletal Pathology. *Proc. Natl. Acad. Sci. U. S. A.* 1986, 83 (13), 4913–4917.
- (30) Hashiguchi, M.; Sobue, K.; Paudel, H. K. 14-3-3zeta Is an Effector of Tau Protein Phosphorylation. *J. Biol. Chem.* 2000, 275 (33), 25247–25254.
- (31) Yuan, Z.; Agarwal-Mawal, A.; Paudel, H. K. 14-3-3 Binds to and Mediates Phosphorylation of Microtubule-Associated Tau Protein by Ser9-Phosphorylated Glycogen Synthase Kinase 3beta in the Brain. *J. Biol. Chem.* 2004, 279 (25), 26105–26114.
- (32) Li, T.; Paudel, H. K. 14-3-3zeta Facilitates GSK3beta-Catalyzed Tau Phosphorylation in HEK-293 Cells by a Mechanism That Requires Phosphorylation of GSK3beta on Ser9. *Neurosci. Lett.* 2007, 414 (3), 203–208.

- (33) Qureshi, H. Y.; Li, T.; MacDonald, R.; Cho, C. M.; Leclerc, N.; Paudel, H. K. Interaction of 14-3-3 ζ with Microtubule-Associated Protein Tau within Alzheimer's Disease Neurofibrillary Tangles. *Biochemistry (Mosc.)* 2013, 52 (37), 6445–6455.
- (34) Li, T.; Paudel, H. K. 14-3-3 ζ Mediates Tau Aggregation in Human Neuroblastoma M17 Cells. *PloS One* 2016, 11 (8), e0160635.
- (35) Sillen, A.; Barbier, P.; Landrieu, I.; Lefebvre, S.; Wieruszeski, J.-M.; Leroy, A.; Peyrot, V.; Lippens, G. NMR Investigation of the Interaction between the Neuronal Protein Tau and the Microtubules. *Biochemistry (Mosc.)* 2007, 46 (11), 3055–3064.
- (36) Lou, K.; Yao, Y.; Hoye, A. T.; James, M. J.; Cornec, A.-S.; Hyde, E.; Gay, B.; Lee, V. M.-Y.; Trojanowski, J. Q.; Smith, A. B.; et al. Brain-Penetrant, Orally Bioavailable Microtubule-Stabilizing Small Molecules Are Potential Candidate Therapeutics for Alzheimer's Disease and Related Tauopathies. *J. Med. Chem.* 2014, 57 (14), 6116–6127.
- (37) Grüninger, F. Invited Review: Drug Development for Tauopathies. *Neuropathol. Appl. Neurobiol.* 2015, 41 (1), 81–96.
- (38) Dammers, C.; Yolcu, D.; Kukuk, L.; Willbold, D.; Pickhardt, M.; Mandelkow, E.; Horn, A. H. C.; Sticht, H.; Malhis, M. N.; Will, N.; et al. Selection and Characterization of Tau Binding D-Enantiomeric Peptides with Potential for Therapy of Alzheimer Disease. *PloS One* 2016, 11 (12), e0167432.
- (39) Molzan, M.; Schumacher, B.; Ottmann, C.; Baljuls, A.; Polzien, L.; Weyand, M.; Thiel, P.; Rose, R.; Rose, M.; Kuhenne, P.; et al. Impaired Binding of 14-3-3 to C-RAF in Noonan Syndrome Suggests New Approaches in Diseases with Increased Ras Signaling. *Mol. Cell. Biol.* 2010, 30 (19), 4698–4711.
- (40) Bailey, D. J.; O'Hagan, D.; Tavasli, M. A Short Synthesis of (S)-2-(Diphenylmethyl)Pyrrolidine, a Chiral Solvating Agent for NMR Analysis. *Tetrahedron Asymmetry* 1997, 8 (1), 149–153.
- (41) Stevers, L. M.; Lam, C. V.; Leysen, S. F. R.; Meijer, F. A.; van Scheppingen, D. S.; de Vries, R. M. J. M.; Carlile, G. W.; Milroy, L. G.; Thomas, D. Y.; Brunsveld, L.; et al. Characterization and Small-Molecule Stabilization of the Multisite Tandem Binding between 14-3-3 and the R Domain of CFTR. *Proc. Natl. Acad. Sci. U. S. A.* 2016, 113 (9), E1152-1161.

- (42) Landrieu, I.; Lacosse, L.; Leroy, A.; Wieruszeski, J.-M.; Trivelli, X.; Sillen, A.; Sibille, N.; Schwalbe, H.; Saxena, K.; Langer, T.; et al. NMR Analysis of a Tau Phosphorylation Pattern. *J. Am. Chem. Soc.* 2006, 128 (11), 3575–3583.
- (43) Lippens, G.; Wieruszeski, J.-M.; Leroy, A.; Smet, C.; Sillen, A.; Buée, L.; Landrieu, I. Proline-Directed Random-Coil Chemical Shift Values as a Tool for the NMR Assignment of the Tau Phosphorylation Sites. *Chembiochem Eur. J. Chem. Biol.* 2004, 5 (1), 73–78.
- (44) Mukrasch, M. D.; Bibow, S.; Korukottu, J.; Jeganathan, S.; Biernat, J.; Griesinger, C.; Mandelkow, E.; Zweckstetter, M. Structural Polymorphism of 441-Residue Tau at Single Residue Resolution. *PLoS Biol.* 2009, 7 (2), e34.
- (45) Smet, C.; Leroy, A.; Sillen, A.; Wieruszeski, J.-M.; Landrieu, I.; Lippens, G. Accepting Its Random Coil Nature Allows a Partial NMR Assignment of the Neuronal Tau Protein. *ChemBioChem* 2004, 5 (12), 1639–1646.
- (46) Powell, H. R.; Johnson, O.; Leslie, A. G. W. Autoindexing Diffraction Images with IMosflm. *Acta Crystallogr. D Biol. Crystallogr.* 2013, 69 (Pt 7), 1195–1203.
- (47) McCoy, A. J. Solving Structures of Protein Complexes by Molecular Replacement with Phaser. *Acta Crystallogr. D Biol. Crystallogr.* 2007, 63 (1), 32–41.
- (48) Adams, P. D.; Grosse-Kunstleve, R. W.; Hung, L. W.; Ioerger, T. R.; McCoy, A. J.; Moriarty, N. W.; Read, R. J.; Sacchettini, J. C.; Sauter, N. K.; Terwilliger, T. C. PHENIX: Building New Software for Automated Crystallographic Structure Determination. *Acta Crystallogr. D Biol. Crystallogr.* 2002, 58 (Pt 11), 1948–1954.
- (49) Emsley, P.; Lohkamp, B.; Scott, W. G.; Cowtan, K. Features and Development of Coot. *Acta Crystallogr. D Biol. Crystallogr.* 2010, 66 (4), 486–501.
- (50) Danis, C.; Despres, C.; Bessa, L. M.; Malki, I.; Merzougui, H.; Huvent, I.; Qi, H.; Lippens, G.; Cantrelle, F.-X.; Schneider, R.; et al. Nuclear Magnetic Resonance Spectroscopy for the Identification of Multiple Phosphorylations of Intrinsically Disordered Proteins. *J. Vis. Exp. JoVE* 2016, No. 118.
- (51) Qi, H.; Despres, C.; Prabakaran, S.; Cantrelle, F.-X.; Chambraud, B.; Gunawardena, J.; Lippens, G.; Smet-Nocca, C.; Landrieu, I. The Study of Posttranslational Modifications of Tau Protein by Nuclear Magnetic Resonance Spectroscopy: Phosphorylation of Tau Protein by

ERK2 Recombinant Kinase and Rat Brain Extract, and Acetylation by Recombinant Creb-Binding Protein. *Methods Mol. Biol.* Clifton NJ 2017, 1523, 179–213.

Inhibition of 14-3-3/Tau by hybrid small-molecule-peptides operating via two different binding modes.

Sebastian A. Andrei,[†] ζ Femke A. Meijer,[†] ζ João Filipe Neves,[§] Luc Brunsveld,[†] Isabelle Landrieu,^{§} Christian Ottmann,[†] ζ * and Lech-Gustav Milroy^{†*}*

[†] Department of Biomedical Engineering and Institute of Complex Molecular Systems, Laboratory of Chemical Biology, Technische Universiteit Eindhoven, Den Dolech 2, 5612 AZ Eindhoven, The Netherlands

[§] UMR 8576 CNRS-Lille University, 59000 Villeneuve d'Ascq, France

^{ζ} Department of Chemistry, University of Duisburg-Essen, Universitätsstrasse 7, 45117 Essen, Germany

^{ζ} These authors contributed equally to the work.

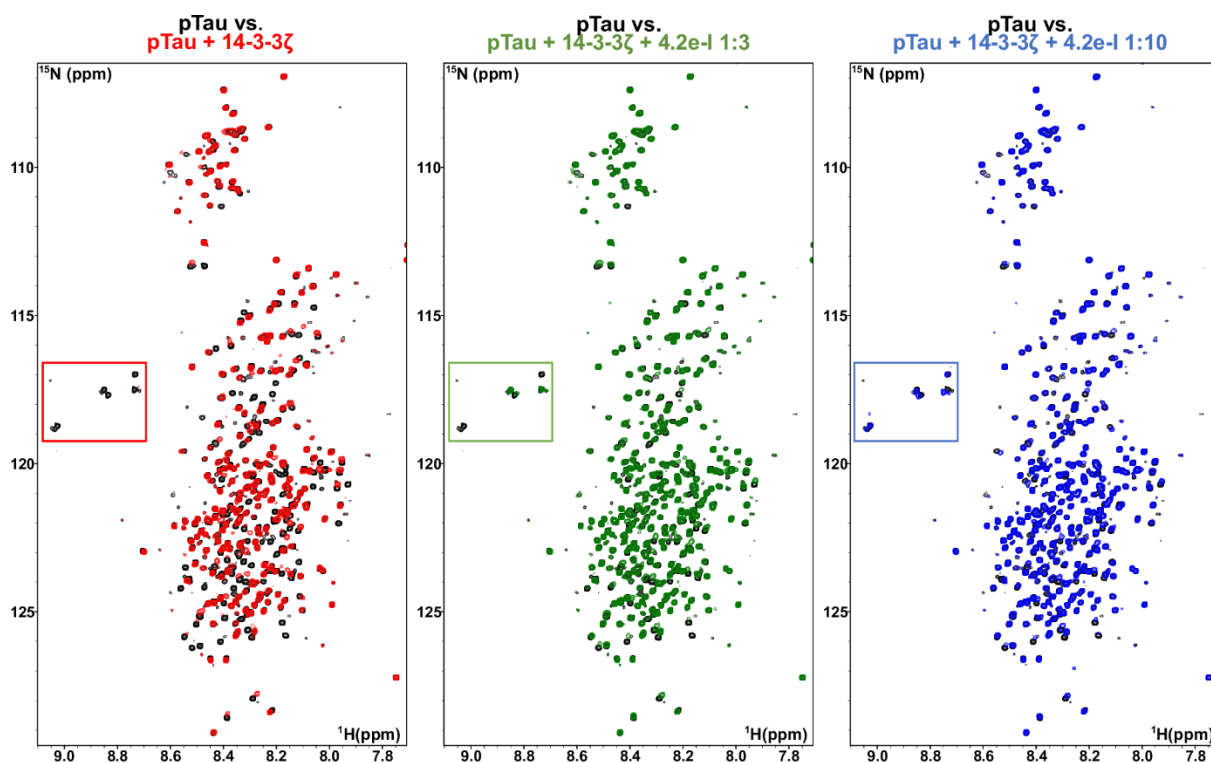


Figure S36 - Superimposed ^{15}N - ^1H HSQC spectra of $60\ \mu\text{M}$ ^{15}N labelled pTau (black spectrum) and $60\ \mu\text{M}$ ^{15}N labelled pTau + 14-3-3 ζ 120 μM (overlaid red spectrum); $60\ \mu\text{M}$ ^{15}N labelled pTau + 14-3-3 ζ 120 μM + 4.2e-I 360 μM (overlaid green spectrum) and $60\ \mu\text{M}$ ^{15}N labelled pTau + 14-3-3 ζ 120 μM + 4.2e-I 1200 μM (overlaid blue spectrum). The boxed regions in the spectra are enlarged in Figure 6 of the manuscript.

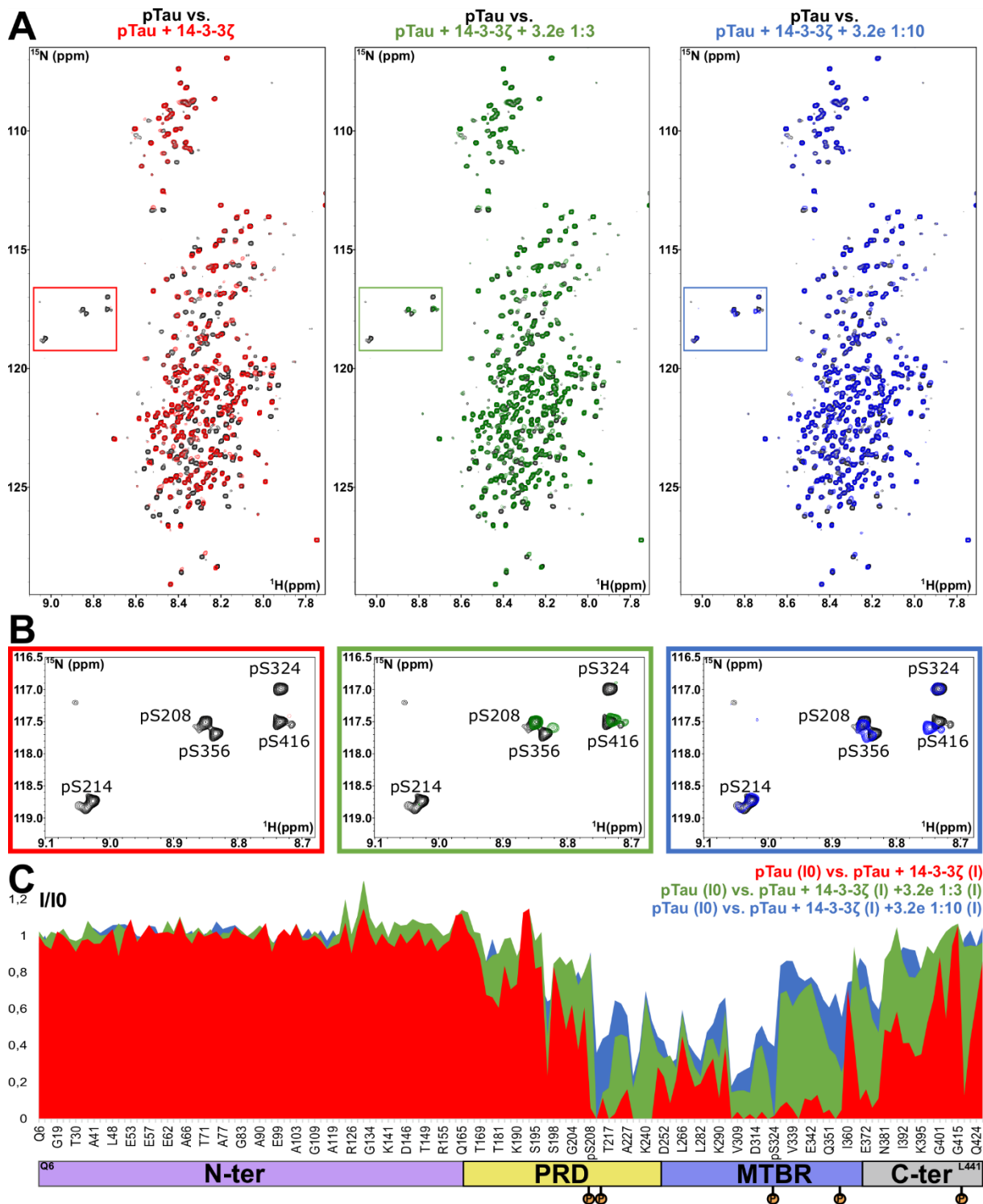


Figure S37 - **3.2e** inhibits the binding of full-length PKA-phosphorylated Tau (pTau) to 14-3-3 ζ in a concentration-dependent manner. A) Superimposed ^{15}N - ^1H HSQC spectra of 60 μM ^{15}N labelled pTau (black spectrum) and 60 μM ^{15}N labelled pTau + 14-3-3 ζ 120 μM (overlaid red spectrum); 60 μM ^{15}N labelled pTau + 14-3-3 ζ 120 μM + **3.2e** 360 μM (overlaid green spectrum) and 60 μM ^{15}N labelled pTau + 14-3-3 ζ 120 μM + **3.2e** 1200 μM (overlaid blue spectrum). The boxed regions are enlarged in B), showing the intensity recovery of the correlation

peaks correspondent to the amide groups of the PKA-phosphorylated Serines after the addition of **3.2e**. C) Plot of the ratios of the bound (I)/free (I0) ^1H - ^{15}N correlation peak intensities of full length pTau 60 μM (y axis) versus the amino acid sequence (x axis) in the presence of 14-3-3 ζ 120 μM (red plot); 14-3-3 ζ 120 μM + **3.2e** 360 μM (green plot) and 14-3-3 ζ 120 μM + **3.2e** 1200 μM (blue plot). A total of 155 correlation peak intensities are shown. The x axis is not proportional. The domains of full-length pTau (N-ter for N-terminal; PRD for Proline-Rich Domain; MTBR for Microtubule Binding Region; C-ter for C-terminal) and the phosphorylation sites (S208, S214, S356, S314 and S416) are identified bellow the x axis.

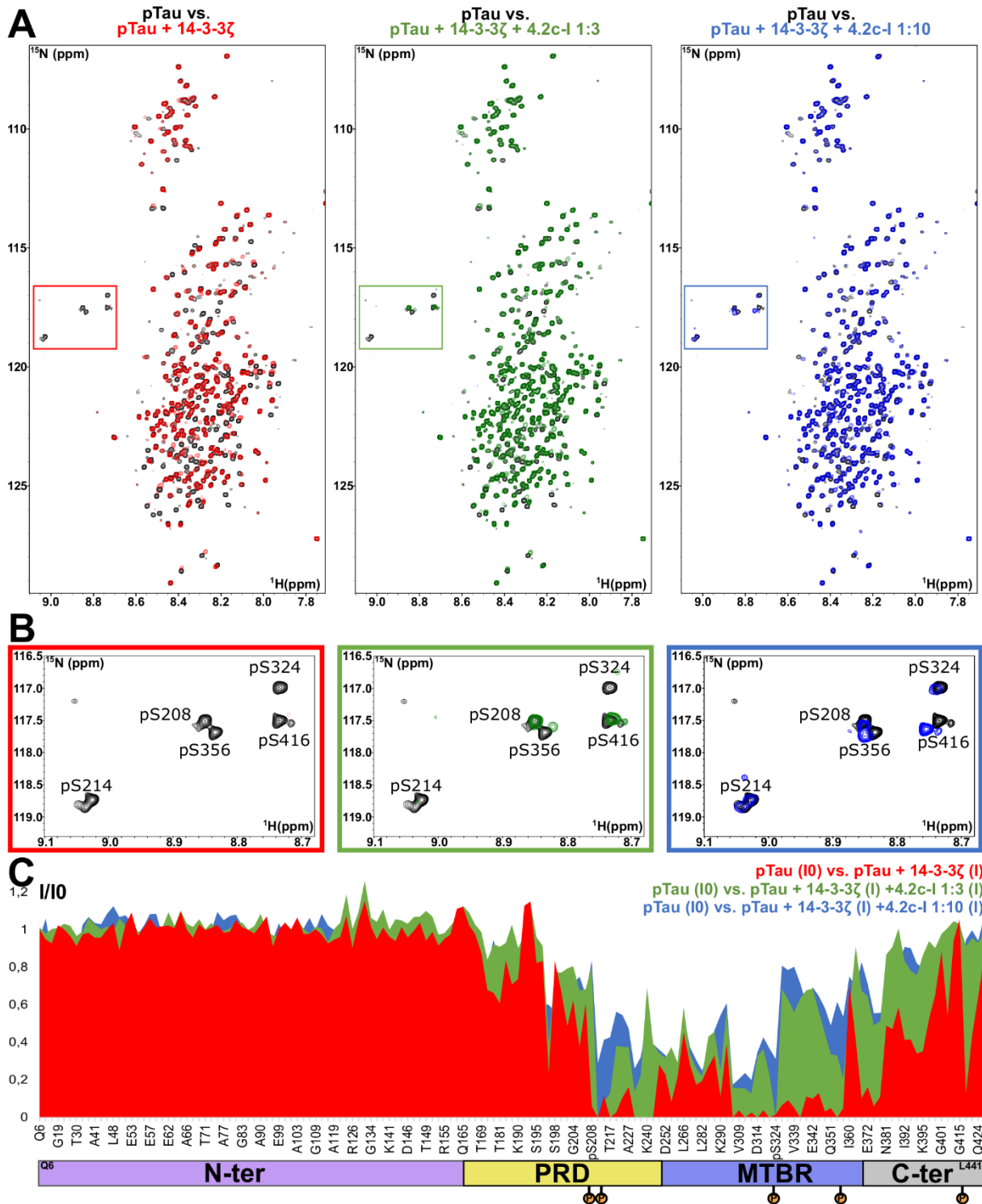


Figure S38 - **4.2c-I** inhibits the binding of full-length PKA-phosphorylated Tau (pTau) to 14-3-3 ζ in a concentration-dependent manner. A) Superimposed ^{15}N - ^1H HSQC spectra of 60 μM ^{15}N labelled pTau (black spectrum) and 60 μM ^{15}N labelled pTau + 14-3-3 ζ 120 μM (overlaid red spectrum); 60 μM ^{15}N labelled pTau + 14-3-3 ζ 120 μM + **4.2c-I** 360 μM (overlaid green spectrum) and 60 μM ^{15}N labelled pTau + 14-3-3 ζ 120 μM + **4.2c-I** 1200 μM (overlaid blue spectrum). The boxed regions are enlarged in B), showing the intensity recovery of the correlation

peaks correspondent to the amide groups of the PKA-phosphorylated Serines after the addition of **4.2c-I**. C) Plot of the ratios of the bound (I)/free (I0) ^1H - ^{15}N correlation peak intensities of full length pTau 60 μM (y axis) versus the amino acid sequence (x axis) in the presence of 14-3-3 ζ 120 μM (red plot); 14-3-3 ζ 120 μM + **4.2c-I** 360 μM (green plot) and 14-3-3 ζ 120 μM + **4.2c-I** 1200 μM (blue plot). A total of 155 correlation peak intensities are shown. The x axis is not proportional. The domains of full-length pTau (N-ter for N-terminal; PRD for Proline-Rich Domain; MTBR for Microtubule Binding Region; C-ter for C-terminal) and the phosphorylation sites (S208, S214, S356, S314 and S416) are identified bellow the x axis.

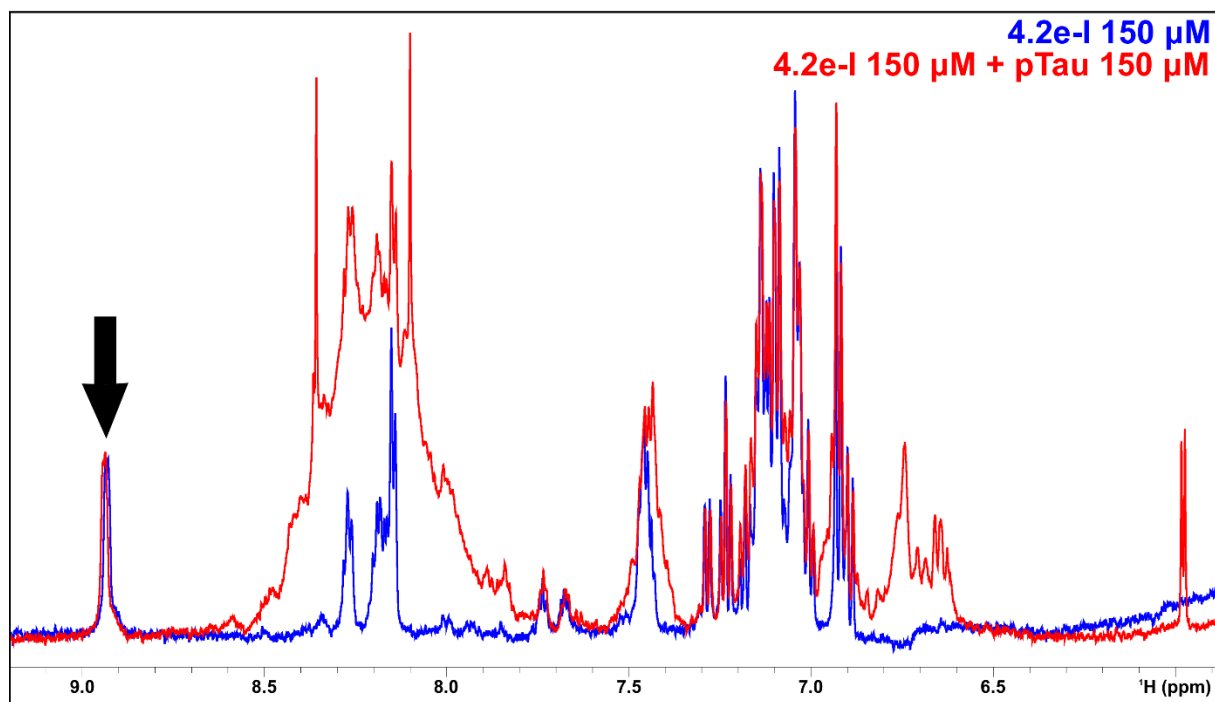


Figure S39 - Section of overlaid ¹H spectra of **4.2e-I** 150 μM alone (blue) and in the presence of pTau 150 μM (red). The black arrow points to a well-isolated resonance from **4.2e-I**, which is not affected in the presence of pTau.

7 Stabilization of the 14-3-3/p65pS45 PPI by Fusicoccin-A

7.1 The 14-3-3 role on the NF- κ B interaction

The Nuclear factor kappa-light-chain-enhancer of activated B cells (NF- κ B) is a protein complex with extreme influence in the control of DNA transcription (Nabel & Verma, 1993). Activation of the NF- κ B complex occurs under conditions of cellular stress and leads to the activation of many genes involved in important processes such as inflammation and immune response. The activity of NF- κ B is inhibited by the NF- κ B Inhibitor, alpha (I κ B α). The human genome encodes for 5 polypeptides (p50, p52, p65, c-Rel, RelB) that constitute the NF- κ B complex. The five proteins associate in other to form different combinations of dimers (Huxford & Ghosh, 2009).

14-3-3 was shown to bind to one of the NF- κ B subunits, the p65 protein, in response to TNF α . It was also shown that the exposure to TNF α was directly linked to the phosphorylation of S42 and S281 of p65, two theoretical 14-3-3 binding motifs located in the loops of the Rel homology regions of p65 (Aguilera et al., 2006). Cellular studies on three mutants of p65 (S42A, S281A and S340A) shown that the mutations have a considerable impact on the interaction with 14-3-3. The same study concludes that 14-3-3 was shown to be essential for the nuclear export of the p65/ I κ B α complex and therefore for the well-functioning of the NF- κ B signaling (Aguilera et al., 2006). Although more studies are needed, the available information points to the reasoning that the stabilization of the 14-3-3/p65 PPI may be of interest for a number of NF- κ B related pathologies (Aguilera et al., 2006; Inglés-Esteve et al., 2012).

7.2 Context of the collaboration

Our collaborators resolved the crystal structure of 14-3-3 σ in the presence of the p65pS45 and p65pS281 epitopes. Fluorescence anisotropy assays showed that Fusicoccanes, including FC-A, could stabilize the 14-3-3 σ /p65pS45 PPI. Surprisingly, our collaborators could not find electron density corresponding to FC-A when they soaked the compound in pre-formed crystals of the binary complex 14-3-3 σ /p65pS45. Our collaboration was therefore

requested in order to use our NMR assignment of 14-3-3 σ for confirming the binding pocket of FC-A and the stabilization of the 14-3-3 σ /p65pS45 PPI by this compound.

7.3 Materials and Methods

7.3.1 NMR spectroscopy

^1H - ^{15}N TROSY-HSQC (Transverse Relaxation Optimized Spectroscopy- Heteronuclear Single Quantum Coherence Spectroscopy) spectra were acquired in 3 mm tubes (sample volume 200 μL) using a 900 MHz Bruker Avance NEO spectrometer, equipped with a cryoprobe. The spectra were recorded at 32 $^\circ\text{C}$, in a buffer containing 100 mM sodium phosphate, 50 mM NaCl, pH 6.8, 4% (v/v) DMSO- d_6 , 1 mM DTT, EDTA-free protease inhibitor cocktail (Roche, Basel, Switzerland) and 10% (v/v) D $_2$ O. The experiments were recorded with 3426 complex data points in the direct dimension and 128 complex data points in the indirect dimension, with 300 scans per increment. The spectra for accessing the stabilization of the 14-3-3/p65 PPI were performed with samples containing 125 μM $^{15}\text{N}^{13}\text{C}^2\text{H}$ labeled 14-3-3 σ in the presence of 125 μM Fusicoccin-A and/or 625 μM p65pS45 peptide. A ^1H - ^{15}N TROSY-HSQC spectrum was acquired as reference with 125 μM $^{15}\text{N}^{13}\text{C}^2\text{H}$ -labeled 14-3-3 σ . 14-3-3 σ ΔC17 ^1H - ^{15}N TROSY-HSQC spectrum obtained in the same experimental conditions was used to confirm tryptophan side chain assignments. The reference for the ^1H chemical shift was relative to trimethylsilyl propionate. ^{15}N chemical shift values were referenced indirectly. Spectra were collected and processed with Topspin 4.0 (Bruker Biospin, Karlsruhe, Germany) and analyzed with Sparky 3.12 (T. D. Goddard and D. G. Kneller, SPARKY 3, University of California, San Francisco).

7.4 Results and discussion

As an alternative to obtain structural information on FC-A binding to the binary complex, NMR measurements were performed, based on the assignments of 14-3-3 σ signals (Neves et al., 2019). Chemical shift perturbations in the resonances corresponding to specific residues along 14-3-3 σ confirmed that FC-A binds in its previously reported binding pocket, in the

presence and in the absence of the p65pS45 peptide (**Figure S1**). In order to confirm the stabilization by NMR, an increase in the complex formation with the peptide has to be detected in the presence of the stabilizing compound. This can be achieved by detecting an increase of the chemical shift perturbations of resonances specifically affected by the peptide binding, but not directly by the stabilizer compound binding. The p65pS45 peptide was shown to bind at the phospho-binding pocket of the amphipathic binding groove of 14-3-3 (**Figure 1 A**). The natural stabilizer FC-A is accommodated in the FC-binding pocket, away from the phospho-binding pocket (**Figure 1 A**). We decided therefore to monitor the isolated resonance corresponding to the N ϵ -H ϵ bond of residue W230 of 14-3-3 σ on the ^1H - ^{15}N TROSY-HSQC of $^{15}\text{N}^{13}\text{C}^2\text{H}$ labeled 14-3-3 σ , which is specifically affected by the peptide binding, but not by the FC-A binding (**Figure 1 A**). This resonance corresponds to a residue that interacts directly with the peptide but that is remote from the FC binding pocket. The assignment of this resonance is unambiguous (**Figure S2**). Because the peptide binding induced broadening of a number of resonances, including N ϵ -H ϵ W230, the resonance intensity of N ϵ -H ϵ W230 was monitored in a series of spectra acquired in the same experimental conditions. Comparison of the intensities of N ϵ -H ϵ W230 in the spectrum of 14-3-3 σ in the presence of FC-A (I) with the reference spectrum acquired for 14-3-3 σ with 4% DMSO-d₆ (I0) showed that the intensity of this resonance is, as expected, not affected by the presence of FC-A (**Figure 1 B,C**). Once the p65pS45 peptide is added, the resonance broadens due to the interaction and consequently its intensity drops to 83% compared to the reference spectrum (**Figure 1 D**). When FC-A was added together with the p65pS45 peptide, the intensity of the N ϵ -H ϵ W230 resonance further decreased, down to 18% (**Figure 1E**). Since the binding of FC-A does not cause any perturbation on this particular resonance, the intensity decrease was linked to an increased amount of complex formation in solution. This data independently confirms the stabilization of the p65pS45/14-3-3 σ complex in the presence of FC-A.

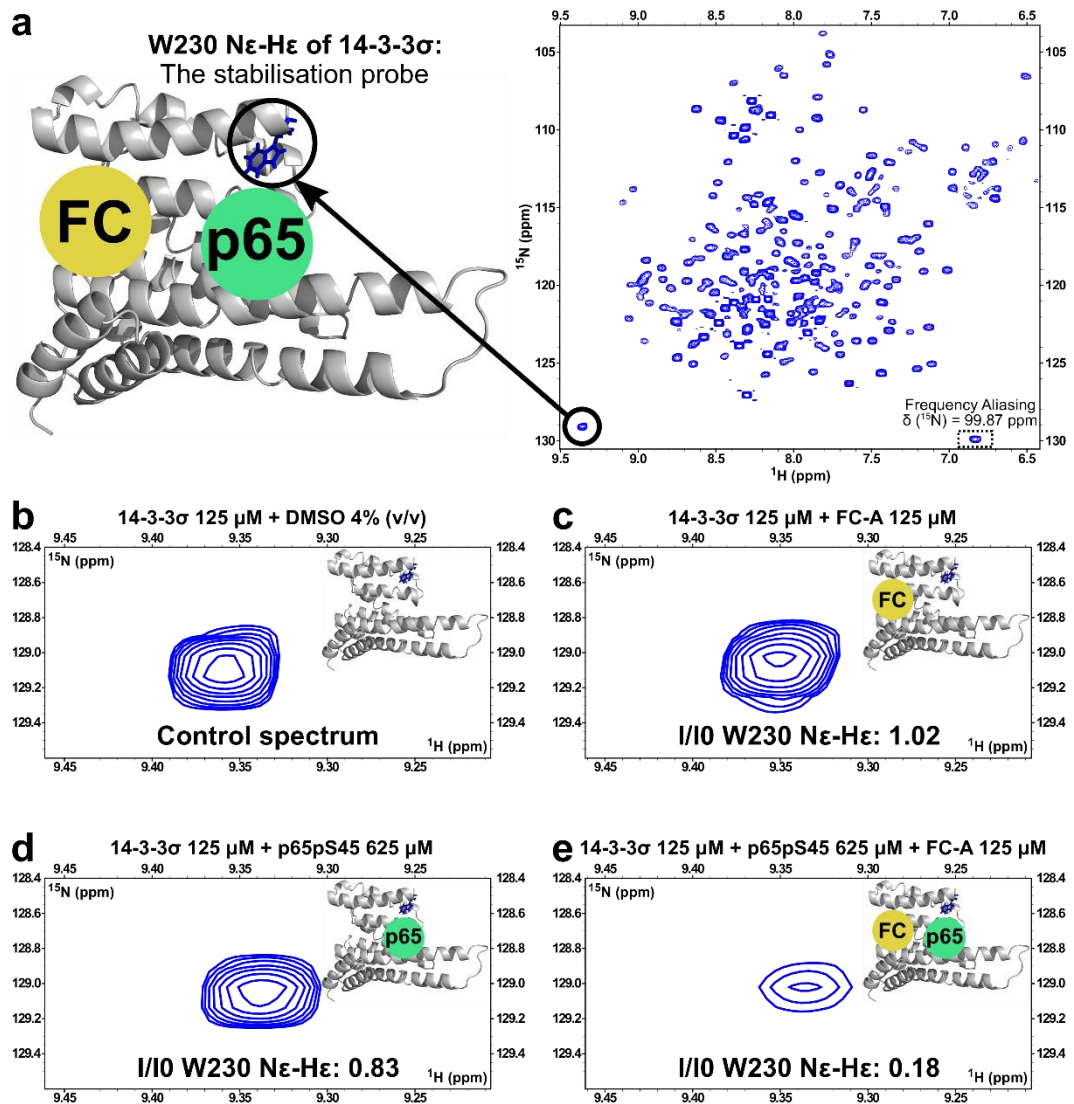


Figure 1 – Fusicoccin stabilizes the 14-3-3/p65pS45 PPI. (A) The resonance corresponding to the W230 N ϵ -H ϵ bond of 14-3-3 σ was monitored to detect the stabilization of this PPI. This resonance is circled in black on the ^1H - ^{15}N TROSY-HSQC spectrum of $^{15}\text{N}^{13}\text{C}^2\text{H}$ -labeled 14-3-3 σ (shown on the right) and the corresponding residue W230 is represented as sticks, colored in blue and circled in black on the crystal structure (shown on the left, represented as white surface). This residue is close to the peptide-binding site (represented with a green circle) and away from the FC-A binding site (represented with a yellow circle). (B-E) The enlarged spectral region of the ^1H - ^{15}N TROSY-HSQC containing the resonance corresponding to the W230 N ϵ -H ϵ bond of 14-3-3 σ (125 μM) is shown in the presence of: DMSO- d_6 4% (v/v), present in all samples (B), FC-A 125 μM (C), p65pS45 peptide 625 μM (D) and p65pS45 peptide 625 μM and FC-A 125 μM (E).

7.5 Conclusions

In this work, we have shown that FC-A binds in its typical binding pocket when 14-3-3 σ is in the presence of the p65pS45 peptide. Moreover, using NMR we observed, through a single resonance, the stabilization of the 14-3-3 σ /p65pS45 complex by FC-A, confirming the results from fluorescence anisotropy. To our knowledge, this is the first use of NMR to report on a complex stabilization. Further work in this project includes the test of more FC-A derivatives in order to find potent stabilizers of this complex and on the replacement of the Fusicocanes by smaller molecules.

7.6 Supporting Information

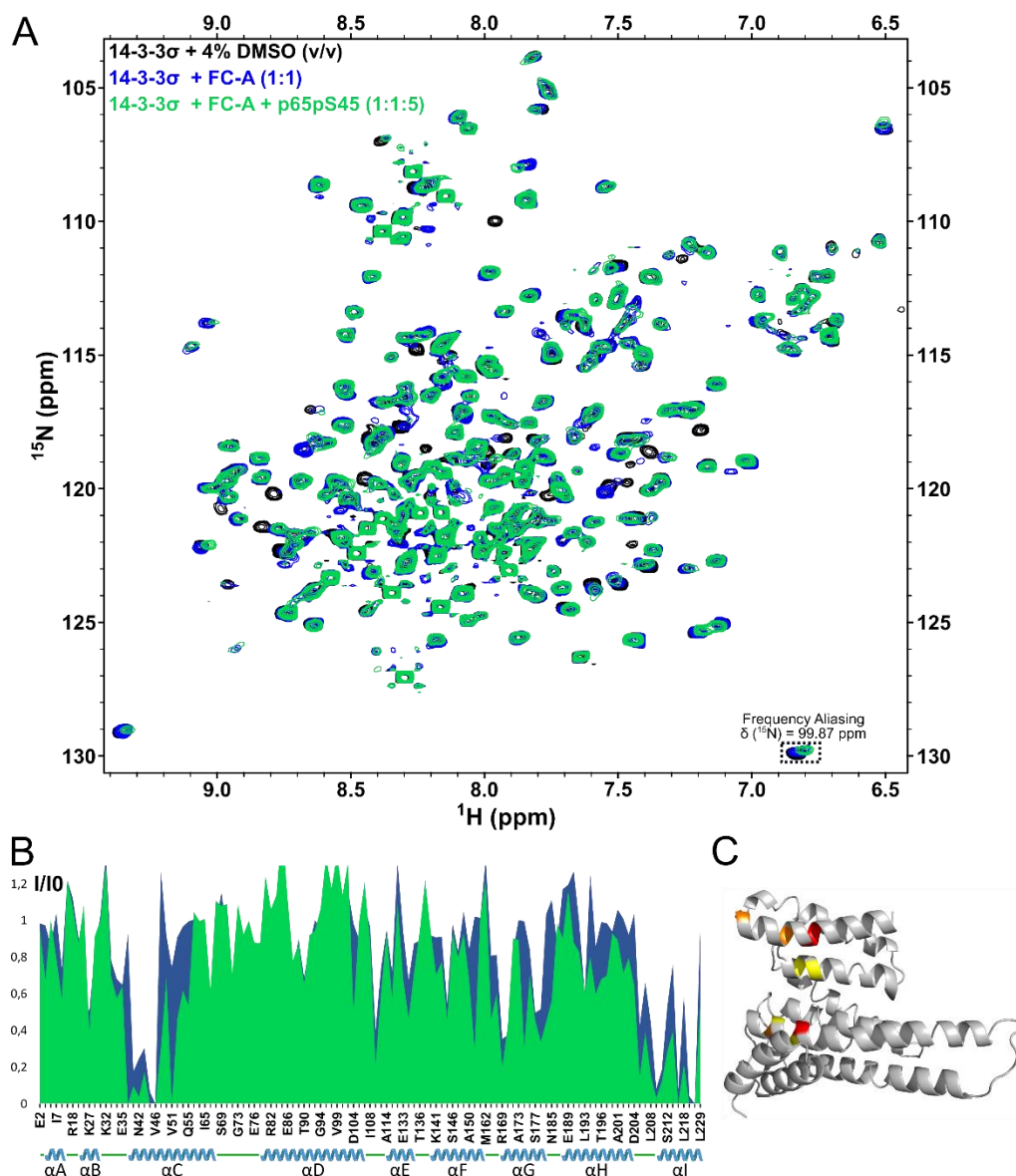


Figure S1 - FC-A binds in its usual binding pocket in the presence or absence of the p65pS45 peptide. A) Superimposed ^1H - ^{15}N TROSY-HSQC spectra of $^{15}\text{N}^{13}\text{C}$ 14-3-3 σ 125 μM in the presence of 4% DMSO- d_6 (v/v) (in black), FC-A 125 μM (in blue) and FC-A 125 μM + p65pS45 625 μM (in green). B) Plot of the ratios of the bound (I)/free (I0) ^1H - ^{15}N correlation peak intensities of 14-3-3 σ (y axis) versus the amino acid sequence (x axis) in the presence of FC-A 125 μM (blue plot) and FC-A 125 μM + p65pS45 625 μM (green plot). A total of 121 correlation peak intensities are shown. The x axis is not proportional to the sequence length. The helices of 14-3-3 σ are identified below the x axis as a blue cartoon, while disordered regions are represented as a green line. Note that the areas affected by the binding of FC-A alone (blue plot) are also affected when the peptide is added (green plot). C) Mapping on the crystal structure of 14-3-3 σ (PDB ID: 6QHL-unreleased) of the amino acid residues whose

correspondent correlation peak intensities were the most affected by the presence of FC-A 125 μM alone. The 1-4 residues whose correspondent correlation peak intensities were the most affected are colored in red, the 5-8 are colored in brown and the 9-12 are colored in yellow.

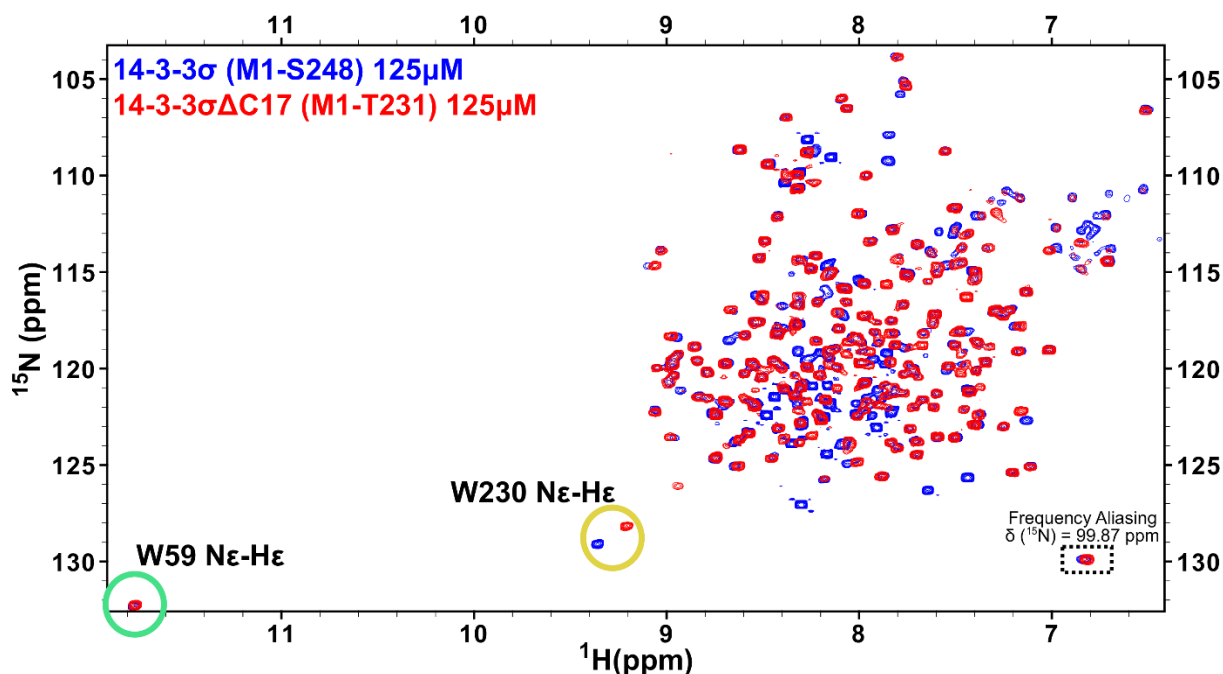


Figure S2 - Assignment of the two Tryptophan N ϵ -H ϵ resonances on the ^1H - ^{15}N TROSY HSQC spectrum of 14-3-3 σ . Overlaid ^1H - ^{15}N TROSY HSQC spectra of full-length $^{15}\text{N}^{13}\text{C}^2\text{H}$ labeled 14-3-3 σ 125 μM (blue) and $^{15}\text{N}^{13}\text{C}^2\text{H}$ labeled 14-3-3 $\sigma\Delta\text{C17}$ (red). After truncation of the C-terminus (A232-S248), a chemical shift value modification was, as expected, only observed for one of the Tryptophan side chain resonances (surrounded by a yellow circle). Therefore, this resonance ($\delta(^{15}\text{N}) = 129.1$ ppm; $\delta(^1\text{H}) = 9.35$ ppm) corresponds to the N ϵ -H ϵ bond of W230, since it is close to the truncation site. The other Tryptophan N ϵ -H ϵ resonance ($\delta(^{15}\text{N}) = 132.3$ ppm; $\delta(^1\text{H}) = 11.76$ ppm), surrounded by a green circle, is not affected upon truncation of the C-terminus and therefore corresponds to the W59 N ϵ -H ϵ bond.

8 Stabilization of the 14-3-3/p53 Protein-Protein Interaction

8.1 Context of the collaboration

Our collaborators performed a crystallography-based screening for the identification of compounds binding to the 14-3-3/p53pT387 complex. They identified a family of compounds binding in the amphipathic binding groove of 14-3-3 σ adjacently to the p53pT387 peptide. They further designed and screened derivatives of the initial hits by fluorescence-based methods and X-ray crystallography. They indeed observed electron density for some derivatives in the amphipathic binding groove of 14-3-3. One compound (AK-008) showed a very promising activity when tested by the fluorescence-based method but our collaborators did not manage to observe any electron density correspondent to the compound by X-ray crystallography. Our collaboration was requested in order to confirm that AK-008 was binding in the amphipathic binding groove and if possible, to characterize the modulatory activity of this compound on the 14-3-3/p53pT387 complex.

8.2 Materials and Methods

8.2.1 WaterLOGSY experiments

WaterLOGSY spectra were acquired in 5 mm tubes (sample volume 530 μ L) using a 600 MHz Bruker Avance I spectrometer equipped with a CPQCI cryogenic probe. The spectra were recorded with 32768 complex data points, with 1024 scans per increment and with a mixing time of 1.7s (acquisition time of 94 minutes). The spectra were acquired at 16 °C, in a buffer containing 100 mM sodium phosphate, 50 mM NaCl, pH 6.8 and 10% (v/v) D₂O. The final concentration of DMSO-d₆ was 2% (v/v) and was kept constant for all the experiments. For the evaluation of the binding of AK-008 to the 14-3-3 σ /p53 complex, WaterLOGSY spectra were recorded on solutions containing 14-3-3 σ 25 μ M in the presence and absence of 500 μ M AK-008, 50 μ M p53pT387 peptide, and simultaneously 50 μ M p53pT387 peptide and 500 μ M AK-008. An additional control experiment consisted of the acquisition of a WaterLOGSY spectrum in the presence of 500 μ M AK-008 and in the absence of protein and peptide. A ¹H

spectrum with water-suppression was additionally recorded for each sample. Spectra were collected, processed and analyzed with Topspin 4.0 (Bruker Biospin, Karlsruhe, Germany).

8.2.2 ^1H - ^{15}N TROSY-HSQC NMR spectroscopy

^1H - ^{15}N TROSY-HSQC (Transverse Relaxation Optimized Spectroscopy- Heteronuclear Single Quantum Coherence Spectroscopy) spectra were acquired in 3 mm tubes (sample volume 200 μL) using a 900 MHz Bruker Avance Neo spectrometer, equipped with a cryoprobe. The spectra were recorded at 32 $^\circ\text{C}$, in a buffer containing 100 mM sodium phosphate, 50 mM NaCl, pH 6.8, 2% (v/v) DMSO- d_6 , 1 mM DTT, EDTA-free protease inhibitor cocktail (Roche, Basel, Switzerland) and 10% (v/v) D_2O . The experiments were recorded with 3072 complex data points in the direct dimension and 128 complex data points in the indirect dimension, with 184 scans per increment. For the evaluation of the binding of AK-008 to the 14-3-3 σ /p53 complex, spectra of $^{15}\text{N}^2\text{H}$ labeled 14-3-3 $\sigma\Delta\text{C}$ 100 μM were recorded in the presence and absence of 2000 μM AK-008, 500 μM p53pT387 peptide, and simultaneously 500 μM p53pT387 peptide and 2000 μM AK-008. Assignments of the backbone resonances of $^{15}\text{N}^2\text{H}$ labeled 14-3-3 $\sigma\Delta\text{C}$ were previously reported (Neves et al., 2019). A ^1H spectrum with water-suppression was additionally recorded for each sample for monitoring the peptide signals. The reference for the ^1H chemical shift was relative to DSS (4,4-dimethyl-4-silapentane-1-sulfonic acid) while ^{15}N chemical shift values were referenced indirectly. Spectra were collected and processed with Topspin 4.0 (Bruker Biospin, Karlsruhe, Germany) and analyzed with Sparky 3.12 (T. D. Goddard and D. G. Kneller, SPARKY 3, University of California, San Francisco).

8.3 Results and discussion

Our collaborators were not able to detect any electronic density by X-ray crystallography for compound AK-008, one rationally designed extended fragment targeting the 14-3-3/p53pT387 complex. We thus next used WaterLOGSY NMR experiments to detect the potential interaction of AK-008 with 14-3-3 σ . Detection of the interaction by this experiment is based on the differential behavior of the compound free in solution, experimenting fast

tumbling, or bound to the protein, in slower motion (Dalvit et al., 2001). Positive ^1H signals of the ligand in the presence of the protein are indicative of binding. Using this approach, positive NMR signals in the WaterLOGSY spectra of AK-008 mixed with 14-3-3 σ , both in the presence or absence of the p53pT387 peptide, confirmed the interactions (**Figure S1**). The two-dimensional spectrum (^1H - ^{15}N TROSY-HSQC) of 14-3-3 $\sigma\Delta\text{C}$ ($^{15}\text{N}^2\text{H}$ labeled) was next used as reporter to further characterize the binding. Because the resonances in this spectrum are sensitive to the chemical environment of the corresponding residues, a modification in the presence of a ligand of a resonance chemical shift value, and/or intensity, reports an interaction. In addition, chemical shift assignments of 14-3-3 $\sigma\Delta\text{C}$ have been performed, allowing to link a specific resonance in the spectrum to an amino acid residue in 14-3-3 $\sigma\Delta\text{C}$ sequence (Neves et al., 2019). The addition of AK-008 to 14-3-3 $\sigma\Delta\text{C}$ or 14-3-3 $\sigma\Delta\text{C}$ in the presence of the p53pT387 peptide resulted in detectable broadening (intensity decrease) of a few resonances in the ^1H - ^{15}N 2D spectrum of the protein (**Figure S2, 1 A, 1 C**). Based on the signal assignments, we concluded that addition of AK-008 affected mainly residues R41, N42, E115 and F119 of 14-3-3 σ , with no variation in the presence of p53pT387 peptide (**Figure 1 A, C**). These experiments indicated that binding of AK-008 occurs in the same pocket in both cases, with or without the p53pT387 peptide. Visualizing the corresponding amino acid perturbation induced by AK-008 on 14-3-3 σ structure clearly highlighted a binding site (**Figure 1 B**), which can be matched to data from the co-crystal structure of 14-3-3 σ and p53pT387 in the presence of its analogs (data not shown). The binding pose resulting from docking AK-008 to the 14-3-3 σ /p53pT387 complex is in accordance with both the NMR data and the bound-conformation adopted by other fragments based on this scaffold (not shown). In conclusion, AK-008 bound 14-3-3 σ , even in the absence of p53pT387, in a pocket similar to the one observed in the co-crystal structure of 14-3-3 σ /p53pT387 in the presence of close analogs of this fragment.

Interestingly, addition of AK-008 also induced chemical shift perturbations (CSP) of the ^1H NMR signals of the bound peptide (**Figure 1 D, S3**). In particular, the ^1H signals (**Figure 1 D**) of the H_δ methyl protons of L383 of the p53pT387 peptide are affected by AK-008 binding, despite the fact that they are not close to the fragment binding site. Perturbation of these signals thus did not correspond to a direct effect due to the local change of environment. This

data suggests that the binding of the fragment impacted the global binding of the peptide to 14-3-3 σ . Moreover, the extent of decrease of the intensity of specific resonances in the 2D spectrum of 14-3-3 σ Δ C in the presence AK-008 reports on the amount of complex present in the solution. The intensity of resonances corresponding to amino acid residues located in, or close, to the p53pT387 binding site specifically decreased with the addition of AK-008 to a solution containing the complex (**Figure 1 E, F**). Therefore, the amount of 14-3-3 σ /p53pT387 complex that was present in solution was increased when both ligands were present, indicating that the complex was stabilized in the presence of AK-008.

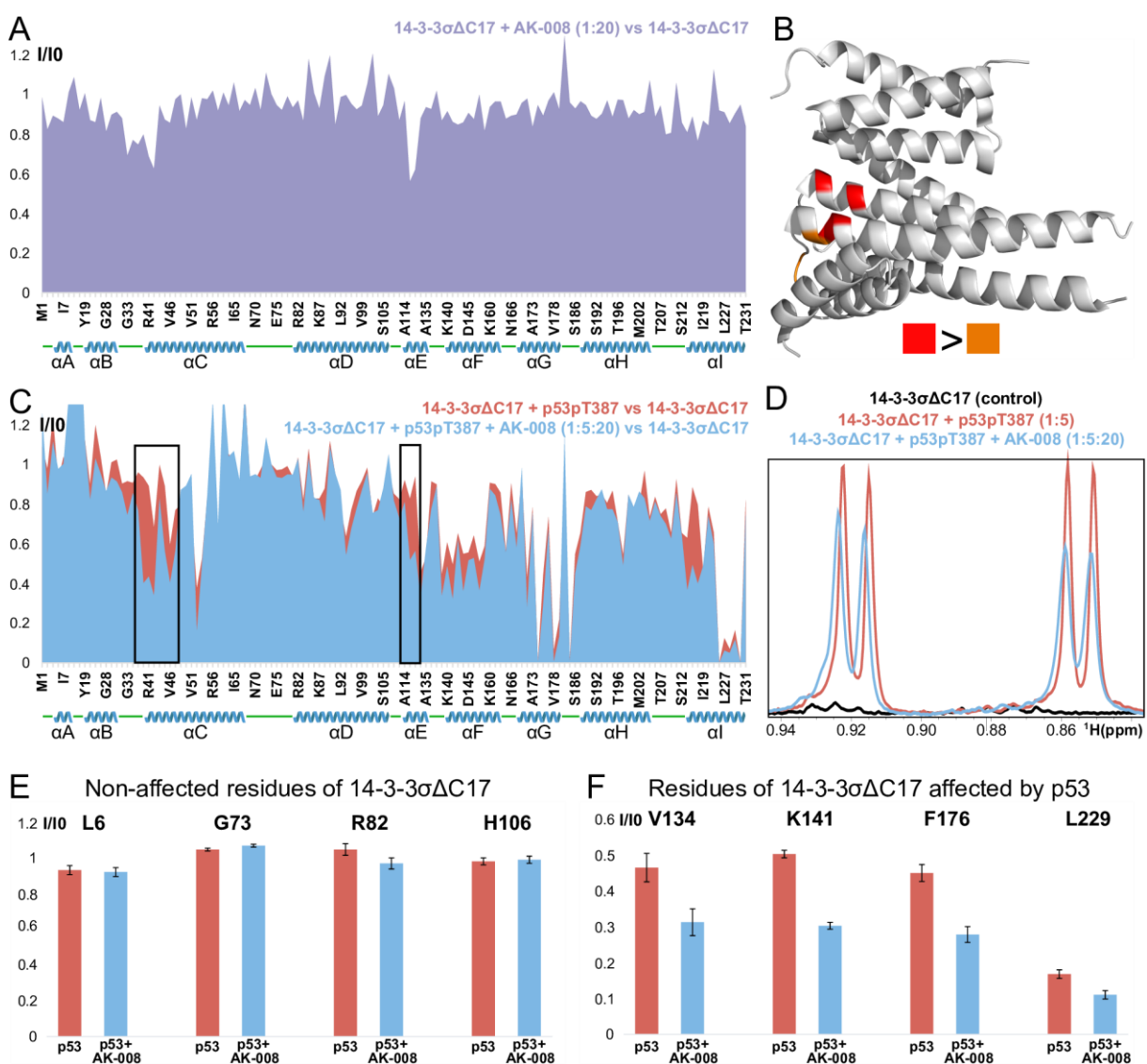


Figure 1 - AK-008 binds to the amphipathic binding groove of 14-3-3 σ and stabilizes the 14-3-3 σ /p53pT387 complex. (A) Plot of the intensity ratios I/I_0 of corresponding 1H - ^{15}N correlation peaks in the 2D 14-3-3 σ Δ C spectra

corresponding to the bound 14-3-3 σ Δ C (100 μ M 14-3-3 σ Δ C in the presence of 2000 μ M AK-008, I) and free 14-3-3 σ Δ C (100 μ M 14-3-3 σ I0) protein (y axis) versus 14-3-3 σ Δ C amino acid sequence (x axis). A total of 133 correlation peak intensities are shown. The x axis is not proportional to the sequence length. The helices of 14-3-3 σ are identified below the x axis as blue cartoons, while disordered regions are represented by green lines. B) Mapping on the crystal structure of 14-3-3 σ (PDB ID: 1YZ5) of the amino acid residues corresponding to the most affected resonances by the presence of AK-008. Residues whose corresponding correlation peak intensities were the most affected are colored in red and an additional 5-8 are colored in brown. (C) Plot of the intensity ratios I/I0 (y-axis) of corresponding ^1H - ^{15}N correlation peaks in the 2D 14-3-3 σ Δ C spectra of, in red: the peptide-bound 14-3-3 σ Δ C (100 μ M 14-3-3 σ Δ C in the presence of 500 μ M p53pT387, I) and free 14-3-3 σ Δ C (100 μ M 14-3-3 σ I0), and in blue: corresponding to the peptide and fragment-bound 14-3-3 σ Δ C (100 μ M 14-3-3 σ Δ C with 500 μ M p53pT387 and 2000 μ M AK-008, I) and free 14-3-3 σ Δ C (100 μ M 14-3-3 σ Δ C, I0) protein. Note that the boxed regions correspond to the same areas affected in panel A and therefore show that the binding site of the fragment is the same when the peptide is present or not. (D) ^1H NMR signals of the spectrum of 100 μ M 14-3-3 σ Δ C (in black), 100 μ M 14-3-3 σ Δ C in the presence of 500 μ M p53pT387 (in red) and 100 μ M 14-3-3 σ Δ C in the simultaneous presence of 500 μ M p53pT387 and 2000 μ M AK-008 (in blue). The NMR signals correspond to the H_δ protons of L383 of the p53pT387 peptide. CSP in the peptide signals can be observed when AK-008 is added to the solution containing the 14-3-3 σ /p53pT387 complex. (E, F) Plot of the ratios of the bound (I)/free (I0) ^1H - ^{15}N TROSY-HSQC correlation peak intensities of individual resonances corresponding to residues of 100 μ M 14-3-3 σ Δ C, remote from the interaction site (E) or close to the p53pT387 interaction site (F) of, in the presence of 500 μ M p53pT387 (in red) and 100 μ M 14-3-3 σ Δ C in the simultaneous presence of 500 μ M p53pT387 and 2000 μ M AK-008 (in blue). Error bars of I/I0 ratios were calculated based on the maximum noise estimate of each spectrum. Note that the resonances corresponding to regions affected by the p53pT387 peptide binding were considerably more affected in the presence of AK-008.

8.4 Conclusions

Our experiments suggest that AK-008 binds in the amphipathic binding groove of 14-3-3 σ and stabilizes the 14-3-3 σ /p53pT387. Our collaborators performed docking simulations, which agree with the binding site suggested by our NMR experiments. Further SPR and FP experiments also confirmed our hypothesis that this compound stabilizes the 14-3-3 σ /p53pT387 PPI. The results of these *in vitro* assays of this compound are extremely promising given the binding at the protein-protein interface and the stabilization. These results pave the way to the development of derivatives of AK-008 in order to develop potent stabilizers of the 14-3-3 σ /p53pT387 PPI. These results are also a proof of concept that NMR

spectroscopy can be of great utility to characterize the stabilization of a PPI, which is often extremely challenging.

8.5 Supporting Information

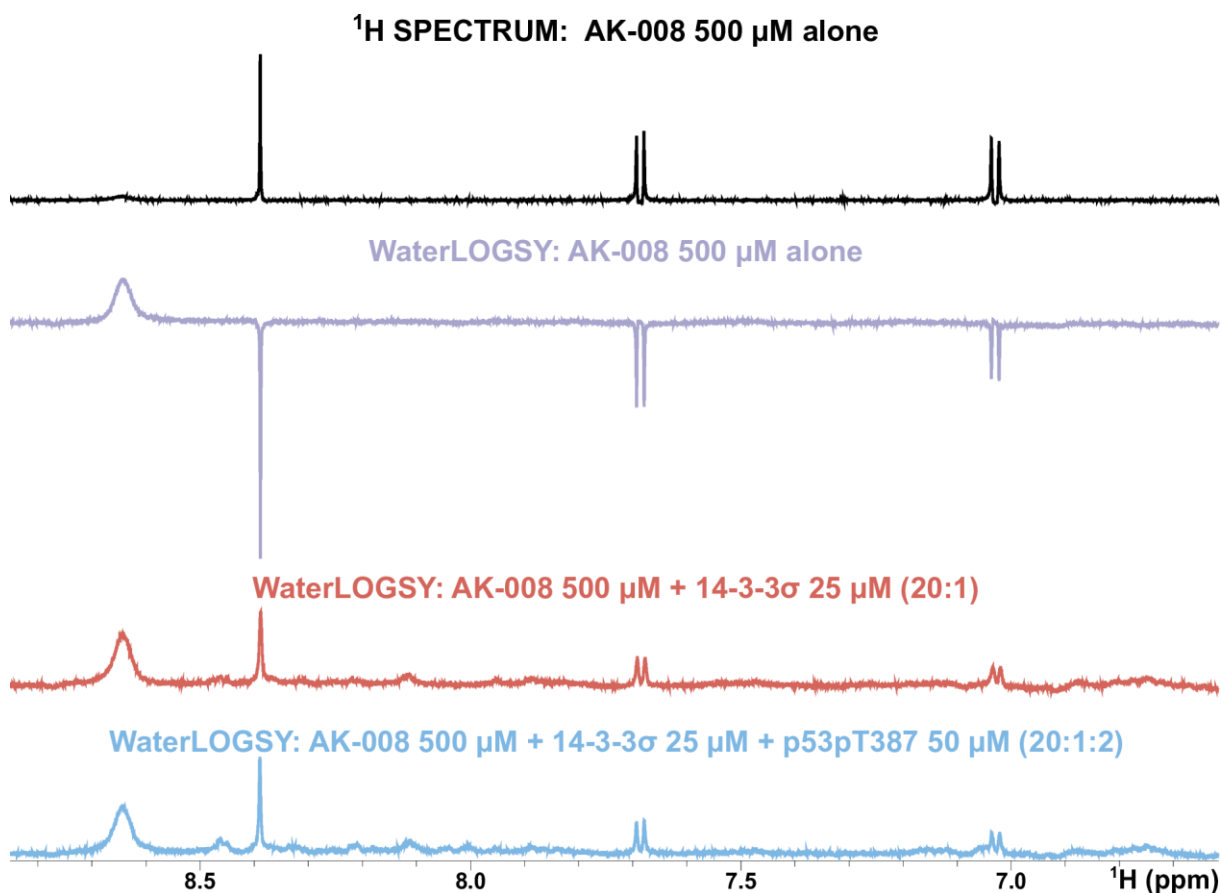


Figure S1 - WaterLOGSY detects the binding of AK-008 to 14-3-3 σ and to 14-3-3 σ /p53 pT387 complex. ^1H spectrum of AK-008 500 μM (black spectrum, on top). WaterLOGSY spectrum of AK-008 500 μM (in purple): NMR signals are all phased negative, except the one at 8.65 ppm. WaterLOGSY spectrum of a solution containing 14-3-3 σ 25 μM and AK-008 500 μM (in red): NMR signals of the small molecule are all phased positive, indicating binding. WaterLOGSY spectrum of a solution containing 14-3-3 σ 25 μM , p53pT387 50 μM and AK-008 500 μM (in blue): NMR signals of the small molecule are all phased positive, indicating binding.

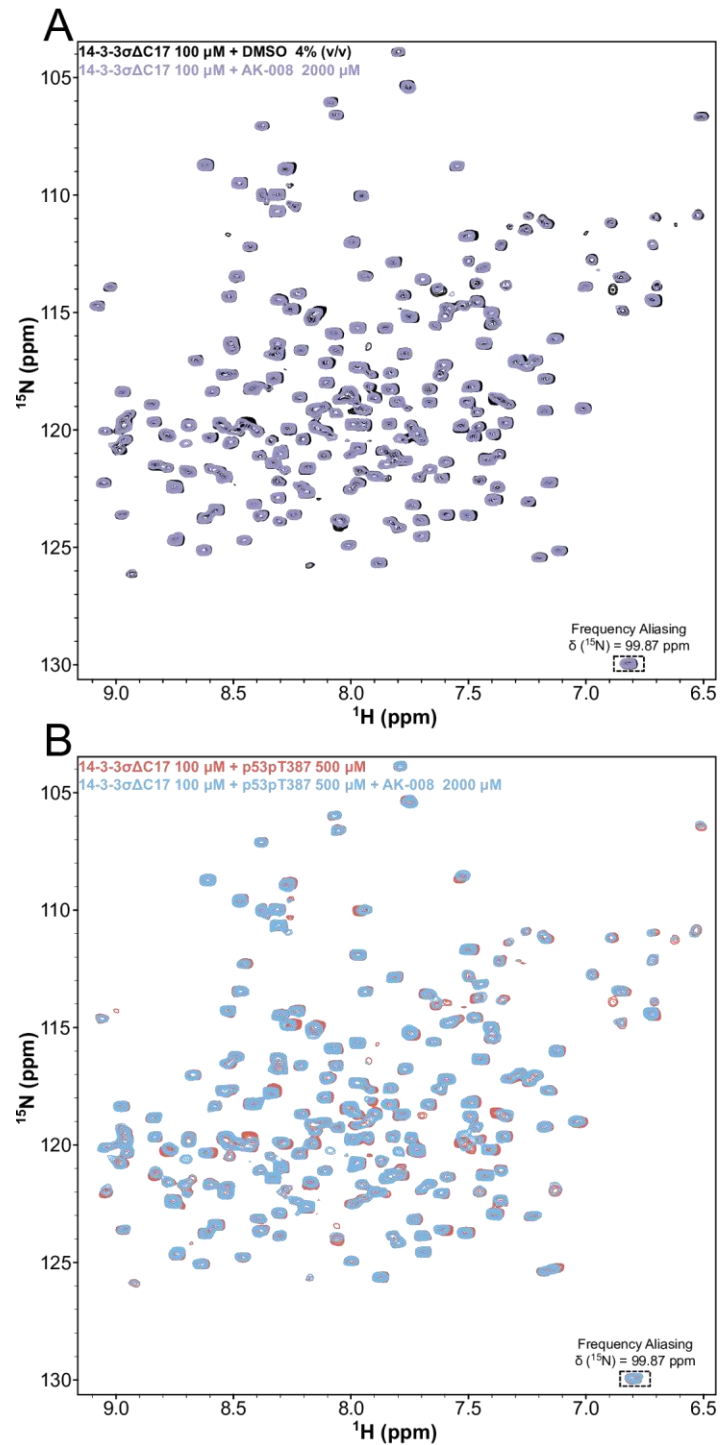


Figure S2 – ^1H - ^{15}N TROSY-HSQC spectra of $^{15}\text{N}^2\text{H}$ labeled 14-3-3. A) Superimposed spectra of $^{15}\text{N}^2\text{H}$ labeled 14-3-3 $\sigma\Delta\text{C}$ 100 μM , alone (in black), or in the presence of 2000 μM AK-008 (superimposed in purple). B) Spectra of $^{15}\text{N}^2\text{H}$ labeled 14-3-3 $\sigma\Delta\text{C}$ 100 μM in the presence of 500 μM p53pT387 (in red), and $^{15}\text{N}^2\text{H}$ labeled 14-3-3 $\sigma\Delta\text{C}$ 100 μM in the presence of both 500 μM p53pT387 and 2000 μM AK-008 (superimposed in blue).

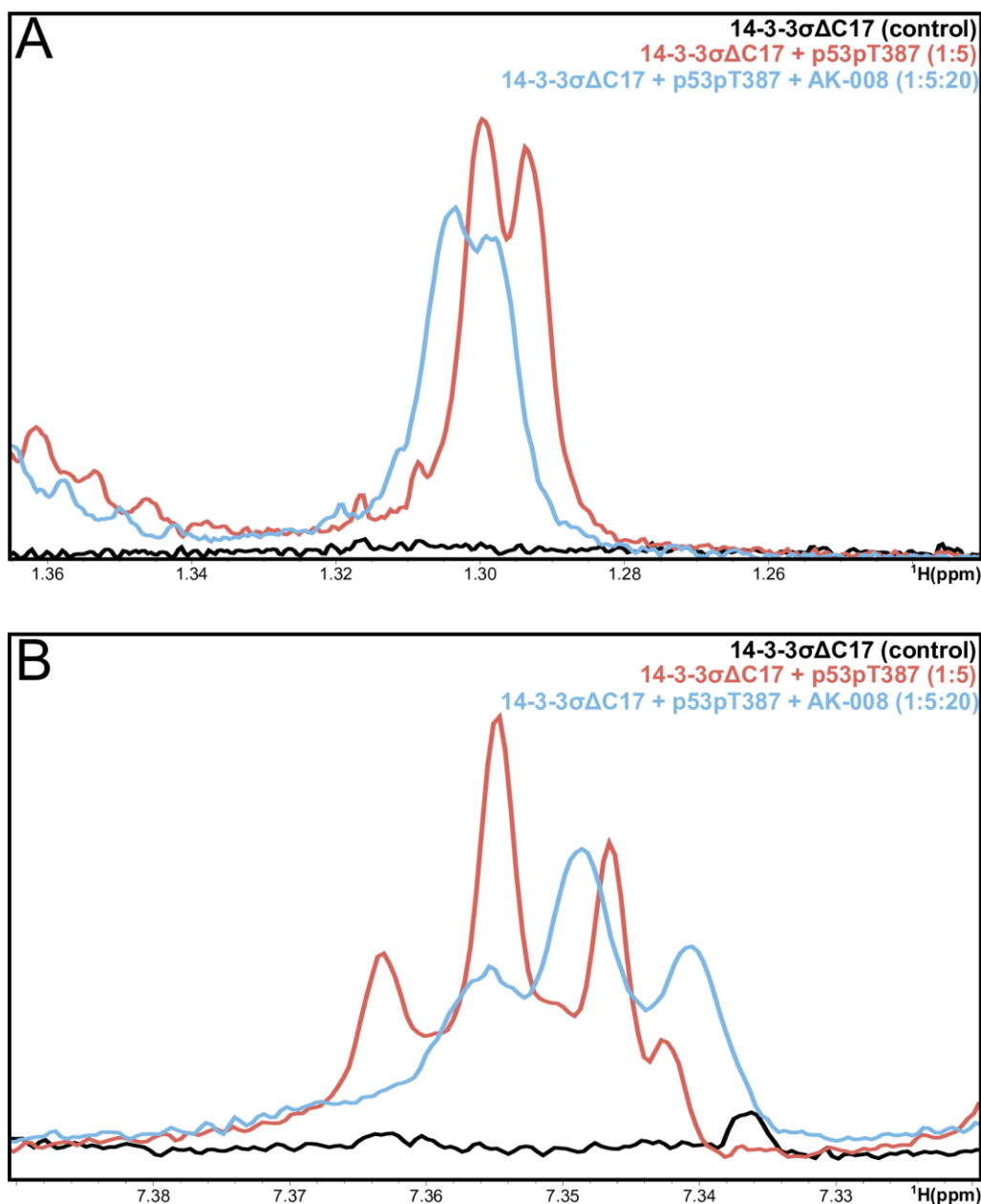


Figure S3 - ¹H NMR signals corresponding to peptide protons show that the peptide is affected by the binding of AK-008. The panels show superimposed ¹H NMR signals of enlarged regions of the spectrum of 14-3-3σΔC 100 μM (in black), 14-3-3σΔC 100 μM in the presence of 500 μM p53pT387 (in red) and 14-3-3σΔC 100 μM in the simultaneous presence of 500 μM p53pT387 and AK-008 2000 μM (in blue). In A) the NMR signal corresponding to the H β proton of pT387 of the p53pT387 peptide is shown, whereas in B), the NMR signals corresponding to aromatic protons of F385 of the p53pT387 peptide are observed. CSP on the peptide signals can be observed in both cases when the fragment AK-008 is added to the solution containing the 14-3-3σ/p53pT387 complex.

GENERAL CONCLUSION AND PERSPECTIVES

This work was performed on the scope of the Targeted small-molecule stabilization of protein-protein Interactions (TASPPI) European Training Network. Our project in the consortium was focused on the Tau/14-3-3 PPI in the context of AD. Additionally we have developed the conditions to collaborate with other partner institutions for carrying out studies on 14-3-3 PPIs and on the screening and characterization of small molecules modulating these targets. Due to the collaborative character of the TASPPI network, this work includes several projects divided in three main topics:

- Backbone chemical shift assignments of human 14-3-3 σ ;
- Study of 14-3-3 protein-protein interactions;
- Screening and characterization of compounds targeting 14-3-3 or 14-3-3 PPIs.

General conclusions and perspectives per topic

Backbone chemical shift assignments of human 14-3-3 σ

The backbone chemical shift assignment of 14-3-3 σ was an important milestone on the TASPPI project. Prior to the beginning of the TASPPI project, a partial backbone chemical shift assignment of 14-3-3 ζ was already available (BMRB Entry #25231) (Killoran et al., 2015). Despite having already a backbone assignment available, we considered very important to assign the isoform σ of 14-3-3 for several reasons. First, the availability of two assigned isoforms would allow the study of isoform specific partners/small molecules. A second reason concerns the study of the 14-3-3/Tau PPI since 14-3-3 σ was shown to be linked to Tau-mediated toxicity in cells (Joo et al., 2015). Another reason for having assigned 14-3-3 σ is the fact that it is, according to the Protein Data Bank, by far, the preferred human 14-3-3 isoform for structural studies (88 PDB entries for human 14-3-3 σ against 79 PDB entries for all other isoforms, according to the PDB as per June 2019). Due to the high MW of 14-3-3 σ Δ C (53.1 KDa), a number of strategies were put in place in order to achieve the most complete assignment as possible. These strategies included protein deuteration, protein truncation, specific amino acid labelling, use of TROSY pulse sequences and use of automatic assignment software and servers. In the end we were able to assign 177 out of 226 $^1\text{H}^{\text{N}}$ and ^{15}N resonances

(78%), 200 out of 231 $^{13}\text{C}_\alpha$ resonances (87%), 187 out of 219 $^{13}\text{C}_\beta$ resonances (85%) and 176 out of 231 ^{13}CO resonances (77%). This assignment covered most of the protein's sequence and proved to be a powerful tool for the study of interactions of 14-3-3 σ with proteins, peptides and small-molecules. New advances in NMR spectrometers, with magnetic strengths of 1.2 GHz (28.2 T) being available soon, may probably permit the complete backbone assignments of 14-3-3 proteins in a near future.

Study of 14-3-3 protein-protein interactions

The 14-3-3/Tau PPI

The 14-3-3/Tau PPI has been studied for almost 20 years with considerable progress from the structural and functional points of view. In this work we addressed several aspects on the structural study of the 14-3-3/Tau PPI that were not fully understood. We have first showed that, as suggested in other studies, phosphorylation by PKA enhances the affinity of Tau to 14-3-3. We additionally show that the interaction between wt-Tau and 14-3-3 is too weak to form a complex in solution detectable by AUC-SV. Our data from AUC-SV and NMR experiments suggests that Tau-PKA can occupy both monomers of 14-3-3 and interacts exclusively within the amphipathic binding groove. This information can be of great relevance for drug discovery projects aiming to develop inhibitors of the 14-3-3/Tau PPI. The information available on the literature is not consensual regarding the affinity of the interaction between 14-3-3 and phosphorylated Tau, with one study pointing to the low μM range (Joo et al., 2015) and another one pointing to the low nM range (Sadik et al., 2009). In this work we addressed this particular issue through the determination of the dissociation constant by two different techniques and showed that the affinity of the 14-3-3 σ /Tau-PKA interaction is in the low μM range. Altogether our data shed some light on unconfirmed questions on the 14-3-3/Tau PPI such as the stoichiometry, affinity and contact surface.

Despite 20 years of research on the 14-3-3/Tau PPI, there is still a lot to investigate both at structural and functional levels. One of the areas for potential significant work would be the study of the interaction of Tau phosphorylated by different kinases with 14-3-3. Despite the fact that the Tau phosphorylation sites presenting more similarity with 14-3-3 binding

epitopes are phosphorylated by PKA (Sluchanko et al., 2017), this does not exclude that other residues phosphorylated by other kinases cannot create anchoring points on 14-3-3. Another interesting study would be the investigation of the interaction of O-GlcNAcylated Tau with 14-3-3. Recently, it was shown that O-GlcNAc motifs can mimic the phosphate group and create an anchoring point on the phospho-accepting pocket of 14-3-3 proteins (Toleman et al., 2018). Moreover, a recent study showed that O-GlcNAcylation of Tau can be performed *in vitro* and monitored in a residue specific way by NMR (Bourré et al., 2018). NMR studies with ¹⁵N labeled O-GlcNAcylated Tau in the presence of 14-3-3 would be a promising approach for identifying new epitopes of Tau for binding to 14-3-3. After exploring new phosphoepitopes and O-GlcNAcylated epitopes for binding to 14-3-3, it would be of great relevance to study the functional impact of these putative epitopes on the “14-3-3-induced aggregation” of Tau and on 14-3-3 mediated Tau cytotoxicity.

Taken into account that the first inhibitors of this interaction have already been produced (Andrei, Meijer, et al., 2018; Milroy et al., 2015) and that there is considerable structural information about this PPI, more efforts should be made towards the development of more potent and more selective small-molecule inhibitors. Given the poor PK profile conferred by the phosphate group, research should ideally be more directed to non-phosphate containing inhibitors. Moreover, successful compounds should be tested against other 14-3-3 complexes for selectivity. Another alternative is to target the 14-3-3/Tau PPI with nanobodies, also called variable heavy-chain domain (VHH) antibodies, which correspond to the antigen-binding fragment of heavy chain only antibodies. These nanobodies can be isolated from the Heavy-chain only antibodies contained in the sera of animals from the *camelidae* family (S. Muyldermans, 2001; Serge Muyldermans, 2013). Compared to monoclonal antibodies, VHH antibodies are smaller, more stable and therefore possess certain advantages from a PK point of view such as higher permeability of the blood-brain barrier (Jank et al., 2019). For these and other reasons VHH are seen as the new generation of biologics. Having this in mind, we have already initiated a collaboration with partners from the VIB institute in Brussels for the development of nanobodies that recognize selectively the 14-3-3/Tau complex. For this purpose, animals from the *camelidae* family were immunized with 14-3-3 σ in complex with the F1 fragment of Tau (an N-terminal truncated fragment containing

residues Q165-L441) phosphorylated by PKA. The nanobodies are currently being screened for their selectivity to the complex over the isolated proteins. We believe that if we identify selective nanobodies for this complex, they can be the basis of the development of interesting biological tools or even be starting points for the development of therapeutic biologics for AD.

The 14-3-3/p53 PPI

On the scope of a collaboration, we investigated why five p53 peptides of different lengths containing the pT387 epitope interacted with such different affinities with 14-3-3 despite the fact that all the peptides contained the essential residues for the interaction. Thanks to protein-observed and peptide-observed NMR experiments, we were able to confirm that the difference in affinity between the p53 peptides was related to the higher propensity of the peptide to adopt a turn conformation in solution. Our observations were further confirmed by MD simulations, which suggested that intramolecular interactions between the positively charged N-terminal residues of the peptide with the negatively charged C-terminal residues were promoting a turn conformation and enhancing the binding to 14-3-3.

Although the evidence from our NMR studies is supported by MD simulations, further experiments with a mutant peptide would clearly confirm our conclusions. In this case, the substitution of one of the N-terminal positively charged residues of the p53 peptide should cause a decrease in affinity for 14-3-3. It would also be interesting to study the impact of this intramolecular interaction in the activity of the full-length p53 protein in a cellular setting.

Screening and characterization of compounds targeting 14-3-3 or 14-3-3 PPIs

One of the central roles of this work was to find small-molecule starting points binding to 14-3-3 or complexes of 14-3-3 with target phosphopeptides/proteins with the potential to be optimized into selective modulators of 14-3-3 PPIs. In this context, we set-up the conditions for Ligand-based experiments, namely STD and WaterLOGSY, which allowed us to increase our screening throughput and provide us different information from Protein-based experiments. We have also applied our backbone assignment of 14-3-3 σ for screening, detecting binding sites and characterizing the binding of small-molecules to 14-3-3 or 14-3-3/phosphopeptide complexes.

Taros Chemicals, one of our partners from the TASPPI consortium set-up a library containing more than 1000 fragments with optimized chemical properties for PPI modulation. From this library, 785 were selected to be screened, in cocktails of 5, for binding to 14-3-3 σ . The fragments were primarily screened with DSF, and either WaterLOGSY or ^1H - ^{15}N TROSY HSQC. Cocktails containing hits were further screened with ^1H - ^{15}N TROSY HSQC and the individual fragments were finally confirmed by both WaterLOGSY and ^1H - ^{15}N TROSY HSQC. We found 3 fragments binding to different regions of the protein. Notably, ^1H - ^{15}N TROSY HSQC experiments showed that these fragments bind remotely from the amphipathic binding groove. This fact can constitute an opportunity to target selectively the interaction of 14-3-3 with partner proteins that interact with areas other than the binding groove. Initial future perspectives for this work might include X-ray crystallography studies for getting more detailed information of the binding site of these 3 fragments on 14-3-3 σ . This detailed structural information can then pave the way for the fragment elaboration step. Once more potent molecules are synthesized, they can be tested for the modulation of 14-3-3 PPIs with proteins binding remotely from the binding groove of 14-3-3.

Regarding other collaborations aiming the development of 14-3-3 PPI modulators, we screened and/or characterized the binding of several molecules to eight different 14-3-3 complexes. Apart from detecting the binding of several compounds and their respective binding sites using NMR, we were also able to access the inhibition (for the 14-3-3/Tau-PKA inhibition by peptidomimetic compounds) and also the stabilization of 14-3-3 PPIs (stabilization of 14-3-3/p65pS45 by FC-A and stabilization of 14-3-3/p53pT387 by a fragment). Future perspectives change according to the project. These might include, for example, X-ray crystallography studies for compounds that were not yet crystallized in complex with 14-3-3 or a 14-3-3/peptide complex. Other perspectives are the synthesis of analogs of the identified compounds in order to increase their potency and selectivity towards one particular 14-3-3 PPI. Other perspectives may include the screening and evaluation of the activity of the compounds against other 14-3-3 complexes. Successful compounds should also be tested in cellular assays for accessing the modulation of the PPIs in a physiological environment. Proximity Ligation assays (PLA) or Fluorescence Resonance Energy Transfer (FRET)

experiments would be good ways for accessing in a quantitative and specific manner the inhibition or stabilization of a 14-3-3 PPI in a cellular context.

Final remarks

As a general conclusion, during these three years we have applied several biophysical techniques, mostly NMR spectroscopy, to the study of 14-3-3 PPIs and to the discovery of modulators thereof. We have now more structural insights into the 14-3-3/Tau and 14-3-3/p53 PPIs and, together with our partners from the TASPPI consortium, we enriched the portfolio of small-molecules binding to 14-3-3 or 14-3-3 complexes. Undoubtedly, this work and the TASPPI consortium in general were a step further in the long path to find potent and selective stabilizers of 14-3-3 PPIs. Notably we contributed with structural information, biophysical assays and small-molecule starting points that can be used in the future for accomplishing the objective of having 14-3-3 PPI modulators as clinical candidates. The greatest challenge in the future will be the optimization of the compounds born in the TASPPI project towards potent and selective modulators of 14-3-3 PPIs. The road will be long, but we are definitely closer.

RÉSUMÉ SUBSTANTIEL EN FRANÇAIS

Les protéines 14-3-3 sont des protéines régulatrices qui lient des protéines phosphorylées. Ces protéines n'ont pas d'activité intrinsèque mais exercent leur fonction physiologique en se liant à d'autres protéines. En conséquence, les protéines cibles voient leur activité enzymatique, leur localisation cellulaire ou leur capacité à lier d'autres partenaires modulées. On connaît aujourd'hui plus de 800 partenaires des protéines 14-3-3. Grâce à ce grand nombre de partenaires, les protéines 14-3-3 ont une grande importance au niveau de la régulation de voies de signalisation cellulaires. Par conséquent, les protéines 14-3-3 sont liées à de nombreuses maladies comme la maladie d'Alzheimer, certains types de cancers ou la maladie de Parkinson. Dans ce contexte, la stabilisation ou l'inhibition sélective d'interactions protéine-protéine (IPP) de 14-3-3 sont considérées comme des approches prometteuses pour trouver des thérapies innovantes. L'objectif du projet de thèse est la découverte de petites molécules capables de stabiliser ou inhiber les interactions de 14-3-3 avec certains de ses partenaires. Pour atteindre cet objectif, il est nécessaire d'obtenir une caractérisation structurale détaillée pour les interactions concernées.

La première étape de notre travail a donc été l'étude, au niveau moléculaire, par Résonance magnétique nucléaire (RMN) des protéines 14-3-3. Les protéines 14-3-3 sont des protéines de grande taille dont l'étude a nécessité la mise en place d'une méthodologie adaptée. Nous avons ainsi attribué les déplacements chimiques des atomes du squelette de 14-3-3 σ . L'attribution de ce spectre RMN de 14-3-3 σ nous a permis d'étudier son interaction avec ses partenaires et avec des petites molécules.

Nous nous sommes tout particulièrement focalisés sur l'étude de l'interaction entre la protéine 14-3-3 et la protéine Tau. La protéine neuronale Tau est impliquée dans le développement de la maladie d'Alzheimer par des mécanismes moléculaires qu'il reste encore à éclaircir. Cette protéine Tau est le constituant majeur des agrégats fibrillaires observés dans les neurones qui vont graduellement envahir le cerveau au cours de la maladie. La protéine Tau présente dans ces agrégats est sous forme modifiée, hyperphosphorylée. D'autre part, des partenaires protéiques peuvent faciliter son agrégation. C'est le cas de la protéine 14-3-3 qui est associée à Tau dans les agrégats neurofibrillaires. Nous avons étudié cette interaction

et montré que Tau se lie strictement dans la cavité amphipathique de 14-3-3 et peut s'ancrer aux deux monomères du dimère de 14-3-3.

Nous avons aussi étudié l'interaction entre la protéine 14-3-3 et la protéine anti tumorale p53. L'interaction entre la protéine 14-3-3 et la région C-terminale de p53 phosphorylé en T387 permet de protéger p53 de la dégradation par MDM2 et par conséquent de préserver l'activité anti tumorale de p53. La stabilisation de l'interaction 14-3-3/p53 serait donc une approche thérapeutique prometteuse pour le traitement de cancers. Nous avons étudié les détails moléculaires de cette interaction et avons montré, en utilisant la RMN, que l'affinité du peptide p53 envers 14-3-3 est liée à des interactions intramoléculaires au niveau du peptide.

Nous nous sommes enfin focalisés, avec le soutien de nos partenaires universitaires et industriels Européens, sur l'optimisation d'expériences RMN visant le criblage et la caractérisation de l'activité de petites molécules qui se lient à 14-3-3 ou à des complexes de 14-3-3 avec des peptides phosphorylés. Nous avons mis en place les conditions nécessaires pour réaliser des expériences RMN de criblage primaire permettant l'obtention de résultats rapides, ainsi que des expériences de criblage secondaire permettant l'obtention de résultats plus robustes et l'identification du site d'interaction. Nous avons ainsi criblé une bibliothèque de fragments contre 14-3-3 σ et trouvé trois *hits* qui se lient à des régions différentes de la protéine. Des expériences RMN ont ensuite permis de caractériser l'activité de certaines petites molécules actives sur des complexes de 14-3-3 avec, par exemple des peptides de kinases, p53 ou p65. Nous avons aussi démontré la capacité de certains de ces composés à stabiliser les complexes 14-3-3/p53 et 14-3-3/p65, qui constituent des cibles thérapeutiques prometteuses pour le traitement du cancer et l'inflammation, respectivement. Nous avons également poursuivi une stratégie différente, basée sur l'activité de peptides phospho-mimétiques pour inhiber l'interaction 14-3-3/Tau, une cible prometteuse pour le traitement de la maladie d'Alzheimer.

Notre travail a permis de mieux comprendre les IPP 14-3-3/Tau et 14-3-3/p53 et d'augmenter le nombre de petites molécules capables de cibler 14-3-3 ou des complexes de 14-3-3 avec ses partenaires. Ces molécules peuvent maintenant être optimisées pour devenir plus puissantes et sélectives contre des complexes de 14-3-3 spécifiques.

REFERENCES

- Agarwal-Mawal, A., Qureshi, H. Y., Cafferty, P. W., Yuan, Z., Han, D., Lin, R., & Paudel, H. K. (2003). 14-3-3 Connects Glycogen Synthase Kinase-3 to Tau within a Brain Microtubule-associated Tau Phosphorylation Complex. *Journal of Biological Chemistry*, *278*(15), 12722–12728. <https://doi.org/10.1074/jbc.M211491200>
- Agrawal, P. (2014). NMR Spectroscopy in Drug Discovery and Development. *Materials and Methods*, *4*. <https://doi.org/10.13070/mm.en.4.599>
- Aguilera, C., Fernández-Majada, V., Inglés-Esteve, J., Rodilla, V., Bigas, A., & Espinosa, L. (2006). Efficient nuclear export of p65-IkBa complexes requires 14-3-3 proteins. *Journal of Cell Science*, *119*(17), 3695–3704. <https://doi.org/10.1242/jcs.03086>
- Aguirre, C., Cala, O., & Krimm, I. (2015). Overview of Probing Protein-Ligand Interactions Using NMR. *Current Protocols in Protein Science*, *81*, 17.18.1-24. <https://doi.org/10.1002/0471140864.ps1718s81>
- Alblova, M., Smidova, A., Docekal, V., Vesely, J., Herman, P., Obsilova, V., & Obsil, T. (2017). Molecular basis of the 14-3-3 protein-dependent activation of yeast neutral trehalase Nth1. *Proceedings of the National Academy of Sciences of the United States of America*, *114*(46), E9811–E9820. <https://doi.org/10.1073/pnas.1714491114>
- Anders, C., Higuchi, Y., Koschinsky, K., Bartel, M., Schumacher, B., Thiel, P., ... Ottmann, C. (2013). A Semisynthetic Fusicoccane Stabilizes a Protein-Protein Interaction and Enhances the Expression of K⁺ Channels at the Cell Surface. *Chemistry & Biology*, *20*(4), 583–593. <https://doi.org/10.1016/j.chembiol.2013.03.015>
- Andrei, S. A., de Vink, P., Sijbesma, E., Han, L., Brunsveld, L., Kato, N., ... Higuchi, Y. (2018). Rationally Designed Semisynthetic Natural Product Analogues for Stabilization of 14-

- 3-3 Protein-Protein Interactions. *Angewandte Chemie International Edition*, 57(41), 13470–13474. <https://doi.org/10.1002/anie.201806584>
- Andrei, S. A., Meijer, F. A., Neves, J. F., Brunsveld, L., Landrieu, I., Ottmann, C., & Milroy, L.-G. (2018). Inhibition of 14-3-3/Tau by Hybrid Small-Molecule Peptides Operating via Two Different Binding Modes. *ACS Chemical Neuroscience*, 9(11), 2639–2654. <https://doi.org/10.1021/acschemneuro.8b00118>
- Angulo, J., Enríquez-Navas, P. M., & Nieto, P. M. (2010). Ligand-Receptor Binding Affinities from Saturation Transfer Difference (STD) NMR Spectroscopy: The Binding Isotherm of STD Initial Growth Rates. *Chemistry - A European Journal*, 16(26), 7803–7812. <https://doi.org/10.1002/chem.200903528>
- Antanasijevic, A., Ramirez, B., & Caffrey, M. (2014). Comparison of the sensitivities of WaterLOGSY and saturation transfer difference NMR experiments. *Journal of Biomolecular NMR*, 60(1), 37–44. <https://doi.org/10.1007/s10858-014-9848-9>
- Bahrami, A., Assadi, A. H., Markley, J. L., & Eghbalnia, H. R. (2009). Probabilistic Interaction Network of Evidence Algorithm and its Application to Complete Labeling of Peak Lists from Protein NMR Spectroscopy. *PLOS Computational Biology*, 5(3), e1000307. <https://doi.org/10.1371/journal.pcbi.1000307>
- Bai, N., Roder, H., Dickson, A., & Karanicolas, J. (2019). Isothermal Analysis of ThermoFluor Data can readily provide Quantitative Binding Affinities. *Scientific Reports*, 9(1), 2650. <https://doi.org/10.1038/s41598-018-37072-x>
- Bakota, L., & Brandt, R. (2016). Tau Biology and Tau-Directed Therapies for Alzheimer's Disease. *Drugs*, 76, 301–313. <https://doi.org/10.1007/s40265-015-0529-0>

- Ballone, A., Centorrino, F., & Ottmann, C. (2018). 14-3-3: A Case Study in PPI Modulation. *Molecules*, *23*(6), 1386. <https://doi.org/10.3390/molecules23061386>
- Barber, K. W., Muir, P., Szeligowski, R. V., Rogulina, S., Gerstein, M., Sampson, J. R., ... Rinehart, J. (2018). Encoding human serine phosphopeptides in bacteria for proteome-wide identification of phosphorylation-dependent interactions. *Nature Biotechnology*, *36*(7), 638–644. <https://doi.org/10.1038/nbt.4150>
- Barile, E., & Pellecchia, M. (2014). NMR-Based Approaches for the Identification and Optimization of Inhibitors of Protein–Protein Interactions. *Chemical Reviews*, *114*(9), 4749–4763. <https://doi.org/10.1021/cr500043b>
- Barnes, J., Dickerson, B., Frost, C., Jiskoot, L. C., Wolk, D., & van der Flier, W. M. (2015). Alzheimer’s disease first symptoms are age dependent: Evidence from the NACC dataset. *Alzheimer’s & Dementia : The Journal of the Alzheimer’s Association*, *11*(11), 1349–1357. <https://doi.org/10.1016/j.jalz.2014.12.007>
- Becker, W., Bhattiprolu, K. C., Gubensäk, N., & Zangger, K. (2018). Investigating Protein–Ligand Interactions by Solution Nuclear Magnetic Resonance Spectroscopy. *Chemphyschem*, *19*(8), 895–906. <https://doi.org/10.1002/cphc.201701253>
- Begley, D. W., Moen, S. O., Pierce, P. G., & Zartler, E. R. (2013). Saturation Transfer Difference NMR for Fragment Screening. *Current Protocols in Chemical Biology*, *5*(2), 251–268. <https://doi.org/10.1002/9780470559277.ch130118>
- Benzinger, A., Popowicz, G. M., Joy, J. K., Majumdar, S., Holak, T. A., & Hermeking, H. (2005). The crystal structure of the non-liganded 14-3-3 [sigma] protein: Insights into determinants of isoform specific ligand binding and dimerization. *Cell Research*, *15*(4), 219.

- Bergsdorf, C., & Wright, S. K. (2018). Chapter Seven—A Guide to Run Affinity Screens Using Differential Scanning Fluorimetry and Surface Plasmon Resonance Assays. In C. A. Lesburg (Ed.), *Methods in Enzymology* (pp. 135–165). <https://doi.org/10.1016/bs.mie.2018.09.015>
- Bibow, S., Ozenne, V., Biernat, J., Blackledge, M., Mandelkow, E., & Zweckstetter, M. (2011). Structural Impact of Proline-Directed Pseudophosphorylation at AT8, AT100, and PHF1 Epitopes on 441-Residue Tau. *Journal of the American Chemical Society*, *133*(40), 15842–15845. <https://doi.org/10.1021/ja205836j>
- Bier, D., Mittal, S., Bravo-Rodriguez, K., Sowislok, A., Guillory, X., Briels, J., ... Ottmann, C. (2017). The Molecular Tweezer CLR01 Stabilizes a Disordered Protein–Protein Interface. *Journal of the American Chemical Society*, *139*(45), 16256–16263. <https://doi.org/10.1021/jacs.7b07939>
- Bier, D., Rose, R., Bravo-Rodriguez, K., Bartel, M., Ramirez-Anguila, J. M., Dutt, S., ... Ottmann, C. (2013). Molecular tweezers modulate 14-3-3 protein–protein interactions. *Nature Chemistry*, *5*(3), 234–239. <https://doi.org/10.1038/nchem.1570>
- Bourré, G., Cantrelle, F.-X., Kamah, A., Chambraud, B., Landrieu, I., & Smet-Nocca, C. (2018). Direct Crosstalk Between O-GlcNAcylation and Phosphorylation of Tau Protein Investigated by NMR Spectroscopy. *Frontiers in Endocrinology*, *9*. <https://doi.org/10.3389/fendo.2018.00595>
- Brautigam, C. A. (2015). Chapter Five: Calculations and Publication-Quality Illustrations for Analytical Ultracentrifugation Data. In J. L. Cole (Ed.), *Methods in Enzymology* (pp. 109–133). <https://doi.org/10.1016/bs.mie.2015.05.001>

- Brion, J. P., Flament-Durand, J., & Dustin, P. (1986). Alzheimer's disease and tau proteins. *Lancet (London, England)*, 2(8515), 1098. [https://doi.org/10.1016/s0140-6736\(86\)90495-2](https://doi.org/10.1016/s0140-6736(86)90495-2)
- Brummer, T., Larance, M., Abreu, M. T. H., Lyons, R. J., Timpson, P., Emmerich, C. H., ... Daly, R. J. (2008). Phosphorylation-dependent binding of 14-3-3 terminates signalling by the Gab2 docking protein. *The EMBO Journal*, 27(17), 2305–2316. <https://doi.org/10.1038/emboj.2008.159>
- Buée, L., Bussièrè, T., Buée-Scherrer, V., Delacourte, A., & Hof, P. R. (2000). Tau protein isoforms, phosphorylation and role in neurodegenerative disorders¹¹These authors contributed equally to this work. *Brain Research Reviews*, 33(1), 95–130. [https://doi.org/10.1016/S0165-0173\(00\)00019-9](https://doi.org/10.1016/S0165-0173(00)00019-9)
- Burnouf, S., Martire, A., Derisbourg, M., Laurent, C., Belarbi, K., Leboucher, A., ... Blum, D. (2013). NMDA receptor dysfunction contributes to impaired brain-derived neurotrophic factor-induced facilitation of hippocampal synaptic transmission in a Tau transgenic model. *Aging Cell*, 12(1), 11–23. <https://doi.org/10.1111/accel.12018>
- B.W. Moore, & V. J. Perez. (1967). Specific acidic proteins of the nervous system. In *Physiological and Biochemical Aspects of Nervous Intergration* (F.D. Carlson, pp. 343–359). MA: Prentice-Hall, Woods Hole.
- Cala, O., & Krimm, I. (2015). Ligand-Orientation Based Fragment Selection in STD NMR Screening. *Journal of Medicinal Chemistry*, 58(21), 8739–8742. <https://doi.org/10.1021/acs.jmedchem.5b01114>
- Cavanagh, J., Fairbrother, W. J., III, A. G. P., Skelton, N. J., & Rance, M. (2010). *Protein NMR Spectroscopy: Principles and Practice*. Elsevier.

- Chen, J., Kanai, Y., Cowan, N. J., & Hirokawa, N. (1992). Projection domains of MAP2 and tau determine spacings between microtubules in dendrites and axons. *Nature*, *360*(6405), 674–677. <https://doi.org/10.1038/360674a0>
- Chirita, C. N., Congdon, E. E., Yin, H., & Kuret, J. (2005). Triggers of Full-Length Tau Aggregation: A Role for Partially Folded Intermediates. *Biochemistry*, *44*(15), 5862–5872. <https://doi.org/10.1021/bi0500123>
- Chow, M. L., Troussicot, L., Martin, M., Doumèche, B., Guillière, F., & Lancelin, J.-M. (2016). Predicting and Understanding the Enzymatic Inhibition of Human Peroxiredoxin 5 by 4-Substituted Pyrocatechols by Combining Funnel Metadynamics, Solution NMR, and Steady-State Kinetics. *Biochemistry*, *55*(24), 3469–3480. <https://doi.org/10.1021/acs.biochem.6b00367>
- Cimpmperman, P., Baranauskienė, L., Jachimovičiūtė, S., Jachno, J., Torresan, J., Michailovienė, V., ... Matulis, D. (2008). A Quantitative Model of Thermal Stabilization and Destabilization of Proteins by Ligands. *Biophysical Journal*, *95*(7), 3222–3231. <https://doi.org/10.1529/biophysj.108.134973>
- Ciulli, A. (2013). Biophysical Screening for the Discovery of Small-Molecule Ligands. *Methods in Molecular Biology (Clifton, N.J.)*, *1008*, 357–388. https://doi.org/10.1007/978-1-62703-398-5_13
- Coblitz, B., Wu, M., Shikano, S., & Li, M. (2006). C-terminal binding: An expanded repertoire and function of 14-3-3 proteins. *FEBS Letters*, *580*(6), 1531–1535. <https://doi.org/10.1016/j.febslet.2006.02.014>

- Cole, J. L., Lary, J. W., Moody, T., & Laue, T. M. (2008). Analytical Ultracentrifugation: Sedimentation Velocity and Sedimentation Equilibrium. *Methods in Cell Biology*, *84*, 143–179. [https://doi.org/10.1016/S0091-679X\(07\)84006-4](https://doi.org/10.1016/S0091-679X(07)84006-4)
- Congreve, M., Carr, R., Murray, C., & Jhoti, H. (2003). A ‘Rule of Three’ for fragment-based lead discovery? *Drug Discovery Today*, *8*(19), 876–877. [https://doi.org/10.1016/S1359-6446\(03\)02831-9](https://doi.org/10.1016/S1359-6446(03)02831-9)
- Corradi, V., Mancini, M., Manetti, F., Petta, S., Santucci, M. A., & Botta, M. (2010). Identification of the first non-peptidic small molecule inhibitor of the c-Abl/14-3-3 protein–protein interactions able to drive sensitive and Imatinib-resistant leukemia cells to apoptosis. *Bioorganic & Medicinal Chemistry Letters*, *20*(20), 6133–6137. <https://doi.org/10.1016/j.bmcl.2010.08.019>
- Corradi, V., Mancini, M., Santucci, M. A., Carlomagno, T., Sanfelice, D., Mori, M., ... Botta, M. (2011). Computational techniques are valuable tools for the discovery of protein–protein interaction inhibitors: The 14-3-3 σ case. *Bioorganic & Medicinal Chemistry Letters*, *21*(22), 6867–6871. <https://doi.org/10.1016/j.bmcl.2011.09.011>
- Crowther, R. A. (1991). Straight and paired helical filaments in Alzheimer disease have a common structural unit. *Proceedings of the National Academy of Sciences of the United States of America*, *88*(6), 2288–2292.
- Cummings, J., Lee, G., Ritter, A., & Zhong, K. (2018). Alzheimer’s disease drug development pipeline: 2018. *Alzheimer’s & Dementia: Translational Research & Clinical Interventions*, *4*, 195–214. <https://doi.org/10.1016/j.trci.2018.03.009>

- Dalvit, C., Caronni, D., Mongelli, N., Veronesi, M., & Vulpetti, A. (2006). NMR-based quality control approach for the identification of false positives and false negatives in high throughput screening. *Current Drug Discovery Technologies*, 3(2), 115–124.
- Dalvit, C., & Dalvit, C. (2003). *World Intellectual Property Organization Patent No. WO2003104824A2*. Retrieved from <https://patents.google.com/patent/WO2003104824A2/en>
- Dalvit, C., Fagerness, P. E., Hadden, D. T. A., Sarver, R. W., & Stockman, B. J. (2003). Fluorine-NMR experiments for high-throughput screening: Theoretical aspects, practical considerations, and range of applicability. *Journal of the American Chemical Society*, 125(25), 7696–7703. <https://doi.org/10.1021/ja034646d>
- Dalvit, C., Fogliatto, G., Stewart, A., & Veronesi, M. (2001). *WaterLOGSY as a method for primary NMR screening: Practical aspects and range of applicability*. 21(4), 349–359.
- Dalvit, C., & Vulpetti, A. (2019). Ligand-Based Fluorine NMR Screening: Principles and Applications in Drug Discovery Projects. *Journal of Medicinal Chemistry*, 62(5), 2218–2244. <https://doi.org/10.1021/acs.jmedchem.8b01210>
- Dam, J., Velikovskiy, C. A., Mariuzza, R. A., Urbanke, C., & Schuck, P. (2005). Sedimentation Velocity Analysis of Heterogeneous Protein-Protein Interactions: Lamm Equation Modeling and Sedimentation Coefficient Distributions $c(s)$. *Biophysical Journal*, 89(1), 619–634. <https://doi.org/10.1529/biophysj.105.059568>
- Danis, C., Despres, C., Bessa, L. M., Malki, I., Merzougui, H., Huvent, I., ... Landrieu, I. (2016). Nuclear Magnetic Resonance Spectroscopy for the Identification of Multiple Phosphorylations of Intrinsically Disordered Proteins. *JoVE (Journal of Visualized Experiments)*, (118), e55001. <https://doi.org/10.3791/55001>

- Davare, M. A., Saneyoshi, T., Guire, E. S., Nygaard, S. C., & Soderling, T. R. (2004). Inhibition of calcium/calmodulin-dependent protein kinase kinase by protein 14-3-3. *The Journal of Biological Chemistry*, *279*(50), 52191–52199. <https://doi.org/10.1074/jbc.M409873200>
- De Vries-van Leeuwen, I. J., da Costa Pereira, D., Flach, K. D., Piersma, S. R., Haase, C., Bier, D., ... de Boer, A. H. (2013). Interaction of 14-3-3 proteins with the Estrogen Receptor Alpha F domain provides a drug target interface. *Proceedings of the National Academy of Sciences*, *110*(22), 8894–8899. <https://doi.org/10.1073/pnas.1220809110>
- Derome, A. E. (Ed.). (1987). Chapter 5: The Nuclear Overhauser Effect. In *Tetrahedron Organic Chemistry Series* (pp. 97–127). <https://doi.org/10.1016/B978-0-08-032513-2.50012-7>
- Dias, D. M., Van Molle, I., Baud, M. G. J., Galdeano, C., Geraldès, C. F. G. C., & Ciulli, A. (2014). Is NMR Fragment Screening Fine-Tuned to Assess Druggability of Protein–Protein Interactions? *ACS Medicinal Chemistry Letters*, *5*(1), 23–28. <https://doi.org/10.1021/ml400296c>
- Doveston, R. G., Kuusk, A., Andrei, S. A., Leysen, S., Cao, Q., Castaldi, M. P., ... Ottmann, C. (2017). Small-molecule stabilization of the p53–14-3-3 protein-protein interaction. *FEBS Letters*, *591*(16), 2449–2457. <https://doi.org/10.1002/1873-3468.12723>
- Erlanson, D. (2016, October 3). Practical Fragments: Poll results: affiliation, metrics, and fragment-finding methods. Retrieved 16 May 2019, from Practical Fragments website: <http://practicalfragments.blogspot.com/2016/10/poll-results-affiliation-metrics-and.html>

- Fertalova, T., & Ondrioiva, I. (2019). Non-pharmacological Treatment of Alzheimer's. *Redirecting Alzheimer Strategy - Tracing Memory Loss to Self Pathology*.
<https://doi.org/10.5772/intechopen.84893>
- Fielding, L. (2007). NMR methods for the determination of protein–ligand dissociation constants. *Progress in Nuclear Magnetic Resonance Spectroscopy*, 51(4), 219–242.
<https://doi.org/10.1016/j.pnmrs.2007.04.001>
- Fischer, M., Leech, A. P., & Hubbard, R. E. (2011). Comparative assessment of different histidine-tags for immobilization of protein onto surface plasmon resonance sensorchips. *Analytical Chemistry*, 83(5), 1800–1807.
<https://doi.org/10.1021/ac103168q>
- Fitzpatrick, A. W. P., Falcon, B., He, S., Murzin, A. G., Murshudov, G., Garringer, H. J., ... Scheres, S. H. W. (2017). Cryo-EM structures of tau filaments from Alzheimer's disease. *Nature*, 547(7662), 185–190. <https://doi.org/10.1038/nature23002>
- Freed-Pastor, W. A., & Prives, C. (2012). Mutant p53: One name, many proteins. *Genes & Development*, 26(12), 1268–1286. <https://doi.org/10.1101/gad.190678.112>
- Frost, B., Hemberg, M., Lewis, J., & Feany, M. B. (2014). Tau promotes neurodegeneration through global chromatin relaxation. *Nature Neuroscience*, 17(3), 357–366.
<https://doi.org/10.1038/nn.3639>
- Frueh, D. P. (2014). Practical aspects of NMR signal assignment in larger and challenging proteins. *Progress in Nuclear Magnetic Resonance Spectroscopy*, 0, 47–75.
<https://doi.org/10.1016/j.pnmrs.2013.12.001>

- Fu, H., Coburn, J., & Collier, R. J. (1993). The Eukaryotic Host Factor that Activates Exoenzyme S of *Pseudomonas aeruginosa* is a Member of the 14-3-3 Protein Family. *Proceedings of the National Academy of Sciences of the United States of America*, *90*(6), 2320–2324.
- Fu, H., Subramanian, R. R., & Masters, S. C. (2000). 14-3-3 proteins: Structure, function, and regulation. *Annual Review of Pharmacology and Toxicology*, *40*(1), 617–647.
- Ganguly, S., Weller, J. L., Ho, A., Chemineau, P., Malpoux, B., & Klein, D. C. (2005). Melatonin synthesis: 14-3-3-dependent activation and inhibition of arylalkylamine N-acetyltransferase mediated by phosphoserine-205. *Proceedings of the National Academy of Sciences*, *102*(4), 1222–1227. <https://doi.org/10.1073/pnas.0406871102>
- Gardner, K. H., & Kay, L. E. (1998). The use of ²H, ¹³C, ¹⁵N multidimensional NMR to study the structure and dynamics of proteins. *Annual Review of Biophysics and Biomolecular Structure*, *27*, 357–406. <https://doi.org/10.1146/annurev.biophys.27.1.357>
- Gibbs, E. B., Cook, E. C., & Showalter, S. A. (2017). Application of NMR to studies of intrinsically disordered proteins. *Archives of Biochemistry and Biophysics*, *628*, 57–70. <https://doi.org/10.1016/j.abb.2017.05.008>
- Gigante, A., Grad, J.-N., Briels, J., Bartel, M., Hoffmann, D., Ottmann, C., & Schmuck, C. (2019). A new class of supramolecular ligands stabilizes 14-3-3 protein–protein interactions by up to two orders of magnitude. *Chemical Communications*, *55*(1), 111–114. <https://doi.org/10.1039/C8CC07946C>
- Glas, A., Bier, D., Hahne, G., Rademacher, C., Ottmann, C., & Grossmann, T. N. (2014). Constrained Peptides with Target-Adapted Cross-Links as Inhibitors of a Pathogenic Protein–Protein Interaction. *Angewandte Chemie International Edition*, *53*(9), 2489–2493. <https://doi.org/10.1002/anie.201310082>

- Goldman, E. H., Chen, L., & Fu, H. (2004). Activation of apoptosis signal-regulating kinase 1 by reactive oxygen species through dephosphorylation at serine 967 and 14-3-3 dissociation. *The Journal of Biological Chemistry*, 279(11), 10442–10449. <https://doi.org/10.1074/jbc.M311129200>
- Gorania, M., Seker, H., & Haris, P. I. (2010). Predicting a protein's melting temperature from its amino acid sequence. *Conference Proceedings: ... Annual International Conference of the IEEE Engineering in Medicine and Biology Society. IEEE Engineering in Medicine and Biology Society. Annual Conference, 2010*, 1820–1823. <https://doi.org/10.1109/IEMBS.2010.5626421>
- Gossert, A. D., & Jahnke, W. (2016). NMR in drug discovery: A practical guide to identification and validation of ligands interacting with biological macromolecules. *Progress in Nuclear Magnetic Resonance Spectroscopy*, 97, 82–125. <https://doi.org/10.1016/j.pnmrs.2016.09.001>
- Grundke-Iqbal, I., Iqbal, K., Tung, Y. C., Quinlan, M., Wisniewski, H. M., & Binder, L. I. (1986). Abnormal phosphorylation of the microtubule-associated protein tau (tau) in Alzheimer cytoskeletal pathology. *Proceedings of the National Academy of Sciences*, 83(13), 4913–4917. <https://doi.org/10.1073/pnas.83.13.4913>
- Guo, T., Noble, W., & Hanger, D. P. (2017). Roles of tau protein in health and disease. *Acta Neuropathologica*, 133(5), 665–704. <https://doi.org/10.1007/s00401-017-1707-9>
- Hafsa, N. E., Arndt, D., & Wishart, D. S. (2015). CSI 3.0: A web server for identifying secondary and super-secondary structure in proteins using NMR chemical shifts. *Nucleic Acids Research*, 43(W1), W370-377. <https://doi.org/10.1093/nar/gkv494>

- Hajduk, P. J. (2006). SAR by NMR: Putting the pieces together. *Molecular Interventions*, 6(5), 266–272. <https://doi.org/10.1124/mi.6.5.8>
- Hajduk, P. J., Augeri, D. J., Mack, J., Mendoza, R., Yang, J., Betz, S. F., & Fesik, S. W. (2000). NMR-Based Screening of Proteins Containing ¹³C-Labeled Methyl Groups. *Journal of the American Chemical Society*, 122(33), 7898–7904. <https://doi.org/10.1021/ja000350l>
- Hajduk, P. J., Meadows, R. P., & Fesik, S. W. (1997). Discovering High-Affinity Ligands for Proteins. *Science*, 278(5337), 497–499. <https://doi.org/10.1126/science.278.5337.497>
- Hamdane, M., Bretteville, A., Sambo, A.-V., Schindowski, K., Bégard, S., Delacourte, A., ... Buée, L. (2005). P25/Cdk5-mediated retinoblastoma phosphorylation is an early event in neuronal cell death. *Journal of Cell Science*, 118(6), 1291–1298. <https://doi.org/10.1242/jcs.01724>
- Hanseeuw, B. J., Betensky, R. A., Jacobs, H. I. L., Schultz, A. P., Sepulcre, J., Becker, J. A., ... Johnson, K. (2019). Association of Amyloid and Tau With Cognition in Preclinical Alzheimer Disease: A Longitudinal Study. *JAMA Neurology*. <https://doi.org/10.1001/jamaneurol.2019.1424>
- Harding, S. E. (1993). Analytical Ultracentrifugation and the Genetic Engineering of Macromolecules. *Biotechnology and Genetic Engineering Reviews*, 11(1), 317–356. <https://doi.org/10.1080/02648725.1993.10647905>
- Harding, S. E., & Rowe, A. J. (2010). Insight into protein–protein interactions from analytical ultracentrifugation. *Biochemical Society Transactions*, 38(4), 901–907. <https://doi.org/10.1042/BST0380901>

- Haribabu, B., Hook, S. S., Selbert, M. A., Goldstein, E. G., Tomhave, E. D., Edelman, A. M., ... Means, A. R. (1995). Human calcium-calmodulin dependent protein kinase I: CDNA cloning, domain structure and activation by phosphorylation at threonine-177 by calcium-calmodulin dependent protein kinase I kinase. *The EMBO Journal*, *14*(15), 3679–3686.
- Harner, M. J., Frank, A. O., & Fesik, S. W. (2013). Fragment-based drug discovery using NMR spectroscopy. *Journal of Biomolecular NMR*, *56*(2), 65–75.
<https://doi.org/10.1007/s10858-013-9740-z>
- Hasegawa, M. (2016). Molecular Mechanisms in the Pathogenesis of Alzheimer's disease and Tauopathies-Prion-Like Seeded Aggregation and Phosphorylation. *Biomolecules*, *6*(2), 24. <https://doi.org/10.3390/biom6020024>
- Hashiguchi, M., Sobue, K., & Paudel, H. K. (2000). 14-3-3 ζ Is an Effector of Tau Protein Phosphorylation. *Journal of Biological Chemistry*, *275*(33), 25247–25254.
<https://doi.org/10.1074/jbc.M003738200>
- Hermeking, H. (2003). The 14-3-3 cancer connection. *Nature Reviews Cancer*, *3*(12), 931–943.
<https://doi.org/10.1038/nrc1230>
- Hernández, F., Cuadros, R., & Avila, J. (2004). Zeta 14-3-3 protein favours the formation of human tau fibrillar polymers. *Neuroscience Letters*, *357*(2), 143–146.
<https://doi.org/10.1016/j.neulet.2003.12.049>
- Hippius, H., & Neundörfer, G. (2003). The discovery of Alzheimer's disease. *Dialogues in Clinical Neuroscience*, *5*(1), 101–108.
- Hirata, S., Marotta, A., Gui, Y., Hanami, K., & Tanaka, Y. (2015). Serum 14-3-3 η level is associated with severity and clinical outcomes of rheumatoid arthritis, and its

- pretreatment level is predictive of DAS28 remission with tocilizumab. *Arthritis Research & Therapy*, 17, 280. <https://doi.org/10.1186/s13075-015-0799-7>
- Howard, S., Abell, C., & Royal Society of Chemistry (Great Britain) (Eds.). (2015). *Fragment-based drug discovery*. Cambridge: Royal Society of Chemistry.
- Huth, J. R., Park, C., Petros, A. M., Kunzer, A. R., Wendt, M. D., Wang, X., ... Hajduk, P. J. (2007). Discovery and Design of Novel HSP90 Inhibitors Using Multiple Fragment-based Design Strategies. *Chemical Biology & Drug Design*, 70(1), 1–12. <https://doi.org/10.1111/j.1747-0285.2007.00535.x>
- Huxford, T., & Ghosh, G. (2009). A Structural Guide to Proteins of the NF- κ B Signaling Module. *Cold Spring Harbor Perspectives in Biology*, 1(3). <https://doi.org/10.1101/cshperspect.a000075>
- Ichimura, T., Taoka, M., Hozumi, Y., Goto, K., & Tokumitsu, H. (2008). 14-3-3 Proteins directly regulate Ca(2+)/calmodulin-dependent protein kinase kinase alpha through phosphorylation-dependent multisite binding. *FEBS Letters*, 582(5), 661–665. <https://doi.org/10.1016/j.febslet.2008.01.037>
- Inglés-Esteve, J., Morales, M., Dalmases, A., Garcia-Carbonell, R., Jené-Sanz, A., López-Bigas, N., ... Espinosa, L. (2012). Inhibition of Specific NF- κ B Activity Contributes to the Tumor Suppressor Function of 14-3-3 σ in Breast Cancer. *PLOS ONE*, 7(5), e38347. <https://doi.org/10.1371/journal.pone.0038347>
- Iralde-Lorente, L., Cau, Y., Clementi, L., Franci, L., Tassone, G., Valensin, D., ... Botta, M. (2019). Chemically stable inhibitors of 14-3-3 protein–protein interactions derived from BV02. *Journal of Enzyme Inhibition and Medicinal Chemistry*, 34(1), 657–664. <https://doi.org/10.1080/14756366.2019.1574779>

- Jadhav, S., Avila, J., Schöll, M., Kovacs, G. G., Kövari, E., Skrabana, R., ... Zilka, N. (2019). A walk through tau therapeutic strategies. *Acta Neuropathologica Communications*, 7(1), 22. <https://doi.org/10.1186/s40478-019-0664-z>
- Jahnke, W., Rüdiger, S., & Zurini, M. (2001). Spin Label Enhanced NMR Screening. *Journal of the American Chemical Society*, 123(13), 3149–3150. <https://doi.org/10.1021/ja005836g>
- James Chou. (2008). *Introduction to Protein NMR Spectroscopy*. Presented at the Harvard University. Harvard University.
- Jank, L., Pinto-Espinoza, C., Duan, Y., Koch-Nolte, F., Magnus, T., & Rissiek, B. (2019). Current Approaches and Future Perspectives for Nanobodies in Stroke Diagnostic and Therapy. *Antibodies*, 8(1), 5. <https://doi.org/10.3390/antib8010005>
- Jin, M., Shepardson, N., Yang, T., Chen, G., Walsh, D., & Selkoe, D. J. (2011). Soluble amyloid beta-protein dimers isolated from Alzheimer cortex directly induce Tau hyperphosphorylation and neuritic degeneration. *Proceedings of the National Academy of Sciences of the United States of America*, 108(14), 5819–5824. <https://doi.org/10.1073/pnas.1017033108>
- Joo, Y., Schumacher, B., Landrieu, I., Bartel, M., Smet-Nocca, C., Jang, A., ... Suh, Y.-H. (2015). Involvement of 14-3-3 in tubulin instability and impaired axon development is mediated by Tau. *The FASEB Journal*, 29(10), 4133–4144. <https://doi.org/10.1096/fj.14-265009>
- Jung, Y.-S., & Zweckstetter, M. (2004). Mars—Robust automatic backbone assignment of proteins. *Journal of Biomolecular NMR*, 30(1), 11–23. <https://doi.org/10.1023/B:JNMR.0000042954.99056.ad>

- Kaiser, M., & Ottmann, C. (2010). The First Small-Molecule Inhibitor of 14-3-3s: Modulating the Master Regulator. *ChemBioChem*, *11*(15), 2085–2087. <https://doi.org/10.1002/cbic.201000483>
- Kaplan, A., Morquette, B., Kroner, A., Leong, S., Madwar, C., Sanz, R., ... Fournier, A. E. (2017). Small-Molecule Stabilization of 14-3-3 Protein-Protein Interactions Stimulates Axon Regeneration. *Neuron*, *93*(5), 1082-1093.e5. <https://doi.org/10.1016/j.neuron.2017.02.018>
- Kaplan, A., Ottmann, C., & Fournier, A. E. (2017). 14-3-3 adaptor protein-protein interactions as therapeutic targets for CNS diseases. *Pharmacological Research*, *125*, 114–121. <https://doi.org/10.1016/j.phrs.2017.09.007>
- Kawarazaki, Y., Ichijo, H., & Naguro, I. (2014). Apoptosis signal-regulating kinase 1 as a therapeutic target. *Expert Opinion on Therapeutic Targets*, *18*(6), 651–664. <https://doi.org/10.1517/14728222.2014.896903>
- Kemp, B. E., Graves, D. J., Benjamini, E., & Krebs, E. G. (1977). Role of multiple basic residues in determining the substrate specificity of cyclic AMP-dependent protein kinase. *The Journal of Biological Chemistry*, *252*(14), 4888–4894.
- Kerfah, R., Plevin, M. J., Sounier, R., Gans, P., & Boisbouvier, J. (2015). Methyl-specific isotopic labeling: A molecular tool box for solution NMR studies of large proteins. *Current Opinion in Structural Biology*, *32*, 113–122. <https://doi.org/10.1016/j.sbi.2015.03.009>
- Kidd, M. (1963). Paired Helical Filaments in Electron Microscopy of Alzheimer's Disease. *Nature*, *197*(4863), 192. <https://doi.org/10.1038/197192b0>

- Killoran, R. C., Fan, J., Yang, D., Shilton, B. H., & Choy, W.-Y. (2015). Structural Analysis of the 14-3-3 ζ /Chibby Interaction Involved in Wnt/ β -Catenin Signaling. *PLOS ONE*, *10*(4), e0123934. <https://doi.org/10.1371/journal.pone.0123934>
- Kim, Y., Kim, H., Jang, S.-W., & Ko, J. (2011). The role of 14-3-3 β in transcriptional activation of estrogen receptor α and its involvement in proliferation of breast cancer cells. *Biochemical and Biophysical Research Communications*, *414*(1), 199–204. <https://doi.org/10.1016/j.bbrc.2011.09.056>
- Kolarova, M., García-Sierra, F., Bartos, A., Ricny, J., & Ripova, D. (2012). Structure and Pathology of Tau Protein in Alzheimer Disease. *International Journal of Alzheimer's Disease*, *2012*, 1–13. <https://doi.org/10.1155/2012/731526>
- Kosek, D., Kylarova, S., Psenakova, K., Rezabkova, L., Herman, P., Vecer, J., ... Obsil, T. (2014). Biophysical and Structural Characterization of the Thioredoxin-binding Domain of Protein Kinase ASK1 and Its Interaction with Reduced Thioredoxin. *Journal of Biological Chemistry*, *289*(35), 24463–24474. <https://doi.org/10.1074/jbc.M114.583807>
- Kranz, J. K., & Schalk-Hihi, C. (2011). Protein thermal shifts to identify low molecular weight fragments. *Methods in Enzymology*, *493*, 277–298. <https://doi.org/10.1016/B978-0-12-381274-2.00011-X>
- Krishnan, V. V. (2005). Ligand screening by saturation-transfer difference (STD) NMR spectroscopy. *Current Analytical Chemistry*, *1*(3), 307–320.
- Krüger, D. M., Glas, A., Bier, D., Pospiech, N., Wallraven, K., Dietrich, L., ... Grossmann, T. N. (2017). Structure-Based Design of Non-natural Macrocyclic Peptides That Inhibit Protein–Protein Interactions. *Journal of Medicinal Chemistry*, *60*(21), 8982–8988. <https://doi.org/10.1021/acs.jmedchem.7b01221>

- Lakin, N. D., & Jackson, S. P. (1999). Regulation of p53 in response to DNA damage. *Oncogene*, *18*(53), 7644–7655. <https://doi.org/10.1038/sj.onc.1203015>
- Lanctôt, K. L., Amatniek, J., Ancoli-Israel, S., Arnold, S. E., Ballard, C., Cohen-Mansfield, J., ... Boot, B. (2017). Neuropsychiatric signs and symptoms of Alzheimer's disease: New treatment paradigms. *Alzheimer's & Dementia: Translational Research & Clinical Interventions*, *3*(3), 440–449. <https://doi.org/10.1016/j.trci.2017.07.001>
- Landrieu, I., Lacosse, L., Leroy, A., Wieruszeski, J.-M., Trivelli, X., Sillen, A., ... others. (2006). NMR analysis of a Tau phosphorylation pattern. *Journal of the American Chemical Society*, *128*(11), 3575–3583.
- Lankhorst, D., Schriever, J., & Leyte, J. C. (1982). Determination of the Rotational Correlation Time of Water by Proton NMR Relaxation in H₂O and Some Related Results. *Berichte Der Bunsengesellschaft Für Physikalische Chemie*, *86*(3), 215–221. <https://doi.org/10.1002/bbpc.19820860308>
- LaPlante, S. R., Carson, R., Gillard, J., Aubry, N., Coulombe, R., Bordeleau, S., ... Beaulieu, P. L. (2013). Compound Aggregation in Drug Discovery: Implementing a Practical NMR Assay for Medicinal Chemists. *Journal of Medicinal Chemistry*, *56*(12), 5142–5150. <https://doi.org/10.1021/jm400535b>
- Lasorsa, A., Malki, I., Cantrelle, F.-X., Merzougui, H., Boll, E., Lambert, J.-C., & Landrieu, I. (2018). Structural Basis of Tau Interaction With BIN1 and Regulation by Tau Phosphorylation. *Frontiers in Molecular Neuroscience*, *11*, 421. <https://doi.org/10.3389/fnmol.2018.00421>

- Layfield, R., Fergusson, J., Aitken, A., Lowe, J., Landon, M., & Mayer, R. J. (1996). Neurofibrillary tangles of Alzheimer's disease brains contain 14-3-3 proteins. *Neuroscience Letters*, *209*(1), 57–60.
- Lebowitz, J., Lewis, M. S., & Schuck, P. (2002). Modern analytical ultracentrifugation in protein science: A tutorial review. *Protein Science*, *11*(9), 2067–2079. <https://doi.org/10.1110/ps.0207702>
- Lee, G., Newman, S. T., Gard, D. L., Band, H., & Panchamoorthy, G. (1998). Tau interacts with src-family non-receptor tyrosine kinases. *Journal of Cell Science*, *111* (Pt 21), 3167–3177.
- Lee, Gloria. (2005). Tau and src family tyrosine kinases. *Biochimica Et Biophysica Acta*, *1739*(2–3), 323–330. <https://doi.org/10.1016/j.bbadis.2004.09.002>
- Lepre, C. A., Moore, J. M., & Peng, J. W. (2004). Theory and Applications of NMR-Based Screening in Pharmaceutical Research. *Chemical Reviews*, *104*(8), 3641–3676. <https://doi.org/10.1021/cr030409h>
- Li, T., & Paudel, H. K. (2016). 14-3-3 ζ Mediates Tau Aggregation in Human Neuroblastoma M17 Cells. *PLOS ONE*, *11*(8), e0160635. <https://doi.org/10.1371/journal.pone.0160635>
- Lipinski, C. A., Lombardo, F., Dominy, B. W., & Feeney, P. J. (1997). Experimental and computational approaches to estimate solubility and permeability in drug discovery and development settings. *Advanced Drug Delivery Reviews*, *23*(1), 3–25. [https://doi.org/10.1016/S0169-409X\(96\)00423-1](https://doi.org/10.1016/S0169-409X(96)00423-1)
- Lippens, G., Landrieu, I., Smet, C., Huvent, I., Gandhi, N. S., Gigant, B., ... Lopez, J. (2016). NMR Meets Tau: Insights into Its Function and Pathology. *Biomolecules*, *6*(2), 28. <https://doi.org/10.3390/biom6020028>

- Liu, C., Song, X., Nisbet, R., & Götz, J. (2016). Co-immunoprecipitation with Tau Isoform-specific Antibodies Reveals Distinct Protein Interactions and Highlights a Putative Role for 2N Tau in Disease. *Journal of Biological Chemistry*, 291(15), 8173–8188.
<https://doi.org/10.1074/jbc.M115.641902>
- Ludwig, C., Michiels, P. J. A., Wu, X., Kavanagh, K. L., Pilka, E., Jansson, A., ... Günther, U. L. (2008). SALMON: Solvent Accessibility, Ligand binding, and Mapping of ligand Orientation by NMR Spectroscopy. *Journal of Medicinal Chemistry*, 51(1), 1–3.
<https://doi.org/10.1021/jm701020f>
- Ma, R., Wang, P., Wu, J., & Ruan, K. (2016). Process of Fragment-Based Lead Discovery—A Perspective from NMR. *Molecules*, 21(7), 854.
<https://doi.org/10.3390/molecules21070854>
- Madeira, F., Tinti, M., Murugesan, G., Berrett, E., Stafford, M., Toth, R., ... Barton, G. J. (2015). 14-3-3-Pred: Improved methods to predict 14-3-3-binding phosphopeptides. *Bioinformatics (Oxford, England)*, 31(14), 2276–2283.
<https://doi.org/10.1093/bioinformatics/btv133>
- Makin, S. (2018). The amyloid hypothesis on trial. *Nature*, 559, S4.
<https://doi.org/10.1038/d41586-018-05719-4>
- Marsh, J. A., Singh, V. K., Jia, Z., & Forman-Kay, J. D. (2006). Sensitivity of secondary structure propensities to sequence differences between α - and γ -synuclein: Implications for fibrillation. *Protein Science : A Publication of the Protein Society*, 15(12), 2795–2804.
<https://doi.org/10.1110/ps.062465306>

- Martin, L., Latypova, X., Wilson, C. M., Magnaudeix, A., Perrin, M.-L., Yardin, C., & Terro, F. (2013). Tau protein kinases: Involvement in Alzheimer's disease. *Ageing Research Reviews, 12*(1), 289–309. <https://doi.org/10.1016/j.arr.2012.06.003>
- Masliah, E., Mallory, M., Alford, M., DeTeresa, R., Hansen, L. A., McKeel, D. W., & Morris, J. C. (2001). Altered expression of synaptic proteins occurs early during progression of Alzheimer's disease. *Neurology, 56*(1), 127–129.
- Matsushita, M., & Nairn, A. C. (1999). Inhibition of the Ca²⁺/Calmodulin-dependent Protein Kinase I Cascade by cAMP-dependent Protein Kinase. *Journal of Biological Chemistry, 274*(15), 10086–10093. <https://doi.org/10.1074/jbc.274.15.10086>
- Mayer, M., & James, T. L. (2002). Detecting Ligand Binding to a Small RNA Target via Saturation Transfer Difference NMR Experiments in D₂O and H₂O. *Journal of the American Chemical Society, 124*(45), 13376–13377. <https://doi.org/10.1021/ja027526z>
- Mayer, M., & Meyer, B. (1999). Characterization of Ligand Binding by Saturation Transfer Difference NMR Spectroscopy. *Angewandte Chemie International Edition, 38*(12), 1784–1788. [https://doi.org/10.1002/\(SICI\)1521-3773\(19990614\)38:12<1784::AID-ANIE1784>3.0.CO;2-Q](https://doi.org/10.1002/(SICI)1521-3773(19990614)38:12<1784::AID-ANIE1784>3.0.CO;2-Q)
- Mayer, M., & Meyer, B. (2001). Group Epitope Mapping by Saturation Transfer Difference NMR To Identify Segments of a Ligand in Direct Contact with a Protein Receptor. *Journal of the American Chemical Society, 123*(25), 6108–6117. <https://doi.org/10.1021/ja0100120>
- Medina, M. (2018). An Overview on the Clinical Development of Tau-Based Therapeutics. *International Journal of Molecular Sciences, 19*(4). <https://doi.org/10.3390/ijms19041160>

- Megy, S., Bertho, G., Gharbi-Benarous, J., Baleux, F., Benarous, R., & Girault, J.-P. (2006). STD and TRNOESY NMR studies for the epitope mapping of the phosphorylation motif of the oncogenic protein β -catenin recognized by a selective monoclonal antibody. *FEBS Letters*, *580*(22), 5411–5422. <https://doi.org/10.1016/j.febslet.2006.08.084>
- Meyer, B., & Peters, T. (2003). NMR spectroscopy techniques for screening and identifying ligand binding to protein receptors. *Angewandte Chemie (International Ed. in English)*, *42*(8), 864–890. <https://doi.org/10.1002/anie.200390233>
- Milroy, L.-G., Bartel, M., Henen, M. A., Leysen, S., Adriaans, J. M. C., Brunsveld, L., ... Ottmann, C. (2015). Stabilizer-Guided Inhibition of Protein-Protein Interactions. *Angewandte Chemie International Edition*, *54*(52), 15720–15724. <https://doi.org/10.1002/anie.201507976>
- Milroy, L.-G., Brunsveld, L., & Ottmann, C. (2013). Stabilization and Inhibition of Protein-Protein Interactions: The 14-3-3 Case Study. *ACS Chemical Biology*, *8*(1), 27–35. <https://doi.org/10.1021/cb300599t>
- Molzan, M., Schumacher, B., Ottmann, C., Baljuls, A., Polzien, L., Weyand, M., ... Ottmann, C. (2010). Impaired Binding of 14-3-3 to C-RAF in Noonan Syndrome Suggests New Approaches in Diseases with Increased Ras Signaling. *Molecular and Cellular Biology*, *30*(19), 4698–4711. <https://doi.org/10.1128/MCB.01636-09>
- Molzan, Manuela, Kasper, S., Röglin, L., Skwarczynska, M., Sassa, T., Inoue, T., ... Ottmann, C. (2013). Stabilization of Physical RAF/14-3-3 Interaction by Cotylenin A as Treatment Strategy for RAS Mutant Cancers. *ACS Chemical Biology*, *8*(9), 1869–1875. <https://doi.org/10.1021/cb4003464>

- Musi, N., Valentine, J. M., Sickora, K. R., Baeuerle, E., Thompson, C. S., Shen, Q., & Orr, M. E. (2018). Tau protein aggregation is associated with cellular senescence in the brain. *Aging Cell*, 17(6). <https://doi.org/10.1111/accel.12840>
- Muyldermans, S. (2001). Single domain camel antibodies: Current status. *Journal of Biotechnology*, 74(4), 277–302.
- Muyldermans, Serge. (2013). Nanobodies: Natural single-domain antibodies. *Annual Review of Biochemistry*, 82, 775–797. <https://doi.org/10.1146/annurev-biochem-063011-092449>
- Nabel, G. J., & Verma, I. M. (1993). Proposed NF-kappa B/I kappa B family nomenclature. *Genes & Development*, 7(11), 2063. <https://doi.org/10.1101/gad.7.11.2063>
- Navratilova, I., & Hopkins, A. L. (2010). Fragment Screening by Surface Plasmon Resonance. *ACS Medicinal Chemistry Letters*, 1(1), 44–48. <https://doi.org/10.1021/ml900002k>
- Neugroschl, J., & Wang, S. (2011). Alzheimer's Disease: Diagnosis and Treatment Across the Spectrum of Disease Severity. *The Mount Sinai Journal of Medicine, New York*, 78(4), 596–612. <https://doi.org/10.1002/msj.20279>
- Neves, J. F., Landrieu, I., Merzougui, H., Boll, E., Hanouille, X., & Cantrelle, F.-X. (2019). Backbone chemical shift assignments of human 14-3-3 σ . *Biomolecular NMR Assignments*, 13(1), 103–107. <https://doi.org/10.1007/s12104-018-9860-1>
- Nieba, L., Nieba-Axmann, S. E., Persson, A., Hämäläinen, M., Edebratt, F., Hansson, A., ... Plückthun, A. (1997). BIACORE analysis of histidine-tagged proteins using a chelating NTA sensor chip. *Analytical Biochemistry*, 252(2), 217–228. <https://doi.org/10.1006/abio.1997.2326>

- Nomura, M., Shimizu, S., Sugiyama, T., Narita, M., Ito, T., Matsuda, H., & Tsujimoto, Y. (2003). 14-3-3 Interacts directly with and negatively regulates pro-apoptotic Bax. *The Journal of Biological Chemistry*, 278(3), 2058–2065. <https://doi.org/10.1074/jbc.M207880200>
- Obsil, T., Ghirlando, R., Klein, D. C., Ganguly, S., & Dyda, F. (2001). Crystal structure of the 14-3-3zeta:serotonin N-acetyltransferase complex. A role for scaffolding in enzyme regulation. *Cell*, 105(2), 257–267.
- Obsil, Tomas, & Obsilova, V. (2011). Structural basis of 14-3-3 protein functions. *Seminars in Cell & Developmental Biology*, 22(7), 663–672. <https://doi.org/10.1016/j.semcd.2011.09.001>
- O’Grady, C., Rempel, B. L., Sokaribo, A., Nokhrin, S., & Dmitriev, O. Y. (2012). One-step amino acid selective isotope labeling of proteins in prototrophic Escherichia coli strains. *Analytical Biochemistry*, 426(2), 126–128. <https://doi.org/10.1016/j.ab.2012.04.019>
- Okuno, S., Kitani, T., & Fujisawa, H. (2001). Regulation of Ca²⁺/Calmodulin-Dependent Protein Kinase Kinase α by cAMP-Dependent Protein Kinase: I. Biochemical Analysis. *The Journal of Biochemistry*, 130(4), 503–513. <https://doi.org/10.1093/oxfordjournals.jbchem.a003013>
- Ottmann, C. (2013). Small-molecule modulators of 14-3-3 protein–protein interactions. *Bioorganic & Medicinal Chemistry*, 21(14), 4058–4062. <https://doi.org/10.1016/j.bmc.2012.11.028>
- Ottmann, C., Marco, S., Jaspert, N., Marcon, C., Schauer, N., Weyand, M., ... Oecking, C. (2007). Structure of a 14-3-3 coordinated hexamer of the plant plasma membrane H⁺-ATPase by combining X-ray crystallography and electron cryomicroscopy. *Molecular Cell*, 25(3), 427–440. <https://doi.org/10.1016/j.molcel.2006.12.017>

- Ottmann, C., Weyand, M., Sassa, T., Inoue, T., Kato, N., Wittinghofer, A., & Oecking, C. (2009). A Structural Rationale for Selective Stabilization of Anti-tumor Interactions of 14-3-3 proteins by Cotylenin A. *Journal of Molecular Biology*, 386(4), 913–919. <https://doi.org/10.1016/j.jmb.2009.01.005>
- Papanikolopoulou, K., Grammenoudi, S., Samiotaki, M., & Skoulakis, E. M. C. (2018). Differential effects of 14-3-3 dimers on Tau phosphorylation, stability and toxicity in vivo. *Human Molecular Genetics*, 27(13), 2244–2261. <https://doi.org/10.1093/hmg/ddy129>
- Penfold, L., Woods, A., Muckett, P., Nikitin, A. Y., Kent, T. R., Zhang, S., ... Carling, D. (2018). CAMKK2 promotes prostate cancer independently of AMPK via increased lipogenesis. *Cancer Research*, canres.0585.2018. <https://doi.org/10.1158/0008-5472.CAN-18-0585>
- Peng, C. Y., Graves, P. R., Thoma, R. S., Wu, Z., Shaw, A. S., & Piwnica-Worms, H. (1997). Mitotic and G2 checkpoint control: Regulation of 14-3-3 protein binding by phosphorylation of Cdc25C on serine-216. *Science (New York, N.Y.)*, 277(5331), 1501–1505. <https://doi.org/10.1126/science.277.5331.1501>
- Pennington, K. L., Chan, T. Y., Torres, M. P., & Andersen, J. L. (2018). The dynamic and stress-adaptive signaling hub of 14-3-3: Emerging mechanisms of regulation and context-dependent protein–protein interactions. *Oncogene*, 37(42), 5587. <https://doi.org/10.1038/s41388-018-0348-3>
- Pervushin, K., Riek, R., Wider, G., & Wüthrich, K. (1997). Attenuated T2 relaxation by mutual cancellation of dipole-dipole coupling and chemical shift anisotropy indicates an avenue to NMR structures of very large biological macromolecules in solution.

Proceedings of the National Academy of Sciences of the United States of America,
94(23), 12366–12371.

Petosa, C., Masters, S. C., Bankston, L. A., Pohl, J., Wang, B., Fu, H., & Liddington, R. C. (1998).

14-3-3 ζ Binds a Phosphorylated Raf Peptide and an Unphosphorylated Peptide via Its Conserved Amphipathic Groove. *Journal of Biological Chemistry*, 273(26), 16305–16310. <https://doi.org/10.1074/jbc.273.26.16305>

Petros, A. M., Dinges, J., Augeri, D. J., Baumeister, S. A., Betebenner, D. A., Bures, M. G., ...

Fesik, S. W. (2006). Discovery of a Potent Inhibitor of the Antiapoptotic Protein Bcl-x_L from NMR and Parallel Synthesis. *Journal of Medicinal Chemistry*, 49(2), 656–663. <https://doi.org/10.1021/jm0507532>

Petrvalska, O., Kosek, D., Kukacka, Z., Tosner, Z., Man, P., Vecer, J., ... Obsil, T. (2016). Structural

Insight into the 14-3-3 Protein-Dependent Inhibition of Protein Kinase ASK1. *Journal of Biological Chemistry*, 291(39), 20753–20765. <https://doi.org/10.1074/jbc.M116.724310>

Price, D. J., Drewry, D. H., Schaller, L. T., Thompson, B. D., Reid, P. R., Maloney, P. R., ... Wang,

T. Y. (2018). An orally available, brain-penetrant CAMKK2 inhibitor reduces food intake in rodent model. *Bioorganic & Medicinal Chemistry Letters*, 28(10), 1958–1963. <https://doi.org/10.1016/j.bmcl.2018.03.034>

Psenakova, K., Petrvalska, O., Kylarova, S., Lentini Santo, D., Kalabova, D., Herman, P., ... Obsil,

T. (2018). 14-3-3 protein directly interacts with the kinase domain of calcium/calmodulin-dependent protein kinase kinase (CaMKK2). *Biochimica Et Biophysica Acta. General Subjects*, 1862(7), 1612–1625. <https://doi.org/10.1016/j.bbagen.2018.04.006>

- Qi, H., Cantrelle, F.-X., Benhelli-Mokrani, H., Smet-Nocca, C., Buée, L., Lippens, G., ... Landrieu, I. (2015). Nuclear magnetic resonance spectroscopy characterization of interaction of Tau with DNA and its regulation by phosphorylation. *Biochemistry*, *54*(7), 1525–1533. <https://doi.org/10.1021/bi5014613>
- Qureshi, H. Y., Han, D., MacDonald, R., & Paudel, H. K. (2013). Overexpression of 14-3-3 ζ Promotes Tau Phosphorylation at Ser262 and Accelerates Proteosomal Degradation of Synaptophysin in Rat Primary Hippocampal Neurons. *PLOS ONE*, *8*(12), e84615. <https://doi.org/10.1371/journal.pone.0084615>
- Qureshi, H. Y., Li, T., MacDonald, R., Cho, C. M., Leclerc, N., & Paudel, H. K. (2013). Interaction of 14-3-3 ζ with Microtubule-Associated Protein Tau within Alzheimer's Disease Neurofibrillary Tangles. *Biochemistry*, *52*(37), 6445–6455. <https://doi.org/10.1021/bi400442d>
- Racioppi, L., & Means, A. R. (2012). Calcium/calmodulin-dependent protein kinase kinase 2: Roles in signaling and pathophysiology. *The Journal of Biological Chemistry*, *287*(38), 31658–31665. <https://doi.org/10.1074/jbc.R112.356485>
- Rajagopalan, S., Jaulent, A. M., Wells, M., Veprintsev, D. B., & Fersht, A. R. (2008). 14-3-3 activation of DNA binding of p53 by enhancing its association into tetramers. *Nucleic Acids Research*, *36*(18), 5983–5991. <https://doi.org/10.1093/nar/gkn598>
- Rega, M. F., Wu, B., Wei, J., Zhang, Z., Cellitti, J. F., & Pellecchia, M. (2011). SAR by Interligand Nuclear Overhauser Effects (ILOEs) Based Discovery of Acylsulfonamide Compounds Active against Bcl-xL and Mcl-1. *Journal of Medicinal Chemistry*, *54*(17), 6000–6013. <https://doi.org/10.1021/jm200826s>

- Richter, A., Rose, R., Hedberg, C., Waldmann, H., & Ottmann, C. (2012). An Optimised Small-Molecule Stabiliser of the 14-3-3–PMA2 Protein–Protein Interaction. *Chemistry – A European Journal*, *18*(21), 6520–6527. <https://doi.org/10.1002/chem.201103761>
- Röglin, L., Thiel, P., Kohlbacher, O., & Ottmann, C. (2012). Covalent attachment of pyridoxal-phosphate derivatives to 14-3-3 proteins. *Proceedings of the National Academy of Sciences*, *109*(18), E1051–E1053. <https://doi.org/10.1073/pnas.1116592109>
- Rose, R., Erdmann, S., Bovens, S., Wolf, A., Rose, M., Hennig, S., ... Ottmann, C. (2010). Identification and Structure of Small-Molecule Stabilizers of 14–3–3 Protein–Protein Interactions. *Angewandte Chemie International Edition*, *49*(24), 4129–4132. <https://doi.org/10.1002/anie.200907203>
- Rudenko, I. N., & Cookson, M. R. (2010). 14-3-3 proteins are promising LRRK2 interactors. *Biochemical Journal*, *430*(3), e5–e6. <https://doi.org/10.1042/BJ20101200>
- S. Raghothama. (2010). NMR of peptides. *Journal of the Indian Institute of Science*, *90*(1).
- Sadik, G., Tanaka, T., Kato, K., Yamamori, H., Nessa, B. N., Morihara, T., & Takeda, M. (2009). Phosphorylation of tau at Ser214 mediates its interaction with 14-3-3 protein: Implications for the mechanism of tau aggregation. *Journal of Neurochemistry*, *108*(1), 33–43. <https://doi.org/10.1111/j.1471-4159.2008.05716.x>
- Salzmann, M., Pervushin, K., Wider, G., Senn, H., & Wüthrich, K. (1998). TROSY in triple-resonance experiments: New perspectives for sequential NMR assignment of large proteins. *Proceedings of the National Academy of Sciences of the United States of America*, *95*(23), 13585–13590.
- Santiago, A. da S., Couñago, R. M., Ramos, P. Z., Godoi, P. H. C., Massirer, K. B., Gileadi, O., & Elkins, J. M. (2018). Structural Analysis of Inhibitor Binding to CAMKK1 Identifies

- Features Necessary for Design of Specific Inhibitors. *Scientific Reports*, 8.
<https://doi.org/10.1038/s41598-018-33043-4>
- Sato, S., Jung, H., Nakagawa, T., Pawlosky, R., Takeshima, T., Lee, W.-R., ... Uyeda, K. (2016). Metabolite Regulation of Nuclear Localization of Carbohydrate-response Element-binding Protein (ChREBP) ROLE OF AMP AS AN ALLOSTERIC INHIBITOR. *Journal of Biological Chemistry*, 291(20), 10515–10527.
<https://doi.org/10.1074/jbc.M115.708982>
- Sattler, M., & Fesik, S. W. (1996). Use of deuterium labeling in NMR: Overcoming a sizeable problem. *Structure*, 4(11), 1245–1249. [https://doi.org/10.1016/S0969-2126\(96\)00133-5](https://doi.org/10.1016/S0969-2126(96)00133-5)
- Schneider, A., Biernat, J., von Bergen, M., Mandelkow, E., & Mandelkow, E.-M. (1999). Phosphorylation that Detaches Tau Protein from Microtubules (Ser262, Ser214) Also Protects It against Aggregation into Alzheimer Paired Helical Filaments. *Biochemistry*, 38(12), 3549–3558. <https://doi.org/10.1021/bi981874p>
- Schuck, P. (2000). Size-distribution analysis of macromolecules by sedimentation velocity ultracentrifugation and lamm equation modeling. *Biophysical Journal*, 78(3), 1606–1619. [https://doi.org/10.1016/S0006-3495\(00\)76713-0](https://doi.org/10.1016/S0006-3495(00)76713-0)
- Scott, D. E., Coyne, A. G., Hudson, S. A., & Abell, C. (2012). Fragment-Based Approaches in Drug Discovery and Chemical Biology. *Biochemistry*, 51(25), 4990–5003.
<https://doi.org/10.1021/bi3005126>
- Seifert, R., & Wieland, T. (Eds.). (2005). *G protein-coupled receptors as drug targets: Analysis of activation and constitutive activity*. Weinheim: Wiley-VCH.

- Selkoe, D. J. (2002). Alzheimer's Disease Is a Synaptic Failure. *Science*, 298(5594), 789–791.
<https://doi.org/10.1126/science.1074069>
- Selkoe, D. J., & Hardy, J. (2016). The amyloid hypothesis of Alzheimer's disease at 25 years. *EMBO Molecular Medicine*, 8(6), 595–608.
<https://doi.org/10.15252/emmm.201606210>
- Sevigny, J., Chiao, P., Bussière, T., Weinreb, P. H., Williams, L., Maier, M., ... Sandrock, A. (2016). The antibody aducanumab reduces A β plaques in Alzheimer's disease. *Nature*, 537(7618), 50–56. <https://doi.org/10.1038/nature19323>
- Shen, Y., & Bax, A. (2013). Protein backbone and sidechain torsion angles predicted from NMR chemical shifts using artificial neural networks. *Journal of Biomolecular NMR*, 56(3), 227–241. <https://doi.org/10.1007/s10858-013-9741-y>
- Shen, Y., Delaglio, F., Cornilescu, G., & Bax, A. (2009). TALOS+: A hybrid method for predicting protein backbone torsion angles from NMR chemical shifts. *Journal of Biomolecular NMR*, 44(4), 213–223. <https://doi.org/10.1007/s10858-009-9333-z>
- Shiizaki, S., Naguro, I., & Ichijo, H. (2013). Activation mechanisms of ASK1 in response to various stresses and its significance in intracellular signaling. *Advances in Biological Regulation*, 53(1), 135–144. <https://doi.org/10.1016/j.jbior.2012.09.006>
- Shuker, S. B., Hajduk, P. J., Meadows, R. P., & Fesik, S. W. (1996). Discovering High-Affinity Ligands for Proteins: SAR by NMR. *Science*, 274(5292), 1531–1534.
<https://doi.org/10.1126/science.274.5292.1531>
- Sigurdsson, E. M. (2018). Tau Immunotherapies for Alzheimer's Disease and Related Tauopathies: Progress and Potential Pitfalls. *Journal of Alzheimer's Disease : JAD*, 64(Suppl 1), S555–S565. <https://doi.org/10.3233/JAD-179937>

- Sijbesma, E., Hallenbeck, K. K., Leysen, S., de Vink, P., Skora, L., Jahnke, W., ... Ottmann, C. (2019). Site-Directed Fragment-based Screening for the Discovery of Protein-Protein Interaction Stabilizers. *Journal of the American Chemical Society*. <https://doi.org/10.1021/jacs.8b11658>
- Silhan, J., Obsilova, V., Vecer, J., Herman, P., Sulc, M., Teisinger, J., & Obsil, T. (2004). 14-3-3 Protein C-terminal Stretch Occupies Ligand Binding Groove and Is Displaced by Phosphopeptide Binding. *Journal of Biological Chemistry*, 279(47), 49113–49119. <https://doi.org/10.1074/jbc.M408671200>
- Sillen, A., Barbier, P., Landrieu, I., Lefebvre, S., Wieruszeski, J.-M., Leroy, A., ... Lippens, G. (2007). NMR investigation of the interaction between the neuronal protein tau and the microtubules. *Biochemistry*, 46(11), 3055–3064. <https://doi.org/10.1021/bi061920i>
- Sluchanko, N. N. (2018). Association of Multiple Phosphorylated Proteins with the 14-3-3 Regulatory Hubs: Problems and Perspectives. *Journal of Molecular Biology*, 430(1), 20–26. <https://doi.org/10.1016/j.jmb.2017.11.010>
- Sluchanko, N. N., Beelen, S., Kulikova, A. A., Weeks, S. D., Antson, A. A., Gusev, N. B., & Strelkov, S. V. (2017). Structural basis for the interaction of a human small heat shock protein with the 14-3-3 universal signaling regulator. *Structure (London, England : 1993)*, 25(2), 305–316. <https://doi.org/10.1016/j.str.2016.12.005>
- Sluchanko, N. N., Seit-Nebi, A. S., & Gusev, N. B. (2009). Phosphorylation of more than one site is required for tight interaction of human tau protein with 14-3-3 ζ . *FEBS Letters*, 583(17), 2739–2742. <https://doi.org/10.1016/j.febslet.2009.07.043>

- Sluchanko, N. N., Sudnitsyna, M. V., Seit-Nebi, A. S., Antson, A. A., & Gusev, N. B. (2011). Properties of the Monomeric Form of Human 14-3-3 ζ Protein and Its Interaction with Tau and HspB6. *Biochemistry*, *50*(45), 9797–9808. <https://doi.org/10.1021/bi201374s>
- Sprangers, R., & Kay, L. E. (2007). Quantitative dynamics and binding studies of the 20S proteasome by NMR. *Nature*, *445*(7128), 618–622. <https://doi.org/10.1038/nature05512>
- Sprangers, R., Li, X., Mao, X., Rubinstein, J. L., Schimmer, A. D., & Kay, L. E. (2008). TROSY-based NMR evidence for a novel class of 20S proteasome inhibitors. *Biochemistry*, *47*(26), 6727–6734. <https://doi.org/10.1021/bi8005913>
- Stark, J. L., Eghbalnia, H. R., Lee, W., Westler, W. M., & Markley, J. L. (2016). NMRmix: A Tool for the Optimization of Compound Mixtures in 1D ^1H NMR Ligand Affinity Screens. *Journal of Proteome Research*, *15*(4), 1360–1368. <https://doi.org/10.1021/acs.jproteome.6b00121>
- Stark, J. L., & Powers, R. (2011). Application of NMR and Molecular Docking in Structure-Based Drug Discovery. In G. Zhu (Ed.), *NMR of Proteins and Small Biomolecules* (Vol. 326, pp. 1–34). https://doi.org/10.1007/128_2011_213
- Steinacker, P., Aitken, A., & Otto, M. (2011). 14-3-3 proteins in neurodegeneration. *Seminars in Cell & Developmental Biology*, *22*(7), 696–704. <https://doi.org/10.1016/j.semcdb.2011.08.005>
- Stevens, L. M., Lam, C. V., Leysen, S. F. R., Meijer, F. A., van Scheppingen, D. S., de Vries, R. M. J. M., ... Ottmann, C. (2016). Characterization and small-molecule stabilization of the multisite tandem binding between 14-3-3 and the R domain of CFTR. *Proceedings of*

the National Academy of Sciences, 113(9), E1152–E1161.

<https://doi.org/10.1073/pnas.1516631113>

Stevens, L. M., Sijbesma, E., Botta, M., MacKintosh, C., Obsil, T., Landrieu, I., ... Ottmann, C.

(2018). Modulators of 14-3-3 Protein–Protein Interactions. *Journal of Medicinal Chemistry*, 61(9), 3755–3778. <https://doi.org/10.1021/acs.jmedchem.7b00574>

Takahashi, S., Wakui, H., Gustafsson, J.-Å., Zilliacus, J., & Itoh, H. (2000). Functional Interaction

of the Immunosuppressant Mizoribine with the 14-3-3 Protein. *Biochemical and Biophysical Research Communications*, 274(1), 87–92.

<https://doi.org/10.1006/bbrc.2000.3104>

Taoka, K., Ohki, I., Tsuji, H., Furuita, K., Hayashi, K., Yanase, T., ... Shimamoto, K. (2011). 14-3-

3 proteins act as intracellular receptors for rice Hd3a florigen. *Nature*, 476(7360), 332–335. <https://doi.org/10.1038/nature10272>

Teich, A. F., & Arancio, O. (2012). Is the Amyloid Hypothesis of Alzheimer's disease therapeutically relevant? *Biochemical Journal*, 446(2), 165–177.

<https://doi.org/10.1042/BJ20120653>

Teodor Parella. (n.d.). NMR guide 3.5: ¹H Chemical Shifts of aminoacids. Retrieved 26 April

2019, from <http://triton.iqfr.csic.es/guide/eNMR/proteins/chempro5.html>

Terwel, D., Dewachter, I., & Van Leuven, F. (2002). Axonal transport, tau protein, and neurodegeneration in Alzheimer's disease. *Neuromolecular Medicine*, 2(2), 151–165.

<https://doi.org/10.1385/NMM:2:2:151>

Thandavarayan, R. A., Watanabe, K., Ma, M., Veeraveedu, P. T., Gurusamy, N., Palaniyandi, S.

S., ... Aizawa, Y. (2008). 14-3-3 protein regulates Ask1 signaling and protects against

- diabetic cardiomyopathy. *Biochemical Pharmacology*, 75(9), 1797–1806.
<https://doi.org/10.1016/j.bcp.2008.02.003>
- Thiel, P., Kaiser, M., & Ottmann, C. (2012). Small-Molecule Stabilization of Protein-Protein Interactions: An Underestimated Concept in Drug Discovery? *Angewandte Chemie International Edition*, 51(9), 2012–2018. <https://doi.org/10.1002/anie.201107616>
- Toleman, C. A., Schumacher, M. A., Yu, S.-H., Zeng, W., Cox, N. J., Smith, T. J., ... Boyce, M. (2018). Structural basis of O-GlcNAc recognition by mammalian 14-3-3 proteins. *Proceedings of the National Academy of Sciences*, 115(23), 5956–5961.
<https://doi.org/10.1073/pnas.1722437115>
- Tugaeva, K. V., Tsvetkov, P. O., & Sluchanko, N. N. (2017). Bacterial co-expression of human Tau protein with protein kinase A and 14-3-3 for studies of 14-3-3/phospho-Tau interaction. *PLOS ONE*, 12(6), e0178933.
- Tugarinov, V., Kanelis, V., & Kay, L. E. (2006). Isotope labeling strategies for the study of high-molecular-weight proteins by solution NMR spectroscopy. *Nature Protocols*, 1(2), 749–754. <https://doi.org/10.1038/nprot.2006.101>
- Umahara, T., Uchihara, T., Tsuchiya, K., Nakamura, A., Iwamoto, T., Ikeda, K., & Takasaki, M. (2004). 14-3-3 proteins and zeta isoform containing neurofibrillary tangles in patients with Alzheimer's disease. *Acta Neuropathologica*, 108(4), 279–286.
<https://doi.org/10.1007/s00401-004-0885-4>
- Unione, L., Galante, S., Díaz, D., Cañada, F. J., & Jiménez-Barbero, J. (2014). NMR and molecular recognition. The application of ligand-based NMR methods to monitor molecular interactions. *MedChemComm*, 5(9), 1280–1289.
<https://doi.org/10.1039/C4MD00138A>

- Valenti, D., Hristeva, S., Tzalis, D., & Ottmann, C. (2019). Clinical candidates modulating protein-protein interactions: The fragment-based experience. *European Journal of Medicinal Chemistry*, *167*, 76–95. <https://doi.org/10.1016/j.ejmech.2019.01.084>
- Vanwetswinkel, S., Heetebrij, R. J., van Duynhoven, J., Hollander, J. G., Filippov, D. V., Hajduk, P. J., & Siegal, G. (2005). TINS, Target Immobilized NMR Screening: An Efficient and Sensitive Method for Ligand Discovery. *Chemistry & Biology*, *12*(2), 207–216. <https://doi.org/10.1016/j.chembiol.2004.12.004>
- Velvadapu, V., Farmer, B. T., & Reitz, A. B. (2015). Fragment-Based Drug Discovery. In C. G. Wermuth, D. Aldous, P. Raboisson, & D. Rognan (Eds.), *The Practice of Medicinal Chemistry (Fourth Edition)* (pp. 161–180). <https://doi.org/10.1016/B978-0-12-417205-0.00007-9>
- Viegas, A., Manso, J., Nobrega, F. L., & Cabrita, E. J. (2011). Saturation-Transfer Difference (STD) NMR: A Simple and Fast Method for Ligand Screening and Characterization of Protein Binding. *Journal of Chemical Education*, *88*(7), 990–994. <https://doi.org/10.1021/ed101169t>
- Vishal, S., Sourabh, A., & Harkirat, S. (2011). Alois Alzheimer (1864-1915) and the Alzheimer syndrome. *Journal of Medical Biography*, *19*(1), 32–33. <https://doi.org/10.1258/jmb.2010.010037>
- Wakui, H., Wright, A. P., Gustafsson, J., & Zilliacus, J. (1997). Interaction of the ligand-activated glucocorticoid receptor with the 14-3-3 eta protein. *The Journal of Biological Chemistry*, *272*(13), 8153–8156. <https://doi.org/10.1074/jbc.272.13.8153>

- Wang, C., Grey, M. J., & Palmer, A. G. (2001). CPMG sequences with enhanced sensitivity to chemical exchange. *Journal of Biomolecular NMR*, 21(4), 361–366. <https://doi.org/10.1023/A:1013328206498>
- Wang, X., Li, J.-P., Kuo, H.-K., Chiu, L.-L., Dement, G. A., Lan, J.-L., ... Tan, T.-H. (2012). Down-regulation of B cell receptor signaling by hematopoietic progenitor kinase 1 (HPK1)-mediated phosphorylation and ubiquitination of activated B cell linker protein (BLNK). *The Journal of Biological Chemistry*, 287(14), 11037–11048. <https://doi.org/10.1074/jbc.M111.310946>
- Waterman, M. J., Stavridi, E. S., Waterman, J. L., & Halazonetis, T. D. (1998). ATM-dependent activation of p53 involves dephosphorylation and association with 14-3-3 proteins. *Nature Genetics*, 19(2), 175–178. <https://doi.org/10.1038/542>
- Weingarten, M. D., Lockwood, A. H., Hwo, S. Y., & Kirschner, M. W. (1975). A protein factor essential for microtubule assembly. *Proceedings of the National Academy of Sciences of the United States of America*, 72(5), 1858–1862.
- Weller, J., & Budson, A. (2018). Current understanding of Alzheimer’s disease diagnosis and treatment. *F1000Research*, 7. <https://doi.org/10.12688/f1000research.14506.1>
- Williamson, M. P. (2013). Using chemical shift perturbation to characterise ligand binding. *Progress in Nuclear Magnetic Resonance Spectroscopy*, 73, 1–16. <https://doi.org/10.1016/j.pnmrs.2013.02.001>
- Wishart, D. S., & Sykes, B. D. (1994). Chemical shifts as a tool for structure determination. *Methods in Enzymology*, 239, 363–392.

- Wishart, David S., & Sykes, B. D. (1994). The ^{13}C Chemical-Shift Index: A simple method for the identification of protein secondary structure using ^{13}C chemical-shift data. *Journal of Biomolecular NMR*, 4(2), 171–180. <https://doi.org/10.1007/BF00175245>
- World Alzheimer Report 2018: The state of the art of dementia research: New frontiers. (2018). *NEW FRONTIERS*, 48.
- Würtele, M., Jelic-Ottmann, C., Wittinghofer, A., & Oecking, C. (2003). Structural view of a fungal toxin acting on a 14-3-3 regulatory complex. *The EMBO Journal*, 22(5), 987–994.
- Wüthrich, K., Spitzfaden, C., Memmert, K., Widmer, H., & Wider, G. (1991). Protein secondary structure determination by NMR Application with recombinant human cyclophilin. *FEBS Letters*, 285(2), 237–247. [https://doi.org/10.1016/0014-5793\(91\)80808-G](https://doi.org/10.1016/0014-5793(91)80808-G)
- Xu, J., & Van Doren, S. R. (2016). Binding Isotherms and Time Courses Readily from Magnetic Resonance. *Analytical Chemistry*, 88(16), 8172–8178. <https://doi.org/10.1021/acs.analchem.6b01918>
- Yagishita, S., Itoh, Y., Nan, W., & Amano, N. (1981). Reappraisal of the fine structure of Alzheimer's neurofibrillary tangles. *Acta Neuropathologica*, 54(3), 239–246. <https://doi.org/10.1007/BF00687747>
- Yang, H.-Y., Wen, Y.-Y., Chen, C.-H., Lozano, G., & Lee, M.-H. (2003). 14-3-3 sigma positively regulates p53 and suppresses tumor growth. *Molecular and Cellular Biology*, 23(20), 7096–7107. <https://doi.org/10.1128/mcb.23.20.7096-7107.2003>
- Zauner, D., Taskinen, B., Eichinger, D., Flattinger, C., Ruttmann, B., Knoglinger, C., ... Hytönen, V. P. (2016). Regenerative biosensor chips based on switchable mutants of avidin—A systematic study. *Sensors and Actuators B: Chemical*, 229, 646–654. <https://doi.org/10.1016/j.snb.2016.02.039>

- Zhang, H., Neal, S., & Wishart, D. S. (2003). RefDB: A database of uniformly referenced protein chemical shifts. *Journal of Biomolecular NMR*, 25(3), 173–195.
<https://doi.org/10.1023/A:1022836027055>
- Zhang, L., Chen, J., & Fu, H. (1999). Suppression of apoptosis signal-regulating kinase 1-induced cell death by 14-3-3 proteins. *Proceedings of the National Academy of Sciences of the United States of America*, 96(15), 8511–8515.
<https://doi.org/10.1073/pnas.96.15.8511>
- Zhao, J., Du, Y., Horton, J. R., Upadhyay, A. K., Lou, B., Bai, Y., ... Fu, H. (2011). Discovery and structural characterization of a small molecule 14-3-3 protein-protein interaction inhibitor. *Proceedings of the National Academy of Sciences*, 108(39), 16212–16216.
<https://doi.org/10.1073/pnas.1100012108>

NMR STUDY OF 14-3-3 PROTEIN-PROTEIN INTERACTIONS AND MODULATION THEREOF BY SMALL MOLECULES

14-3-3 proteins are adapter proteins that exert their biological functions by modulating the activity of hundreds of proteins. This remarkable interactome makes 14-3-3 proteins influent actors in many cellular events and, by consequence, in several pathologies. The selective stabilization or inhibition of 14-3-3 protein-protein interactions (PPIs) are therefore seen as promising approaches for finding innovative therapies for a number of conditions like Alzheimer's, cancer or Parkinson. Our first objective towards finding small molecule modulators of these targets was to obtain the molecular detail of 14-3-3 PPIs. To this end, using Nuclear Magnetic Resonance (NMR), we assigned the backbone chemical shifts of 14-3-3 σ . We then studied the 14-3-3/phosphorylated Tau interaction and found that Tau binds strictly within the amphipathic binding groove of 14-3-3 and can anchor in both monomers of the 14-3-3 dimer. We also studied the 14-3-3/p53 interaction and showed by NMR, that intramolecular interactions within the peptide define a conformation that drives the affinity towards 14-3-3. We then focused on the optimization of NMR assays for screening and characterization of the effect of small-molecules binding to 14-3-3 or 14-3-3 complexes with target's phosphopeptides. We used, for example, phospho-mimetic peptides to inhibit the Tau/14-3-3 interaction. In a different strategy, we screened a fragment library against 14-3-3 σ and found three hits binding to different regions of the protein. Using our NMR assays we further characterized small molecules binding 14-3-3 complexes with, for example, p53 and p65 peptides and demonstrated the stabilization capacity of some compounds.

Keywords: Nuclear magnetic resonance, 14-3-3, Protein-protein interactions, drug discovery

ÉTUDE PAR RÉSONANCE MAGNÉTIQUE NUCLÉAIRE DES INTERACTIONS PROTÉINE-PROTÉINE DE 14-3-3 ET LEUR MODULATION AVEC DES PETITES MOLÉCULES

Les protéines 14-3-3 sont des protéines adaptatrices qui exercent leurs fonctions biologiques en modulant l'activité de centaines d'autres protéines. De part leur impressionnant interactome, les protéines 14-3-3 sont des acteurs qui influencent de nombreux événements cellulaires et, par conséquent, de maladies associées. La stabilisation ou l'inhibition sélective d'interactions protéine-protéine (IPP) de 14-3-3 sont considérées comme des approches prometteuses pour trouver des thérapies innovantes contre des maladies comme la maladie d'Alzheimer, certains cancers ou la maladie de Parkinson. Notre premier but afin de trouver des petites molécules capables de moduler ces cibles a été d'étudier au niveau moléculaire des IPP de 14-3-3. Dans ce but, nous avons utilisé la Résonance Magnétique Nucléaire (RMN) pour attribuer les déplacements chimiques des atomes du squelette de 14-3-3 σ . Nous avons ensuite étudié l'interaction entre 14-3-3 et la protéine Tau phosphorylée. Nous avons découvert que Tau se lie strictement dans la cavité amphipathique de 14-3-3 et peut s'ancrer aux deux monomères du dimère de 14-3-3. Nous avons aussi étudié l'interaction 14-3-3/p53 et avons découvert, en utilisant la RMN, que l'affinité du peptide p53 envers 14-3-3 est liée à des interactions intramoléculaires au niveau du peptide. Nous nous sommes enfin focalisés sur l'optimisation d'expériences RMN visant le criblage et la caractérisation de l'activité des petites molécules qui se lient à 14-3-3 ou à des complexes de 14-3-3 avec des peptides phosphorylés. Nous avons aussi utilisé des peptides phospho-mimétiques pour inhiber l'interaction 14-3-3/Tau. D'autre part, nous avons criblé une bibliothèque de fragments contre 14-3-3 σ et trouvé trois *hits* qui se lient à des régions différentes de la protéine. Des expériences RMN ont ensuite permis de caractériser l'activité de certaines petites molécules actives sur des complexes de 14-3-3 avec, par exemple des peptides de p53 ou p65, et nous avons aussi démontré la capacité de certains de ces composés à stabiliser les complexes.

Mots-clés : Résonance magnétique nucléaire, 14-3-3, interactions protéine-protéine, découverte de médicaments